

A NEW GENERATION OF ORGANIC LIGHT-EMITTING MATERIALS AND DEVICES

EDITED BY: Shi-Jian Su, Lian Duan and Hisahiro Sasabe
PUBLISHED IN: Frontiers in Chemistry





frontiers

Frontiers eBook Copyright Statement

The copyright in the text of individual articles in this eBook is the property of their respective authors or their respective institutions or funders. The copyright in graphics and images within each article may be subject to copyright of other parties. In both cases this is subject to a license granted to Frontiers.

The compilation of articles constituting this eBook is the property of Frontiers.

Each article within this eBook, and the eBook itself, are published under the most recent version of the Creative Commons CC-BY licence.

The version current at the date of publication of this eBook is CC-BY 4.0. If the CC-BY licence is updated, the licence granted by Frontiers is automatically updated to the new version.

When exercising any right under the CC-BY licence, Frontiers must be attributed as the original publisher of the article or eBook, as applicable.

Authors have the responsibility of ensuring that any graphics or other materials which are the property of others may be included in the CC-BY licence, but this should be checked before relying on the CC-BY licence to reproduce those materials. Any copyright notices relating to those materials must be complied with.

Copyright and source acknowledgement notices may not be removed and must be displayed in any copy, derivative work or partial copy which includes the elements in question.

All copyright, and all rights therein, are protected by national and international copyright laws. The above represents a summary only. For further information please read Frontiers' Conditions for Website Use and Copyright Statement, and the applicable CC-BY licence.

ISSN 1664-8714

ISBN 978-2-88963-163-6

DOI 10.3389/978-2-88963-163-6

About Frontiers

Frontiers is more than just an open-access publisher of scholarly articles: it is a pioneering approach to the world of academia, radically improving the way scholarly research is managed. The grand vision of Frontiers is a world where all people have an equal opportunity to seek, share and generate knowledge. Frontiers provides immediate and permanent online open access to all its publications, but this alone is not enough to realize our grand goals.

Frontiers Journal Series

The Frontiers Journal Series is a multi-tier and interdisciplinary set of open-access, online journals, promising a paradigm shift from the current review, selection and dissemination processes in academic publishing. All Frontiers journals are driven by researchers for researchers; therefore, they constitute a service to the scholarly community. At the same time, the Frontiers Journal Series operates on a revolutionary invention, the tiered publishing system, initially addressing specific communities of scholars, and gradually climbing up to broader public understanding, thus serving the interests of the lay society, too.

Dedication to Quality

Each Frontiers article is a landmark of the highest quality, thanks to genuinely collaborative interactions between authors and review editors, who include some of the world's best academicians. Research must be certified by peers before entering a stream of knowledge that may eventually reach the public - and shape society; therefore, Frontiers only applies the most rigorous and unbiased reviews.

Frontiers revolutionizes research publishing by freely delivering the most outstanding research, evaluated with no bias from both the academic and social point of view. By applying the most advanced information technologies, Frontiers is catapulting scholarly publishing into a new generation.

What are Frontiers Research Topics?

Frontiers Research Topics are very popular trademarks of the Frontiers Journals Series: they are collections of at least ten articles, all centered on a particular subject. With their unique mix of varied contributions from Original Research to Review Articles, Frontiers Research Topics unify the most influential researchers, the latest key findings and historical advances in a hot research area! Find out more on how to host your own Frontiers Research Topic or contribute to one as an author by contacting the Frontiers Editorial Office: researchtopics@frontiersin.org

A NEW GENERATION OF ORGANIC LIGHT-EMITTING MATERIALS AND DEVICES

Topic Editors:

Shi-Jian Su, South China University of Technology, China

Lian Duan, Tsinghua University, China

Hisahiro Sasabe, Yamagata University, Japan

Since the invention of the first efficient organic light-emitting diodes (OLEDs) by C. T. Tang and S. VanSlyke, OLEDs have attracted close interest as a promising candidate for next-generation full-color displays and future solid-state lighting sources because of a number of advantages like high brightness and contrast, high luminous efficiency, fast response time, wide viewing angle, low power consumption, and light weight. The recombination of holes and electrons under electrical excitation typically generates 25% singlet excitons and 75% triplet excitons. For traditional fluorescent OLEDs, only 25% singlet excitons can be utilized to emit light, while the other 75% triplet excitons are generally wasted through nonradiative transition. By adopting noble metal phosphorescent complexes, an internal quantum efficiency (IQE) of 100% could be achieved by utilizing both the 25% singlet excitons and 75% triplet excitons. However, these phosphors usually contain nonrenewable and high-cost iridium or platinum noble metals.

Most recently, unity IQE has been readily achieved through noble metal-free purely organic emitters, such as thermally activated delayed fluorescence (TADF) emitters, hybridized local and charge-transfer state (HLCT) “hot exciton” emitters, binary- or ternary-mixed donor-acceptor exciplex emitters, and neutral π radical emitters, etc. In addition, the combination of conventional p-type hole-transport and n-type electron-transport materials in an appropriate device structure can also provide an uncommon efficiency. Both strategies are essential and attractive for high-performance and low-cost full-color displays and white OLED applications.

This Research Topic mainly focus on this new generation of organic light-emitting materials and devices, including design, synthesis, and characterization of light-emitting organic molecules with tunable excited states, and their structural, electrical, and photophysical properties. Contributions relating to carrier transporting materials and corresponding device engineering are also included. Two mini reviews and thirteen original research articles by recognized academic experts in their respective fields are collected in this Research Topic, which will offer a broad perspective of noble metal-free organic light emitters, including conventional fluorescent emitters, TADF emitters, HLCT emitters, exciplex emitters, aggregation-induced emission (AIE) luminogens, and their corresponding devices.

We believe this eBook should attract the attention of multidisciplinary researchers in the fields of materials science, organic synthesis, and electronic device engineering, especially for those engaged in OLED-related areas.

Citation: Su, S.-J., Duan, L., Sasabe, H., eds. (2019). A New Generation of Organic Light-Emitting Materials and Devices. Lausanne: Frontiers Media SA.
doi: 10.3389/978-2-88963-163-6

Table of Contents

MINI REVIEW

06 Recent Applications of Interfacial Exciplex as Ideal Host of Power-Efficient OLEDs

Baohua Zhang and Zhiyuan Xie

14 Recent Advances in Organic Light-Emitting Diodes Based on Pure Organic Room Temperature Phosphorescence Materials

Ge Zhan, Zhiwei Liu, Zuqiang Bian and Chunhui Huang

ORIGINAL RESEARCH

20 Modulation of Excited State Property Based on Benzo[a, c]phenazine Acceptor: Three Typical Excited States and Electroluminescence Performance

Changjiang Zhou, Shengbing Xiao, Man Wang, Wenzhe Jiang, Haichao Liu, Shitong Zhang and Bing Yang

30 Thiophene Disubstituted Benzothiadiazole Derivatives: An Effective Planarization Strategy Toward Deep-Red to Near-Infrared (NIR) Organic Light-Emitting Diodes

Wentao Xie, Binbin Li, Xinyi Cai, Mengke Li, Zhenyang Qiao, Xiaohui Tang, Kunkun Liu, Cheng Gu, Yuguang Ma and Shi-Jian Su

38 Highly Efficient Thermally Activated Delayed Fluorescence Emitter Developed by Replacing Carbazole With 1,3,6,8-Tetramethyl-Carbazole

Jia-Lin Cai, Wei Liu, Kai Wang, Jia-Xiong Chen, Yi-Zhong Shi, Ming Zhang, Cai-Jun Zheng, Si-Lu Tao and Xiao-Hong Zhang

48 High-Efficiency Sky Blue-To-Green Fluorescent Emitters Based on 3-Pyridinecarbonitrile Derivatives

Yuki Masuda, Hisahiro Sasabe, Hiroki Arai, Natsuki Onuma and Junji Kido

55 Suppressing Efficiency Roll-Off of TADF Based OLEDs by Constructing Emitting Layer With Dual Delayed Fluorescence

Yuewei Zhang, Zhiqiang Li, Chenglong Li and Yue Wang

64 Pyrazine-Based Blue Thermally Activated Delayed Fluorescence Materials: Combine Small Singlet–Triplet Splitting With Large Fluorescence Rate

Junyuan Liu, Keren Zhou, Dan Wang, Chao Deng, Ke Duan, Qi Ai and Qisheng Zhang

73 Phenothiazinen-Dimesitylarylborane-Based Thermally Activated Delayed Fluorescence: High-Performance Non-doped OLEDs With Reduced Efficiency Roll-Off at High Luminescence

Xiangyang Tang, Yanchun Tao, Hui Liu, Futong Liu, Xin He, Qiming Peng, Jinyu Li and Ping Lu

85 Synthesis, Structures, and Photophysical Properties of Novel Four-Coordinate Cu(I) Complexes Supported by Chelating N-Heterocyclic Carbene Ligands

Zhiqiang Wang, Xiaojuan Sun, Chen Xu and Baoming Ji

- 95** *New Aggregation-Induced Delayed Fluorescence Luminogens With Through-Space Charge Transfer for Efficient Non-doped OLEDs*
Panpan Zhang, Jiajie Zeng, Jingjing Guo, Shijie Zhen, Biao Xiao, Zhiming Wang, Zujin Zhao and Ben Zhong Tang
- 106** *Design of Efficient Exciplex Emitters by Decreasing the Energy Gap Between the Local Excited Triplet (β LE) State of the Acceptor and the Charge Transfer (CT) States of the Exciplex*
Xiaofang Wei, Yanwei Liu, Taiping Hu, Zhiyi Li, Jianjun Liu, Ruifang Wang, Honglei Gao, Xiaoxiao Hu, Guanhao Liu, Pengfei Wang, Chun-sing Lee and Ying Wang
- 115** *Development of Red Exciplex for Efficient OLEDs by Employing a Phosphor as a Component*
Ming Zhang, Kai Wang, Cai-Jun Zheng, De-Qi Wang, Yi-Zhong Shi, Hui Lin, Si-Lu Tao, Xing Li and Xiao-Hong Zhang
- 124** *N-Benzoimidazole/Oxadiazole Hybrid Universal Electron Acceptors for Highly Efficient Exciplex-Type Thermally Activated Delayed Fluorescence OLEDs*
Wenbo Yuan, Hannan Yang, Mucan Zhang, Die Hu, Ning Sun and Youtian Tao
- 134** *Efficient Organic Light Emitting Diodes Using Solution-Processed Alkali Metal Carbonate Doped ZnO as Electron Injection Layer*
Guo Chen, Feiyang Liu, Zhitian Ling, Pengpeng Zhang, Bin Wei and Wenqing Zhu



Recent Applications of Interfacial Exciplex as Ideal Host of Power-Efficient OLEDs

Baohua Zhang^{1*} and Zhiyuan Xie^{2*}

¹ Center for Advanced Analytical Science, School of Chemistry and Chemical Engineering, Guangzhou University, Guangzhou, China, ² State Key Laboratory of Polymer Physics and Chemistry, Changchun Institute of Applied Chemistry, Chinese Academy of Sciences, Changchun, China

OPEN ACCESS

Edited by:

Lian Duan,
Tsinghua University, China

Reviewed by:

CaiJun Zheng,
University of Electronic Science and
Technology of China, China
Lixin Xiao,
Peking University, China

*Correspondence:

Baohua Zhang
ccbhzhang@gzhu.edu.cn
Zhiyuan Xie
xiezy_n@ciac.ac.cn

Specialty section:

This article was submitted to
Organic Chemistry,
a section of the journal
Frontiers in Chemistry

Received: 29 January 2019

Accepted: 16 April 2019

Published: 07 May 2019

Citation:

Zhang B and Xie Z (2019) Recent
Applications of Interfacial Exciplex as
Ideal Host of Power-Efficient OLEDs.
Front. Chem. 7:306.
doi: 10.3389/fchem.2019.00306

Currently, exploring the applications of intermolecular donor-acceptor exciplex couple as host of OLEDs with phosphorescence, thermally activated delayed fluorescence (TADF) or fluorescence emitter as dopant is a hot topic. Compared to other host strategies, interfacial exciplex has the advantage in various aspects, such as barrier-free charge injection, unimpeded charge transport, and the energy-saving direct exciton formation process at the “Well”-like heterojunction interface region. Most importantly, due to a very fast and efficient reverse intersystem-crossing (RISC) process, such a host is capable of regulating singlet/triplet exciton populations in itself as well as in the dopant emitters both under photoluminescent (PL) and electroluminescent (EL) driving conditions. In this mini-review, we briefly summarize and comment on recent applications of this ideal host in OLEDs (including both thermal-evaporation OLEDs and solution-processed OLEDs) with diverse emitters, e.g., fluorescence, phosphorescence, delayed fluorescence, or others. Special attention is given to illustrate the peculiar achievement of high overall EL performance with superiorities of low driving voltages, slow roll-off rate, high power efficiencies and satisfied device lifetime using this host strategy, which is then concluded by personal perspectives on the relevant next-step in this field.

Keywords: OLED, exciplex, thermally activated delayed fluorescence, phosphorescence, power efficiency

Since their invention in 1987 (Tang and Vanslyke, 1987), OLEDs have received persistent attention considering their great advantage in modern displays and lighting applications (Burroughes et al., 1990; Kido et al., 1995). With the development of phosphorescent emitters (Baldo et al., 1998), efficiencies of OLEDs have been significantly improved (Wang et al., 2018). Endo et al. (2011) launched new generation OLEDs by inventing efficient thermal-activated delayed fluorescence (TADF) emitters purely from aromatic carbon materials. On the basis of a high RISC rate and a high radiative decay rate ($S_1 \rightarrow S_0$) in TADF emitters (Uoyama et al., 2012; Higuchi et al., 2015; Noda et al., 2018), or exciplex couples (Goushi and Adachi, 2012; Goushi et al., 2012; Hung et al., 2013, 2014; Liu et al., 2015a,c), highly efficient monochromatic and white TADF OLEDs have been achieved. Other candidates such as hybridized local and charge-transfer (HLCT) excited state molecules (Li et al., 2014) and radical-based double emission molecules (Ai et al., 2018) have also been reported and well-documented, showing the analogous cost and performance merits.

However, irrespective of emitter categories, e.g., phosphorescent, TADF or fluorescent emitters, it is highly pursued ideal hosts that maximize their EL performance since critical parameters of OLEDs e.g., external quantum efficiency (EQE), power efficiency (PE), roll-off rate and device lifetime, are highly determined by host choices. Among those host strategies (Tao et al., 2011; Yook and Lee, 2014; Wang et al., 2019), interfacial exciplex seems an ideal choice since all these expected characteristics are simultaneously satisfied. Based on relevant publications and our understanding, this mini-review presents a short introduction on its application status and remarks on the future research direction.

INTERFACIAL EXCIPLEX AS HOST IN THERMAL-EVAPORATED OLEDs

At a type II P/N organic/organic (O/O) heterojunction interface between an electron-donating molecule and an electron-accepting molecule, there is a high tendency to form a charge-transfer excited-state complex, also known as an exciplex (Jenekhe and Osaheni, 1994; Itano et al., 1998; Giro et al., 2000; Morteani et al., 2003). Simultaneously, HOMO and LUMO levels of hole transporting material (HTM) and electron transporting material (ETM) display a distinct gap at the heterojunction interface (**Figure 1A**). It is barely possible to generate exciton on either constituting molecule. By contrast, exciplex formation is energetically allowed, in which one of them locates in the excited state while another one is in the ground state being coupled. There is an experimental guideline on exciplex formation (Matsumoto et al., 2008), i.e., coexistence of huge gap, e.g., larger than 0.3 eV, for both HOMO and LUMO levels. However, it is not necessarily the case. A certain constituting material couple could be switched to exciplex or not simply by altering the substrate (Ng et al., 2014). From the electronic viewpoint, Ng et al. (2014) illustrated how the local molecular interactions and interfacial energetics at PN heterojunction play a role in exciplex formation (**Figure 1B**). It corresponds to $P^{\delta-}-N^{\delta+}$ contact at the PN heterojunction, in which the N-type material donates electrons to the LUMO level of the P-type material at the interface. Bounded immobile charges (CTC) formed thus guarantee the exciplex formation. From the classic viewpoint of semiconductor physics, exciplex is a universal concept, i.e., including organic exciplex but not limited to it, such as hybrid exciplex in a lead halide perovskite ($\text{MAPbI}_{3-x}\text{Cl}_x$)/quantum dot (core/shell PbS/CdS) heterojunction (Sanchez et al., 2016).

Previously, exciplex was frequently observed during fabrication of thermal-evaporated OLEDs (e-OLEDs), but unwelcomed due to its low PL quantum efficiency (PLQE) as an emitter and quenching effect in host-guest-doping devices. For instance, interfacial exciplex was discovered (or generated but not noticed by researchers) at the interface between the emissive layer (EML) and hole transporting layer (HTL), or between the EML and electron transporting layer (ETL). As the singlet and triplet levels (S_1/T_1) of the exciplex were less than those of emissive constituents of the EML, EL spectra and device efficiency were deteriorated via a back-energy transfer from them

to the exciplex (Jenekhe and Osaheni, 1994; Gebler et al., 1997, 1998; Itano et al., 1998; Giro et al., 2000; Matsumoto et al., 2008). One useful exception is white OLEDs, since exciplex featured in color-adjustable and very broad PL/EL spectra (Chao and Chen, 1998). However, restricted by its low PLQE, the corresponding device performance was very limited.

Exciplex was confirmed to be intermolecular TADF materials due to its extremely low HOMO-LUMO overlap and thus low exchange energy ΔE_{ST} (0–100 meV) (Graves et al., 2014). **Figure 1C** depicted PL/EL transient decay results of a typical exciplex couple of 4,4',4''-tris[3-methylphenyl(phenyl)amino]triphenylamine (m-MTDATA) and 2-(biphenyl-4-yl)-5-(4-tert-butylphenyl)-1,3,4-oxadiazole (t-Bu-PBD), which was characteristic of the distinct delay fluorescent component (Goushi et al., 2012). Their difference, was due to high initial triplet excitons formed on exciplex emitters under EL driving, e.g., triplets/(singlets+triplets) ~ 0.75 in general, which enhanced the delayed fluorescence component significantly. As indicated, its RISC rate and efficiency (k_{RISC} , Φ_{RISC}) were very efficient. Along with the explorations of novel exciplex emitters with enhanced PLQE, big progress has been achieved, e.g., even close to the best TADF or phosphorescent OLEDs in performance (Goushi et al., 2012; Hung et al., 2013, 2014; Liu et al., 2015a,c). Alternatively, considering the unique merits of exciplex couple, e.g., the lowest HOMO-LUMO transport gap under a certain T_1 energy, bipolar transporting properties and triplet-to-singlet upconversion capability via RISC process, exciplex has also been used as host OLEDs to obtain ultrahigh EQE/PE performance. A representative example is a bulk exciplex-forming cohost in phosphorescent- and TADF-doped OLEDs (PhOLEDs, TADF OLEDs) by Kim et al., e.g., achieving a high EQE/PE of 29.1%/124 lm W⁻¹ with slow roll-off (Park et al., 2013; Lee et al., 2014; Sun et al., 2014), and exciplex-sensitized fluorescent OLED (FOLEDs) (peak EQE/PE of 14.5%/46.1 lm W⁻¹) and hybrid white OLEDs (forward-viewing peak EQE/PE of 25.5%/84.1 lm W⁻¹) by Liu et al. (2015a,b). Compared to bulk exciplex, in which the constituents are physically blended and doped with guests, an interfacial exciplex host is a simplified bilayer structure doped with guests in either layer or both. Recent results show that an interfacial exciplex host can also be well-applied to OLEDs (Park et al., 2011; Seino et al., 2014; Wang et al., 2015; Zhang et al., 2016; Xu et al., 2017; Lin et al., 2018), with some unique characteristics (Al Attar and Monkman, 2016; Chen et al., 2016; He et al., 2016; Nakanotani et al., 2016; Lin et al., 2017). The key results of reported OLEDs using interfacial exciplex host are summarized in the **Supplementary Materials**.

The schematic energy transfer (ET) mechanisms on PhOLEDs, TADF OLEDs and FOLEDs using the interfacial exciplex as a sensitizing host are shown in **Figures 1D–F** (Park et al., 2011; Seino et al., 2014; Liu et al., 2015a,b; Wang et al., 2015; Zhang et al., 2016). The sensitizing function of the exciplex host is ascribed to its TADF property, in which initial populations of triplets on them are efficiently up-converted into singlets, followed by Förster ET to a guest. While the guest is phosphorescent or TADF emitters, such a process is unique in lowering local exciton density of long-lived triplets on guests, therefore sharply increasing EQE/PE performance and also

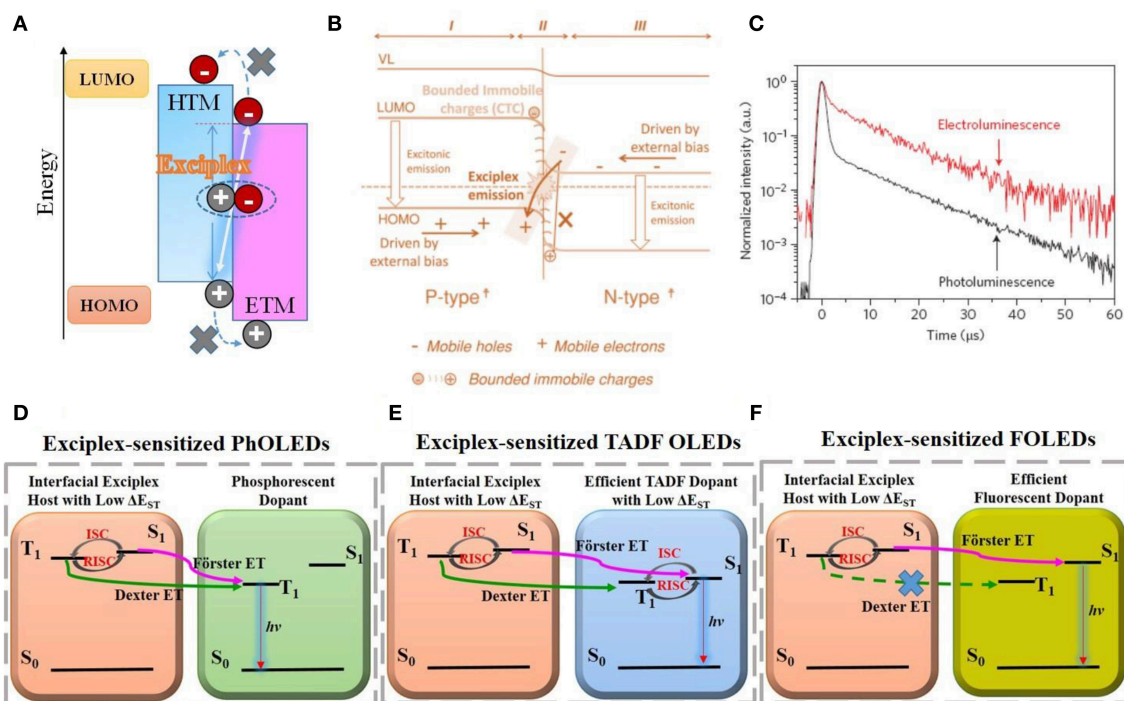


FIGURE 1 | (A) Schematic illustration on interfacial exciplex formation. **(B)** Electronic energy-level alignments of exciplex-forming P/N heterojunction mentioned in Ng et al. (2014). Reprinted with permission from Ng et al. (2014), Copyright 2014 Wiley-VCH. **(C)** EL/PL transient of m-MTDATA:t-Bu-PBD exciplex shown in Goushi et al. (2012). Reprinted by permission from Goushi et al. (2012), Copyright 2012 Springer Nature. **(D–F)** exciplex-to-dopant ET process in exciplex-sensitized PhOLEDs, TADF OLEDs, and FOLEDs, respectively.

distinctly alleviating triplet-involved quenching processes, e.g., triplet-triplet annihilation (TTA), triplet-polaron annihilation (TPA) etc (Moon et al., 2017). Due to the RISC process in the exciplex host, enhanced Förster ET is believed to be the main PL/EL ET mechanism. However, debates still exist (Seino et al., 2014; Zhou et al., 2014), i.e., Förster or Dexter ET or both. In some reports the doping concentration in PhOLEDs and TADF OLEDs is as high as 10–20 wt.% (Seino et al., 2014; Wang et al., 2015; Liu et al., 2016; Lin et al., 2018). Dexter ET is thus unavoidable, playing positive roles on triplet-harvesting. However, in FOLEDs (Figure 1F), such Dexter ET, also trap-assisted recombination on guest itself, should be well-removed (Nakanotani et al., 2014; Zhang et al., 2014; Liu et al., 2015b), which was realized by minimizing doping concentration of guest and novel guest (Zhang et al., 2018).

Seino et al. (2014) firstly reported blue PhOLEDs via an interfacial exciplex host, in which a combination of di-[4-(N,N-ditoly-amino)-phenyl]cyclohexane (TAPC) and home-made 5',5'''-sulfonyl-di-1,1':3',1''-terphenyl (BTPS) was used as the exciplex (S_1/T_1 : 2.97/2.82 eV) and blue phosphor phosphoriridium(III) bis[(4,6-difluorophenyl)-pyridine-N,C^{2'}]picolinate (FIrpic) (S_1/T_1 : 2.78/2.77 eV) was doped into the BTPS layer. Direct exciton confinement occurred at the TAPC/BTPS exciplex interface, followed by Förster and Dexter ET to the dopant. It achieved a satisfied PE_{100} of 50.1 lm W⁻¹ merely at a low voltage of 2.90 V, along with an ultralow turn-on voltage (V_{on}) of 2.5 V. Compared to the control device,

without using the exciplex host, the efficiencies were moderately enhanced, but the turn-on/driving voltages were dramatically lowered, e.g., 2.80 \rightarrow 2.50 V, 3.32 \rightarrow 2.90 V for V_{on}/V_{100} . They further developed power-efficient TADF OLEDs with a similar structure (Seino et al., 2016). For example, the constructed EML consisted of CBP:5 wt.% 4CzIPN/B4PYMPM, in which 4,4'-N,N'-dicarbazolylbiphenyl (CBP)/B4PYMPM was an interfacial exciplex couple and 1,2,3,5-tetrakis (carbazol-9-yl)-4,6-dicyanobenzene (4CzIPN) was the TADF emitter. The charge and exciton formation route were analogous to that of PhOLEDs, and the EL mechanism is shown in Figure 1E. The resultant device displayed ultralow V_{on} of 2.33 V, EQE_{max}/PE_{max} of 25.7% and 106.9 lm W⁻¹, slightly declined to 24.8% and 79.4 lm W⁻¹ at high luminance of 1,000 cd m⁻². Such performance came close to the best PhOLED counterpart ever developed.

Duan's group provided an illustration on applications of the exciplex host (Zhang et al., 2016), and provided direct comparisons on the interfacial exciplex vs. the bulk exciplex host, from the viewpoint of device efficiencies, roll-off performance and device lifetime. The constituting materials were one bipolar host (3'-(4,6-diphenyl-1,3,5-triazin-2-yl)-(1,1'-biphenyl)-3-yl)-9-carbazole (CzTrz), and a donor molecule tris(4-(9H-carbazol-9-yl)phenyl)amine (TCTA) to form the CzTrz:TCTA bulk exciplex or CzTrz/TCTA interfacial exciplex host, respectively, where orange phosphor was (acetylacetonato)bis[2-(thieno[3,2-c]pyridin-4-yl)phenyl]-iridium(III) (PO-01). Very surprisingly, the interfacial exciplex

host based PhOLED comprehensively outperformed the bulk exciplex host based PhOLED. $\text{EQE}_{\text{max.}}/\text{EQE}_{5000}/\text{EQE}_{10000}$ and $\text{PE}_{\text{max.}}/\text{PE}_{5000}/\text{PE}_{10000}$ of the former device reached to 27.0/25.6/24.0% and 73.1/52.1/44.6 lm W^{-1} , as compared to 23.5/21.5/19.5% and 58.5/41.1/33.2 lm W^{-1} achieved for the latter. Obviously, the interfacial exciplex host rendered the PhOLED much higher EQEs/PEs along with the alleviated roll-off rate. As disclosed, it was due to the enhanced Förster ET from the CzTrz/TCTA to the dopant in the EML [CzTrz:PO-01(1–3 wt.%)]. Despite relatively high local exciton density at the exciplex interface, fast and efficient long-range Förster ET spread these excitons throughout the EML, thereby overcoming TTA, TPA quenching limitations. Besides, with the CzTrz/TCTA interfacial exciplex host, the device lifetime of PhOLED was enhanced by almost two orders of a magnitude compared to the device counterpart with a bulk exciplex host (L_0 : 1,000 cd m^{-2}), since this structure avoided the formation of easily dissociated high-energy aromatic amines, TCTA in this case, donor excited states (Zhang et al., 2016). The formation possibility of unstable high-energy TCTA excitons was largely lowered in the interfacial exciplex host device structure, which was indicated by a condition experiment, i.e., a much longer device lifetime using a lower content of the TCTA constitute. It was not mentioned why the bulk exciplex host based PhOLEDs exhibited much lower efficiencies (as well as quicker roll-off rates), compared to the interfacial exciplex host PhOLEDs. Probably, the TCTA-excitonic involved a degradation process. As indicated, accelerated TPA and/or TTA quenching also distinctly deteriorated device efficiencies and roll-off behaviors. In short, this report might have referential significance in solving efficiency and lifetime issues of other OLEDs with host-guest structures that were not mentioned. The same group further used such geometry in red PhOLEDs, in which the exploration of constituting materials to form suitable interfacial exciplex was proven to be important (Song et al., 2018).

Xu et al. (2017) further reported a new emitting sub-unit design in tandem OLEDs, using an ultra-thin emissive layer (UEML), i.e., green-color phosphor bis[2-(2-pyridinyl-N)phenyl-C](acetylacetonato)-iridium(III) [$\text{Ir}(\text{ppy})_2(\text{acac})$], sandwiched between a layer of 1,1-bis[(di-4-tolylamino)phenyl]cyclohexane (TAPC) and a layer of 1,3,5-tri(p-pyrid-3-yl-phenyl)benzene (TmPyPB), in which TAPC/TmPyPB could form an interfacial exciplex. It displayed a peak LE/EQE of 135.74 cd A^{-1} /36.85%, which is among the best efficiencies of OLEDs using non-doped EML without using an out-coupling method. Despite indirect contact, exciplex excited states were generated efficiently via long-range coupling under device operation (Al Attar and Monkman, 2016; Nakanotani et al., 2016), followed by sufficient Förster/Dexter ET to the UEML. As the complexed co-evaporation operation is avoided, such architecture is significant in simplifying the manufacturing process of OLEDs and enhancing yield and repeatability of OLED products.

Su's group conducted systematic works on interfacial exciplex host application in FOLEDs (Li et al., 2018). FOLEDs with different EML structures were fabricated, i.e., TAPC:1% DBP/TmPyTz (device 1), TAPC:1% DBP/TAPC(3 nm)/TmPyTz

(device 2), TAPC:1% DBP/mCP(3 nm)/TmPyTz (device 3), in which TAPC/TmPyTz formed exciplex directly at the interface (device 1 and 2) or even long-range distance (device 3, with mCP spacer) (see the **Supplementary Materials** for a detailed performance) and DBP was a common fluorescent emitter. Among all of them, device 3 with a spatially separated exciplex couple host was the best, i.e., simultaneously achieving a low driving voltage, a high luminance and efficiency, e.g., $V_{\text{on}}/L_{\text{max.}}/\text{EQE}_{\text{max.}}/\text{PE}_{\text{max.}}$ of 2.18 V, 2956.8 cd m^{-2} , 14.8% and 38.8 lm W^{-1} . As illustrated, the merits of such FOLEDs using a spatially separated exciplex host lie in separating exciton generation and energy transferring areas, and also restraining the charge trapping effect of the dopant emitter, which is basically different from common FOLEDs.

Moreover, Lin et al. (2017) successfully constructed prototypical up-conversion OLEDs on the basis of a so-called exciplex-sensitized TTA (ESTTA) mechanism, featuring ultra-low sub-bandgap EL driving voltages, e.g., light turn-on merely at 2.2 V for high energy blue emission (2.9 eV for its bandgap). As verified, low-energy exciplex triplets formed at the interface of 4, 4', 4''-tris[3-methylphenyl(phenyl)amino]triphenylamine (m-MTDATA)/9,10-bis(2'-naphthyl) anthracene (ADN) are harvested by ADN themselves and then trigger their TTA processes to realize high-energy blue emission ($S_1 \rightarrow S_0$). At first glance, such ESTTA-OLED featured in low-voltage driving but suffered from low EQE performance (0.1%) due to back energy transfer quenching from S_1 of ADN to S_1 of the exciplex. After incorporating the "triplet diffusion and singlet blocking (TDSB)" layer and/or a more efficient fluorescent dopant, e.g., DPAVB, the corresponding EQE performance was sharply enhanced to 3.8%. Impressively, for TTA emissive material, this configuration theoretically requires only one-half of the driving voltage equal to its singlet photonics energy. This work provides a novel clue toward developing ultralow driving-voltage and power-efficient OLEDs (especially for the blue one).

INTERFACIAL EXCIPLEX AS HOST IN SOLUTION-PROCESSED OLEDs

Solution-processed OLEDs (s-OLEDs) are appealing since the adopted wet-process approach is cost-effective, and more suitable for future flexible, stretchable and large-size displaying and lighting applications via high-speed printing, "roll-to-roll" coating industrial techniques. However, one of the unsolved challenges lies in how to realize sufficient high EL performance, especially low power consumption. To this goal, among various strategies, interfacial exciplex was found to be an ideal host in various types of s-OLEDs, i.e., acquiring sufficient low driving condition, high PE while using a very simplified device structure.

Zhang and Wang et al. first reported power-efficient phosphorescent s-OLEDs (s-PhOLEDs) using an interfacial exciplex host, i.e., m-MTDATA/TmPyPB (Wang et al., 2015). The achieved $\text{PE}_{\text{max.}}$ of orange s-PhOLED reached a record value of 97.2 lm W^{-1} , along with ultra-low V_{on} of 2.36 V, and extremely low driving voltages of 2.60/3.03 V at the luminance of 100/1,000 cd m^{-2} . Such PE is the best among all-reported

s-OLEDs and even superior to thermal-evaporated PhOLEDs with the same color. **Figures 2A,B** depicts the device structure and the proposed EL driving mechanisms, in which both holes and electrons were barrier-freely injected, transported and then combined at the m-MTDATA/TmPyPB heterojunction to form exciplex excitons, and then transferred to dopants of the EML via Förster/Dexter ET. A negligible influence on current density-voltage (J-V) characteristics was observed by doping the guests, indicating that notorious charge trapping/scattering effects of dopants (Wang et al., 2018) were absent in such an architecture. By contrast, s-PhOLEDs using bulk exciplex of m-MTDATA:TmPyPB (1:1 w/w) was unsatisfied, corresponding to a low PE_{max} of 35.2 lm W^{-1} mainly due to sharply increased driving voltages, e.g., $V_{on}/V_{100}/V_{1000}$: 4.15/5.18/5.80 V. Two reasons were involved; i) low charge transporting capability of the bulk exciplex couple due to their intrinsic incompatibility (Yao et al., 2018); ii) the serious charge trapping tendency of dopant in the EML structure of m-MTDATA:TmPyPB:dopant (Wang et al., 2015). Accordingly, interfacial exciplex rather than bulk exciplex shown here is more suitable for s-PhOLEDs as a host.

By replacing the orange phosphor to other ones (**Figures 2C–F**), power-efficient s-PhOLEDs with similar EL driving features were realized, e.g., 81.1 lm W^{-1} for green (Wang et al., 2015) and 44.5 lm W^{-1} for red (Liu et al., 2016, 2018a), respectively, confirming its universal application potential.

Komatsu et al. (2015) fabricated efficient TADF s-OLEDs using 4CzIPN as the dopant dispersed within the CBP matrix, and an interfacial exciplex couple of CBP (35 nm)/bis-4,6-(3,5-di-4-pyridylphenyl)-2-methylpyrimidine (B4PyMPM) as the host. With the analogous ET mechanisms shown in **Figure 1E** and EL driving process shown in **Figure 2B**, the device was also satisfied in performance, achieving a very low V_{on} of 2.5 V and high PE of 55 lm W^{-1} . It was one of the best ever developed TADF s-OLEDs with a TADF small molecular emitter (Kim et al., 2016; Liu et al., 2018b). On the topic of TADF polymer s-OLEDs (Nikolaenko et al., 2015; Nobuyasu et al., 2016; Zhang and Cheng, 2019), the interfacial exciplex host strategy was also confirmed as a wise choice. For instance, the application of interfacial exciplex TAPC/TmPyPB as the host of polymer PAPTC endowed the device with a very satisfied overall EL performance, with

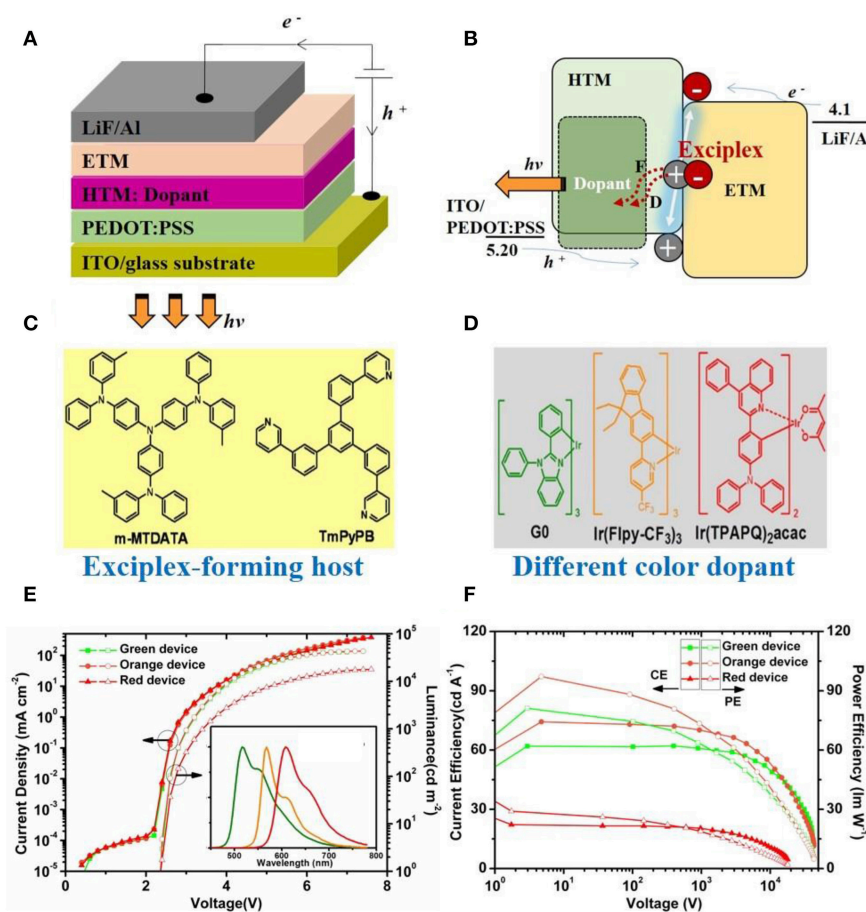


FIGURE 2 | (A) Device structure of s-OLEDs with interfacial exciplex host. **(B)** Schematic EL driving mechanisms for them, in which F, D denotes Förster and Dexter ET, respectively shown in Wang et al. (2015) and Liu et al. (2018a). **(C)** chemical structures of the m-MTDATA:TmPyPB exciplex couple. **(D)** Example of dopants used with different colors. **(E,F)** J-V-L and LE-V-PE characteristics of G/O/R color s-PhOLEDs illustrated in Wang et al. (2015).

extremely low voltages of 2.50/2.91/3.51 V at a luminance of 1/100/1,000 cd m^{-2} , high peak EQE/PE of 14.9%/50.1 lm W^{-1} , and a wonderful slow roll-off rate, of J_{50} of 63.16 cm^{-2} and L_{50} of approx. fifteen thousand cd m^{-2} (Lin et al., 2018). It is distinctly superior to that of a control device using pure PAPTC EML. Especially, efficiency roll-off was enhanced nearly 3-fold. Further studied disclosed that, with respect to the pure PAPTC layer, the optimized structure of TAPC:PAPTC (20 wt.%) / TmPyPB not only gained a much higher PLQE (79.5 vs. 36.3%) by largely restraining aggregation-induced Dexter triplet-quenching (Lee et al., 2017), but also sharply reduced triplet population on PAPTC itself by 4-fold enhancement of its k_{RSIC} to as high as $1.48 \times 10^7 \text{ s}^{-1}$ (Moon et al., 2017). These two aspects were combined to explain the promotions of the EL performance presented.

CONCLUDING REMARKS

Over the past several years, successful applications of an interfacial exciplex host in OLEDs were presented. Due to its merits in barrier-free exciton generation, “Well”-like exciton confinement and high ET efficiencies, simultaneous low voltage, high EQE/PE, low roll-off rate and even much higher device stability were representatively achieved, irrespective of dopant types. It should be strengthened that, compared to a traditional host, RISC up-conversion of the exciplex host renders the interfacial exciplex with an enhanced Förster ET process, guaranteeing low exciton density on emitters, thereby removing the risk of accelerating exciton-aggregation quenching. Moreover, local high charge/exciton density at the interfacial exciplex region is not a drawback but a special advantage that is not accessible in the bulk exciplex counterpart. For instance, a simple manipulation of the category of the major carrier (hole-rich or electron-rich or balanced) at the donor/accepter heterojunction, was found to induce exciplex recombination or Auger recombination or both (He et al., 2016). After doping with an appropriate guest, the novel EL driving mechanism is anticipated and may be significant. Unfortunately, the corresponding phenomena and mechanisms were not found in bulk exciplex counterparts. In addition, an

interesting long-ranging coupling property of exciplex has been discovered recently but has still not been widely used in host applications (Al Attar and Monkman, 2016; Nakanotani et al., 2016). In this respect, interfacial exciplex architecture is also an ideal choice.

It must be noted that compared to bulk exciplex, relevant interfacial exciplex host applications in OLEDs are still limited and required. It is believed that if the structural advantages of interfacial exciplex are further utilized, there are more opportunities to construct OLEDs with a much higher performance and can also enrich our understanding of the related physical processes. Both of them are crucial from an OLED science and technology point of view.

AUTHOR CONTRIBUTIONS

All authors listed have made a substantial, direct and intellectual contribution to the work, and approved it for publication.

FUNDING

This work is funded by the National Key Basic Research and Development Program of China (2015CB655001) founded by MOST, and the National Natural Science Foundation of China (No. 51773195, 51473162).

ACKNOWLEDGMENTS

We appreciate all our colleagues, collaborators and students for giving fruitful contributions on our achievements in this topic, especially Prof. L. X. Wang, Prof. W. Y. Wong, Prof. J. Q. Ding, Prof. Y. X. Cheng, Prof. L. Niu, Prof. Y. W. Zhang, Dr. S. M. Wang, and Dr. X. J. Liu.

SUPPLEMENTARY MATERIAL

The Supplementary Material for this article can be found online at: <https://www.frontiersin.org/articles/10.3389/fchem.2019.00306/full#supplementary-material>

REFERENCES

- Ai, X., Evans, E. W., Dong, S., Gillett, A. J., Guo, H., Chen, Y., et al. (2018). Efficient radical-based light-emitting diodes with doublet emission. *Nature* 563, 536–540. doi: 10.1038/s41586-018-0695-9
- Al Attar, H. A., and Monkman, A. P. (2016). Electric field induce blue shift and intensity enhancement in 2D exciplex organic light emitting diodes; controlling electron-hole separation. *Adv. Mater.* 28:8014. doi: 10.1002/adma.201600965
- Baldo, M. A., O'Brien, D. F., You, Y., Shoustikov, A., Sibley, S., Thompson, M. E., et al. (1998). Highly efficient phosphorescent emission from organic electroluminescent devices. *Nature* 395, 151–154.
- Burroughes, J. H., Bradley, D. D. C., Brown, A. R., Marks, R. N., Mackay, K., Friend, R. H., et al. (1990). Light-emitting-diodes based on conjugated polymers. *Nature* 347, 539–541. doi: 10.1038/347539a0
- Chao, C. I., and Chen, S. A. (1998). White light emission from exciplex in a bilayer device with two blue light-emitting polymers. *Appl. Phys. Lett.* 73, 426–428. doi: 10.1063/1.121888
- Chen, D., Xie, G., Cai, X., Liu, M., Cao, Y., and Su, S.-J. (2016). Fluorescent organic planar pn heterojunction light-emitting diodes with simplified structure, extremely low driving voltage, and high efficiency. *Adv. Mater.* 28, 239–244. doi: 10.1002/adma.201504290
- Endo, A., Sato, K., Yoshimura, K., Kai, T., Kawada, A., Miyazaki, H., et al. (2011). Efficient up-conversion of triplet excitons into a singlet state and its application for organic light emitting diodes. *Appl. Phys. Lett.* 98, 083302–083304. doi: 10.1063/1.3558906
- Gebler, D. D., Wang, Y. Z., Blatchford, J. W., Jessen, S. W., Fu, D. K., Swager, T. M., et al. (1997). Exciplex emission in bilayer polymer light-emitting devices. *Appl. Phys. Lett.* 70, 1644–1646. doi: 10.1063/1.118657
- Gebler, D. D., Wang, Y. Z., Fu, D.-K., Swager, T. M., and Epstein, A. J. (1998). Exciplex emission from bilayers of poly(vinyl carbazole) and pyridine based conjugated copolymers. *J. Chem. Phys.* 108, 7842–7848. doi: 10.1063/1.476221
- Giro, G., Cocchi, M., Kalinowski, J., Di Marco, P., and Fattori, V. (2000). Multicomponent emission from organic light emitting diodes based on

- polymer dispersion of an aromatic diamine and an oxadiazole derivative. *Chem. Phys. Lett.* 318, 137–141. doi: 10.1016/S0009-2614(99)01456-6
- Goushi, K., and Adachi, C. (2012). Efficient organic light-emitting diodes through up-conversion from triplet to singlet excited states of exciplexes. *Appl. Phys. Lett.* 101:023306. doi: 10.1063/1.4737006
- Goushi, K., Yoshida, K., Sato, K., and Adachi, C. (2012). Organic light-emitting diodes employing efficient reverse intersystem crossing for triplet-to-singlet state conversion. *Nat. Photonics* 6, 253–258. doi: 10.1038/nphoton.2012.31
- Graves, D., Jankus, V., Dias, F. B., and Monkman, A. (2014). Photophysical investigation of the thermally activated delayed emission from films of m-MTDATA:PBD exciplex. *Adv. Funct. Mater.* 24, 2343–2351. doi: 10.1002/adfm.201303389
- He, S.-J., Wang, D.-K., Jiang, N., Tse, J. S., and Lu, Z.-H. (2016). Tunable excitonic processes at organic heterojunctions. *Adv. Mater.* 28, 649–654. doi: 10.1002/adma.201504287
- Higuchi, T., Nakanotani, H., and Adachi, C. (2015). High-efficiency white organic light-emitting diodes based on a blue thermally activated delayed fluorescent emitter combined with green and red fluorescent emitters. *Adv. Mater.* 27, 2019–2023. doi: 10.1002/adma.201404967
- Hung, W.-Y., Fang, G.-C., Chang, Y.-C., Kuo, T.-Y., Chou, P.-T., Lin, S.-W., et al. (2013). Highly efficient bilayer interface exciplex for yellow organic light-emitting diode. *ACS Appl. Mater. Interfaces* 5, 6826–6831. doi: 10.1021/am402032z
- Hung, W. Y., Fang, G. C., Lin, S. W., Cheng, S. H., Wong, K. T., Kuo, T. Y., et al. (2014). The First tandem, all-exciplex-based WOLED. *Sci. Rep.* 4:5161. doi: 10.1038/srep05161
- Itano, K., Ogawa, H., and Shirota, Y. (1998). Exciplex formation at the organic solid-state interface: yellow emission in organic light-emitting diodes using green-fluorescent tris(8-quinolinolato)aluminum and hole-transporting molecular materials with low ionization potentials. *Appl. Phys. Lett.* 72, 636–638. doi: 10.1063/1.120826
- Jenekhe, S. A., and Osaheni, J. A. (1994). Excimers and exciplexes of conjugated polymers. *Science* 265, 765–768. doi: 10.1126/science.265.5173.765
- Kido, J., Kimura, M., and Nagai, K. (1995). Multilayer white light-emitting organic electroluminescent device. *Science* 267, 1332–1334. doi: 10.1126/science.267.5202.1332
- Kim, Y. H., Wolf, C., Cho, H., Jeong, S. H., and Lee, T. W. (2016). Highly efficient, simplified, solution-processed thermally activated delayed-fluorescence organic light-emitting diodes. *Adv. Mater.* 28, 734–741. doi: 10.1002/adma.201504490
- Komatsu, R., Sasabe, H., Inomata, S., Pu, Y.-J., and Kido, J. (2015). High efficiency solution processed OLEDs using a thermally activated delayed fluorescence emitter. *Synth. Met.* 202, 165–168. doi: 10.1016/j.synthmet.2015.02.009
- Lee, J., Aizawa, N., Numata, M., Adachi, C., and Yasuda, T. (2017). Versatile molecular functionalization for inhibiting concentration quenching of thermally activated delayed fluorescence. *Adv. Mater.* 29, 1604856–1604861. doi: 10.1002/adma.201604856
- Lee, J.-H., Lee, S., Yoo, S.-J., Kim, K.-H., and Kim, J.-J. (2014). Langevin and trap-assisted recombination in phosphorescent organic light emitting diodes. *Adv. Funct. Mater.* 24, 4681–4688. doi: 10.1002/adfm.201303453
- Li, B. B., Gan, L., Cai, X. Y., Li, X. L., Wang, Z. H., Gao, K., et al. (2018). An effective strategy toward high-efficiency fluorescent OLEDs by radiative coupling of spatially separated electron-hole pairs. *Adv. Mater. Interfaces* 5:1800025. doi: 10.1002/admi.201800025
- Li, W., Pan, Y., Xiao, R., Peng, Q., Zhang, S., Ma, D., et al. (2014). Employing ~100% excitons in OLEDs by utilizing a fluorescent molecule with hybridized local and charge-transfer excited state. *Adv. Funct. Mater.* 24, 1609–1614. doi: 10.1002/adfm.201301750
- Lin, B.-Y., Easley, C. J., Chen, C.-H., Tseng, P.-C., Lee, M.-Z., Sher, P.-H., et al. (2017). Exciplex-sensitized triplet-triplet annihilation in heterojunction organic thin-film. *ACS Appl. Mater. Interfaces* 9, 10963–10970. doi: 10.1021/acsami.6b16397
- Lin, X., Zhu, Y., Zhang, B., Zhao, X., Yao, B., Cheng, Y., et al. (2018). Highly efficient TADF polymer electroluminescence with reduced efficiency roll-off via interfacial exciplex host strategy. *ACS Appl. Mater. Interfaces* 10, 47–52. doi: 10.1021/acsami.7b16887
- Liu, X., Yao, B., Wang, H., Zhang, B., Lin, X., Zhao, X., et al. (2018a). Efficient solution-processed yellow/orange phosphorescent OLEDs based on heteroleptic Ir(III) complexes with 2-(9,9-diethylfluorene-2-yl) pyridine main ligand and various ancillary ligands. *Org. Electron.* 54, 197–203. doi: 10.1016/j.orgel.2017.12.050
- Liu, X., Yao, B., Zhang, Z., Zhao, X., Zhang, B., Wong, W.-Y., et al. (2016). Power-efficient solution-processed red organic light-emitting diodes based on exciplex host and novel phosphorescent iridium complex. *J. Mater. Chem. C* 4:5787. doi: 10.1039/c6tc01270a
- Liu, X.-K., Chen, Z., Qing, J., Zhang, W.-J., Wu, B., Tam, H. L., et al. (2015a). Remanagement of singlet and triplet excitons in single-emissive-layer hybrid white organic light-emitting devices using thermally activated delayed fluorescent blue exciplex. *Adv. Mater.* 27, 7079–7085. doi: 10.1002/adma.201502897
- Liu, X.-K., Chen, Z., Zheng, C.-J., Chen, M., Liu, W., Zhang, X.-H., et al. (2015b). Nearly 100% triplet harvesting in conventional fluorescent dopant-based organic light-emitting devices through energy transfer from exciplex. *Adv. Mater.* 27, 2025–2030. doi: 10.1002/adma.201500013
- Liu, X.-K., Chen, Z., Zheng, C.-J., Liu, C.-L., Lee, C.-S., Li, F., et al. (2015c). Prediction and design of efficient exciplex emitters for high-efficiency, thermally activated delayed-fluorescence organic light-emitting diodes. *Adv. Mater.* 27, 2378–2383. doi: 10.1002/adma.201405062
- Liu, Y., Li, C., Ren, Z., Yan, S., and Bryce, M. R. (2018b). All-organic thermally activated delayed fluorescence materials for organic light-emitting diodes. *Nat. Rev. Mater.* 3:18020. doi: 10.1038/natrevmats.2018.20
- Matsumoto, N., Nishiyama, M., and Adachi, C. (2008). Exciplex formations between tris(8-hydroxyquinolato)aluminum and hole transport materials and their photoluminescence and electroluminescence characteristics. *J. Phys. Chem. C* 112, 7735–7741. doi: 10.1021/jp800443r
- Moon, C.-K., Suzuki, K., Shizu, K., Adachi, C., Kaji, H., and Kim, J.-J. (2017). Combined inter- and intramolecular charge-transfer processes for highly efficient fluorescent organic light-emitting diodes with reduced triplet exciton quenching. *Adv. Mater.* 29, 1606448–1606452. doi: 10.1002/adma.201606448
- Morteani, A. C., Dhoot, A. S., Kim, J. S., Silva, C., Greenham, N. C., Murphy, C., et al. (2003). Barrier-free electron-hole capture in polymer blend heterojunction light-emitting diodes. *Adv. Mater.* 15, 1708–1712. doi: 10.1002/adma.200305618
- Nakanotani, H., Furukawa, T., Morimoto, K., and Adachi, C. (2016). Long-range coupling of electron-hole pairs in spatially separated organic donor-acceptor layers. *Sci. Adv.* 2:e1501470. doi: 10.1126/sciadv.1501470
- Nakanotani, H., Higuchi, T., Furukawa, T., Masui, K., Morimoto, K., Numata, M., et al. (2014). High-efficiency organic light-emitting diodes with fluorescent emitters. *Nat. Commun.* 5:4016. doi: 10.1038/ncomms5016
- Ng, T.-W., Lo, M.-F., Fung, M.-K., Zhang, W.-J., and Lee, C.-S. (2014). Charge-transfer complexes and their role in exciplex emission and near-infrared photovoltaics. *Adv. Mater.* 26, 5569–5574. doi: 10.1002/adma.201400563
- Nikolaenko, A. E., Cass, M., Bourcet, F., Mohamad, D., and Roberts, M. (2015). Thermally activated delayed fluorescence in polymers: a new route toward highly efficient solution processable OLEDs. *Adv. Mater.* 27, 7236–7240. doi: 10.1002/adma.201501090
- Nobuyasu, R. S., Ren, Z., Griffiths, G. C., Batsanov, A. S., Data, P., Yan, S., et al. (2016). Rational design of TADF polymers using a donor-acceptor monomer with enhanced TADF efficiency induced by the energy alignment of charge transfer and local triplet excited states. *Adv. Opt. Mater.* 4, 597–607. doi: 10.1002/adom.201500689
- Noda, H., Nakanotani, H., and Adachi, C. (2018). Excited state engineering for efficient reverse intersystem crossing. *Sci. Adv.* 4:eaa06910. doi: 10.1126/sciadv.aao6910
- Park, Y.-S., Jeong, W.-I., and Kim, J.-J. (2011). Energy transfer from exciplexes to dopants and its effect on efficiency of organic light-emitting diodes. *J. Appl. Phys.* 110:124519. doi: 10.1063/1.3672836
- Park, Y.-S., Lee, S., Kim, K.-H., Kim, S.-Y., Lee, J.-H., and Kim, J.-J. (2013). Exciplex-forming co-host for organic light-emitting diodes with ultimate efficiency. *Adv. Funct. Mater.* 23, 4914–4920. doi: 10.1002/adfm.201300547
- Sanchez, R. S., de la Fuente, M. S., Suarez, I., Muñoz-Matutano, G., Martinez-Pastor, J. P., and Mora-Sero, I. (2016). Tunable light emission by exciplex state formation between hybrid halide perovskite and core/shell quantum dots: implications in advanced LEDs and photovoltaics. *Sci. Adv.* 2:e1501104. doi: 10.1126/sciadv.1501104

- Seino, Y., Inomata, S., Sasabe, H., Pu, Y. J., and Kido, J. (2016). High-performance green OLEDs using thermally activated delayed fluorescence with a power efficiency of over 100 lm W⁻¹. *Adv. Mater.* 28:2638. doi: 10.1002/adma.201503782
- Seino, Y., Sasabe, H., Pu, Y.-J., and Kido, J. (2014). High-performance blue phosphorescent OLEDs using energy transfer from exciplex. *Adv. Mater.* 26, 1612–1616. doi: 10.1002/adma.201304253
- Song, X., Zhang, D., Huang, T., Cai, M., and Duan, L. (2018). Efficient red phosphorescent OLEDs based on the energy transfer from interface exciplex: the critical role of constituting molecules. *Sci. China Chem.* 61, 836–843. doi: 10.1007/s11426-018-9242-1
- Sun, J. W., Lee, J.-H., Moon, C.-K., Kim, K.-H., Shin, H., and Kim, J.-J. (2014). A fluorescent organic light-emitting diode with 30% external quantum efficiency. *Adv. Mater.* 26, 5684–5688. doi: 10.1002/adma.201401407
- Tang, C. W., and Vanslyke, S. A. (1987). Organic electroluminescent diodes. *Appl. Phys. Lett.* 51, 913–915. doi: 10.1063/1.98799
- Tao, Y., Yang, C., and Qin, J. (2011). Organic host materials for phosphorescent organic light-emitting diodes. *Chem. Soc. Rev.* 40, 2943–2970. doi: 10.1039/c0cs00160k
- Uoyama, H., Goushi, K., Shizu, K., Nomura, H., and Adachi, C. (2012). Highly efficient organic light-emitting diodes from delayed fluorescence. *Nature* 492, 234–238. doi: 10.1038/nature11687
- Wang, S., Wang, X., Yao, B., Zhang, B., Ding, J., Xie, Z., et al. (2015). Solution-processed phosphorescent organic light-emitting diodes with ultralow driving voltage and very high power efficiency. *Sci. Rep.* 5:12487. doi: 10.1038/srep12487
- Wang, S., Zhao, L., Zhang, B., Ding, J., Xie, Z., Wang, L., et al. (2018). High-energy-level blue phosphor for solution-processed white organic light-emitting diodes with efficiency comparable to fluorescent tubes. *iScience* 6, 128–137. doi: 10.1016/j.isci.2018.07.016
- Wang, Z., Wang, C., Zhang, H., Liu, Z., Zhao, B., and Li, W. (2019). The application of charge transfer host based exciplex and thermally activated delayed fluorescence materials in organic light-emitting diodes. *Org. Electron.* 66, 227–241. doi: 10.1016/j.orgel.2018.12.039
- Xu, T., Zhou, J.-G., Huang, C.-C., Zhang, L., Fung, M. K., Murtaza, I., et al. (2017). Highly simplified tandem organic light-emitting devices incorporating a green phosphorescence ultrathin emitter within a novel interface exciplex for high efficiency. *ACS Appl. Mater. Interfaces* 9, 10955–10962. doi: 10.1021/acsami.6b16094
- Yao, B., Lin, X., Zhang, B., Wang, H., Liu, X., and Xie, Z. (2018). Power-efficient and solution-processed red phosphorescent organic light-emitting diodes by choosing combinations of small molecular materials to form a well-dispersed exciplex co-host. *J. Mater. Chem. C* 6, 4409–4417. doi: 10.1039/c8tc00592c
- Yook, K. S., and Lee, J. Y. (2014). Small molecule host materials for solution processed phosphorescent organic light-emitting diodes. *Adv. Mater.* 26, 4218–4233. doi: 10.1002/adma.201306266
- Zhang, B., and Cheng, Y. (2019). Recent advances in conjugated TADF polymer featuring in backbone-donor/pendant-acceptor structure: material and device perspectives. *Chem. Rec.* doi: 10.1002/tcr.201800152. [Epub ahead of print].
- Zhang, D., Cai, M., Zhang, Y., Bin, Z., Zhang, D., and Duan, L. (2016). Simultaneous enhancement of efficiency and stability of phosphorescent OLEDs based on efficient forster energy transfer from interface exciplex. *ACS Appl. Mater. Interfaces* 8, 3825–3832. doi: 10.1021/acsami.5b10561
- Zhang, D., Duan, L., Li, C., Li, Y., Li, H., Zhang, D., et al. (2014). High-efficiency fluorescent organic light-emitting devices using sensitizing hosts with a small singlet-triplet exchange energy. *Adv. Mater.* 26, 5050–5055. doi: 10.1002/adma.201401476
- Zhang, D., Song, X., Cai, M., and Duan, L. (2018). Blocking energy-loss pathways for ideal fluorescent organic light-emitting diodes with thermally activated delayed fluorescent sensitizers. *Adv. Mater.* 30, 1705250. doi: 10.1002/adma.201705250
- Zhou, D.-Y., Zamani Siboni, H., Wang, Q., Liao, L.-S., and Aziz, H. (2014). Host to guest energy transfer mechanism in phosphorescent and fluorescent organic light-emitting devices utilizing exciplex-forming hosts. *J. Phys. Chem. C* 118, 24006–24012. doi: 10.1021/jp508228z

Conflict of Interest Statement: The authors declare that the research was conducted in the absence of any commercial or financial relationships that could be construed as a potential conflict of interest.

Copyright © 2019 Zhang and Xie. This is an open-access article distributed under the terms of the Creative Commons Attribution License (CC BY). The use, distribution or reproduction in other forums is permitted, provided the original author(s) and the copyright owner(s) are credited and that the original publication in this journal is cited, in accordance with accepted academic practice. No use, distribution or reproduction is permitted which does not comply with these terms.



Recent Advances in Organic Light-Emitting Diodes Based on Pure Organic Room Temperature Phosphorescence Materials

Ge Zhan, Zhiwei Liu*, Zuqiang Bian and Chunhui Huang

Beijing National Laboratory for Molecular Sciences, Beijing Engineering Technology Research Centre of Active Display, College of Chemistry and Molecular Engineering, Peking University, Beijing, China

OPEN ACCESS

Edited by:

Lian Duan,
Tsinghua University, China

Reviewed by:

Jang Hyuk Kwon,
Kyung Hee University, South Korea
Basem Moosa,
KAUST Catalysis Center (KCC),
Saudi Arabia

*Correspondence:

Zhiwei Liu
zwliu@pku.edu.cn

Specialty section:

This article was submitted to
Organic Chemistry,
a section of the journal
Frontiers in Chemistry

Received: 31 January 2019

Accepted: 16 April 2019

Published: 07 May 2019

Citation:

Zhan G, Liu Z, Bian Z and Huang C
(2019) Recent Advances in Organic
Light-Emitting Diodes Based on Pure
Organic Room Temperature
Phosphorescence Materials.
Front. Chem. 7:305.
doi: 10.3389/fchem.2019.00305

Pure organic room temperature phosphorescence (RTP) materials have attracted extensive attention in recent years due to their unique characteristics, such as flexible design method, low toxicity, low cost, as well as the ease of production at scale. The involvement of triplet state and direct radiative transition from the triplet state show that RTP materials have great potential as a new generation emitter in organic light-emitting diodes (OLEDs). Based on the mechanism of phosphorescence, various methods have been developed to achieve RTP emissions in the crystal state. However, the observation of RTP in the thin film state is much more difficult to achieve because of the lower degree of rigidity and suppression of the non-radiative transition. In this mini-review, molecular design strategies developed to achieve RTP emissions and their application in OLEDs are summarized and discussed. The conclusion and outlook point to great potential as well as the challenges for the continued study of pure organic RTP materials-based OLEDs.

Keywords: organic light-emitting diodes, room-temperature phosphorescence, external quantum efficiency, lifetime, optoelectronic functional devices

INTRODUCTION

The early stage of organic light-emitting diodes (OLEDs) are based on fluorescent materials (Tang and Vanslyke, 1987), which could not utilize the triplet excitons that accounted for 75% of the total excitons (Baldo et al., 1999), and caused incomplete energy utilization and low device efficiency. In 1998, Ma et al. (1998) and Baldo et al. (1998) introduced osmium complex and platinum complex as luminescent materials into OLEDs, which increased the theoretical maximum internal quantum efficiency (IQE) of the device from 25% of the fluorescent material to 100% of the phosphorescent material. So far, phosphorescent OLEDs have achieved great success and has even been applied in commercial devices, such as mobile phones, televisions, and so on.

However, the noble metals contained in phosphorescent complexes are expensive, low in abundance and toxic, which restricts the further development and popularization of OLEDs. Therefore, metal-free luminescent materials have attracted increased interests in OLEDs, among which thermally activated delayed fluorescent (TADF) materials and pure organic room temperature phosphorescence (RTP) materials are successively introduced into OLEDs as emitters, while the OLEDs also showed a theoretical maximum IQE up to 100%.

Different from TADF materials, which have been demonstrated great success in OLEDs, the application of pure organic RTP materials in OLEDs is still in its initial stage, because high efficiency and short-lived RTP molecules suitable for OLEDs are rare. Nevertheless, RTP materials will provide more possibilities for high performance OLEDs and deserve to be explored further. This mini-review starts with an introduction to basic concepts such as RTP and OLEDs, and then discusses representative work on the electroluminescence study of pure organic RTP materials as well as the reported pure organic RTP materials potentially using in fabricating OLEDs. Finally, the potential and challenges of the study of electroluminescence on pure organic RTP materials are summarized.

BASIC PRINCIPLES FOR RTP

In general, the production of phosphorescence in pure organics involves two necessary processes: (i) intersystem crossing (ISC) from the lowest excited singlet state (S_1) to a triplet state (T_n) and (ii) radiative transition from the lowest excited triplet state (T_1) to the ground state (S_0) (Figure 1A). However, the excited triplet state can only be generated by ISC process from an excited singlet state (Reineke and Baldo, 2014). Therefore, $k_{ISC} > 0$ is a necessary condition for generating phosphorescence emission, where k_{ISC} is the ISC rate (Hirata, 2017). Only the energy level and electronic configuration determine k_{ISC} . The ISC process can be accelerated by a small energy gap between S_1 and T_1 (ΔE_{ST}). Experiments have shown that the ISC and reverse ISC (RISC) process are both accelerated when ΔE_{ST} is extremely small (<100 meV), and TADF emission can be obtained under this condition (Uoyama et al., 2012). However, TADF showed a different photophysical process to phosphorescence, as TADF contains both a prompt and delayed radiative transition from S_1 to S_0 , while phosphorescence is a radiative transition from T_1 to S_0 . The effect of electronic configuration on ISC has been confirmed by El-Sayed (Kalyanasundaram et al., 1977). He found that the spin-orbit coupling could be promoted by mixing different electronic configuration singlet and triplet states, such as (π , π^*) and (n , π^*). In addition, the heavy atom effect is also widely used to accelerate the k_{ISC} process (Plummer et al., 1993). Therefore, introducing n electrons containing atoms such as O and N, and heavy atoms like Br and I, are strategies frequently used to design efficient RTP materials.

Due to a longer lifetime, the excited triplet state can be easily quenched under ambient conditions (Schulman and Parker, 1977). The second necessary condition for obtaining high efficiency phosphorescence is $k_p > k_{nr}$, where k_p and k_{nr} are a radiative and non-radiative transition rate from T_1 to S_0 , respectively. The non-radiative process can be divided into external losses caused by the interaction with environmental conditions and intramolecular losses (Liu et al., 2016). At room temperature, k_p is generally less than k_{nr} in pure organic compounds, which is the main reason for the low photoluminescence quantum yield (PLQY) of pure organic RTP materials. Therefore, suppressing non-radiative transitions may

be the most important and challenging part of achieving effective RTP in pure organic materials.

BRIEF INTRODUCTION TO OLEDs

A typical OLEDs (Figure 1B) includes a hole transport layer (HTL), an emitting layer (EML), an electron transport layer (ETL), an anode, and a cathode. In addition, a hole injection layer (HIL) and an electron injection layer (EIL) are widely used to reduce the carrier injection barrier from the electrode to the organic layer, while a hole blocking layer (HBL) and an electron blocking layer (EBL) are usually used to effectively confine the hole and electron within the EML. Based on the working mechanism (Figure 1C), the external quantum efficiency (EQE) of OLEDs could be deduced as $EQE = \eta_{eh} \times \eta_{PL} \times \eta_{exciton} \times \eta_{out}$, where η_{eh} is the recombination efficiency of injected holes and electrons, η_{PL} is the intrinsic photoluminescence efficiency, i.e., PLQY of the EML, $\eta_{exciton}$ is the radiative exciton ratio, and η_{out} is the light out-coupling efficiency. Since the theoretical $\eta_{exciton}$ and η_{out} are 100% and ca. 20% respectively, the challenge for RTP based OLEDs is to achieve high PLQY in a thin film.

OLEDs BASED ON PURE ORGANIC RTP MATERIALS

Though pure organic RTP materials have great potential as emitters in OLEDs, there are only a few examples of the study of electroluminescence in pure organic RTP materials, since most reported pure organic RTP materials showed low PLQY and a long excited lifetime (Kabe and Adachi, 2017), which is not suitable for fabricating high efficiency OLEDs.

In 2013, Bergamini et al. synthesized **RTP-1** (Figure 2) consisting of a hexathio-benzene core and peripheral tolyl substituents (Bergamini et al., 2013). The compound showed outstanding phosphorescence in solid state at room temperature, while no luminescence was observed in solution. The authors attributed the luminescence behavior to a rigid environment and limited conformational migration of the tolyl substituent, which suppresses the non-radiative deactivation process from T_1 . Since the compound showed a high PLQY up to 80% in solid powder, the authors applied **RTP-1** in OLEDs as an emitter and fabricated OLEDs with a structure of indium tin oxide (ITO)/poly(3,4-ethylenedioxythiophene)-poly-(styrenesulfonic acid) (PEDOT:PSS)/polyvinylcarbazole (PVK):2-(4-biphenyl)-5-(4-tert-butylphenyl)-1,3,4-oxadiazole (PBD):**RTP-1**/Ba/Al. The device showed EQE and current efficiency of 0.1% and 0.5 cd A^{-1} at 11 V, respectively. The performance was not satisfactory because the device architecture was not optimized and the PLQY measured in the same blend film (PVK:PBD:**RTP-1**) was only 2%, which is much lower than that measured in the powder. The result demonstrated that the low rigidity of blend film cannot effectively suppress the competitive deactivation process of the excited triplet state. Although the device performance was poor, this work is the first attempt at using pure organic RTP materials as an emitter in OLEDs. Pure organic RTP materials then became a new choice for OLEDs after fluorescence materials,

phosphorescence materials and TADF materials. It should be noted that the luminescence mechanism of **RTP-1** in the film has not been well-studied, and the device exhibited different electroluminescence spectra under various voltages, which indicates that the device performance could be further improved by using proper host matrix and device structures.

Later in 2013, Chaudhuri et al. developed two pure organic RTP materials **RTP-2** and **RTP-3** (Figure 2) and their OLEDs were fabricated with a structure of ITO/PEDOT:PSS/N,N'-bis(3-methylphenyl)-N,N'-diphenylbenzidine (TPD)/PVK:**RTP-2** (or **RTP-3**)/PBD/CsF/Al (Chaudhuri et al., 2013). The electroluminescence spectra showed two distinct peaks, 560 and 690 nm for **RTP-2**, and 630 and 760 nm for **RTP-3**. Such dual emissions contain both singlet and triplet transitions of the molecule under electrical excitation and reveal a long-lived triplet afterglow. However, **RTP-2** and **RTP-3** showed low PLQY of 4.6 and 1.3% and their corresponding device also showed very low EQE of 2.54×10^{-4} and 5.58×10^{-5} , respectively. In this work and subsequent work, the authors studied the photoluminescence properties of these RTP materials in doped polymer films in detail (Ratzke et al., 2016). Through characterization and attribution of different emission peaks in the spectra, the authors provided a new understanding on the behavior of RTP materials in film, which is useful for RTP materials to be applied as emitters in OLEDs.

In 2016, Kabe et al. dispersed **RTP-4** (Figure 2) into the host molecule of 3-(N-carbazolyl)-androst-2-ene (CzSte) and observed dual emissions of blue fluorescent and green phosphorescent under photoexcitation (Kabe et al., 2016). By using **RTP-4** doped CzSte as the EML, they fabricated an OLEDs with a device structure of ITO/4,4'-bis[N-(1-naphthyl)-N-phenyl-amino]biphenyl (α -NPD) (30 nm)/1,3-bis(N-carbazolyl)benzene (mCP) (10 nm)/**RTP-4**:CzSte (1 %, 30 nm)/1,3,5-tris(N-phenylbenzimidazol-2-yl)benzene (TPBi) (60 nm)/LiF (0.8 nm)/Al (80 nm). The device emitted a blue emission with an EQE around 1% under the external electric current excitation. When the external electric current excitation was turned off, the device could still emit a green permanent emission with a lifetime of 0.39 s. The significant improvement of the device performance compared with the aforementioned two examples may arise from a better device fabrication method, i.e., thermal evaporation vs. solution spin coating, which provides more choices for host materials and other functional layers.

OTHER PURE ORGANIC RTP MATERIALS POTENTIAL FOR OLEDs

The requirements for luminescent materials in OLEDs are often combined with the advantages of high PLQY and a short-excited state lifetime, in order to produce devices with a high efficiency and low efficiency roll-off. Screening by these requirements, there are a few pure organic RTP materials reported in the literature, based on which OLEDs are expected to have good performance.

In 2014, Koch et al. designed and synthesized a series of boron-based RTP materials (Koch et al., 2014). The photophysical

results showed that the compounds **RTP-5–RTP-11** (Figure 2) have a high PLQY (29–104%) and a short-excited state lifetime (1233–5413 ns) that is suitable for OLEDs. In particular, the compound **RTP-7** showed a high PLQY up to 104% and a short-excited state lifetime of 1,382 ns in a diluted dichloromethane solution, as well as a high PLQY up to 118% in poly(methyl methacrylate) (PMMA). This indicates that the non-radiative transition in these compounds can be well-suppressed even in a less rigid atmosphere, leading to a high PLQY and short excited state lifetime comparable to phosphorescent complexes (Endo et al., 2008). However, OLEDs based on these RTP materials are yet to be fabricated and explored.

In 2016, Shimizu et al. reported **RTP-12–RTP-16** (Figure 2) as a new class of RTP materials (Shimizu et al., 2016). The crystals of these compounds showed photoluminescence under ambient conditions. Intermolecular interactions were observed in each crystal, which contributed to the restriction of intramolecular motion and suppressed non-radiative transitions. The excited state lifetimes were dozens of microseconds and the PLQY was 14 and 8% for **RTP-13** and **RTP-14**, respectively. Though these compounds were not emissive either in solution or in a doped polymer film, the short-excited state lifetime in microseconds is attractive for the high efficiency OLEDs, which deserves to be explored in more detail.

Later in 2016, Gutierrez et al. reported red phosphorescence from **RTP-17–RTP-20** (Figure 2) at room temperature (Gutierrez et al., 2016). The photophysical properties of these compounds in deoxygenated cyclohexane are presented. The excited state lifetime of 2.8–5.4 μ s is similar to that of traditional phosphorescent complexes, making them suitable for OLEDs. However, the PLQYs of this class of compound in a solution are very low (<1%). The reason is probably due to the presence of long alkyl chains. In the low-rigid solution, the twisting of the alkyl chain may lead to an increase in the non-radiative transition. Reducing the length of the alkyl chain or incorporating the luminescent molecules into more rigid host materials could upgrade the PLQY of these compounds.

In 2018, Huang et al. proposed a series of donor-acceptor-donor (D–A–D) compounds **RTP-21–RTP-24** (Figure 2) (Huang et al., 2018). The unsubstituted compound **RTP-21** exists in both equatorial and axial forms in the ground state, but the equatorial conformer prevails in the excited state. The changing in conformers lead to enhancement of RTP emissions with a high PLQY up to 71% in zeonex solid films. The excited state lifetime of 63.3 μ s also indicates that the molecule is suitable for application in OLEDs. The phosphorescence quantum yield of **RTP-21** is the highest among all current reported RTP molecules, and highly efficient OLEDs are expected when using **RTP-21** as the emitter.

CONCLUSION AND OUTLOOK

In recent years, a variety of RTP materials have been designed and synthesized, the color of which can cover the entire visible region (Li et al., 2018). However, the application of pure organic RTP materials in OLEDs is still in its infancy. The reasons are as follows: (i) The PLQYs of pure organic RTP materials in the thin

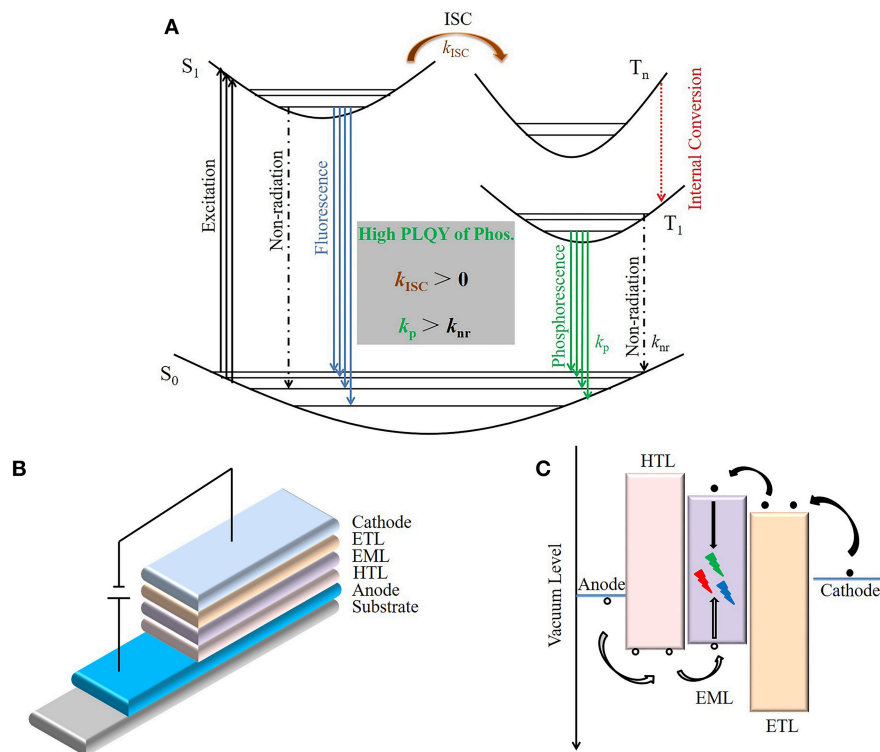


FIGURE 1 | Schematic diagram of OLEDs based on RTP materials. **(A)** Schematic Jablonski diagram of photoluminescence for RTP materials. **(B)** The typical structure of three-layer OLEDs. **(C)** The schematic injection, transport, and recombination process of holes (black circles) and electrons (black dots) in OLEDs.

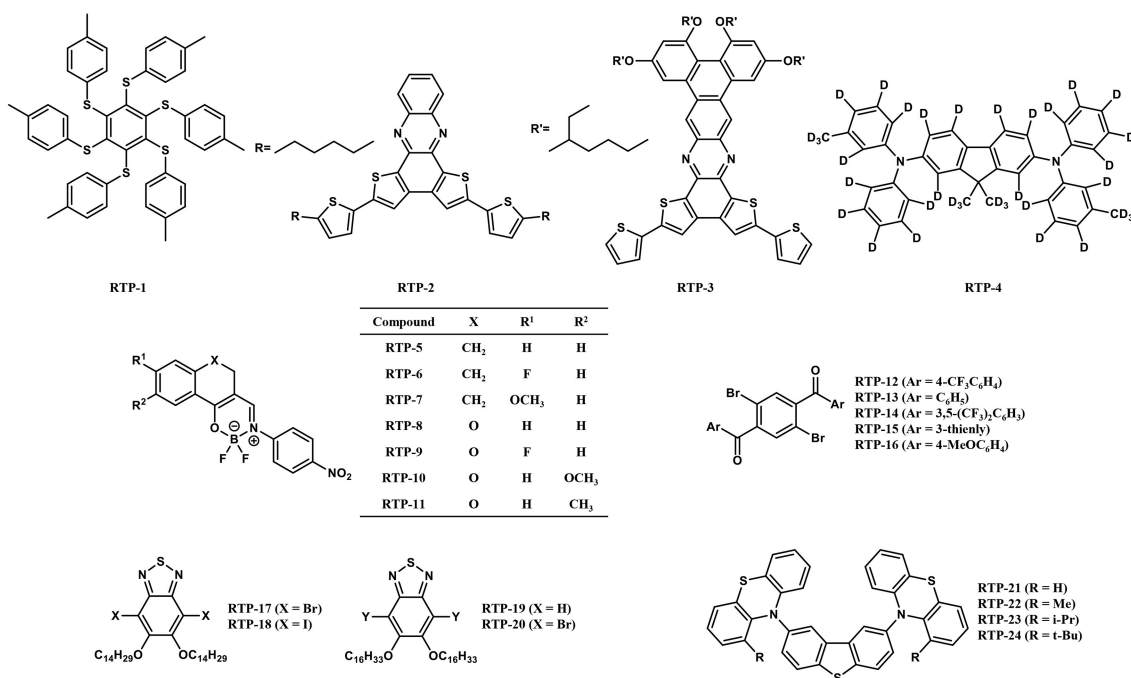


FIGURE 2 | Chemical structure of RTP materials used or potential to be used in OLEDs.

film state tend to be very low. Compared with the phosphorescent complexes or TADF materials commonly used in OLEDs, the PLQYs of pure organic RTP materials are still at low levels, and the effects of non-radiative transitions are significant. Most pure organic RTP materials tend to exhibit high PLQY in crystals or at low temperatures, while their PLQYs decrease significantly in a solution or a thin film at room temperature. The reason is that the rotation and vibration of the molecules are suppressed in a rigid environment or at a low temperature, where the rate of non-radiative transition is greatly reduced; (ii) The pure organic RTP materials have low radiative transition rates and long excited state lifetimes. Most of the reported pure organic RTP materials have lifetimes in the order of milliseconds or even seconds, and RTP materials with short lifetimes of several microseconds have hardly been reported. The long-excited state lifetime may result in serious triplet-triplet annihilation, leading to obvious efficiency roll-off in OLEDs.

Though the current performance of pure organic RTP based OLEDs is poor, it can theoretically achieve 100% IQE like noble metal complexes and TADF materials, which provide more possibilities for high performance OLEDs. The design and synthesis of pure organic RTP materials with a high PLQY and a short-excited state lifetime, especially in the thin film state, is the key goal in this field, since the EML in OLEDs is often a spin-coated or vapor-deposited thin film. To achieve this, it

is conceivable to introduce n electrons containing atoms and heavy atoms (Saigusa and Azumi, 1979) into the luminescent molecule to accelerate k_{ISC} and k_p , to improve the PLQY of the RTP materials. It is also possible to introduce a more rigid host material or a full-deuterated host to suppress non-radiative transitions. Moreover, OLEDs architecture optimization, using proper functional materials for balanced charge transport, favorable exciton confinement, and efficient energy transfer is also critical in improving the performance of RTP based OLEDs.

AUTHOR CONTRIBUTIONS

GZ wrote the manuscript. ZL, ZB, and CH helped to revise the manuscript.

FUNDING

This work was funded by The National Key R&D Program of China (No. 2016YFB0401001).

ACKNOWLEDGMENTS

We gratefully acknowledge the invitation from Prof. Shijian Su and the financial support from the National Key R&D Program of China (No. 2016YFB0401001).

REFERENCES

- Baldo, M. A., O'Brien, D. F., You, Y., Shoustikov, A., Sibley, S., Thompson, M. E., et al. (1998). Highly efficient phosphorescent emission from organic electroluminescent devices. *Nature* 395, 151–154.
- Baldo, M. A., Thompson, M. E., and Forrest, S. R. (1999). Phosphorescent materials for application to organic light emitting devices. *Pure Appl. Chem.* 71, 2095–2106. doi: 10.1351/pac199971112095
- Bergamini, G., Fermi, A., Botta, C., Giovanella, U., Di Motta, S., Negri, F., et al. (2013). A persulfurated benzene molecule exhibits outstanding phosphorescence in rigid environments: from computational study to organic nanocrystals and OLED applications. *J. Mater. Chem. C* 1, 2717–2724. doi: 10.1039/c3tc00878a
- Chaudhuri, D., Sigmund, E., Meyer, A., Röck, L., Klemm, P., Lautenschlager, S., et al. (2013). Metal-Free OLED triplet emitters by side-stepping Kasha's rule. *Angew. Chem. Int. Ed.* 52, 13449–13452. doi: 10.1002/anie.201307601
- Endo, A., Suzuki, K., Yoshihara, T., Tobita, S., Yahiro, M., and Adachi, C. (2008). Measurement of photoluminescence efficiency of Ir(III) phenylpyridine derivatives in solution and solid-state films. *Chem. Phys. Lett.* 460, 155–157. doi: 10.1016/j.cplett.2008.05.064
- Gutierrez, G. D., Sazama, G. T., Wu, T., Baldo, M. A., and Swager, T. M. (2016). Red Phosphorescence from Benzo[2,1,3]thiadiazoles at Room Temperature. *J. Organ. Chem.* 81, 4789–4796. doi: 10.1021/acs.joc.6b00789
- Hirata, S. (2017). Recent advances in materials with room-temperature phosphorescence: photophysics for triplet exciton stabilization. *Adv. Opt. Mater.* 5:1700116. doi: 10.1002/adom.201700116
- Huang, R. J., Ward, J. S., Kukhta, N. A., Avo, J., Gibson, J., Penfold, T., et al. (2018). The influence of molecular conformation on the photophysics of organic room temperature phosphorescent luminophores. *J. Mater. Chem. C* 6, 9238–9247. doi: 10.1039/c8tc02987c
- Kabe, R., and Adachi, C. (2017). Organic long persistent luminescence. *Nature* 550, 384–387. doi: 10.1038/nature24010
- Kabe, R., Notsuka, N., Yoshida, K., and Adachi, C. (2016). Afterglow organic light-emitting diode. *Adv. Mater.* 28, 655–660. doi: 10.1002/adma.201504321
- Kalyanasundaram, K., Grieser, F., and Thomas, J. K. (1977). Room-temperature phosphorescence of aromatic-hydrocarbons in aqueous micellar solutions. *Chem. Phys. Lett.* 51, 501–505. doi: 10.1016/0009-2614(77)85410-9
- Koch, M., Perumal, K., Blacque, O., Garg, J. A., Saiganesh, R., Kabilan, S., et al. (2014). Metal-free triplet phosphors with high emission efficiency and high tunability. *Angew. Chem. Int. Ed.* 53, 6378–6382. doi: 10.1002/anie.201402199
- Li, D. F., Lu, F. F., Wang, J., Hu, W. D., Cao, X. M., Ma, X., et al. (2018). Amorphous metal-free room-temperature phosphorescent small molecules with multicolor photoluminescence via a host-guest and dual-emission strategy. *J. Am. Chem. Soc.* 140, 1916–1923. doi: 10.1021/jacs.7b12800
- Liu, Y., Zhan, G., Liu, Z. W., Bian, Z. Q., and Huang, C. H. (2016). Room-temperature phosphorescence from purely organic materials. *Chin. Chem. Lett.* 27, 1231–1240. doi: 10.1016/j.ccl.2016.06.029
- Ma, Y. G., Zhang, H. Y., Shen, J. C., and Che, C. M. (1998). Electroluminescence from triplet metal-ligand charge-transfer excited state of transition metal complexes. *Synth. Met.* 94, 245–248. doi: 10.1016/S0379-6779(97)04166-0
- Plummer, B. F., Steffen, L. K., Braley, T. L., Reese, W. G., Zych, K., Vandyke, G., et al. (1993). Study of geometry-effects on heavy-atom perturbation of the electronic-properties of derivatives of the nonalternant polycyclic aromatic-hydrocarbons fluoranthene and Acenaphtho[1,2-K]Fluoranthene. *J. Am. Chem. Soc.* 115, 11542–11551. doi: 10.1021/ja00077a061
- Ratzke, W., Schmitt, L., Matsuoka, H., Bannwarth, C., Retegan, M., Bange, S., et al. (2016). Effect of conjugation pathway in metal-free room-temperature dual singlet triplet emitters for organic light-emitting diodes. *J. Phys. Chem. Lett.* 7, 4802–4808. doi: 10.1021/acs.jpclett.6b01907
- Reineke, S., and Baldo, M. A. (2014). Room temperature triplet state spectroscopy of organic semiconductors. *Sci. Rep.* 4:3797. doi: 10.1038/srep03797
- Saigusa, H., and Azumi, T. (1979). Internal heavy-atom effect on the triplet spin sublevels of the lowest triplet-state of Naphthalene. I. Radiative and nonradiative decays of the spin sublevels of 1-Halonaphthalenes. *J. Chem. Phys.* 71, 1408–1413. doi: 10.1063/1.438443
- Schulman, E. M., and Parker, R. T. (1977). Room-temperature phosphorescence of organic-compounds - effects of moisture, oxygen, and nature of support-phosphor

- interaction. *J. Phys. Chem.* 81, 1932–1939. doi: 10.1021/j100535a010
- Shimizu, M., Kimura, A., and Sakaguchi, H. (2016). Room-temperature phosphorescence of Crystalline 1,4-Bis(aryloyl)-2,5-dibromobenzenes. *Eur. J. Organ. Chem.* 2016, 467–473. doi: 10.1002/ejoc.201501382
- Tang, C. W., and Vanslyke, S. A. (1987). Organic electroluminescent diodes. *Appl. Phys. Lett.* 51, 913–915. doi: 10.1063/1.98799
- Uoyama, H., Goushi, K., Shizu, K., Nomura, H., and Adachi, C. (2012). Highly efficient organic light-emitting diodes from delayed fluorescence. *Nature* 492, 234–238. doi: 10.1038/nature11687

Conflict of Interest Statement: The authors declare that the research was conducted in the absence of any commercial or financial relationships that could be construed as a potential conflict of interest.

Copyright © 2019 Zhan, Liu, Bian and Huang. This is an open-access article distributed under the terms of the Creative Commons Attribution License (CC BY). The use, distribution or reproduction in other forums is permitted, provided the original author(s) and the copyright owner(s) are credited and that the original publication in this journal is cited, in accordance with accepted academic practice. No use, distribution or reproduction is permitted which does not comply with these terms.



Modulation of Excited State Property Based on Benzo[a, c]phenazine Acceptor: Three Typical Excited States and Electroluminescence Performance

Changjiang Zhou¹, Shengbing Xiao¹, Man Wang¹, Wenzhe Jiang¹, Haichao Liu¹, Shitong Zhang^{1,2*} and Bing Yang^{1*}

¹ State Key Laboratory of Supramolecular Structure and Materials, College of Chemistry, Jilin University, Changchun, China,

² Institute of Theoretical Chemistry, Jilin University, Changchun, China

OPEN ACCESS

Edited by:

Lian Duan,
Tsinghua University, China

Reviewed by:

Silu Tao,
University of Electronic Science and
Technology of China, China
Zhiyuan Chen,
Jiangxi Normal University, China

*Correspondence:

Shitong Zhang
stzhang@jlu.edu.cn
Bing Yang
yangbing@jlu.edu.cn

Specialty section:

This article was submitted to
Organic Chemistry,
a section of the journal
Frontiers in Chemistry

Received: 24 January 2019

Accepted: 26 February 2019

Published: 22 March 2019

Citation:

Zhou C, Xiao S, Wang M, Jiang W,
Liu H, Zhang S and Yang B (2019)
Modulation of Excited State Property
Based on Benzo[a, c]phenazine
Acceptor: Three Typical Excited States
and Electroluminescence
Performance. *Front. Chem.* 7:141.
doi: 10.3389/fchem.2019.00141

Throwing light upon the structure-property relationship of the excited state properties for next-generation fluorescent materials is crucial for the organic light emitting diode (OLED) field. Herein, we designed and synthesized three donor-acceptor (D-A) structure compounds based on a strong spin orbit coupling (SOC) acceptor benzo[a, c]phenazine (DPPZ) to research on the three typical types of excited states, namely, the locally-excited (LE) dominated excited state (CZP-DPPZ), the hybridized local and charge-transfer (HLCT) state (TPA-DPPZ), and the charge-transfer (CT) dominated state with TADF characteristics (PXZ-DPPZ). A theoretical combined experimental research was adopted for the excited state properties and their regulation methods of the three compounds. Benefiting from the HLCT character, TPA-DPPZ achieves the best non-doped device performance with maximum brightness of 61,951 cd m⁻² and maximum external quantum efficiency of 3.42%, with both high photoluminescence quantum efficiency of 40.2% and high exciton utilization of 42.8%. Additionally, for the doped OLED, PXZ-DPPZ can achieve a max EQE of 9.35%, due to a suppressed triplet quenching and an enhanced SOC.

Keywords: OLED, phenazine, donor-acceptor, spin-orbit coupling, hybridization state

INTRODUCTION

Over the past few decades, organic light-emitting diodes (OLEDs) have attracted much attention from academia to industry due to their advantages for high quality flat panel display and lighting applications (Tang and VanSlyke, 1987; Cao et al., 1999; Xiang et al., 2013; Jin et al., 2014; Yao et al., 2014; Krotkus et al., 2016; Chen et al., 2017, 2018; Liu et al., 2017a). For the cheap, metal-free pure organic fluorescent molecules, effective utilization of triplet exciton is the major issue to achieve high performance device according to the spin statistics rules in electro-excitons that are generated through the combination of hole- and electron-carriers (Atkins and Friedman, 2011; Lee et al., 2014; Chen et al., 2016; Guo F. et al., 2017). By now, three main mechanisms have been proposed to utilize the 75% electro-triplet excitons: the thermally-activated delayed fluorescence (TADF)(Uoyama et al., 2012; Zhang et al., 2014a,b; Zhang D. et al., 2015; Guo J. et al., 2017), the

triplet-triplet annihilation (TTA)(Luo and Aziz, 2010; Chiang et al., 2013) and the hybridized local and charge-transfer (HLCT) state(Li et al., 2012; Yao et al., 2015; Zhang S. et al., 2015; Wang et al., 2016, 2017; Tang et al., 2018). Recently, Li et al also reported a highly efficient near-infrared OLED utilizing doublet excited state, which is a promising method for 100% electro-exciton utilization (Peng et al., 2015; Ai et al., 2018a,b). Especially, the HLCT excited state is decent for fast triplet utilization and high photoluminescent (PL) efficiency, which is a promising method for the next-generation OLED materials. Generally, the excited states of pure organic material can be mainly divided into two kinds: the locally-excited (LE) state and the charge-transfer (CT) state (Gao et al., 2016; Zhou et al., 2018a). The LE state possesses large orbital overlap between the hole and electron wave functions, which usually possesses higher oscillator strength, corresponding to a larger radiative transition probability; while the CT state exhibits separated wave functions between hole and electron, and it is usually considered of non-emissive. However, the CT excited state is in favor of harvesting triplet excitons through a narrowed energy splitting between singlet and triplet states. Thus, the HLCT excited state contains a coexistence of LE and CT characters, and simultaneous high PL efficiency with high exciton utilization in OLED is expected to achieve through rational state regulation(Li et al., 2014b; Liu et al., 2015, 2017b; Zhou et al., 2017).

The explanation of high electro-triplet utilization of HLCT excited state is currently explained as going through a “hot-exciton” channel(Li et al., 2014a; Pan et al., 2014), but the essential mechanism is still under researching. Generally, the triplet utilization relies on the reversed intersystem crossing (RISC) process. Inspiring by the works on the room-temperature phosphorescence (RTP) materials, enhancing the spin-orbit coupling (SOC) can be a decent method to further accelerate the RISC for triplet utilization(Mao et al., 2015; Xu et al., 2016; Liu et al., 2018; Sun et al., 2018). Recently we have reported a singles-molecular white emissive material benzo[a, c]phenazine (DPPZ), which can realize a ternary emission of T₂-RTP, T₁-RTP, and S₁-RTP (Figure 1) (Zhou et al., 2018b). We have proved that the two sp²-hybridized nitrogen atoms greatly contribute to the enhanced SOC in DPPZ (~10 cm⁻¹) according to the El-Sayed rule(El-Sayed, 1963, 1964), and obviously, for the same reason, it can also be a suitable acceptor for the donor-acceptor (D-A) material, which is expectable for realizing decent electroluminescent (EL) performances. However, the sp²-hybridized nitrogen atom also causes problem in efficient emission, since the n → π* transition always performance badly in oscillator strength. Therefore, to overcome this problem, rational remolding of the excited state of DPPZ is necessary. In our previous work, introducing a proper CT excited state component to build up a HLCT excited state is an effective solution. Considering the energy-level arrangement of LE and CT origin excited states, three kinds of possible energy structures could be concluded between LE and CT states: (1) low-lying LE and high-lying CT, (2) LE lies close to CT, and (3) high-lying LE and low-lying CT (Scheme 1). Obviously, (1) and (3) are not desired model for DPPZ derivates, since the LE (originate from DPPZ) and the CT (Donor moiety → DPPZ)

are neither emissive. Judging from the state-mixing principle (Equation 1 and 2):

$$\psi(S_1) = \psi(LE) + \lambda \times \psi(CT) \quad (1)$$

$$\lambda = \left| \frac{\langle \psi_{LE} | H | \psi_{CT} \rangle}{E_{LE} - E_{CT}} \right| \quad (2)$$

where λ is the mixing coefficient that represents the degree of hybridization between LE and CT, and λ is mainly determined by two factors: the energy gap of the non-adiabatic LE and CT states $E_{LE} - E_{CT}$, and the magnitude of their interstate coupling $\langle \psi_{LE} | H | \psi_{CT} \rangle$. Obviously, it is easier to regulate $E_{LE} - E_{CT}$ by choosing different donor units, and at the same time, its essential structure-property relationship can be further understood.

In this work, based on the DPPZ acceptor, we designed and synthesized three D-A compounds with three typical donor moieties (CZP, phenyl-carbazole; TPA, triphenylamine; PXZ, phenoxazine), which corresponds to three typical excited states characteristics: the LE-dominated excited state (CZP-DPPZ), the HLCT (TPA-DPPZ) and CT state with TADF characters (PXZ-DPPZ). Among these three molecules, the HLCT material TPA-DPPZ obtains both high quantum efficiency of 40.2% and high exciton utilization of 42.8% in the non-doped OLED, benefiting from the HLCT character that arises the radiative transition rate and restrains the non-radiative transition, and eventually achieves the best non-doped OLED performance among the three materials with a maximum external quantum efficiency (EQE) of 3.42%. Additionally, The TADF material PXZ-DPPZ also demonstrates an efficient orange-red electro-fluorescence in doped OLED with an EQE of 9.35%.

MATERIALS AND METHODS

Synthesis

All the reagents and solvents used for the synthesis were purchased from Aldrich or Acros and used as received. All reactions were performed under nitrogen atmosphere. The synthesis of precursor reactants can be found in our previous work.

11-bromodibenzo[a, c]phenazine

A mixture of phenanthrene-9,10-dione (5 mmol) and 4-bromobenzene-1,2-diamine (5 mmol) in acetic acid (80 mL) was heated to reflux for 8 h. After cooling to room temperature, the resulting mixture was poured into ethanol (200 mL), and then filtered. The solid was washed with ethanol several times. The crude product was purified by column chromatography on silica gel (eluent: dichloromethane) and dried under vacuum to give the desired compound as a yellow solid in 90% yield (1.62 g). ¹H NMR (500 MHz, CDCl₃): δ 9.46–9.32 (m, 2H), 8.59 (d, *J* = 8.1 Hz, 2H), 8.56 (d, *J* = 2.0 Hz, 1H), 8.23 (d, *J* = 9.0 Hz, 1H), 7.94 (dd, *J* = 9.0, 2.1 Hz, 1H), 7.84 (t, *J* = 7.5 Hz, 2H), 7.78 (t, *J* = 7.5 Hz, 2H). MALDI-TOF MS (mass *m/z*): 361.4 [M(H)]⁺.



refluxed at 90°C for 48 h under nitrogen. After the mixture was cooled down, 40 mL water was added to the resulting solution and the mixture was extracted with CH₂Cl₂ for several times. The organic phase was dried over Na₂SO₄. After filtration and solvent evaporation, the liquid was purified by chromatography using the mixture of CH₂Cl₂/petroleum ether as the eluent to afford a pale green solid in 75% yield (0.78 g). ¹H NMR (500 MHz, CDCl₃):

δ 9.59 (d, $J = 7.9$ Hz, 1H), 9.53 (d, $J = 7.6$ Hz, 1H), 8.84 (s, 1H), 8.64 (d, $J = 7.6$ Hz, 2H), 8.58 (d, $J = 8.8$ Hz, 1H), 8.30 (dd, $J = 8.8$, 1.6 Hz, 1H), 8.21 (d, $J = 7.8$ Hz, 2H), 8.15 (d, $J = 8.3$ Hz, 2H), 7.86 (ddd, $J = 22.6$, 14.0, 7.6 Hz, 6H), 7.58 (d, $J = 8.2$ Hz, 2H), 7.50 (t, $J = 7.3$ Hz, 2H), 7.36 (t, $J = 7.4$ Hz, 2H). MALDI-TOF MS (mass m/z): 522.7 $[M(H)]^+$. Anal. calcd for $C_{38}H_{23}N_3$: C 87.50, H 4.44, N 8.06; found: C 87.13, H 4.68, N 8.16.

4-(dibenzo[a, c]phenazin-11-yl)-N,N-diphenylaniline (TPA-DPPZ)

A mixture of N,N-diphenyl-4-(4,4,5,5-tetramethyl-1,3,2-dioxaborolan-2-yl)aniline (2.6 mmol), 11-bromodibenzo[a, c]phenazine (2.0 mmol), sodium carbonate (20 mmol), toluene (15 mL), absolute alcohol (10 mL) and deionized water (10 mL), with $Pd(PPh_3)_4$ (60 mg) acting as catalyst was refluxed at $90^\circ C$ for 48 h under nitrogen. After the mixture was cooled down, 40 mL water was added to the resulting solution and the mixture was extracted with CH_2Cl_2 for several times. The organic phase was dried over Na_2SO_4 . After filtration and solvent evaporation, the liquid was purified by chromatography using the mixture of CH_2Cl_2 /petroleum ether as the eluent to afford a yellow-green solid in 75% yield (0.78 g). 1H NMR (500 MHz, $CDCl_3$): δ 9.59 (d, $J = 7.8$ Hz, 1H), 9.49 (d, $J = 6.9$ Hz, 1H), 8.73 (s, 1H), 8.62 (dd, $J = 7.8$, 3.7 Hz, 2H), 8.48 (d, $J = 8.8$ Hz, 1H), 8.21 (dd, $J = 8.9$, 1.9 Hz, 1H), 7.92–7.74 (m, 6H), 7.40–7.32 (m, 4H), 7.27–7.18 (m, 6H), 7.12 (t, $J = 7.4$ Hz, 2H). MALDI-TOF MS (mass m/z): 524.2 $[M(H)]^+$. Anal. calcd for $C_{38}H_{25}N_3$: C 87.16, H 4.81, N 8.02; found: C 86.92, H 4.75, N 8.32.

10-(dibenzo[a, c]phenazin-11-yl)-10H-phenoxazine (PXZ-DPPZ)

A mixture of 10H-phenoxazine (2.0 mmol), 11-bromodibenzo[a, c]phenazine (2.2 mmol), $HfBu_3BF_4$ (0.1 mmol), Sodium tert-butoxide (2.3 mmol), toluene (10 mL), with $Pd_2(dba)_3$ (0.06

mmol) acting as catalyst was refluxed at $110^\circ C$ for 48 h under nitrogen. After the mixture was cooled down, 40 mL water was added to the resulting solution and the mixture was extracted with CH_2Cl_2 for several times. The organic phase was dried over Na_2SO_4 . After filtration and solvent evaporation, the liquid was purified by chromatography using the mixture of CH_2Cl_2 /petroleum ether as the eluent to afford a red solid in 60% yield (0.55 g). 1H NMR (500 MHz, $CDCl_3$): δ 9.47 (dd, $J = 8.0$, 1.1 Hz, 1H), 9.44 (dd, $J = 8.0$, 1.0 Hz, 1H), 8.60 (dd, $J = 14.0$, 8.5 Hz, 3H), 8.48 (d, $J = 2.2$ Hz, 1H), 7.94–7.72 (m, 5H), 6.81 (dd,

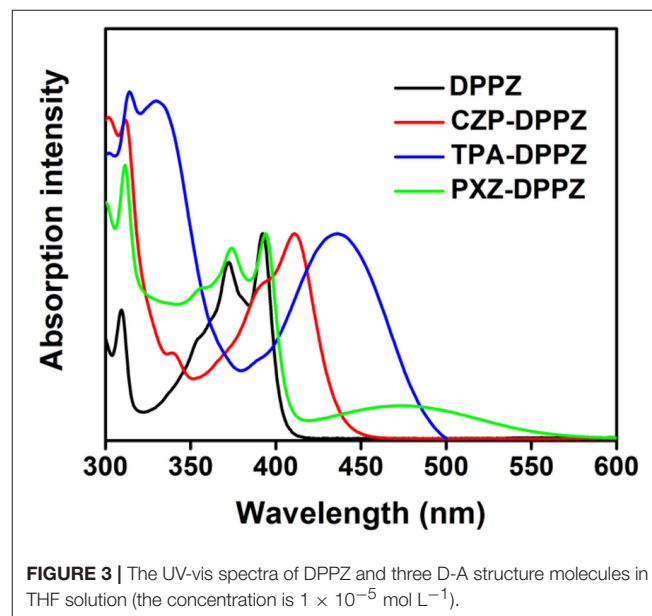


FIGURE 3 | The UV-vis spectra of DPPZ and three D-A structure molecules in THF solution (the concentration is 1×10^{-5} mol L^{-1}).

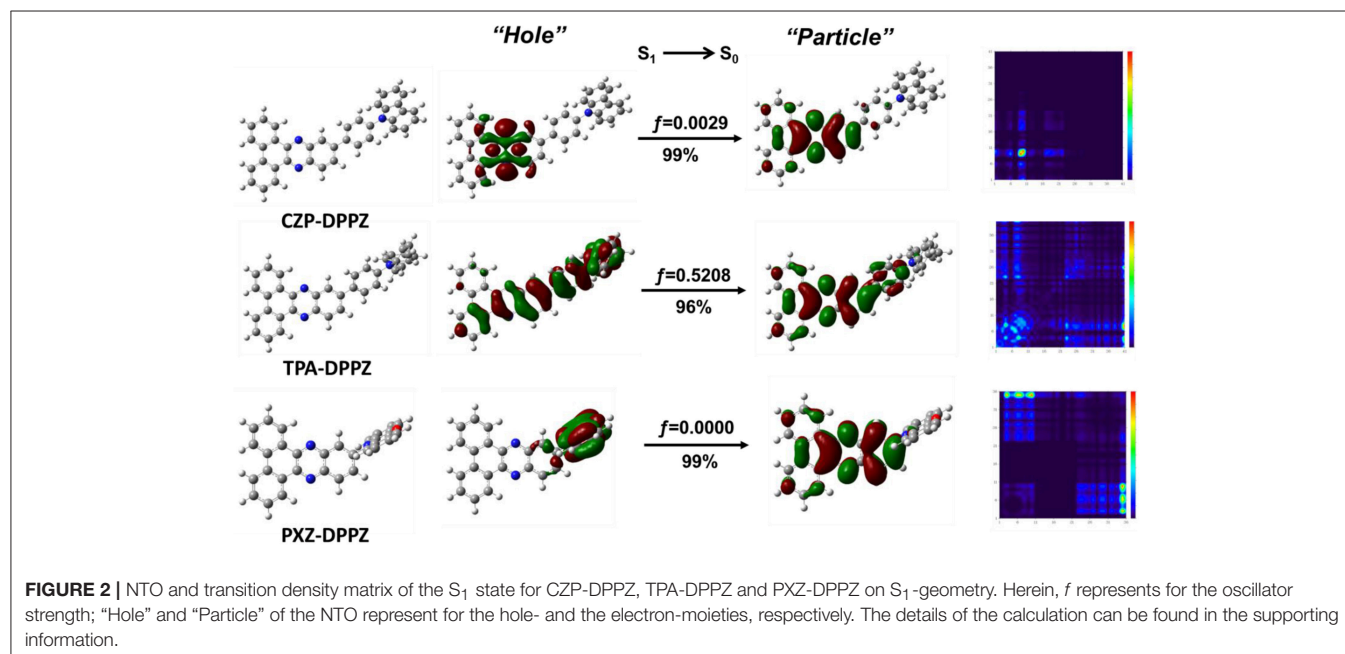


FIGURE 2 | NTO and transition density matrix of the S_1 state for CZP-DPPZ, TPA-DPPZ and PXZ-DPPZ on S_1 -geometry. Herein, f represents for the oscillator strength; “Hole” and “Particle” of the NTO represent for the hole- and the electron-moieties, respectively. The details of the calculation can be found in the supporting information.

$J = 7.9, 1.5 \text{ Hz, 2H}$), 6.75 (td, $J = 7.7, 1.4 \text{ Hz, 2H}$), 6.66 (td, $J = 7.7, 1.5 \text{ Hz, 2H}$), 6.20 (dd, $J = 8.0, 1.3 \text{ Hz, 2H}$). MALDI-TOF MS (mass m/z): 462.8 $[M(H)]^+$. Anal. calcd for $C_{32}H_{19}N_3O$: C 83.28, H 4.15, N 9.10, O 3.47; found: C 83.02, H 4.41, N 9.22, O 3.24.

RESULTS AND DISCUSSION

Molecular Design

Structures

The structures of the compounds are illustrated in **Figure 1**. To gain a primary understanding of these compounds, we carried out the geometrical optimization and calculated their frontier orbital distributions (the highest occupied molecular orbital, HOMO; the lowest unoccupied molecular orbital, LUMO; in **Figure S1**) (Zhao and Truhlar, 2008; Frisch et al., 2009). The three compounds are all of separated HOMO and LUMO, in which the HOMOs locate on the donor moieties, whereas the LUMOs distribute on DPPZ. This bipolar molecule character is

beneficial for the balanced carrier transport in OLED. Notably, the twist angle between donor and acceptor for PXZ-DPPZ is as large as 78° due to the large steric hindrance, while the dihedral angles for the other two compounds are around 35° (**Table S1**). Such an orthogonal molecular conformation may largely break the conjugation between PXZ and DPPZ, leading to a strong CT transition of its emissive excited state. The HOMO energy level of CZP-DPPZ, TPA-DPPZ and PXZ-DPPZ are measured as -5.58 eV , -5.26 eV , and -5.09 eV , respectively, which also implies that PXZ-DPPZ may possess an obvious CT character, while CZP-DPPZ can be a LE-like material.

Electron Transition Properties

To better understand the nature and character of excited states, we optimized the excited state geometries and calculated the natural transition orbital (NTO) of the emissive singlet state ($S_1 \rightarrow S_0$) for these compounds. As shown in **Figure 2**, the NTO “hole” and “particle” of CZP-DPPZ both localize on the DPPZ

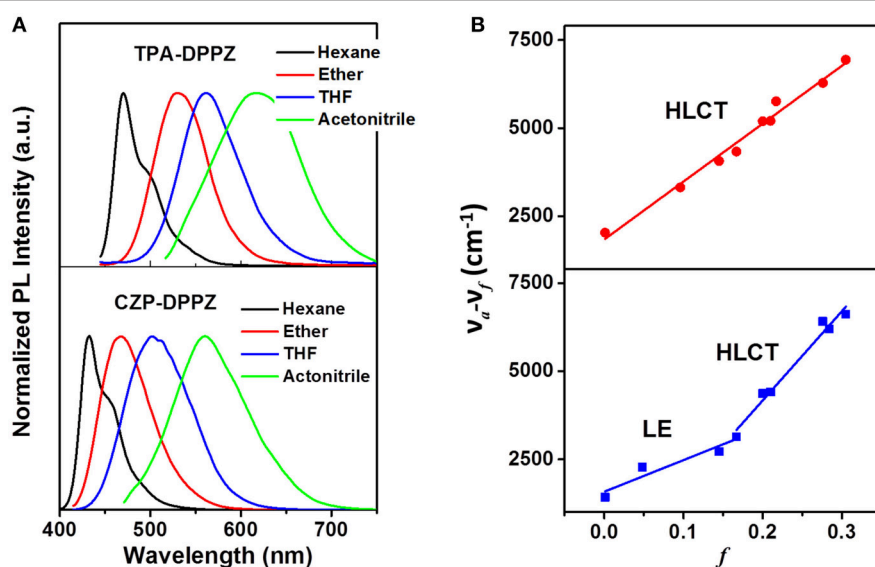


FIGURE 4 | (A) Solvent effect on the PL spectra of CZP-DPPZ, TPA-DPPZ and PXZ-DPPZ, in which the polarity f of the four solvents are $f_{\text{hexane}} = 0.0012$, $f_{\text{ether}} = 0.167$, $f_{\text{THF}} = 0.210$ and $f_{\text{acetonitrile}} = 0.305$. **(B)** Refined Lippert-Mataga model of CZP-DPPZ, TPA-DPPZ, and PXZ-DPPZ between Stokes shift and solvent polarity in more solvents. The details of the building of Lippert-Mataga model are in **Table S2**.

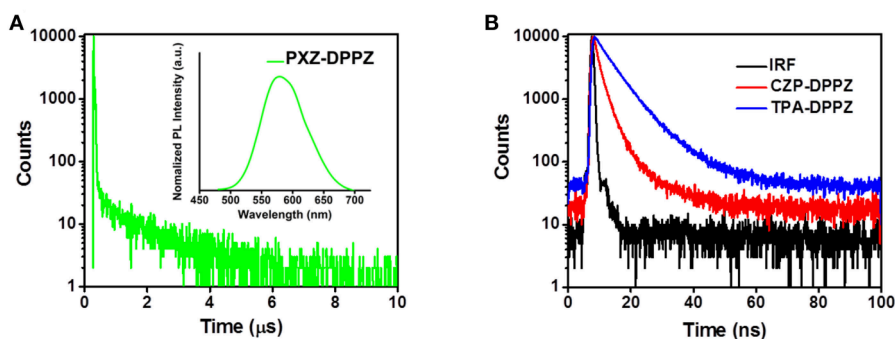


FIGURE 5 | (A) Lifetime and PL spectra of PXZ-DPPZ and **(B)** lifetimes of CZP-DPPZ and TPA-DPPZ in doped film.

moiety, which is almost the same to NTO of pure DPPZ (**Figure S2**). The oscillator strength of the S_1 state of CZP-DPPZ is 0.0029, which is only a little increasing comparing to that of DPPZ (0.0011), revealing that although certain state hybridization may occur, the S_1 state of CZP-DPPZ mainly exhibits an obvious LE character of $n \rightarrow \pi^*$ transition, which can result in a quenched fluorescence. On the other hand, the S_1 state of PXZ-DPPZ shows totally vertical, separated “hole” and “particle,” assigning to an obvious CT character. And just for this reason, the oscillator strength of the S_1 excited state is calculated to be zero, which indicates that the radiative transition in DPPZ can be very poor. Additionally, the ΔE_{ST} ($E_{S1} - E_{T1}$) of PXZ-DPPZ is estimated as 0.0238 eV, suggesting that the strong donor PXZ can potentially contribute to TADF property for PXZ-DPPZ. Therefore, neither LE-dominated nor CT-dominated is a good state regulation method of DPPZ in enhancing its emission.

Different from the nearly absolute overlap (LE) or separated (CT) character, For the S_1 state of TPA-DPPZ, its “hole” and “particle” are partially overlapped, that is, LE and CT characters simultaneously exists in the S_1 excited state, according with the HLCT state character. Thanks to this efficient state hybridization, the oscillator strength of TPA-DPPZ S_1 excited state grows up to 0.5208, which is 170 times that of the LE-dominated CZP-DPPZ, indicating that TPA-DPPZ can be an emissive material by HLCT modulation. Additionally, the LE and CT compositions of the three materials can be quantitatively estimated using the transition density matrix method (Gao et al., 2016) (**Figure S3**) to verify our judge on the excited state categories. The LE: CT proportions of the S_1 excited states of CZP-DPPZ, TPA-DPPZ and PXZ-DPPZ are 0.97:0.3, 0.49:0.51 and 0.13:0.87, respectively, which agrees well with their excited state properties of LE-dominated, HLCT and CT-dominated.

Photophysical Properties

The UV spectra of these compounds were recorded in tetrahydrofuran (THF) solution (**Figure 3**) in reference to that of the acceptor unit DPPZ. The DPPZ unit shows vibronic fine absorption with peaks at 371 nm and 391 nm, which is a typical character for the rigid condensed ring structure. Upon substitution of different donor moieties, characteristic absorptions can be observed to judge the excited state essences that we have predicted in the theoretical calculations. First, a single broadened absorption peak at 436 nm is observed in TPA-DPPZ, owing to the well hybridization of LE and CT. In the case of the strongest donor moiety, PXZ-DPPZ shows a new

absorption with onset of 570 nm, and the original absorption peak of DPPZ is fully reserved. The newly generated, weak absorption is of a small molar absorption coefficient of below $1,000 \text{ L mol}^{-1} \text{ cm}^{-1}$ which should be ascribed to a forbidden electron transition for the small orbital overlap and large twist angle, indicating a CT-dominate absorption character, reflecting that the LE and CT components are independent, or a de-hybridized LE and CT excited state components in PXZ-DPPZ. Surprisingly, the LE-like CZP-DPPZ does not display an overlapped absorption as DPPZ or PXZ-DPPZ, instead a red-shifted spectrum with a residual fine structure is observed, which indicates that its S_1 state is still mainly of LE state transition character of DPPZ, but certain state-hybridization of LE and CT has taken place, which may also affect its OLED performance.

The solvatochromic PL measurements are then conducted for further confirm the different excited state formation of these compounds. First, CZP-DPPZ and TPA-DPPZ both exhibit red-shifted emissions in the polarity-increasing solvents, assigning to CT character (**Figure 4**). In their refined Lippert-Mataga model (**Table S2**) (Grabowski et al., 2003), obviously, CZP-DPPZ shows a two-section line with two slopes, demonstrating a non-equivalent hybridization state with two different characters of excited state, which is in accordance to its absorption: though very little, certain CT component is actually hybridized into the emissive excited state of CZP-DPPZ. The dipole moment (μ_e) of CZP-DPPZ can be estimated to 13.57 D in low-polarity solvents and 22.74 D in high-polarity solvents, which could be assigned to a set of independent LE state and HLCT state, respectively. Different from CZP-DPPZ, in TPA-DPPZ, a good linear relation of the polarity factor f and the Stokes shift in all solvents is observed, corresponding to an undistinguished dipole moment of 18.41 D, assigning to the quasi-equivalent hybridization between LE and CT states. Besides, the single exponential lifetimes of TPA-DPPZ in different solvents are also

TABLE 1 | Photoluminescence quantum yields (PLQYs) of compounds in different states.

PLQY	CZP-DPPZ (%)	TPA-DPPZ (%)	PXZ-DPPZ (%)
Hexane	12	51	12
Ether	36	97	–
THF	81	93	–
Doped film	31	91	22
Powder	23	40	11

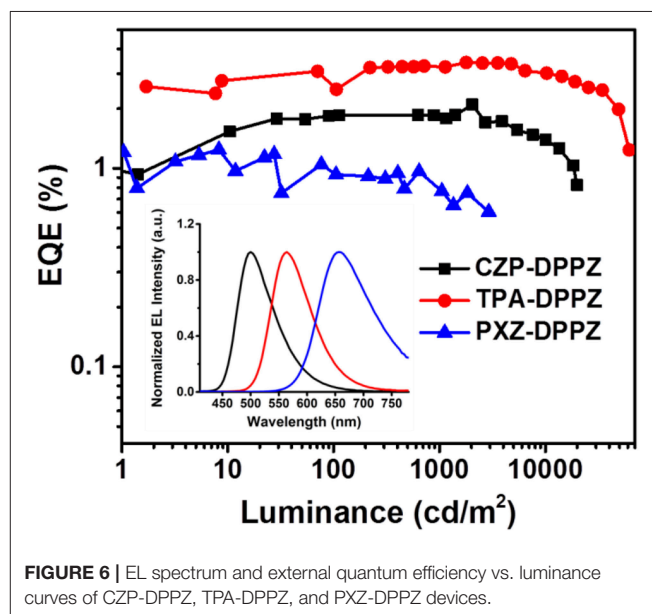


FIGURE 6 | EL spectrum and external quantum efficiency vs. luminance curves of CZP-DPPZ, TPA-DPPZ, and PXZ-DPPZ devices.

evidence that the excited state is one hybridized state (**Figure S4**), not a simple mix of two excited states (**Table S3**).

The “pure” CT compound PXZ-DPPZ demonstrates quite different PL compared to the other two compounds. We can only observe a very weak fluorescence in the lowest polarity solvent hexane with a PL peak at 566 nm (**Figure S5**), which is quite a red-shifted emission comparing to those of CZP-DPPZ and TPA-DPPZ, due to its obvious CT character caused by state de-hybridization. However, in higher-polarity solvents, the even strengthened CT character of PXZ-DPPZ causes totally non-emissive, so that its Lippert-Mataga model cannot be built. In order to figure out its PL properties, we prepared a 5% doped film (w/w, PXZ-DPPZ in PMMA,) on neat quartz plate. As shown in **Figure 5A**, the doped film of PXZ-DPPZ shows an orange emission with a PL peak at 579 nm. Different from the other two compounds (**Figure 5B**), the CT compound PXZ-DPPZ demonstrates a typical TADF character, whose PL decay spectrum can be fitted as a bi-exponential model, where the delayed component (τ_d) exhibits a longer lifetime of 1.3 μ s in the time range of 10 μ s at room temperature, and the prompt component (τ_p) is estimated as 10.0 ns in the time range of 200 ns (**Figure S6**). Owing to the joint action of strong donor and orthogonal configuration, PXZ-DPPZ demonstrates a nearly zero overlap of wave functions, resulting in the small ΔE_{ST} and strong CT with TADF characters.

In addition, the photoluminescent quantum yield (PLQY) of three compounds are measured for different statuses (Solutions, doped films, and neat powder) in **Table 1**. As a result, the HLCT compound TPA-DPPZ keeps the highest quantum yields than others in any status, suggesting that the HLCT compound TPA-DPPZ is more promising than CZP-DPPZ and PXZ-DPPZ in non-doped OLED. Furthermore, the radiative and non-radiative transition rate constants of the three compounds are given out by theoretical calculation (**Table S4**) using the Molecular Materials Property Prediction Package (MOMAP) to understand the PLQY variation of the compounds (Peng et al., 2007, 2013). CZP-DPPZ displays a low radiative transition rate of $7.32 \times 10^6 \text{ s}^{-1}$, which

originate from the non-emissive $n \rightarrow \pi^*$ character of LE state. Similarly, owing to the forbidden transition of CT state, PXZ-DPPZ exhibits the lowest k_r of $1.82 \times 10^3 \text{ s}^{-1}$ and corresponding to a low PLQY. But in the case of the HLCT material TPA-DPPZ, the k_r largely increases to $1.23 \times 10^8 \text{ s}^{-1}$, more importantly, its k_{nr} also shows a significant suppression comparing to the LE compound CZP-DPPZ, which is in accordance to our previous work (Zhang et al., 2013).

Additionally, the seemingly non-emissive pure-CT compound PXZ-DPPZ is actually of considerable PLQY (11%). Although hard evidence has not been found yet, this phenomenon can be tentatively understood that the nuclear motion, such as the vibration and the rotation of D-A connection bond, i.e., electron-vibrational coupling (EVC) is expected to affect the emission of pure CT excited state in solid state (Chen et al., 2015; Etherington et al., 2016), which could be the basis that the TADF doped OLED is always highly efficient.

Electroluminescence Performances

The energy levels of the frontier orbital measured by cyclic voltammetry (CV) method for the three materials are listed in **Table S5**. The thermal gravimetric analysis (TGA) measurements are also carried out to examine their thermal stabilities. All the three compounds exhibit good thermal stability with thermal-decomposition temperature (T_d) over 430°C (**Figure S7**). The good thermal performance of these emissive materials will benefit the device stability in OLED.

The non-doped OLED using the three compounds as emitters are fabricated with typical multi-layer structure: indium tin oxide (ITO)/ hexaazatriphenylenehexacarbonitrile (HATCN) (5 nm)/ 1,1'-bis(di-4-tolyl-aminophenyl)cyclohexane (TAPC) (40 nm)/4,4',4''-tri(N-carbazolyl)-triphenylamine (TCTA) (10 nm)/ emitter layer (20 nm)/ 1, 3, 5-tri(phenyl-2-benzimidazolyl)-benzene (TPBi) (40 nm)/ LiF (1 nm)/ Al (100 nm). Considering that the HOMO energy level of CZP is too deep (-5.58 eV), we add 4,4'-Bis(9H-carbazol-9-yl) biphenyl (CBP, HOMO = -5.91 eV) between TCTA and CZP-DPPZ as an

TABLE 2 | The electroluminescence device performances of emissive materials.

Emitter layer	$V_{on} \text{ (V)}^a$	$\lambda_{max} \text{ (nm)}^b$	$L_{max} \text{ (cd m}^{-2}\text{)}^c$	$\eta_{LE}/\text{max (cd A}^{-1}\text{)}^d$	$\eta_{PE}/\text{max (lm W}^{-1}\text{)}^e$	$\eta_{EQE}/\text{max (\%)}^f$	$\eta_s \text{ (\%)}^g$
CZP-DPPZ	3.9	502	19,860	6.22	3.43	2.10	45.8
TPA-DPPZ	3.0	568	61,951	11.05	8.18	3.42	42.8
PXZ-DPPZ	3.6	656	2,918	0.61	0.52	1.24	49.0

^a Turn-on voltage at a luminance of 1 cd m^{-2} ; ^b Maximum peak of EL spectra; ^c maximum luminance; ^d Maximum luminous efficiency; ^e Maximum power efficiency; ^f maximum external quantum efficiency; ^g Electro-excitation utilization.

TABLE 3 | Doped device performances of CZP-DPPZ, TPA-DPPZ, and PXZ-DPPZ.

Emitter layer	doping (wt%)	$V_{on} \text{ (V)}$	$\lambda_{max} \text{ (nm)}$	$L_{max} \text{ (cd m}^{-2}\text{)}$	$\eta_{LE}/\text{max (cd A}^{-1}\text{)}$	$\eta_{PE}/\text{max (lm W}^{-1}\text{)}$	$\eta_{EQE}/\text{max (\%)}^f$
CZP-DPPZ	40	3.8	492	14,030	3.59	2.38	1.46
TPA-DPPZ	10	3.6	532	15,740	12.74	10.07	3.73
PXZ-DPPZ	5	3.6	616	10,430	14.30	11.49	9.35

The device structure is: HATCN(5 nm)/TAPA(30 nm)/TCTA(10 nm)/CBP: emitter(wt%)(20 nm)/TPBi(30 nm) /LiF(1 nm)/Al(100 nm).

electron-blocking layer to avoid the formation of exciplex. The device performances are summarized in **Figure 6** and **Table 2**. The device based on CZP-DPPZ exhibits a green emission with a peak at 502 nm, and device of PXZ-DPPZ displays a red emission peaking at 656 nm (**Figure S8**), corresponding to the maximum external quantum efficiency (EQE) of 2.10 and 1.24%, respectively. Comparing to them, TPA-DPPZ based OLED shows significantly improved electroluminescence performance. It exhibits a lower turn-on voltage of 3.0 V, a larger maximum brightness of 61,951 cd m⁻², reflecting quite excellent stability of device (**Figure S10**). What's more, it achieves a max EQE of 3.42%, which 1.5 times that of CZP-DPPZ and 3 times that of PXZ-DPPZ. This efficiency increase can be assigned to the PLQY increasing brought about by HLCT, since the electro-exciton utilization of the three materials are just similar to each other, which is the result that the three compounds are all of certain CT excited state character (**Figure S9**), and non-negligibly, the strong SOC between singlet and triplet from DPPZ can also be a possible structural reason in parallel comparison to the acridine based D-A compounds that we have reported before (Zhou et al., 2017, 2018a).

The last but not the least, in previous works, the HLCT materials perform well in the non-doped OLED but the TADF materials do well in the doped OLED, although the k_r of TADF materials can be very limited. To investigate this issue, we also fabricated the doped OLED for these compounds, and the data are summarized in **Table 3**. Although the EQE of LE-dominated compound CZP-DPPZ and the HLCT compound TPA-DPPZ are kept at the same level as their non-doped OLED, the TADF material PXZ-DPPZ demonstrates an efficient orange-red emission with an 8-fold EQE (9.35%) that of its non-doped OLED (**Figure S11**), benefiting from its greatly suppressed triplet quenching and the probably existed EVC interaction that can drive the pure CT excited state be emissive.

CONCLUSIONS

In this work, to make the best use of the large SOC acceptor DPPZ, we synthesized three D-A compounds, which represent three typical excited states in fluorescent OLED: LE-dominated (CZP-DPPZ), HLCT (TPA-DPPZ), and CT (PXZ-DPPZ), and discussed the relationships between the structure and excited-state properties. Among them, the HLCT material TPA-DPPZ merits the highest k_r that is assigned to its enhanced oscillator

strength. As a result, TPA-DPPZ performs better than the other two materials in the non-doped OLED. For the doped OLED, despite its limited k_r , PXZ-DPPZ demonstrates a maximum EQE of 9.35%, which benefits from the greatly suppressed triplet quenching, high SOC originated from DPPZ acceptor and probably existed EVC. This work further proves that the regulation of HLCT excited state can be a decent method to design highly efficient organic functional materials, and also provides a new understanding to the structure-property relationship in fluorescent OLED.

DATA AVAILABILITY

All datasets generated for this study are included in the manuscript and/or the **Supplementary Files**.

AUTHOR CONTRIBUTIONS

CZ conducted the synthesis and the theoretical calculations. CZ, SX, MW, and WJ conducted the photophysical and OLED characterizations. SZ and CZ discussed the results and wrote the manuscript. SZ, HL and BY supervised the whole work and provided the funding of this work.

FUNDING

This work was supported by the National Basic Research Program of China (2015CB655003 and 2016YFB0401001), the National Natural Science Foundation of China (51673083, 51873077, and 51803071), the Postdoctoral Innovation Talent Support Project (BX20170097, BX20180121) and the China Postdoctoral Science Foundation (2017M620108 and 2018M641767).

ACKNOWLEDGMENTS

We thank our colleagues, Dr. Yu Gao, Dr. Jinyu Li, Yue Shen, Xiaohui Tang, Yating Wen, Hui Liu, Xiangyu Zhang, and Guocui Pan for experimental assistances and helpful discussions.

SUPPLEMENTARY MATERIAL

The Supplementary Material for this article can be found online at: <https://www.frontiersin.org/articles/10.3389/fchem.2019.00141/full#supplementary-material>

REFERENCES

- Ai, X., Chen, Y., Feng, Y., and Li, F. (2018a). A stable room-temperature luminescent biphenylmethyl radical. *Angew. Chem. Int. Ed.* 57, 2869–2873. doi: 10.1002/anie.201713321
- Ai, X., Evans, E. W., Dong, S., Gillett, A. J., Guo, H., Chen, Y., et al. (2018b). Efficient radical-based light-emitting diodes with doublet emission. *Nature* 563, 536–540. doi: 10.1038/s41586-018-0695-9
- Atkins, P. W., and Friedman, R. S. (2011). *Molecular Quantum Mechanics*. London: Oxford University Press.
- Cao, Y., Parker, I. D., Yu, G., Zhang, C., and Heeger, A. J. (1999). Improved quantum efficiency for electroluminescence in semiconducting polymers. *Nature* 397, 414–417. doi: 10.1038/17087
- Chen, H.-W., Lee, J.-H., Lin, B.-Y., Chen, S., and Wu, S.-T. (2018). Liquid crystal display and organic light-emitting diode display: present status and future perspectives. *Light Sci. Appl.* 7:17168. doi: 10.1038/lsa.2017.168
- Chen, X.-K., Zhang, S.-F., Fan, J.-X., and Ren, A.-M. (2015). Nature of highly efficient thermally activated delayed fluorescence in organic light-emitting diode emitters: nonadiabatic effect between excited states. *J. Phys. Chem. C* 119, 9728–9733. doi: 10.1021/acs.jpcc.5b00276

- Chen, Y.-H., Ma, D.-G., Sun, H.-D., Chen, J.-S., Guo, Q.-X., Wang, Q., et al. (2016). Organic semiconductor heterojunctions: electrode-independent charge injectors for high-performance organic light-emitting diodes. *Light Sci. Appl.* 5:e16042. doi: 10.1038/lsa.2016.42
- Chen, Z., Zhang, C., Jiang, X.-F., Liu, M., Xia, R., Shi, T., et al. (2017). High-performance color-tunable perovskite light emitting devices through structural modulation from bulk to layered film. *Adv. Mater.* 29:1603157. doi: 10.1002/adma.201603157
- Chiang, C.-J., Kimyonok, A., Etherington, M. K., Griffiths, G. C., Jankus, V., Turksoy, F., et al. (2013). Ultrahigh efficiency fluorescent single and bi-layer organic light emitting diodes: the key role of triplet fusion. *Adv. Funct. Mater.* 23, 739–746. doi: 10.1002/adfm.201201750
- El-Sayed, M. (1963). Spin-orbit coupling and the radiationless processes in nitrogen heterocycles. *J. Chem. Phys.* 38, 2834–2838. doi: 10.1063/1.1733610
- El-Sayed, M. (1964). Vanishing first- and second-order intramolecular heavy-atom effects on the ($\pi^* \rightarrow n$) phosphorescence in carbonyls. *J. Chem. Phys.* 41, 2462–2467. doi: 10.1063/1.1726288
- Etherington, M. K., Gibson, J., Higginbotham, H. F., Penfold, T. J., and Monkman, A. P. (2016). Revealing the spin-vibronic coupling mechanism of thermally activated delayed fluorescence. *Nat. Commun.* 7:13680. doi: 10.1038/ncomms13680
- Frisch, M., Trucks, G., Schlegel, H., Scuseria, G., Robb, M., Cheeseman, J., et al. (2009). Gaussian 09 Revision D. 01. Wallingford, CT: Gaussian Inc.
- Gao, Y., Zhang, S., Pan, Y., Yao, L., Liu, H., Guo, Y., et al. (2016). Hybridization and de-hybridization between the locally-excited (LE) state and the charge-transfer (CT) state: a combined experimental and theoretical study. *Phys. Chem. Chem. Phys.* 18, 24176–24184. doi: 10.1039/C6CP02778D
- Grabowski, Z. R., Rotkiewicz, K., and Rettig, W. (2003). Structural changes accompanying intramolecular electron transfer: focus on twisted intramolecular charge-transfer states and structures. *Chem. Rev.* 103, 3899–4031. doi: 10.1021/cr940745l
- Guo, F., Karl, A., Xue, Q.-F., Tam, K. C., Forberich, K., and Brabec, C. J. (2017). The fabrication of color-tunable organic light-emitting diode displays via solution processing. *Light Sci. Appl.* 6:e17094. doi: 10.1038/lsa.2017.94
- Guo, J., Li, X.-L., Nie, H., Luo, W., Gan, S., Hu, S., et al. (2017). Achieving high-performance nondoped OLEDs with extremely small efficiency roll-off by combining aggregation-induced emission and thermally activated delayed fluorescence. *Adv. Funct. Mater.* 27:1606458. doi: 10.1002/adfm.201606458
- Jin, J., Zhang, W., Wang, B., Mu, G., Xu, P., Wang, L., et al. (2014). construction of high Tg bipolar host materials with balanced electron-hole mobility based on 1,2,4-thiadiazole for phosphorescent organic light-emitting diodes. *Chem. Mater.* 26, 2388–2395. doi: 10.1021/cm403388s
- Krotkus, S., Kasemann, D., Lenk, S., Leo, K., and Reineke, S. (2016). Adjustable white-light emission from a photo-structured micro-OLED array. *Light Sci. Appl.* 5:e16121. doi: 10.1038/lsa.2016.121
- Lee, J., Sloatsky, M., Lee, K., Zhang, Y., and Forrest, S. R. (2014). An electrophosphorescent organic light emitting concentrator. *Light Sci. Appl.* 3:e181. doi: 10.1038/lsa.2014.62
- Li, W., Liu, D., Shen, F., Ma, D., Wang, Z., Feng, T., et al. (2012). A twisting donor-acceptor molecule with an intercrossed excited state for highly efficient, deep-blue electroluminescence. *Adv. Funct. Mater.* 22, 2797–2803. doi: 10.1002/adfm.201200116
- Li, W., Pan, Y., Xiao, R., Peng, Q., Zhang, S., Ma, D., et al. (2014a). Employing similar to 100% excitons in OLEDs by utilizing a fluorescent molecule with hybridized local and charge-transfer excited state. *Adv. Funct. Mater.* 24, 1609–1614. doi: 10.1002/adfm.201301750
- Li, W., Pan, Y., Yao, L., Liu, H., Zhang, S., Wang, C., et al. (2014b). A hybridized local and charge-transfer excited state for highly efficient fluorescent OLEDs: molecular design, spectral character, and full exciton utilization. *Adv. Opt. Mater.* 2, 892–901. doi: 10.1002/adom.201400154
- Liu, H., Bai, Q., Yao, L., Zhang, H., Xu, H., Zhang, S., et al. (2015). Highly efficient near ultraviolet organic light-emitting diode based on a meta-linked donor-acceptor molecule. *Chem. Sci.* 6, 3797–3804. doi: 10.1039/C5SC01131K
- Liu, H., Gao, Y., Cao, J., Li, T., Wen, Y., Ge, Y., et al. (2018). Efficient room-temperature phosphorescence based on a pure organic sulfur-containing heterocycle: folding-induced spin-orbit coupling enhancement. *Mater. Chem. Front.* 2, 1853–1858. doi: 10.1039/C8QM00320C
- Liu, T., Zhu, L., Gong, S., Zhong, C., Xie, G., Mao, E., et al. (2017a). A red fluorescent emitter with a simultaneous hybrid local and charge transfer excited state and aggregation-induced emission for high-efficiency, low efficiency roll-off OLEDs. *Adv. Opt. Mater.* 5:1700145. doi: 10.1002/adom.201700145
- Liu, T., Zhu, L., Zhong, C., Xie, G., Gong, S., Fang, J., et al. (2017b). Naphthothiadiazole-based near-infrared emitter with a photoluminescence quantum yield of 60% in neat film and external quantum efficiencies of up to 3.9% in nondoped OLEDs. *Adv. Funct. Mater.* 27:1606384. doi: 10.1002/adfm.201606384
- Luo, Y., and Aziz, H. (2010). Correlation between triplet triplet annihilation and electroluminescence efficiency in doped fluorescent organic light-emitting devices. *Adv. Funct. Mater.* 20, 1285–1293. doi: 10.1002/adfm.200902329
- Mao, Z., Yang, Z., Mu, Y., Zhang, Y., Wang, Y. F., Chi, Z., et al. (2015). Linearly tunable emission colors obtained from a fluorescent-phosphorescent dual-emission compound by mechanical stimuli. *Angew. Chem. Int. Ed.* 54, 6270–6273. doi: 10.1002/anie.201500426
- Pan, Y., Li, W., Zhang, S., Yao, L., Gu, C., Xu, H., et al. (2014). High yields of singlet excitons in organic electroluminescence through two paths of cold and hot excitons. *Adv. Opt. Mater.* 2, 510–515. doi: 10.1002/adom.201300467
- Peng, Q., Niu, Y., Shi, Q., Gao, X., and Shuai, Z. (2013). Correlation function formalism for triplet excited state decay: combined spin-orbit and nonadiabatic couplings. *J. Chem. Theory Comput.* 9, 1132–1143. doi: 10.1021/ct300798t
- Peng, Q., Obolda, A., Zhang, M., and Li, F. (2015). Organic light-emitting diodes using a neutral pi radical as emitter: the emission from a doublet. *Angew. Chem. Int. Ed.* 54, 7091–7095. doi: 10.1002/anie.201500242
- Peng, Q., Yi, Y., Shuai, Z., and Shao, J. (2007). Toward quantitative prediction of molecular fluorescence quantum efficiency: role of Duschinsky rotation. *J. Am. Chem. Soc.* 129, 9333–9339. doi: 10.1021/ja067946e
- Sun, C., Ran, X., Wang, X., Cheng, Z., Wu, Q., Cai, S., et al. (2018). A twisted molecular structure on tuning ultralong organic phosphorescence. *J. Phys. Chem. Lett.* 9, 335–339. doi: 10.1021/acs.jpclett.7b02953
- Tang, C. W., and VanSlyke, S. A. (1987). Organic electroluminescent diodes. *Appl. Phys. Lett.* 51, 913–915. doi: 10.1063/1.98799
- Tang, X., Li, X.-L., Liu, H., Gao, Y., Shen, Y., Zhang, S., et al. (2018). Efficient near-infrared emission based on donor-acceptor molecular architecture: the role of ancillary acceptor of cyanophenyl. *Dyes Pigments* 149, 430–436. doi: 10.1016/j.dyepig.2017.10.033
- Uoyama, H., Goushi, K., Shizu, K., Nomura, H., and Adachi, C. (2012). Highly efficient organic light-emitting diodes from delayed fluorescence. *Nature* 492, 234–238. doi: 10.1038/nature11687
- Wang, C., Li, X., Pan, Y., Zhang, S., Yao, L., Bai, Q., et al. (2016). Highly efficient nondoped green organic light-emitting diodes with combination of high photoluminescence and high exciton utilization. *ACS Appl. Mater. Interfaces* 8, 3041–3049. doi: 10.1021/acsami.5b10129
- Wang, C., Li, X.-L., Gao, Y., Wang, L., Zhang, S., Zhao, L., et al. (2017). Efficient near-infrared (NIR) organic light-emitting diodes based on donor-acceptor architecture: an improved emissive state from mixing to hybridization. *Adv. Opt. Mater.* 5:1700441. doi: 10.1002/adom.201700441
- Xiang, C., Koo, W., So, F., Sasabe, H., and Kido, J. (2013). A systematic study on efficiency enhancements in phosphorescent green, red and blue microcavity organic light emitting devices. *Light Sci. Appl.* 2:e74. doi: 10.1038/lsa.2013.30
- Xu, S., Chen, R., Zheng, C., and Huang, W. (2016). Excited state modulation for organic afterglow: materials and applications. *Adv. Mater.* 28, 9920–9940. doi: 10.1002/adma.201602604
- Yao, L., Pan, Y., Tang, X., Bai, Q., Shen, F., Li, F., et al. (2015). Tailoring excited-state properties and electroluminescence performance of donor acceptor molecules through tuning the energy level of the charge-transfer state. *J. Phys. Chem. C* 119, 17800–17808. doi: 10.1021/acs.jpcc.5b03996
- Yao, L., Zhang, S., Wang, R., Li, W., Shen, F., Yang, B., et al. (2014). Highly efficient near-infrared organic light-emitting diode based on a butterfly-shaped donor-acceptor chromophore with strong solid-state fluorescence and a large proportion of radiative excitons. *Angew. Chem. Int. Ed.* 53, 2119–2123. doi: 10.1002/anie.201308486
- Zhang, D., Duan, L., Zhang, Y., Cai, M., Zhang, D., and Qiu, Y. (2015). Highly efficient hybrid warm white organic light-emitting diodes using a

- blue thermally activated delayed fluorescence emitter: exploiting the external heavy-atom effect. *Light Sci. Appl.* 4:e232. doi: 10.1038/lsa.2015.5
- Zhang, Q., Kuwabara, H., Potscavage, W. J. Jr., Huang, S., Hatae, Y., Shibata, T., et al. (2014a). Anthraquinone-based intramolecular charge-transfer compounds: computational molecular design, thermally activated delayed fluorescence, and highly efficient red electroluminescence. *J. Am. Chem. Soc.* 136, 18070–18081. doi: 10.1021/ja510144h
- Zhang, Q., Li, B., Huang, S., Nomura, H., Tanaka, H., and Adachi, C. (2014b). Efficient blue organic light-emitting diodes employing thermally activated delayed fluorescence. *Nat. Photonics* 8, 326–332. doi: 10.1038/nphoton.2014.12
- Zhang, S., Li, W., Yao, L., Pan, Y., Shen, F., Xiao, R., et al. (2013). Enhanced proportion of radiative excitons in non-doped electro-fluorescence generated from an imidazole derivative with an orthogonal donor-acceptor structure. *Chem. Commun.* 49, 11302–11304. doi: 10.1039/c3cc47130f
- Zhang, S., Yao, L., Peng, Q., Li, W., Pan, Y., Xiao, R., et al. (2015). Achieving a significantly increased efficiency in nondoped pure blue fluorescent OLED: a quasi-equivalent hybridized excited state. *Adv. Funct. Mater.* 25, 1755–1762. doi: 10.1002/adfm.201404260
- Zhao, Y., and Truhlar, D. G. (2008). The M06 suite of density functionals for main group thermochemistry, thermochemical kinetics, noncovalent interactions, excited states, and transition elements: two new functionals and systematic testing of four M06-class functionals and 12 other functionals. *Theor. Chem. Acc* 120, 215–241. doi: 10.1007/s00214-007-0310-x
- Zhou, C., Gong, D., Gao, Y., Liu, H., Li, J., Zhang, S., et al. (2018a). Enhancing the electroluminescent efficiency of acridine-based donor-acceptor materials: quasi-equivalent hybridized local and charge-transfer state. *J. Phys. Chem. C* 122, 18376–18382. doi: 10.1021/acs.jpcc.8b07083
- Zhou, C., Zhang, S., Gao, Y., Liu, H., Shan, T., Liang, X., et al. (2018b). Ternary emission of fluorescence and dual phosphorescence at room temperature: a single-molecule white light emitter based on pure organic aza-aromatic material. *Adv. Funct. Mater.* 28:1802407. doi: 10.1002/adfm.201802407
- Zhou, C., Zhang, T., Zhang, S., Liu, H., Gao, Y., Su, Q., et al. (2017). Isomerization effect of triphenylamine-acridine derivatives on excited-state modification, photophysical property and electroluminescence performance. *Dyes Pigments* 146, 558–566. doi: 10.1016/j.dyepig.2017.07.056
- Conflict of Interest Statement:** The authors declare that the research was conducted in the absence of any commercial or financial relationships that could be construed as a potential conflict of interest.
- Copyright © 2019 Zhou, Xiao, Wang, Jiang, Liu, Zhang and Yang. This is an open-access article distributed under the terms of the Creative Commons Attribution License (CC BY). The use, distribution or reproduction in other forums is permitted, provided the original author(s) and the copyright owner(s) are credited and that the original publication in this journal is cited, in accordance with accepted academic practice. No use, distribution or reproduction is permitted which does not comply with these terms.



Thiophene Disubstituted Benzothiadiazole Derivatives: An Effective Planarization Strategy Toward Deep-Red to Near-Infrared (NIR) Organic Light-Emitting Diodes

Wentao Xie, Binbin Li, Xinyi Cai, Mengke Li, Zhenyang Qiao, Xiaohui Tang, Kunkun Liu, Cheng Gu, Yuguang Ma and Shi-Jian Su*

State Key Laboratory of Luminescent Materials and Devices, Institute of Polymer Optoelectronic Materials and Devices, South China University of Technology, Guangzhou, China

OPEN ACCESS

Edited by:

Naohiko Yoshikai,
Nanyang Technological University,
Singapore

Reviewed by:

Bing Yang,
Jilin University, China
Silu Tao,
University of Electronic Science and
Technology of China, China

*Correspondence:

Shi-Jian Su
mssjsu@scut.edu.cn

Specialty section:

This article was submitted to
Organic Chemistry,
a section of the journal
Frontiers in Chemistry

Received: 06 March 2019

Accepted: 03 April 2019

Published: 18 April 2019

Citation:

Xie W, Li B, Cai X, Li M, Qiao Z,
Tang X, Liu K, Gu C, Ma Y and Su S-J
(2019) Thiophene Disubstituted
Benzothiadiazole Derivatives: An
Effective Planarization Strategy
Toward Deep-Red to Near-Infrared
(NIR) Organic Light-Emitting Diodes.
Front. Chem. 7:276.
doi: 10.3389/fchem.2019.00276

As one of the three primary colors that are indispensable in full-color displays, the development of red emitters is far behind the blue and green ones. Here, three novel orange-yellow to near-infrared (NIR) emitters based on 5,6-difluorobenzo[c][1,2,5]thiadiazole (BTDF) namely BTDF-TPA, BTDF-TTPA, and BTDF-TtTPA were designed and synthesized. Density functional theory analysis and photophysical characterization reveal that these three materials possess hybridized local and charge-transfer (HLCT) state feature and a feasible reverse intersystem crossing (RISC) from the high-lying triplet state to the singlet state may conduce to an exciton utilization exceeding the limit of 25% of traditional fluorescence materials under electrical excitation. The insertion of thiophene with small steric hindrance as π -bridge between the electron-donating (D) moiety triphenylamine (TPA) and the electron-accepting (A) moiety BTDF not only results in a remarkable 67 nm red-shift of the emission peak but also brings about a large overlap of frontier molecular orbitals to guarantee high radiative transition rate that is of great significance to obtain high photoluminescence quantum yield (PLQY) in the “energy-gap law” dominated long-wavelength emission region. Consequently, an attractive high maximum external quantum efficiency (EQE) of 5.75% was achieved for the doped devices based on these thiophene π -bridged emitters, giving a deep-red emission with small efficiency roll-off. Remarkably, NIR emission could be obtained for the non-doped devices, achieving an excellent maximum EQE of 1.44% and Commission Internationale de l’Éclairage (CIE) coordinates of (0.71, 0.29). These results are among the highest efficiencies in the reported deep-red to NIR fluorescent OLEDs and offer a new π -bridge design strategy in D- π -A and D- π -A- π -D red emitter design.

Keywords: organic light-emitting diodes, donor-acceptor chromophores, deep-red to near-infrared (NIR) emission, hybridized local and charge-transfer state (HLCT), hot-exciton

INTRODUCTION

Since the creative invention of organic light-emitting diodes (OLEDs) by Tang and VanSlyke (1987), OLEDs have been receiving intense research for more than 30 years for the potential applications in flat panel display (Pfeiffer et al., 2002), solid state lighting (Kido et al., 1995) and other applications outside the visible range (Tessler et al., 2002). According to spin statistics rule, the branching ratio of singlet and triplet excitons is 1:3, meaning one singlet exciton is generated for every three triplet excitons under electrical excitation (Baldo et al., 1999). Therefore, since radiative transition of triplets is spin-forbidden, internal quantum efficiency (η_{int}) is limited to 25% for traditional fluorescence. Transition metals such as iridium and platinum were introduced into organic aromatic frameworks by Baldo et al. (1998), to harvest triplets by increasing spin-orbit coupling (SOC) between the first singlet excited state (S_1) and the first triplet excited state (T_1), and nearly 100% internal quantum efficiency can be theoretically obtained. However, the usage of noble metals like Ir and Pt are expensive and non-renewable, which are fatal to large area, low cost production in future. Hence, searching for high efficiency and noble metal-free purely organic emitting materials is imperative (Chen et al., 2016).

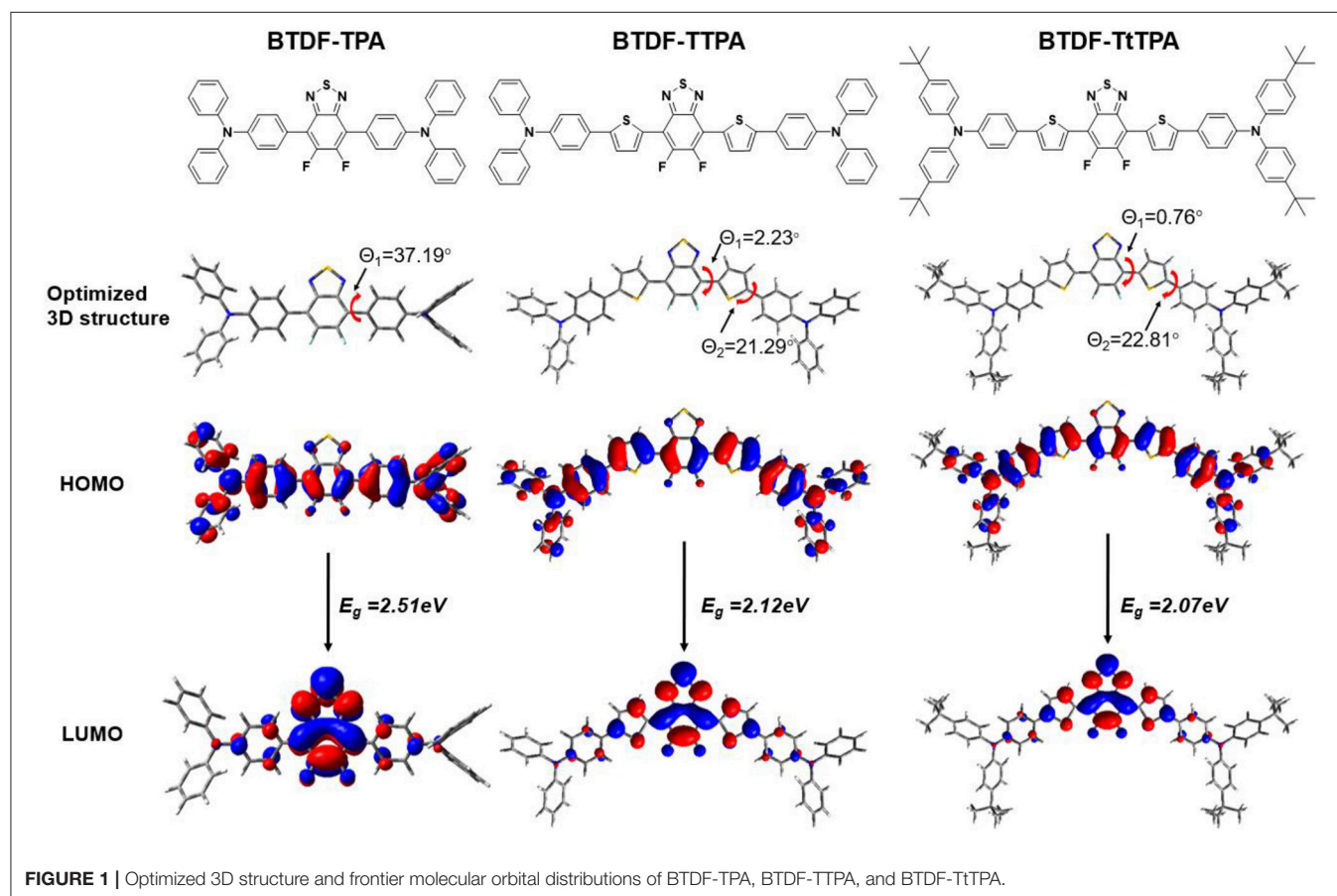
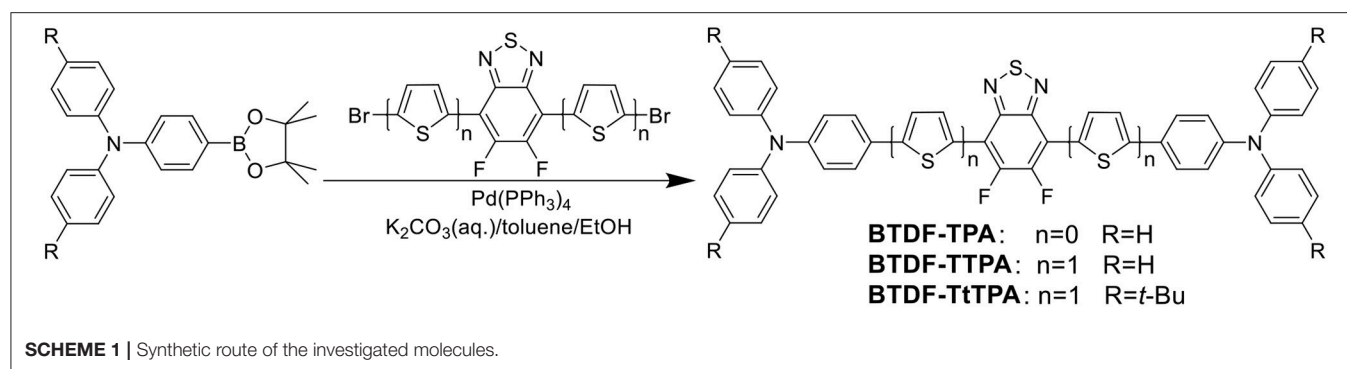
Recently, many purely organic luminescence mechanisms with internal quantum efficiency over 25% were proposed by different research groups around the world, such as thermally activated delayed fluorescence (TADF) (Uoyama et al., 2012), triplet-triplet annihilation (TTA) (Kondakov et al., 2009), hybridized local and charge-transfer state (HLCT) (Li et al., 2012) and neutral π radical doublet emission (Peng et al., 2015). Among these luminescence mechanisms, TADF materials were regarded as the most promising next generation luminescent materials for their fascinating advantages: (1) concise design concept (Cai et al., 2016b); (2) tunable full spectrum emission (Park et al., 2016); and (3) high efficiency that can rival those of phosphorescent OLEDs (Liu M. et al., 2017). Unfortunately, TADF-OLEDs are often suffered from severe efficiency roll-off at high current density due to triplet-triplet annihilation (TTA) and triplet-polaron annihilation (TPA) induced by their long triplet exciton lifetimes, regardless of high EQEs at low current density (Zhang et al., 2012). Yet, the most essential reason is the small radiative transition rate (k_f) of these TADF materials (Chen et al., 2019). As one of the three primary colors that are indispensable in full-color display, the research progress in red OLEDs still lags behind the development of highly efficient blue and green OLEDs (Lin et al., 2016; Wu et al., 2018). The reason for the slow development of red luminescent materials can be attributed to the “energy-gap law,” i.e., when the energy gap decreased, the coupling (or vibrational overlap) between the zero-vibrational level of S_1 and the higher levels of S_0 state is enhanced (Furue et al., 2018). As a result, the red luminescent materials often suffered from the accelerated energy loss caused by the enhanced non-radiative internal conversion (IC) (Chen et al., 2018). Therefore, the common large twist donor-acceptor structure in blue and green TADF-OLEDs is not suitable for the design of highly efficient red OLEDs with small efficiency roll-off due to the small k_f .

Fortunately, the HLCT state is likely suitable for the design of red emission materials, where the locally excited (LE) state contributes to a high photoluminescence (PL) efficiency and the charge-transfer (CT) state contributes to a large fraction of triplet exciton utilization in electroluminescence (EL) (Li et al., 2014b). Therefore, to achieve a highly efficient and small efficiency roll-off deep-red to NIR purely organic luminescent materials, three BTDF-based compounds were designed and synthesized (Scheme 1 and Figure S1). By incorporating a thiophene unit with small steric hindrance as π -bridge in the common D-A-D skeleton, a remarkable 67 nm red-shift of the emission peak was achieved with the maintenance of high radiative transition rate that is of great significance to obtain high PLQY in “energy-gap law” dominated long-wavelength emission region (Zhang et al., 2014).

RESULTS AND DISCUSSION

Theoretical Calculation

In order to explore the relationship between the material property and molecular structure of these compounds, density functional theory (DFT) simulation was performed firstly using the Gaussian suite of programs (Gaussian 09-B01 package). The ground-state geometries of the investigated compounds were optimized at the B3LYP/6-31G (d, p) level, and geometries and frontier molecular orbital (FMO) distributions were depicted in Figure 1. As shown, the highest occupied molecular orbitals (HOMOs) of these compounds are distributed throughout the whole molecular skeleton, but the lowest unoccupied molecular orbitals (LUMOs) are mainly located on the BTDF acceptor and slightly extended to the benzene or thiophene π -bridges. The large overlaps of HOMOs and LUMOs imply a decent radiative transition rate for these materials to achieve high PLQY (Gan et al., 2018). Comparing BTDF-TTPA (or BTDF-TtTPA) with BTDF-TPA, the introduction of the five-membered ring thiophene bridge between the electron donor (D) and the electron acceptor (A) not only extends the conjugation length of the whole molecule to ensure a red-shift of the emission wavelength, but also reduces the dihedral angle between D and A by a wide margin to obtain a large oscillator strength for the sake of moderate PLQY (Cai et al., 2016a). Furthermore, to deeply describe the excited state properties of these investigated materials, natural transition orbitals (NTOs) and the energy levels of singlets (S_1 to S_5) and triplets (T_1 to T_5) were calculated at the level of TD-M062X/6-31G (d, p) on the basis of the optimized S_0 state configuration (Figure 2 and Figure S2) (Han et al., 2015). For the lowest singlet excited states (S_1), the particles are obviously localized on the BTDF acceptor component, but the holes are dispersed on the whole molecules. Therefore, a majority of LE transition of BTDF and a minority of CT transition from TPA to BTDF can be predicted. The overlap of holes and particles demonstrated the coexistence of LE and CT components, implying the existence of the HLCT state, which was proposed by Li et al. (2014a) in recent years. However, the lowest triplet excited states (T_1) were a LE state, and its holes and particles were localized on the BTDF acceptor moiety and almost completely overlapped. The configuration of the high-lying triplet excited states T_2 is quite similar to that of the S_1

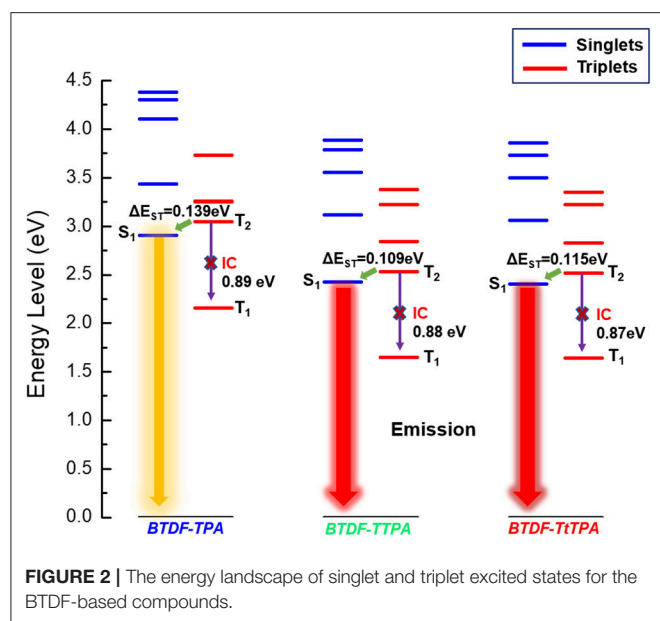


states, indicating the T_2 states also possess the HLCT feature. The coexistence of the LE and CT states in the S_1 and T_2 states are in favor of the reverse intersystem crossing (RISC) according to the permissible SOC between the singlet state and the triplet state, and the RISC rate can be greatly enhanced since the sulfur atoms in the thiophene and BTDF heterocyclics are able to improve SOC (Yao et al., 2014). As depicted in **Figure 2**, a significantly large energy gaps (0.87–0.89 eV) between T_2 and T_1 may inhibit the IC from T_2 to T_1 according to the energy-gap law, and the small energy split (0.109–0.139 eV) between T_2 and S_1 may facilitate the RISC from T_2 to S_1 (Liu T. et al., 2017). Such energy level landscape meets the requirement of “hot exciton” mechanism

very well, leading to a high-lying RISC process from T_2 to S_1 , and an exciton utilization exceeding 25% under electrical excitation can be expected (Tang et al., 2018).

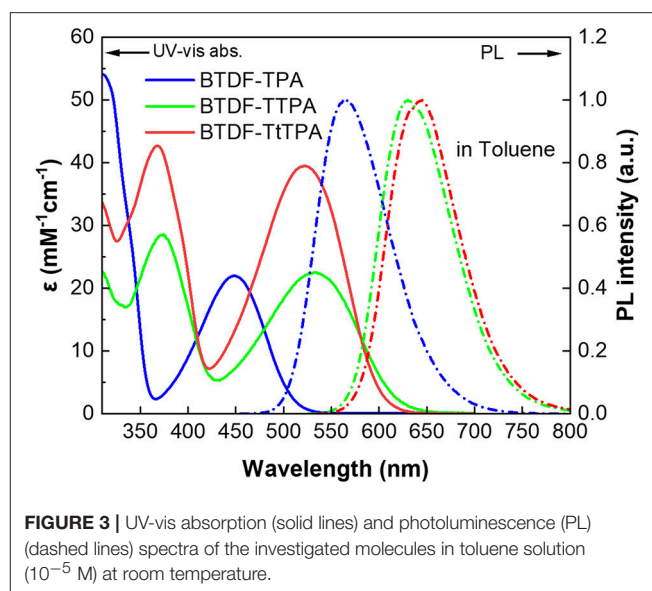
Photophysical Properties

To clarify the photophysical properties of the BTDF-based compounds, ultra-violet and visible (UV-vis) absorption and PL spectra were firstly measured in different polar solvents (**Figure 3**, **Figure S6** and **Table S2**). As depicted in **Figure 3**, the short-wavelength absorption bands at around 325 and 375 nm could be associated with π - π^* transition, while the weak absorption bands at around 375–525 and 425–625 nm could be



attributed to the intramolecular charge-transfer (ICT) transition from the TPA moiety to the BTDF moiety (Tsai et al., 2015). As the polarity of the solvent increases (Figure S6), the absorption spectra change slightly in shape, which means that the dipoles change in the ground state is quite small in different polar solvents (Yao et al., 2014). Furthermore, despite the introduction of the thiophene bridge results in about 67 nm red shift of the emission spectra, the molar extinction coefficients (ϵ) of the ICT transitions in toluene solution still remain a relatively high level (about $2\text{--}4 \times 10^4 \text{ L mol}^{-1} \text{ cm}^{-1}$), which should most likely be ascribed to the effective planarization molecular design strategy (Jiang et al., 2017). The emission colors of these materials in dilute toluene solution (10^{-5} M) are in a range from orange-yellow (BTDF-TPA: $\lambda_{\text{em}} = 563 \text{ nm}$) to deep-red (BTDF-TTPA: $\lambda_{\text{em}} = 630 \text{ nm}$; BTDF-TtTPA: $\lambda_{\text{em}} = 645 \text{ nm}$). Besides, the PL spectra of these BTDF-based compounds in different polar solvents show a significant red-shift phenomenon as the solvent polarity increases: the emission peak wavelength moves from 605 nm in low polar solvent n-hexane to 689 nm in high polar solvent acetone for BTDF-TTPA. These remarkable solvatochromic phenomena in solution indicate that the excited states of these investigated compounds have a strong CT characteristic and the dipoles change a lot (Zhao et al., 2018). Considering the emissions of BTDF-TTPA and BTDF-TtTPA in toluene solution are located in the deep-red region, UV-vis absorption and PL spectra of these two materials in neat thin film have also been characterized (Figure S3). They exhibit an emission peak of 663 nm, indicating the possibility to fabricate a non-doped NIR device.

Moreover, in order to deeply understand the relationship between the excited state properties and the solvent polarity, the dipole moment of the excited state (μ_e) on the basis of the Lippert–Mataga relation was measured for these three compounds. As shown in Figure 4, the linear relation of the Stokes shift ($\nu_a - \nu_f$) vs. the orientation polarizability $f(\epsilon, n)$ was fitted for BTDF-TPA, BTDF-TTPA, and BTDF-TtTPA. They all

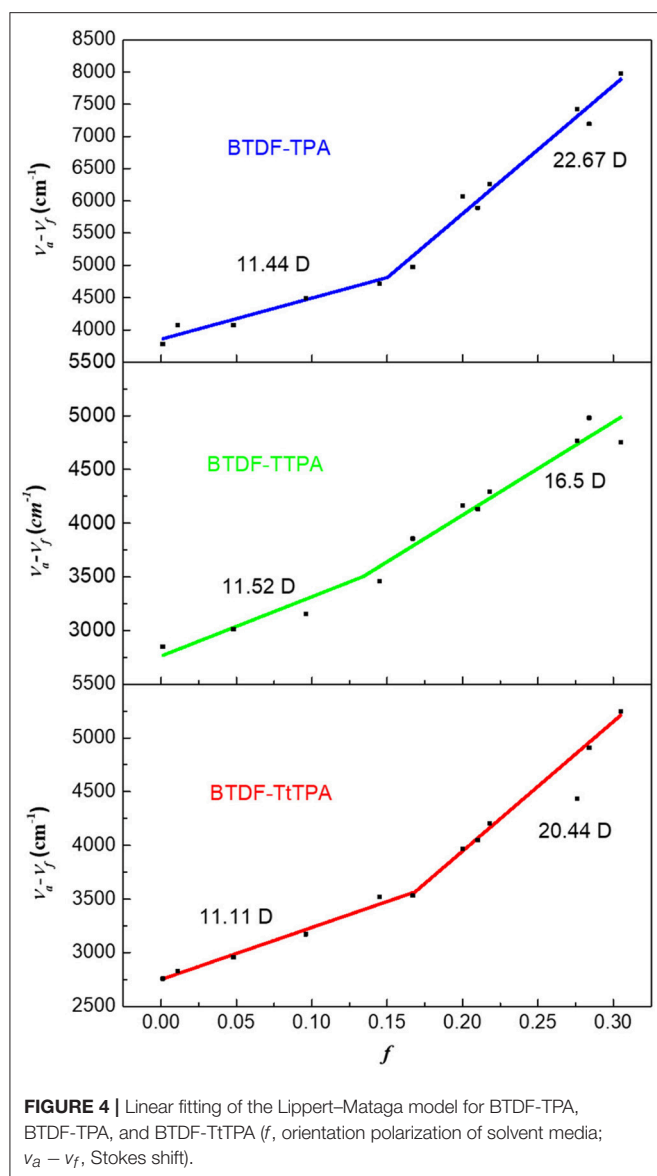


displayed two different linear relations in low-polarity and high-polarity region, respectively. Taken BTDF-TPA as an example, the dipole moment μ_e of 11.44 Debye in low polar solvents indicate a LE-state dominated character, while the μ_e of 22.67 Debye in high polar solvents can be attributed to CT-state. Based on the above analysis, the inter-crossing and the coexistence of LE and CT components can facilitate the HLCT state in medium polarity solvents for the BTDF-based compounds (Li et al., 2014a).

Transient PL decay characteristics of these compounds were also investigated in toluene solution, doped film and neat film (Figure S5 and Table S1). The transient PL decay curves of these materials in toluene solution exhibit a single-exponential fluorescence decay process with a lifetime of 1.28, 0.96 and 1.10 ns for BTDF-TPA, BTDF-TTPA, and BTDF-TtTPA, respectively. No delayed fluorescence was observed from the transient PL decay curves, suggesting these compounds are not TADF emitters. With the combination of the PLQY in toluene solution, radiative rate constants could be calculated as 7.4×10^8 , 8.9×10^8 , and $7.5 \times 10^8 \text{ s}^{-1}$ for BTDF-TPA, BTDF-TTPA, and BTDF-TtTPA, respectively, by the equation $k_f = \frac{1}{\tau_f}$. Obviously, throughout the above analysis one can know that the effective thiophene-bridge planarization strategy not only results in a remarkable red-shift of the emission peak but also brings about a large overlap of frontier molecular orbitals to guarantee high radiative transition rate that is of great significance to obtain high PLQY in the “energy-gap law” dominated long-wavelength emission region.

Thermal Properties and Electrochemical Characterization

As a good thermal stability helps to form an uniform evaporated amorphous film during the fabrication of OLED devices, these compounds were also subjected to thermal analysis by differential scanning calorimetry (DSC) and thermogravimetry (TG) (Zhang et al., 2017). Figure S7 shows the TG and DSC curves of these compounds. High decomposition temperatures (T_d) from 453 to



493°C were found for the materials corresponding to 5% mass loss. Different from BTDF-TPA and BTDF-TtTPA that show no glass transition temperature (T_g) and crystallization temperature

(T_c) in the range of 50–200°C, BTDF-TTPA exhibits a T_g at 117°C and a clear T_c at 161°C. The observed T_g and T_c for BTDF-TTPA can be attributed to the more planar molecular structure and closer molecular packing due to the introduction of the small steric thiophene as the bridge and the absence of *tert*-butyl substituent group (Qian et al., 2009).

Electrochemical properties of these materials were obtained by cyclic voltammetry (CV) measurement. The HOMO energy levels of BTDF-TPA, BTDF-TTPA, and BTDF-TtTPA were estimated as −5.32, −5.03, and −5.06 eV, respectively. The oxidation potentials were obviously lowered by the introduced electron-rich thiophene bridge, as clearly presented in Figure S8. With the combination of the band-gap obtained from the absorption edge in toluene solution, their LUMO energy levels were estimated to be −2.89, −2.97, and −3.05 eV, respectively. Considering the oxidation potential was measured in a solution, which may be somewhat different from the film state in devices, ionization potentials of BTDF-TTPA (5.30 eV) and BTDF-TtTPA (5.12 eV) in a neat film were also measured by photoelectron yield spectroscopy (Figure S9). Their electron affinities were estimated by adding the corresponding optical energy gaps (E_g), which were determined from the onset of the neat film absorption spectra (Figure S3). The key parameters of the BTDF-based compounds are summarized in Table 1.

OLED Characterization

According to the PL spectra of these materials in toluene solution, BTDF-TTPA and BTDF-TtTPA are promising deep-red and NIR emitters for OLED applications. Firstly, in order to avoid aggregation caused quenching (ACQ) which may affect device performance, BTDF-TTPA and BTDF-TtTPA were used as dopants dispersed in a common host CBP (4,4'-bis(carbazol-9-yl) biphenyl) in a concentration of 1 wt.% (Xie et al., 2016). As depicted in Figure 5A, a simple device architecture of indium tin oxide (ITO)/TAPC (40 nm)/EML (25 nm)/TmPyPB (55 nm)/LiF (1 nm)/Al (100 nm) was fabricated, in which 1,1-bis(4-(*N,N*-di(*p*-tolyl)-amino)-phenyl)cyclohexane (TAPC), 1,3,5-tri(*m*-pyrid-3-ylphenyl)benzene (TmPyPB) and LiF play the roles of hole-transport and electron-blocking, electron-transport and hole-blocking and electron-injection layers, respectively (Figure S10). Meanwhile, a non-doped emission layer (EML) was also adopted in the same device structure to obtain NIR emissions. As the HOMO and LUMO energy levels of all guest molecules are

TABLE 1 | Photophysical, thermal, and electrochemical properties of the investigated compounds.

Compounds	λ_{abs} [nm] ^a	λ_{em} [nm] ^a	T_d/T_g [°C] ^b	HOMO/LUMO/ E_g [eV] ^c	ϕ_{PL} [%] ^d
BTDF-TPA	310, 451	563	453/N.A.	5.32/2.89/2.43	95.2
BTDF-TTPA	368, 524	630	490/124	5.03/2.97/2.06	85.8
BTDF-TtTPA	371, 531	645	493/N.A.	5.06/3.05/2.01	82.9

^aUV-vis absorption and PL spectra measured in toluene solution (10^{-5} M) at room temperature.

^bDecomposition (T_d) (at 5% weight loss) and glass transition temperatures (T_g).

^cHOMO energy levels calculated from the empirical formula: $E_{\text{HOMO}} = -(E_{\text{ox}} + 4.4 \text{ eV})$, LUMO energy levels estimated from the absorption edge in toluene solution (λ_{onset}) and E_{HOMO} , using empirical formula: $E_{\text{LUMO}} = E_{\text{HOMO}} + 1,240/\lambda_{\text{onset}}$.

^dPL quantum yields were measured in toluene solution (10^{-5} M) at room temperature using an integrating sphere.

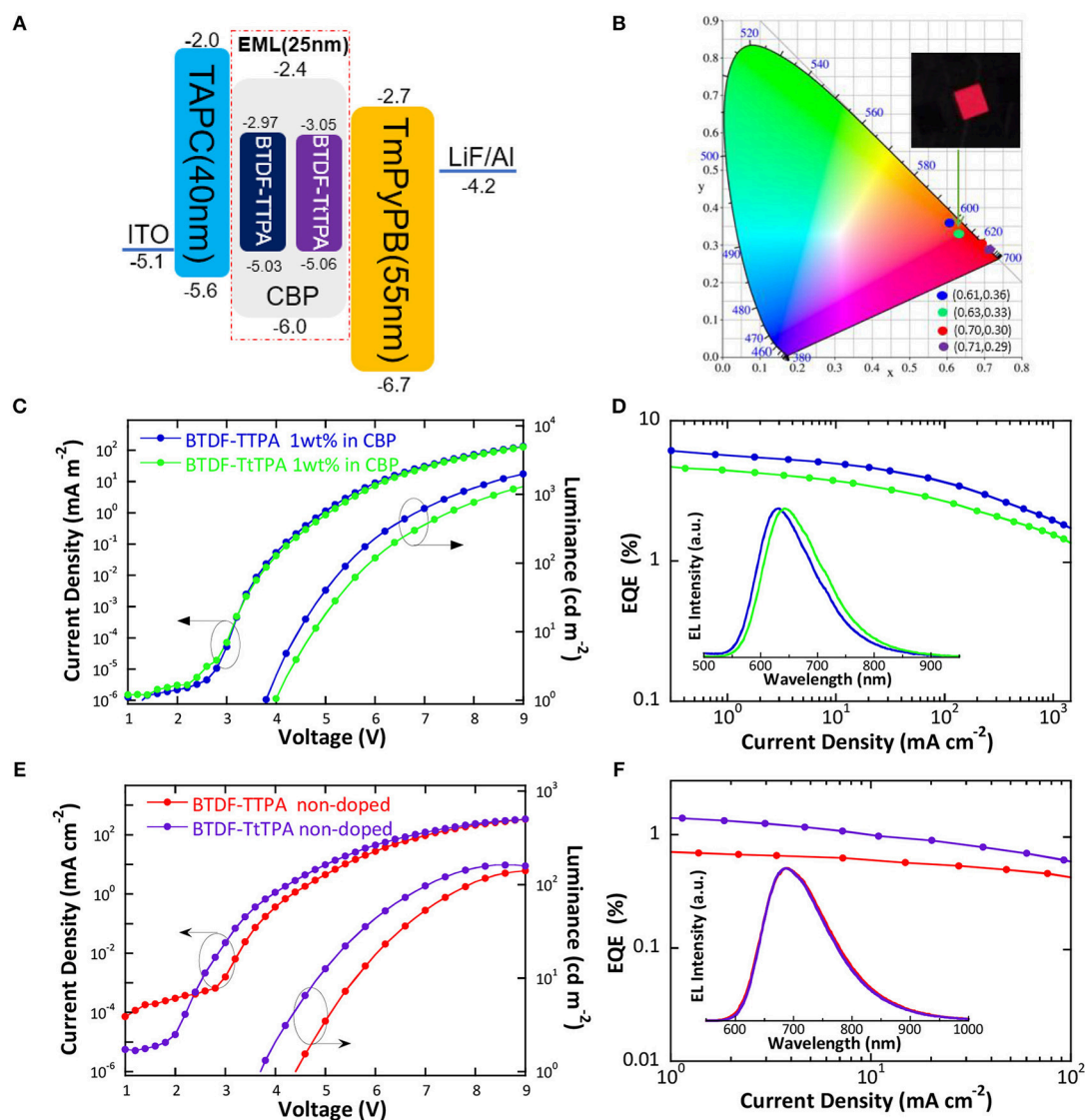


FIGURE 5 | (A) Schematic energy level diagram of the doped and non-doped devices based on BTDF-TTPA and BTDF-TtTPA; **(B)** CIE coordinates of the doped and non-doped devices using BTDF-TTPA and BTDF-TtTPA as the emitter at the current density of 1 mA cm^{-2} (the inset photograph is the device of BTDF-TtTPA 1 wt.% in CBP); **(C)** Current density-voltage-luminance and **(D)** external quantum efficiency-current density characteristics of the doped devices (Inset: EL spectra of the doped devices at the current density of 1 mA cm^{-2}); **(E)** Current density-voltage-luminance and **(F)** external quantum efficiency-current density characteristics of the non-doped devices (Inset: EL spectra of the non-doped devices at the current density of 1 mA cm^{-2}).

TABLE 2 | EL performance of the doped and non-doped devices using BTDF-TTPA and BTDF-TtTPA as emitters.

EMLs	V_{on}^a	EQE (%) / CE (cd A^{-1})/PE (lm W^{-1})			Luminance (cd m^{-2})	CIE ^b
		Max	@100 mA cm^{-2}	@200 mA cm^{-2}		
BTDF-TTPA 1 wt.% in CBP	3.8	5.75/5.15/4.27	1.54/1.67/0.58	1.00/1.10/0.33	2,644	(0.61, 0.36)
BTDF-TtTPA 1 wt.% in CBP	4.0	4.94/2.98/2.60	1.43/1.17/0.41	0.99/0.84/0.25	2,004	(0.63, 0.33)
BTDF-TTPA	4.6	0.83/0.11/0.09	0.40/0.06/0.03	0.32/0.06/0.02	147	(0.70, 0.30)
BTDF-TtTPA	3.8	1.44/0.19/0.16	0.60/0.09/0.04	0.35/0.06/0.02	163	(0.71, 0.29)

^aAt the luminance of 1 cd m^{-2} .

^bAt the current density of 1 mA cm^{-2} .

shallower and deeper than that of the host (CBP), relatively equilibrium hole and electron capture abilities can be anticipated.

The results of the EL performance are recorded in **Figures 5C–F**, including current density-voltage-luminance (J-V-L), external quantum efficiency (EQE) vs. current density curves for the devices, and the key device parameters are summarized in **Table 2**. All the devices displayed EL spectra similar to the corresponding PL spectra in doped or neat films, confirming the EL emission was generated solely from the developed emitters (**Figures S3, S4**). The doped devices exhibit excellent deep-red emission with the emission peaks of 630 and 642 nm, and the device based on 1 wt.% BTDF-TtTPA in CBP shows a Commission Internationale de l'Éclairage (CIE) coordinates of (0.63, 0.33) (**Figure 5B**), which is quite close to the standard red of (0.67, 0.33) defined by the National Television System Committee (NTSC). A maximum EQE of 5.75% was achieved with small efficiency roll-off, which is among the highest device performance in the reported red fluorescent OLEDs. Besides, the non-doped devices of these two materials appear the same NIR EL emission with a maximum wavelength (λ_{el}) of 690 nm and CIE coordinates of (0.70, 0.30) and (0.71, 0.29) (**Figure 5B**). Although the emission of the non-doped devices is in the NIR range, the highest EQE value of 1.44% obtained by BTDF-TtTPA is also one of the best device performances at the same emission wavelength.

Moreover, exciton utilization efficiency (η_s) of the devices can be calculated according to the following equation:

$$EQE = (\gamma \times \eta_s \times \phi_{PL}) \times \eta_{out} \quad (1)$$

where γ is the ideal recombination efficiency of the injected holes and electrons under electrical excitation ($\approx 100\%$); η_{out} is the light out-coupling efficiency (≈ 0.2); ϕ_{PL} is the intrinsic photoluminescence efficiency of the emitters. η_s s of 34.8% and 54.4% were estimated for the doped devices based on BTDF-TTPA and BTDF-TtTPA, respectively. For the non-doped devices, η_s s of 66.9 and 97.3% were achieved for BTDF-TTPA and BTDF-TtTPA, respectively. Both are exceeding the limit of the radiative exciton ratio of 25% for traditional fluorescence OLEDs, strongly proving the contribution of triplet excitons to the electroluminescence thanks to the ultrafast high-lying RISC process, namely, the “hot exciton” channels.

CONCLUSION

In summary, aiming to exploit highly efficient organic deep-red to NIR OLEDs, we have designed and synthesized three novel BTDF-based emitters, and their photophysical, thermal

and electrochemical properties were thoroughly investigated. By incorporating thiophene as π -bridge into the D-A-D skeleton, the emission peak was successfully red-shifted 67 nm without sacrifice in efficiency. Among the three emitters, BTDF-TTPA and BTDF-TtTPA exhibit deep-red emission that possesses the potential to fabricate deep-red to NIR fluorescence OLEDs. In the EL performance, a maximum EQE of 5.75% was achieved with a very low efficiency roll-off for the doped devices thanks to the large overlap of frontier molecular orbitals that induced high PLQY. Besides, non-doped devices have also been fabricated and a maximum EQE of 1.44% was obtained for the NIR emission with a peak of 690 nm. In short, the new thiophene-bridge planarization strategy provides us a successful avenue for designing high efficiency D- π -A and D- π -A- π -D organic deep-red to NIR emitters.

DATA AVAILABILITY

All datasets generated for this study are included in the manuscript and/or the **Supplementary Files**.

AUTHOR CONTRIBUTIONS

WX, XC, and KL designed the whole work. WX and XC synthesized the investigated compounds. BL fabricated and characterized the electroluminescent devices. WX and ML carried out the theoretical calculation. WX, XT, and ZQ measured the photophysical, thermal, and electrochemical properties of the investigated compounds. WX wrote the paper with the support from XC and S-JS. All authors contributed to the general discussion.

FUNDING

The authors greatly appreciate the financial support from the National Natural Science Foundation of China (91833304, 51625301, U1601651, and 51573059), the National Key R&D Program of China (2016YFB0401004), 973 Project (2015CB655003), and Guangdong Provincial Department of Science and Technology (2016B090906003 and 2016TX03C175).

SUPPLEMENTARY MATERIAL

The Supplementary Material for this article can be found online at: <https://www.frontiersin.org/articles/10.3389/fchem.2019.00276/full#supplementary-material>

REFERENCES

- Baldo, M. A., O'Brien, D. F., You, Y., Shoustikov, A., Sibley, S., Thompson, M. E., et al. (1998). Highly efficient phosphorescent emission from organic electroluminescent devices. *Nature* 395:151. doi: 10.1038/25954
- Baldo, M. A., O'Brien, D. F., Thompson, M. E., and Forrest, S. R. (1999). Excitonic singlet-triplet ratio in a semiconducting organic thin film. *Phys. Rev. B* 60, 14422–14428. doi: 10.1103/PhysRevB.60.14422

- Cai, X., Gao, B., Li, X., Cao, Y., and Su, S. J. (2016a). Singlet-triplet splitting energy management via acceptor substitution: comprehension molecular design for deep-blue thermally activated delayed fluorescence emitters and organic light-emitting diodes application. *Adv. Funct. Mater.* 26, 8042–8052. doi: 10.1002/adfm.201603520
- Cai, X., Li, X., Xie, G., He, Z., Gao, K., Liu, K., et al. (2016b). “Rate-limited effect” of reverse intersystem crossing process: the key for tuning thermally activated delayed fluorescence lifetime and efficiency roll-off of

- organic light emitting diodes. *Chem. Sci.* 7, 4264–4275. doi: 10.1039/c6sc00542j
- Chen, D., Xie, G., Cai, X., Liu, M., Cao, Y., and Su, S. J. (2016). Fluorescent organic planar pn heterojunction light-emitting diodes with simplified structure, extremely low driving voltage, and high efficiency. *Adv. Mater.* 28, 239–244. doi: 10.1002/adma.201504290
- Chen, J., Tao, W., Xiao, Y., Tian, S., Chen, W., Wang, K., et al. (2019). Isomeric thermally activated delayed fluorescence emitters based on indolo[2,3-b]acridine electron-donor: a compromising optimization for efficient orange-red organic light-emitting diodes. *J. Mater. Chem. C* 7, 2898–2904. doi: 10.1039/c8tc06081a
- Chen, J., Wang, K., Zheng, C., Zhang, M., Shi, Y., Tao, S., et al. (2018). Red organic light-emitting diode with external quantum efficiency beyond 20% based on a novel thermally activated delayed fluorescence emitter. *Adv. Sci.* 5:1800436. doi: 10.1002/advs.201800436
- Furue, R., Matsuo, K., Ashikari, Y., Ooka, H., Amanokura, N., and Yasuda, T. (2018). Highly efficient red-orange delayed fluorescence emitters based on strong π -accepting dibenzophenazine and dibenzoquinoxaline cores: toward a rational pure-red OLED design. *Adv. Opt. Mater.* 6:1701147. doi: 10.1002/adom.201701147
- Gan, L., Gao, K., Cai, X., Chen, D., and Su, S. J. (2018). Achieving efficient triplet exciton utilization with large ΔE_{ST} and nonobvious delayed fluorescence by adjusting excited state energy levels. *J. Phys. Chem. Lett.* 9, 4725–4731. doi: 10.1021/acs.jpclett.8b01961
- Han, X., Bai, Q., Yao, L., Liu, H., Gao, Y., Li, J., et al. (2015). Highly efficient solid-state near-infrared emitting material based on triphenylamine and diphenylfumarone with an EQE of 2.58% in nondoped organic light-emitting diode. *Adv. Funct. Mater.* 25, 7521–7529. doi: 10.1002/adfm.201503344
- Jiang, J., Li, X., Hanif, M., Zhou, J., Hu, D., Su, S., et al. (2017). Pyridal[2,1,3]thiadiazole as strong electron-withdrawing and less sterically-hindered acceptor for highly efficient donor-acceptor type NIR materials. *J. Mater. Chem. C* 5, 11053–11058. doi: 10.1039/c7tc03978f
- Kido, J., Kimura, M., and Nagai, K. (1995). Multilayer white light-emitting organic electroluminescent device. *Science* 267, 1332–1334. doi: 10.1126/science.267.5202.1332
- Kondakov, D. Y., Pawlik, T. D., Hatwar, T. K., and Spindler, J. P. (2009). Triplet annihilation exceeding spin statistical limit in highly efficient fluorescent organic light-emitting diodes. *J. Appl. Phys.* 106:124510. doi: 10.1063/1.3273407
- Li, W., Liu, D., Shen, F., Ma, D., Wang, Z., Feng, T., et al. (2012). A twisting donor-acceptor molecule with an intercrossed excited state for highly efficient, deep-blue electroluminescence. *Adv. Funct. Mater.* 22, 2797–2803. doi: 10.1002/adfm.201200116
- Li, W., Pan, Y., Xiao, R., Peng, Q., Zhang, S., Ma, D., et al. (2014a). Employing $\sim 100\%$ excitons in OLEDs by utilizing a fluorescent molecule with hybridized local and charge-transfer excited state. *Adv. Funct. Mater.* 24, 1609–1614. doi: 10.1002/adfm.201301750
- Li, W., Pan, Y., Yao, L., Liu, H., Zhang, S., Wang, C., et al. (2014b). A hybridized local and charge-transfer excited state for highly efficient fluorescent OLEDs: molecular design, spectral character, and full exciton utilization. *Adv. Opt. Mater.* 2, 892–901. doi: 10.1002/adom.201400154
- Lin, T. A., Chatterjee, T., Tsai, W. L., Lee, W. K., Wu, M. J., Jiao, M., et al. (2016). Sky-blue organic light emitting diode with 37% external quantum efficiency using thermally activated delayed fluorescence from spiroacridine-triazine hybrid. *Adv. Mater.* 28, 6976–6983. doi: 10.1002/adma.201601675
- Liu, M., Komatsu, R., Cai, X., Hotta, K., Sato, S., Liu, K., et al. (2017). Horizontally orientated sticklike emitters: enhancement of intrinsic out-coupling factor and electroluminescence performance. *Chem. Mater.* 29, 8630–8636. doi: 10.1021/acs.chemmater.7b02403
- Liu, T., Zhu, L., Zhong, C., Xie, G., Gong, S., Fang, J., et al. (2017). Naphthothiadiazole-based near-infrared emitter with a photoluminescence quantum yield of 60% in neat film and external quantum efficiencies of up to 3.9% in nondoped OLEDs. *Adv. Funct. Mater.* 27:1606384. doi: 10.1002/adfm.201606384
- Park, I. S., Lee, S. Y., Adachi, C., and Yasuda, T. (2016). Full-color delayed fluorescence materials based on wedge-shaped phthalonitriles and dicyanopyrazines: systematic design, tunable photophysical properties, and OLED performance. *Adv. Funct. Mater.* 26, 1813–1821. doi: 10.1002/adfm.201505106
- Peng, Q., Obolda, A., Zhang, M., and Li, F. (2015). Organic light-emitting diodes using a neutral pi Radical as emitter: the emission from a doublet. *Angew. Chem. Int. Ed.* 54, 7091–7095. doi: 10.1002/anie.201500242
- Pfeiffer, M., Forrest, S. R., Leo, K., and Thompson, M. E. (2002). Electrophosphorescent p-i-n organic light-emitting devices for very-high-efficiency flat-panel displays. *Adv. Mater.* 14, 1633–1636. doi: 10.1002/1521-4095(20021118)14:22<1633::Aid-adma1633>3.0.Co;2-#
- Qian, G., Zhong, Z., Luo, M., Yu, D., Zhang, Z., Wang, Z., et al. (2009). Simple and efficient near-infrared organic chromophores for light-emitting diodes with single electroluminescent emission above 1000 nm. *Adv. Mater.* 21, 111–116. doi: 10.1002/adma.200801918
- Tang, C. W., and VanSlyke, S. A. (1987). Organic electroluminescent diodes. *Appl. Phys. Lett.* 51, 913–915. doi: 10.1063/1.98799
- Tang, X., Li, X., Liu, H., Gao, Y., Shen, Y., Zhang, S., et al. (2018). Efficient near-infrared emission based on donor-acceptor molecular architecture: the role of ancillary acceptor of cyanophenyl. *Dyes Pigments* 149, 430–436. doi: 10.1016/j.dyepig.2017.10.033
- Tessler, N., Medvedev, V., Kazes, M., Kan, S., and Banin, U. (2002). Efficient near-infrared polymer nanocrystal light-emitting diodes. *Science* 295, 1506–1508. doi: 10.1126/science.1068153
- Tsai, W. L., Huang, M. H., Lee, W. K., Hsu, Y. J., Pan, K. C., Huang, Y. H., et al. (2015). A versatile thermally activated delayed fluorescence emitter for both highly efficient doped and non-doped organic light emitting devices. *Chem. Commun.* 51, 13662–13665. doi: 10.1039/c5cc05022g
- Uoyama, H., Goushi, K., Shizu, K., Nomura, H., and Adachi, C. (2012). Highly efficient organic light-emitting diodes from delayed fluorescence. *Nature* 492, 234–238. doi: 10.1038/nature11687
- Wu, T. L., Huang, M. J., Lin, C. C., Huang, P. Y., Chou, T. Y., Chen Cheng, R. W., et al. (2018). Diboron compound-based organic light-emitting diodes with high efficiency and reduced efficiency roll-off. *Nat. Photon.* 12, 235–240. doi: 10.1038/s41566-018-0112-9
- Xie, G., Li, X., Chen, D., Wang, Z., Cai, X., Chen, D., et al. (2016). Evaporation- and solution-process-feasible highly efficient thianthrene-9,9',10,10'-tetraoxide-based thermally activated delayed fluorescence emitters with reduced efficiency roll-off. *Adv. Mater.* 28, 181–187. doi: 10.1002/adma.201503225
- Yao, L., Zhang, S., Wang, R., Li, W., Shen, F., Yang, B., et al. (2014). Highly efficient near-infrared organic light-emitting diode based on a butterfly-shaped donor-acceptor chromophore with strong solid-state fluorescence and a large proportion of radiative excitons. *Angew. Chem. Int. Ed.* 53, 2119–2123. doi: 10.1002/anie.201308486
- Zhang, D., Qiao, J., Zhang, D., and Duan, L. (2017). Ultrahigh-efficiency green PHOLEDs with a voltage under 3 V and a power efficiency of nearly 110 lm W⁻¹ at luminance of 10 000 cd m⁻². *Adv. Mater.* 29:1702847. doi: 10.1002/adma.201702847
- Zhang, Q., Kuwabara, H., Potschavage, W. J. Jr., Huang, S., Hatae, Y., Shibata, T., et al. (2014). Anthraquinone-based intramolecular charge-transfer compounds: computational molecular design, thermally activated delayed fluorescence, and highly efficient red electroluminescence. *J. Am. Chem. Soc.* 136, 18070–18081. doi: 10.1021/ja510144h
- Zhang, Q., Li, J., Shizu, K., Huang, S., Hirata, S., Miyazaki, H., et al. (2012). Design of efficient thermally activated delayed fluorescence materials for pure blue organic light emitting diodes. *J. Am. Chem. Soc.* 134, 14706–14709. doi: 10.1021/ja306538w
- Zhao, J., Liu, B., Wang, Z., Tong, Q., Du, X., Zheng, C., et al. (2018). EQE climbing over 6% at high brightness of 14350 cd/m² in deep-blue OLEDs based on hybridized local and charge-transfer fluorescence. *ACS Appl. Mater. Interfaces* 10, 9629–9637. doi: 10.1021/acsami.7b19646

Conflict of Interest Statement: The authors declare that the research was conducted in the absence of any commercial or financial relationships that could be construed as a potential conflict of interest.

Copyright © 2019 Xie, Li, Cai, Li, Qiao, Tang, Liu, Gu, Ma and Su. This is an open-access article distributed under the terms of the Creative Commons Attribution License (CC BY). The use, distribution or reproduction in other forums is permitted, provided the original author(s) and the copyright owner(s) are credited and that the original publication in this journal is cited, in accordance with accepted academic practice. No use, distribution or reproduction is permitted which does not comply with these terms.



Highly Efficient Thermally Activated Delayed Fluorescence Emitter Developed by Replacing Carbazole With 1,3,6,8-Tetramethyl-Carbazole

Jia-Lin Cai¹, Wei Liu², Kai Wang², Jia-Xiong Chen², Yi-Zhong Shi², Ming Zhang¹, Cai-Jun Zheng^{1*}, Si-Lu Tao^{1*} and Xiao-Hong Zhang^{2*}

¹ School of Optoelectronic Science and Engineering, University of Electronic Science and Technology of China, Chengdu, China, ² Institute of Functional Nano and Soft Materials, Jiangsu Key Laboratory for Carbon-Based Functional Materials and Devices, Soochow University, Suzhou, China

OPEN ACCESS

Edited by:

Shi-Jian Su,
South China University of Technology,
China

Reviewed by:

Qisheng Zhang,
Zhejiang University, China
Chuluo Yang,
Wuhan University, China

*Correspondence:

Cai-Jun Zheng
zhengcaijun@uestc.edu.cn
Si-Lu Tao
silutao@uestc.edu.cn
Xiao-Hong Zhang
xiaohong_zhang@suda.edu.cn

Specialty section:

This article was submitted to
Organic Chemistry,
a section of the journal
Frontiers in Chemistry

Received: 16 November 2018

Accepted: 08 January 2019

Published: 28 January 2019

Citation:

Cai J-L, Liu W, Wang K, Chen J-X,
Shi Y-Z, Zhang M, Zheng C-J, Tao S-L
and Zhang X-H (2019) Highly Efficient
Thermally Activated Delayed
Fluorescence Emitter Developed by
Replacing Carbazole With
1,3,6,8-Tetramethyl-Carbazole.
Front. Chem. 7:17.
doi: 10.3389/fchem.2019.00017

Carbazole (Cz) is the one of the most popular electron donors to develop thermally activated delayed fluorescence (TADF) emitters, but additional groups are generally required in the molecules to enhance the steric hindrance between Cz and electron acceptor segments. To address this issue, we replaced Cz with its derivative 1,3,6,8-tetramethyl-carbazole (tMCz) to develop TADF emitters. Two novel compounds, 6-(4-(carbazol-9-yl)phenyl)-2,4-diphenylnicotinonitrile (CzPN) and 2,4-diphenyl-6-(4-(1,3,6,8-tetramethyl-carbazol-9-yl)phenyl) nicotinonitrile (tMCzPN) were designed and synthesized accordingly. With the same and simple molecular framework, tMCzPN successfully exhibits TADF behavior, while CzPN is a non-TADF fluorophor, as the additional steric hindrance of methyl groups leads to a more twisted structure of tMCzPN. In the organic light-emitting diodes (OLEDs), tMCzPN exhibits extremely high forward-viewing maximum external quantum efficiency of 26.0%, without any light out-coupling enhancement, which is significantly higher than that of 5.3% for CzPN. These results indicate that tMCzPN is an excellent TADF emitter and proves that tMCz is a more appropriate candidate than Cz to develop TADF emitters.

Keywords: thermally activated delayed fluorescence, steric hindrance, OLED, 1, 3, 6, 8-tetramethyl-carbazole, dihedral angle

INTRODUCTION

Organic light-emitting diodes (OLEDs) have attracted great attention and are considered as next-generation solid-state lighting and displays because of their flexibility, light weight, and low-cost fabrication (Pope et al., 1963; Tang and VanSlyke, 1987; Baldo et al., 1998; Goushi et al., 2012; Uoyama et al., 2012; Zheng et al., 2013; Liu et al., 2015b,c; Li et al., 2018; Shi et al., 2018). Based on spin quantum statistics, electrical excitation generates 25% singlet excitons and 75% triplet excitons in the devices (Segal et al., 2003). OLEDs based on traditional fluorescent emitters can only utilize singlet excitons with a maximum internal quantum efficiency (IQE) of 25% (Baldo et al., 1999; Segal et al., 2003). To harvest triplet excitons, phosphorescent OLEDs, using heavy metal complexes as emitters, were developed, and successfully realized with 100% IQE, due to the strong spin-orbit coupling effect of heavy metal irons (Baldo et al., 1998; Adachi et al., 2001; Sajoto et al., 2009; Yersin et al., 2011). However, noble metal complexes also lead to expensive costs and environmental hazards, which further constrains the development of phosphorescent OLEDs (Méhes et al., 2012; Zhang et al., 2014c, 2015).

To address this issue, Adachi and co-workers firstly introduced pure organic molecules with thermally activated delayed fluorescence (TADF) characteristic as emitters for OLEDs (Uoyama et al., 2012). TADF emitters can convert non-radiative triplet excitons to radiative singlet excitons through an efficient reverse intersystem crossing (RISC) process, thus TADF-based OLEDs can also theoretically achieve 100% IQE (Endo et al., 2009). As a TADF emitter, it is key to realize an extremely small singlet and triplet energy splitting (ΔE_{ST}) for an efficient RISC process (Peng et al., 2013). Therefore, nearly all reported TADF emitters were developed by connecting electron-donor (D) and electron-acceptor (A) segments with a highly twisted structure (Zhang et al., 2014a, 2017; Liu et al., 2016; Chen et al., 2017; Wang et al., 2017), as such a highly twisted D-A molecular framework can naturally separate the highest occupied molecular orbital (HOMO) and lowest unoccupied molecular orbital (LUMO) on the D and A segments respectively, which is the general requirement for extremely small ΔE_{ST} s (Endo et al., 2011; Zhang et al., 2012, 2014a,b). Among the reported TADF emitters, carbazole (Cz) is one of the most popular D candidates due to its planar aromaticity, appropriate energy levels, feasible modification and good chemical stability (Uoyama et al., 2012; Liu et al., 2015a; Mounnggon et al., 2015; Chan et al., 2018; Pashazadeh et al., 2018). However, with the relatively small steric hindrance of the Cz segment, Cz-A structure TADF emitters usually possess moderate dihedral angles between the Cz and A segments around 45° (Hirata et al., 2014; Zhang et al., 2018), which induces higher ΔE_{ST} s and hinders the RISC process. Thus, to develop Cz-A structure TADF emitters, additional groups are generally required to enhance the steric hindrance between the Cz and A segments, which lead to complicated synthetic procedures and high costs.

To address this issue, Cz's derivative group 1,3,6,8-tetramethyl-carbazole (tMCz) has been proposed to replace the Cz group in the development of TADF emitters. Compared with Cz, the methyl groups at 1, 8 positions on tMCz can enhance the steric hindrance between tMCz and A segments, thus leading to more twisted structures of the compounds without other additional groups. In 2017, Adachi and co-workers developed a TADF emitter Cz-TRZ2 with tMCz group and realized a maximum EQE of 22.0% in the OLED (Cui et al., 2017). In this work, we designed and synthesized two novel compounds 6-(4-(carbazol-9-yl)phenyl)-2,4-diphenylnicotinonitrile (CzPN) and 2,4-diphenyl-6-(4-(1,3,6,8-tetramethyl-carbazol-9-yl)phenyl)nicotinonitrile (tMCzPN) by combining Cz or tMCz with electron-acceptor diphenylnicotinonitrile (Liu et al., 2015a), in a simple molecular framework. With the same molecular framework, the dihedral angles between the Cz (or tMCz) and phenylnicotinonitrile segments are 52° for CzPN and 84.9° for tMCzPN, respectively, proving that tMCz can better separate the HOMO and LUMO than Cz can. Moreover, tMCzPN successfully exhibits TADF characteristic with a small ΔE_{ST} of 0.10 eV, while CzPN is a non-TADF fluorophor with a large ΔE_{ST} of 0.32 eV. In these devices, CzPN exhibits low forward-viewing maximum current efficiency (CE), power efficiency (PE), and external quantum efficiency (EQE) of 4.7 cd A⁻¹ (Pope et al., 1963), 4.7 lm W⁻¹, and 5.3%, respectively, consistent with

common traditional fluorescent emitters. Additionally, the tMCzPN-based OLED shows high forward-viewing maximum efficiencies of 26.0% for EQE, 65.9 cd A⁻¹ for CE, and 62.7 lm W⁻¹ for PE, without any light out-coupling enhancement. To the best of our knowledge, these high efficiencies are among the best reported TADF-based OLEDs, proving that tMCz is a more appropriate candidate than Cz to develop TADF emitters.

EXPERIMENTAL

General Methods

¹H nuclear magnetic resonance (NMR) and ¹³C NMR spectral data were obtained by using an AVANCZ spectrometer. Mass spectral (MS) data were measured using a Finnigan 4021C gas chromatography mass spectrometry instrument. Absorption and Photoluminescence (PL) spectra were obtained using a Hitachi UV-vis spectrophotometer U-3010 and a Hitachi fluorescence spectrometer F-4600, respectively. Cyclic voltammetry (CV) measurements were performed using a CHI660E electrochemical analyzer, while the oxidation potential of saturated calomel electrode (SCE) relative to the vacuum level is calibrated to be 4.56 eV in dimethylformamide (DMF). Transient PL spectra were obtained using Edinburgh Instruments FLS980 spectrometer. The photoluminescence quantum yields (PLQYs) of mixed DPEPO (bis[2-(di-(phenyl)phosphino)-phenyl]ether oxide) solid films were investigated using a QY-2000 fluorescence spectrometer and estimated via a F-3018 Integrating Sphere. Thermogravimetric analysis (TGA) and differential scanning calorimetry (DSC) measurements were performed using a TAQ 500 thermogravimeter and a NETZSCH DSC204 instrument in N₂, respectively.

Synthesis

The commercially available reagents and materials were used directly without purification.

(E)-1-(4-bromophenyl)-3-phenylprop-2-en-1-one

A mixture of 1-(4-bromophenyl)ethan-1-one (2.0 g, 10 mmol) and benzaldehyde (2.12 g, 20 mmol) was stirred in 20 ml of ethanol and a 10% NaOH solution for 30 min at room temperature. The reaction mixture was allowed to stand for 1 h and then filtered and recrystallized from ethanol to obtain a light yellow powder (E)-1-(4-bromophenyl)-3-phenylprop-2-en-1-one (2.5 g, 87% yield). The crude product was dried in a vacuum oven directly for the next step.

6-(4-bromophenyl)-2,4-diphenylnicotinonitrile

3-oxo-3-phenylpropanenitrile (1.45 g, 10 mmol), (E)-1-(4-bromophenyl)-3-phenylprop-2-en-1-one (2.87 g, 10 mmol) and anhydrous ammonium acetate (4.01 g, 52 mmol) was dissolved in glacial acid (8 mL). The mixture was refluxed under stirring for 2 h at 110°C. After cooling to room temperature, the reaction was neutralized using a 10% NaOH solution and extracted with dichloromethane. The dichloromethane phase was then dried with anhydrous sodium sulfate. After evaporation of

the solvent, the crude product was purified through silica gel column chromatography, using 1:3 dichloromethane/petroleum as eluent to obtain a white solid powder 6-(4-bromophenyl)-2,4-diphenylnicotinonitrile (1.0 g, 24.3% yield). ^1H NMR (600 MHz, Chloroform-*d*) δ 8.09–8.00 (m, 4H), 7.79 (s, 1H), 7.73–7.61 (m, 4H), 7.56 (dt, J = 7.7, 5.8 Hz, 6H). ^{13}C NMR (151 MHz, Chloroform-*d*) δ 162.62, 158.05, 155.80, 137.95, 136.74, 136.51, 132.32, 130.32, 130.16, 129.48, 129.18, 128.79, 128.69, 125.43, 118.50, 117.70, 104.81. MS (EI) m/z : [M]⁺ calcd for $\text{C}_{24}\text{H}_{15}\text{BrN}_2$, 411.30; found, 411.05.

6-(4-(Carbazol-9-yl)phenyl)-2,4-diphenylnicotinonitrile (CzPN)

A mixture of 6-(4-bromophenyl)-2,4-diphenylnicotinonitrile (0.411 g, 1 mmol), Cz (0.200 g, 1.2 mmol), sodium tert-butoxide (0.192 g, 2 mmol), tris(dibenzylideneacetone)dipalladium (0.018 g, 0.02 mmol) and tri-tert-butylphosphine tetrafluoroborate (0.023 g, 0.008 mmol) was added into toluene (10 mL) under N_2 and then refluxed at 110°C for 12 h. After cooling to room temperature, the mixture was filtered with diatomite. The solvent of the filtrate was removed under reduced pressure. The crude product was purified through silica gel column chromatography, using 1:3 dichloromethane/petroleum as eluent to obtain a green solid powder (0.425 g, 86% yield). ^1H NMR (600 MHz, Chloroform-*d*) δ 8.45–8.42 (m, 2H), 8.16 (d, J = 7.7 Hz, 2H), 8.11–8.07 (m, 2H), 7.92 (d, J = 1.6 Hz, 1H), 7.75 (ddd, J = 11.0, 7.5, 1.7 Hz, 4H), 7.63–7.54 (m, 6H), 7.51 (d, J = 8.2 Hz, 2H), 7.46–7.42 (m, 2H), 7.32 (t, J = 7.4 Hz, 2H). ^{13}C NMR (151 MHz, Chloroform-*d*) δ 162.56, 158.15, 155.66,

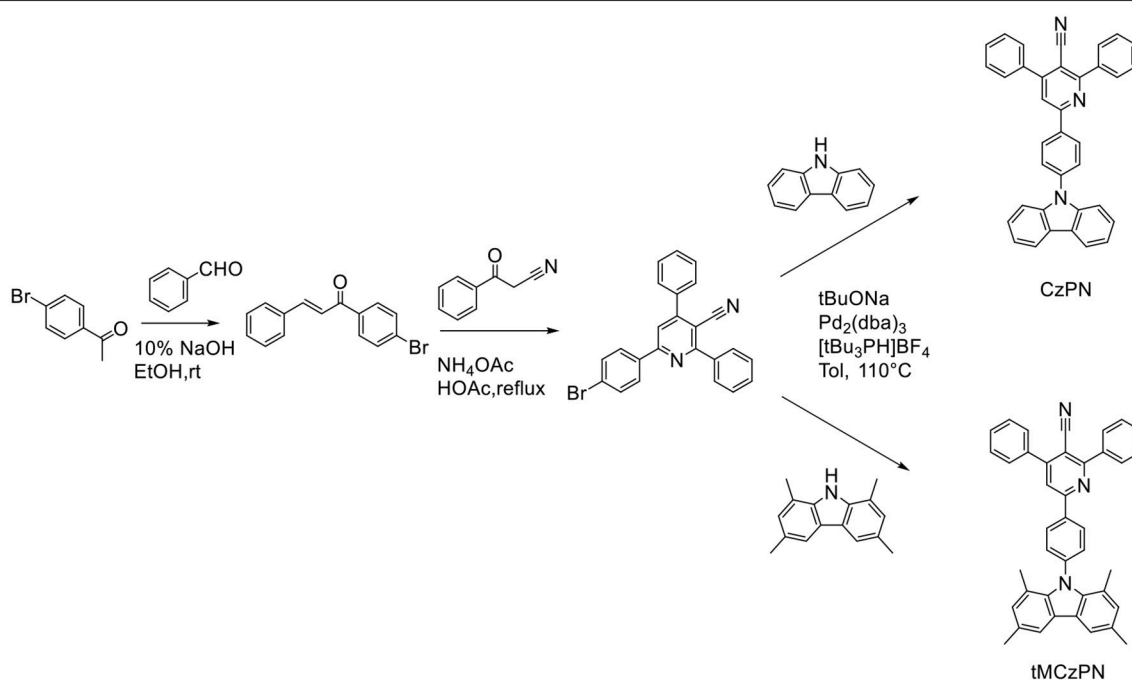
140.44, 139.83, 137.88, 136.66, 136.27, 130.17, 130.02, 129.36, 129.11, 129.04, 128.67, 128.56, 127.17, 126.09, 123.64, 120.41, 120.32, 118.61, 117.62, 109.76, 104.55. MS (EI) m/z : [M]⁺ calcd for $\text{C}_{36}\text{H}_{23}\text{N}_3$, 497.60; found, 497.19.

2,4-diphenyl-6-(4-(1,3,6,8-tetramethylcarbazol-9-yl)phenyl)nicotinonitrile (tMCzPN)

tMCzPN was synthesized according to the same procedure as CzPN, by using tMCz instead of Cz. After cooling to room temperature, the mixture was filtered with diatomite. The solvent of filtrate was removed under reduced pressure; the crude product was purified through silica gel column chromatography using 1:3 dichloromethane/petroleum as eluent to obtain a yellow solid powder (0.25 g, 45% yield). ^1H NMR (600 MHz, Chloroform-*d*) δ 8.32 (d, J = 8.4 Hz, 2H), 8.08 (dd, J = 8.0, 1.6 Hz, 2H), 7.95 (s, 1H), 7.80–7.69 (m, 4H), 7.66–7.53 (m, 8H), 6.92 (s, 2H), 2.48 (s, 6H), 1.93 (s, 6H). ^{13}C NMR (151 MHz, Chloroform-*d*) δ 162.75, 158.04, 155.92, 144.86, 139.51, 138.07, 137.75, 136.85, 132.03, 130.46, 130.44, 130.25, 129.58, 129.36, 129.26, 128.87, 128.82, 127.52, 124.45, 121.36, 118.98, 118.05, 117.78, 104.95, 21.32, 19.82. MS (EI) m/z : [M]⁺ calcd for $\text{C}_{40}\text{H}_{31}\text{N}_3$, 553.71; found, 553.25.

Device Fabrication and Measurements

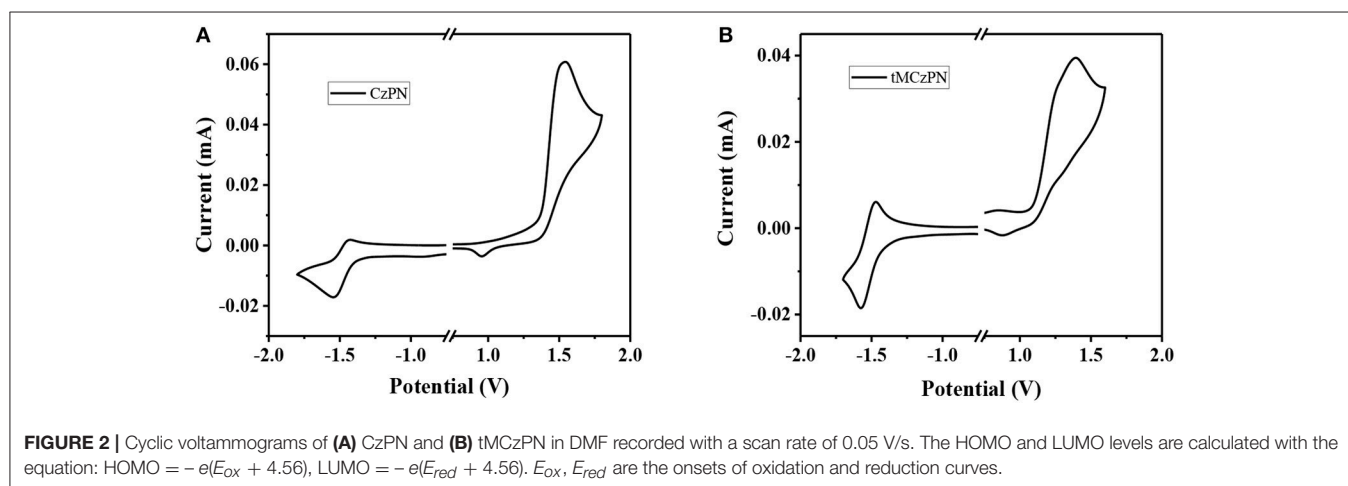
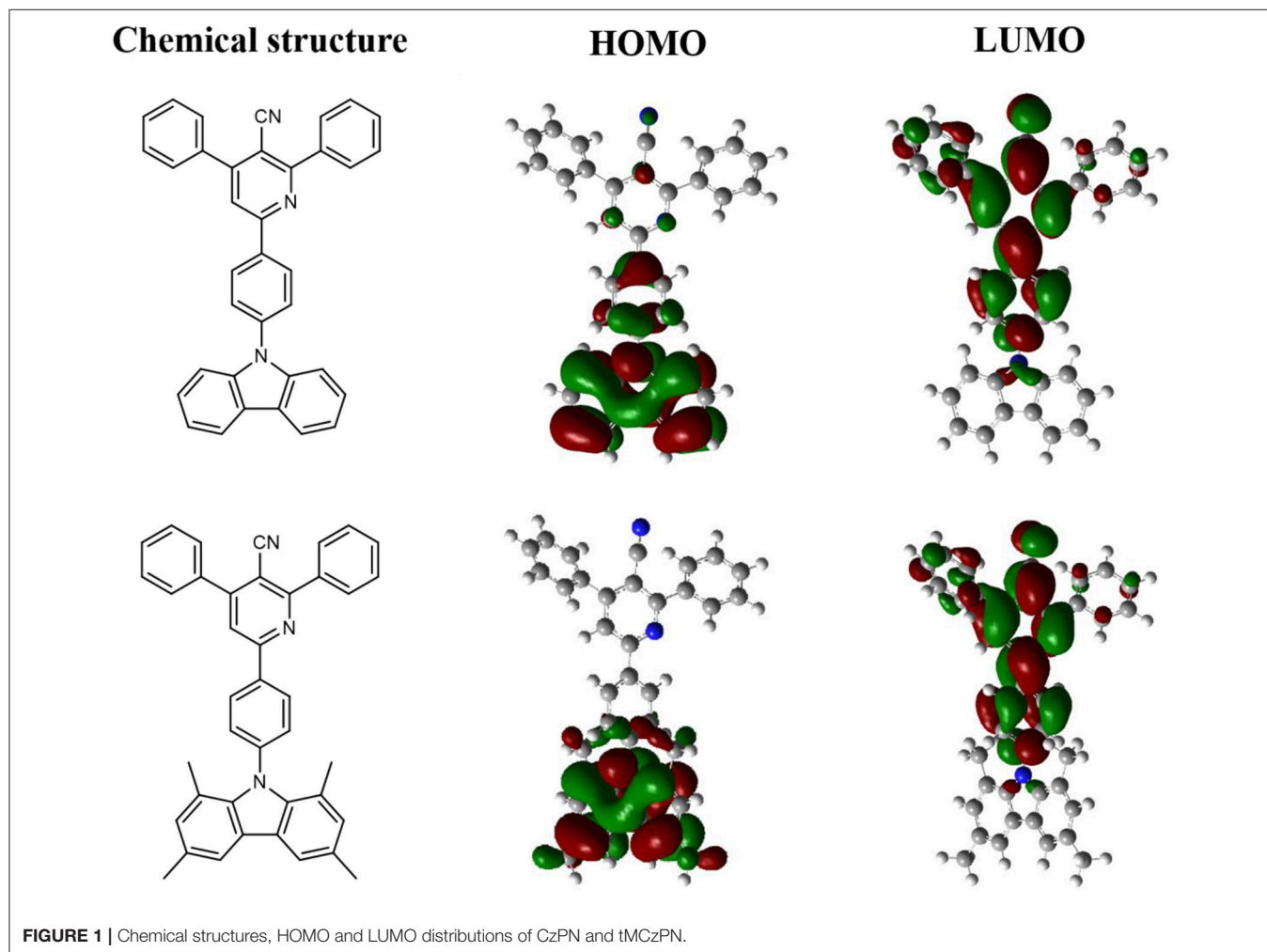
ITO-coated glass substrates with a sheet resistance of 30 Ω per square, were cleaned with acetone and ethanol, then washed with deionized water for 5 min, and then oven-dried at 120°C and treated with UV-ozone for 5 min. The cleaned substrates were then moved into the vacuum evaporation chamber. The



SCHEME 1 | Synthetic routes and molecular structures of CzPN and tMCzPN.

organic layers were deposited onto the substrates through thermal evaporation under 1×10^{-6} Torr with the rate of $1\text{--}2 \text{ \AA s}^{-1}$. The rate was 0.1 \AA s^{-1} for LiF, and 10 \AA s^{-1} for Al. The electroluminescence (EL) spectra and CIE color coordinates

were measured using a Spectrascan PR650 instrument. The current density-voltage characteristics were obtained using a Keithley 2400 Source Meter controlled by a computer. The EQE was calculated from the current density, luminance, and EL



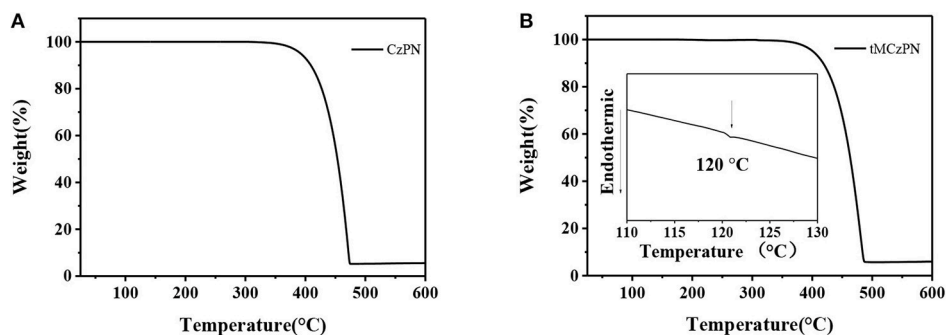


FIGURE 3 | TGA and DSC measurements of (A) CzPN and (B) tMCzPN recorded with a heating rate of 10°C/min.

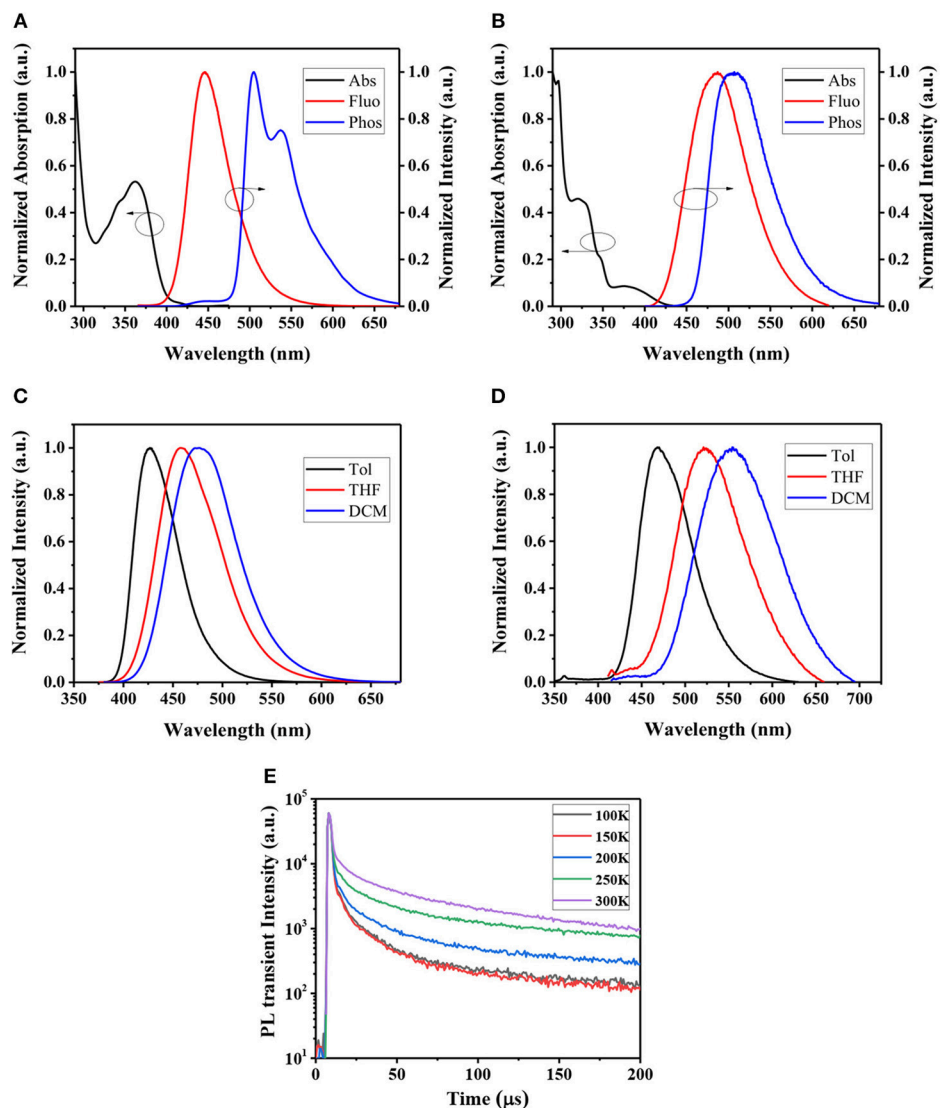


FIGURE 4 | UV-Vis absorption spectra in toluene, fluorescence spectrum in DPEPO film at room temperature, and phosphorescence spectra in DPEPO film at 77K of (A) CzPN and (B) tMCzPN. Fluorescence spectra of (C) CzPN and (D) tMCzPN in different solvent (Tol, toluene; DCM, dichloromethane; and THF, tetrahydrofuran). (E) Temperature-dependent transient PL decay spectra of tMCzPN doped in DPEPO film by exciting at 300 nm (20 wt.%).

spectrum, assuming a Lambertian distribution (Okamoto et al., 2001).

RESULTS AND DISCUSSION

Synthesis

As shown in **Scheme 1**, both two compounds were synthesized through three steps. The (E)-1-(4-bromophenyl)-3-phenylprop-2-en-1-one was synthesized by aldol reaction between benzaldehyde and 1-(4-bromophenyl)ethan-1-one. And the cyanopyridine derivative was synthesized by cyclizing a pyridine ring between 3-oxo-3-phenylpropanenitrile and (E)-1-(4-bromophenyl)-3-phenylprop-2-en-1-one with ammonium acetate as the source of nitrogen. Then, the final products were synthesized through the Buchwald-Hartwig coupling reaction between cyanopyridine derivative and the corresponding Cz derivatives. The chemical structure of CzPN and tMCzPN were characterized and confirmed by ^1H NMR and ^{13}C NMR spectroscopies and mass spectrometry. Moreover, CzPN and tMCzPN were purified by sublimation before further characterizations.

Theoretical Calculations and Electrochemical Properties

To analyze the relationships between the structures and properties of CzPN and tMCzPN at the molecular level, we performed the density function theory (DFT) calculation for both compounds at the B3LYP/6-31G(d) level. The optimized ground-state conformations and HOMO and LUMO distributions of the two compounds are shown in **Figure 1**. In the CzPN molecule, the dihedral angle between the Cz and phenylnicotinonitrile segments was optimized to 52° , which is close to other reported common Cz-A structure compounds, without steric hindrance between the D and A segments (Choi et al., 2017; Rajamalli et al., 2017; Liang et al., 2018). Caused by such insufficient twist, both the HOMO and LUMO of CzPN are extended to the central benzene bridge. The obvious overlap between HOMO and LUMO leads to an evident conjugation and a large ΔE_{ST} for CzPN, which suppresses the TADF behavior. Reversely, due to the large hindrance of the two methyl groups at 1, 8 positions on the Cz, tMCzPN possesses a nearly vertical dihedral angle between the Cz and phenylnicotinonitrile segments of 84.9° . The HOMO is mainly confined on the tMCz segment and the LUMO is located on the phenylnicotinonitrile unit, realizing a nearly full separation between HOMO and LUMO. Thus, by replacing Cz with tMCz, tMCzPN successfully possesses a more twisted

molecular structure and is predicted to have an extremely small ΔE_{ST} and the TADF characteristic theoretically.

We further investigated the electrochemical properties of both compounds by CV in DMF. As shown in **Figure 2**, from the onsets of oxidation curves, the HOMO energy levels of CzPN and tMCzPN are estimated to be -5.93 and -5.66 eV, respectively. As the electron-donating ability of the four methyl groups, tMCz has a much higher HOMO energy level than Cz. Whereas, from the onsets of reduction curves, the LUMO energy levels of CzPN and tMCzPN are calculated to be of similar values of -3.16 and -3.13 eV, respectively.

Thermal Properties

The thermal properties of CzPN and tMCzPN were characterized by TGA and DSC measurements under a nitrogen atmosphere. As shown in **Figure 3**, two compounds exhibit high decomposition temperatures ($T_{\text{d}5}$) (corresponding to 5.0 % weight loss) of 392°C for CzPN and 400°C for tMCzPN, respectively, suggesting that both are capable of vacuum purification and evaporation. The glass transition temperature (T_{g}) of tMCzPN is determined to be 120°C , and no glass transition was observed for CzPN from 25 to 250°C . The high T_{g} of tMCzPN would be beneficial to its morphological stability and reduce the phase separation rate of the guest-host system.

Photophysical Properties

Room temperature UV-Vis absorption spectra of CzPN and tMCzPN in toluene are shown in **Figure 4**. At the long-wavelength region, both compounds show broad absorption bands with peaks at 362 and 375 nm, respectively for CzPN, and tMCzPN which are assigned to the intramolecular charge transfer (ICT) transition from the electron donor Cz to the electron acceptor phenylnicotinonitrile. Additionally, the ICT absorption of tMCzPN was much weaker than that of CzPN, which is ascribed to its better separation between the HOMO and LUMO as shown in **Figure 2**. With the ICT transition characteristic, both compounds exhibit obvious solvatochromic effects in varied solvents as shown in **Figures 4C,D**. From low-polar toluene to high-polar dichloromethane, the emission peak of CzPN is red-shifted from 427 to 477 nm, while the emission peak of tMCzPN is red-shifted from 468 to 554 nm. As the solvatochromic effect is related to structure relaxation of the ICT molecule, CzPN, which has a higher molecular restriction due to stronger conjugation between the D and A segments, exhibits a much weaker red-shift compared to tMCzPN accordingly.

The PL spectra of the two compounds doped in DPEPO films were further studied. At room temperature, CzPN and

TABLE 1 | Key physical properties of two compounds.

Compounds	λ_{abs} (nm) ^a	λ_{fluor} (nm) ^b	λ_{phos} (nm) ^c	ΔE_{ST} (eV) ^d	HOMO (eV) ^e	LUMO (eV) ^f	$T_{\text{d}}/T_{\text{g}}$ ($^\circ\text{C}$)	PLQY (%)
CzPN	362	446	505	0.32	-5.93	-3.16	392/	93.3
tMCzPN	375	487	507	0.10	-5.66	-3.13	400/120	70.5

^aMeasured in toluene solution at room temperature. ^bMeasured in DPEPO film at room temperature. ^cMeasured in DPEPO film at 77 K . ^dEstimated from the peak of fluorescence and phosphorescence spectra. ^eCalculated from the onset of oxidation potential. ^fCalculated from the onset of reduction potential.

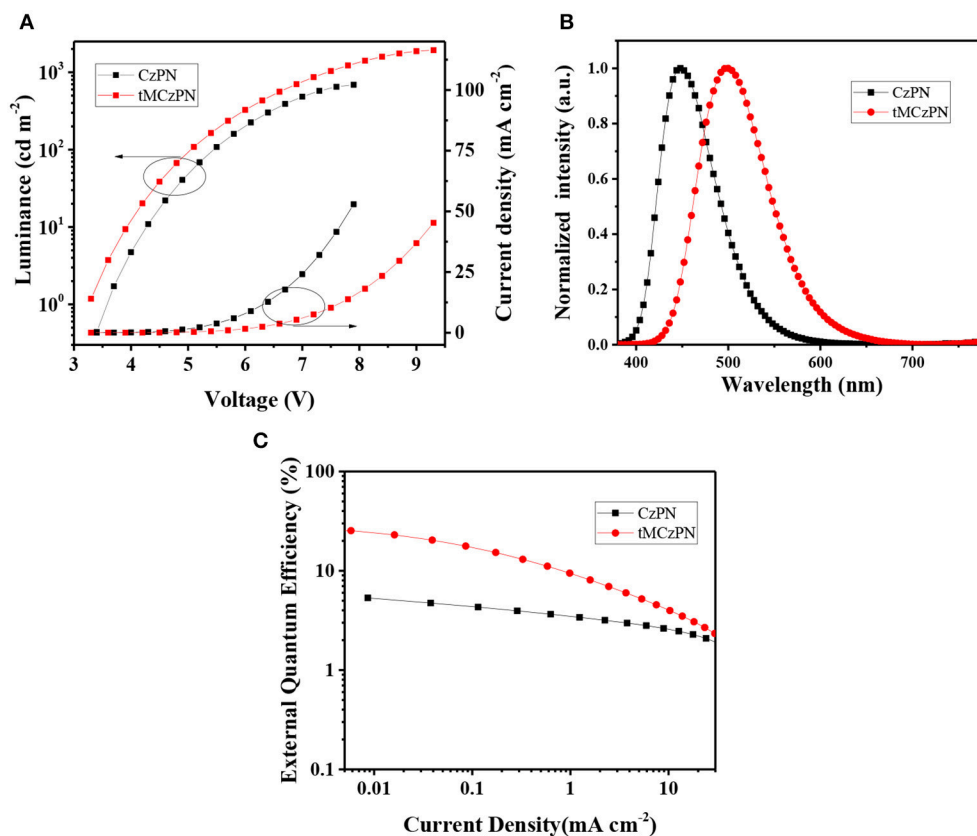


FIGURE 5 | (A) Current density-voltage-luminance characteristics, **(B)** EL spectra, and **(C)** Current density-EQE characteristics of the devices based on CzPN and tMCzPN.

TABLE 2 | Electroluminescence properties of the devices.

Emitters	V_{on} (V) ^a	CE_{max} (cd A ⁻¹) ^b	PE_{max} (lm W ⁻¹) ^c	EQE_{max} (%) ^d	Peak (nm)	FWHM (nm) ^e	CIE
CzPN	3.4	5.1	4.7	5.3	448	72	(0.15, 0.11)
tMCzPN	3.3	65.9	62.7	26.0	500	90	(0.20, 0.42)

^a Turn-on voltage, measured at the luminance of 1 cd m⁻². ^b Maximum current efficiency. ^c Maximum power efficiency. ^d Maximum external quantum efficiency. ^e Full-width at half-maximum.

tMCzPN both exhibit shapeless fluorescent spectra peaked at 446 and 487 nm, respectively. Due to the stronger electron-donating ability of tMCz, the fluorescence of tMCzPN is evidently red-shifted. At 77 K, we obtained the phosphorescent spectra of two compounds. CzPN showed a local-excited feature phosphorescence with two sharp peaks, because the extended conjugation lowers the triplet energy level of Cz. While tMCzPN exhibits a shapeless and broad phosphorescence, suggesting its T₁ state is still ICT characteristic. From the peaks of fluorescent and phosphorescent spectra, the S₁ and T₁ energy levels are estimated to be 2.78 and 2.46 eV for CzPN, and 2.55 and 2.45 eV for tMCzPN. As listed in Table 1, the ΔE_{ST} s of CzPN and tMCzPN are estimated to be 0.32 and 0.10 eV, respectively. With a large ΔE_{ST} and different features of S₁ and T₁ states, the up-conversion from triplet to singlet excitons will be inhibited, making it difficult for CzPN to possess TADF characteristic. Reversely, the

small ΔE_{ST} of 0.10 eV will lead tMCzPN to realize an efficient RISC process and exhibit TADF behavior. In DPEPO films at room temperature, the PLQYs of CzPN and tMCzPN were measured to be 93.3 and 70.5%, respectively. With a significant overlap between HOMO and LUMO, the fluorescence process of singlet excitons is efficient for CzPN, and it can be an excellent conventional fluorescent emitter. Additionally, tMCzPN also realizes quite a high PQLY for TADF emitters.

To further prove their TADF characteristics, the transient PL decays of the two compounds doped into DPEPO films were measured. In the order of a microsecond, no delayed component was observed for CzPN, indicating its non-TADF characteristic. While for tMCzPN, a delayed decay with a lifetime of 14.29 μ s was obtained at room temperature. We also measured the temperature-dependent transient PL decays of the tMCzPN doped DPEPO film from 100 to 300 K. As shown in Figure 4E,

the delayed component clearly enhanced with the increasing temperature, due to the acceleration of the up-conversion from triplet to singlet excitons by thermal activation, which directly demonstrated the TADF characteristic of tMCzPN. By replacing the common Cz with tMCz, CzPN, and tMCzPN exhibit significant differences in some key photophysical properties. Thus, compared to Cz, tMCz is more convenient to develop TADF emitters.

Electroluminescence Properties

To investigate the EL performance of two compounds, devices with structures of ITO/TAPC (35 nm)/TCTA (10 nm)/CzSi (10 nm)/DPEPO: CzPN or tMCzPN (20 wt%) (20 nm)/TmPyPb (40 nm)/LiF (1 nm)/Al were fabricated. Herein, indium tin oxide (ITO) was the anode, 4,4'-cyclohexylidenebis[N,N-bis(4-methylphenyl)aniline (TAPC) and 4,4',4''-tris(carbazolyl)triphenylamine (TCTA) were the hole-transporting layers, 9-(triphenyl-silyl)-9H-carbazole (CzSi) was the exciton-blocking layer, 1,3,5-tri(m-pyrid-3-yl-phenyl)benzene (TmPyPb) was electron-transporting, hole-blocking, and exciton-blocking layer, LiF was the electron injection layer, and Al was the cathode, respectively. CzPN or tMCzPN doped DPEPO was used as the emitting layers, and the doping concentration was optimized to 20 wt%.

As shown in **Figure 5** and listed in **Table 2**, both devices show close turn on voltages of 3.4 V and 3.3 V, respectively for CzPN and tMCzPN. The similar turn on voltages should be attributed to the use of the same host material, which is consistent with the results of the reported devices using DPEPO as the host. In the devices, CzPN exhibits a stable blue emission with a peak at 448 nm and a CIE coordinate of (0.15, 0.11), while tMCzPN shows a stable cyan emission with a peak at 500 nm and a CIE coordinate of (0.20, 0.42). The red-shift between two EL spectra should be mainly ascribed to the stronger electron-donating ability of tMCz compared with Cz, and is consistent with their PL spectra in DPEPO films. Additionally, from the EL spectra, the full-width at half-maximum is 72 nm for CzPN, evidently narrower than 90 nm for tMCzPN. This is because CzPN has a higher conjugation between the D and A segments, and thereby possesses a stronger molecular restriction to confine structural relaxation. The maximum forward-viewing efficiencies of CzPN-based OLED are 4.7 cd A⁻¹ for CE, 4.7 lm W⁻¹ for PE, and 5.3% for EQE, respectively. The EQE of 5.3% is consistent with the theoretical limitation of the OLEDs based on traditional fluorescent emitters, demonstrating the non-TADF characteristic of CzPN yet again. Without any light out-coupling enhancement, the tMCzPN-based device exhibits extremely high forward-viewing maximum CE, PE and EQE of 65.9 cd A⁻¹, 62.7 lm W⁻¹

and 26.0%, respectively. To the best of our knowledge, such a high EQE of 26.0% is among the best performance for TADF-based OLEDs. Thus, by simply replacing common Cz with tMCz, the non-TADF fluorophor CzPN is successfully transformed to an excellent TADF emitter tMCzPN, indicating that tMCz is a more appropriate candidate than Cz, for developing TADF emitters.

CONCLUSION

Due to the insufficient steric hindrance of Cz, additional groups are generally required to enhance the separation between HOMO and LUMO for Cz-based TADF emitters, resulting in complicated synthetic procedures and high costs. To address this issue, we replaced Cz with its derivative tMCz to develop TADF emitters, and designed and synthesized two novel compounds CzPN and tMCzPN accordingly. With the same and simple molecular framework, two compounds exhibit evident differences due to the additional methyl groups on tMCz. tMCzPN possesses a more twisted molecular structure and successfully realizes the TADF characteristic with a small ΔE_{ST} of 0.10 eV, while CzPN is a non-TADF fluorophor. In the devices, tMCzPN exhibits an extremely high forward-viewing maximum EQE of 26.0%, without any light out-coupling enhancement, which is significantly higher than that of 5.3% for CzPN. These results indicate that tMCzPN is an excellent TADF emitter and proves that tMCz is a more appropriate candidate than Cz for developing TADF emitters with a simple molecular framework.

AUTHOR CONTRIBUTIONS

J-LC and WL contributed equally to this work. C-JZ, S-LT, and X-HZ designed whole work. J-LC, WL, and J-XC synthesized the organic compounds. J-LC, KW, and Y-ZS characterize the physical properties of compounds. WL and MZ fabricated and optimized the devices. J-LC and WL wrote the paper with support from C-JZ, S-LT, and X-HZ. All authors contributed to the general discussion.

ACKNOWLEDGMENTS

This work was supported by the National Natural Science Foundation of China (Grant No. 51773029, 61775029, 51533005, 51373190), the National Key Research & Development Program of China (Grant No. 2016YFB0401002), the Collaborative Innovation Center of Suzhou Nano Science & Technology, the Priority Academic Program Development of Jiangsu Higher Education Institutions (PAPD) and the 111 Project and Qing Lan Project, P. R. China.

REFERENCES

Adachi, C., Baldo, M. A., Thompson, M. E., and Forrest, S. R. (2001). Nearly 100% internal phosphorescence efficiency in an organic light-emitting device. *J. Appl. Phys.* 90, 5048–5051. doi: 10.1063/1.1409582

Baldo, M. A., O'Brien, D. F., Thompson, M. E., and Forrest, S. R. (1999). Excitonic singlet-triplet ratio in a semiconducting organic thin film. *Phys.Rev.B.* 60, 14422–14428.

Baldo, M. A., O'Brien, D. F., You, Y., Shoustikov, A., Sibley, S., Thompson, M. E., et al. (1998). Highly efficient phosphorescent emission from organic electroluminescent devices. *Nature* 395, 151–154. doi: 10.1038/25954

- Chan, C. Y., Cui, L. S., Uk, K. J., Hajime, N., and Chihaya, A. (2018). Efficient and stable sky-blue delayed fluorescence organic light-emitting diodes with CIEy below 0.4. *Adv. Funct. Mater.* 28:1706023. doi: 10.1002/adfm.201706023
- Chen, J.-X., Liu, W., Zheng, C. J., Wang, K., Liang, K., Shi, Y. Z., et al. (2017). Coumarin-based thermally activated delayed fluorescence emitters with high external quantum efficiency and low efficiency roll-off in the devices. *ACS APPL. Mater. Interfaces* 9, 8848–8854. doi: 10.1021/acsami.6b15816
- Choi, S., Godumala, M., Lee, J. H., Kim, G. H., Moon, J. S., Kim, J. Y., et al. (2017). Optimized structure of silane-core containing host materials for highly efficient blue TADF OLEDs. *J. Mater. Chem. C* 5, 6570–6577. doi: 10.1039/C7TC01357D
- Cui, L.-S., Nomura, H., Geng, Y., Kim, J. U., Nakanotani, H., and Adachi, C. (2017). Controlling singlet–triplet energy splitting for deep-blue thermally activated delayed fluorescence emitters. *Angew. Chem. Int. Ed.* 56, 1571–1575. doi: 10.1002/anie.201609459
- Endo, A., Ogasawara, M., Takahashi, A., Yokoyama, D., Kato, Y., and Adachi, C. (2009). Thermally activated delayed fluorescence from Sn(4+)-porphyrin complexes and their application to organic light emitting diodes—a novel mechanism for electroluminescence. *Adv. Mater.* 21, 4802–4806. doi: 10.1002/adma.200900983
- Endo, A., Sato, K., Yoshimura, K., Kai, T., Kawada, A., Miyazaki, H., et al. (2011). Efficient up-conversion of triplet excitons into a singlet state and its application for organic light emitting diodes. *Appl. Phys. Lett.* 98:083302. doi: 10.1063/1.3558906
- Goushi, K., Kou, Y., Sato, K., and Adachi, C. (2012). Organic light-emitting diodes employing efficient reverse intersystem crossing for triplet-to-singlet state conversion. *Nat. Photonics* 6, 253–258. doi: 10.1038/nphoton.2012.31
- Hirata, S., Sakai, Y., Masui, K., Tanaka, H., Lee, S. Y., Nomura, H., et al. (2014). Highly efficient blue electroluminescence based on thermally activated delayed fluorescence. *Nat. Mater.* 14, 330–336. doi: 10.1038/nmat4154
- Li, W., Zhao, J., Li, L., Du, X., Fan, C., Zheng, C., et al. (2018). Efficient solution-processed blue and white OLEDs based on a high-triplet bipolar host and a blue TADF emitter. *Org. Electron.* 58, 276. doi: 10.1016/j.orgel.2018.04.027
- Liang, J., Li, C., Zhuang, X., Ye, K., Liu, Y., and Wang, Y. (2018). Novel blue bipolar thermally activated delayed fluorescence material as host emitter for high-efficiency hybrid warm-white OLEDs with stable high color-rendering index. *Adv. Funct. Mater.* 28:1707002. doi: 10.1002/adfm.201707002
- Liu, W., Chen, J. X., Zheng, C. J., Wang, K., Chen, D. Y., Li, F., et al. (2016). Novel strategy to develop exciplex emitters for high-performance OLEDs by employing thermally activated delayed fluorescence materials. *Adv. Funct. Mater.* 26, 2002–2008. doi: 10.1002/adfm.201505014
- Liu, W., Chen, Z., Zheng, C. J., Liu, X. K., Wang, K., Li, F., et al. (2015b). A novel nicotinonitrile derivative as an excellent multifunctional blue fluorophore for highly efficient hybrid white organic light-emitting devices. *J. Mater. Chem. C* 3, 8817–8823. doi: 10.1039/C5TC01415H
- Liu, W., Zheng, C. J., Wang, K., Chen, Z., Chen, D. Y., Li, F., et al. (2015a). Novel carbazol-pyridine-carbonitrile derivative as excellent blue thermally activated delayed fluorescence emitter for highly efficient organic light-emitting devices. *ACS Appl. Mater. Interfaces* 7, 18930–18936. doi: 10.1021/acsami.5b05648
- Liu, X. K., Zhan, C., Zheng, C. J., Liu, C. L., Lee, C. S., Li, F., et al. (2015c). Prediction and design of efficient exciplex emitters for high-efficiency, thermally activated delayed-fluorescence organic light-emitting diodes. *Adv. Mater.* 27, 2378–2383. doi: 10.1002/adma.201405062
- Méhes, G., Nomura, H., Zhang, Q., Nakagawa, T., and Adachi, C. (2012). Enhanced electroluminescence efficiency in a spiro-acridine derivative through thermally activated delayed fluorescence. *Angew. Chem. Int. Ed.* 51, 11311–11315. doi: 10.1002/anie.201206289
- Mounggon, K., Kyu, J. S., Seok-Ho, H., and Yeob, L. J. (2015). Stable blue thermally activated delayed fluorescent organic light-emitting diodes with three times longer lifetime than phosphorescent organic light-emitting diodes. *Adv. Mater.* 27, 2515–2520. doi: 10.1002/adma.201500267
- Okamoto, S., Tanaka, K., Izumi, Y., Adachi, H., Yamaji, T., and Suzuki, T. (2001). Simple measurement of quantum efficiency in organic electroluminescent devices. *J. Appl. Phys.* 40, 783–784. doi: 10.1143/JAP.40.L783
- Pashazadeh, R., Pander, P., Lazauskas, A., Dias, F. B., and Grazulevicius, J. V. (2018). Multicolor luminescence switching and controllable thermally activated delayed fluorescence turn on/turn off in carbazole–quinoxaline–carbazole triads. *J. Phys. Chem. Lett.* 9, 1172–1177. doi: 10.1021/acs.jpclett.8b00136
- Peng, Q., Li, W., Zhang, S., Chen, P., Li, F., and Ma, Y. (2013). Evidence of the reverse intersystem crossing in intra-molecular charge transfer fluorescence based organic light-emitting devices through magneto-electroluminescence measurements. *Adv. Opt. Mater.* 1, 362–366. doi: 10.1002/adom.201300028
- Pope, M., Kallmann, H. P., and Magnante, P. (1963). Electroluminescence in Organic Crystals. *J. Chem. Phys.* 38, 2042–2043. doi: 10.1063/1.1733929
- Rajamalli, P., Thangaraji, V., Senthilkumar, N., Ren-Wu, C. C. Lin, H. W., and Cheng, C. H. (2017). Thermally activated delayed fluorescence emitters with a *m,m*-di-*tert*-butyl-carbazoyl benzoylpyridine core achieving extremely high blue electroluminescence efficiencies. *J. Mater. Chem. C* 5, 2919–2926. doi: 10.1039/C7TC00457E
- Sajoto, T., Djurovich, P. I., Tamayo, A. B., Oxgaard, J., Goddard, W. A. III, and Thompson, M. E. (2009). Temperature dependence of blue phosphorescent cyclometalated Ir(III) complexes. *J. Am. Chem. Soc.* 131, 9813–9822. doi: 10.1021/ja903317w
- Segal, M., Baldo, M. A., Holmes, R. J., Forrest, S. R., and Soos, Z. G. (2003). Excitonic singlet–triplet ratios in molecular and polymeric organic materials. *PhRvB* 68, 338–344. doi: 10.1103/PhysRevB.68.075211
- Shi, Y. Z., Wang, K., Li, X., Dai, G. L., Liu, W., Ke, K., et al. (2018). Intermolecular charge-transfer transition emitter showing thermally activated delayed fluorescence for efficient non-doped OLEDs. *Angew. Chem. Int. Ed.* 57:9480. doi: 10.1002/anie.201804483
- Tang, C. W., and VanSlyke, S. A. (1987). Organic electroluminescent diodes. *Appl. Phys. Lett.* 51, 913–915. doi: 10.1063/1.98799
- Uoyama, H., Goushi, K., Shizu, K., Nomura, H., and Adachi, C. (2012). Highly efficient organic light-emitting diodes from delayed fluorescence. *Nature* 492, 234–238. doi: 10.1038/nature11687
- Wang, K., Zheng, C. J., Liu, W., Liang, K., Shi, Y. Z., Tao, S. L., et al. (2017). Avoiding energy loss on TADF emitters: controlling the dual conformations of D-A structure molecules based on the pseudoplanar segments. *Adv. Mater.* 29:1701476. doi: 10.1002/adma.201701476
- Yersin, H., Rausch, A. F., Czerwieniec, R., Hofbeck, T., and Fischer, T. (2011). The triplet state of organo-transition metal compounds. Triplet harvesting and singlet harvesting for efficient OLEDs. *Coord. Chem. Rev.* 255, 2622–2652. doi: 10.1016/j.ccr.2011.01.042
- Zhang, D., Duan, L., Li, C., Li, Y., Li, H., Zhang, D., et al. (2014a). High-efficiency fluorescent organic light-emitting devices using sensitizing hosts with a small singlet–triplet exchange energy. *Adv. Mater.* 26, 5050–5055. doi: 10.1002/adma.201401476
- Zhang, D., Song, X., Cai, M., Kaji, H., and Duan, L. (2018). Versatile indolocarbazole-isomer derivatives as highly emissive emitters and ideal hosts for thermally activated delayed fluorescent OLEDs with alleviated efficiency roll-off. *Adv. Mater.* 30:1705406. doi: 10.1002/adma.201705406
- Zhang, D., Wei, P., Zhang, D., and Duan, L. (2017). Sterically shielded electron transporting material with nearly 100% internal quantum efficiency and long lifetime for thermally activated delayed fluorescent and phosphorescent OLEDs. *ACS Appl. Mater. Interfaces* 9, 19040–19047. doi: 10.1021/acsami.7b04391
- Zhang, Q., Kuwabara, H., Potsavage, W. J., Huang, S., Hatae, Y., Shibata, T., et al. (2014b). Anthraquinone-based intramolecular charge-transfer compounds: computational molecular design, thermally activated delayed fluorescence, and highly efficient red electroluminescence. *J. Am. Chem. Soc.* 136, 18070–18081. doi: 10.1021/ja510144h

- Zhang, Q., Li, B., Huang, S., Nomura, H., Tanaka, H., and Adachi, C. (2014c). Efficient blue organic light-emitting diodes employing thermally activated delayed fluorescence. *Nat. Photonics*. 8, 326–332. doi: 10.1038/nphoton.2014.12
- Zhang, Q., Li, J., Shizu, K., Huang, S., Hirata, S., Miyazaki, H., et al. (2012). Design of efficient thermally activated delayed fluorescence materials for pure blue organic light emitting diodes. *J. Am. Chem. Soc.* 134, 14706–14709. doi: 10.1021/ja306538w
- Zhang, S., Yao, L., Peng, Q., Li, W., Pan, Y., Xiao, R., et al. (2015). Achieving a significantly increased efficiency in nondoped pure blue fluorescent OLED: a quasi-equivalent hybridized excited state. *Adv. Funct. Mater.* 25, 1755–1762. doi: 10.1002/adfm.201404260
- Zheng, C. J., Wang, J., Ye, J., Lo, M. F., Liu, X. K., Fung, M. K., et al. (2013). Novel efficient blue fluorophors with small singlet-triplet splitting: Hosts for highly

efficient fluorescence and phosphorescence hybrid WOLEDs with simplified structure. *Adv. Mater.* 25, 2205–2211. doi: 10.1002/adma.201204724

Conflict of Interest Statement: The authors declare that the research was conducted in the absence of any commercial or financial relationships that could be construed as a potential conflict of interest.

Copyright © 2019 Cai, Liu, Wang, Chen, Shi, Zhang, Zheng, Tao and Zhang. This is an open-access article distributed under the terms of the Creative Commons Attribution License (CC BY). The use, distribution or reproduction in other forums is permitted, provided the original author(s) and the copyright owner(s) are credited and that the original publication in this journal is cited, in accordance with accepted academic practice. No use, distribution or reproduction is permitted which does not comply with these terms.



High-Efficiency Sky Blue-To-Green Fluorescent Emitters Based on 3-Pyridinecarbonitrile Derivatives

Yuki Masuda¹, Hisahiro Sasabe^{1,2,3*}, Hiroki Arai¹, Natsuki Onuma¹ and Junji Kido^{1,2,3*}

¹ Department of Organic Materials Science, Graduate School of Organic Materials Science, Yamagata University, Yamagata, Japan, ² Frontier Center for Organic Materials (FROM) Yamagata University, Yamagata, Japan, ³ Research Center for Organic Electronics (ROEL), Yamagata University, Yamagata, Japan

OPEN ACCESS

Edited by:

Guigen Li,
Texas Tech University, United States

Reviewed by:

You-Xuan Zheng,
Nanjing University, China
Lian Duan,
Tsinghua University, China
Bo Jiang,
Jiangsu Normal University, China

*Correspondence:

Hisahiro Sasabe
h-sasabe@yz.yamagata-u.ac.jp
Junji Kido
kido@yz.yamagata-u.ac.jp

Specialty section:

This article was submitted to
Organic Chemistry,
a section of the journal
Frontiers in Chemistry

Received: 31 January 2019

Accepted: 01 April 2019

Published: 24 April 2019

Citation:

Masuda Y, Sasabe H, Arai H,
Onuma N and Kido J (2019)
High-Efficiency Sky Blue-To-Green
Fluorescent Emitters Based on
3-Pyridinecarbonitrile Derivatives.
Front. Chem. 7:254.
doi: 10.3389/fchem.2019.00254

The pyridinecarbonitrile derivative is well known as an acceptor unit in fluorescent materials. However, its use in thermally activated delayed fluorescent (TADF) emitters is very limited compared with its benzenecarbonitrile counterparts. Very recently, we developed a series of 4-pyridinecarbonitrile, so-called isonicotinonitrile derivatives, as a highly efficient sky blue-to-green TADF emitters realizing low-drive-voltage organic light-emitting devices (OLEDs). In this work, we contributed new design and development for three 3-pyridinecarbonitrile-based TADF emitters named **2AcNN**, **2PXZNN**, and **5PXZNN**. Among these emitters, a sky blue emitter, **2AcNN**, showed a maximum external quantum efficiency ($\eta_{\text{ext,max}}$) of 12% with CIE (0.19, 0.36). While green emitters, **5PXZNN** and **2PXZNN**, realized highly efficient TADF OLEDs with a $\eta_{\text{ext,max}}$ of 16–20%. Introduction of electron-donor moiety into the 2-position of 3-pyridinecarbonitrile contributes a larger overlapping of frontier molecular orbitals (FMOs) and stronger intramolecular charge transfer (ICT) interaction generating efficient TADF emitters.

Keywords: solid-state emission, organic light-emitting device, donor-acceptor system, thermally activated delayed fluorescence, photochemistry

INTRODUCTION

High-efficiency organic light-emitting devices (OLEDs) have attracted significant attention due to their ability to yield energy savings in small- to large-area flat-panel displays and general lighting applications (Walzer et al., 2007; Sasabe and Kido, 2013; Adachi, 2014; Im et al., 2017; Wong and Z.-Colman, 2017; Yang et al., 2017; Kim and Kim, 2018; Komatsu et al., 2018). Organic phosphorescent and thermally activated delayed fluorescent (TADF) emitters can convert all electrogenerated molecular excitons such as singlets and triplets to photons achieving an electron-to-photon conversion efficiency of up to 100%. Recently, the development of pure organic TADF emitters has been focused on simultaneously realizing cost-effective and high-performance OLEDs compared with its phosphorescent counterparts (Uoyama et al., 2012; Adachi, 2014; Kaji et al., 2015; Lin et al., 2016; Seino et al., 2016; Im et al., 2017; Liu et al., 2017; Rajamalli et al., 2017; Wong and Z.-Colman, 2017; Yang et al., 2017; dos Santo et al., 2018; Komatsu et al., 2018; Sasabe et al., 2018; Wu et al., 2018). In principle, TADF emitters consist of electron-donor (D) and electron-acceptor (A) moieties realizing efficient intramolecular charge transfer (ICT). The connection between D and A moieties is generally accompanied with a small overlap in the frontier molecular orbital (FMO) between the highest occupied molecular orbital (HOMO) and the lowest unoccupied molecular orbital (LUMO), in other words, a small energy difference between singlet and triplet energies

(ΔE_{ST}). Among the A units, cyano-containing aromatic moieties, such as benzenecarbonitriles and pyridinecarbonitriles, are very effective in developing high-performance TADF emitters. However, compared with well-known benzenecarbonitrile derivatives, more electron-deficient pyridinecarbonitrile-based counterparts have been relatively unexplored.

In 2015, Liu et al. reported a pyridinedicarbonitrile/carbazole-conjugated molecule, namely **CPC**, in which pyridinedicarbonitrile and carbazole units are directly linked, showing a photoluminescent quantum yield (η_{PL}) of 49.7% in host doped film (Liu et al., 2015). The **CPC** showed efficient sky blue emission with a maximum external quantum efficiency ($\eta_{ext,max}$) of 21% and Commission Internationale de l'Éclairage (CIE) coordinates (0.20, 0.35). This is the first report to use pyridinecarbonitrile as an acceptor moiety of a TADF emitter. In 2016, Pan and co-workers developed several pyridinedicarbonitrile/dimethylacridine-conjugated molecules (Pan et al., 2016). Among these molecules, **Py2** and **Py5** showed a high η_{PL} of 89–92% and yielded efficient greenish blue OLED with $\eta_{ext,max}$ at 23–24%. CIE coordinates were (0.24, 0.49) for **Py2** and (0.28, 0.54) for **Py5**. In 2017, Sasabe et al. developed a series of 4-pyridinecarbonitrile, so-called isonicotinonitrile derivatives, as highly efficient sky blue-to-green TADF emitters realizing low-drive-voltage OLEDs (Sasabe et al., 2017). Sky blue emitter **26AcINN** exhibited a low turn-on voltage of 2.9 V, a maximum power efficiency ($\eta_{p,max}$) of 66 lm W⁻¹, and a $\eta_{ext,max}$ of 22% with CIE coordinates (0.22, 0.45). Meanwhile, green emitter **26PXZINN** exhibited a low turn-on voltage of 2.2 V, a high $\eta_{p,max}$ of 99 lm W⁻¹, and a $\eta_{ext,max}$ of 22% with CIE coordinates (0.37, 0.58). As mentioned above, although pyridinecarbonitrile-based TADF emitters exhibited very promising OLED performances, they have been relatively unexplored so far.

In this work, we focused on 3-pyridinecarbonitrile derivatives as TADF emitters aiming bluer emission based on a larger energy gap than that of the corresponding 4-pyridinecarbonitrile derivatives, and aimed to enrich the materials science of cyano-containing aromatic compounds. We designed and developed three 3-pyridinecarbonitrile-based TADF emitters labeled **2AcNN**, **2PXZNN**, and **5PXZNN**. Among these emitters, a blue emitter, **2AcNN**, exhibited a sky blue emission with CIE coordinates (0.19, 0.36), $\eta_{ext,max}$ of 12%, and $\eta_{p,max}$ of 28.8 lm W⁻¹. Meanwhile, a green emitter, **2PXZNN**, realized a high efficiency TADF OLED with CIE coordinates (0.35, 0.55) and $\eta_{ext,max}$ of 20.8%.

RESULTS AND DISCUSSION

Density Functional Theory Calculation and Synthesis

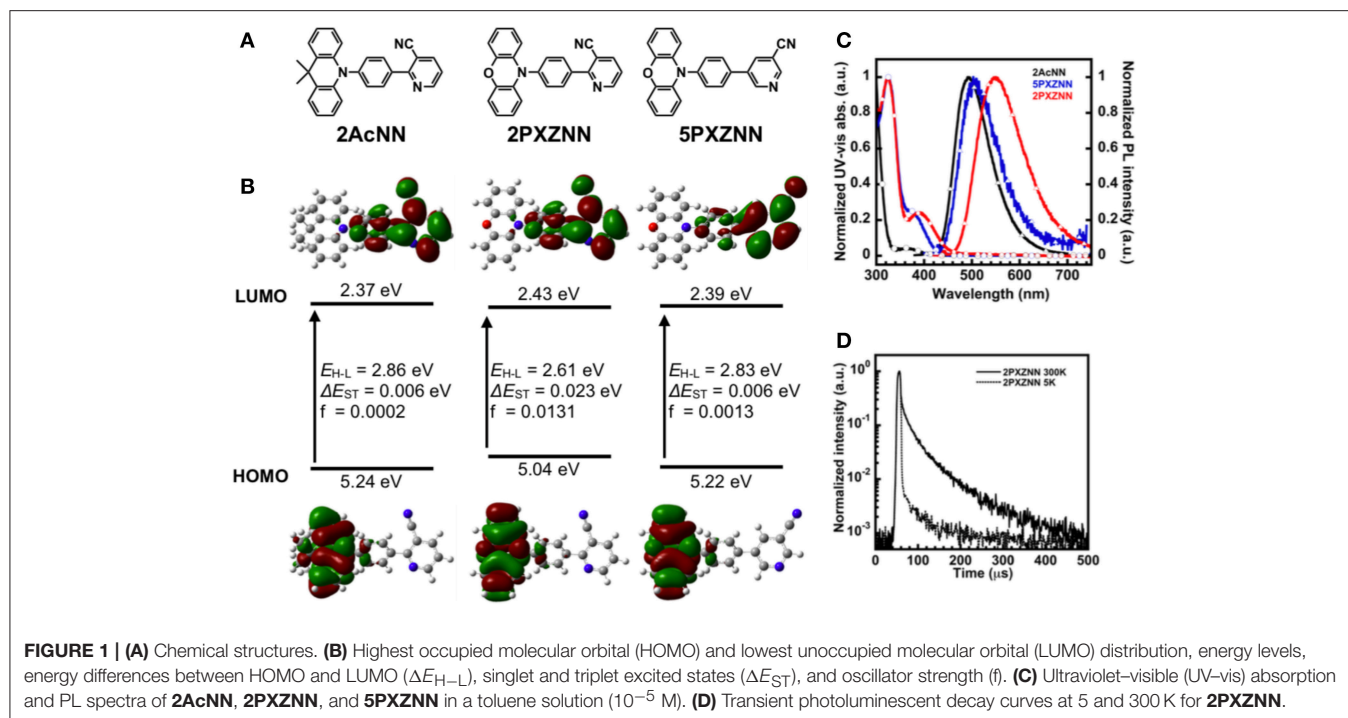
In previous work, we successfully developed a sky blue TADF emitter, **26AcINN**, with a $\eta_{ext,max}$ of 22% (Sasabe et al., 2017). However, color coordinates were not located in the blue region. Therefore, in order to obtain bluer emission compared with the 4-pyridinecarbonitrile derivatives, we used 3-pyridinecarbonitrile with reduced π -conjugation as an A

unit. In addition, to get an effective molecular design and expand the materials chemistry of the pyridinecarbonitrile derivatives, we designed three types of 3-pyridinecarbonitrile-based TADF emitters, **2AcNN**, **2PXZNN**, and **5PXZNN**, using dimethylacridine (**Ac**) and phenoxiazine (**PXZ**) donors. Prior to preparing the emitters, we conducted density functional theory (DFT) calculations to estimate the geometric structure, the energy difference between HOMO and LUMO (ΔE_{H-L}), and the E_S , E_T , and ΔE_{ST} of **2AcNN**, **2PXZNN**, and **5PXZNN** (Figure 1A and Table S1). These derivatives exhibited small ΔE_{ST} (<0.02 eV) values, which is consistent with TADF emissions. The electron cloud distribution in Figure 1B shows that the HOMO was located on the donor unit, whereas the LUMO was located on the phenylpyridinecarbonitrile skeleton. Among the PXZ derivatives, **5PXZNN** showed a larger energy gap than **2PXZNN**. To verify these differences, we also conducted DFT calculations of the phenylpyridinecarbonitrile skeleton (Figure S1). As a result, **5PXZNN** showed smaller electron distributions of LUMO on the phenyl ring compared with **2PXZNN**, resulting in smaller overlapping of FMO and weaker ICT interaction causing a larger energy gap. The FMOs were almost completely separated with a small overlap. The synthetic routes of the target compounds are shown in Schemes S1–3. These compounds were readily synthesized through a Suzuki–Miyaura coupling reaction between a halogenated 3-pyridinecarbonitrile precursor and a donor-substituted 4-phenylboronate (Komatsu et al., 2016) with 67–78% yield, and multigram amounts of product were readily obtained. The target compounds were characterized using ¹H NMR, ¹³C NMR, mass spectrometry, and elemental analysis.

Thermal and Photophysical Properties

Products were purified through train sublimation before device fabrication. The purity of the compounds was evaluated at over 99% using high-performance liquid chromatography. The compounds can be used for further thermal and photophysical investigation, and OLED evaluation with no influence from impurities. The thermal properties of the materials were estimated via thermogravimetric analysis (TGA) and differential scanning calorimetry (DSC). The materials exhibited high thermal stability with a weight loss of 5% (T_{d5}) at temperatures over 300°C. The glass transition temperatures (T_g) were observed at 56°C for **2AcNN**, 50°C for **2PXZNN**, and 57°C for **5PXZNN**. The T_g values were relatively low due to the low molecular weight of these emitters. The physical properties of the materials were evaluated in the solid-state film. The ionization potential (I_p) levels, measured via photoelectron yield spectroscopy (PYS), were observed at \sim -5.7 to -5.8 eV. The optical energy gap (E_g) was taken as the point of intersection of the normalized ultraviolet–visible (UV–vis) absorption spectra. The electron affinity (E_a) levels were estimated at \sim -3.0 eV, by subtracting the optical E_g from the I_p level.

The optical properties of the materials were evaluated under a dilute toluene solution (10⁻⁵ M). The UV–vis absorption and PL spectra of the pyridinecarbonitrile derivatives obtained at room temperature are on display in Figure 1C. The PL peak wavelength was observed at 492 nm for **2AcNN**, 550 nm for **2PXZNN**, and



503 nm for **5PXZNN**. As predicted from the DFT calculations, **2AcNN** showed sky blue emission and a shorter wavelength based on the weaker ICT character among these three emitters. On the other hand, **2PXZNN** showed green emission and a longer wavelength due to the stronger ICT character as shown in the UV-vis absorption spectra.

With regard to the application of OLEDs, the photophysical properties of the thin film have to be evaluated. Because a TADF emitter can harvest all the molecular excitons from singlets and triplets, the E_T of host materials should be higher than that of the emitters suppressing the triplet exciton quenching for high-efficiency OLEDs. Therefore, the PL spectra were subsequently investigated in a host matrix of bis[2-(diphenylphosphino)phenyl]ether oxide (DPEPO) with a high triplet energy (E_T) of 3.30 eV and a host matrix of 4,4'-bis(carbazol-9-yl)biphenyl (CBP) with E_T of 2.60 eV. As shown in **Figure S2**, the emission peaks in DPEPO films doped with 10 wt% **2AcNN**, **5PXZNN**, and **2PXZNN** were located at 477, 492, and 521 nm, respectively. Furthermore, the emission peaks in CBP films doped with 10 wt% **5PXZNN** and **2PXZNN** were almost the same as those observed in the DPEPO host. η_{PL} differed between the DPEPO and CBP hosts. The η_{PL} value of **5PXZNN** was lowered in CBP ($\eta_{PL} = 31\%$) compared with that in DPEPO ($\eta_{PL} = 59\%$), but in the case of **2PXZNN**, it remained unchanged (η_{PL} values: 68% in DPEPO and 69% in CBP). These results suggested that **5PXZNN** had higher E_T than that of CBP and was quenched by CBP. The TADF character was subsequently confirmed by examining the PL decay curves of the emitter doped host films at various temperatures (i.e., 5 and 300 K; **Figure 1D**; **Figure S3**). The delayed PL intensities of the three materials increased at 300 K, thereby indicating the

presence of TADF. The transient PL decay curves of the 10 wt%-doped DPEPO or CBP films exhibited double-exponential decay with delayed lifetimes (τ_d) of 264, 175, and 53 μ s for **2AcNN**, **5PXZNN**, and **2PXZNN**, respectively. The τ_d are relatively long compared with the well-known green TADF emitters, such as **4CzIPN** ($\tau_d = 5.1$ μ s; Uoyama et al., 2012), most likely because of the relatively large ΔE_{ST} of ~ 0.4 eV. Considering the combined results from the DFT calculations and photophysical experiments, an electron-donor should be introduced into the 2-position of 3-pyridinecarbonitrile to create a superior TADF emitter. The introduction of an electron-donor into the 2-position contributes a larger overlapping of FMOs and stronger ICT interaction for efficient TADF behaviors leading to shorter τ_d . All thermal and photophysical properties of the pyridinecarbonitrile derivatives are summarized in **Table 1** and **Table S2**.

Organic Light-Emitting Device Performance

Next, we evaluated the OLED performance for three emitters, **2AcNN**, **5PXZNN**, and **2PXZNN**. We used a carrier- and exciton-confining device to maximize OLED performance. We employed di-[4-(*N,N*-ditolyl-amino)-phenyl]cyclohexane (TAPC) as a hole transport layer (HTL), and TAPC with a shallow E_a of -2.0 eV to effectively block electrons. 3,3'',5,5'-Tetra(3-pyridyl)-1,1';3',1''-terphenyl (B3PyPB; Sasabe et al., 2008a,b) was used as an electron transport layer (ETL), and B3PyPB with a deep I_p of -6.6 eV effectively blocked the hole leakage. By using a combination of TAPC and B3PyPB, we were able to confine all holes and electrons in the emission layer

TABLE 1 | Thermal and optical properties.

Compound	Mw.	$T_g/T_m/T_{d5}$ [°C] ^a	$I_p/E_a/E_g$ [eV] ^b	$E_S/E_T/\Delta E_{ST}$ [eV] ^c	τ_d [μs] ^d	η_{PL} [%]
2AcNN	387.5	56/195/317	−5.73/−2.99/2.74	3.08/2.71/0.37	264	64 ^e
2PXZNN	361.4	50/161/322	−5.70/−3.12/2.58	2.74/2.60/0.14	53 ^f	68 ^e /69 ^f
5PXZNN	361.4	57/239/321	−5.80/−3.06/2.74	2.91/2.52/0.40	175	59 ^e /31 ^f

^a T_g and T_m were measured by DSC, and T_{d5} was measured by TGA.

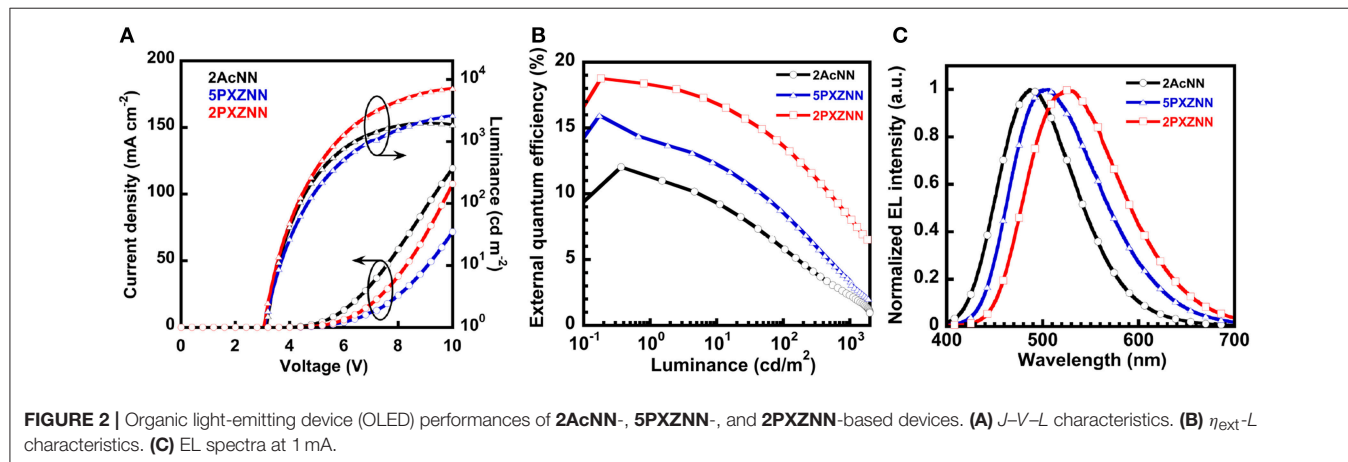
^b I_p was measured by PYS, E_g was taken as the point of intersection of the normalized absorption spectra, and E_a was calculated from I_p and E_g .

^cThe onset of delayed PL of the neat film was measured using a streak camera and $\Delta E_{ST} = E_S - E_T$.

^dDelayed fluorescent lifetime of the 10 wt%-doped DPEPO film.

^ePL quantum yield of the 10 wt%-doped DPEPO film.

^fCBP was used instead of DPEPO.



(EML) to create superior carrier balance. In addition, *N,N*-dicarbazoyl-3,5-benzene (mCP) was inserted at the interface between HTL and EML to prevent the exciton-quenching between TAPC and emitter molecules. This is because the η_{PL} value of **2AcNN** was lower in TAPC ($\eta_{PL} = 42\%$) compared with neat film of **2AcNN** ($\eta_{PL} = 60\%$). DPEPO was used as a host material, and the E_T levels of TAPC, mCP, DPEPO, and B3PyPB were 2.98, 3.00, 3.30, and 2.77 eV, respectively. The chemical structures of the materials used in this study are shown in **Figure S4**. Therefore, we were able to suppress exciton quenching from the perspective of E_T confinement and maximize OLED performance. All chemical structures for the materials used in this study are shown in **Figure S4**. Three types of OLEDs with the structures of [ITO/triphenylamine-containing polymer: 4-isopropyl-4'-methyl-diphenyl-iodonium tetrakis(pentafluorophenyl)borate (PPBI; Kido et al., 1997) (20 nm)/TAPC (25 nm)/mCP (5 nm)/10 wt% emitter-doped DPEPO (20 nm)/B3PyPB (50 nm)/LiF (0.5 nm)/Al (100 nm)] were fabricated. **Figure S5A** shows the energy diagrams for these devices. All peaks in the EL spectra originate from emitters with no emissions arising from neighboring materials. The current density–voltage–luminance (J – V – L) characteristics are shown in **Figure 2A**, and the external quantum efficiency–luminance (η_{ext} – L) characteristics are shown in **Figure 2B**. OLED performance is summarized in **Table 2**. The EL emission peaks located at 486, 506, and 527 nm are linked to **2AcNN**, **5PXZNN**, and **2PXZNN**, respectively (**Figure 2C**). Among these, a blue emitter, **2AcNN**,

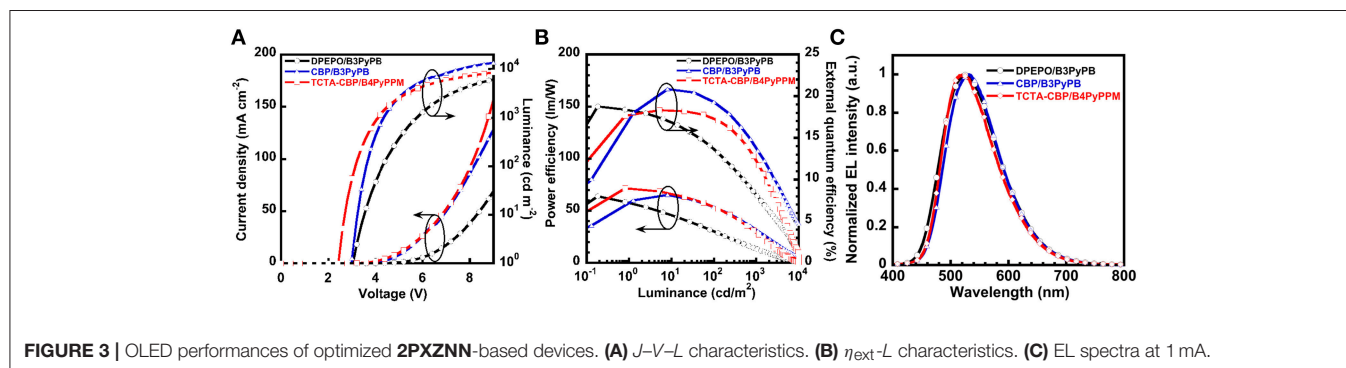
showed a sky blue emission with CIE (0.19, 0.36), $\eta_{ext,max}$ of 12%, and $\eta_{p,max}$ of 28.8 lm W⁻¹. The operating voltage at 1 cd m⁻² was relatively low, at 3.1 V. By contrast, a green emitter, **2PXZNN**, realized a high-efficiency TADF OLED with CIE (0.35, 0.53) and $\eta_{ext,max}$ of 18.8%. The operating voltage at 1 cd m⁻² was recorded at 3.0 V and was almost identical to the **2AcNN**-based sky blue OLED. Compared with state-of-the-art green OLEDs, the operating voltage can be reduced significantly.

Low-Operating-Voltage 2PXZNN-Based Organic Light-Emitting Devices

In the previous section, we also used DPEPO as a host material for a green emitter, **2PXZNN**. As a result, **2PXZNN**-based OLED showed a relatively high operating voltage of 3.0 V at 1 cd m⁻². To further reduce operating voltage, we simply substituted host material DPEPO with CBP. Note that the **2PXZNN**-doped CBP film exhibited a η_{PL} value of 69%, similar to that of a DPEPO film. An OLED with an EML of 10 wt% **2PXZNN**-doped CBP (20 nm) was fabricated. **Figure S5B** shows the energy diagram. The J – V – L characteristics are shown in **Figure 3A**, and the η_{ext} – L – η_p characteristics are shown in **Figure 3B**. The peak in the EL spectra at 532 nm originates from **2PXZNN**, with no emissions arising from neighboring materials (**Figure 3C**). The device showed green emission with CIE (0.35, 0.55), higher $\eta_{ext,max}$ of 20.8%, and $\eta_{p,max}$ of 65 lm W⁻¹. Compared with a DPEPO-based device, the CBP-based device exhibited slightly higher $\eta_{ext,max}$ value. The operating voltage was recorded at

TABLE 2 | Summary of OLED performances.

Emitter	V_{on} [V] ^a	$V_{100}/\eta_p, 100/\eta_c, 100/\eta_{ext}, 100$ [V/lm W ⁻¹ /cd A ⁻¹ /%] ^b	$V_{1000}/\eta_p, 1000/\eta_c, 1000/\eta_{ext}, 1000$ [V/lm W ⁻¹ /cd A ⁻¹ /%] ^c	$\eta_{p,max}/\eta_c,max/\eta_{ext,max}$ [lm W ⁻¹ /cd A ⁻¹ /%] ^d	CIE (x, y) ^e
2AcNN	3.1	4.4/9.7/13.4/5.9	6.4/2.5/5.1/2.3	28.8/27.5/12.0	(0.19, 0.36)
5PXZNN	3.1	4.7/15.8/23.4/8.6	7.0/4.1/9.1/3.4	48.9/43.6/15.9	(0.25, 0.45)
2PXZNN	3.0	4.3/30.5/41.6/13.7	5.8/13.5/24.8/8.2	64.0/57.0/18.8	(0.33, 0.53)
2PXZNN^f	3.0	3.6/53.7/61.5/19.3	4.4/31.8/44.0/13.8	65.2/66.4/20.8	(0.35, 0.55)
2PXZNN^g	2.4	3.1/54.1/53.8/17.3	4.1/29.2/38.0/12.3	71.6/56.8/18.3	(0.37, 0.56)

^a Turn-on voltage (V) at 1 cd m⁻².^b Power efficiency (η_p), current efficiency (η_c), voltage (V), and external quantum efficiency (η_{ext}) at 100 cd m⁻².^c η_p , η_c , V, and η_{ext} at 1,000 cd m⁻².^d η_p , η_c , and η_{ext} at maximum.^e CIE at 100 cd m⁻².^f Device using CBP-doped 2PXZNN.^g Device using TCTA-doped and CBP-doped 2PXZNN as a double emission layer and B4PyPPM.**FIGURE 3** | OLED performances of optimized **2PXZNN**-based devices. **(A)** J - V - L characteristics. **(B)** η_{ext} - L characteristics. **(C)** EL spectra at 1 mA.

3.0 V, similar to that of a DPEPO-based device. However, much higher current density and luminance were obtained using a CPB host. This is most likely due to the improved carrier balance in the EML. The CBP host was considered to contribute an increase in hole carrier in the EML compared with a DPEPO host. Encouraged by these results, we further improved the device structure using a double EML device using 4,4'-tris(N-carbazolyl)triphenylamine (TCTA) with shallower I_p and E_a than CBP to increase the density of the hole carriers. Note that the η_{PL} value of a 10 wt% **2PXZNN**-doped TCTA film was recorded to be 64%. In addition, we used B4PyPPM as an ETL (Sasabe et al., 2008a,b, 2011). B4PyPPM has a deeper E_a than B3PyPB, enabling efficient electron injection leading to low-operating-voltages. An OLED with the structure [ITO/triphenylamine-containing polymer: PPBI (20 nm)/TAPC (30 nm)/10 wt% **2PXZNN**-doped TCTA (10 nm)/10 wt% **2PXZNN**-doped CBP (10 nm)/B4PyPPM (50 nm)/LiF (0.5 nm)/Al (100 nm)] was fabricated. **Figure S5C** displays the energy diagram. OLED performance is summarized in **Table 2**. The EL emission peak is located at 523 nm with CIE (0.37, 0.56), high $\eta_{ext,max}$ of 18%, and $\eta_{p,max}$ of 72 lm W⁻¹. The operating voltage was recorded as 2.4 V, a reduction of 0.6 V compared with the previous device, leading to a much higher $\eta_{p,max}$ of 71.6 lm W⁻¹.

CONCLUSION

In this work, we focused on relatively unexplored pyridinecarbonitrile derivatives, particularly on 3-pyridinecarbonitrile derivatives for an efficient TADF emitter aiming for bluer emission, and aimed to enrich the science of cyano-containing aromatic compounds. We developed three new types of 3-pyridinecarbonitrile-based TADF emitters, labeled **2AcNN**, **2PXZNN**, and **5PXZNN**. These compounds can be readily prepared through one-step Suzuki–Miyaura cross-coupling reaction with 67–78% yields. These emitters exhibited relatively high η_{PL} s of 59–69% with low ΔE_{ST} values of 0.14–0.40 eV in host matrices, such as DPEPO and CBP. Following photophysical investigations of the EML, three emitters appeared to achieve TADF behavior at high temperature and hence are expected to yield efficient TADF OLEDs. A sky blue emitter, **2AcNN**, showed a $\eta_{ext,max}$ of 12% and a $\eta_{p,max}$ of 28.8 lm W⁻¹ with CIE (0.19, 0.36). Meanwhile, a green emitter, **2PXZNN**, realized a highly efficient TADF OLED realizing a $\eta_{ext,max}$ of 20.8% with CIE (0.35, 0.55). Furthermore, by improving the carrier balance factor in the EML, the **2PXZNN**-based OLED achieved a low-operating voltage of 2.4 V at 1 cd m⁻² and a high $\eta_{p,max}$ of 71.6 lm W⁻¹. We believe that these results clearly demonstrate the capability of pyridinecarbonitrile derivatives as

TADF emitters, and contribute an effective molecular design for novel TADF emitters. Further study is ongoing in our laboratory.

EXPERIMENTAL SECTION

General Considerations

Quantum chemical calculations were performed using the Gaussian 09 program packages. An optimized structure was calculated at the B3LYP/6-31G(d) level for the ground state. The single-point energies were evaluated in accordance with the time-dependent density functional calculations in B3LYP/6-311 G+(d,p). ^1H NMR and ^{13}C NMR spectra were recorded on a JEOL 400 (400 MHz) spectrometer. Mass spectra were obtained using a Waters SQD2 mass spectrometer with an atmospheric pressure solid analysis probe (ASAP). DSC was performed using a Perkin-Elmer Diamond DSC Pyris instrument under a nitrogen atmosphere at a heating rate of $10^\circ\text{C min}^{-1}$. TGA was undertaken using a SEIKO EXSTAR 6000 TG/DTA 6200 unit under a nitrogen atmosphere at a heating rate of $10^\circ\text{C min}^{-1}$. UV-vis spectra were measured using a Shimadzu UV-3150 UV-vis-NIR spectrophotometer. Photoluminescence spectra were measured using a FluoroMax-2 (Jobin-Yvon-Spex) luminescence spectrometer. I_p was determined by a PYS under vacuum ($=10^{-3}$ Pa). Transient PL decay curves and time-resolved photoluminescence spectra were measured using a streak camera (C4334 from Hamamatsu Photonics) at 5 and 300 K.

Device Fabrication and Characterization

The substrates were cleaned with ultrapurified water and organic solvents (acetone, then isopropanol), and then dry-cleaned for 30 min through exposure to UV-ozone. Organic layers were deposited onto ITO substrates under vacuum ($=10^{-5}$ Pa), successively. LiF and Al were patterned using a shadow mask with an array of $2\text{ mm} \times 2\text{ mm}$ openings without breaking the vacuum ($=10^{-5}$ Pa). The electroluminescent (EL) were taken using an optical multichannel analyzer Hamamatsu Photonics PMA-11. The current density-voltage and luminance-voltage characteristics were measured using a Keithley 2400 source measure unit and a Minolta CS200 luminance meter, respectively.

Syntheses of Materials

Synthesis of 2AcNN

AcPhBpin (1.16 g, 2.8 mmol), 2-chloro-3-pyridinecarbonitrile (0.39 g, 2.8 mmol), and aqueous K_3PO_4 (1.35 M, 7.4 ml) were added to a round bottom flask. 1,4-Dioxane (35 ml) was added, and nitrogen bubbled through the mixture for an hour. Then, $\text{Pd}_2(\text{dba})_3$ (0.13 g, 0.10 mmol) and S-phos (0.06 g, 0.10 mmol) were added, and the resultant mixture was stirred for 14 h at reflux temperature under N_2 flow. The precipitate was filtered and washed with brine, dried over anhydrous MgSO_4 , filtered, and evaporated to dryness. The resulting solid was purified by chromatography on silica gel (eluent: toluene) to afford **2AcNN** (0.74 g, 67%) as a white solid: ^1H NMR (400 MHz, $\text{DMSO}-d_6$): δ = 9.01 (d, J = 5.0 Hz, 1H), 8.51 (d, J = 6.8 Hz, 1H), 8.20 (d, J = 8.2 Hz, 2H), 7.68 (dd, J = 7.9, 4.8 Hz, 1H), 7.59 (d, J = 8.2 Hz, 2H), 7.52 (d, J = 7.2 Hz, 2H), 7.02 (t, J = 7.5 Hz, 2H), 6.94 (t, J =

7.5 Hz, 2H), 6.23 (d, J = 8.2 Hz, 2H), 1.64 (s, 6H); ^{13}C NMR (100 MHz, CDCl_3): δ = 160.11, 152.82, 143.21, 142.04, 140.57, 136.91, 131.72, 131.49, 130.11, 126.44, 125.26, 121.95, 120.79, 117.54, 114.18, 107.56, 35.98, 31.20; MS: m/z = 388 $[\text{M}+1]^+$; Anal calcd for $\text{C}_{27}\text{H}_{21}\text{N}_3$: C, 83.69; H, 5.46; N, 10.84%. Found: C, 83.73; H, 5.38; N, 10.80%.

Synthesis of 2PXZNN

PXZPhBpin (1.28 g, 3.3 mmol), 2-chloro-3-pyridinecarbonitrile (0.48 g, 3.3 mmol), and aqueous K_3PO_4 (1.2 M, 8.7 ml) were added to a round bottom flask. 1,4-Dioxane (42 ml) was added, and nitrogen bubbled through the mixture for an hour. Then, $\text{Pd}_2(\text{dba})_3$ (0.31 g, 0.33 mmol) and S-phos (0.14 g, 0.33 mmol) were added, and the resultant mixture was stirred for 18 h at reflux temperature under N_2 flow. The precipitate was filtered and washed with brine, dried over anhydrous MgSO_4 , filtered, and evaporated to dryness. The resulting solid was purified by chromatography on silica gel (eluent: dichloromethane/hexane = 4:1) to afford **2PXZNN** (0.94 g, 78%) as an orange solid: ^1H NMR (400 MHz, $\text{DMSO}-d_6$): δ = 8.98 (dd, J = 4.8, 1.6 Hz, 1H), 8.49 (dd, J = 7.9, 1.6 Hz, 1H), 8.16 (d, J = 8.6 Hz, 2H), 7.62–7.68 (m, 3H), 6.67–6.78 (m, 6H), 5.91–5.94 (m, 2H) ppm; ^{13}C NMR (100 MHz, CDCl_3): δ = 159.93, 152.84, 143.88, 142.01, 140.90, 137.17, 133.92, 131.68, 131.26, 123.31, 122.03, 121.59, 117.48, 115.53, 113.37, 107.55; MS: m/z = 362 $[\text{M}+1]^+$; Anal calcd for $\text{C}_{24}\text{H}_{15}\text{N}_3\text{O}$: C, 79.76; H, 4.18; N, 11.63; O, 4.43%. Found: C, 79.73; H, 4.35; N, 11.54%.

Synthesis of 5PXZNN

PXZPhBpin (1.28 g, 3.3 mmol), 5-bromo-3-pyridinecarbonitrile (0.606 g, 3.3 mmol), and aqueous K_3PO_4 (1.2 M, 8.7 ml) were added to a round bottom flask. 1,4-Dioxane (42 ml) was added, and nitrogen bubbled through the mixture for an hour. Then, $\text{Pd}_2(\text{dba})_3$ (0.31 g, 0.33 mmol) and S-phos (0.14 g, 0.33 mmol) were added, and the resultant mixture was stirred for 17 h at reflux temperature under N_2 flow. The precipitate was filtered and washed with brine, dried over anhydrous MgSO_4 , filtered, and evaporated to dryness. The resulting solid was purified by chromatography on silica gel (eluent: dichloromethane) to afford **5PXZNN** (0.91 g, 76%) as a yellow solid: ^1H NMR (400 MHz, $\text{DMSO}-d_6$): δ = 9.31 (d, J = 2.3 Hz, 1H), 9.07 (d, J = 1.4 Hz, 1H), 8.77 (t, J = 2.0 Hz, 1H), 8.13 (d, J = 8.6 Hz, 2H), 7.60 (d, J = 8.6 Hz, 2H), 6.65–6.77 (m, 6H), 5.91–5.93 (m, 2H) ppm; ^{13}C NMR (100 MHz, CDCl_3): δ = 151.48, 151.12, 143.91, 140.22, 137.34, 136.00, 135.56, 133.93, 132.12, 129.89, 123.27, 121.71, 116.41, 115.65, 113.16, 110.26; MS: m/z = 362 $[\text{M}+1]^+$; Anal calcd for $\text{C}_{24}\text{H}_{15}\text{N}_3\text{O}$: C, 79.76; H, 4.18; N, 11.63; O, 4.43%. Found: C, 79.71; H, 4.04; N, 11.63%.

AUTHOR CONTRIBUTIONS

HS conceived the project. HS and YM interpreted the data. HS and JK supervised the project. HS, NO, and YM designed the experiments. YM, HA, and NO prepared the samples and performed the data analyses. YM and HA synthesized and characterized the materials. YM and HA performed the quantum chemical calculations. YM and

HS prepared the manuscript and supplementary materials. All authors discussed the results and commented on the manuscript.

ACKNOWLEDGMENTS

We greatly acknowledge the partial financial support from the Center of Innovation (COI) Program from Japan Science and

Technology Agency, JST. HS acknowledges financial support in part by JSPS KAKENHI (17H03131) from JSPS.

SUPPLEMENTARY MATERIAL

The Supplementary Material for this article can be found online at: <https://www.frontiersin.org/articles/10.3389/fchem.2019.00254/full#supplementary-material>

REFERENCES

- Adachi, C. (2014). Third-generation organic electroluminescence materials. *Jpn. J. Appl. Phys.* 53:60101. doi: 10.7567/JJAP.53.060101
- dos Santo, P. L., Ward, J. S., Congrave, D. G., Batsanov, A. S., Eng, J., Stacey, J. E., et al. (2018). Triazatruxene: a rigid central donor unit for a D-A3 thermally activated delayed fluorescence material exhibiting sub-microsecond reverse intersystem crossing and unity quantum yield via multiple singlet-triplet state pairs. *Adv. Sci.* 5:1700989. doi: 10.1002/advs.201700989
- Im, Y., Kim, M., Cho, Y.-J., Seo, J.-A., Yook, K.-S., and Lee, J.-Y. (2017). Molecular design strategy of organic thermally activated delayed fluorescence emitters. *Chem. Mater.* 29, 1946–1963. doi: 10.1021/acs.chemmater.6b05324
- Kaji, H., Suzuki, H., Fukushima, T., Shizu, K., Suzuki, K., Kubo, S., et al. (2015). Purely organic electroluminescent material realizing 100% conversion from electricity to light. *Nat. Commun.* 6:8476. doi: 10.1038/ncomms9476
- Kido, J., Harada, G., Komada, M., Shionoya, H., and Nagai, K. (1997). Aromatic-amine-containing polymers for organic electroluminescent devices. *ACS Symp. Ser.* 672, 381–394. doi: 10.1021/bk-1997-0672.ch025
- Kim, K.-H., and Kim, J.-J. (2018). Origin and control of orientation of phosphorescent and TADF dyes for high-efficiency OLEDs. *Adv. Mater.* 30:1705600. doi: 10.1002/adma.201705600
- Komatsu, R., Sasabe, H., and Kido, J. (2018). Recent progress of pyrimidine derivatives for high-performance organic light-emitting devices. *J. Phon. Ener.* 8:32108. doi: 10.1117/1.JPE.8.032108
- Komatsu, R., Sasabe, H., Seino, Y., Nakao, K., and Kido, J. (2016). Light-blue thermally activated delayed fluorescence emitters realizing a high external quantum efficiency of 25% and unprecedented low drive voltages in OLEDs. *J. Mater. Chem. C* 4, 2274–2278. doi: 10.1039/C5TC04057D
- Lin, T.-A., Chatterjee, T., Tsai, W.-L., Lee, W.-K., Wu, M.-J., Jiao, M., et al. (2016). Sky-blue organic light emitting diode with 37% external quantum efficiency using thermally activated delayed fluorescence from spiroacridine-triazine hybrid. *Adv. Mater.* 28, 6976–6983. doi: 10.1002/adma.201601675
- Liu, M., Komatsu, R., Cai, X., Hotta, K., Sato, S., Liu, K., et al. (2017). Horizontally orientated sticklike emitters: enhancement of intrinsic out-coupling factor and electroluminescence performance. *Chem. Mater.* 29, 8630–8636. doi: 10.1021/acs.chemmater.7b02403
- Liu, W., Zheng, C.-J., Wang, K., Chen, Z., Chen, D.-Y., Li, F., et al. (2015). Novel carbazol-pyridine-carbonitrile derivative as excellent blue thermally activated delayed fluorescence emitter for highly efficient organic light-emitting devices. *ACS Appl. Mater. Interf.* 7, 18930–18936. doi: 10.1021/acsami.5b05648
- Pan, K.-C., Li, S.-W., Ho, Y.-Y., Shiu, Y.-J., Tsai, W.-L., Jiao, M., et al. (2016). Efficient and tunable thermally activated delayed fluorescence emitters having orientation-adjustable CN-substituted pyridine and pyrimidine acceptor units. *Adv. Funct. Mater.* 26, 7560–7571. doi: 10.1002/adfm.201602501
- Rajamalli, P., Senthilkumar, N., Huang, P.-Y., Ren-Wu, C.-C., Lin, H.-W., and Cheng, C.-H. (2017). New molecular design concurrently providing superior pure blue, thermally activated delayed fluorescence and optical out-coupling efficiencies. *J. Am. Chem. Soc.* 139, 10948–10951. doi: 10.1021/jacs.7b03848
- Sasabe, H., Chiba, T., Su, S.-J., Pu, Y.-J., Nakayama, K.-I., and Kido, J. (2008a). 2-Phenylpyrimidine skeleton-based electron-transport materials for extremely efficient green organic light-emitting devices. *Chem. Commun.* 5821–5823. doi: 10.1039/b812270a
- Sasabe, H., Gonmori, E., Chiba, T., Li, Y.-J., Tanaka, D., Su, S.-J., et al. (2008b). Wide-energy-gap electron-transport materials containing 3,5-dipyridylphenyl moieties for an ultra high efficiency blue organic light-emitting device. *Chem. Mater.* 20, 5951–5953. doi: 10.1021/cm801727d
- Sasabe, H., and Kido, J. (2013). Development of high performance OLEDs for general lighting. *J. Mater. Chem. C* 1, 1699–1707. doi: 10.1039/c2tc00584k
- Sasabe, H., Onuma, N., Nagai, Y., Ito, T., and Kido, J. (2017). High power efficiency blue-to-green organic light-emitting diodes using isonicotinonitrile-based fluorescent emitters. *Chem. Asian J.* 12, 648–654. doi: 10.1002/asia.201601641
- Sasabe, H., Sato, R., Suzuki, K., Watanabe, Y., Adachi, C., Kaji, H., et al. (2018). Ultrahigh power efficiency thermally activated delayed fluorescent OLEDs by the strategic use of electron-transport materials. *Adv. Opt. Mater.* 6:1800376. doi: 10.1002/adom.201800376
- Sasabe, H., Tanaka, D., Yokoyama, D., Chiba, T., Pu, Y.-J., Nakayama, K., et al. (2011). Influence of substituted pyridine rings on physical properties and electron mobilities of 2-methylpyrimidine skeleton-based electron transporters. *Adv. Funct. Mater.* 21, 336–342. doi: 10.1002/adfm.201001252
- Seino, Y., Inomata, S., Sasabe, H., Pu, Y.-J., and Kido, J. (2016). High-performance green OLEDs using thermally activated delayed fluorescence with a power efficiency of over 100 lm W⁻¹. *Adv. Mater.* 28, 2638–2643. doi: 10.1002/adma.201503782
- Uoyama, H., Goushi, K., Shizu, K., Nomura, H., and Adachi, C. (2012). Highly efficient organic light-emitting diodes from delayed fluorescence. *Nature* 492, 234–238. doi: 10.1038/nature11687
- Walzer, K., Maennig, B., Pfeiffer, M., and Leo, K. (2007). Highly efficient organic devices based on electrically doped transport layers. *Chem. Rev.* 107, 1233–1271. doi: 10.1021/cr050156n
- Wong, M.-Y., and Z.-Colman, E. (2017). Purely organic thermally activated delayed fluorescence materials for organic light-emitting diodes. *Adv. Mater.* 29:1605444. doi: 10.1002/adma.201605444
- Wu, T.-L., Huang, M.-J., Lin, C.-C., Huang, P.-Y., Chou, T.-Y., Chen-Cheng, R.-W., et al. (2018). Diboron compound-based organic light-emitting diodes with high efficiency and reduced efficiency roll-off. *Nat. Photonics* 12, 235–240. doi: 10.1038/s41566-018-0112-9
- Yang, Z., Mao, Z., Xie, Z., Zhang, Y., Liu, S., Zhao, J., et al. (2017). Recent advances in organic thermally activated delayed fluorescence materials. *Chem. Soc. Rev.* 46, 915–1016. doi: 10.1039/C6CS00368K

Conflict of Interest Statement: The authors declare that the research was conducted in the absence of any commercial or financial relationships that could be construed as a potential conflict of interest.

Copyright © 2019 Masuda, Sasabe, Arai, Onuma and Kido. This is an open-access article distributed under the terms of the Creative Commons Attribution License (CC BY). The use, distribution or reproduction in other forums is permitted, provided the original author(s) and the copyright owner(s) are credited and that the original publication in this journal is cited, in accordance with accepted academic practice. No use, distribution or reproduction is permitted which does not comply with these terms.



Suppressing Efficiency Roll-Off of TADF Based OLEDs by Constructing Emitting Layer With Dual Delayed Fluorescence

Yuewei Zhang¹, Zhiqiang Li¹, Chenglong Li^{1,2*} and Yue Wang^{1*}

¹ State Key Laboratory of Supramolecular Structure and Materials, Jilin University, Changchun, China, ² State Key Laboratory on Integrated Optoelectronics, Key Laboratory of Advanced Gas Sensors, College of Electronic Science and Engineering, Jilin University, Changchun, China

OPEN ACCESS

Edited by:

Lian Duan,
Tsinghua University, China

Reviewed by:

Zuo-Quan Jiang,
Soochow University, China
Albert Moyano,
University of Barcelona, Spain

*Correspondence:

Chenglong Li
chenglongli@jlu.edu.cn
Yue Wang
yuewang@jlu.edu.cn

Specialty section:

This article was submitted to
Organic Chemistry,
a section of the journal
Frontiers in Chemistry

Received: 27 January 2019

Accepted: 15 April 2019

Published: 30 April 2019

Citation:

Zhang Y, Li Z, Li C and Wang Y (2019)
Suppressing Efficiency Roll-Off of
TADF Based OLEDs by Constructing
Emitting Layer With Dual Delayed
Fluorescence. *Front. Chem.* 7:302.
doi: 10.3389/fchem.2019.00302

To suppress efficiency roll-off induced by triplet-triplet annihilation (TTA) and singlet-triplet annihilation (STA) in thermally activated delayed fluorescence (TADF) based organic light emitting diodes (OLEDs) is still a challenge. This issue was efficiently addressed by generating dual delayed fluorescence in the emitting layer of OLEDs. A novel TADF compound, PXZ-CMO, featuring a D-A structure was designed and synthesized. By dispersing the emitter into different hosts, devices G1 (MCP host) and G2 (DPEPO host) with identical configurations were carefully fabricated, which showed similar maximum EQE/CE of 12.1%/38.2 cd A⁻¹ and 11.8%/33.1 cd A⁻¹, respectively. Despite severe efficiency roll-off in device G2 with only 6.4% EQE remaining at a luminance of 1,000 cd m⁻², a remarkably reduced efficiency roll-off was attained in device G1, retaining EQE as high as 10.4% at the same luminance of 1,000 cd m⁻². The excellent device performance with reduced roll-off in device G1 should result from the dual delayed fluorescence in the emitting layer, which possesses great advantages in achieving dynamic and adaptive exciton distribution for radiation acceleration and quench suppression.

Keywords: thermally activated delayed fluorescence, organic light emitting diodes, dual delayed fluorescence, efficiency roll-off, donor-acceptor

INTRODUCTION

Recently, thermally activated delayed fluorescence (TADF) materials based on pure organic aromatic molecules have drawn great attention for their nature to achieve 100% exciton utilization in organic light emitting diodes (OLEDs) (Uoyama et al., 2012; Tao et al., 2014; Zhang et al., 2014a; Kaji et al., 2015; Liu et al., 2015, 2017; Cho et al., 2016; Data et al., 2016; Li et al., 2016; Chen et al., 2017). TADF-OLEDs with high external quantum efficiencies (EQEs) of over 20% have been reported within the visible light spectrum region. However, they still suffer from severe efficiency roll-offs and often exhibited quite low EQEs at a brightness of over 1,000 cd m⁻², which is the required value for the practical application (Wang et al., 2014; Lin et al., 2016; Rajamalli et al., 2016; Huang et al., 2017; Wu et al., 2018; Zeng et al., 2018). For most of TADF emitters this is a great issue, which can induce the increase of power consumption, reduction of device lifetime, and limitation of their extensive applications. For TADF-OLEDs, the electrically generated triplet excitons contribute to emission through reverse intersystem crossing (RISC) process (Figure 1A), which can result in the transformation from triplet (T₁) to singlet (S₁) and sequential single excited state radiation transition.

To accomplish the RISC process, a relatively long time is essential. Therefore, in emitting layer (EML), the accumulation of T_1 excitons is unavoidable, leading to intense T_1 - T_1 annihilation (TTA), and S_1 - T_1 annihilation (STA). The TTA and STA can result in remarkable efficiency roll-off. In principle, the efficiency roll-off can be suppressed by reducing delayed lifetime and concentration of T_1 excitons. It was demonstrated that the TADF emitters with shorter delayed lifetimes displayed relatively smaller efficiency roll-offs (Numata et al., 2015; Lee et al., 2016, 2017). On the other hand, to promote both of phosphorescence and delayed fluorescence in OLEDs could also suppress the efficiency roll-off (Zhang et al., 2016a; Wei et al., 2017; Yu et al., 2017). To dilute the T_1 excitons within an EML, a scheme for establishing the single molecule based dual- or multi- T_1 excited states with different lifetimes and similar emission maxima was proposed (Figure 1B). It is rational to expect a breakthrough in EL performance based on this dual delayed fluorescence mechanism from both S_1 and T_1 states, which theoretically possesses great advantages in achieving dynamic and adaptive exciton distribution for radiation acceleration and quench suppression. However, so far, the construction of TADF systems with dual- or multi- T_1 excited states still remains a great challenge.

To achieve TADF, the excited states generally have intramolecular-charge-transfer (ICT) characteristic and the molecules are composed of spatially separated donor (D) and acceptor (A) moieties. Upon transformation from ground state to excited state, the molecules undergo internal electron transfer from D to A, which is usually accompanied by molecular conformation change resulting a new dipolar state to stabilize the excited state. It was demonstrated that the above process could be dominated by the environment polarity when the TADF molecules were doped in some matrixes (Grabowski et al., 2003; Aydemir et al., 2015, 2017; Data et al., 2016). Upon a kind of TADF molecules are doped into a host, the molecules may exist under different polarity and rigidity circumstances, which can induce different excited states. Additionally, the D-A type molecules containing pseudo-planar fragments, such as xanthone (XO), 9,9-dimethyl-9,10-dihydroacridine (DMAC), and phenoxazine (PXZ), have the potential to adopt different molecular configurations (Zhang et al., 2016b, 2017; Wang et al., 2017). Therefore, by dispersing the emitters in suitable hosts with distinct polarity and steric hindrance, dual- or multi- T_1 excited states may be generated from one kind of TADF molecules (Méhes et al., 2014; Zhang et al., 2014b). To evaluate our hypothesis, 4H-chromen-4-one (CMO) and phenoxazine (PXZ) were selected as the electron A and D moieties, respectively, to construct a target TADF molecule PXZ-CMO (Figure 2A). 1,3-bis(carbazol-9-yl)benzene (MCP) with weak polarity and bis(2-(diphenylphosphino)phenyl)ether oxide (DPEPO) with strong polarity were employed as the hosts to prepare the emitting layer of OLEDs, respectively (Lee et al., 2014). In this contribution, we successfully develop an effective strategy to reduce the efficiency roll-off of TADF-OLEDs based on the dual delayed fluorescence in the emitting layer.

RESULTS AND DISCUSSION

Synthesis, Crystal and Photophysical Properties

A TADF emitter 6-(10H-phenoxazin-10-yl)-4H-chromen-4-one, namely PXZ-CMO, was synthesized via Buchwald-Hartwig cross coupling between 6-bromo-4H-chromen-4-one and PXZ with high yields (Scheme S1) (Wolfe et al., 1998; Littke et al., 2002; Hooper et al., 2003; Fu, 2008). The single-crystal X-ray diffraction analyses demonstrated that both the PXZ and CMO moieties adopt perfect planar π -conjugated structure feature. The D and A planes are linked together by a single bond, which is beneficial to the regulation of molecular conformation. The crystal is generated based on moderate intermolecular $\pi\cdots\pi$ stacking interactions (acceptor \cdots acceptor contacts) accompanied by noncovalent bonds such as C-H \cdots O, O=C \cdots H-C, and C-H $\cdots\pi$ interactions (Figures 2C,D), which can enhance the charge transfer ability (Wang et al., 2013). Since the highly twisted structure with large dihedral angle of 83° between D and A planes, the highest occupied molecular orbital (HOMO) and the lowest unoccupied molecular orbital (LUMO) of PXZ-CMO are mainly localized on the D and A moieties (Figure 2B and Figure S1), respectively. Therefore, the energy gap (ΔE_{ST}) between the lowest singlet excited state (S_1) and triplet excited state (T_1) is as small as 0.02 eV, which was calculated based on spectroscopic data in Figure S2. Obviously, the ΔE_{ST} value is small enough to promote the reverse intersystem crossing (RISC) from T_1 to S_1 (Yang et al., 2017).

The UV-vis absorption and emission spectra of PXZ-CMO in various solvents with different polarity were shown in Figure S3 and the photophysical data were summarized in Table S1. The strong absorption band at around 310 nm can be attributed to the π - π^* transition of the PXZ, and the other weak and broad absorption band at longer wavelengths from 345 to 420 nm can be assigned to the ICT absorption from D (PXZ) to A (CMO). PXZ-CMO emission spectra displayed a significant solvatochromic phenomenon and the emission maxima displayed red-shift from 398 nm in toluene to 524 nm in dichloromethane. The largely solvatochromic red-shift indicated a typical ICT feature of PXZ-CMO, suggesting a large change of dipole moment in the electronically excited state (Guo et al., 2014; Wang et al., 2015; Li et al., 2017). Moreover, emissions that originated from local excited (LE) states could also be observed in toluene and THF solutions, which further demonstrated a weak electronic coupling between PXZ and CMO units. The transient PL decays for PXZ-CMO were measured in dilute solutions under nitrogen atmosphere (Figure S4). Unlike the behavior of conventional TADF molecules, its long-lived TADF emission was completely quenched by non-radiative decay in solution and only the prompt components with nanosecond-scale lifetimes were observed (Zhang et al., 2012, 2014c). In solid state, PXZ-CMO displayed a prompt lifetime of 93 ns and a delayed lifetime of 1.6 μ s (Figure S5). The PXZ-CMO solid exhibited photoluminescence quantum yield (PLQY) of 27.6% and emission maximum of 518 nm (Table S1 and Figure S6). Thermogravimetric analysis (TGA) and differential scanning calorimetry (DSC) measurements revealed that PXZ-CMO

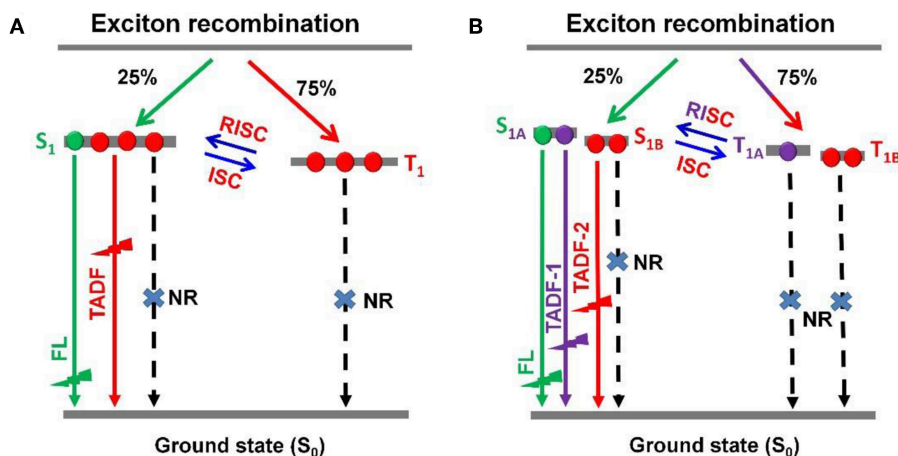


FIGURE 1 | Schematic representations of RISC processes of emitters with (A) single delayed excited state and (B) dual delayed excited states.

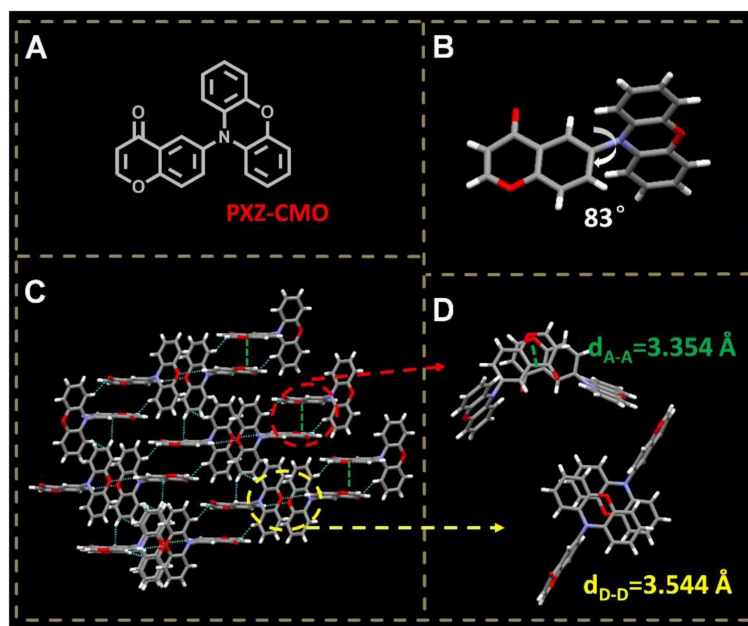


FIGURE 2 | (A) Molecular structure of PXZ-CMO. (B) Single crystal structure of PXZ-CMO: twisted molecular structure. (C,D) Intermolecular interactions and molecular packing mode.

possessed a good thermal stability with a thermal decomposition temperature (T_{d5} , corresponding to 5% weight loss) of 261°C and a melting point (T_m) of 187°C (Figure S7). The HOMO (-5.95 eV) and LUMO (-3.35 eV) energy levels of PXZ-CMO were obtained from the onsets of the oxidation and reduction curves (Figure S8).

Electroluminescence Performance

To evaluate the electroluminescent (EL) performance of PXZ-CMO, we fabricated multi-layer OLEDs with a structure of [ITO/HATCN (5 nm)/NPB (60 nm)/MCP (5 nm)/EML (30 nm)/TSPO1 (5 nm)/TPBi (30 nm)/LiF (0.5 nm)/Al (150 nm)]

(Figure 3). ITO (indium-tin oxide) and LiF/Al (lithium fluoride/aluminum) were used as anode and cathode, respectively. HATCN (1,4,5,8,9,11-hexaazatriphenylene hexacarbonitrile), NPB (1,4-bis[(1-naphthylphenyl)amino]-biphenyl), and TPBi (1,3,5-tris[(N-phenylbenzimidazol-2-yl)benzene]) were selected as hole-injection (HIL), hole-transporting (HTL) and electron-transporting layers (ETL), respectively. MCP ($T_1 = 2.90\text{ eV}$) and TSPO1 (diphenyl-4-triphenylsilylphenyl-phosphine oxide with high T_1 (3.36 eV)) were acted as the exciton-blocking layers (Kim and Lee, 2014). The doped thin films of PXZ-MCO (dopant) in solid hosts of MCP or DPEPO ($T_1 = 3.10\text{ eV}$) with different dopant

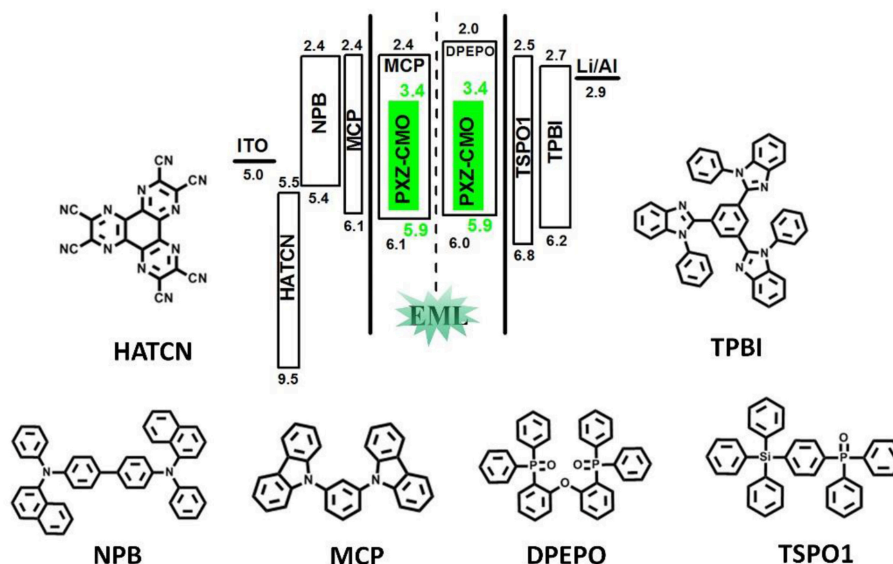


FIGURE 3 | The energy-level diagram of the four devices and chemical structures of the used materials.

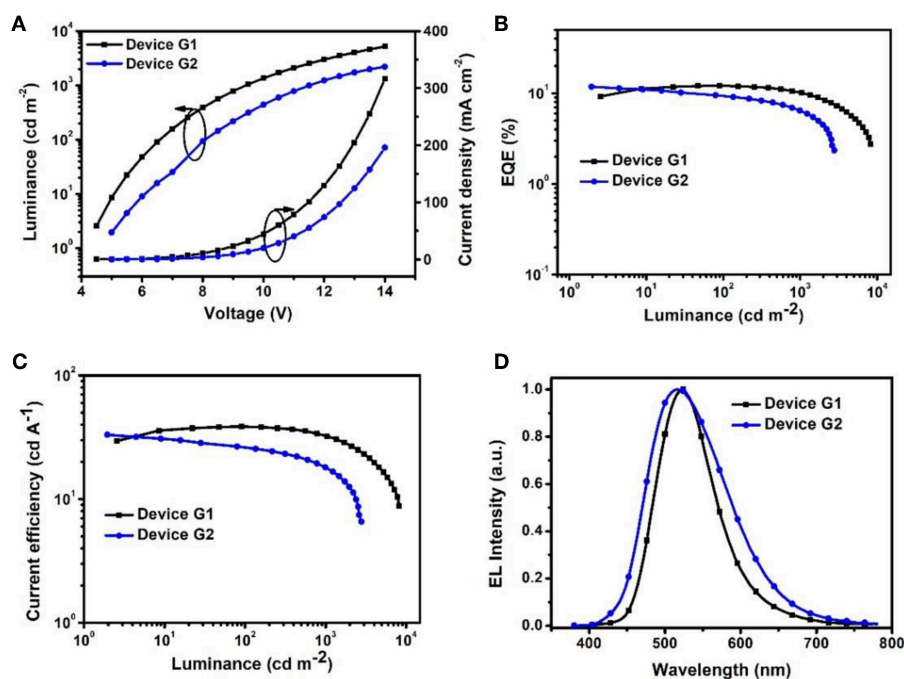


FIGURE 4 | (A) Current density–voltage–luminance ($J-V-L$). (B) EQE vs. luminance curves. (C) Current efficiency vs. luminance curves. (D) EL spectra measured at 10 mA cm^{-2} .

concentrations from 5 to 30 wt% were employed as the emitting layers (EMLs). **Table 1** presents the key EL parameters of PXZ-CMO based OLEDs with various dopant concentrations (5, 15, 25 wt% PXZ-CMO doped in MCP and 10, 15, 20, 30 wt% PXZ-CMO doped in DPEPO). Obviously, the DPEPO-based devices all showed more severe efficiency roll-offs than that of the MCP-based ones. When 15 and 20 wt% dopant

concentrations were employed, the MCP- and DPEPO-based devices displayed the best performances with the highest external quantum efficiencies (EQEs) of 12.1 and 11.8%, respectively. The photoluminescence quantum yields (PLQYs) of film A (15 wt% PXZ-CMO:MCP) and film B (20 wt% PXZ-CMO:DPEPO) were 48.7% and 35.0% (**Table S1**), respectively. Thus, almost all T_1 excitons were up-converted into S_1 excitons and utilized

TABLE 1 | Summary of the EL data of OLEDs based on PXZ-CMO doped in MCP/DPEPO with different doping concentrations.

Device	$V_{\text{turn-on}}$ (V) ^a	L_{max} /cd m ⁻² (V at L_{max})	CE^b /cd A ⁻¹	EQE^b /%	Roll-offs ^c /%	EL λ_{max} /nm, CIE (x, y) ^d
5 wt% PXZ-CMO:MCP	4.0	6,968 (16.5)	28.63/24.13	10.20/10.20/8.40	17.65	504 (0.26, 0.51)
15 wt% PXZ-CMO:MCP	4.5	8,214 (16.5)	38.20/32.70	12.10/12.10/10.40	10.05	524 (0.28, 0.55)
25 wt% PXZ-CMO:MCP	5.0	7,475 (16.0)	29.90/27.71	9.79/9.75/9.10	7.05	516 (0.29, 0.56)
10 wt% PXZ-CMO:DPEPO	5.0	2,606 (15.0)	27.48/17.78	10.37/8.20/5.87	43.39	524 (0.28, 0.54)
15 wt% PXZ-CMO:DPEPO	4.9	2,685 (15.0)	29.04/15.12	10.77/9.20/5.37	50.14	516 (0.31, 0.48)
20 wt% PXZ-CMO:DPEPO	5.0	2,780 (16.0)	33.10/18.10	11.80/6.40	45.76	517 (0.30, 0.48)
30 wt% PXZ-CMO:DPEPO	5.1	2,494 (16.0)	32.42/17.95	11.43/6.33	44.62	516 (0.30, 0.48)

^aObtained at 1 cd m⁻².
^bMaximum efficiencies/efficiencies at 100 cd m⁻²/efficiencies at 1,000 cd m⁻².
^cEQE roll-offs at 1,000 cd m⁻².
^dRecorded at 10 mA cm⁻².

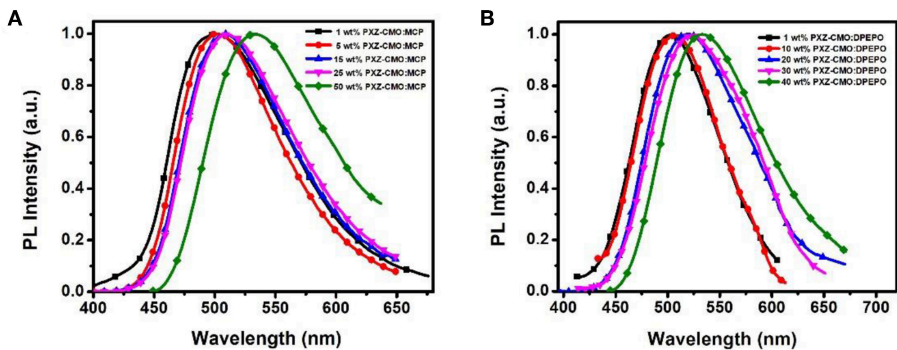


FIGURE 5 | The normalized PL spectra of films based on PXZ-CMO doped in (A) MCP and (B) DPEPO with different doping concentrations.

for electroluminescence, resulting in high EQEs. The finally optimized EMLs are 15 wt% PXZ-CMO:MCP (Device G1) and 20 wt% PXZ-CMO:DPEPO (Device G2). The current density–voltage–luminance (J – V – L), EQE–luminance (EQE – L), current efficiency–luminance (CE – L) characteristics, and EL spectra of devices G1 and G2 were present in **Figure 4**. Devices G1 and G2 exhibited emission maxima at 524 and 517 nm with corresponding Commission Internationale de l’Eclairage (CIE) color coordinates of (0.28, 0.55) and (0.30, 0.48), respectively (**Figure 3D**). Additionally, the EL spectra demonstrated negligible change with increasing driving voltages (**Figure S9**). Devices G1 and G2 showed comparable highest EQE values, however, the efficiency roll-off of device G1 was remarkably small compared with that of device G2. Under a high luminance of 1,000 cd m⁻², G1 maintained its EQE at 10.4%, while the EQE of G2 reduced to 6.4%.

Carrier Transport and Transient PL Spectra Properties

Firstly, we evaluate the carrier transport properties of PXZ-CMO doped in MCP and DPEPO. The single-carrier devices with the structures of [ITO/NPB (10 nm)/15% PXZ-CMO:MCP or 20% PXZ-CMO:DPEPO (80 nm)/NPB (10 nm)/Al (100 nm)] for the hole-only device and [ITO/TPBI (10 nm)/15% PXZ-CMO:MCP or 20% PXZ-CMO:DPEPO (80 nm)/TPBI (10 nm)/LiF (1 nm)/Al

(100 nm)] for the electron-only device were fabricated. The NPB and TPBI layers are used to prevent the electron and hole injection from the cathode and anode, respectively. As depicted in **Figure S10**, both hole and electron current density of 15% PXZ-CMO:MCP are higher than that of 20% PXZ-CMO:DPEPO at the same driving voltage, suggesting better ability for conducting both electrons and holes. However, both two doped films exhibit balanced carrier transport property, indicating that the different efficiency roll-off behaviors of devices G1 and G2 should not be attributed to be the difference of the carrier transport. To further understand the reasons of the different efficiency roll-off behaviors of devices G1 and G2, detail photophysical investigations of PXZ-CMO:MCP and PXZ-CMO:DPEPO doped films were performed and detailed data were summarized in **Table S2**. As shown in **Figures 5, 6**, the delayed PL emissions all presented similar spectral distributions as that of the prompt PL emissions, implying that the delayed and prompt fluorescence of these films originated from the same emissive singlet states (Kim et al., 2018). Upon fitting the transient PL decays of PXZ-CMO:MCP doped films, a clear third-order exponential decay could be found, revealing the presence of two delayed fluorescence processes with characteristic time constants of around 1.1 and 9.1 μ s, respectively. Moreover, for PXZ-CMO:MCP films, the integral ration of the relatively shorter delayed lifetime

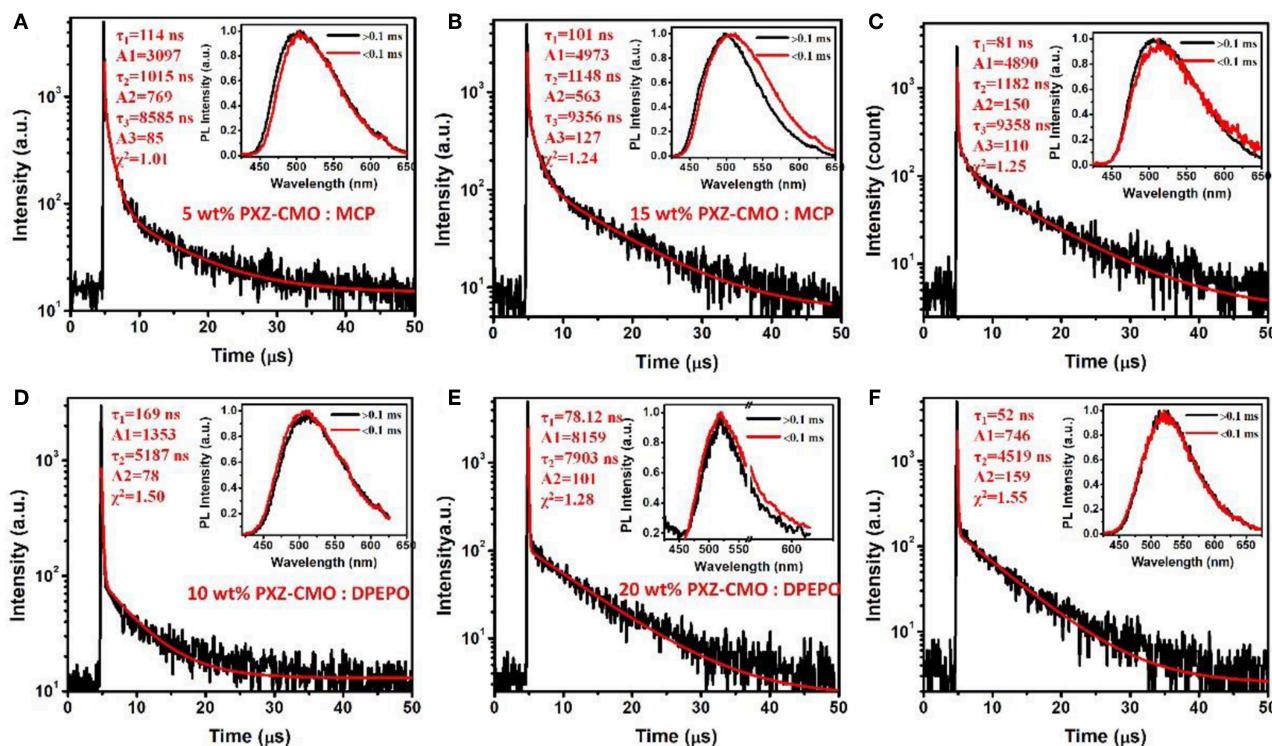


FIGURE 6 | Transient decay spectra of films: **(A)** 5 wt% PXZ-CMO:MCP, **(B)** 5 wt% PXZ-CMO:MCP, **(C)** 25 wt% PXZ-CMO:MCP, **(D)** 10 wt% PXZ-CMO:DPEPO, **(E)** 20 wt% PXZ-CMO:DPEPO, and **(F)** 30 wt% PXZ-CMO:DPEPO at 300 K. Red curves are three or double exponential fitting data. Inset: Emission spectra of TADF components measured by HORIBA Scientific FluoroMax-4 spectrofluorometer.

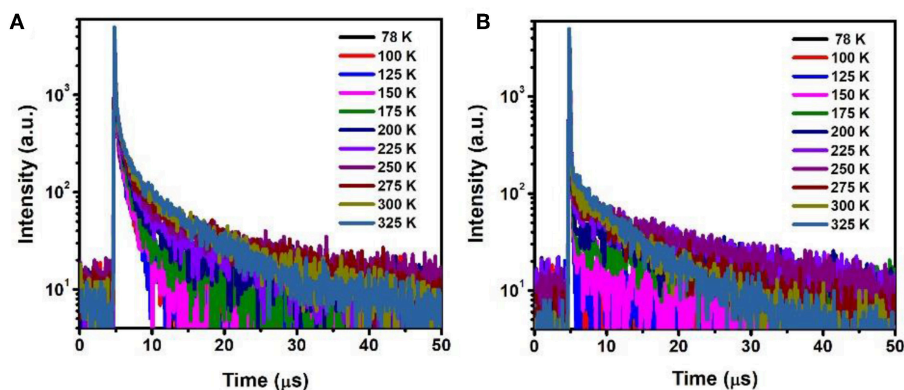


FIGURE 7 | Temperature dependence of time decay characteristics for **(A)** film A and **(B)** film B in the range of 78–325 K.

remarkably decreased and the longer delayed lifetime showed a reverse tendency with increasing the doped concentration. While the PXZ-CMO:DPEPO doped films showed only one delayed lifetime (around 6.5 μ s), testifying the typical TADF feature with a single delayed fluorescence process. In films with the doped concentration of over 5 wt%, the PXZ-CMO molecules should not adopt mono-dispersed state and assemble into small aggregates, which could be proved by the obvious spectral redshift of the green emission in both MCP- and DPEPO-based

films as the doping concentration is increased (**Figure 5**). Since MCP is a weakly polar host, DPEPO is a strongly polar host, and the polarity of PXZ-CMO molecule with D-A structural feature is also very strong. Therefore, from the perspective of polarity, PXZ-CMO and DPEPO are similar with each other, while PXZ-CMO and MCP are different. For the PXZ-CMO aggregates within MCP matrix, the PXZ-CMO molecules should be in strong polarity environment (the inside of aggregates) or weak polarity environment (the surface of aggregates). The

different polarity environment can not only induce different excited state characteristics (two kinds of delayed lifetimes in MCP-based films), but also increase the distance between these two T_1 states to prevent the TTA process, which occurs by a diffusion-limited, short-range electron exchange process (Dexter mechanism) (O'Brien et al., 2009). Differently, in PXZ-CMO:DPEPO doped films, both the dopant and host molecules possess strong polarity, therefore only one delayed lifetime was observed, similar to the PXZ-CMO solids. In addition, the singlet CT state in a polar matrix of DPEPO will be more stabilized than that of MCP, resulting in a theoretically smaller ΔE_{ST} values as well as faster RISC rates (shorter TADF lifetimes) in DPEPO-based films. However, according to the formula $\tau_{av} = \sum A_i \tau_i^2 / \sum A_i \tau_i$ (Zhang et al., 2014c), the average lifetime of film A (6.5 μ s) is actually similar to that of PXZ-CMO:DPEPO doped films (5.2–7.9 μ s) at 300 K. This phenomenon indicates that not only the polarity of the host but also some potential interactions (such as π - π interactions) between the emitter and the host affect the RISC rate (Cai et al., 2017), because MCP has the potential π - π interaction groups of carbazole, while DPEPO doesn't. Thus, the dual delayed fluorescence in the MCP-based films played an important role in realizing the slow efficiency roll-offs.

The temperature dependent photophysical properties of doped films A (15 wt% PXZ-CMO:MCP) and B (20 wt% PXZ-CMO:DPEPO) were presented in **Figure 7** and **Tables S3, S4**. Within the temperature region from 78 to 325 K, film A displayed two delayed fluorescence lifetimes at around 1.0 (τ_{d1}) μ s and 5.0–12.0 (τ_{d2}) μ s, respectively. The integral ratio of the longer τ_{d2} gradually improved upon temperature increasing, suggesting a typical TADF feature (Uoyama et al., 2012; Kaji et al., 2015). For the shorter τ_{d1} , the integral ratio displayed slight improvement upon temperature increasing from 78 to 175 K and then obviously decreased upon temperature increasing from 175 to 325 K. Therefore, it is possible that certain conformation transformation mechanism may be included in the emission spectra of film A at high temperature region (above 200 K). In particular, it still exhibited two delayed lifetimes at 77 K, which further suggested the presence of two T_1 excited states of film A (**Table S3**). For film B, the delayed fluorescence was observed when the temperature was improved to 200 K and the delayed lifetime exhibited successive decrease tendency. Therefore, in DPEPO matrix, the triple excited state of PXZ-CMO may be easily quenched and the TADF behavior was only observed at relatively high temperature, which can provide enough energy to promote the RISC process. Thus, for device G1, the existence of dual delayed fluorescence makes it possible to decrease the concentrations of every kind of T_1 excited state and suppress

the TTA processes to realize an extremely low efficiency roll-off in TADF-OLED. In addition, the delayed lifetimes (τ_d) began to decrease when the dopant concentration ≥ 30 wt% in both MCP- and DPEPO-based films (**Figure S11**), which could be attributed to that the TTA induced excited state quenching is stronger in the high dopant concentration films. To further verify the molecular structure of PXZ-CMO, 1H and ^{13}C NMR spectroscopies were measured (**Figures S12, S13**).

CONCLUSION

In summary, a TADF compound PXZ-CMO featuring a D-A structure was designed and synthesized. The PXZ-CMO:MCP doped films displayed two delayed fluorescence lifetimes at around 1.1 and 9.1 μ s, respectively. The PXZ-CMO:MCP films were employed as emitting layer to fabricate high performance TADF-OLEDs that exhibited low efficiency roll-offs. The MCP matrix with weak polarity can promote the generation of dual delayed fluorescence for PXZ-CMO molecules. The achievement of dual delayed fluorescence can dilute the concentration of T_1 excited states and suppress the TTA processes in the emitting layer, which is beneficial to the reduction of efficiency roll-off. Therefore, this study provided an efficient approach to achieve the high-efficiency TADF-OLEDs with low efficiency roll-offs.

AUTHOR CONTRIBUTIONS

YZ, CL, and YW proposed the idea of this manuscript and analyzed the experiment results. YZ and ZL contributed to the synthesis of the materials and the fabrication of the OLEDs. YW wrote the paper.

FUNDING

This work was supported by the National Basic Research Program of China (2015CB655003), the National Natural Science Foundation of China (91333201 and 51803069), China Postdoctoral Science Foundation (2018M630319 and 2018T110244), Program for JLU Science and Technology Innovative Research Team and Jilin Province-University Program (SXGJSF2017-3).

SUPPLEMENTARY MATERIAL

The Supplementary Material for this article can be found online at: <https://www.frontiersin.org/articles/10.3389/fchem.2019.00302/full#supplementary-material>

REFERENCES

- Aydemir, M., Haykir, G., Türksoy, F., Gümüş, S., Dias, F. B., and Monkman, A. P. (2015). Synthesis and investigation of intra-molecular charge transfer state properties of novel donor-acceptor-donor pyridine derivatives: the effects of temperature and environment on molecular configurations and the origin of delayed fluorescence. *Phys. Chem. Chem. Phys.* 17, 25572–25582. doi: 10.1039/C5CP03937A
- Aydemir, M., Xu, S., Chen, C., Bryce, M. R., Chi, Z., and Monkman, A. P. (2017). Photophysics of an asymmetric donor-acceptor-donor' TADF molecule and reinterpretation of aggregation-induced TADF emission in these materials. *J. Phys. Chem. C* 121, 17764–17772. doi: 10.1021/acs.jpcc.7b06299
- Cai, M., Song, X., Zhang, D., Qiao, J., and Duan, L. (2017). π - π stacking: a strategy to improve the electron mobilities of bipolar hosts for TADF and phosphorescent devices with low efficiency roll-off. *J. Mater. Chem. C* 5, 3372–3381. doi: 10.1039/C7TC00733G

- Chen, J.-X., Liu, W., Zheng, C.-J., Wang, K., Liang, K., Shi, Y.-Z., et al. (2017). Coumarin-Based thermally activated delayed fluorescence emitters with high external quantum efficiency and low efficiency roll-off in the devices. *ACS Appl. Mater. Interfaces* 9, 8848–8854. doi: 10.1021/acsami.6b15816
- Cho, Y. J., Jeon, S. K., and Lee, J. Y. (2016). Molecular engineering of high efficiency and long lifetime blue thermally activated delayed fluorescent emitters for vacuum and solution processed organic light emitting diodes. *Adv. Optical Mater.* 4, 688–693. doi: 10.1002/adom.201500634
- Data, P., Pander, P., Okazaki, M., Takeda, Y., Minakata, S., and Monkman, A. P. (2016). Dibenzo[a,j]phenazine-cored donor-acceptor-donor compounds as green-to-red/NIR thermally activated delayed fluorescence organic light emitters. *Angew. Chem. Int. Ed.* 55, 5739–5744. doi: 10.1002/anie.201600113
- Fu, G. C. (2008). The development of versatile methods for palladium-catalyzed coupling reactions of aryl electrophiles through the use of P(t-Bu)₃ and PCy₃ as ligands. *Acc. Chem. Res.* 41, 1555–1564. doi: 10.1021/ar800148f
- Grabowski, Z. R., Rotkiewicz, K., and Rettig, W. (2003). Structural changes accompanying intramolecular electron transfer: focus on twisted intramolecular charge-transfer states and structures. *Chem. Rev.* 103, 3899–4032. doi: 10.1021/cr940745l
- Guo, Z.-H., Jin, Z.-X., Wang, J.-Y., and Pei, J. (2014). A donor-acceptor-donor conjugated molecule: twist intramolecular charge transfer and piezochromic luminescent properties. *Chem. Commun.* 50, 6088–6090. doi: 10.1039/c3cc48980a
- Hooper, M. W., Utsunomiya, M., and Hartwig, J. F. (2003). Scope and mechanism of palladium-catalyzed amination of five-membered heterocyclic halides. *J. Org. Chem.* 68, 2861–2873. doi: 10.1021/jo0266339
- Huang, J., Nie, H., Zeng, J., Zhuang, Z., Gan, S., Cai, Y., et al. (2017). Highly efficient nondoped OLEDs with negligible efficiency roll-off fabricated from aggregation-induced delayed fluorescence luminogens. *Angew. Chem. Int. Ed.* 56, 12971–12976. doi: 10.1002/anie.201706752
- Kaji, H., Suzuki, H., Fukushima, T., Shizu, K., Suzuki, K., Kubo, S., et al. (2015). Purely organic electroluminescent material realizing 100% conversion from electricity to light. *Nat. Commun.* 6:8476. doi: 10.1038/ncomms9476
- Kim, B. S., and Lee, J. Y. (2014). Phosphine oxide type bipolar host material for high quantum efficiency in thermally activated delayed fluorescent device. *ACS Appl. Mater. Interfaces* 6, 8396–8400. doi: 10.1021/am501301g
- Kim, D.-H., D'Aléo, A., Chen, X.-K., Sandanayaka, A. D. S., Yao, D., Zhao, L., et al. (2018). High-efficiency electroluminescence and amplified spontaneous emission from a thermally activated delayed fluorescent near-infrared emitter. *Nat. Photonics* 12, 98–104. doi: 10.1038/s41566-017-0087-y
- Lee, D. R., Choi, J. M., Lee, C. W., and Lee, J. Y. (2016). Ideal molecular design of blue thermally activated delayed fluorescent emitter for high efficiency, small singlet-triplet energy splitting, low efficiency roll-off, and long lifetime. *ACS Appl. Mater. Interfaces* 8, 23190–23196. doi: 10.1021/acsami.6b05877
- Lee, J., Aizawa, N., and Yasuda, T. (2017). Isobenzofuranone- and chromone-based blue delayed fluorescence emitters with low efficiency roll-off in organic light-emitting diodes. *Chem. Mater.* 29, 8012–8020. doi: 10.1021/acs.chemmater.7b03371
- Lee, S. Y., Yasuda, T., Yang, Y. S., Zhang, Q., and Adachi, C. (2014). Luminous butterflies: efficient exciton harvesting by benzophenone derivatives for full-color delayed fluorescence OLEDs. *Angew. Chem. Int. Ed.* 53, 6402–6406. doi: 10.1002/anie.201402992
- Li, C., Duan, R., Liang, B., Han, G., Wang, S., Ye, K., et al. (2017). Deep-red to near-infrared thermally activated delayed fluorescence in organic solid films and electroluminescent devices. *Angew. Chem. Int. Ed.* 56, 11525–11529. doi: 10.1002/anie.201706464
- Li, Y., Li, X.-L., Chen, D., Cai, X., Xie, G., He, Z., et al. (2016). Design strategy of blue and yellow thermally activated delayed fluorescence emitters and their all-fluorescence white OLEDs with external quantum efficiency beyond 20%. *Adv. Funct. Mater.* 26, 6904–6912. doi: 10.1002/adfm.201602507
- Lin, T.-A., Chatterjee, T., Tsai, W.-L., Lee, W.-K., Wu, M.-J., Jiao, M., et al. (2016). Sky-blue organic light emitting diode with 37% external quantum efficiency using thermally activated delayed fluorescence from spiroacridine-triazine hybrid. *Adv. Mater.* 28, 6976–6983. doi: 10.1002/adma.201601675
- Littke, A. F., Schwarz, L., and Fu, G. C. (2002). Pd/P(t-Bu)₃: a mild and general catalyst for stille reactions of aryl chlorides and aryl bromides. *J. Am. Chem. Soc.* 124, 6343–6348. doi: 10.1021/ja020012f
- Liu, M., Komatsu, R., Cai, X., Sasabe, H., Kamata, T., Nakao, K., et al. (2017). Introduction of twisted backbone: a new strategy to achieve efficient blue fluorescence emitter with delayed emission. *Adv. Optical Mater.* 5:1700334. doi: 10.1002/adom.201700334
- Liu, X.-K., Chen, Z., Zheng, C.-J., Liu, C.-L., Lee, C.-S., Li, F., et al. (2015). Prediction and design of efficient exciplex emitters for high-efficiency, thermally activated delayed-fluorescence organic light-emitting diodes. *Adv. Mater.* 27, 2378–2383. doi: 10.1002/adma.201405062
- Méhes, G., Goushi, K., Potscavage, W. J., and Adachi, C. (2014). Influence of host matrix on thermally-activated delayed fluorescence: effects on emission lifetime, photoluminescence quantum yield, and device performance. *Org. Electron.* 15, 2027–2037. doi: 10.1016/j.orgel.2014.05.027
- Numata, M., Yasuda, T., and Adachi, C. (2015). High efficiency pure blue thermally activated delayed fluorescence molecules having 10H-phenoxaborin and acridan units. *Chem. Commun.* 51, 9443–9446. doi: 10.1039/C5CC00307E
- O'Brien, J. A., Rallabandi, S., Tripathy, U., Paige, M. F., and Steer, R. P. (2009). Efficient S2 state production in ZnTPP-PMMA thin films by triplet-triplet annihilation: Evidence of solute aggregation in photon upconversion systems. *Chem. Phys. Lett.* 475, 220–222. doi: 10.1016/j.cplett.2009.05.039
- Rajamalli, P., Senthilkumar, N., Gandeepan, P., Huang, P.-Y., Huang, M.-J., Ren-Wu, C.-Z., et al. (2016). A new molecular design based on thermally activated delayed fluorescence for highly efficient organic light emitting diodes. *J. Am. Chem. Soc.* 138, 628–634. doi: 10.1021/jacs.5b10950
- Tao, Y., Yuan, K., Chen, T., Xu, P., Li, H., Chen, R., et al. (2014). Thermally activated delayed fluorescence materials towards the breakthrough of organoelectronics. *Adv. Mater.* 26, 7931–7958. doi: 10.1002/adma.201402532
- Uoyama, H., Goushi, K., Shizu, K., Nomura, H., and Adachi, C. (2012). Highly efficient organic light-emitting diodes from delayed fluorescence. *Nature* 492, 234–238. doi: 10.1038/nature11687
- Wang, H., Xie, L., Peng, Q., Meng, L., Wang, Y., Yi, Y., et al. (2014). Novel thermally activated delayed fluorescence materials-thioxanthone derivatives and their applications for highly efficient OLEDs. *Adv. Mater.* 26, 5198–5204. doi: 10.1002/adma.201401393
- Wang, K., Zhao, F., Wang, C., Chen, S., Chen, D., Zhang, H., et al. (2013). High-performance red, green, and blue electroluminescent devices based on blue emitters with small singlet-triplet splitting and ambipolar transport property. *Adv. Funct. Mater.* 23, 2672–2680. doi: 10.1002/adfm.201202981
- Wang, K., Zheng, C.-J., Liu, W., Liang, K., Shi, Y.-Z., Tao, S.-L., et al. (2017). Avoiding energy loss on TADF emitters: controlling the dual conformations of D-A structure molecules based on the pseudoplanar segments. *Adv. Mater.* 29:1701476. doi: 10.1002/adma.201701476
- Wang, S., Yan, X., Cheng, Z., Zhang, H., Liu, Y., and Wang, Y. (2015). Highly efficient near-infrared delayed fluorescence organic light emitting diodes using a phenanthrene-based charge-transfer compound. *Angew. Chem. Int. Ed.* 54, 13068–13072. doi: 10.1002/anie.201506687
- Wei, X., Chen, Y., Duan, R., Liu, J., Wang, R., Liu, Y., et al. (2017). Triplet decay-induced negative temperature dependence of the transient photoluminescence decay of thermally activated delayed fluorescence emitter. *J. Mater. Chem. C* 5, 12077–12084. doi: 10.1039/C7TC04025C
- Wolfe, J. P., Wagaw, S., Marcoux, J.-F., and Buchwald, S. L. (1998). Rational development of practical catalysts for aromatic carbon-nitrogen bond formation. *Acc. Chem. Res.* 31, 805–818. doi: 10.1021/ar9600650
- Wu, T.-L., Huang, M.-J., Lin, C.-C., Huang, P.-Y., Chou, T.-Y., Chen-Cheng, R.-W., et al. (2018). Diboron compound-based organic light-emitting diodes with high efficiency and reduced efficiency roll-off. *Nat. Photonics* 12, 235–240. doi: 10.1038/s41566-018-0112-9
- Yang, Z., Mao, Z., Xie, Z., Zhang, Y., Liu, S., Zhao, J., et al. (2017). Recent advances in organic thermally activated delayed fluorescence materials. *Chem. Soc. Rev.* 46, 915–1016. doi: 10.1039/C6CS00368K
- Yu, L., Wu, Z., Zhong, C., Xie, G., Zhu, Z., Ma, D., et al. (2017). Pure organic emitter with simultaneous thermally activated delayed fluorescence and room-temperature phosphorescence: thermal-controlled triplet recycling channels. *Adv. Optical Mater.* 5:1700588. doi: 10.1002/adom.201700588
- Zeng, W., Lai, H.-Y., Lee, W.-K., Jiao, M., Shiu, Y.-J., Zhong, C., et al. (2018). Achieving nearly 30% external quantum efficiency for orange-red organic light emitting diodes by employing thermally activated delayed fluorescence emitters

- composed of 1,8-naphthalimide-acridine hybrids. *Adv. Mater.* 30:1704961. doi: 10.1002/adma.201704961
- Zhang, D., Duan, L., Li, C., Li, Y., Li, H., Zhang, D., et al. (2014a). High-efficiency fluorescent organic light-emitting devices using sensitizing hosts with a small singlet-triplet exchange energy. *Adv. Mater.* 26, 5050–5055. doi: 10.1002/adma.201401476
- Zhang, J., Duan, C., Han, C., Yang, H., Wei, Y., and Xu, H. (2016a). Balanced dual emissions from tridentate phosphine-coordinate copper(i) complexes toward highly efficient yellow OLEDs. *Adv. Mater.* 28, 5975–5979. doi: 10.1002/adma.201600487
- Zhang, Q., Kuwabara, H., Potscavage, W. J., Huang, S., Hatae, Y., Shibata, T., et al. (2014b). Anthraquinone-based intramolecular charge-transfer compounds: computational molecular design, thermally activated delayed fluorescence, and highly efficient red electroluminescence. *J. Am. Chem. Soc.* 136, 18070–18081. doi: 10.1021/ja510144h
- Zhang, Q., Li, B., Huang, S., Nomura, H., Tanaka, H., and Adachi, C. (2014c). Efficient blue organic light-emitting diodes employing thermally activated delayed fluorescence. *Nat. Photonics* 8, 326–332. doi: 10.1038/nphoton.2014.12
- Zhang, Q., Li, J., Shizu, K., Huang, S., Hirata, S., Miyazaki, H., et al. (2012). Design of efficient thermally activated delayed fluorescence materials for pure blue organic light emitting diodes. *J. Am. Chem. Soc.* 134, 14706–14709. doi: 10.1021/ja306538w
- Zhang, Y., Ma, H., Wang, S., Li, Z., Ye, K., Zhang, J., et al. (2016b). Supramolecular structure-dependent thermally-activated delayed fluorescence (TADF) properties of organic polymorphs. *J. Phys. Chem. C*, 120, 19759–19767. doi: 10.1021/acs.jpcc.6b05537
- Zhang, Y., Miao, Y., Song, X., Gao, Y., Zhang, Z., Ye, K., et al. (2017). Single-molecule-based white-light emissive organic solids with molecular-packing-dependent thermally activated delayed fluorescence. *J. Phys. Chem. Lett.* 8, 4808–4813. doi: 10.1021/acs.jpclett.7b02213

Conflict of Interest Statement: The authors declare that the research was conducted in the absence of any commercial or financial relationships that could be construed as a potential conflict of interest.

Copyright © 2019 Zhang, Li, Li and Wang. This is an open-access article distributed under the terms of the Creative Commons Attribution License (CC BY). The use, distribution or reproduction in other forums is permitted, provided the original author(s) and the copyright owner(s) are credited and that the original publication in this journal is cited, in accordance with accepted academic practice. No use, distribution or reproduction is permitted which does not comply with these terms.



Pyrazine-Based Blue Thermally Activated Delayed Fluorescence Materials: Combine Small Singlet-Triplet Splitting With Large Fluorescence Rate

Junyuan Liu[†], Keren Zhou[†], Dan Wang, Chao Deng, Ke Duan, Qi Ai^{*} and Qisheng Zhang^{*}

OPEN ACCESS

Edited by:

Lian Duan,
Tsinghua University, China

Reviewed by:

Zujin Zhao,
South China University of
Technology, China
Bing Yang,
Jilin University, China

*Correspondence:

Qi Ai
0617289@zju.edu.cn
Qisheng Zhang
qishengzhang@zju.edu.cn

[†]These authors have contributed
equally to this work

Specialty section:

This article was submitted to
Organic Chemistry,
a section of the journal
Frontiers in Chemistry

Received: 27 February 2019

Accepted: 18 April 2019

Published: 21 May 2019

Citation:

Liu J, Zhou K, Wang D, Deng C,
Duan K, Ai Q and Zhang Q (2019)
Pyrazine-Based Blue Thermally
Activated Delayed Fluorescence
Materials: Combine Small
Singlet-Triplet Splitting With Large
Fluorescence Rate.
Front. Chem. 7:312.
doi: 10.3389/fchem.2019.00312

MOE Key Laboratory of Macromolecular Synthesis and Functionalization, Department of Polymer Science and Engineering,
Zhejiang University, Hangzhou, China

Metal-free thermally activated delayed fluorescence (TADF) emitters have emerged as promising candidate materials for highly efficient and low-cost organic light-emitting diodes (OLEDs). Here, a novel acceptor 2-cyanopyrazine is selected for the construction of blue TADF molecules via computer-assisted molecular design. Both theoretical prediction and experimental photophysical data indicate a small S_1 - T_1 energy gap (ΔE_{ST}) and a relative large fluorescence rate (k_F) in an *o*-phenylene-bridged 2-cyanopyrazine/3,6-di-*tert*-butylcarbazole compound (TCzPZCN). The k_F value of $3.7 \times 10^7 \text{ s}^{-1}$ observed in a TCzPZCN doped film is among the highest in the TADF emitters with a ΔE_{ST} smaller than 0.1 eV. Blue TADF emission is observed in a TCzPZCN doped film with a short TADF lifetime of 1.9 μs . The OLEDs using TCzPZCN as emitter exhibit a maximum external quantum efficiency (EQE) of 7.6% with low-efficiency roll-off. A sky-blue device containing a derivative of TCzPZCN achieves an improved EQE maximum of 12.2% by suppressing the non-radiative decay at T_1 .

Keywords: thermally activated delayed fluorescence (TADF), pyrazine, blue organic light-emitting diodes (OLED), fluorescence rate constant, singlet-triplet splitting

INTRODUCTION

Owing to the small energy gap (ΔE_{ST}) between the lowest singlet (S_1) and triplet (T_1) excited states, metal-free thermally activated delayed fluorescence (TADF) molecules can upconvert from their T_1 to S_1 by absorbing environmental thermal energy and then decay radiatively from the S_1 . Organic light-emitting diodes (OLEDs) employing TADF emitters can convert both singlet and triplet excitons into light with a theoretical yield up to 100% (Wex and Kaafarani, 2017; Yang et al., 2017; Cai and Su, 2018; Cai et al., 2018; Liu Y. et al., 2018), and have emerged as a new representation for highly efficient and low-cost OLEDs (Liu et al., 2014; Li W. et al., 2014; Ai et al., 2018; Bian et al., 2018). A twisted donor-phenylene-acceptor (D-Ph-A) structure has been demonstrated to be an effective strategy for the design of TADF materials (Zhang et al., 2012). A number of efficient blue, green, and red TADF materials with small ΔE_{ST} have been developed by using this strategy in

recent years (Uoyama et al., 2012; Wang et al., 2014, 2017; Zhang et al., 2014a,b; Chen et al., 2016; Chen X.-L. et al., 2017; Li et al., 2017; Yuan et al., 2017; Wu et al., 2018; Zhang D. et al., 2018).

Except for ΔE_{ST} , the value of fluorescence rate (k_F) for TADF emitters has attracted more and more attention in recent years, because it is a key for not only the quantum efficiency of the emitter but also the TADF lifetime and the device stability (Zhang et al., 2014a,b; Liu Z. et al., 2018). The D-Ph-A-type TADF emitters with small twisting angles between the neighboring planes can have high k_F values but suffer from large ΔE_{ST} , which leads to significant efficiency roll-off in their devices (Zhang et al., 2012; Li et al., 2013; Hirata et al., 2015; Chen X.-K. et al., 2017). Although increasing the twisting angle can reduce ΔE_{ST} , the k_F value also decreases due to the reduced overlap of the orbitals involved in the S_1 transition (Zhang et al., 2014a). Especially, for blue TADF emitters with large band gaps, large twisting angle cannot ensure a small ΔE_{ST} , because the molecules may have a low-lying triplet state localized at the D or A moieties (Zhang et al., 2014b). Overall, the difficulty of TADF material design is to have small ΔE_{ST} and high k_F at the same time. To enlarge the ratio of k_F to ΔE_{ST} , the D-A couple should be carefully selected, and the twisting geometry should be well-designed.

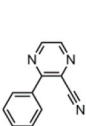
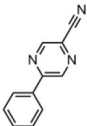
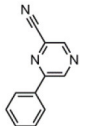
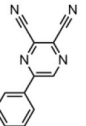
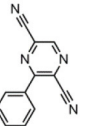
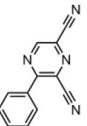
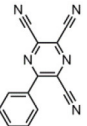
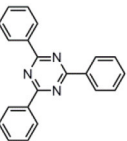
Cyano (Uoyama et al., 2012; Li B. et al., 2014; Lee and Lee, 2015; Taneda et al., 2015; Zhang et al., 2016; Chan et al., 2018; Sommer et al., 2018) and aromatic imines [i.e., triazine (Endo et al., 2011; Lee et al., 2012; Tanaka et al., 2012; Hirata et al., 2015; Kaji et al., 2015; Cha et al., 2016; Lin et al., 2016; Zhu et al., 2016; Chen X.-K. et al., 2017; Cui et al., 2017; Shao et al., 2017; Liu Z. et al., 2018; Oh et al., 2018; Zhang Q. et al., 2018; Wang Q. et al., 2019; Zhang et al., 2019) pyrimidine (Gómez-Bombarelli et al., 2016; Komatsu et al., 2016; Pan et al., 2016; Wu et al., 2016; Ganesan et al., 2017; Nakao et al., 2017; Park et al., 2017; Xiang et al., 2017; Zhang Q. et al., 2018; Zhang et al., 2019), and pyridine (Tang et al., 2015; Pan et al., 2016; Rajamalli et al., 2017; Sasabe et al., 2017; Chen et al., 2018)] are the most used groups for the construction of acceptor moieties in TADF molecules. The electron-withdrawing capability of an aromatic

imine increases with an increase in the number of nitrogen atoms in the ring. 2,4,6-Triphenyl-1,3,5-triazine (TRZ) is a promising acceptor for blue and green TADF materials because of the high T_1 energy level and the relatively strong electron-withdrawing capability (Tanaka et al., 2012; Hirata et al., 2015; Kaji et al., 2015; Cha et al., 2016; Lin et al., 2016; Chen X.-K. et al., 2017; Cui et al., 2017; Shao et al., 2017; Liu Z. et al., 2018; Oh et al., 2018; Zhang D. et al., 2018; Wang Q. et al., 2019). The aromatic heterocyclic rings containing one or two imine groups have a relatively weak electron-withdrawing character, which can be strengthened by introducing additional cyano groups (Tang et al., 2015; Pan et al., 2016; Sasabe et al., 2017; Chen et al., 2018). Although a series of red fluorophores based on pyrazine-2,3-dicarbonitrile has been reported (Gao et al., 2006), the pyrazine-based acceptor hasn't been used to construct a TADF molecule so far. In this paper, the T_1 energy levels and reduction potentials of various cyano-substituted pyrazines are theoretical investigated. A blue TADF emitter with small ΔE_{ST} and relatively large k_F values is successfully designed and synthesized by employing 2-cyanopyrazine as the acceptor.

RESULTS AND DISCUSSION

The CT transition energy is significantly related to the electron-donating ability of the donor and the electron-withdrawing ability of the acceptor in a D-A molecule. To avoid a low-lying locally excited triplet state (3LE) existing under the S_1 (1CT), both donor and acceptor moieties should have a limited conjugation length, and the conjugation between donor and acceptor should be broken (Zhang et al., 2014b). The electron-withdrawing capability of pyrazine is weaker than that of 1,3,5-triazine, which is an ideal acceptor for blue and green TADF materials. To enhance the electron-withdrawing capability of pyrazine, one to three cyano groups are attached onto the pyrazine ring in 2-phenylpyrazine, in which the phenyl ring is used as a π -bridge between the donor and acceptor moieties. The

TABLE 1 | Computed vertical absorption energies (E_{VA}), zero-zero energies (E_{0-0}), lowest unoccupied molecular orbital energies (E_{LUMO}), and reduction potentials (E_{RED}) of cyano-substituted triazine, pyrimidine, and pyridine moieties.

No.	1	2	3	4	5	6	7	TRZ
Molecular structure ^a								
								
$E_{VA}(T_1)$ (eV) ^b	3.03	2.72	2.95	2.63	2.74	2.78	2.57	3.02
$E_{0-0}(T_1)$ (eV) ^c	2.88	2.58	2.80	2.49	2.59	2.60	2.42	2.87
E_{LUMO} (eV) ^d	-2.45	-2.71	-2.52	-3.18	-3.37	-3.13	-3.81	-2.05
E_{RED} (V) ^e	2.94	3.14	2.99	3.51	3.66	3.47	4.01	2.63

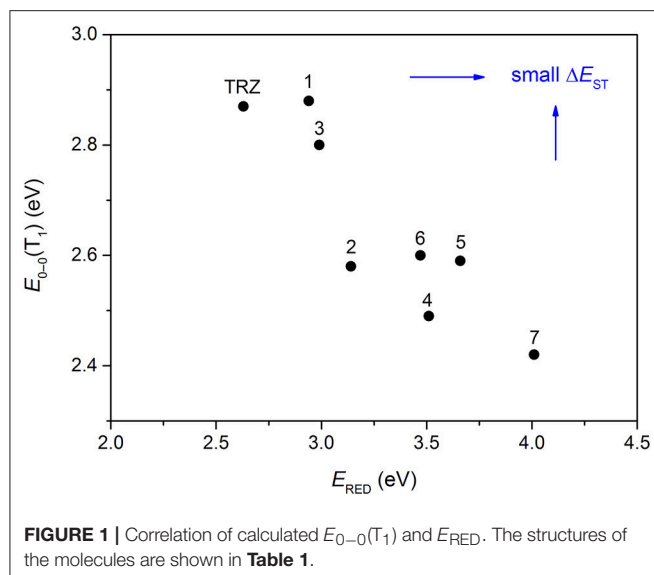
^a The geometries are optimized via DFT at the B3LYP/6-311G(d,p) level in vacuum.

^b Calculated by TD-DFT/B3LYP/6-31G(d) in vacuum.

^c Calculated from $E_{VA}(T_1)$ with a correlation of $E_{0-0}(T_1) = E_{VA}(T_1)/1.02 - 0.09$ (Huang et al., 2013).

^d Derived from DFT/PBE0/6-311++G(d,p) in acetonitrile.

^e Referred to an electron in the vacuum state (Mazur and Hipps, 1995) and calculated from the E_{LUMO} with a correlation of $E_{RED} = 0.79 \times (-E_{LUMO}) + 1.01$ (Wang D. et al., 2019).



calculated zero-zero energy of T_1 [$E_{0-0}(T_1)$] and the reduction potentials (E_{RED}) of the substituted pyrazine fragments are listed in **Table 1** and compared with those of TRZ (Mazur and Hipps, 1995; Huang et al., 2013; Wang D. et al., 2019). As shown in **Figure 1**, there is a roughly proportional relationship between $E_{0-0}(T_1)$ and E_{RED} , i.e., reducing the conjugation length of a moiety generally decreases its electron-withdrawing capability. The theoretical $E_{0-0}(T_1)$ of 3-phenylpyrazine-2-carbonitrile (Liu Y. et al., 2018) (2.88 eV) is as high as that of TRZ (2.87 eV), while the electron-withdrawing capability of **1** ($E_{RED} = 2.94$ eV) is even higher than that of TRZ ($E_{RED} = 2.63$ eV) (Mazur and Hipps, 1995), indicating that 2-cyanopyrazine is a promising acceptor for blue and green TADF molecules.

Using 3-phenylpyrazine-2-carbonitrile (Liu Y. et al., 2018) as the π -bridge attached acceptor and 3,6-di-tertbutylcarbazole as the donor, two molecules TCzPZCN and 2TCzPZCN are designed (**Figure 2A**). TCzPZCN has only one 3,6-di-tertbutylcarbazole donor group, which links to the acceptor group 2-cyanopyrazine via the ortho position of the phenylene (Ph) bridge (Wang R. et al., 2018). The ground-state geometry of TCzPZCN is optimized by DFT/B3LYP/6-31G*. The dihedral angle between carbazole donor and Ph-bridge is 69° , while that between 2-cyanopyrazine acceptor and Ph-bridge is 55° (**Figure 2B**). Such moderate dihedral angles allow a small overlap of the orbitals involved in the CT transition on the Ph-bridge but effectively break the conjugation between the donor and the acceptor. For 2TCzPZCN, there are two 3,6-di-tertbutylcarbazole groups attached to the ortho and meta positions of the Ph-bridge. Although the meta-linked carbazole and the Ph-bridge have a relatively small dihedral angle of 52° , the meta linkage prevents the orbitals on the donor from extending to the acceptor (**Figure 2B**). Using the K -OHF method, a semiempirical descriptor selection method based on time-dependent DFT (Wang et al., 2018), the vertical absorption energies (E_{VA}) of TCzPZCN and 2TCzPZCN are calculated to be 3.15 and

TABLE 2 | A comparison of theoretical predictions and experimental data on photophysical and electrochemistry of the investigated molecules.

	Theoretical data		Experimental data	
	TCzPZCN	2TCzPZCN	TCzPZCN	2TCzPZCN
In Toluene				
$E_{VA}(S_1)$ (eV)	3.15	3.16		
$E_{0-0}(S_1)$ (eV) ^a	2.91	2.92	2.91	2.82
ΔE_{ST} (eV)	0.05	0.05	0.07	0.06
f^b	0.0157	0.0184		
λ_{em} (nm) ^c			490	503
Φ^d			0.10	0.05
$\tau_1/\tau_2/\tau_3$ (ns)			0.14/2.6/8.4	0.12/3.2/9.8
In mCP Film (10 wt%)				
λ_{em} (nm)			483	493
Φ/Φ_F			0.47/0.36	0.44/0.16
τ_F (ns)			9.7	7.2
τ_{TADF} (μ s)			1.9	8.1
k_F ($\times 10^7$ s ⁻¹)			3.7	2.2
In Dichloromethane				
E_{OX} (V) ^e	5.46	5.41	5.57	5.53
In Acetonitrile				
E_{RED} (V) ^e	2.90	2.98	2.92	2.95

^aCalculated from $E_{VA}(S_1)$ with a correlation of $E_{0-0}(S_1) = E_{VA}(S_1) - 0.24$ eV (Huang et al., 2013).

^bOscillator strength.

^cEmission maximum.

^dPhotoluminescence quantum yield.

^eReferred to the vacuum state.

The theoretical potentials are calculated in the same way as those in **Table 1**.

3.16 eV, respectively. Assuming that their absorption is a 0–1 transition, the commonest transition for TADF emitters in weak polar medium, the $E_{0-0}(S_1)$ values of TCzPZCN and 2TCzPZCN in toluene are evaluated to be 2.91 and 2.92 eV, respectively (Huang et al., 2013). The ΔE_{ST} and the oscillator strength (f) are calculated to be 0.05 and 0.0157 for TCzPZCN, respectively, and 0.05 and 0.0184 for 2TCzPZCN, respectively. The ratios of f to ΔE_{ST} are among the highest values for the TADF emitters ($\Delta E_{ST} < 0.15$ eV) calculated using the K -OHF method (**Table S1**). Using a rough relationship between the theoretical frontier orbital energies and the measured redox potentials (Wang D. et al., 2019), the oxidation potentials (E_{OX}) of TCzPZCN and 2TCzPZCN are calculated to be 5.46 and 5.41 V, respectively, in dichloromethane, while the E_{RED} of TCzPZCN and 2TCzPZCN are calculated to be 2.90 and 2.98 V, respectively, in acetonitrile (**Table 2**).

The synthesis of TCzPZCN and 2TCzPZCN is described in the **Supplementary Material**. Their absorption and emission spectra in toluene and 10 wt% *m*-bis(N-carbazolyl)benzene (mCP) films are presented in **Figure 3** and **Figure S1**. As shown in **Figure 3A**, the absorption shoulders in the wavelength region of 350–430 nm can be ascribed to the intramolecular charge-transfer (CT) transitions. The fluorescence (1–2 ns component) and phosphorescence (1–2 ms component) spectra in toluene at 77 K are all smooth and broad. The ΔE_{ST}

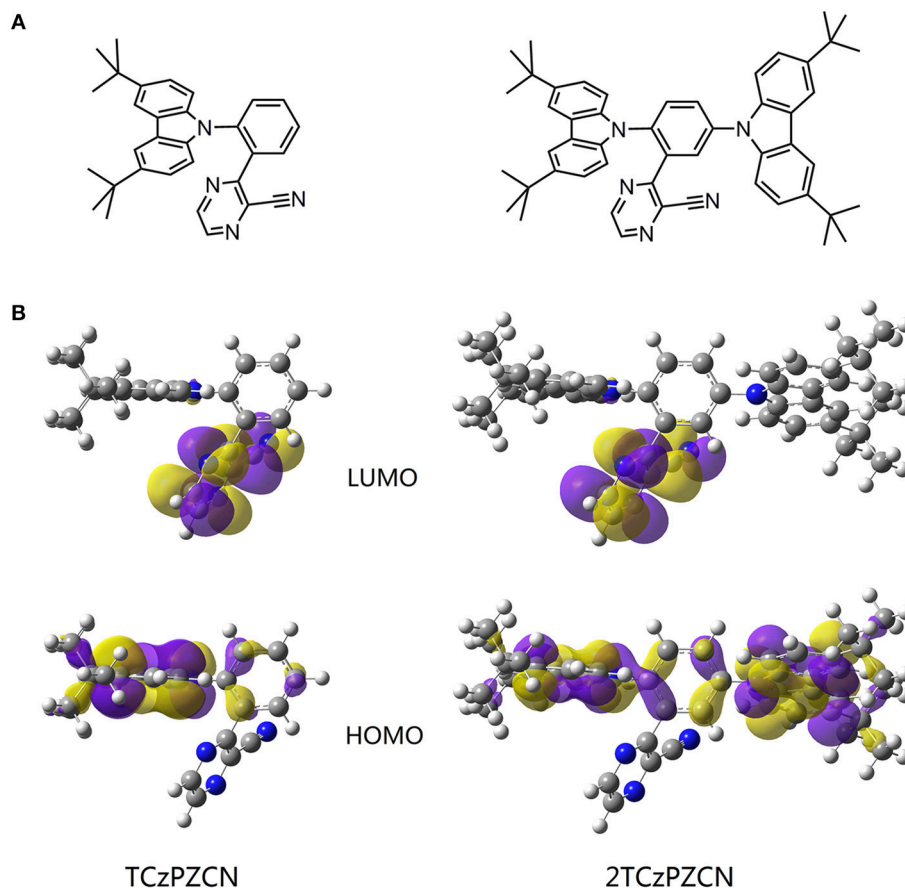


FIGURE 2 | (A) Structures of the investigated molecules. **(B)** The highest occupied and lowest unoccupied molecular orbitals (HOMO and LUMO) of the investigated molecules in their S0 state in vacuum. The geometries are optimized via density functional theory (DFT) at the B3LYP/6-311G (d,p) level.

values can be estimated from the energy difference between the fluorescence and phosphorescence peaks. The measured ΔE_{ST} of 0.07 eV for TCzPZCN and 0.06 eV for 2TCzPZCN are close to the theoretical values (Table 2). From the onset of the fluorescence bands at room temperature (RT; Figure S1), the 0–0 energies of TCzPZCN and 2TCzPZCN in toluene are estimated to be 2.91 and 2.82 eV, respectively, which are also in good agreement with the above theoretical estimation. These two compounds emit brightly at 77 K but dimly at RT with photoluminescence quantum yields (PLQY) <0.10 (Figure 3A inset and Table 2). In comparison to the emission spectra in solvent glass, those in the fluid solution (Figure S1) exhibit a significant redshift, indicating a correlation between the serious non-radiative decay in RT toluene and the excited-state geometrical relaxation process.

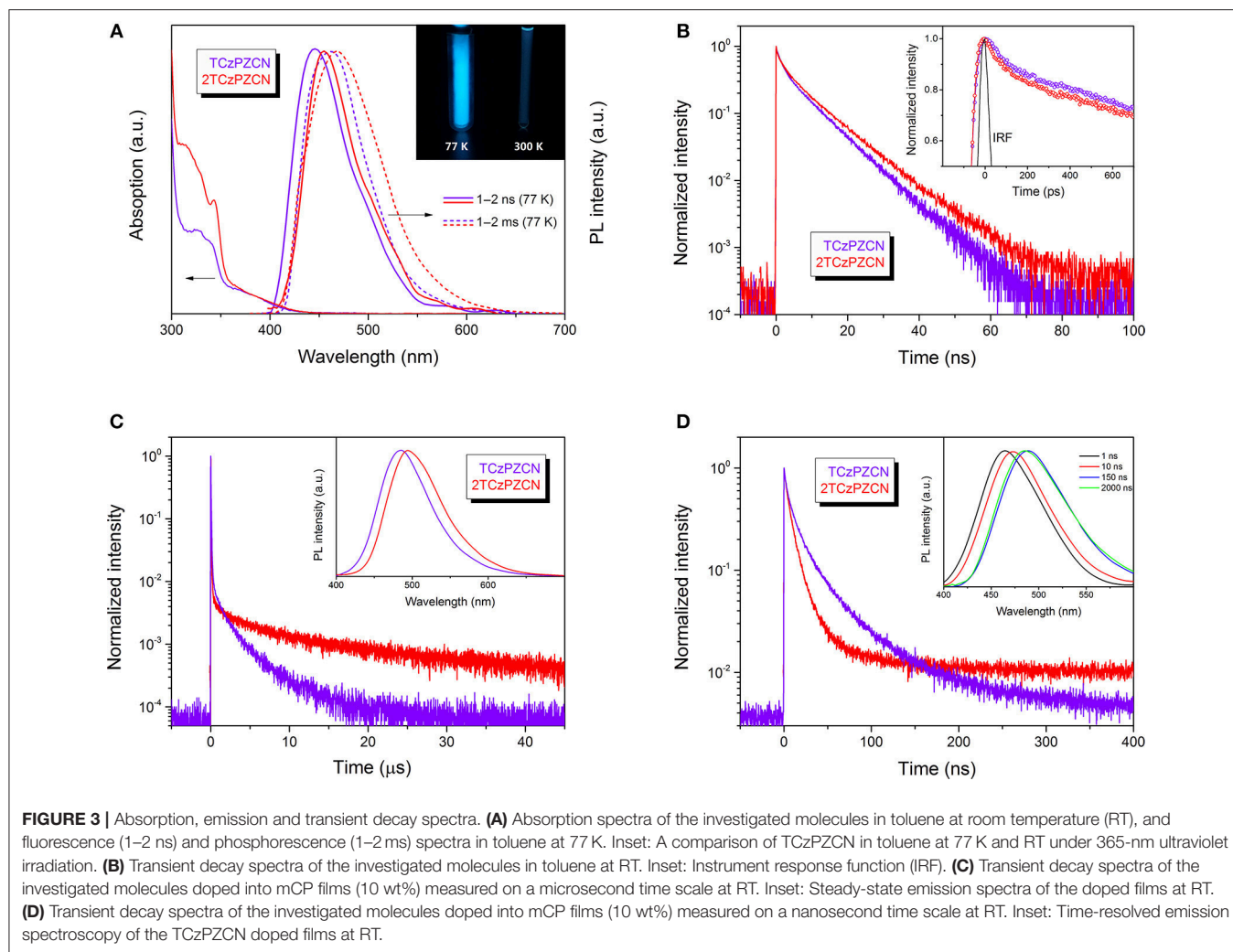
The transient decay spectra in degassed toluene at RT are presented in Figure 3B. No obvious TADF component is observed in the microsecond time range. Besides the single-exponential nanosecond fluorescence decay, a quick decay in the picosecond time scale is recorded by using an ultrafast time-correlated single photon counting (TCSPC). This fast decay could be resolved into two exponentially decaying components with the lifetimes (τ) of 0.14 and 2.6 ns for TCzPZCN and 0.12 and

3.2 ns for 2TCzPZCN. It is reasonable to expect that the non-radiative decay rate (k_{nr}) is not a constant during the fluorescence decay process. It is known that the excited-state solvation and relaxation process can be completed in a few picoseconds in fluid solution (Castner et al., 1987; Kinoshita and Nishi, 1988), resulting in a very fast non-radiative decay via a so-called free rotor and loose bolt effects (Turro et al., 2010). If the radiative and non-radiative decay rates are constants in the total luminescence process, the k_F value can be obtained by the following formula:

$$k_F = \Phi_F / \tau_F \quad (1)$$

where Φ_F and τ_F are the PLQY and lifetime of the fluorescence component, respectively. Given that both the k_F and k_{nr} in the first few nanoseconds are the same as the values after that, the PLQYs of these two compounds in toluene will be significantly higher than the observed ones. Consequently, if we calculate k_F from the measured Φ_F and the dominant nanosecond τ with Equation 1, the k_F value will be considerably underestimated.

In 10-wt%-doped mCP films, TCzPZCN and 2TCzPZCN exhibit blueshifted emission peaks at 483 and 493 nm, respectively (Figure 3C), with respect to that in toluene. Meanwhile, the PLQYs of TCzPZCN and 2TCzPZCN in the



doped films increase to 0.47 and 0.44, respectively, owing to the suppression of the collision-induced non-radiative decay (Turro et al., 2010; Zhang et al., 2014a). However, it was previously demonstrated that there is enough free volume in amorphous organic semiconductor films (Sun et al., 2017). The large-amplitude excited-state distortion cannot be fully inhibited in the films, leading to the moderate PLQYs for these films. TADF decay can be observed from the doped films, with a short lifetime of 1.9 μs for TCzPZCN and 8.1 μs for 2TCzPZCN (Figure 3C).

It is known that the solvation effect increases the separation of the electron and hole in a CT state (Sun et al., 2017; Wang and Zhang, 2019) and consequently decreases the fluorescence rate. According to the time-resolved emission spectroscopy shown in Figure 3D, the solvation process in a doped mCP film can last for dozens of nanoseconds, which is much slower than that in fluid solutions (Deng et al., 2019). The fluorescence rate of a TADF emitter in organic thin films decreases gradually in this time region and therefore can have a higher average value than that in solution. Since the fluorescence decays in organic thin films are always best fit by multiple exponentials (Figure 3D), an average

lifetime determined from the time the fluorescence intensity decays to $1/e$ of the initial value (Table 2) is used to calculate the k_F values. The k_F value of TCzPZCN in doped mCP films is then calculated to be $3.7 \times 10^7 \text{ s}^{-1}$, which is considerably higher than those of the TADF emitters having a ΔE_{ST} smaller than 0.1 eV (Table S2). In comparison to TCzPZCN, 2TCzPZCN has a lower k_F of $2.2 \times 10^7 \text{ s}^{-1}$, probably because of the reduced distance between the charge centroids of the donor and acceptor orbitals (Figure 2). According to first-principles calculation, the square root of the CT transition rate is approximately proportional to the effective D/A separation distance and the orbital overlap integral (Phifer and McMillin, 1986; Zhang et al., 2014a).

The oxidation and reduction behaviors of TCzPZCN and 2TCzPZCN are measured by cyclic voltammetry in dichloromethane and acetonitrile, respectively (Figure S2). From the onsets of the quasi-reversible redox couples, the vacuum-state-referenced E_{OX} and E_{RED} of TCzPZCN are determined to be 5.57 and 2.92 V, respectively, while those of 2TCzPZCN are determined to be 5.53 and 2.95 V, respectively. These potential values are all close to their

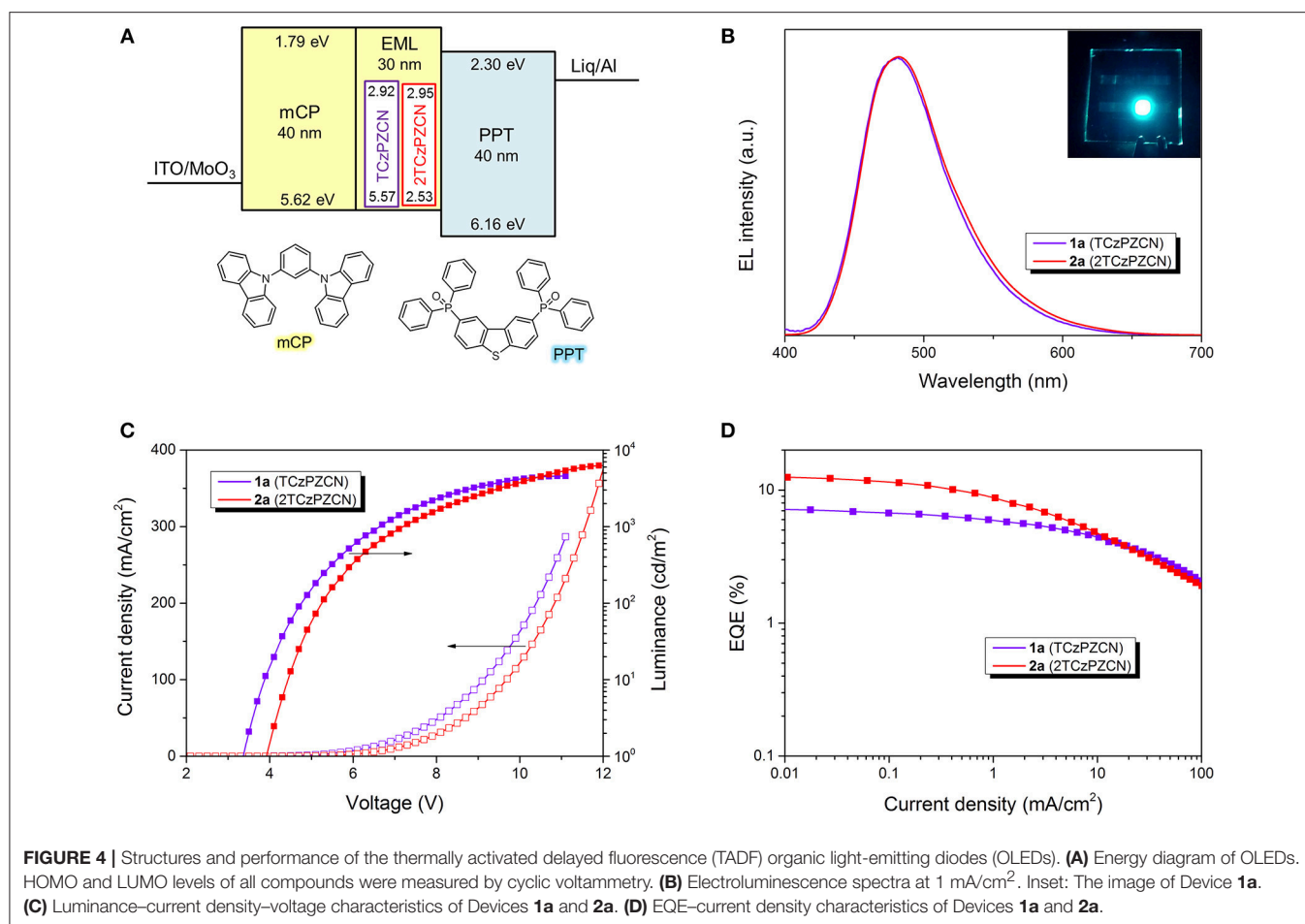


TABLE 3 | Emissive layer (EML) component, turn-on voltage (V_{on}), maximum luminance (L_{max}), external quantum efficiency maximum (EQE_{max}), emission maximum (λ_{max}), full width at half maxima (FWHM), and CIE coordinates of the TADF OLEDs.

Device	EML	V_{on} (V)	L_{max} (cd/m ²)	EQE_{max} (%)	λ_{max} (nm)	FWHM (nm)	CIE
1a	10 wt% TCzPZCN in mCP	3.4	4,579	7.1	480	70	(0.15, 0.26)
1b	30 wt% TCzPZCN in mCP	3.2	5,339	7.6	483	73	(0.15, 0.29)
1c	neat TCzPZCN	3.3	6,053	5.4	485	80	(0.17, 0.32)
2a	10 wt% 2TCzPZCN in mCP	3.9	6,257	12.2	480	70	(0.15, 0.26)
2b	30 wt% 2TCzPZCN in mCP	3.9	7,885	10.4	489	76	(0.17, 0.35)
2c	neat 2TCzPZCN	3.7	6,375	4.9	494	80	(0.20, 0.42)

theoretical ones. In comparison to TRZ-based compounds, TCzPZCN and 2TCzPZCN have higher E_{RED} values in favor of electron injection into the emitting layers of their devices.

Six OLEDs containing TCzPZCN and 2TCzPZCN are fabricated using a very simple device structure, as shown in **Figure 4A**. The 30-nm-thick emissive layers of the six devices are TCzPZCN or 2TCzPZCN doped mCP films and their neat films (see **Table 3**). At a doping concentration of 10 wt%, both TCzPZCN- (**1a**) and 2TCzPZCN-based (**2a**) OLEDs display a sky-blue emission with a maximum at 480 nm (**Figure 4B**). Devices **1a** and **2a** turn-on at 3.4 and 3.9 V, respectively, and

reach a maximum luminance of 4579 and 6257 cd/m² at 11 and 12 V, respectively (**Figure 4C**). The maximum external quantum efficiencies (EQEs) of Devices **1a** and **2a** are found to be 7.1 and 12.2%, respectively (**Figure 4D**), which are both higher than the upper limit of the traditional fluorescent OLEDs (5%). Although the PLQYs of these two compounds are approximate in 10-wt%-doped mCP films, the maximum EQEs of their devices are quite different. The internal quantum efficiency (IQE) of a TADF OLED can approach the PLQY of the emitter only when the internal conversion from S_1 to S_0 is the principal deactivation pathway for the emitter (Zhang et al., 2014a). The maximum IQE for Device **1a** is lower than the PLQY of the emissive layer

(0.47) when a light out-coupling efficiency of 0.2–0.3 is assumed, indicating that the non-radiative decay at T_1 for TCzPZCN cannot be ignored in the doped films. In comparison to Device 2a, Device 1a shows a reduced EQE roll-off that can be attributed to the short TADF lifetime of 1.9 μ s for TCzPZCN in doped film (Zhang et al., 2014a,b).

The influence of doping concentration on device performance is shown in **Figures S3, S4** and **Table 3**. The performance of TCzPZCN-based OLEDs is rather insensitive to the doping concentration of the emissive layer owing to the highly twisted configuration of the emitter (Zhang et al., 2015; Cha et al., 2016; Chen X.-L. et al., 2017). The electroluminescence (EL) spectra and EQE–current density curves of 10- and 30-wt%-doped devices almost coincide with each other respectively (**Figure S3**). Even the undoped device exhibits similar EQE–current density characteristics in the current density range from 1 to 100 mA/cm^2 with a slightly broader EL spectrum in comparison to the 10-wt%-doped device. In contrast, increasing the doping concentration of 2TCzPZCN-based OLEDs produces clear redshifts of the EL spectrum and decreases the EQE maximum. The lower steric hindrance surrounding the meta-linked carbazole may be responsible for the relatively strong intermolecular interaction between emitters in 2TCzPZCN doped films.

CONCLUSION

On the basis of a novel acceptor 2-cyanopyrazine, a type of blue emissive TADF molecule with small ΔE_{ST} (<0.1 eV) is successfully designed and synthesized. The fluorescence kinetics investigation indicates that the non-radiative decay rates of these molecules in toluene are far from constants. The ultrafast fluorescence decay ($1/\tau$) in the first hundred picoseconds after the excitation is related to a significant excited-state structural distortion. In doped mCP films, an *o*-phenylene-bridged 2-cyanopyrazine/3,6-di-*tert*butylcarbazole

compound (TCzPZCN) shows a fast TADF decay with a lifetime of 1.9 μ s, as well as a high fluorescence rate of $3.7 \times 10^7 \text{ s}^{-1}$ that can be comparable to those of the TADF emitters having relatively large orbital overlap and ΔE_{ST} (>0.2 eV). Although the pyrazine-based TADF emitters in solid films exhibit only moderate quantum yields on PL and EL suffered by the structural distortion process, it is one step toward a TADF emitter with both small ΔE_{ST} and large k_{F} . Additionally, we have demonstrated that 2-cyanopyrazine is a promising acceptor for the construction of blue TADF emitters. By suppressing the structural distortion induced non-radiative decay, efficient pyrazine-based TADF emitters with short TADF lifetime can be expected.

DATA AVAILABILITY

The datasets generated for this study are available on request to the corresponding author.

AUTHOR CONTRIBUTIONS

All authors listed have made a substantial, direct and intellectual contribution to the work, and approved it for publication.

FUNDING

This work is supported by the National Key R&D Program of China (grant no. 2016YFB0401004) and the National Natural Science Foundation of China (grant no. 51673164, 51873183).

SUPPLEMENTARY MATERIAL

The Supplementary Material for this article can be found online at: <https://www.frontiersin.org/articles/10.3389/fchem.2019.00312/full#supplementary-material>

REFERENCES

- Ai, X., Evans, E. W., Dong, S., Gillett, A. J., Guo, H., Chen, Y., et al. (2018). Efficient radical-based light-emitting diodes with doublet emission. *Nature* 563, 536–540. doi: 10.1038/s41586-018-0695-9
- Bian, M., Zhao, Z., Li, Y., Li, Q., Chen, Z., Zhang, D., et al. (2018). Positional isomerism effect of spirobifluorene and terpyridine moieties of “(A)_n-D-(A)_n” type electron transport materials for long-lived and highly efficient TADF-PhOLEDs. *J. Mater. Chem. C* 6, 745–753. doi: 10.1039/C7TC04685E
- Cai, M., Zhang, D., and Duan, L. (2018). High performance thermally activated delayed fluorescence sensitized organic light-emitting diodes. *Chem. Rec.* 18, 1–14. doi: 10.1002/tcr.201800148
- Cai, X., and Su, S. J. (2018). Marching toward highly efficient, pure-blue, and stable thermally activated delayed fluorescent organic light-emitting diodes. *Adv. Funct. Mater.* 28:1802558. doi: 10.1002/adfm.201802558
- Castner, E. W., Maroncelli, M., and Fleming, G. R. (1987). Subpicosecond resolution studies of solvation dynamics in polar aprotic and alcohol solvents. *J. Chem. Phys.* 86, 1090–1097. doi: 10.1063/1.452249
- Cha, J.-R., Lee, C. W., Lee, J. Y., and Gong, M. S. (2016). Design of *ortho*-linkage carbazole-triazine structure for high-efficiency blue thermally activated delayed fluorescent emitters. *Dyes Pigments* 134, 562–568. doi: 10.1016/j.dyepig.2016.08.023
- Chan, C.-Y., Cui, L.-S., Uk Kim, J., Nakanotani, H., and Adachi, C. (2018). Rational molecular design for deep-blue thermally activated delayed fluorescence emitters. *Adv. Funct. Mater.* 28:1706023. doi: 10.1002/adfm.201706023
- Chen, D., Liu, K., Gan, L., Liu, M., Gao, K., Xie, G., et al. (2016). Modulation of exciton generation in organic active planar pn heterojunction: toward low driving voltage and high efficiency OLEDs employing conventional and thermally activated delayed fluorescent emitters. *Adv. Mater.* 28, 6758–6765. doi: 10.1002/adma.201600612
- Chen, X.-K., Tsuchiya, Y., Ishikawa, Y., Zhong, C., Adachi, C., and Brédas, J. L. (2017). A new design strategy for efficient thermally activated delayed fluorescence organic emitters: from twisted to planar structures. *Adv. Mater.* 29:1702767. doi: 10.1002/adma.201702767
- Chen, X.-L., Jia, J.-H., Yu, R., Liao, J.-Z., Yang, M.-X., and Lu, C. Z. (2017). Combining charge-transfer pathways to achieve unique thermally activated delayed fluorescence emitters for high-performance solution-processed, non-doped blue OLEDs. *Angew. Chem. Int. Ed.* 56, 15006–15009. doi: 10.1002/anie.201709125
- Chen, Z., Wu, Z., Ni, F., Zhong, C., Zeng, W., Wei, D., et al. (2018). Emitters with a pyridine-3,5-dicarbonitrile core and short delayed fluorescence lifetimes of

- about 1.5 μ s: orange-red TADF-based OLEDs with very slow efficiency roll-offs at high luminance. *J. Mater. Chem. C* 6, 6543–6548. doi: 10.1039/C8TC01698D
- Cui, L.-S., Nomura, H., Geng, Y., Kim, J. U., Nakanotani, H., and Adachi, C. (2017). Controlling singlet–triplet energy splitting for deep-blue thermally activated delayed fluorescence emitters. *Angew. Chem. Int. Ed.* 56, 1571–1575. doi: 10.1002/anie.201609459
- Deng, C., Zhang, L., Wang, D., Tsuboi, T., and Zhang, Q. (2019). Exciton- and polaron-induced reversible dipole reorientation in amorphous organic semiconductor films. *Adv. Opt. Mater.* 7:1801644. doi: 10.1002/adom.201801644
- Endo, A., Sato, K., Yoshimura, K., Kai, T., Kawada, A., Miyazaki, H., et al. (2011). Efficient up-conversion of triplet excitons into a singlet state and its application for organic light emitting diodes. *Appl. Phys. Lett.* 98:083302. doi: 10.1063/1.3558906
- Ganesan, P., Ranganathan, R., Chi, Y., Liu, X.-K., Lee, C.-S., Liu, S.-H., et al. (2017). Functional pyrimidine-based thermally activated delay fluorescence emitters: photophysics, mechanochromism, and fabrication of organic light-emitting diodes. *Chem. Eur. J.* 23, 2858–2866. doi: 10.1002/chem.201604883
- Gao, B., Zhou, Q., Geng, Y., Cheng, Y., Ma, D., Xie, Z., et al. (2006). New fluorescent dipolar pyrazine derivatives for non-doped red organic light-emitting diodes. *Mater. Chem. Phys.* 99, 247–252. doi: 10.1016/j.matchemphys.2005.10.020
- Gómez-Bombarelli, R., Aguilera-Iparraguirre, J., Hirzel, T. D., Duvenaud, D., Maclaurin, D., Blood-Forsythe, M. A., et al. (2016). Design of efficient molecular organic light-emitting diodes by a high-throughput virtual screening and experimental approach. *Nat. Mater.* 15, 1120–1127. doi: 10.1038/nmat4717
- Hirata, S., Sakai, Y., Masui, K., Tanaka, H., Lee, S. Y., Nomura, H., et al. (2015). Highly efficient blue electroluminescence based on thermally activated delayed fluorescence. *Nat. Mater.* 14, 330–336. doi: 10.1038/nmat4154
- Huang, S., Zhang, Q., Shiota, Y., Nakagawa, T., Kuwabara, K., Yoshizawa, K., et al. (2013). Computational prediction for singlet- and triplet-transition energies of charge-transfer compounds. *J. Chem. Theory Comput.* 9, 3872–3877. doi: 10.1021/ct400415r
- Kaji, H., Suzuki, H., Fukushima, T., Shizu, K., Suzuki, K., Kubo, S., et al. (2015). Purely organic electroluminescent material realizing 100% conversion from electricity to light. *Nat. Comm.* 6:8476. doi: 10.1038/ncomms9476
- Kinoshita, S., and Nishi, N. (1988). Dynamics of fluorescence of a dye molecule in solution. *J. Chem. Phys.* 89, 6612–6622. doi: 10.1063/1.455383
- Komatsu, R., Sasabe, H., Seino, Y., Nakao, K., and Kido, J. (2016). Light-blue thermally activated delayed fluorescent emitters realizing a high external quantum efficiency of 25% and unprecedented low drive voltages in OLEDs. *J. Mater. Chem. C* 4, 2274–2278. doi: 10.1039/C5TC04057D
- Lee, C. W., and Lee, J. Y. (2015). Systematic control of photophysical properties of host materials for high quantum efficiency above 25% in green thermally activated delayed fluorescent devices. *ACS Appl. Mater. Interfaces* 7, 2899–2904. doi: 10.1021/am508259u
- Lee, S. Y., Yasuda, T., Nomura, H., and Adachi, C. (2012). High-efficiency organic light-emitting diodes utilizing thermally activated delayed fluorescence from triazine-based donor-acceptor hybrid molecules. *Appl. Phys. Lett.* 101:093306. doi: 10.1063/1.4749285
- Li, B., Nomura, H., Miyazaki, H., Zhang, Q., Yoshida, K., Suzuma, Y., et al. (2014). Dicarbazolyldicyanobenzenes as thermally activated delayed fluorescence emitters: effect of substitution position on photoluminescent and electroluminescent Properties. *Chem. Lett.* 43, 319–321. doi: 10.1246/cl.130907
- Li, C., Duan, R., Liang, B., Han, G., Wang, S., Ye, K., et al. (2017). Deep-red to near-infrared thermally activated delayed fluorescence in organic solid films and electroluminescent devices. *Angew. Chem. Int. Ed.* 56, 11525–11529. doi: 10.1002/anie.201706464
- Li, J., Nakagawa, T., MacDonald, J., Zhang, Q., Nomura, H., Miyazaki, H., et al. (2013). Highly efficient organic light-emitting diode based on a hidden thermally activated delayed fluorescence channel in a heptazine derivative. *Adv. Mater.* 25, 3319–3323. doi: 10.1002/adma.201300575
- Li, W., Pan, Y., Yao, L., Liu, H., Zhang, S., Wang, C., et al. (2014). A hybridized local and charge-transfer excited state for highly efficient fluorescent OLEDs: molecular design, spectral character, and full exciton utilization. *Adv. Opt. Mater.* 2, 892–901. doi: 10.1002/adom.201400154
- Lin, T.-A., Chatterjee, T., Tsai, W.-L., Lee, W.-K., Wu, M.-J., Jiao, M., et al. (2016). Sky-blue organic light emitting diode with 37% external quantum efficiency using thermally activated delayed fluorescence from spiroacridine-triazine hybrid. *Adv. Mater.* 28, 6976–6983. doi: 10.1002/adma.201601675
- Liu, Y., Li, C., Ren, Z., Yan, S., and Bryce, M. R. (2018). All-organic thermally activated delayed fluorescence materials for organic light-emitting diodes. *Nat. Rev. Mater.* 3, 1–20. doi: 10.1038/natrevmats.2018.20
- Liu, Z., Cao, F., Tsuboi, T., Yue, Y., Deng, C., Ni, X., et al. (2018). A high fluorescence rate is key for stable blue organic light-emitting diodes. *J. Mater. Chem. C* 6, 7728–7733. doi: 10.1039/C8TC01471J
- Liu, Z., Qiu, J., Wei, F., Wang, J., Liu, X., Helander, M., et al. (2014). Simple and high efficiency phosphorescence organic light-emitting diodes with codeposited copper(I) emitter. *Chem. Mater.* 26, 2368–2373. doi: 10.1021/cm5006086
- Mazur, U., and Hipps, K. W. (1995). Resonant tunneling bands and electrochemical reduction potentials. *J. Phys. Chem.* 99, 6684–6688. doi: 10.1021/j100017a060
- Nakao, K., Sasabe, H., Komatsu, R., Hayasaka, Y., Ohsawa, T., and Kido, J. (2017). Significant enhancement of blue OLED performances through molecular engineering of pyrimidine-based emitter. *Adv. Opt. Mater.* 5:1600843. doi: 10.1002/adom.201600843
- Oh, C. S., de Sa Pereira, D., Han, H., Park, H. J., Higginbotham, H. F., Monkman, A. P., et al. (2018). Dihedral angle control of blue thermally activated delayed fluorescent emitters through donor substitution position for efficient reverse intersystem crossing. *ACS Appl. Mater. Interfaces* 10, 35420–35429. doi: 10.1021/acsami.8b10595
- Pan, K.-C., Li, S.-W., Ho, Y.-Y., Shiu, Y.-J., Tsai, W.-L., Jiao, M., et al. (2016). Efficient and tunable thermally activated delayed fluorescence emitters having orientation-adjustable CN-substituted pyridine and pyrimidine acceptor units. *Adv. Funct. Mater.* 26, 7560–7571. doi: 10.1002/adfm.201602501
- Park, S., Komiyama, H., and Yasuda, T. (2017). Pyrimidine-based twisted donor-acceptor delayed fluorescence molecules: a new universal platform for highly efficient blue electroluminescence. *Chem. Sci.* 8, 953–960. doi: 10.1039/C6SC03793C
- Phifer, C. C., and McMillin, D. R. (1986). The basis of aryl substituent effects on charge-transfer absorption intensities. *Inorg. Chem.* 25, 132–1333. doi: 10.1021/ic00229a008
- Rajamalli, P., Senthilkumar, N., Huang, P.-Y., Ren-Wu, C.-C., Lin, H.-W., and Cheng, C.-H. (2017). New molecular design concurrently providing superior pure blue, thermally activated delayed fluorescence and optical out-coupling efficiencies. *J. Am. Chem. Soc.* 139, 10948–10951. doi: 10.1021/jacs.7b03848
- Sasabe, H., Onuma, N., Nagai, Y., Ito, T., and Kido, J. (2017). High power efficiency blue-to-green organic light-emitting diodes using isonicotinonitrile-based fluorescent emitters. *Chem. Asian J.* 12, 648–654. doi: 10.1002/asia.201601641
- Shao, S., Hu, J., Wang, X., Wang, L., Jing, X., and Wang, F. (2017). Blue thermally activated delayed fluorescence polymers with nonconjugated backbone and through-space charge transfer effect. *J. Am. Chem. Soc.* 139, 17739–17742. doi: 10.1021/jacs.7b10257
- Sommer, G. A., Mataranga-Popa, L. N., Czerwieniec, R., Hofbeck, T., Homeier, H. H., Muller, T. J., et al. (2018). Design of conformationally distorted donor-acceptor dyads showing efficient thermally activated delayed fluorescence. *J. Phys. Chem. Lett.* 9, 3692–3697. doi: 10.1021/acs.jpclett.8b01511
- Sun, H., Hu, Z., Zhong, C., Chen, X., Sun, Z., and Bredas, J.-L. (2017). Impact of dielectric constant on the singlet-triplet gap in thermally activated delayed fluorescence materials. *J. Phys. Chem. Lett.* 8, 2393–2398. doi: 10.1021/acs.jpclett.7b00688
- Tanaka, H., Shizu, K., Miyazaki, H., and Adachi, C. (2012). Efficient green thermally activated delayed fluorescence (TADF) from a phenoxazine-triphenyltriazine (PXZ-TRZ) derivative. *Chem. Comm.* 48, 11392–11394. doi: 10.1039/c2cc36237f
- Taneda, M., Shizu, K., Tanaka, H., and Adachi, C. (2015). High efficiency thermally activated delayed fluorescence based on 1,3,5-tris(4-(diphenylamino)phenyl)-2,4,6-tricyanobenzene. *Chem. Comm.* 51, 5028–5031. doi: 10.1039/C5CC00511F
- Tang, C., Yang, T., Cao, X., Tao, Y., Wang, F., Zhong, C., et al. (2015). Tuning a weak emissive blue host to highly efficient green dopant by a CN in tetracarbazolepyridines for solution-processed thermally activated delayed fluorescence devices. *Adv. Opt. Mater.* 3, 786–790. doi: 10.1002/adom.201500016

- Turro, N. J., Ramamurthy, V., and Scaiano, J. C. (2010). *Modern Molecular Photochemistry of Organic Molecules*. Sausalito, CA: University Science Books.
- Uoyama, H., Goushi, K., Shizu, K., Nomura, H., and Adachi, C. (2012). Highly efficient organic light-emitting diodes from delayed fluorescence. *Nature* 492, 234–238. doi: 10.1038/nature11687
- Wang, C., Deng, C., Wang, D., and Zhang, Q. (2018). Prediction of Intramolecular charge-transfer excitation for thermally activated delayed fluorescence molecules from a descriptor-tuned density functional. *J. Phys. Chem. C* 122, 7816–7823. doi: 10.1021/acs.jpcc.7b10560
- Wang, C., and Zhang, Q. (2019). Understanding solid-state solvation-enhanced thermally activated delayed fluorescence using a descriptor-tuned screened range-separated functional. *J. Phys. Chem. C* 123, 4407–4416. doi: 10.1021/acs.jpcc.8b08228
- Wang, D., Huang, S., Wang, C., Yue, Y., and Zhang, Q. (2019). Computational prediction for oxidation and reduction potentials of organic molecules used in organic light-emitting diodes. *Org. Electron.* 64, 216–222. doi: 10.1016/j.orgel.2018.10.038
- Wang, H., Xie, L., Peng, Q., Meng, L., Wang, Y., Yi, Y., et al. (2014). Novel thermally activated delayed fluorescence materials–thioxanthone derivatives and their applications for highly efficient OLEDs. *Adv. Mater.* 26, 5198–5204. doi: 10.1002/adma.201401393
- Wang, K., Zheng, C.-J., Liu, W., Liang, K., Shi, Y.-Z., Tao, S.-L., et al. (2017). Avoiding energy loss on TADF emitters: controlling the dual conformations of D–A structure molecules based on the pseudoplanar segments. *Adv. Mater.* 29:1701476. doi: 10.1002/adma.201701476
- Wang, Q., Zhang, Y.-X., Yuan, Y., Hu, Y., Tian, Q.-S., Jiang, Z.-Q., et al. (2019). Alleviating efficiency roll-off of hybrid single-emitting layer WOLED utilizing bipolar TADF material as host and emitter. *ACS Appl. Mater. Interfaces* 11, 2197–2204. doi: 10.1021/acsami.8b18665
- Wang, R., Wang, Y.-L., Lin, N., Zhang, R., Duan, L., and Qiao, J. (2018). Effects of ortho-linkages on the molecular stability of organic light-emitting diode materials. *Chem. Mater.* 30, 8771–8781. doi: 10.1021/acs.chemmater.8b03142
- Wex, B., and Kaafarani, B. R. (2017). Perspective on carbazole-based organic compounds as emitters and hosts in TADF applications. *J. Mater. Chem. C* 5, 8622–8653. doi: 10.1039/C7TC02156A
- Wu, K., Zhang, T., Zhan, L., Zhong, C., Gong, S., Jiang, N., et al. (2016). Optimizing optoelectronic properties of pyrimidine-based TADF emitters by changing the substituent for organic light-emitting diodes with external quantum efficiency close to 25% and slow efficiency Roll-Off. *Chem. Eur. J.* 22, 10860–10866. doi: 10.1002/chem.201601686
- Wu, T.-L., Huang, M.-J., Lin, C.-C., Huang, P.-Y., Chou, T.-Y., Chen-Cheng, R.-W., et al. (2018). Diboron compound-based organic light-emitting diodes with high efficiency and reduced efficiency roll-off. *Nat. Photonics* 12, 235–240. doi: 10.1038/s41566-018-0112-9
- Xiang, Y., Zhao, Y., Xu, N., Gong, S., Ni, F., Wu, K., et al. (2017). Halogen-induced internal heavy-atom effect shortening the emissive lifetime and improving the fluorescence efficiency of thermally activated delayed fluorescence emitters. *J. Mater. Chem. C* 5, 12204–12210. doi: 10.1039/C7TC04181K
- Yang, Z., Mao, Z., Xie, Z., Zhang, Y., Liu, S., Zhao, J., et al. (2017). Recent advances in organic thermally activated delayed fluorescence materials. *Chem. Soc. Rev.* 46, 915–1016. doi: 10.1039/C6CS00368K
- Yuan, Y., Hu, Y., Zhang, Y.-X., Lin, J.-D., Wang, Y.-K., Jiang, Z.-Q., et al. (2017). Light-emitting diodes: Over 10% EQE near-infrared electroluminescence based on a thermally activated delayed fluorescence emitter. *Adv. Funct. Mater.* 27:1700986. doi: 10.1002/adfm.201700986
- Zhang, D., Cai, M., Zhang, Y., Zhang, D., and Duan, L. (2016). Sterically shielded blue thermally activated delayed fluorescence emitters with improved efficiency and stability. *Mater. Horiz.* 3, 145–151. doi: 10.1039/C5MH00258C
- Zhang, D., Song, X., Cai, M., Kaji, H., and Duan, L. (2018). Versatile indolocarbazole-isomer derivatives as highly emissive emitters and ideal hosts for thermally activated delayed fluorescent OLEDs with alleviated efficiency roll-off. *Adv. Mater.* 30:1705406. doi: 10.1002/adma.201705406
- Zhang, D.-D., Suzuki, K., Song, X.-Z., Wada, Y., Kubo, S., Duan, L., et al. (2019). Thermally activated delayed fluorescent materials combining intra- and intermolecular charge transfers. *ACS Appl. Mater. Interfaces* 11, 7192–7198. doi: 10.1021/acsami.8b19428
- Zhang, Q., Kuwabara, H., Potscavage, W. J., Huang, S., Hatae, Y., Shibata, T., et al. (2014a). Anthraquinone-based intramolecular charge-transfer compounds: computational molecular design, thermally activated delayed fluorescence, and highly efficient red electroluminescence. *J. Am. Chem. Soc.* 136, 18070–18081. doi: 10.1021/ja510144h
- Zhang, Q., Li, B., Huang, S., Nomura, H., Tanaka, H., and Adachi, C. (2014b). Efficient blue organic light-emitting diodes employing thermally activated delayed fluorescence. *Nat. Photonics* 8, 326–332. doi: 10.1038/nphoton.2014.12
- Zhang, Q., Li, J., Shizu, K., Huang, S., Hirata, S., Miyazaki, H., et al. (2012). Design of efficient thermally activated delayed fluorescence materials for pure blue organic light emitting diodes. *J. Am. Chem. Soc.* 134, 14706–14709. doi: 10.1021/ja306538w
- Zhang, Q., Tsang, D., Kuwabara, H., Hatae, Y., Li, B., Takahashi, T., et al. (2015). Nearly 100% internal quantum efficiency in undoped electroluminescent devices employing pure organic emitters. *Adv. Mater.* 27, 2096–2100. doi: 10.1002/adma.201405474
- Zhang, Q., Xiang, S., Huang, Z., Sun, S., Ye, S., Lv, X., et al. (2018). Molecular engineering of pyrimidine-containing thermally activated delayed fluorescence emitters for highly efficient deep-blue (CIEy < 0.06) organic light-emitting diodes. *Dyes Pigments* 155, 51–58. doi: 10.1016/j.dyepig.2018.03.004
- Zhu, Y., Zhang, Y., Yao, B., Wang, Y., Zhang, Z., Zhan, H., et al. (2016). Synthesis and electroluminescence of a conjugated polymer with thermally activated delayed fluorescence. *Macromolecules* 49, 4373–4377. doi: 10.1021/acs.macromol.6b00430

Conflict of Interest Statement: The authors declare that the research was conducted in the absence of any commercial or financial relationships that could be construed as a potential conflict of interest.

Copyright © 2019 Liu, Zhou, Wang, Deng, Duan, Ai and Zhang. This is an open-access article distributed under the terms of the Creative Commons Attribution License (CC BY). The use, distribution or reproduction in other forums is permitted, provided the original author(s) and the copyright owner(s) are credited and that the original publication in this journal is cited, in accordance with accepted academic practice. No use, distribution or reproduction is permitted which does not comply with these terms.



Phenothiazinen-Dimesitylarylborane-Based Thermally Activated Delayed Fluorescence: High-Performance Non-doped OLEDs With Reduced Efficiency Roll-Off at High Luminescence

OPEN ACCESS

Edited by:

Lian Duan,
Tsinghua University, China

Reviewed by:

Junqiao Ding,
Changchun Institute of Applied
Chemistry (CAS), China
Xin Xin Ban,
Huaihai Institute of Technology, China
Yanqin Miao,
Taiyuan University of
Technology, China

*Correspondence:

Ping Lu
lup@jlu.edu.cn

[†]These authors have contributed
equally to this work

Specialty section:

This article was submitted to
Organic Chemistry,
a section of the journal
Frontiers in Chemistry

Received: 31 January 2019

Accepted: 06 May 2019

Published: 29 May 2019

Citation:

Tang X, Tao Y, Liu H, Liu F, He X,
Peng Q, Li J and Lu P (2019)
Phenothiazinen-Dimesitylarylborane-
Based Thermally Activated Delayed
Fluorescence: High-Performance
Non-doped OLEDs With Reduced
Efficiency Roll-Off at High
Luminescence. *Front. Chem.* 7:373.
doi: 10.3389/fchem.2019.00373

Xiangyang Tang^{1†}, Yanchun Tao^{1†}, Hui Liu¹, Futong Liu¹, Xin He¹, Qiming Peng², Jinyu Li¹
and Ping Lu^{1*}

¹ State Key Lab of Supramolecular Structure and Materials, Jilin University, Changchun, China, ² Key Laboratory of Flexible Electronics (KLOFE) and Institute of Advanced Materials (IAM), Jiangsu National Synergetic Innovation Center for Advanced Materials (SICAM), Nanjing Tech University (NanjingTech), Nanjing, China

We report a phenothiazinen-dimesitylarylborane thermally activated delayed fluorescence (TADF) molecule that exhibits high external quantum efficiency (EQE) in non-doped organic light-emitting diodes (OLEDs) at high luminescence. The non-doped device shows green electroluminescence with an emission peak of 540 nm and a maximum EQE of 19.66% obtained at a luminescence of $\sim 170 \text{ cd m}^{-2}$. The EQE is still as high as 17.31% at a high luminescence of $1,500 \text{ cd m}^{-2}$ with small efficiency roll-off.

Keywords: thermally activated delayed fluorescence, organic light-emitting diodes, non-doped device, high efficiency, low efficiency roll-off

INTRODUCTION

Thermally activated delayed fluorescence (TADF) materials are emerging as third-generation organic electroluminescence materials and are expected to replace Ir- or Pt-based phosphorescent complexes in practical application (Adachi, 2014; Reineke, 2014; Chen H.-W. et al., 2018). In organic light-emitting diodes (OLEDs), the singlet/triplet exciton branching ratio upon electrical excitation is generally believed to be 1:3 according to spin statistics. Phosphorescent materials can make the triplet state emissive *via* strong spin-orbit coupling caused by heavy metal atoms and are widely applied in full-color displays and white lightings (Zhang et al., 2015; Liu et al., 2016; Guo et al., 2017a; Miao et al., 2018a,b). However, the resource of Ir and Pt is limited. Therefore, developing low-cost alternatives is demanding. For fluorescent molecules, only the 25% singlet excitons can be emissive and the 75% triplet excitons are thus deactivated *via* thermal motion. Hence, how to utilize triplet exciton is the intrinsic issue in terms of boosting the efficiency of fluorescent OLEDs.

TADF materials can up-convert the lowest triplet (T_1) exciton to the lowest singlet (S_1) excited state *via* reverse intersystem crossing (RISC) by absorbing thermal energy of surroundings provided that the energy splitting (ΔE_{ST}) between T_1 and S_1 is sufficiently small, enabling the internal quantum efficiency (IQE) to approach unity without introducing noble metal elements (Endo et al., 2009; Uoyama et al., 2012; Zhang et al., 2012, 2014b). A general molecular design strategy toward small ΔE_{ST} proposed by Adachi et al. is linking electron donor and acceptor with high triplet energy in a twisted manner so that the highest occupied molecular orbital (HOMO) and the lowest unoccupied molecular orbital (LUMO) can be separated to get a small exchange energy (Endo et al., 2011; Lee et al., 2012). Though TADF materials can readily realize high device efficiency comparable to phosphorescent OLEDs, some critical issues still cannot be well resolved, which impede TADF materials toward practical application. One is that TADF materials normally need to be doped into appropriate host in device (Lee et al., 2012). The other is that the device efficiency decreases rapidly at high luminescence (Zhang et al., 2012, 2014a). The polarity, carrier transporting property, triplet energy of host, etc. can all remarkably influence TADF device performance (Lee et al., 2012; Komino et al., 2013; Li et al., 2016; Zhang J. et al., 2016). Hence, selecting or synthesizing proper host materials is necessary to obtain the desired device efficiency. Optimizing doping concentration is also needed in order to acquire high device performance (Lee et al., 2012; Zhang D. et al., 2016). A low doping concentration may result in incomplete energy transfer from host to dopant while a high doping level can cause concentration quenching. Both would lead to inferior device performance. Therefore, developing TADF materials that can achieve high efficiency at high luminescence in non-doped device is of great significance in terms of academic research as well as practical application. For TADF materials, the device efficiency roll-off at high luminescence and the necessity of fabricating doped device intrinsically inherit from two aspects: the fluorescence quenching in aggregate state and the triplet exciton quenching at high current density. A majority of TADF molecules are weakly emissive in solution while strongly emissive in aggregate states (Guo et al., 2017b,c). This is owing to the small overlap between HOMO and LUMO orbitals, which would result in a relatively slow fluorescence radiative decay constant that can barely compete with the active non-radiative processes such as molecular vibrations and motions in solution. In contrast, these non-radiative processes are greatly limited in aggregate state partially because of the rigid twisted molecular configuration. Consequently, the emission in aggregate state is greatly enhanced compared to that in solution. However, the D-A molecular structure of the TADF material would result in strong dipole-dipole interactions in the neat film and consequently induces fluorescence quenching. In addition, close π - π stacking can also quench fluorescence. Moreover, the weak binding energy of S_1 exciton arising from the CT attribute of S_1 state renders high probability of spin flip of the excited electron in singlet manifold, indicating remarkable intersystem crossing (ISC) from singlet to triplet. However, instead of being converted back to singlet state to produce fluorescence, the long-lived triplet

exciton is subject to deactivation by intermolecular interactions, thermal motions, oxygen, etc., causing appreciable decrease of fluorescence efficiency (Méhes et al., 2012). Hence, the neat film of some TADF materials normally suffers from relatively low fluorescence quantum yield. As a result, TADF molecules usually need to be dispersed in proper host materials. On the other hand, the relatively slow RISC process from T_1 to S_1 induces triplet excitons to accumulate at high current density and go through various quenching processes such as triplet-singlet quenching and triplet-charge quenching. A fundamental solution for this is accelerating the RISC process from T_1 to S_1 to the extent of fluorescence decay rate, which seems impossible without introducing heavy atoms such as Ir or Pt. Even though reducing ΔE_{ST} is feasible to speed up the RISC process, a microsecond or even longer delay component still exists for TADF molecules (Uoyama et al., 2012; Zhang et al., 2014b). Herein, we propose an alternative strategy toward high-efficiency non-doped OLEDs with reduced efficiency roll-off at high luminescence. Introducing a steric hindrance group to increase intermolecular distance can reduce intermolecular interactions. Accordingly, fluorescence quenching as well as triplet exciton quenching caused by intermolecular interactions can be alleviated. In this work, we adopt dimesitylarylborane (Mes_2B) as a steric repulsive electron acceptor. The vacant p orbital of boron atom endows it with electron-withdrawing ability. As a result, boron derivatives are widely applied as optoelectronic materials and sensors (Shirota et al., 2000; Yamaguchi et al., 2001; Jia et al., 2005; Welch et al., 2006; Bonn and Wenger, 2015; Hirai et al., 2015; Kitamoto et al., 2015, 2016a,b; Na et al., 2015; Numata et al., 2015; Suzuki et al., 2015; Dou et al., 2016; Hatakeyama et al., 2016; Park et al., 2016; Shiu et al., 2016; Chen et al., 2017; D'Aléo et al., 2017; Lee et al., 2017; Lien et al., 2017; Matsuo and Yasuda, 2017; Nakanotani et al., 2017; Neena et al., 2017; Chen D.-G. et al., 2018; Kim et al., 2018). The peripheral methyl groups around boron can shield the boron atom from the outer environment to protect it from protonic agents such as moisture. The additional effect of these methyl groups is their steric repulsion to adjacent molecules so that intermolecular interactions can be reduced. As a result, a high photoluminescence quantum yield (PLQY) in the neat film and reduced efficiency roll-off are expected. Using phenothiazine (PTZ) as electron donor, the Mes_2B is attached to the *N* position of PTZ and the resulting molecule PTZ Mes_2B presents a twisted configuration to ensure the separation between HOMO and LUMO. The PTZ Mes_2B shows intense green emission with a relatively high PLQY of 65% in the neat film. We fabricated both non-doped and doped devices with doping level ranging from low to high concentration. The performance of doped device enhances as the doping concentration increases. The non-doped device exhibits higher efficiency than these doped devices with a maximum external quantum efficiency (EQE_{max}) of 19.66%, which is acquired at a luminescence of ~ 170 cd m $^{-2}$. The EQE can still remain 17.31% at a luminescence of $\sim 1,500$ cd m $^{-2}$, showing only 12% efficiency roll-off. In contrast to the fact that a large majority of TADF materials only suit for doped device and suffer from severe efficiency roll-off, we have achieved high efficiency at high luminescence in the non-doped device and the device performance is comparable to some reported non-doped

TADF OLEDs (Numata et al., 2015; Guo et al., 2017b,c; Yang et al., 2018; Rao et al., 2019).

EXPERIMENTAL

General Methods

All the reagents and solvents used for the synthesis and characterization were purchased from Aldrich and Acros and used without further purification. The ^1H and ^{13}C NMR data were recorded on a Bruker AVANCE 500 spectrometer at 500 and 125 MHz, respectively, using tetramethylsilane (TMS) as the internal standard and DMSO- D_6 or CDCl_3 as solvent. Elemental analysis was performed on a Flash EA 1112, CHNS-O elemental analysis instrument. The MALDI-TOF-MS mass spectra were measured using an AXIMA-CFRTM plus instrument. Thermal gravimetric analysis (TGA) was measured on a Perkin-Elmer thermal analysis system from 30 to 900°C at a heating rate of 10 K min^{-1} under a nitrogen flow rate of 80 ml min^{-1} . Differential scanning calorimetry (DSC) was performed on a NETZSCH (DSC-204) unit from 50 to 380°C at a heating rate of 10 K min^{-1} under nitrogen atmosphere. UV-Vis spectra were recorded on a Shimadzu UV-3100 spectrophotometer. Steady-state photoluminescence spectra were measured by an RF-5301PC spectrophotometer. Time-resolved photoluminescence spectra were performed on Edinburgh spectrometer LP920 with 355-nm laser flash as excitation source. The PL lifetime was measured using an FLS920 spectrometer with a 375-nm picosecond pulsed light-emitting diode excitation source (pulse width: 898.3 ps). The PLQY (Φ) is measured by integrating sphere. Single crystal measurement was carried out at room temperature on a Rigaku RAXIS RAPID diffractometer equipped with a graphite monochromated Mo-K α radiation source. The crystal structure was determined *via* SHELXL-97 software program.

Electrochemical Measurement

The electrochemical properties (oxidation and reduction potentials) were carried out *via* cyclic voltammetry (CV) measurements by using a standard one-compartment, three-electrode electrochemical cell given by a BAS 100B/W electrochemical analyzer. Tetrabutylammoniumhexafluorophosphate (TBAPF $_6$) in anhydrous dimethyl formamide (DMF) or anhydrous dichloromethane (0.1 M) were used as the electrolyte for negative or positive scan. A glass-carbon disk electrode was used as the working electrode, a Pt wire was used as the counter electrode, and Ag/Ag $^+$ was used as the reference electrode together with ferrocene as the internal standard at a scan rate of 100 mV s^{-1} . According to the literature, the formal potential of Fc $^+$ /Fc is 4.8 eV below vacuum (Pomrèhne et al., 1995). All potentials relative to the Ag/Ag $^+$ electrode obtained from CV measurement are eventually referenced against Fc $^+$ /Fc to calculate HOMO/LUMO energy levels. The HOMO/LUMO levels are calculated according to the following formalism:

$$E_{\text{HOMO}} = -(E_{\text{ox vs. Fc/Fc}^+} + 4.8)\text{eV} \quad (1)$$

$$E_{\text{LUMO}} = -(E_{\text{red vs. Fc/Fc}^+} + 4.8)\text{eV} \quad (2)$$

where the E_{ox} vs. Fc/Fc $^+$ and E_{red} vs. Fc/Fc $^+$ are oxidation and reduction onset potentials relative to Fc/Fc $^+$ internal reference, respectively.

Theoretical Calculations

The ground-state (S_0) and the lowest singlet excited state (S_1) geometries were optimized at the B3LYP/6-31G(d, p) level. Natural transition orbitals (NTOs) of both $S_0 \rightarrow S_1$ and $S_0 \rightarrow T_1$ were calculated using the TD-M06-2X/6-31G(d, p) method on the basis of the optimized ground-state configuration.

Device Fabrication

ITO-coated glass was used as the substrate and the sheet resistance was 20 Ω square $^{-1}$. The ITO glass substrates were cleaned with isopropyl alcohol, acetone, toluene, and deionized water; dried in an oven at 120°C; treated with UV-zone for 20 min; and finally transferred to a vacuum deposition system with a base pressure lower than 5×10^{-6} mbar for organic and metal deposition. The MoO $_3$ was deposited at a rate of 0.1 Å s^{-1} . The deposition rate of all organic layers was 1.0 Å s^{-1} . The cathode LiF (1 nm) was deposited at a rate of 0.1 Å s^{-1} and then the capping Al metal layer (120 nm) was deposited at a rate of 4.0 Å s^{-1} . A mask with an array of 2×2 cm openings was used to define the cathode. The electroluminescent (EL) characteristics were measured using a Keithley 2400 programmable electrometer and a PR-650 Spectroscan spectrometer under ambient condition at room temperature.

Synthesis

Mes $_2$ BBr

Mes $_2$ BBr is synthesized according to literature (Na et al., 2015). ^1H NMR (500 MHz, DMSO- D_6 , 25°C, TMS) δ (ppm): 7.51 (d, J = 8.2 Hz, 2H; Ar H), 7.39 (d, J = 8.2 Hz, 2H; Ar H), 6.85 (s, 4H; Ar H), 2.33 (s, 6H; CH $_3$), 2.01 (s, 12H; CH $_3$).

PTZMes $_2$ B

In a 100-ml round flask, a mixture of 10H-PTZ (995 mg, 5 mmol), Mes $_2$ BBr (2.02 g, 5 mmol), Na t OBu (960 mg, 10 mmol), PH t Bu $_3$ BF $_4$ (72 mg, 0.25 mmol), and Pd $_2$ (dba) $_3$ (137 mg, 0.15 mmol) was dissolved in toluene (30 ml) and stirred at 110°C for 24 h under N $_2$. The reaction was quenched by water and extracted with dichloromethane. The organic layer was collected and evaporated. The residue was purified *via* column chromatography by using petroleum ether/dichloromethane (5:1, v/v) as eluent to afford bluish-green solid (3.35 g, yield: 90%). ^1H NMR (500 MHz, DMSO- D_6 , 25°C, TMS) δ (ppm): 7.45 (d, J = 8.4 Hz, 2H; Ar H), 7.33 (d, J = 6.4 Hz, 2H; Ar H), 7.23 (d, J = 8.4 Hz, 2H; Ar H), 7.18 (t, J = 7.1 Hz, 2H; Ar H), 7.08 (t, J = 7.1 Hz, 2H; Ar H), 6.84 (d, J = 2.6 Hz, 2H; Ar H), 6.83 (s, 4H; Ar H), 2.26 (s, 6H; CH $_3$), 1.99 (s, 12H; CH $_3$); ^{13}C NMR (125 MHz, CDCl_3 , 25°C, TMS) δ (ppm): 145.92 (C), 142.98 (C), 142.75 (C), 141.71 (C), 140.79 (C), 138.82 (CH), 138.64 (C), 128.26 (CH), 127.60 (CH), 126.95 (CH), 125.75 (C), 123.92 (CH), 120.28 (CH), 23.56 (CH $_3$), 21.26 (CH $_3$); MALDI-TOF MS (mass m/z): calcd for C $_{36}$ H $_{34}$ BNS, 523.25; found, 523.84 [M^+]. Anal. calcd (%) for C $_{36}$ H $_{34}$ BNS: C, 82.59; H, 6.55; N, 2.68. Found: C, 82.57; H, 6.56; N, 2.67.

RESULTS AND DISCUSSION

Synthesis

The synthesis of PTZMes₂B is shown in **Scheme 1**. Mes₂BBr is prepared the same way with literature (Na et al., 2015). Then PTZMes₂B is readily acquired *via* Pd-catalyzed Ullmann coupling in high yield starting with PTZ and Mes₂BBr as reactants. The target compound PTZMes₂B is purified by column chromatography and sublimation. The chemical structure and purity are well verified *via* NMR, MS, elemental analysis, and crystallography.

Thermal Properties and Morphology

Thermal property is investigated *via* thermogravimetric analysis (TGA) and DSC. As shown in **Figure S1a**, the decomposition temperature (T_d , corresponding to 5% weight loss) of PTZMes₂B is measured to be 381°C. The DSC curve of as-synthesized amorphous powder is displayed in **Figure S1b**. The weak endothermic signal at 84°C can be assigned to glass transition temperature (T_g). The sharp exothermic peak at 157°C is attributed to crystallization (T_c) and the intense endothermic peak at 262°C is the melting point (T_m). To explore whether PTZMes₂B can be applied in the non-doped device, film-forming ability is assessed by atomic force microscopy (AFM). Non-doped film of ~70 nm was prepared on quartz substrate by vacuum evaporation. An image of 5 × 5 μm area scanned by AFM is presented in **Figure S2**. Though the uniformity of film surface is inferior to that of some solution-processed oligomers (Yao et al., 2012), a root-mean-square (RMS) roughness of only about 0.72 nm is good enough for evaporation-deposited film. Therefore, PTZMes₂B is suitable for non-doped device application.

Electrochemical Properties and Single Carrier Device

CV is performed to calculate HOMO/LUMO energy levels. As can be seen in **Figure 1A**, the oxidation and reduction onsets of PTZMes₂B against ferrocenium/ferrocene (Fc⁺/Fc) redox couple are 0.23 and −2.19 V, respectively, corresponding to a HOMO energy of −5.03 eV and a LUMO energy of −2.61 eV (Equations 1 and 2). The coexistence of donor PTZ and acceptor Mes₂B in one molecule yields proper HOMO/LUMO energy alignment that is in favor of both hole and electron injection from adjacent carrier transporting layers. We also fabricated single carrier devices to find out if PTZMes₂B possesses balanced carrier transporting ability. The device structure of hole- and electron-only devices are ITO/HATCN (6 nm)/NPB (5 nm)/PTZMes₂B (100 nm)/NPB (20 nm)/Al (100 nm) and ITO/TPBi (20 nm)/PTZMes₂B (100 nm)/TPBi (5 nm)/LiF (1 nm)/Al (100 nm), respectively, where ITO is indium-tin oxide, HATCN is hexaazatriphenylenehexacarbonitrile, NPB is *N,N'*-bis(naphthalen-1-yl)-*N,N'*-bis(phenyl)-benzidine, and TPBi is 1,3,5-tris(1-phenyl-1*H*-benzimidazol-2-yl)benzene. Since we only aim to evaluate the carrier transporting property of PTZMes₂B, but not carrier injection ability between electrodes and PTZMes₂B, we have to eliminate energy barriers between electrodes and PTZMes₂B. Hence, for the hole-only device, a

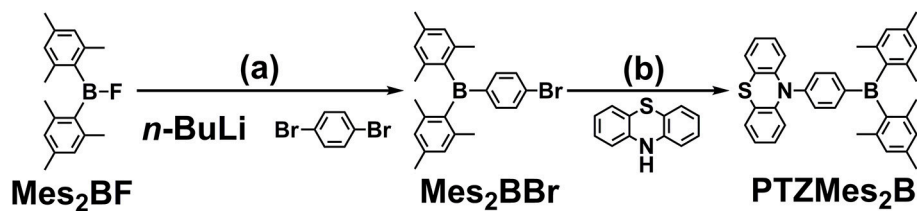
thin layer of HATCN (6 nm)/NPB (5 nm) is inserted between the anode ITO and PTZMes₂B layer to facilitate hole injection. The NPB (20 nm) layer between PTZMes₂B and cathode Al is used to block electrons. Similarly, for the electron-only device, a thin layer of TPBi (5 nm)/LiF (1 nm) inserted between PTZMes₂B and cathode Al is applied to enhance electron injection and the TPBi (20 nm) layer between PTZMes₂B and the anode ITO is designed to prevent hole injection. For both hole- and electron-only devices, the PTZMes₂B layer is much thicker than the NPB or TPBi layers so that the carrier mobility of the whole device is predominated by PTZMes₂B. The result is shown in **Figure 1B**; the inset shows the value derived from current density of the hole-only device divided by that of the electron-only device. At any given voltages within the range of our measurement, we can see in **Figure 1B** that the current density of the hole-only device is always higher than that of the electron-only device, indicating that hole mobility of PTZMes₂B is better than electron mobility. The difference between hole and electron mobility is quite large at low voltages such as 3 V at which the current density of the hole-only device is ~70 times that of the electron-only device. However, with increasing voltages, such difference gradually decreases, as can be seen in the inset of **Figure 1B**. For example, at a voltage of 4 V, the ratio (current density of the hole-only device over that of the electron-only device) is only ~20; at a voltage of 7 V, current density of the hole-only device is only ~1.5 times higher than that of the electron-only device. Nevertheless, PTZMes₂B displays relatively balanced carrier mobility. Such bipolar nature of the D-A molecule is beneficial for balanced charge injection and recombination in the emitting layer, which can alleviate exciton quenching by the free charges. In addition, the bipolar character can widen the carrier recombination zone in the emissive layer, which may reduce the adverse effect of concentration-induced exciton quenching.

Theoretical Calculations

NTOs are calculated by the TD-M062X/6-31G(d, p) method based on the optimized configuration of ground state. As shown in **Figure 2**, for the $S_0 \rightarrow S_1$ transition, the hole and particle distribute separately on the donor PTZ and acceptor dimesitylboryl, respectively, revealing the CT attribute of S_1 state. On the other hand, the hole and particle of $S_0 \rightarrow T_1$ overlap on the donor PTZ moiety, disclosing the locally excited (LE) property of T_1 state. The calculated S_1 and T_1 energies are 3.57 and 3.41 eV, respectively, resulting in a ΔE_{ST} of 0.16 eV. The binding energy of the LE exciton is generally large, which is adverse for spin flip of the excited electron, while the binding energy of the CT exciton tends to be small, which is beneficial for spin flip. Therefore, a reasonable explanation of the TADF emission is that the ³LE exciton is firstly up-converted to ³CT excited state and then goes through RISC process to the S_1 state followed by delayed fluorescence.

Crystal Structure

The donor and acceptor are linked in a torsion fashion with a large dihedral angle of ~87.83° between them as evidenced by single crystal X-ray diffraction (XRD) shown in **Figure 3A**. As can be seen in **Figure 3B**, the adjacent molecules orientate



SCHEME 1 | Synthesis of PTZMes₂B: (a) 1,4-dibromobenzene, *n*-BuLi, −78°C, 3 h; Mes₂BF in THF was added dropwise, stirring at room temperature overnight; (b) PTZ, Mes₂BBr, Na^tOBu, Ph^tBu₃BF₄, Pd₂(dba)₃, toluene, 110°C, 24 h, under N₂.

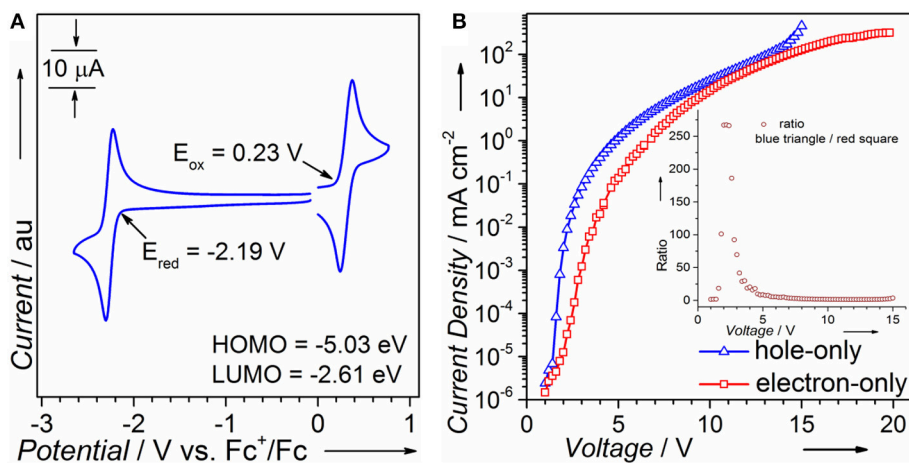


FIGURE 1 | (A) Cyclic voltammetry and (B) single carrier device of PTZMes₂B.

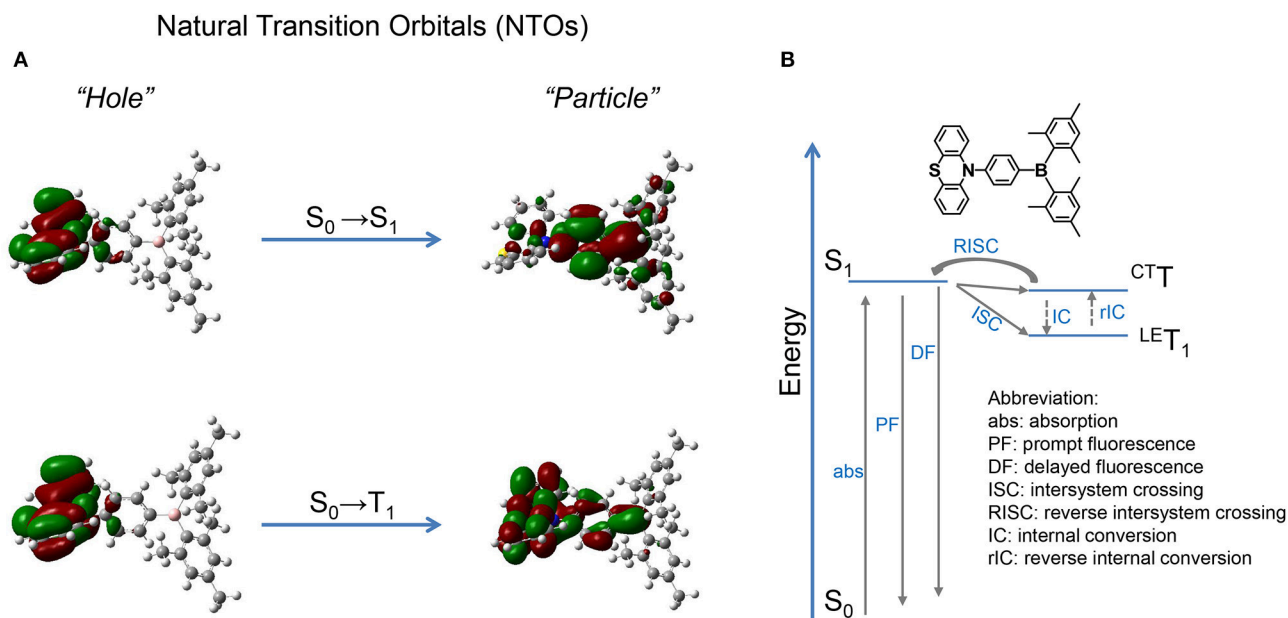
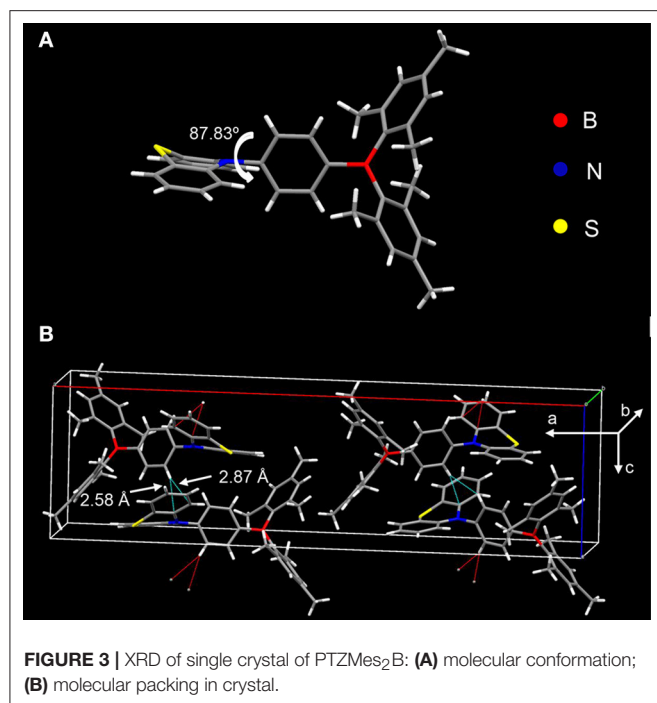


FIGURE 2 | (A) NTOs of PTZMes₂B; (B) possible TADF route.

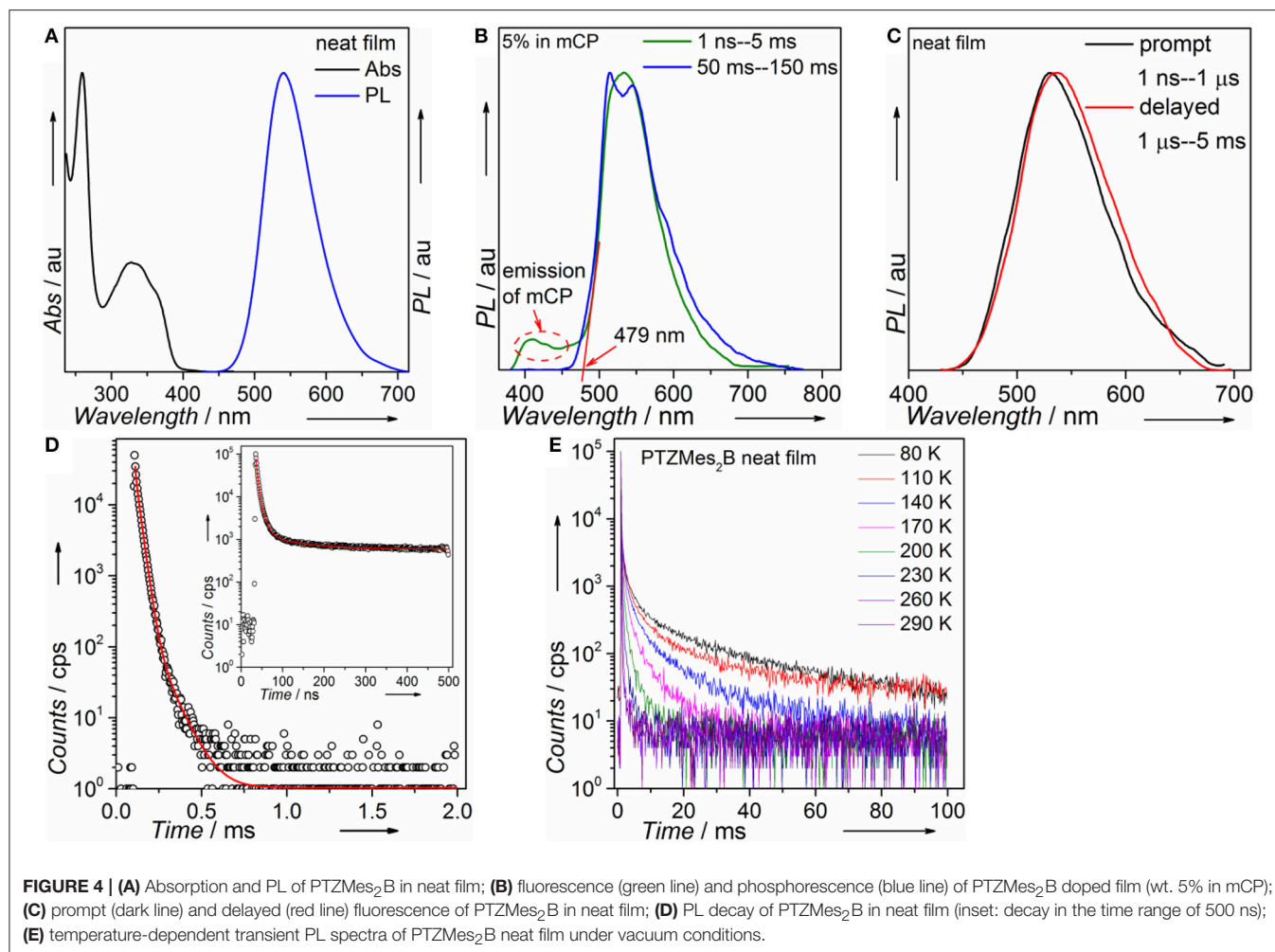


inversely against each other. Considering the steric configuration of the acceptor Mes₂B, a face-to-face packing between adjacent Mes₂B would not be thermodynamically stable. Therefore, the acceptors avoid approaching each other and the arrangement of two adjacent molecules are in an inversion mode so that the resultant crystal can be in its thermodynamic stable state. In addition, PTZMes₂B piles up without parallel face-to-face stacking. As a result, no π - π interactions or hydrogen bonds can be found in the crystal. Only CH- π interactions exist with a distance of \sim 2.58 and 2.87 Å as shown in **Figure 3B**. The weak intermolecular interactions mainly result from the bulky figure of the acceptor, which avoids close intermolecular contact. From the crystallography of PTZMes₂B, we may further deduce that intermolecular interactions in thin film may also be weak, which is in favor of reducing both singlet and triplet quenching. Detailed information about the crystal can be seen in **Table S4**.

Photophysical Properties

Steady-state absorption and photoluminescence spectra of the PTZMes₂B neat film recorded at ambient condition are shown in **Figure 4A**. The absorption band, showing vague vibronic structure peaking at \sim 360 and \sim 325 nm, can be assigned to the $\pi \rightarrow \pi^*$ transition of the molecule. The neat film of PTZMes₂B shows intense green emission with an emission peak at \sim 540 nm and a relatively high PLQY of \sim 65%. The PLQY of doped films with various doping concentrations is also measured and displayed in **Table S1** and **Figure S3**. The PLQY of doped films is higher than that of neat films. For example, the PLQY of wt. 10% (weight ratio) doped film is as high as 93%. Therefore, the neat film of PTZMes₂B experiences a certain degree of concentration quenching. The decrease of PLQY of the neat film may be caused by concentration quenching of singlet or triplet

excitons, or both. The deactivation of singlet excitons would lead to the quenching of both prompt and delayed fluorescence while the deactivation of triplet excitons would only lead to the quenching of delayed fluorescence. Thus, we measured transient PL spectra of these films at ambient condition. As shown in **Figure S4**, with increasing doping concentration, the lifetime of delayed component gradually shortened. This may be due to two possibilities. One is that the RISC of $T_1 \rightarrow S_1$ is more efficient at aggregation state probably because either the ΔE_{ST} tends to be smaller or intermolecular spin-orbit coupling is stronger in aggregates. Thus, heavier doping films show shorter lifetime of the delayed component. The other possibility is that concentration caused triplet quenching that leads to a shorter lifetime of the delayed component at heavier doping level. Combined with the decreased PLQY of the neat film, we temporarily assume that the shortened lifetime of the delayed component is due to concentration quenching. More detailed experiments and analysis are ongoing to further investigate the influence of aggregates on the RISC of $T_1 \rightarrow S_1$. Nevertheless, the neat film shows a relatively high PLQY of 65% and obvious delayed emission. If we consider exciton as hole-electron pair, ISC is essentially the process of spin flip of the excited electron. The binding energy between electron and hole of S_1 state of common TADF emitters is weak as a result of almost completely separated hole-electron distributions (i.e., the CT attribute of S_1 state). Hence, spin flip of the excited electron of S_1 state occurs with high probability and therefore high efficiency of the ISC process. As a result, for TADF emitters, large amounts of S_1 excitons would turn into T_1 excitons *via* ISC. The PLQY of the TADF emitter would decrease dramatically if triplet exciton yields from S_1 state are severely quenched and cannot be converted back to S_1 state (Méhes et al., 2012). The relatively high PLQY of 65% and the obvious delayed component in the neat film show that large amounts of triplet excitons can still be converted back to S_1 state instead of being quenched by intermolecular interactions such as dipole-dipole or π - π interactions. Though singlet and triplet quenching is inevitable in the neat film, our molecular design strategy, i.e., by introducing methyl groups to enhance steric repulsion among molecules, can help to alleviate concentration quenching in the neat film. To attain T_1 energy as well as ΔE_{ST} , time-resolved PL spectra of the doped film of PTZMes₂B were measured at a low temperature of \sim 80 K, as can be seen in **Figure 4B**. The fluorescence or phosphorescence may be affected by aggregation mode. Therefore, we take the doped film of PTZMes₂B as testing sample to try to eliminate the interference of aggregation. The doping concentration is wt. 5% and the host is mCP, which has higher triplet energy than PTZMes₂B. The fluorescence and phosphorescence are collected in the time range of 1 ns–5 ms and 50–150 ms, respectively, when the excitation source is off. The phosphorescence of PTZMes₂B shows a vibronic structure, indicating the LE character of T_1 state. We find that the phosphorescence of PTZMes₂B is similar to that of PTZP while different from that of Mes₂BBr (**Figure S5**). Hence, we may conclude that the T_1 state of PTZMes₂B localizes on the donor moiety. NTOs calculations further confirm this speculation (**Figure 2A**). The first vibronic peak of PTZMes₂B phosphorescence is \sim 515 nm, corresponding



to an energy of 2.41 eV. The fluorescence spectra (1 ns–5 ms) are composed of combined emission of both mCP (fluorescence or phosphorescence or both) and PTZMes₂B (prompt fluorescence or prompt + delayed fluorescence). The onset of the fluorescence is ~ 479 nm, and the energy is ~ 2.59 eV. Thus, the energy splitting ΔE_{ST} between S_1 and T_1 is determined to be 0.18 eV. Different experimental methods may produce different values of ΔE_{ST} . The ΔE_{ST} herein derived from PL spectra of film can only be taken as one of the versions that may approach the true value of ΔE_{ST} . Time-resolved PL spectra of the neat film of PTZMes₂B recorded at ambient condition are displayed in **Figure 4C**. PTZMes₂B exhibits delayed fluorescence (1 μ s–5 ms) matching well with the prompt fluorescence (1 ns–1 μ s), which is a persuasive evidence of TADF. **Figure 4D** is the PL decay of the PTZMes₂B neat film measured at ambient condition. The inset is PL decay within 500 ns. The PL decay is far from finished in the time range of nanoseconds (**Figure 4D**, inset). The PL decay finishes in the timescale of milliseconds with a lifetime of 13.71, 77.45, and 891.40 μ s. We have measured temperature-dependent steady-state PL spectra of doped and neat films from 80 to 290 K under vacuum conditions as shown in **Figure S6**. Generally, radiative rate

constant, either fluorescence or phosphorescence, is independent of temperature. However, some non-radiative transitions are temperature dependent, such as thermal deactivations and RISC of $T_1 \rightarrow S_1$, both of which are positively related to temperature. Therefore, for most TADF molecules, any PL intensity variations at different temperatures can be virtually ascribed to these two factors. However, thermal deactivations and RISC of $T_1 \rightarrow S_1$ exert opposite effects on PL intensity as temperature changes. **Figure S6a** shows the temperature-dependent PL spectra of the doped film (wt. 10% in mCP, weight ratio). From 80 to 290 K, as the temperature increases, the emission intensity of mCP continues to decrease because thermal deactivations become more and more active, which would consume both singlets and triplets without producing photons and therefore weaken PL intensity. On the other hand, the situation is different for PTZMes₂B. From 80 to 200 K, contrary to mCP, the PL intensity increases with temperature. This is because higher temperature can better activate RISC of $T_1 \rightarrow S_1$ and the subsequent delayed fluorescence and therefore enhanced PL intensity. However, further temperature increase from 200 to 290 K results in the gradual decrease of PL intensity due to more and more active thermal deactivation.

The neat film of PTZMes₂B shows similar phenomenon as can be seen in **Figure S6b**: from 80 to 200 K, the PL intensity increases as a result of more and more efficient RISC process of $T_1 \rightarrow S_1$. After 200 K, PL intensity gradually decreases due to thermal deactivation. We have also measured temperature-dependent transient PL spectra of the neat film under vacuum conditions as displayed in **Figure 4E**. At low temperature such as 80 K, PL decay is not completed within 100 ms and the long lifetime component beyond 100 ms can be attributed to phosphorescence, from which we can also conclude that the phosphorescence radiative rate must be very slow. In addition, even at temperature as low as 80 K, we can qualitatively conclude from **Figure 4E** that the proportion of the ultra-long lifetime component, i.e., the phosphorescence, is quite small, indicating that the phosphorescence process cannot compete with the RISC process of $T_1 \rightarrow S_1$. Normally, the phosphorescence radiative rate constant is not affected by temperature. As temperature increases, thermal deactivations of triplet excitons as well as RISC of $T_1 \rightarrow S_1$ become more and more active, and the slow phosphorescence process would not be able to compete with these processes. Indeed, with increasing temperature, the long lifetime component caused by phosphorescence gradually decreases and disappears at a temperature of 290 K. Actually, the PL decays completely within several milliseconds at 290 K. If phosphorescence exists at 290 K, considering its slow decay constant, the PL decay profile would not finish within several milliseconds. This means that the emission profile of **Figure 4C** does not contain any phosphorescence. In fact, under the same experimental conditions of **Figure 4C** at room temperature, no emission signal can be detected by delaying 50 ms. Thus, we can exclude the possibility of phosphorescence at room temperature and the long lifetime component of **Figure 4D** can be safely assigned to the TADF. Some basic photophysical data is listed in **Table 1**.

Electroluminescence Properties

We fabricated both doped and non-doped EL devices *via* vacuum evaporation. The structure of doped devices is as follows: ITO/HATCN (6 nm)/TAPC (20 nm)/TCTA (10 nm)/mCP (10 nm)/mCP: wt. x% PTZMes₂B (20 nm)/TPBi (40 nm)/LiF (1 nm)/Al (100 nm), where ITO (indium tin oxide) is the anode, TAPC [di-(4-(*N,N*-ditolyl-amino)-phenyl)cyclohexan] is the hole transporting layer (HTL),

TCTA [tris(4-carbazoyl-9-ylphenyl)amine] is the buffer layer, mCP [1,3-bis(carbazol-9-yl)benzene] is the host material, TPBi [1,3,5-tris-(*N*-phenylbenzimidazol-2-yl)benzene] is the electron transporting layer (ETL), LiF is the electron injecting layer, and Al is the cathode (**Figure S7**). The emitting layer consists of mCP: wt. x% PTZMes₂B with wt. x% indicating a doping ratio (wt.: weight ratio) of 5% (device A), 10% (device B), 20% (device C), 30% (device D), 50% (device E), and 80% (device F). The device performance can be seen in **Figure S8**. The turn-on voltage decreases as the doping concentration becomes higher as listed in **Table 2**. We believe that, at a low doping ratio such as wt. 5%, charges are injected directly into the host instead of the dopant. Excitons are formed on the host followed by energy transfer to the dopant. Accordingly, the turn-on voltage would be high because of the wide energy gap of the host. However, at high doping concentration, charges are mostly captured by the dopant and form excitons directly on dopant. Since the energy gap of dopant is much narrower than that of host, the turn-on voltage of heavily doped or non-doped devices is correspondingly lowered. Another interesting phenomenon is that the maximum EQE (EQE_{max}) occurs at lower luminescence for low doping concentration devices such as wt. 5 and 10% but at higher luminescence for high doping concentration such as wt. 80% or non-doped devices as can be seen in **Figure 5A**. This essentially means that low doping concentration devices achieve EQE_{max} at low current density whereas high doping concentration or non-doped devices achieve EQE_{max} at high current density. Indeed, for example, EQE_{max} appears at $J = 0.06 \text{ mA cm}^{-2}$ for both wt. 5 and 10% devices and $J = 0.27 \text{ mA cm}^{-2}$ for the non-doped device. A similar phenomenon is also observed by Adachi et al. (Nakanotani et al., 2013). The host mCP does not contain any electron-withdrawing group that can lower its LUMO energy; thus electron injection from TPBi into mCP is not easy. However, the dopant shows both appropriate HOMO and LUMO energy levels that can facilitate balanced charge injection. Therefore, charge injection is more balanced for heavily doped or non-doped devices. Though we did not measure single carrier mobility of doped devices, it is reasonable to deduce that carrier transporting is also more balanced and the recombination zone is much broader, not only at the interface but also in the bulk of the emission layer, for heavily doped or non-doped devices according to the results of Adachi et al. (Nakanotani et al., 2013). Thus, higher current density would

TABLE 1 | Photophysical properties of PTZMes₂B.

Compound	$T_d/T_g/T_c/T_m^a$ [°C]	$\lambda_{\text{max,abs}}^b$ [nm]	$\lambda_{\text{max,PL}}^c$ [nm]	PLQY ^d (%)	HOMO/LUMO ^e [eV]	ΔE_{ST}^f [eV]
PTZMes ₂ B	381/84/157/262	360/325	540	65	−5.03/−2.61	0.169/0.18 ^h

^a T_d , decomposition temperature; T_g , glass transition temperature; T_c , crystalline temperature; T_m , melting point.

^b $\lambda_{\text{max,abs}}$, absorption maximum in neat film.

^c $\lambda_{\text{max,PL}}$, emission peak in neat film.

^dPLQY, photoluminescence quantum yield of neat film measured by integrating sphere.

^eHOMO/LUMO energy levels estimated from cyclic voltammetry measurement.

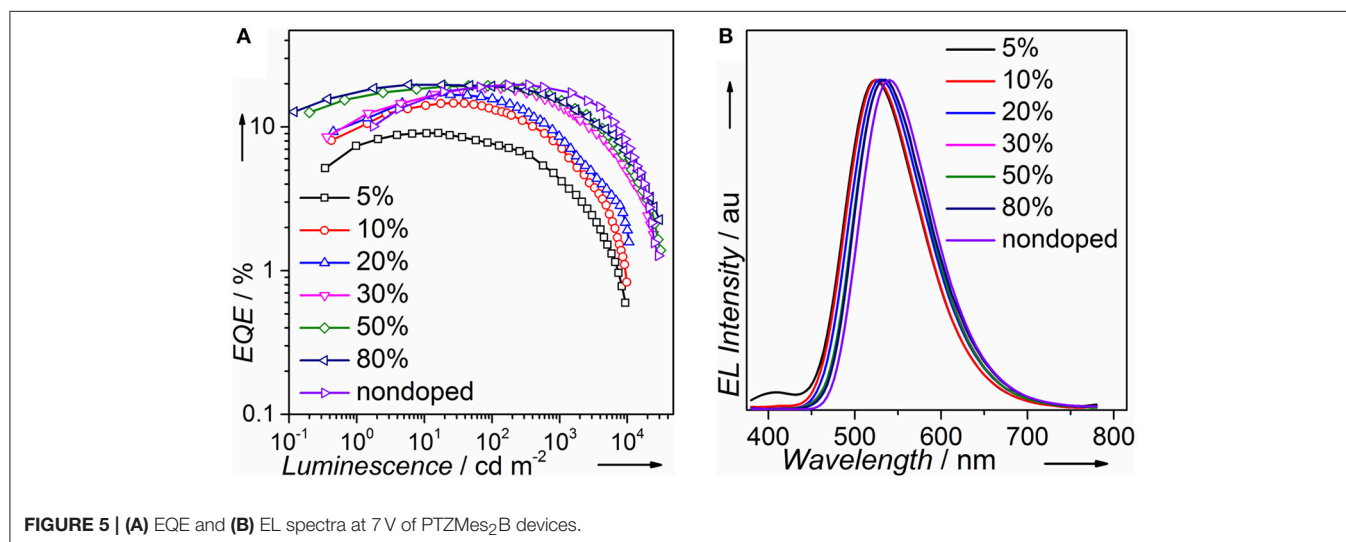
^f ΔE_{ST} , energy splitting between S_1 and T_1 states.

^g ΔE_{ST} derived from theoretical calculations.

^h ΔE_{ST} calculated from emission difference between fluorescence and phosphorescence.

TABLE 2 | EL performance of PTZMes₂B-based devices.

Device	V_{on}^a [V]	L_{max}^b [cd m ⁻²]	CE_{max}^c [cd A ⁻¹]	EQE ^d [%]	EL λ_{max}^e [nm]	CIE ^f [x, y]
				max/100/1000		
wt. 5%	4.4	9,388	26.44	9.07/7.78/4.18	525	0.31, 0.54
wt. 10%	4.2	9,831	45.05	14.66/13.52/7.06	525	0.31, 0.55
wt. 20%	4.0	10,589	52.65	16.79/15.65/8.60	530	0.33, 0.55
wt. 30%	3.6	24,467	61.09	18.90/18.71/13.52	535	0.35, 0.56
wt. 50%	3.6	31,006	62.47	19.40/19.20/15.22	535	0.35, 0.56
wt. 80%	3.4	29,920	63.06	19.73/19.22/14.91	536	0.36, 0.56
Non-doped	2.8	28,845	62.88	19.66/19.66/17.31	540	0.37, 0.57

^a V_{on} , turn-on voltage at the luminescence of ~ 1 cd m⁻².^b L_{max} , maximum luminescence.^c CE_{max} , maximum current efficiency.^dEQE max/1,000/10,000, EQE of maximum/at 1,000 cd m⁻²/10,000 cd m⁻².^eEL λ_{max} , emission peak of EL spectrum at 7 V.^fCIE coordinates at 7 V.**FIGURE 5** | (A) EQE and (B) EL spectra at 7 V of PTZMes₂B devices.

lead to unbalanced charge recombination and bring side effects such as charge-exciton quenching on device efficiency for low doping concentration devices. Moreover, the amount of dopant molecules in heavily doped or non-doped devices is much more than those in low doping concentration devices. If, ideally, each injected charge pair can form an exciton on molecules, then relatively low current density can already excite all dopant molecules when doping concentration is low. A higher current density would lead to redundant charges that would quench excitons. Hence, EQE_{max} occurs at lower current density for low doping concentration devices and higher current density for heavily or non-doped devices. The device performance enhances with increasing doping concentration (Figure 5A and Table 2). At low doping level, for example, wt. 5%, the corresponding EL spectra show a combined emission of both host and dopant with host emission being weaker than that of dopant (Figure 5B or Figure S8d). This means that (Adachi, 2014) excitons generated under electrical excitation are populated on both host and dopant in these doped devices (Reineke, 2014); singlet energy transfer from host to dopant is insufficient at low doping ratio. Generally, the effective radius of triplet energy transfer is much

shorter than that of singlet energy transfer. The inadequate singlet energy transfer from host to dopant at a low doping ratio indicates that triplet energy transfer from host to dopant is even more insufficient. However, the host itself cannot utilize triplet excitons. As a result, triplet excitons localized on host are wasted, leading to incomplete exciton utilization and therefore relatively low efficiency. Indeed, the EQE is only $\sim 9\%$ for the wt. 5% doped device. At a higher doping ratio, wt. 10% for example, the host emission still exists, but is negligible, indicative of efficient singlet energy transfer from host to dopant, and the corresponding EQE is improved to $\sim 14\%$. Further increasing doping ratio, i.e., wt. 20–80%, leads to the disappearance of host emission, which demonstrates more efficient singlet energy transfer from host to dopant. However, the EL originates from a singlet excited state. The triplet state is not emissive. Hence, the disappearance of host emission can only imply complete singlet energy transfer. As stated above, the effective radius of triplet energy transfer is much shorter than that of singlet energy transfer. It would be arbitrary to deduce that triplet excitons formed on host are 100% transferred to the dopant from the phenomenon of the disappearance of host emission in the EL

spectra. Accordingly, for doping ratio ranging from wt. 20 to 80%, though the host emission vanishes, the EQE continues to improve, in part owing to enhanced triplet energy transfer from host to dopant as the doping ratio increases. At a doping ratio as high as wt. 80%, the EQE can reach $\sim 19.73\%$. We also fabricated doped devices based on other hosts such as DPEPO and mCBP and observed similar phenomenon as presented in **Figures S9, S10** and **Tables S2, S3**. The fact that a heavily doped device can achieve better device performance promotes us to explore the potential application of PTZMes₂B in the non-doped device. The device structure of the non-doped device is as follows: ITO/HATCN (6 nm)/TAPC (25 nm)/TCTA (15 nm)/PTZMes₂B (20 nm)/TPBi (40 nm)/LiF (1 nm)/Al (100 nm). The turn-on voltage is 2.8 V and the maximum luminescence is $\sim 28,000$ cd m⁻². The non-doped device shows green emission with EL peak of 540 nm and CIE coordinates of (0.37, 0.57). The maximum current efficiency (CE) and EQE are 62.88 cd A⁻¹ and 19.66%, respectively, which are obtained at a luminescence of ~ 170 cd m⁻². At a high luminescence of $\sim 1,500$ cd m⁻², the EQE is still as high as 17.31%, showing an efficiency roll-off of about 12% compared with the maximum EQE of 19.66%. The discussion of both doped and non-doped devices is not intended to highlight that the performance of non-doped device is superior over doped devices but to emphasize the feasibility of PTZMes₂B as a non-doped emitter. This result verifies that our molecular design strategy works. The methyl in Mes₂B can function as an intermolecular steric group that may relieve triplet exciton quenching caused by intermolecular interactions. However, severe efficiency roll-off still exists when luminescence is much higher, for example, after 5,000 cd m⁻². This may be caused by the slow RISC of T₁ \rightarrow S₁, which is an intrinsic defect of TADF emitter. Large amounts of triplet excitons would accumulate at high current density due to their long-lived attribute, resulting in various active triplet quenching processes such as triplet-triplet annihilation, triplet-charge quenching, etc., and therefore serious efficiency roll-off. The fundamental solution toward relieving efficiency roll-off at high luminescence is by accelerating the T₁ \rightarrow S₁ RISC process to the extent of several nanoseconds so that triplets can transform to singlets in time instead of being quenched. This is a great challenge beyond this paper. Nevertheless, high EQE and relatively small efficiency roll-off are realized in the non-doped device, which, from our point of view, is a tiny advancement among TADF materials.

CONCLUSION

In conclusion, we have demonstrated a phenothiazinen-dimesitylarylborane (PTZMes₂B)-based twisted D-A molecule with TADF for high-performance non-doped OLEDs with reduced efficiency roll-off. PTZMes₂B shows a high PLQY of 65% in the neat film. A maximum EQE of 19.66% is obtained at a luminescence of 170 cd m⁻² in the non-doped device. A relatively small efficiency roll-off is achieved. The EQE is still as high as 17.31% at a high luminescence of 1,500 cd m⁻². Our work proves that introducing steric groups to reduce intermolecular interactions is in favor of acquiring a high PLQY in the neat film as well as alleviating triplet exciton quenching at high current density, both of which are crucial in terms of improving device efficiency and reducing efficiency roll-off. However, a fundamental solution to reduce efficiency roll-off of TADF materials rests upon accelerating the RISC process of T₁ \rightarrow S₁ to the timescale of several nanoseconds, which remains a great challenge for future material development.

AUTHOR CONTRIBUTIONS

XT designed and synthesized the TADF compound and carried out photophysical characterization and wrote the manuscript. YT helped in material synthesis and structural characterization. FL helped in material synthesis and purification. HL helped in device fabrication and characterization. JL helped in CV measurement. QP helped in photophysical characterization. XH helped in theoretical calculations. PL helped revise the manuscript and gave many suggestions.

FUNDING

We appreciate the financial support from the National Natural Science Foundation of China (grant nos. 91833304, 21774047, and 11804156).

SUPPLEMENTARY MATERIAL

The Supplementary Material for this article can be found online at: <https://www.frontiersin.org/articles/10.3389/fchem.2019.00373/full#supplementary-material>

REFERENCES

- Adachi, C. (2014). Third-generation organic electroluminescence materials. *Jpn. J. Appl. Phys.* 53:060101. doi: 10.7567/JJAP.53.060101
- Bonn, A. G., and Wenger, O. S. (2015). Charge transfer emission in oligotriarylamine-triarylborane compounds. *J. Org. Chem.* 80, 4097–4107. doi: 10.1021/acs.joc.5b00416
- Chen, D.-G., Lin, T.-C., Chen, C.-L., Chen, Y.-T., Chen, Y.-A., Lee, G.-H., et al. (2018). Optically triggered planarization of boryl-substituted phenoxazine: another horizon of TADF molecules and high-performance OLEDs. *ACS Appl. Mater. Interfaces* 10, 12886–12896. doi: 10.1021/acsami.8b00053
- Chen, H.-W., Lee, J.-H., Lin, B.-Y., Chen, S., and Wu, S.-T. (2018). Liquid crystal display and organic light-emitting diode display: present status and future perspectives. *Light Sci. Appl.* 7:17168. doi: 10.1038/lsa.2017.168
- Chen, X.-L., Jia, J.-H., Yu, R. M., Liao, J.-Z., Yang, M.-X., and Lu, C.-Z. (2017). Combining charge-transfer pathways to achieve unique thermally activated delayed fluorescence emitters for high-performance solution-processed, non-doped blue OLEDs. *Angew. Chem. Int. Ed.* 56, 15006–15009. doi: 10.1002/anie.201709125
- D'Aléo, A., Sazzad, M. H., Kim, D. H., Choi, E. Y., Wu, J. W., Canard, G., et al. (2017). Boron difluoride hemicurcuminoid as an efficient far red to near-infrared emitter: toward OLEDs and laser dyes. *Chem. Commun.* 53, 7003–7006. doi: 10.1039/c7cc01786c

- Dou, C. D., Long, X. J., Ding, Z. C., Xie, Z. Y., Liu, J., and Wang, L. X. (2016). An electron-deficient building block based on the B₂N unit: an electron acceptor for all-polymer solar cells. *Angew. Chem. Int. Ed.* 55, 1436–1440. doi: 10.1002/anie.201508482
- Endo, A., Ogasawara, M., Takahashi, A., Yokoyama, D., Kato, Y., and Adachi, C. (2009). Thermally activated delayed fluorescence from Sn⁴⁺-porphyrin complexes and their application to organic light-emitting diodes—a novel mechanism for electroluminescence. *Adv. Mater.* 21, 4802–4806. doi: 10.1002/adma.200900983
- Endo, A., Sato, K., Yoshimura, K., Kai, T., Kawada, A., Miyazaki, H., et al. (2011). Efficient up-conversion of triplet excitons into a singlet state and its application for organic light emitting diodes. *Appl. Phys. Lett.* 98:083302. doi: 10.1063/1.3558906
- Guo, F., Karl, A., Xue, Q.-F., Tam, K. C., Forberich, K., and Brabec, C. J. (2017a). The fabrication of color-tunable organic light-emitting diode displays via solution processing. *Light Sci. Appl.* 6:e17094. doi: 10.1038/lsa.2017.94
- Guo, J., Li, X.-L., Nie, H., Luo, W., Gan, S., Hu, S., et al. (2017b). Achieving high-performance nondoped OLEDs with extremely small efficiency roll-off by combining aggregation-induced emission and thermally activated delayed fluorescence. *Adv. Funct. Mater.* 27:1606458. doi: 10.1002/adfm.201606458
- Guo, J., Li, X.-L., Nie, H., Luo, W., Hu, R., Qin, A., et al. (2017c). Robust luminescent materials with prominent aggregation-induced emission and thermally activated delayed fluorescence for high performance organic light-emitting diodes. *Chem. Mater.* 29, 3623–3631. doi: 10.1021/acs.chemmater.7b00450
- Hatakeyama, T., Shiren, K., Nakajima, K., Nomura, S., Nakatsuka, S., Kinoshita, K., et al. (2016). Ultrapure blue thermally activated delayed fluorescence molecules: Efficient HOMO–LUMO separation by the multiple resonance effect. *Adv. Mater.* 28, 2777–2781. doi: 10.1002/adma.201505491
- Hirai, H., Nakajima, K., Nakatsuka, S., Shiren, K., Ni, J. P., Nomura, S., et al. (2015). One-step borylation of 1,3-diaryloxybenzenes towards efficient materials for organic light-emitting diodes. *Angew. Chem. Int. Ed.* 54, 13581–13585. doi: 10.1002/anie.201506335
- Jia, W. L., Feng, X. D., Bai, D. R., Lu, Z. H., Wang, S. N., and Vamvounis, G. (2005). Mes₂B(p-4,4-biphenyl-NPh(1-naphthyl)): a multifunctional molecule for electroluminescent devices. *Chem. Mater.* 17, 164–170. doi: 10.1021/cm048617t
- Kim, D.-H., D'Aléo, A., Chen, X.-K., Sandanayaka, A. D. S., Yao, D. D., Zhao, L., et al. (2018). High-efficiency electroluminescence and amplified spontaneous emission from a thermally activated delayed fluorescent near-infrared emitter. *Nat. Photon.* 12, 98–104. doi: 10.1038/s41566-017-0087-y
- Kitamoto, Y., Namikawa, T., Ikemizu, D., Miyata, Y., Suzuki, T., Kita, H., et al. (2015). Light blue and green thermally activated delayed fluorescence from 10H-phenoxaborin-derivatives and their application to organic light-emitting diodes. *J. Mater. Chem. C* 3, 9122–9130. doi: 10.1039/c5tc01380a
- Kitamoto, Y., Namikawa, T., Suzuki, T., Miyata, Y., Kita, H., Sato, T., et al. (2016a). Design and synthesis of efficient blue thermally activated delayed fluorescence molecules bearing triarylborane and 10,10-dimethyl-5,10-dihydrophenazasiline moieties. *Tetrahedron Lett.* 57, 4914–4917. doi: 10.1016/j.tetlet.2016.09.072
- Kitamoto, Y., Namikawa, T., Suzuki, T., Miyata, Y., Kita, H., Sato, T., et al. (2016b). Dimesitylarylborane-based luminescent emitters exhibiting highly efficient thermally activated delayed fluorescence for organic light emitting diodes. *Org. Electron.* 34, 208–217. doi: 10.1016/j.orgel.2016.04.030
- Komino, T., Nomura, H., Koyanagi, T., and Adachi, C. (2013). Suppression of efficiency roll-off characteristics in thermally activated delayed fluorescence based organic light-emitting diodes using randomly oriented host molecules. *Chem. Mater.* 25, 3038–3047. doi: 10.1021/cm4011597
- Lee, S. Y., Yasuda, T., Nomura, H., and Adachi, C. (2012). High-efficiency organic light-emitting diodes utilizing thermally activated delayed fluorescence from triazine-based donor–acceptor hybrid molecules. *Appl. Phys. Lett.* 101:093306. doi: 10.1063/1.4749285
- Lee, Y. H., Park, S., Oh, J., Shin, J. W., Jung, J., Yoo, S., et al. (2017). Rigidity-induced delayed fluorescence by ortho donor-appended triarylboron compounds: record-high efficiency in pure blue fluorescent organic light-emitting diodes. *ACS Appl. Mater. Interfaces* 9, 24035–24042. doi: 10.1021/acsami.7b05615
- Li, J., Ding, D., Tao, Y., Wei, Y., Chen, R., Xie, L., et al. (2016). A significantly twisted spirocyclic phosphine oxide as a universal host for high-efficiency full-color thermally activated delayed fluorescence diodes. *Adv. Mater.* 28, 3122–3130. doi: 10.1002/adma.201506286
- Lien, Y. J., Lin, T.-C., Yang, C.-C., Chiang, Y.-C., Chang, C.-H., Liu, S.-H., et al. (2017). First N-borylated emitters displaying highly efficient thermally activated delayed fluorescence and high-performance OLEDs. *ACS Appl. Mater. Interfaces* 9, 27090–27101. doi: 10.1021/acsami.7b08258
- Liu, B.-Q., Wang, L., Gao, D.-Y., Zou, J.-H., Ning, H.-L., Peng, J.-B., et al. (2016). Extremely high-efficiency and ultrasimplified hybrid white organic light-emitting diodes exploiting double multifunctional blue emitting layers. *Light Sci. Appl.* 5:e16137. doi: 10.1038/lsa.2016.137
- Matsuo, K., and Yasuda, T. (2017). Enhancing thermally activated delayed fluorescence characteristics by intramolecular B–N coordination in a phenylpyridine-containing donor–acceptor π -system. *Chem. Commun.* 53, 8723–8726. doi: 10.1039/c7cc04875k
- Méhes, G., Nomura, H., Zhang, Q., Nakagawa, T., and Adachi, C. (2012). Enhanced electroluminescence efficiency in a spiro-acridine derivative through thermally activated delayed fluorescence. *Angew. Chem. Int. Ed.* 51, 11311–11315. doi: 10.1002/anie.201206289
- Miao, Y., Wang, K., Gao, L., Zhao, B., Wang, H., Zhu, F., et al. (2018a). Precise manipulation of the carrier recombination zone: a universal novel device structure for highly efficient monochrome and white phosphorescent organic light-emitting diodes with extremely small efficiency roll-off. *J. Mater. Chem. C* 6, 8122–8134. doi: 10.1039/C8TC02479K
- Miao, Y., Wang, K., Zhao, B., Gao, L., Tao, P., Liu, X., et al. (2018b). High-efficiency/CRI/color stability warm white organic light-emitting diodes by incorporating ultrathin phosphorescence layers in a blue fluorescence layer. *Nanophotonics* 7, 295–304. doi: 10.1515/nanoph-2017-0021
- Na, Y.-J., Song, W., Lee, J. Y., and Hwang, S.-H. (2015). Synthesis of dibenzothiophene-based host materials with a dimesitylborane substituent and their green PHOLED performances. *Dalton Trans.* 44, 8360–8363. doi: 10.1039/c4dt03700f
- Nakanotani, H., Furukawa, T., Hosokai, T., Hatakeyama, T., and Adachi, C. (2017). Light amplification in molecules exhibiting thermally activated delayed fluorescence. *Adv. Optical Mater.* 5:1700051. doi: 10.1002/adom.201700051
- Nakanotani, H., Masui, K., Nishide, J., Shibata, T., and Adachi, C. (2013). Promising operational stability of high-efficiency organic light-emitting diodes based on thermally activated delayed fluorescence. *Sci. Rep.* 3:2127. doi: 10.1038/srep02127
- Neena, K. K., Pagidi, S., Dipak, K., and Thilagar, P. (2017). Diarylboryl-phenothiazine based multifunctional molecular siblings. *Chem. Commun.* 53, 3641–3644. doi: 10.1039/C6CC09717K
- Numata, M., Yasuda, T., and Adachi, C. (2015). High efficiency pure blue thermally activated delayed fluorescence molecules having 10H-phenoxaborin and acridan units. *Chem. Commun.* 51, 9443–9446. doi: 10.1039/c5cc00307e
- Park, I. S., Numata, M., Adachi, C., and Yasuda, T. (2016). A phenazaborin-based high efficiency blue delayed fluorescence material. *Bull. Chem. Soc. Jpn.* 89, 375–377. doi: 10.1246/bcsj.20150399
- Pomrnernehe, J., Vestweber, H., Gun, W., Muhr, R. F., Bäessler, H., Porsch, M., et al. (1995). Efficient two layer LEDs on a polymer blend basis. *Adv. Mater.* 7, 551–554. doi: 10.1002/adma.19950070608
- Rao, J., Zhao, C., Wang, Y., Bai, K., Wang, S., Ding, J., et al. (2019). Achieving deep-blue thermally activated delayed fluorescence in nondoped organic light-emitting diodes through a spiro-blocking strategy. *ACS Omega* 4, 1861–1867. doi: 10.1021/acsomega.8b03296
- Reineke, S. (2014). Phosphorescence meets its match. *Nat. Photon.* 8, 269–270. doi: 10.1038/nphoton.2014.78
- Shirota, Y., Kinoshita, M., Noda, T., Okumoto, K., and Ohara, T. (2000). A novel class of emitting amorphous molecular materials as bipolar radical formants: 2,4-bis(4-methylphenyl)amino]phenyl-5-(dimesitylboryl)thiophene and 2,4-bis(9,9-dimethylfluorenyl)amino]phenyl-5-(dimesitylboryl)thiophene. *J. Am. Chem. Soc.* 122, 11021–11022. doi: 10.1021/ja002333z
- Shiu, Y.-J., Cheng, Y.-C., Tsai, W.-L., Wu, C.-C., Chao, C.-T., Lu, C. W., et al. (2016). Pyridyl pyrrolide boron complexes: the facile generation of thermally activated delayed fluorescence and preparation of organic light-emitting diodes. *Angew. Chem. Int. Ed.* 55, 3017–3021. doi: 10.1002/anie.201509231
- Suzuki, K., Kubo, S., Shizu, K., Fukushima, T., Wakamiya, A., Murata, Y., et al. (2015). Triarylboron-based fluorescent organic light-emitting diodes

- with external quantum efficiencies exceeding 20%. *Angew. Chem. Int. Ed.* 54, 15231–15235. doi: 10.1002/anie.201508270
- Uoyama, H., Goushi, K., Shizu, K., Nomura, H., and Adachi, A. (2012). Highly efficient organic light-emitting diodes from delayed fluorescence. *Nature* 492, 234–238. doi: 10.1038/nature11687
- Welch, G. C., Juan, R. R. S., Masuda, J. D., and Stephan, D. W. (2006). Reversible, metal-free hydrogen activation. *Science* 314, 1124–1126. doi: 10.1126/science.1134230
- Yamaguchi, S., Akiyama, S., and Tamao, K. (2001). Colorimetric fluoride ion sensing by boron-containing π -electron system. *J. Am. Chem. Soc.* 123, 11372–11375. doi: 10.1021/ja015957w
- Yang, Y., Zhao, L., Wang, S., Ding, J., and Wang, L. (2018). Red-emitting thermally activated delayed fluorescence polymers with poly(fluorene-co-3,3'-dimethyl diphenyl ether) as the backbone. *Macromolecules* 51, 9933–9942. doi: 10.1021/acs.macromol.8b02050
- Yao, L., Xue, S., Wang, Q., Dong, W., Yang, W., Wu, H., et al. (2012). RGB small molecules based on a bipolar molecular design for highly efficient solution-processed single-layer OLEDs. *Chem. Eur. J.* 18, 2707–2714. doi: 10.1002/chem.201101476
- Zhang, D., Cai, M., Zhang, Y., Bin, Z., Zhang, D., and Duan, L. (2016). Simultaneous enhancement of efficiency and stability of phosphorescent OLEDs based on efficient Förster energy transfer from interface exciplex. *ACS Appl. Mater. Interfaces* 6, 3825–3832. doi: 10.1021/acsami.5b10561
- Zhang, D., Duan, L., Zhang, Y., Cai, M., Zhang, D., and Qiu, Y. (2015). Highly efficient hybrid warm white organic light-emitting diodes using a blue thermally activated delayed fluorescence emitter: exploiting the external heavy-atom effect. *Light Sci. Appl.* 4:e232. doi: 10.1038/lsa.2015.5
- Zhang, J., Ding, D., Wei, Y., Han, F., Xu, H., and Huang, W. (2016). Multiphosphine-oxide hosts for ultralow-voltage-driven true-blue thermally activated delayed fluorescence diodes with external quantum efficiency beyond 20%. *Adv. Mater.* 28, 479–485. doi: 10.1002/adma.201502772
- Zhang, Q., Kuwabara, H., Potscavage, W. J., Huang, S., Hatae, Y., Shibata, T., et al. (2014a). Anthraquinone-based intramolecular charge-transfer compounds: computational molecular design, thermally activated delayed fluorescence, and highly efficient red electroluminescence. *J. Am. Chem. Soc.* 136, 18070–11808. doi: 10.1021/ja510144h
- Zhang, Q., Li, B., Huang, S., Nomura, H., Tanaka, H., and Adachi, C. (2014b). Efficient blue organic light-emitting diodes employing thermally activated delayed fluorescence. *Nat. Photon.* 8, 326–332. doi: 10.1038/nphoton.2014.12
- Zhang, Q., Li, J., Shizu, K., Huang, S., Hirata, S., Miyazaki, H., et al. (2012). Design of efficient thermally activated delayed fluorescence materials for pure blue organic light emitting diodes. *J. Am. Chem. Soc.* 134, 14706–14709. doi: 10.1021/ja306538w

Conflict of Interest Statement: The authors declare that the research was conducted in the absence of any commercial or financial relationships that could be construed as a potential conflict of interest.

Copyright © 2019 Tang, Tao, Liu, Liu, He, Peng, Li and Lu. This is an open-access article distributed under the terms of the Creative Commons Attribution License (CC BY). The use, distribution or reproduction in other forums is permitted, provided the original author(s) and the copyright owner(s) are credited and that the original publication in this journal is cited, in accordance with accepted academic practice. No use, distribution or reproduction is permitted which does not comply with these terms.



Synthesis, Structures, and Photophysical Properties of Novel Four-Coordinate Cu(I) Complexes Supported by Chelating N-Heterocyclic Carbene Ligands

Zhiqiang Wang^{1*}, Xiaojuan Sun¹, Chen Xu^{2*} and Baoming Ji¹

¹ College of Chemistry and Chemical Engineering and Henan Key Laboratory of Function-Oriented Porous Materials, Luoyang Normal University, Luoyang, China, ² College of Food and Pharmacy, Luoyang Normal University, Luoyang, China

OPEN ACCESS

Edited by:

Lian Duan,
Tsinghua University, China

Reviewed by:

Ke Gao,
Central China Normal University, China
Michael Lee Singleton,
Catholic University of
Louvain, Belgium

*Correspondence:

Zhiqiang Wang
wzq197811@163.com
Chen Xu
xubohan@163.com

Specialty section:

This article was submitted to
Organic Chemistry,
a section of the journal
Frontiers in Chemistry

Received: 14 February 2019

Accepted: 21 May 2019

Published: 05 June 2019

Citation:

Wang Z, Sun X, Xu C and Ji B (2019)
Synthesis, Structures, and
Photophysical Properties of Novel
Four-Coordinate Cu(I) Complexes
Supported by Chelating
N-Heterocyclic Carbene Ligands.
Front. Chem. 7:422.
doi: 10.3389/fchem.2019.00422

Luminescent Cu(I) complexes are promising emitting materials for electroluminescent devices due to their low cost and abundant resources, as well as high emission efficiency. It is well-known that N-heterocyclic carbenes (NHCs) are excellent ligands for transition metal complexes. To investigate the photophysical properties of Cu(I)-NHC complexes, a series of new mononuclear four-coordinate Cu(I) complexes supported by the diphosphine ligand bis[2-(diphenylphosphino)phenyl]ether (POP) and the NHC ligands, consisting of imidazolylidene and pyrimidine units, were synthesized and fully characterized. To tune the photophysical properties of these Cu(I)-NHC complexes, the NHC ligands were attached with electron-withdrawing/donating groups (fluorine, chlorine, methyl and methoxyl) at the pyrimidine unit. All of these Cu(I)-NHC complexes adopt the typical distorted tetrahedral configuration. The electron-donating groups can lead to shorter Cu–N bond distances and longer Cu–C bond distances compared to the electron-withdrawing groups. Theoretical calculation results show that the highest occupied molecular orbitals are mainly distributed on the Cu(I) ion, POP, and carbene unit, while the lowest unoccupied molecular orbitals are mostly located on the pyrimidine unit of NHC ligands. The lowest energy electronic transitions of these Cu(I)-NHC complexes are mainly the metal-to-ligand charge transfer transition and ligand-to-ligand charge transfer transition. These Cu(I)-NHC complexes in solid state show tunable emissions from 530 to 618 nm with efficiencies of 0.5–38.1% at room temperature. The photophysical behaviors of these complexes at 298 and 50 K match well with the thermally activated delayed fluorescence (TADF) characteristics.

Keywords: Cu(I) complexes, N-heterocyclic carbene, thermally activated delayed fluorescence, crystal structures, theoretical calculations

INTRODUCTION

Since the efficient organic-light emitting diodes (OLEDs) and light-emitting electrochemical cells (LEECs) based on Cu(I) complexes were reported by Wang group and Armaroli group (Zhang et al., 2004; Armaroli et al., 2006), respectively, luminescent Cu(I) complexes have been attracting considerable attention as the emitting materials for electroluminescent (EL) devices

(Volz et al., 2014; Gneuß et al., 2015; Hofbeck et al., 2015; Kobayashi et al., 2016; Brunner et al., 2017; He et al., 2017; Huang et al., 2017; Su et al., 2017; Brown et al., 2018; Mohankumar et al., 2018; Schinabeck et al., 2018; Jia et al., 2019). According to the recent reports, most of Cu(I) complexes show thermally activated delayed fluorescence (TADF) due to small energy gaps (ΔE_{ST}) between the lowest singlet state (S_1) and the lowest triplet states (T_1) (Gneuß et al., 2015; Hofbeck et al., 2015; Kobayashi et al., 2016; Brunner et al., 2017; Huang et al., 2017; Su et al., 2017; Mohankumar et al., 2018; Schinabeck et al., 2018; Jia et al., 2019). As we all know, singlet and triplet excitons are formed in a ratio of 1:3 during EL device operation. In the EL devices based on TADF materials, T_1 excitons can be translated to S_1 excitons through reverse intersystem crossing (RISC), and all S_1 excitons will be converted into photons by the spin-allowed $S_1 \rightarrow S_0$ transition (Wang K. et al., 2017; Shi et al., 2018). Thus, the EL devices using TADF Cu(I) complexes as emitters can utilize both singlet and triplet excitons to generate photons resulting in high EL efficiencies. For this reason, TADF Cu(I) complexes are seen as promising alternatives to the phosphorescent complexes based on noble metals, such as Ir(III) and Pt(II) complexes.

Photophysical properties of the homoleptic Cu(I) complexes supported by diimine ligands (general formula $[\text{Cu}(\text{N}^{\wedge}\text{N})_2]^+$) have always been the focus of research for a long time (Simon et al., 1996; Felder et al., 2001; Kovalevsky et al., 2003; Kalsani and Schmittel, 2006; Leydet et al., 2007). Although many significant research results were obtained, these Cu(I) complexes only show very low emission efficiencies. In 2002, McMillin group used a chelating diphosphine ligand to prepare heteroleptic Cu(I) complexes first, which brought a great breakthrough in the emission efficiency of luminescent Cu(I) complexes (Cuttell et al., 2002; Kuang et al., 2002). For example, the photoluminescence quantum yield (ϕ_{PL}) of $[\text{Cu}(\text{dbp})(\text{POP})]^+$ is hundreds-fold larger than those of $[\text{Cu}(\text{N}^{\wedge}\text{N})_2]^+$, where POP = bis[2-(diphenylphosphino)phenyl]ether, dbp = 2,9-di-*n*-butyl-1,10-phenanthroline. In recent years, lots of luminescent heteroleptic Cu(I) complexes supported by chelating diphosphine ligands and diimine ligands (general formula $[\text{Cu}(\text{P}^{\wedge}\text{P})(\text{N}^{\wedge}\text{N})]^+$) have been successfully developed, and efficient EL devices based on this kind of Cu(I) complexes have been fabricated (Cheng et al., 2015; Osawa et al., 2015; Liang et al., 2016; Lin et al., 2017; Zhang et al., 2017; Alkan-Zambada et al., 2018; Keller et al., 2018; Liu et al., 2018; Brunner et al., 2019).

It is well known that N-heterocyclic carbenes (NHCs) are excellent ligands for transition metal complexes because of their strong σ -donating ability and modest π -accepting ability. Moreover, it has been proven that two- and three-coordinate Cu(I) complexes supported by NHC ligands can give efficient TADF or phosphorescence (Krylova et al., 2012; Leilt et al., 2014; Marion et al., 2014; Elie et al., 2016; Nishikawa et al., 2016; Hamze et al., 2017; Lu et al., 2018). In view of these findings, we synthesized several four-coordinate Cu(I)-NHC complexes with efficient TADF by replacing the diimine ligands in $[\text{Cu}(\text{P}^{\wedge}\text{P})(\text{N}^{\wedge}\text{N})]^+$ with the chelating NHC ligands consisting of imidazolylidene and pyridine (Wang et al., 2016, 2018), and the Zhao group also carried out similar research (Liu et al., 2017; Wang J. et al., 2017; Xu et al., 2018).

In this paper, we designed a series of new chelating NHC ligands, in which the imidazolylidene unit is connected with the pyrimidine unit (**Scheme 1**). Five luminescent Cu(I)-NHC complexes supported by these NHC ligands and the diphosphine ligand POP were successfully synthesized and fully characterized. Research results indicate that the electron-withdrawing/donating groups at pyrimidine unit can effectively tune the photophysical properties of these Cu(I)-NHC complexes, and the emission behaviors of these complexes at 50 K and 298 K match well with TADF characters.

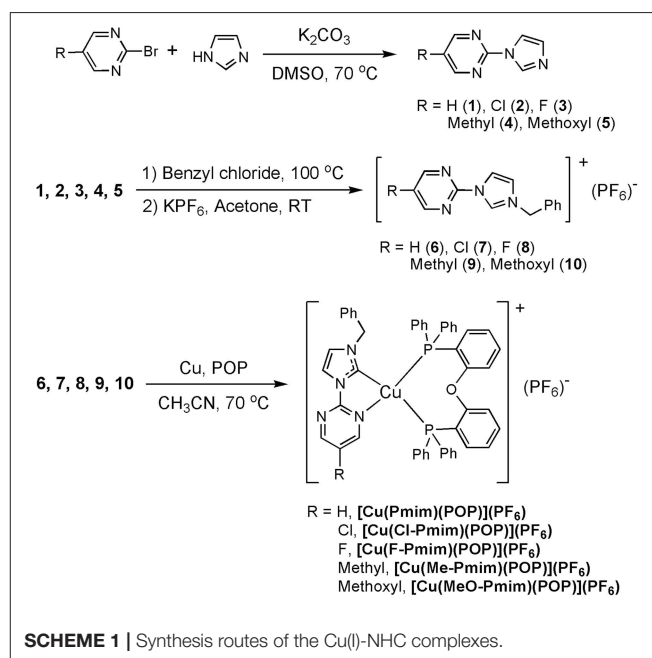
EXPERIMENTAL

General Methods

^1H NMR, ^{13}C NMR, and ^{31}P NMR spectra were recorded on the Bruker Avance 400 spectrometer and Bruker Avance 500 spectrometer. ^1H and ^{13}C chemical shifts are referenced to the internal tetramethylsilane ($\delta = 0$ ppm) and ^{31}P chemical shifts were referenced to the external 85% phosphoric acid ($\delta = 0$ ppm). Mass spectra (MS) were obtained on a Bruker Bruker APEX II FT-ICR instrument. Elemental analysis was performed on a Vario III elemental analyzer. UV-visible absorption spectra were recorded on a Hitachi U-3010 UV-vis spectrophotometer. Photoluminescence (PL) spectra, emission lifetimes, and absolute emission quantum yields were recorded on an Edinburgh FLS980 spectrometer equipped with an integrating sphere.

Synthesis

All starting materials were purchased from commercial suppliers and used as received. Solvents are analytical grade and used without further purification unless otherwise stated.



2-(1H-imidazol-1-yl)pyrimidine (1)

2-bromopyrimidine (790 mg, 5 mmol), imidazole (680 mg, 5 mmol), K_2CO_3 (1.39 g, 10 mmol) and DMSO (15 mL) were added in a round-bottomed flask, then the reaction mixture was stirred vigorously for 24 h at 70°C. After cooling, ethyl acetate (30 mL) was added to the mixture, and then the organic solution was washed with water, dried over anhydrous $MgSO_4$ and evaporated with a rotary evaporator. The residue was purified by column chromatography using ethyl acetate/dichloromethane (1:1 v/v) as a eluent to give the desired product as white powder. Yield: 569 mg (78%). 1H NMR (400 MHz, $CDCl_3$) δ (ppm): 8.70 (2H, d, $J = 4.8$), 8.63 (1H, s), 7.90 (1H, s), 7.21 (1H, t, $J = 4.8$), 7.18 (1H, s). MS (m/z , ESI): 147.1 $[M+H]^+$.

5-chloro-2-(1H-imidazol-1-yl)pyrimidine (2)

2-bromo-5-chloropyrimidine (965 mg, 5 mmol), imidazole (680 mg, 5 mmol), K_2CO_3 (1.39 g, 10 mmol) and DMSO (15 mL) were added in a round-bottomed flask, then the reaction mixture was stirred vigorously for 24 h at 70°C. After cooling, ethyl acetate (30 mL) was added to the mixture, and then the organic solution was washed with water, dried over anhydrous $MgSO_4$ and evaporated with a rotary evaporator. The residue was purified by column chromatography using ethyl acetate/dichloromethane (1:1 v/v) as eluent to give the desired product as white powder. Yield: 730 mg (81%). 1H NMR (400 MHz, $CDCl_3$) δ (ppm): 8.57 (2H, s), 8.50 (1H, s), 7.77 (1H, s), 7.10 (1H, s). MS (m/z , ESI): 181.0 $[M+H]^+$.

5-fluoro-2-(1H-imidazol-1-yl)pyrimidine (3)

2-bromo-5-fluoropyrimidine (885 mg, 5 mmol), imidazole (680 mg, 5 mmol), K_2CO_3 (1.39 g, 10 mmol) and DMSO (15 mL) were added in a round-bottomed flask, then the reaction mixture was stirred vigorously for 24 h at 70°C. After cooling, ethyl acetate (30 mL) was added to the mixture, and then the organic solution was washed with water, dried over anhydrous $MgSO_4$, and evaporated with a rotary evaporator. The residue was purified by column chromatography using ethyl acetate/dichloromethane (1:1 v/v) as eluent to give the desired product as white powder. Yield: 697 mg (85%). 1H NMR (400 MHz, $CDCl_3$) δ (ppm): 8.57 (2H, s), 8.55 (1H, s), 7.83 (1H, d, $J = 0.8$), 7.17 (1H, d, $J = 0.4$). MS (m/z , ESI): 165.1 $[M+H]^+$.

2-(1H-imidazol-1-yl)-5-methylpyrimidine (4)

2-bromo-5-methylpyrimidine (865 mg, 5 mmol), imidazole (680 mg, 5 mmol), K_2CO_3 (1.39 g, 10 mmol) and DMSO (15 mL) were added in a round-bottomed flask, then the reaction mixture was stirred vigorously for 24 h at 70°C. After cooling, ethyl acetate (30 mL) was added to the mixture, and then the organic solution was washed with water, dried over anhydrous $MgSO_4$ and evaporated with a rotary evaporator. The residue was purified by column chromatography using ethyl acetate/dichloromethane (1:1 v/v) as eluent to give the desired product as white powder. Yield: 576 mg (72%). 1H NMR (400 MHz, $CDCl_3$) δ (ppm): 8.58 (1H, s), 8.49 (2H, s), 7.86 (1H, s), 7.15 (1H, s), 2.33 (3H, s). ^{13}C NMR (100 MHz, $CDCl_3$) δ (ppm): 158.66, 153.18, 136.09, 130.58, 128.40, 116.55, 15.21. HRMS (m/z , ESI): 161.0823 $[M+H]^+$.

2-(1H-imidazol-1-yl)-5-methoxypyrimidine (5)

2-bromo-5-methoxypyrimidine (945 mg, 5 mmol), imidazole (680 mg, 5 mmol), K_2CO_3 (1.39 g, 10 mmol) and DMSO (15 mL) were added in a round-bottomed flask, then the reaction mixture was stirred vigorously for 24 h at 70°C. After cooling, ethyl acetate (30 mL) was added to the mixture, and then the organic solution was washed with water, dried over anhydrous $MgSO_4$ and evaporated with a rotary evaporator. The residue was purified by column chromatography using ethyl acetate/dichloromethane (1:1 v/v) as eluent to give the desired product as white powder. Yield: 616 mg (70%). 1H NMR (400 MHz, $CDCl_3$) δ (ppm): 8.52 (1H, s), 8.34 (2H, s), 7.82 (1H, s), 7.15 (1H, s), 3.95 (3H, s). ^{13}C NMR (100 MHz, $CDCl_3$) δ (ppm): 151.97, 148.79, 144.63, 135.88, 130.46, 116.60, 56.47. HRMS (m/z , ESI): 177.0772 $[M+H]^+$.

Compound 6

In a round-bottomed flask, a mixture of benzyl chloride (1.27 g, 10 mmol) 2-(1H-imidazol-1-yl)pyrimidine (584 mg, 4 mmol) was refluxed at 100°C for 2 h. After the excess benzyl chloride was evaporated under vacuum, the residue was put in acetone (20 mL). Then KPF_6 (1.84 g, 10 mmol) was added and stirred for 3 h. The precipitate KCl was filtrated and the organic solvent was evaporated with a rotary evaporator to give the desired product as white powder. Yield: 1.31 g (85%). 1H NMR (400 MHz, Acetone- D_6) δ (ppm): 10.16 (1H, s), 9.04 (2H, d, $J = 4.8$), 8.52 (1H, s), 7.96 (1H, s), 7.77 (1H, t, $J = 4.8$), 7.64–7.62 (2H, m), 7.49–7.41 (3H, m), 5.78 (2H, s). ^{13}C NMR (100 MHz, Acetone- D_6) δ (ppm): 160.86, 153.42, 136.52, 134.61, 130.17, 130.13, 129.72, 124.72, 123.49, 120.75, 54.57. Anal. Calcd. for $C_{14}H_{13}F_6N_4P$: C 43.99, H 3.43, N 14.66; Found: C 44.07, H 3.46, N 14.69.

Compound 7

In a round-bottomed flask, a mixture of benzyl chloride (1.27 g, 10 mmol) 5-chloro-2-(1H-imidazol-1-yl)pyrimidine (720 mg, 4 mmol) was refluxed at 100°C for 2 h. After the excess benzyl chloride was evaporated under vacuum, the residue was put in acetone (20 mL). Then KPF_6 (1.84 g, 10 mmol) was added and stirred for 3 h. The precipitate KCl was filtrated and the organic solvent was evaporated with a rotary evaporator to give the desired product as white powder. Yield: 1.38 g (83%). 1H NMR (400 MHz, Acetone- D_6) δ (ppm): 10.17 (1H, s), 9.11 (2H, s), 8.50 (1H, s), 7.99 (1H, s), 7.63–7.61 (2H, m), 7.48–7.45 (3H, m), 5.79 (2H, s). ^{13}C NMR (100 MHz, Acetone- D_6) δ (ppm): 159.20, 151.60, 136.81, 134.55, 132.51, 130.23, 130.16, 129.75, 124.92, 120.99, 54.67. Anal. Calcd. for $C_{14}H_{12}ClF_6N_4P$: C 40.35, H 2.90, N 13.45; Found: C 40.42, H 2.88, N 13.48.

Compound 8

In a round-bottomed flask, a mixture of benzyl chloride (1.27 g, 10 mmol) 5-fluoro-2-(1H-imidazol-1-yl)pyrimidine (656 mg, 4 mmol) was refluxed at 100°C for 2 h. After the excess benzyl chloride was evaporated under vacuum, the residue was put in acetone (20 mL). Then KPF_6 (1.84 g, 10 mmol) was added and stirred for 3 h. The precipitate KCl was filtrated and the organic solvent was evaporated with a rotary evaporator to give the desired product as white powder. Yield: 1.30 g (81%). 1H NMR

(400 MHz, Acetone- D_6) δ (ppm): 10.14 (1H, s), 9.06 (2H, s), 8.50 (1H, s), 7.98 (1H, s), 7.62–7.56 (2H, m), 7.47–7.43 (3H, m), 5.79 (2H, s). ^{13}C NMR (100 MHz, Acetone- D_6) δ (ppm): 159.00 (J = 261.4), 149.27, 148.72 (J = 24), 136.68, 134.60, 130.21, 130.16, 129.73, 124.85, 121.07, 54.61. Anal. Calcd. for $\text{C}_{14}\text{H}_{12}\text{F}_7\text{N}_4\text{P}$: C 42.01, H 3.02, N 14.00; Found: C 42.08, H 3.04, N 14.03.

Compound 9

In a round-bottomed flask, a mixture of benzyl chloride (1.27 g, 10 mmol) 2-(1H-imidazol-1-yl)-5-methylpyrimidine (640 mg, 4 mmol) was refluxed at 100°C for 2 h. After the excess benzyl chloride was evaporated under vacuum, the residue was put in acetone (20 mL). Then KPF_6 (1.84 g, 10 mmol) was added and stirred for 3 h. The precipitate KCl was filtrated and the organic solvent was evaporated with a rotary evaporator to give the desired product as white powder. Yield: 1.39 g (88%). ^1H NMR (400 MHz, Acetone- D_6) δ (ppm): 10.10 (1H, s), 8.87 (2H, s), 8.47 (1H, s), 7.94 (1H, s), 7.64–7.61 (2H, m), 7.47–7.41 (3H, m), 5.77 (2H, s), 2.46 (3H, s). ^{13}C NMR (100 MHz, Acetone- D_6) δ (ppm): 160.48, 151.60, 136.22, 134.66, 133.81, 130.16, 130.13, 129.73, 124.61, 120.65, 54.53, 15.14. Anal. Calcd. for $\text{C}_{15}\text{H}_{15}\text{F}_6\text{N}_4\text{P}$: C 45.46, H 3.82, N 14.14; Found: C 43.35, H 3.79, N 14.11.

Compound 10

In a round-bottomed flask, a mixture of benzyl chloride (1.27 g, 10 mmol) 2-(1H-imidazol-1-yl)-5-methoxypyrimidine (704 mg, 4 mmol) was refluxed at 100°C for 2 h. After the excess benzyl chloride was evaporated under vacuum, the residue was put in acetone (20 mL). Then KPF_6 (1.84 g, 10 mmol) was added

and stirred for 3 h. The precipitate KCl was filtrated and the organic solvent was evaporated with a rotary evaporator to give the desired product as white powder. Yield: 1.47 g (89%). ^1H NMR (400 MHz, Acetone- D_6) δ (ppm): 10.04 (1H, s), 8.70 (2H, s), 8.43 (1H, s), 7.94 (1H, s), 7.63–7.61 (2H, m), 7.48–7.43 (3H, m), 5.76 (2H, s), 4.09 (3H, s). ^{13}C NMR (100 MHz, Acetone- D_6) δ (ppm): 155.41, 146.59, 146.32, 135.84, 134.73, 130.13, 129.71, 124.56, 120.68, 57.53, 54.46. Anal. Calcd. for $\text{C}_{15}\text{H}_{15}\text{F}_6\text{N}_4\text{OP}$: C 43.70, H 3.67, N 13.59; Found: C 43.61, H 3.63, N 13.56.

[Cu(Pmim)(POP)](PF_6)

Under N_2 atmosphere, compound 6 (382 mg, 1 mmol), copper powder (77 mg, 1.2 mmol) and POP (538 mg, 1 mmol) reacted in CH_3CN (10 mL) at 70 °C overnight. After cooling, the resulting mixture was filtered, then the filtrate was collected and evaporated under vacuum. The residue was dissolved in dichloromethane/ethanol solution, and product was obtained as a pale-yellow crystal by slowly evaporating the solvent. Yield: 0.54 g (55%). ^1H NMR (500 MHz, CD_3CN) δ (ppm): 8.45 (2H, d, J = 5.0), 8.07 (1H, d, J = 2.0), 7.39–7.26 (7H, m), 7.32–7.13 (16H, m), 7.07–6.96 (8H, m), 6.80 (2H, d, J = 7.5), 6.68–6.64 (2H, m), 5.14 (2H, s); ^{13}C NMR (125 MHz, CD_3CN) δ (ppm): 158.75, 158.18, 158.14, 158.09, 155.33, 135.72, 134.19, 133.50, 132.86, 132.20, 130.23, 129.99, 128.81, 128.77, 127.99, 125.10, 123.89, 123.77, 123.66, 122.85, 120.52, 119.75, 117.96, 54.94; ^{31}P NMR (202 MHz, CD_3CN) δ (ppm): −9.75 (s), −144.62 (quint). Anal. Calcd. for

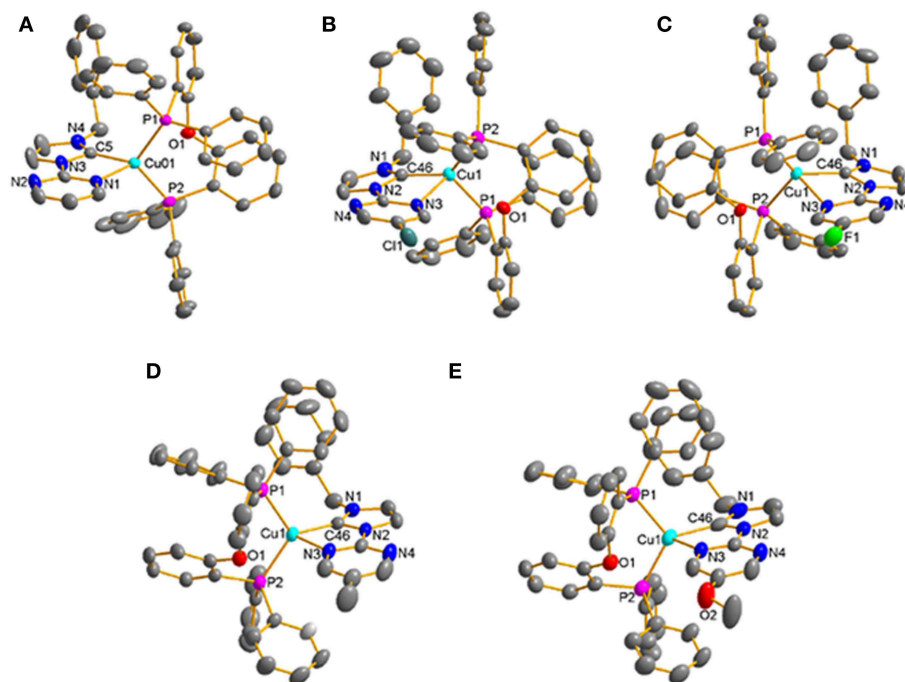


FIGURE 1 | Crystal structures of the Cu(I)-NHC complexes (A) $[\text{Cu}(\text{Pmim})(\text{POP})](\text{PF}_6)$, (B) $[\text{Cu}(\text{Cl-Pmim})(\text{POP})](\text{PF}_6)$, (C) $[\text{Cu}(\text{F-Pmim})(\text{POP})](\text{PF}_6)$, (D) $[\text{Cu}(\text{Me-Pmim})(\text{POP})](\text{PF}_6)$, (E) $[\text{Cu}(\text{MeO-Pmim})(\text{POP})](\text{PF}_6)$ (30% probability ellipsoids, H atoms, solvent molecules and PF_6^- ion are omitted).

$C_{50}H_{40}CuF_6N_4OP_3$: C 61.07, H 4.10, N 5.70; Found: C 61.19, H 4.15, N 5.68.

[Cu(Cl-Pmim)(POP)](PF₆)

Under N₂ atmosphere, compound 7 (416 mg, 1 mmol), copper powder (77 mg, 1.2 mmol) and POP (538 mg, 1 mmol) reacted in CH₃CN (10 mL) at 70°C overnight. After cooling, the resulting mixture was filtered, then the filtrate was collected and evaporated under vacuum. The residue was dissolved in dichloromethane/ethanol solution, and product was obtained as a yellow crystal by slowly evaporating the solvent. Yield: 0.64 g (63%). ¹H NMR (500 MHz, CD₃CN) δ (ppm): 8.31 (2H, s), 8.03 (1H, d, $J = 2.0$), 7.51–7.35 (7H, m), 7.33–7.15 (14H, m), 7.13 (1H, d, $J = 2.0$), 7.09–6.92 (8H, m), 6.83 (2H, d, $J = 7.5$), 6.69–6.63 (2H, m), 5.19 (2H, s); ¹³C NMR (125 MHz, CD₃CN) δ (ppm): 164.33, 158.02, 157.97, 157.92, 156.73, 153.40, 135.54, 134.22, 133.77, 132.73, 132.32, 130.45, 130.00, 128.80, 128.44, 128.07, 125.23, 123.63, 123.51, 123.08, 120.34, 118.21, 55.10; ³¹P NMR (202 MHz, CD₃CN) δ (ppm): –9.53 (s), –144.63 (quint). Anal. Calcd. for $C_{50}H_{39}ClCuF_6N_4OP_3$: C 59.00, H 3.86, N 5.50; Found: C 59.13, H 3.82, N 5.47.

[Cu(F-Pmim)(POP)](PF₆)

Under N₂ atmosphere, compound 8 (400 mg, 1 mmol), copper powder (77 mg, 1.2 mmol) and POP (538 mg, 1 mmol) reacted in CH₃CN (10 mL) at 70°C overnight. After cooling, the resulting mixture was filtered, then the filtrate was collected and evaporated under vacuum. The residue was dissolved in dichloromethane/ethanol solution, and product was obtained as a yellow crystal by slowly evaporating the solvent. Yield: 0.59 g (59%). Yield: 59%. ¹H NMR (500 MHz, CD₃CN) δ (ppm): 8.29 (2H, s), 8.03 (1H, d, $J = 2.0$), 7.49–7.35 (7H, m), 7.33–7.27 (14H, m), 7.13 (1H, d, $J = 2.0$), 7.08–6.95 (8H, m), 6.82 (2H, d, $J = 7.5$), 6.69–6.64 (2H, m), 5.17 (2H, s); ¹³C NMR (125 MHz, CD₃CN) δ (ppm): 158.06, 158.01, 157.96, 156.12 ($J = 258.5$), 151.52, 146.28 ($J = 24$), 135.61, 134.22, 133.66, 132.82, 132.31, 130.36, 130.03, 128.85, 128.05, 127.55, 125.22, 123.62, 123.51, 123.39, 120.41, 118.29, 54.99; ³¹P NMR (202 MHz, CD₃CN) δ (ppm): –9.79 (s), –144.64 (quint). Anal. Calcd. for $C_{50}H_{39}CuF_7N_4OP_3$: C 59.97, H 3.93, N 5.60; Found: C 59.87, H 3.89, N 5.58.

[Cu(Me-Pmim)(POP)](PF₆)

Under N₂ atmosphere, compound 9 (396 mg, 1 mmol), copper powder (77 mg, 1.2 mmol) and POP (538 mg, 1 mmol) reacted

TABLE 1 | Selected Bond Lengths (Å) and Angles (°) of the Cu(I)-NHC complexes.

Compounds	Bond lengths (Å)		Bond angles (°)	
[Cu(Pmim)(POP)](PF ₆)	Cu01–C5	1.968(3)	C5–Cu01–N1	79.10(13)
	Cu01–N1	2.229(2)	C5–Cu01–P1	120.97(9)
	Cu01–P1	2.2470(9)	C5–Cu01–P2	115.61(10)
	Cu01–P2	2.2540(9)	P1–Cu01–P2	110.64(3)
			N1–Cu01–P1	107.92(7)
			N1–Cu01–P2	119.39(7)
[Cu(Cl-Pmim)(POP)](PF ₆)	Cu1–C46	1.957(3)	C46–Cu1–N3	76.55(10)
	Cu1–N3	2.367(2)	C46–Cu1–P1	113.50(9)
	Cu1–P1	2.2660(8)	C46–Cu1–P2	133.30(9)
	Cu1–P2	2.2505(8)	P1–Cu1–P2	112.22(3)
			N3–Cu1–P1	108.23(6)
			N3–Cu1–P2	97.89(6)
[Cu(F-Pmim)(POP)](PF ₆)	Cu1–C46	1.948(2)	C46–Cu1–N3	75.74(9)
	Cu1–N3	2.438(2)	C46–Cu1–P1	132.50(8)
	Cu1–P1	2.2520(7)	C46–Cu1–P2	113.71(8)
	Cu1–P2	2.2668(7)	P1–Cu1–P2	113.23(3)
			N3–Cu1–P1	96.58(5)
			N3–Cu1–P2	107.86(6)
[Cu(Me-Pmim)(POP)](PF ₆)	Cu1–C46	1.993(3)	C46–Cu1–N3	79.26(12)
	Cu1–N3	2.228(3)	C46–Cu1–P1	118.59(9)
	Cu1–P1	2.2882(8)	C46–Cu1–P2	126.83(9)
	Cu1–P2	2.2542(9)	P1–Cu1–P2	112.75(3)
			N3–Cu1–P1	102.87(8)
			N3–Cu1–P2	102.52(8)
[Cu(MeO-Pmim)(POP)](PF ₆)	Cu1–C46	2.083(6)	C46–Cu1–N3	77.79(18)
	Cu1–N3	2.216(4)	C46–Cu1–P1	119.07(13)
	Cu1–P1	2.2735(12)	C46–Cu1–P2	125.53(14)
	Cu1–P2	2.2509(14)	P1–Cu1–P2	113.45(5)
			N3–Cu1–P1	104.64(11)
			N3–Cu1–P2	102.59(11)

in CH₃CN (10 mL) at 70°C overnight. After cooling, the resulting mixture was filtered, then the filtrate was collected and evaporated under vacuum. The residue was dissolved in dichloromethane/ethanol solution, and product was obtained as a colorless crystal by slowly evaporating the solvent. Yield: 0.66 g (66%). ¹H NMR (500 MHz, CD₃CN) δ (ppm): 8.20 (2H, s), 8.04 (1H, d, *J* = 2.0), 7.48–7.34 (7H, m), 7.32–7.26 (14H, m), 7.11 (1H, d, *J* = 2.5), 7.08–6.94 (8H, m), 6.80 (2H, d, *J* = 7.5), 6.69–6.65 (2H, m), 5.16 (2H, s), 2.19 (3H, s); ¹³C NMR (125 MHz, CD₃CN) δ (ppm): 158.26, 158.15, 158.10, 158.06, 153.55, 135.78, 134.16, 133.65, 132.77, 132.20, 130.30, 129.87, 129.69, 127.98, 127.51, 125.11, 123.90, 123.79, 122.62, 120.39, 117.86, 54.94, 14.09; ³¹P NMR (202 MHz, CD₃CN) δ (ppm): –9.43 (s), –144.63 (quint). Anal. Calcd. for C₅₁H₄₂CuF₆N₄OP₃: C 61.42, H 4.24, N 5.62; Found: C 61.31, H 4.20, N 5.65.

[Cu(MeO-Pmim)(POP)](PF₆)

Under N₂ atmosphere, compound 10 (412 mg, 1 mmol), copper powder (77 mg, 1.2 mmol) and POP (538 mg, 1 mmol) reacted in CH₃CN (10 mL) at 70°C overnight. After cooling, the resulting mixture was filtered, then the filtrate was collected and evaporated under vacuum. The residue was dissolved in dichloromethane/ethanol solution, and product was obtained as a greenish crystal by slowly evaporating the solvent. Yield: 0.65 g (64%). ¹H NMR (500 MHz, CD₃CN) δ (ppm): 8.00 (1H, d, *J* = 2.0), 7.99 (2H, s), 7.50–7.38 (7H, m), 7.36–7.28 (14H, m), 7.10 (1H, d, *J* = 2.0), 7.08–6.89 (8H, m), 6.83 (2H, d, *J* = 7.5), 6.65–6.62 (2H, m), 5.25 (2H, s), 3.56 (3H, s); ¹³C NMR (125 MHz, CD₃CN) δ (ppm): 158.06, 157.98, 157.93, 152.25, 135.88, 134.17, 133.60, 132.67, 132.25, 130.26, 128.89, 128.71, 127.97, 127.54, 125.21, 123.82, 123.70, 122.51, 120.32, 117.83, 56.28, 55.03; ³¹P NMR (202 MHz, CD₃CN) δ (ppm): –9.44 (s), –144.65 (quint). Anal. Calcd. for C₅₁H₄₂CuF₆N₄O₂P₃: C 60.45, H 4.18, N 5.53; Found: C 60.33, H 4.12, N 5.56.

X-Ray Crystallographic Analysis

Diffraction data for these complexes were collected on a Bruker SMART APEX-II CCD diffractometer with Mo K α radiation (λ

= 0.71 073 Å). The data were corrected for Lorentz polarization factors as well as for absorption. Structures were solved by direct methods and refined by full-matrix least-squares methods on *F*² with the SHELXL-97 program. All non-hydrogen atoms were refined anisotropically, while H atoms were placed in geometrically calculated positions. CCDC reference numbers for [Cu(Pmim)(POP)](PF₆), [Cu(Cl-Pmim)(POP)](PF₆), [Cu(F-Pmim)(POP)](PF₆), [Cu(Me-Pmim)(POP)](PF₆) and [Cu(MeO-Pmim)(POP)](PF₆) are 1852674, 1852675, 1852676, 1852677 and 1852678, respectively.

Theoretical Calculations

Density functional theory (DFT) calculations were performed with B3LYP functional using Gaussian 09 program. The 6-31G* basis set was used for C, N, H, O, F, Cl and P, and the LanL2DZ was used for Cu. Geometric parameters obtained from X-ray analyses were used as a starting point for geometry optimization in the ground state, and frequency calculations were performed to confirm the optimized structures to be true minima on the potential energy surfaces. Time-dependent density functional (TD-DFT) calculations used the optimized geometries. The hole and electron distributions were analyzed by using the multiwfn 3.5 program.

RESULTS AND DISCUSSION

Synthesis and Structures

Scheme 1 shows the synthesis routes of these Cu(I)-NHC complexes. The N-arylated imidazoles (**1**, **2**, **3**, **4**, **5**) and the imidazolium salts (**6**, **7**, **8**, **9**, **10**) were synthesized through the reported method (Wang et al., 2015, 2016). The target Cu(I)-NHC complexes were synthesized by the simple one-pot method reported by Zhao group (Liu et al., 2017; Wang J. et al., 2017; Xu et al., 2018). All of these complexes are very stable to air and moisture in a solid state at room temperature. The structures of these complexes were characterized by ¹H NMR, ¹³C NMR, and ³¹P NMR, and the characteristic signal peaks from methylene, methyl, methoxyl groups in the NHC ligands and phosphorus

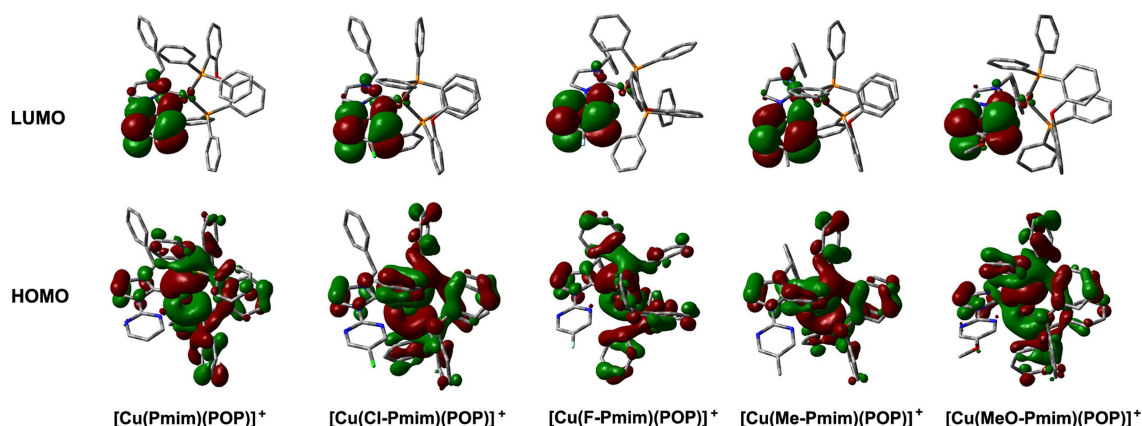


FIGURE 2 | Calculated molecular orbitals for the Cu(I)-NHC complexes. The “+” denotes a positive charge. Figure shows the DFT calculation results. The DFT calculations were performed without regard to the hexafluorophosphate anion in these complexes.

atoms in the ligand POP and hexafluorophosphate anion can be observed clearly in the NMR spectra. Furthermore, the structures of these complexes were confirmed by X-ray crystallography.

All of these complexes adopt the distorted tetrahedral configuration (**Figure 1**), the bond lengths and bond angles around central Cu(I) ions are listed in **Table 1**. It can be found that the Cu–N bond lengths are in agreement with the electron-effect of substituents at the pyrimidine unit of NHC ligands. The electron-donating methyl and methoxyl groups lead to shorter Cu–N bond lengths, while the electron-withdrawing chlorine and fluorine groups lead to longer Cu–N bond lengths, 2.216(4) Å for [Cu(MeO-Pmim)(POP)](PF₆) < 2.228(3) Å for [Cu(Me-Pmim)(POP)](PF₆) < 2.229(2) Å for [Cu(Pmim)(POP)](PF₆) < 2.367(2) Å for [Cu(Cl-Pmim)(POP)](PF₆) < 2.438(2) Å for [Cu(F-Pmim)(POP)](PF₆). It is interesting that the Cu–C bond lengths show an opposite trend to Cu–N bond lengths. The average Cu–P bond lengths

fall in the range 2.2505–2.2712 Å, which are similar to those of reported four-coordinate Cu(I) complexes (Kuang et al., 2002; Gneuß et al., 2015; Liang et al., 2016; Brunner et al., 2017, 2019; Huang et al., 2017; Zhang et al., 2017; Alkan-Zambada et al., 2018; Keller et al., 2018). The dihedral angles between the imidazolydene rings and pyrimidine rings in NHC ligands are 5.5(5)°, 15.5(4)°, 17.3(3)°, 5.1(4)°, and 9.2(6)° for [Cu(Pmim)(POP)](PF₆), [Cu(Cl-Pmim)(POP)](PF₆), [Cu(F-Pmim)(POP)](PF₆), [Cu(Me-Pmim)(POP)](PF₆) and [Cu(MeO-Pmim)(POP)](PF₆), respectively.

Theoretical Calculations

To gain insight into the electronic structures of these complexes, we carried out DFT calculations using the geometric parameters obtained from X-ray analyses as a starting structure. These complexes have similar molecular orbitals (MO) as shown in **Figure 2**. The highest occupied molecular orbitals (HOMOs) are mainly distributed on the Cu(I) ion and the ligand POP, moreover, the imidazolydene unit also has a certain amount of contributions to HOMOs. In contrast, the lowest unoccupied molecular orbitals (LUMOs) are mostly located on the pyrimidine unit and sparingly located on the imidazolydene unit, while the central Cu(I) ion and the ligand POP have minimal contributions. It can be found that the overlaps between the HOMOs and LUMOs of these complexes are very small, which matches with the MO character of TADF materials (Yang et al., 2017; Wang et al., 2019). The TD-DFT calculation results show that the S₁ and T₁ excitations of these complexes mainly involve the HOMO → LUMO transition and HOMO → LUMO+1 transition, while the T₂ excitations involve the lower bonding orbitals and higher anti-bonding orbitals, such as HOMO-1 → LUMO, HOMO-1 → LUMO+1, HOMO-3 → LUMO and so on (**Table S1**). On the basis of TD-DFT results, we analyzed the hole and electron distributions of these complexes at the S₁ and T₁ states. The analysis results show that the lowest energy electronic transitions of these complexes are mainly metal-to-ligand charge transfer (MLCT) transition and

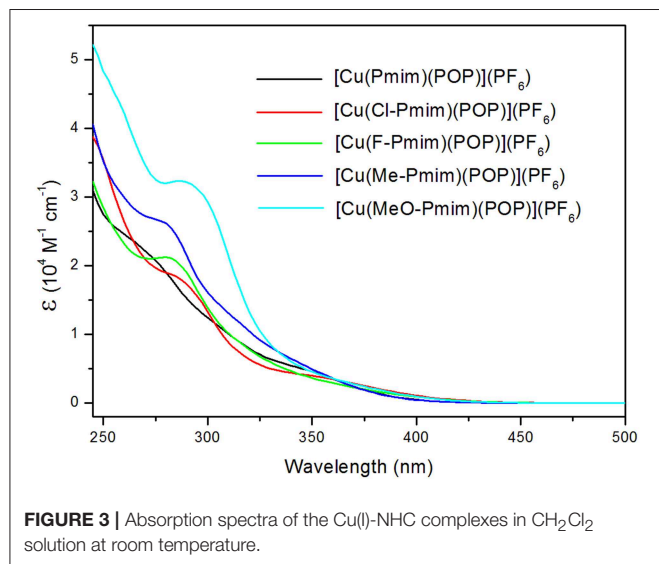


FIGURE 3 | Absorption spectra of the Cu(I)-NHC complexes in CH₂Cl₂ solution at room temperature.

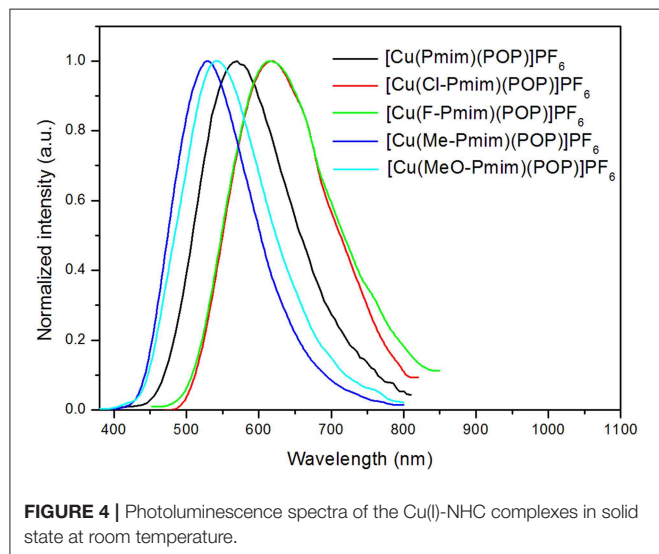


FIGURE 4 | Photoluminescence spectra of the Cu(I)-NHC complexes in solid state at room temperature.

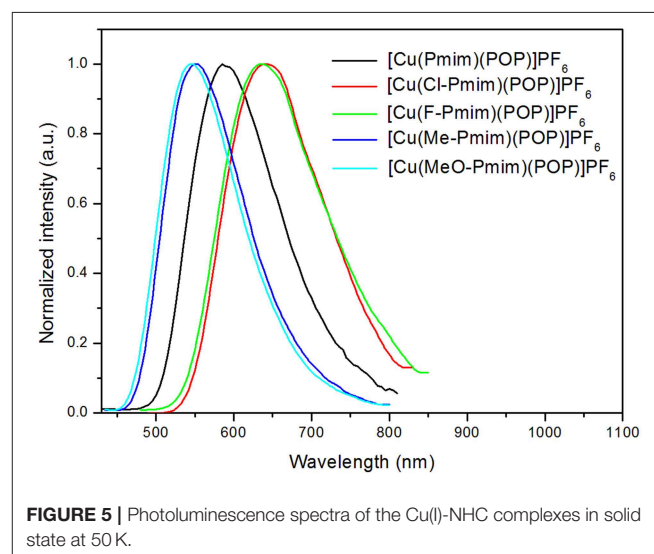


FIGURE 5 | Photoluminescence spectra of the Cu(I)-NHC complexes in solid state at 50 K.

ligand-to-ligand charge transfer (LLCT) transition (**Figure S1**). These calculation results are essentially in agreement with our previous reports and similar to those of other heteroleptic four-coordinate Cu(I) complexes with TADF (Gneuß et al., 2015; Wang et al., 2016, 2018; Huang et al., 2017; Lin et al., 2017).

Photophysical Properties

The UV-visible absorption spectra of these complexes in dichloromethane solution at room temperature are shown in **Figure 3**. All of these complexes exhibit intense absorption bands in the wavelength range <330 nm, which can be assigned to the π - π^* transitions of ligands. By comparing with absorption spectra of the free ligand POP and the NHC ligand precursors **6**, **7**, **8**, **9** and **10** (**Figure S2**), the weaker absorption bands ($\epsilon < 0.85 \times 10^4 \text{ M}^{-1} \text{ cm}^{-1}$) over 330 nm of these complexes can be attributed to the charge transfer (CT) transitions, which include the MLCT and LLCT transitions according to the above calculation results. Because the emission of Cu(I) complexes can be quenched by Jahn-Teller distortion and solvent-induced exciplex (Scaltrito et al., 2000), these complexes do not show luminescence in organic solutions at room temperature.

All of these complexes exhibit obvious emissions in solid state at room temperature, the emission peaks are located at 570 nm for [Cu(Pmim)(POP)](PF₆), 618 nm for [Cu(Cl-Pmim)(POP)](PF₆), 616 nm for [Cu(F-Pmim)(POP)](PF₆), 530 nm for [Cu(Me-Pmim)(POP)](PF₆) and 542 nm for [Cu(MeO-Pmim)(POP)](PF₆), respectively (**Figure 4**). The photoluminescence spectra of these complexes are broad and unstructured which matches with the CT character of emissive state. It is clear that the electron-withdrawing groups (fluorine and chlorine)/electron-donating groups (methyl and methoxyl groups) at the pyrimidine unit of NHC ligands can significantly red-shift/blue-shift emission wavelength. DFT calculation results show that the LUMOs of these complexes mostly locate on the pyrimidine unit of NHC ligands (**Figure 2**), and it is well-known that electron-withdrawing groups can lower LUMO levels and electron-donating groups can raise LUMO levels, which should be the main reason of the emission wavelength red/blue-shifting for these complexes. Similar to previous our reports on Cu(I)-NHC complexes (Wang et al., 2018), the weaker electron-donating methyl group leads to a

shorter emission wavelength in comparison with the stronger electron-donating methoxyl group. The reason should be that the imidazolydene units of these NHC ligands have contributions to both HOMOs and LUMOs, because it means that electron-donating groups can raise HOMO levels as well as LUMO levels. For a similar reason, the emission wavelength of [Cu(Cl-Pmim)(POP)](PF₆) is slightly longer than that of [Cu(F-Pmim)(POP)](PF₆). The absolute photoluminescence quantum yields were measured to 7.4% for [Cu(Pmim)(POP)](PF₆), 0.5% for [Cu(Cl-Pmim)(POP)](PF₆), 0.9% for [Cu(F-Pmim)(POP)](PF₆), 38.1% for [Cu(Me-Pmim)(POP)](PF₆), and 20.1% for [Cu(MeO-Pmim)(POP)](PF₆), respectively. It can be found that the electron-withdrawing/donating groups can obviously decrease/increase the emission efficiencies, which is similar to previous our reports on Cu(I)-NHC complexes (Wang et al., 2016, 2018).

All of these complexes show microsecond-scale emission lifetimes, 6.3 μs for [Cu(Pmim)(POP)](PF₆), 2.8 μs for [Cu(Cl-Pmim)(POP)](PF₆), 4.5 μs for [Cu(F-Pmim)(POP)](PF₆), 20.9 μs for [Cu(Me-Pmim)(POP)](PF₆), and 9.6 μs for [Cu(MeO-Pmim)(POP)](PF₆), respectively. To understand the emissive states of these complexes, photophysical properties under low-temperature condition were measured. The photoluminescence spectra of these complexes in solid state at 50 K are shown in **Figure 5**. The emission spectra measured at 50 K exhibit obvious red-shift (3–25 nm) compared to those acquired at room temperature (298 K). The emission lifetimes increased by a factor of about 3–10 when these complexes are cooled from 298 to 50 K (**Table 2**, **Figure S3**). Moreover, all of these complexes exhibit relatively small ΔE_{ST} from 0.15 to 0.36 eV (**Table 2**). The smaller ΔE_{ST} , red-shift of photoluminescence spectra and increase of emission lifetimes upon decreasing measurement temperature implies that emissions of these complexes at room temperature are TADF.

CONCLUSIONS

In summary, five new cationic mononuclear four-coordinate Cu(I) complexes consisted of the diphosphine ligand POP and the NHC ligands with imidazolydene and pyrimidine units were successfully synthesized. The electron-donating groups at the

TABLE 2 | Emission data of the Cu(I)-NHC complexes in solid state at 298 and 50 K.

Complex	298 K			50 K		S_1^c (eV)	T_1^d (eV)	ΔE_{ST} (eV)
	λ_{em} (nm)	τ^a (μs)	Φ^b (%)	λ_{em} (nm)	τ^a (μs)			
[Cu(Pmim)(POP)](PF ₆)	570	6.3	7.4	586	30.6	2.86	2.61	0.25
[Cu(Cl-Pmim)(POP)](PF ₆)	618	2.8	0.5	643	10.5	2.55	2.40	0.15
[Cu(F-Pmim)(POP)](PF ₆)	616	4.5	0.9	638	15.8	2.65	2.48	0.17
[Cu(Me-Pmim)(POP)](PF ₆)	530	20.9	38.1	552	72.8	3.11	2.75	0.36
[Cu(MeO-Pmim)(POP)](PF ₆)	542	9.6	20.1	545	100.3	3.12	2.78	0.34

^aAverage lifetime which is calculated by the equation $\tau_{\text{ave}} = \sum A_i \tau_i / \sum A_i$ with A_i as the pre-exponential factor for the lifetime. The individual emission lifetimes are listed in **Table S2**.

^bAbsolute photoluminescence quantum yield with relative error = $\pm 10\%$.

^cEstimated from the onset wavelength of emission spectra measured at 298 K.

^dEstimated from the onset wavelength of emission spectra measured at 50 K.

pyrimidine unit of NHC ligands can significantly strengthen the Cu–N bonds and weaken the Cu–C bonds in these complexes, contrarily, the electron-withdrawing groups can lead to longer Cu–N bonds and shorter Cu–C bonds. Theoretical calculations show that these complexes have spatially separated HOMOs and LUMOs, and the lowest energy electronic transitions are mainly MLCT transition and LLCT transition. These complexes in solid state show wavelength-tunable emissions, the electron-donating/withdrawing groups at pyrimidine unit of the NHC ligands can significantly blue/red-shift emission wavelength and can obviously decrease/increase the emission efficiencies. The photophysical behaviors at 298 K and 50 K indicate that emissions of these Cu(I) complexes at room temperature are TADF.

AUTHOR CONTRIBUTIONS

ZW designed whole work. ZW and CX synthesized and characterized these compounds. ZW, XS, and BJ characterized

the physical properties of complexes. All authors contributed to the general discussion.

ACKNOWLEDGMENTS

We are grateful for financial support from the Natural Science Foundation of Henan Province (No. 182300410230), the Training Project for Youth Backbone Teachers in Colleges and Universities of Henan Province (No. 2016GGJS-115), the Innovation Scientists and Technicians Troop Construction Projects of Henan Province (No. 154100510015) and the tackle key problem of science and technology Project of Henan Province (No. 162102210125).

SUPPLEMENTARY MATERIAL

The Supplementary Material for this article can be found online at: <https://www.frontiersin.org/articles/10.3389/fchem.2019.00422/full#supplementary-material>

REFERENCES

- Alkan-Zambada, M., Keller, S., Sessolo, M., Ortí, E., Housecroft, C. E., et al. (2018). [Cu(P[^]P)(N[^]N)](PF₆) compounds with bis(phosphane) and 6-alkoxy, 6-alkylthio, 6-phenyloxy and 6-phenylthio-substituted 2,2'-bipyridine ligands for light-emitting electrochemical cells. *J. Mater. Chem. C* 6, 8460–8471. doi: 10.1039/C8TC02882F
- Armaroli, N., Accorsi, G., Holler, M., Nierengarten, J.-F., Wwnh, R. T., Welter, R., et al. (2006). Highly luminescent Cu^I complexes for light-emitting electrochemical cells. *Adv. Mater.* 18, 1313–1316. doi: 10.1002/adma.200502365
- Brown, C. M., Carta, V., and Wolf, M. O. (2018). Thermochromic solid-state emission of dipyrindyl sulfoxide Cu(I) complexes. *Chem. Mater.* 30, 5786–5795. doi: 10.1021/acs.chemmater.8b02821
- Brunner, F., Babaei, A., Pertegás, A., Ortí, E., Housecroft, C. E., et al. (2019). Phosphane tuning in heteroleptic [Cu(N[^]N)(P[^]P)]⁺ complexes for light-emitting electrochemical cells. *Dalton Trans.* 48, 446–460. doi: 10.1039/C8DT03827A
- Brunner, F., Graber, S., Baumgartner, Y., Häussinger, D., Prescimone, A., Constable, E. C., et al. (2017). The effects of introducing sterically demanding aryl substituents in [Cu(N[^]N)(P[^]P)]⁺ complexes. *Dalton Trans.* 46, 6379–6391. doi: 10.1039/C7DT00782E
- Cheng, G., So, G. K.-M., To, W.-P., Chen, Y., Che, C.-M., et al. (2015). Luminescent zinc(II) and copper(I) complexes for high-performance solution-processed monochromic and white organic light-emitting devices. *Chem. Sci.* 6, 4623–4635. doi: 10.1039/C4SC03161J
- Cuttell, D. G., Kuang, S.-M., Fanwick, P. E., McMillin, D. R., and Walton, R. A. (2002). Simple Cu(I) complexes with unprecedented excited-state lifetimes. *J. Am. Chem. Soc.* 124, 6–7. doi: 10.1021/ja012247h
- Elie, M., Sguerra, F., Linares, M., Hamel, M., Costa, R. D., Gaillard, S., et al. (2016). Designing NHC–copper(I) dipyrindylamine complexes for blue light-emitting electrochemical cells. *ACS. Appl. Mater. Interfaces* 8, 14678–14691. doi: 10.1021/acsami.6b04647
- Felder, D., Nierengarten, J.-F., Barigelletti, F., Ventura, B., and Armaroli, N. (2001). *J. Am. Chem. Soc.* 123, 6291–6299. doi: 10.1021/ja0043439
- Gneuß, T., Leitl, M. J., Finger, L. H., Yersin, H., and Sundermeyer, J. (2015). A new class of deep-blue emitting Cu(I) compounds—effects of counter ions on the emission behavior. *Dalton Trans.* 44, 20045–20055. doi: 10.1039/c5dt03065j
- Hamze, R., Jazzar, R., Soleilhavoup, M., Djurovich, P. I., Bertrand, G., and Thompson, M. E. (2017). Phosphorescent 2-, 3- and 4-coordinate cyclic (alkyl)(amino)carbene (CAAC) Cu(I) complexes. *Chem. Commun.* 53, 9008–9011. doi: 10.1039/C7CC02638B
- He, L.-H., Luo, Y.-S., Chen, J.-L., Ho, C.-L., Wang, J.-Y., Wong, W.-Y., et al. (2017). Luminescent three- and four-coordinate dinuclear copper(I) complexes triply bridged by bis(diphenylphosphino)methane and functionalized 3-(2'-pyridyl)-1,2,4-triazole ligands. *Inorg. Chem.* 56, 10311–10324. doi: 10.1021/acs.inorgchem.7b01159
- Hofbeck, T., Monkowius, U., and Yersin, H. (2015). Highly efficient luminescence of Cu(I) compounds: thermally activated delayed fluorescence combined with short-lived phosphorescence. *J. Am. Chem. Soc.* 137, 399–404. doi: 10.1021/ja5109672
- Huang, C.-H., Wen, M., Wang, C.-Y., Huang, X.-H., Li, H.-H., et al. (2017). A series of pure-blue-light emitting Cu(I) complexes with thermally activated delayed fluorescence: structural, photophysical, and computational studies. *Dalton Trans.* 46, 1413–1419. doi: 10.1039/C6DT03965K
- Jia, J.-H., Chen, X.-L., Liao, J.-Z., Liang, D., Yang, M.-X., Yu, R., et al. (2019). Highly luminescent copper(I) halide complexes chelated with a tetradentate ligand (PNNP): synthesis, structure, photophysical properties and theoretical studies. *Dalton Trans.* 48, 1418–1426. doi: 10.1039/C8DT03452D
- Kalsani, V., and Schmittel, M. (2006). Novel phenanthroline ligands and their kinetically locked copper(I) complexes with unexpected photophysical properties. *Inorg. Chem.* 45, 2061–2067. doi: 10.1021/ic051828v
- Keller, S., Prescimone, A., Bolink, H., Ortí, E., Housecroft, C. E., et al. (2018). Luminescent copper(I) complexes with bisphosphane and halogen-substituted 2,2'-bipyridine ligands. *Dalton Trans.* 47, 14263–14276. doi: 10.1039/C8DT01338A
- Kobayashi, A., Hasegawa, T., Yoshida, M., and Kato, M. (2016). Environmentally friendly mechanochemical syntheses and conversions of highly luminescent Cu(I) dinuclear complexes. *Inorg. Chem.* 55, 1978–1985. doi: 10.1021/acs.inorgchem.5b02160
- Kovalevsky, A. Y., Gembicky, M., Novozhilova, I. V., and Coppens, P. (2003). Solid-state structure dependence of the molecular distortion and spectroscopic properties of the Cu(I) bis(2,9-dimethyl-1,10-phenanthroline) ion. *Inorg. Chem.* 42, 8794–8802. doi: 10.1021/ic0348805
- Krylova, V. A., Djurovich, P. I., Aronson, J. W., Haiges, R., Whited, M. T., and Thompson, M. E. (2012). Dinuclear coinage-metal complexes of bis(NHC) ligands: structural features and dynamic behavior of a Cu–Cu complex. *Organometallics* 31, 7983–7991. doi: 10.1021/om300544g
- Kuang, S.-M., Cuttell, D. G., McMillin, D. R., Fanwick, P. E., and Walton, R. A. (2002). Synthesis and structural characterization of Cu(I) and Ni(II) complexes that contain the bis[2-(diphenylphosphino)phenyl]ether ligand. novel emission properties for the Cu(I) species. *Inorg. Chem.* 41, 3313–3322. doi: 10.1021/ic0201809

- Leitl, M. J., Krylova, V. A., Djurovich, P. I., Thompson, M. E., and Yersin, H. (2014). Phosphorescence versus thermally activated delayed fluorescence. Controlling singlet–triplet splitting in brightly emitting and sublimable Cu(I) compounds. *J. Am. Chem. Soc.* 136, 16032–16038. doi: 10.1021/ja508155x
- Leydet, Y., Bassani, D. M., Jonusauskas, G., and McClenaghan, N. D. (2007). Equilibration between three different excited states in a bichromophoric copper(I) polypyridine complex. *J. Am. Chem. Soc.* 129, 8688–8689. doi: 10.1021/ja072335n
- Liang, D., Chen, X.-L., Liao, J.-Z., Hu, J.-Y., Jia, J.-H., and Lu, C.-Z. (2016). Highly efficient cuprous complexes with thermally activated delayed fluorescence for solution-processed organic light-emitting devices. *Inorg. Chem.* 55, 7467–7475. doi: 10.1021/acs.inorgchem.6b00763
- Lin, L., Chen, D.-H., Yu, R., Chen, X.-L., Lu, C.-Z., et al. (2017). Photo- and electro-luminescence of three TADF binuclear Cu(I) complexes with functional tetraamine ligands. *J. Mater. Chem. C* 5, 4495–4504. doi: 10.1039/C7TC00443E
- Liu, L.-P., Li, Q., Liu, L., Li, G. H., Li, F.-B., Wong, W.-Y., et al. (2018). Near-saturated red emitters: four-coordinate copper(I) halide complexes containing 8-(diphenylphosphino)quinoline and 1-(diphenylphosphino)naphthalene ligands. *Dalton Trans.* 47, 9294–9302. doi: 10.1039/C7DT04528J
- Liu, S., Xu, S., Wang, J., Zhao, F., Xia, H., and Wang, Y. (2017). Four-coordinate N-heterocyclic carbene (NHC) copper(I) complexes with brightly luminescence properties. *J. Coord. Chem.* 70, 584–599. doi: 10.1080/00958972.2016.1278075
- Lu, T., Wang, J.-Y., Shi, L.-X., Chen, Z.-N., Chen, X.-T., and Xue, Z.-L. (2018). Synthesis, structures and luminescence properties of amine-bis(N-heterocyclic carbene) copper(I) and silver(I) complexes. *Dalton Trans.* 47, 6742–6753. doi: 10.1039/C8DT00599K
- Marion, R., Sguerra, F., Linares, M., Hamel, M., Gaillard, S., et al. (2014). NHC copper(I) complexes bearing dipyridylamine ligands: synthesis, structural, and photoluminescent studies. *Inorg. Chem.* 53, 9181–9191. doi: 10.1021/ic501230m
- Mohankumar, M., Holler, M., Nierengarten, J.-F., Sauvage, J.-P., Delavaux-Nicot, B., Armaroli, N., et al. (2018). Heteroleptic copper(I) pseudorotaxanes incorporating macrocyclic phenanthroline ligands of different sizes. *J. Am. Chem. Soc.* 140, 2336–2347. doi: 10.1021/jacs.7b12671
- Nishikawa, M., Sano, T., Washimi, M., Takao, K., and Tsubomura, T. (2016). Emission properties and Cu(I)–Cu(I) interaction in 2-coordinate dicopper(I)-bis(N-heterocyclic)carbene complexes. *Dalton Trans.* 45, 12127–12136. doi: 10.1039/C6DT01239F
- Osawa, M., Hoshino, M., Hashimoto, M., Kawata, I., Igawa, S., and Yashima, M. (2015). Application of three-coordinate copper(I) complexes with halide ligands in organic light-emitting diodes that exhibit delayed fluorescence. *Dalton Trans.* 43, 8369–8378. doi: 10.1039/C4DT02853H
- Scaltrito, D. V., Thompson, D. W., O'Callaghan, J. A., and Meyer, G. J. (2000). *Coord. Chem. Rev.* 208, 243–1016.
- Schinabeck, A., Rau, N., Klein, M., Sundermeyer, J., and Yersin, H. (2018). Deep blue emitting Cu(I) tripod complexes. Design of high quantum yield materials showing TADF-assisted phosphorescence. *Dalton Trans.* 47, 17067–17076. doi: 10.1039/C8DT04093A
- Shi, Y.-Z., Wang, K., Li, X., Dai, G.-L., Liu, W., Zheng, C.-J., et al. (2018). Intermolecular charge-transfer transition emitter showing thermally activated delayed fluorescence for efficient non-doped OLEDs. *Angew. Chem. Int. Ed.* 57, 9480–9484. doi: 10.1002/anie.201804483
- Simon, J. A., Palke, W. E., and Ford, P. C. (1996). Photophysical and *ab initio* studies of mononuclear copper(I) complexes. *Inorg. Chem.* 35, 6413–6421. doi: 10.1021/ic960367y
- Su, Z. C., Zheng, C. C., Cheng, G., Che, C.-M., and Xu, S. J. (2017). Triplet harvesting in luminescent Cu(I) complexes by the thermally activated luminescence transition mechanism: impact of the molecular structure. *J. Mater. Chem. C* 5, 4488–4494. doi: 10.1039/C7TC00773F
- Volz, D., Wallesch, M., Grage, S. L., Heske, C., Weinhardt, L., Baumann, T., Bräse, S., et al. (2014). Labile or stable: can homoleptic and heteroleptic pyrPHOS–copper complexes be processed from solution? *Inorg. Chem.* 53, 7837–7847. doi: 10.1021/ic500135m
- Wang, J., Liu, S., Xu, S., Zhao, F., Xia, H., and Wang, Y. (2017). Four-coordinated copper(I) complexes containing variably substituted N-heterocyclic carbenes (NHCs): Synthesis, photophysical properties and theoretical investigation. *J. Organomet. Chem.* 846, 351–359. doi: 10.1016/j.jorganchem.2017.07.016
- Wang, K., Zheng, C.-J., Liu, W., Liang, K., Lee, C.-S., Zhang, X.-H., et al. (2017). Avoiding energy loss on TADF emitters: controlling the dual conformations of D–A structure molecules based on the pseudoplanar segments. *Adv. Mater.* 29, 1701476. doi: 10.1002/adma.201701476
- Wang, L., Liu, N., and Dai, B. (2015). Metal-free site-selective C–N bond-forming reaction of polyhalogenated pyridines and pyrimidines. *RSC Adv.* 5, 82097–82111. doi: 10.1039/C5RA18653F
- Wang, Z., Cai, J., Zhang, M., Zheng, C., and Ji, B. (2019). A novel yellow thermally activated delayed fluorescence emitter for highly efficient organic light-emitting diodes. *Acta Chim. Sinica* 77:263–268. doi: 10.6023/A18100437
- Wang, Z., Sun, X., Fu, W., Xu, C., and Ji, B. (2018). Four-coordinate Cu(I) complexes supported by N-heterocyclic carbene ligands bearing electron-donating/withdrawing groups: synthesis, structures and photophysical properties. *J. Lumin.* 204, 618–625. doi: 10.1016/j.jlumin.2018.08.064
- Wang, Z., Zheng, C., Wang, W., Xu, C., Ji, B., and Zhang, X. (2016). Synthesis, structure, and photophysical properties of two four-coordinate Cu^I-NHC complexes with efficient delayed fluorescence. *Inorg. Chem.* 55, 2157–2164. doi: 10.1021/acs.inorgchem.5b02546
- Xu, S., Wang, J., Liu, S., Zhao, F., Xia, H., and Wang, Y. (2018). Synthesis, photophysical properties, and computational studies of four-coordinate copper(I) complexes based on benzimidazolylidene N-heterocyclic carbene (NHC) ligands bearing aryl substituents. *J. Mol. Struct.* 1153, 12–19. doi: 10.1016/j.molstruc.2017.09.119
- Yang, Z., Mao, Z., Xie, Z., Zhang, Y., Liu, S., Zhao, J., et al. (2017). Recent advances in organic thermally activated delayed fluorescence materials. *Chem. Soc. Rev.* 46, 915–1016. doi: 10.1039/C6CS00368K
- Zhang, F., Guan, Y., Chen, X., Wang, S., Liang, D., Feng, Y., et al. (2017). Syntheses, photoluminescence, and electroluminescence of a series of sublimable bipolar cationic cuprous complexes with thermally activated delayed fluorescence. *Inorg. Chem.* 56, 3742–3753. doi: 10.1021/acs.inorgchem.6b01847
- Zhang, Q., Zhou, Q., Cheng, Y., Wang, L., Ma, D., Jing, X., et al. (2004). Highly efficient green phosphorescent organic light-emitting diodes based on Cu^I complexes. *Adv. Mater.* 16, 432–436. doi: 10.1002/adma.200306414

Conflict of Interest Statement: The authors declare that the research was conducted in the absence of any commercial or financial relationships that could be construed as a potential conflict of interest.

Copyright © 2019 Wang, Sun, Xu and Ji. This is an open-access article distributed under the terms of the Creative Commons Attribution License (CC BY). The use, distribution or reproduction in other forums is permitted, provided the original author(s) and the copyright owner(s) are credited and that the original publication in this journal is cited, in accordance with accepted academic practice. No use, distribution or reproduction is permitted which does not comply with these terms.



New Aggregation-Induced Delayed Fluorescence Luminogens With Through-Space Charge Transfer for Efficient Non-doped OLEDs

Panpan Zhang¹, Jiajie Zeng¹, Jingjing Guo¹, Shijie Zhen¹, Biao Xiao², Zhiming Wang¹, Zujin Zhao^{1*} and Ben Zhong Tang^{1,3*}

¹ State Key Laboratory of Luminescent Materials and Devices, Center for Aggregation-Induced Emission, South China University of Technology, Guangzhou, China, ² Key Laboratory of Optoelectronic Chemical Materials and Devices, School of Chemical and Environmental Engineering, Jiangnan University, Ministry of Education, Wuhan, China, ³ Department of Chemistry, Hong Kong Branch of Chinese National Engineering Research Center for Tissue Restoration and Reconstruction, The Hong Kong University of Science and Technology, Hong Kong, China

OPEN ACCESS

Edited by:

Lian Duan,
Tsinghua University, China

Reviewed by:

CaiJun Zheng,
University of Electronic Science and
Technology of China, China
Christopher Pigge,
The University of Iowa, United States

*Correspondence:

Zujin Zhao
mszjzhao@scut.edu.cn
Ben Zhong Tang
tangbenz@ust.hk

Specialty section:

This article was submitted to
Organic Chemistry,
a section of the journal
Frontiers in Chemistry

Received: 18 January 2019

Accepted: 15 March 2019

Published: 05 April 2019

Citation:

Zhang P, Zeng J, Guo J, Zhen S,
Xiao B, Wang Z, Zhao Z and Tang BZ
(2019) New Aggregation-Induced
Delayed Fluorescence Luminogens
With Through-Space Charge Transfer
for Efficient Non-doped OLEDs.
Front. Chem. 7:199.
doi: 10.3389/fchem.2019.00199

In this work, two tailor-made luminogens comprising of electron donors (acridine and phenoxazine) and acceptor (triazine) bridged by the through-space conjugated hexaphenylbenzene (HPB) are synthesized and characterized. Their thermal stability, electrochemical behaviors, crystal, and electronic structures, and photophysical properties are systematically investigated. The crystal and electronic structures reveal that the peripheral phenyls in HPB are closely aligned in a propeller-like fashion, rendering efficient through-space charge transfer between donor and electron moieties. These molecules display weak fluorescence with negligible delayed component in solutions but strong fluorescence with greatly increased delayed component upon aggregate formation, namely aggregation-induced delayed fluorescence (AIDF). Their neat films exhibit high photoluminescence quantum yields (PLQY), and prominent delayed fluorescence. The non-doped organic light-emitting diodes (OLEDs) based on these new luminogens exhibit excellent performance with maximum external quantum efficiency of 12.7% and very small efficiency roll-off of 2.7% at 1,000 cd m⁻². Designing AIDF molecules with through-space charge transfer could be a promising strategy to explore robust luminescent materials for efficient non-doped OLEDs.

Keywords: aggregation-induced delayed fluorescence, thermally activated delayed fluorescence, through-space charge transfer, organic light-emitting diodes, hexaphenylbenzene

INTRODUCTION

Organic light-emitting diodes (OLEDs) have been extensively studied owing to their excellent properties, such as flexibility, light weight, energy conservation, and so forth, and have gradually become a highly promising technology for flat panel display and white lighting. Organic electroluminescent materials are the foundation of OLEDs. The first-generation luminescent materials for OLEDs are fluorescent materials, such as tris(8-hydroxyquinolino)aluminum (Alq₃) (Tang and VanSlyke, 1987). But the efficiency of the device is greatly limited because only 25% singlet excitons are harvested for light emission in devices. The second-generation luminescent materials are phosphorescent materials that can achieve almost 100% exciton utilization via strong

spin orbit coupling of heavy metals such as platinum and iridium (Baldo et al., 1998; Adachi et al., 2001; Sasabe and Kido, 2013; Minaev et al., 2014). However, the scarcity and high price of noble metals greatly increase the device cost. So, the search for efficient and cheap luminescent materials still remains an urgent task. In response to these issues, several alternative strategies have been proposed, among which purely organic materials with thermally activated delayed fluorescence (TADF) have received the most interest (Endo et al., 2009; Gong et al., 2011; Wang et al., 2014; Zhang et al., 2014; Hirata et al., 2015; Seino et al., 2016). The OLEDs based on TADF emitters can extract light from both triplet and singlet excitons via spin-converting reverse intersystem crossing (RISC) under thermal activation, theoretically granting excellent internal quantum efficiencies (IQE) of up to 100% of the devices (Sun et al., 2014; Kaji et al., 2015; Lee et al., 2015a).

Generally, TADF emitters adopt highly twisted electron donor-acceptor (D-A) structures to realize small ΔE_{ST} , but the PLQY are often reduced, particularly in the aggregated state, which require doping technique in device fabrication. Recently, an interesting strategy to balance ΔE_{ST} and PLQY by through-space charge transfer effect has been proposed (Kawasumi et al., 2015; Rajamalli et al., 2016; Chen et al., 2017; Tsujimoto et al., 2017). For example, Wang et al. (Shao et al., 2017) took advantage of through-space charge transfer between D and A to realize blue TADF polymers with a non-conjugated polyethylene backbone. Spatial electronic coupling between D and A units results in small ΔE_{ST} (0.019 eV) and high PLQY (60%) in film. The resulting blue polymers exhibited good EL performance with a high EL efficiency of 12.1%. In these materials, D and A are physically separated but are spatially proximate. On one hand, the sufficient separation of highest occupied molecular orbital (HOMO) and lowest unoccupied molecular orbital (LUMO) is achieved, resulting in small ΔE_{ST} and thus delayed fluorescence. On the other hand, the electron clouds of D and A can interact with each other via a through-space manner to expedite the radiative transition rate, and enhanced PLQY can be expected.

It is well-known that most TADF emitters need complicated doping technique to suppress emission quenching and exciton annihilation (Tao et al., 2014; Furue et al., 2016). However, severe efficiency roll-off still happens as luminance increases, which impedes their large-scale commercial application (Cao et al., 2017). According to the recent studies, aggregation-induced delayed fluorescence (AIDF) materials provide an advisable strategy for solving this problem (Guo et al., 2017a, 2018a; Huang et al., 2017; Liu et al., 2018). Aggregation-induced delayed fluorescence (AIDF) luminogens are free of concentration quenching, and can exhibit strong delayed fluorescence upon aggregate formation. And the triplet excitons are rapidly converted to singlet excitons by RISC, inducing increased EL efficiency. Furthermore, AIDF luminogens present a highly twisted conformation, which can weaken intermolecular interactions and thus reduces short-range Dexter energy transfer. In consequence, non-doped OLEDs based on AIDF luminogens provide very small efficiency roll-off (Gan et al., 2016; Guo et al., 2017b).

Hexaphenylbenzene (HPB) derivatives have attracted intense research interest because of their fantastic geometry and wide application prospects (Waldvogel et al., 1999; Geng et al., 2001; Balzani et al., 2003; Tanaka et al., 2010; Lambert et al., 2012). HPB not only exhibits strong toroidal delocalization of π -electrons (Sun et al., 2005; Vij et al., 2016) but also has noteworthy aggregation-induced emission (AIE) property (Cho et al., 2006; Kanibolotsky et al., 2010). Integrating various D-A systems into HPB allows us to regulate molecular orbitals distribution, therefore adjust the ΔE_{ST} value and realize delayed fluorescence. Based on these considerations, herein, we develop two novel luminogens containing an electron D-A system built on HPB. The D and A moieties are positioned in close proximity so that electron clouds of D and A can communicate with each other through spatial interactions. The designed HPB-based molecules exhibit distinct AIDF property, and furnish efficient non-doped OLEDs with very small efficiency roll-off.

EXPERIMENTAL

Synthesis

2-(4-Ethynylphenyl)-4,6-diphenyl-1,3,5-triazine (2): Into a 250 mL two-necked round bottom flask was placed compound **1** (7.765 g, 20 mmol), trimethylsilylacetylene (5.653 mL, 40 mmol), $\text{Pd}(\text{PPh}_3)_2\text{Cl}_2$ (1.404 g, 2 mmol), copper iodide (0.761 g, 4 mmol), and PPh_3 (1.049 g, 4 mmol). The flask was evacuated under vacuum and flushed with dry nitrogen by three times and a mixed solvent system of tetrahydrofuran (THF) and triethylamine (100 mL, v/v = 1: 3) was injected. The reaction mixture was refluxed for 12 h. After cooling to room temperature, the mixture was poured into water and extracted with dichloromethane by three times. The combined organic layers were dried over anhydrous magnesium sulfate. After filtration and solvent evaporation, a mixture of the resulting crude product, KOH (2.0 g, 35.7 mmol) and K_2CO_3 (2.0 g, 14.5 mmol) were added into a mixed solvent system of methanol and THF (60 mL, v/v = 1: 1), and then stirred at room temperature for 12 h. The mixture was poured into water and extracted with dichloromethane by three times. The combined organic layers were dried over anhydrous magnesium sulfate. After filtration and solvent evaporation, the crude product was purified by silica-gel column chromatography (dichloromethane: petroleum ether, v/v = 1: 7). White solid of compound **2** was obtained in 65% yield. ^1H NMR (400 MHz, CDCl_3), δ (TMS, ppm): 8.8–8.73 (m, 6H), 7.70 (d, J = 8.4 Hz, 2H), 7.66–7.56 (m, 6H), 3.27 (s, 1H); ^{13}C NMR (125 MHz, CDCl_3), δ (TMS, ppm): 171.90, 171.06, 136.63, 136.23, 132.78, 132.53, 129.14, 128.94, 128.83, 126.30, 83.55, 79.88. HRMS ($\text{C}_{23}\text{H}_{15}\text{N}_3$): m/z 334.1354 [$\text{M} + \text{H}^+$, calcd 334.1344].

10-(4-((4-(4,6-Diphenyl-1,3,5-triazin-2-yl)phenyl)ethynyl)phenyl)-10-phenoxazine (5a): Into a 250 mL two-necked round bottom flask was placed compound **2** (3.331 g, 10 mmol), compound **3** (1.685 g, 5 mmol), $\text{Pd}(\text{PPh}_3)_2\text{Cl}_2$ (0.351 g, 0.5 mmol), copper iodide (0.190 g, 1 mmol), and PPh_3 (0.262 g, 1 mmol). The flask was evacuated under vacuum and flushed with dry nitrogen by three times and a mixed solvent system of THF and triethylamine (100 mL, v/v = 1: 3) was

injected. The reaction mixture was refluxed for 12 h. After cooling to room temperature, the mixture was poured into water and extracted with dichloromethane by three times. The combined organic layers were dried over anhydrous magnesium sulfate. After filtration and solvent evaporation, the crude product was purified by silica-gel column chromatography (dichloromethane: petroleum ether, v/v = 1: 10). Yellow solid of compound **5a** was obtained in 23% yield. ^1H NMR (500 MHz, CDCl_3), δ (TMS, ppm): 8.82–8.78 (m, 6H), 7.81 (d, J = 7.0 Hz, 2H), 7.76 (d, J = 8.4 Hz, 2H), 7.66–7.58 (m, 6H), 7.38 (d, J = 7.4 Hz, 2H), 6.73–6.59 (m, 6H), 5.97 (s, 2H); ^{13}C NMR (100 MHz, CDCl_3), δ (TMS, ppm): 171.90, 171.10, 146.31, 144.09, 136.35, 136.26, 134.56, 134.17, 132.79, 132.06, 131.21, 129.15, 129.08, 128.84, 127.15, 123.43, 121.73, 116.01, 115.72, 113.40, 91.23, 90.70. HRMS ($\text{C}_{41}\text{H}_{26}\text{N}_4\text{O}$): m/z 590.2086 [M^+ , calcd 590.2107].

10-(4'-((4,6-Diphenyl-1,3,5-triazin-2-yl)phenyl)ethynyl)phenyl-9,9-dimethyl-9,10-dihydroacridine (**5b**): The procedure was analogous to that described for **5a**. White solid of compound **5b** was obtained in 25% yield. ^1H NMR (500 MHz, CDCl_3), δ (TMS, ppm): 8.83–8.78 (m, 6H), 7.85 (d, J = 8.4 Hz, 2H), 7.78 (d, J = 8.6 Hz, 2H), 7.66–7.58 (m, 6H), 7.49–7.46 (m, 2H), 7.38 (d, J = 8.4 Hz, 2H), 7.02–6.98 (m, 2H), 6.97–6.93 (m, 2H), 6.31 (d, J = 8.0 Hz, 2H), 1.7 (s, 6H); ^{13}C NMR (125 MHz, CDCl_3), δ (TMS, ppm): 171.90, 171.12, 141.70, 140.80, 136.29, 136.28, 134.41, 132.78, 132.06, 131.71, 130.30, 129.15, 129.09, 128.84, 127.27, 126.56, 125.45, 123.11, 120.94, 114.17, 91.46, 90.54, 36.15, 31.37. HRMS ($\text{C}_{44}\text{H}_{32}\text{N}_4$): m/z 616.2616 [M^+ , calcd 616.2627].

10-(4''-(4,6-Diphenyl-1,3,5-triazin-2-yl)-3',4',5',6'-tetraphenyl-[1,1':2',1''-terphenyl]-4-yl)-10H-pheno-xazine (TRZ-HPB-PXZ): Into a 50 mL two-necked round bottom flask was placed a mixture of tetraphenylcyclopentadienone (0.922 g, 2.4 mmol) and compound **5a** (1.180 g, 2 mmol) and then diphenyl ether (15 mL) was added. The mixture was refluxed for 10 h and then cooled to room temperature. Ethanol was added into the mixture to precipitate the product, which was collected and washed with ethanol. Yellow solid of TRZ-HPB-PXZ was obtained in 56% yield. ^1H NMR (400 MHz, CDCl_3), δ (TMS, ppm): 8.74–8.69 (m, 4H), 8.47–8.42 (m, 2H), 7.62–7.57 (m, 2H), 7.56–7.51 (m, 4H), 7.15–7.12 (m, 2H), 7.11–7.07 (m, 2H), 6.96–6.87 (m, 20H), 6.84–6.80 (m, 2H), 6.52–6.48 (m, 2H), 6.43–6.30 (m, 4H), 5.48 (d, J = 7.8 Hz, 2H); ^{13}C NMR (125 MHz, CDCl_3), δ (TMS, ppm): 171.63, 171.27, 145.67, 144.85, 143.81, 143.79, 141.49, 141.47, 141.13, 140.95, 140.52, 140.40, 140.37, 140.36, 140.32, 140.18, 139.82, 139.72, 136.31, 134.19, 133.33, 132.59, 132.12, 131.63, 131.53, 131.52, 131.49, 129.04, 128.72, 127.53, 127.09, 126.91, 126.90, 126.87, 125.87, 125.66, 125.61, 125.57, 123.31, 115.81, 115.16, 113.20. HRMS ($\text{C}_{69}\text{H}_{46}\text{N}_4\text{O}$): m/z 946.3687 [M^+ , calcd 946.3672].

10-(4''-(4,6-Diphenyl-1,3,5-triazin-2-yl)-3',4',5',6'-tetraphenyl-[1,1':2',1''-terphenyl]-4-yl)-9,9-dimethyl-9,10-dihydroacridine (TRZ-HPB-DMAC): The procedure was analogous to that described as TRZ-HPB-PXZ. White solid of TRZ-HPB-DMAC was obtained in 60% yield. ^1H NMR (500 MHz, CDCl_3), δ (TMS, ppm): 8.74–8.71 (m, 4H), 8.48 (d, J = 8.2 Hz, 2H), 7.61–7.57 (m, 2H), 7.56–7.52 (m, 4H), 7.27 (s, 1H),

7.17 (d, J = 8.1 Hz, 2H), 7.12 (d, J = 8.0 Hz, 2H), 6.98–6.87 (m, 21H), 6.84–6.79 (m, 4H), 6.61–6.57 (m, 2H), 5.88–5.85 (m, 2H), 1.52 (s, 6H); ^{13}C NMR (125 MHz, CDCl_3), δ (TMS, ppm): 171.52, 171.19, 145.66, 141.05, 140.96, 140.80, 140.55, 140.48, 140.36, 140.32, 140.18, 140.14, 139.97, 139.66, 138.18, 136.24, 133.87, 133.22, 132.46, 132.09, 131.59, 131.47, 131.44, 131.42, 129.77, 129.61, 128.95, 128.62, 127.46, 126.98, 126.81, 126.79, 126.76, 126.30, 125.75, 125.58, 125.50, 125.44, 124.95, 120.19, 113.88, 35.84, 31.23. HRMS ($\text{C}_{72}\text{H}_{52}\text{N}_4$): m/z 972.4164 [M^+ , calcd 972.4192].

X-Ray Crystallography

Crystal data for TRZ-HPB-DMAC (CCDC 1885466): $\text{C}_{72}\text{H}_{52}\text{N}_4$, M_W = 973.17, monoclinic, C 2/c, a = 31.3912(15), b = 10.8163(6), c = 39.535(3) Å, β = 110.8700(10)°, V = 12542.9(13) Å³, Z = 8, D_c = 1.031 g cm⁻³, μ = 0.060 mm⁻¹ (MoK α , λ = 0.71073), $F(000)$ = 4096, T = 173(2) K, $2\theta_{\text{max}}$ = 25.242° (98.2%), 41548 measured reflections, 11317 independent reflections (R_{int} = 0.0914), GOF on F^2 = 1.076, R_1 = 0.1503, wR_2 = 0.1529 (all data), R_1 = 0.0684, wR_2 = 0.1296 [$I > 2\sigma(I)$], Δe 0.206 and -0.251 eÅ⁻³.

OLED Fabrication and Characterization

Glass substrates pre-coated with a 95 nm thin layer of indium tin oxide (ITO) with a sheet resistance of 20 Ω per square were thoroughly cleaned for 10 min in ultrasonic bath of acetone, isopropyl alcohol, detergent, deionized water, and isopropyl alcohol and then treated with O₂ plasma for 5 min in sequence. Organic layers were deposited onto the ITO-coated substrates by high-vacuum ($< 5 \times 10^{-4}$ Pa) thermal evaporation. Deposition rates were controlled by independent quartz crystal oscillators, which were 1 ~ 2 Å s⁻¹ for organic materials, 0.1 Å s⁻¹ for LiF, and 6 Å s⁻¹ for Al, respectively. The emission area of the devices was 3 × 3 mm⁻² as shaped by the overlapping area of the anode and cathode. All the device characterization steps were carried out at room temperature under ambient laboratory conditions without encapsulation except spectrum collection process. EL spectra were taken by an optical analyzer, Photo Research PR705. Current density and luminance vs. driving voltage characteristics were measured by Keithley 2,420 and Konica Minolta chromameter CS-200, respectively. External quantum efficiencies were calculated by assuming that the devices were Lambertian light sources.

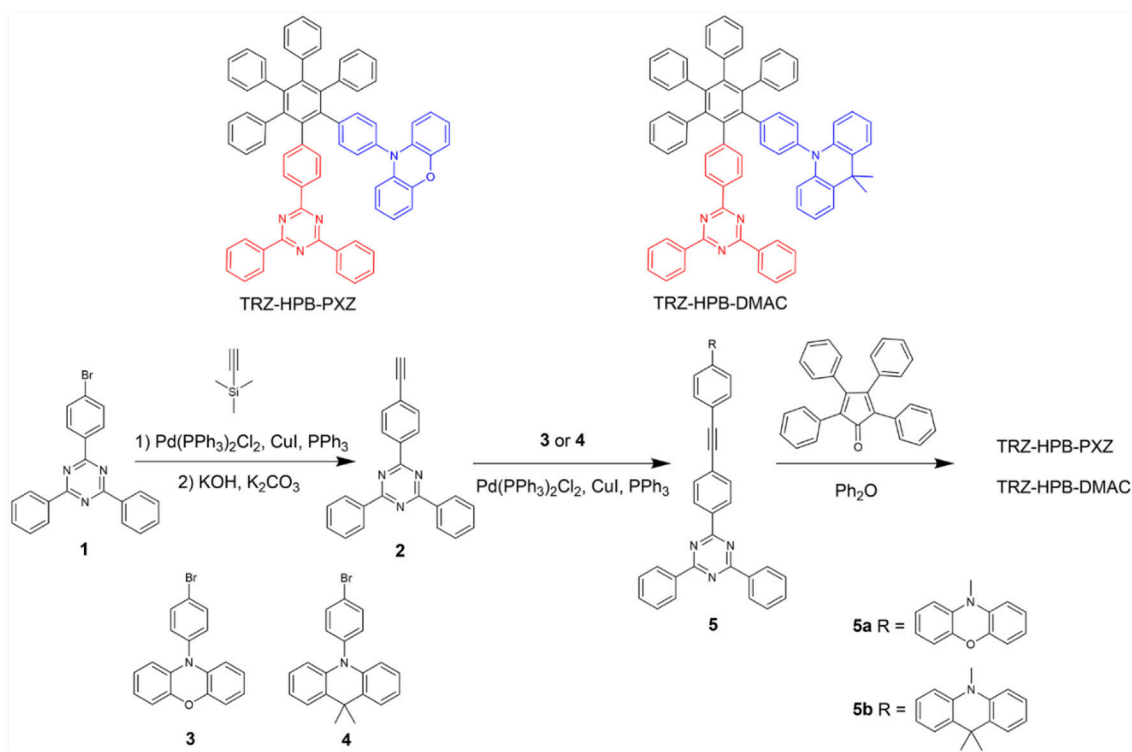
RESULTS AND DISCUSSION

The synthetic procedures of these new HPB-based molecules are described in **Scheme 1**. Intermediates **5a** and **5b** were prepared from compound **1** in two steps by Sonogashira reactions. Subsequently, the target TRZ-HPB-PXZ and TRZ-HPB-DMAC were synthesized through Diels-Alder reactions between **5a** and **5b** with tetraphenylcyclopentadienone, respectively. These HPB-based molecules were identified using ^1H NMR, ^{13}C NMR and high-resolution mass spectroscopy. The thermal stabilities of TRZ-HPB-PXZ and TRZ-HPB-DMAC were evaluated by differential scanning calorimetry (DSC) and thermogravimetric analysis (TGA) methods. They all exhibit good thermal

properties with high decomposition temperatures (T_d) of 450.4 and 464.9°C, respectively (**Figure 1A**). But no glass transition temperatures are observed. The results demonstrate that they are thermally stable and can be used as active layers in OLEDs by vacuum-deposition technique. The cyclic voltammetry was used to test their electrochemical behaviors. They have similar reversible oxidation and reduction processes (**Figure 1B**), indicative of good electrochemical stability. The

HOMO and LUMO energy levels are determined to be -5.02 and -2.68 eV for TRZ-HPB-PXZ, and -5.23 and -2.79 eV for TRZ-HPB-DMAC, respectively.

The single crystals of TRZ-HPB-DMAC were obtained from the THF-hexane mixture by slow solvent evaporation and subject to crystallography analysis. The crystal structure shows that the dihedral angles between 2,4,6-triphenyl-1,3,5-triazine (TRZ) and the central phenyl is 68.94° , and the dihedral



SCHEME 1 | Synthetic routes of TRZ-HPB-PXZ and TRZ-HPB-DMAC.

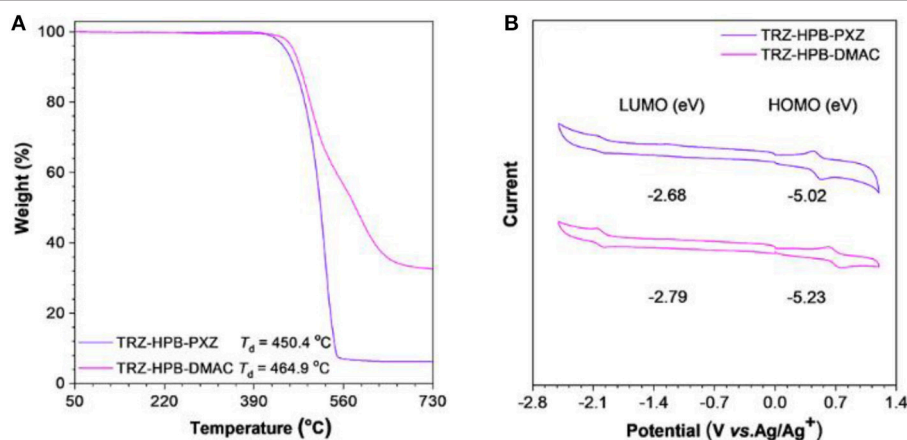


FIGURE 1 | (A) TGA curves of TRZ-HPB-PXZ and TRZ-HPB-DMAC, recorded under nitrogen at a heating rate of $20^\circ\text{C min}^{-1}$. (B) Cyclic voltammograms of TRZ-HPB-PXZ and TRZ-HPB-DMAC, measured in acetonitrile containing 0.1 M tetra-*n*-butylammonium hexafluorophosphate. Scan rate: 100 mV s^{-1} .

angles between 9,9-dimethyl-10-phenyl-acridine (DMAC) and the central phenyl is 68.89° , implying that through-bond conjugation is relatively weak. The six peripheral phenyl groups of HPB are connected to the central phenyl ring in a propeller-like fashion. They are closely aligned with the shortest distances <3.0 Å between adjacent phenyls (**Figure 2A**), indicating that there are strong electronic coupling interactions between these phenyl groups, namely through-space conjugation (Lambert, 2005; Zhen et al., 2018). Furthermore, the shortest distance between TRZ and DMAC is only 2.871 Å, which is close enough to produce intramolecular through-space electronic coupling, providing a charge transfer channel. The screwy architecture is of great importance to the separation of frontier orbitals, resulting in a small ΔE_{ST} . In addition, intermolecular C–H $\cdots\pi$ interactions are also observed (**Figure S1**), which are conducive to increasing the structural rigidity of the molecules and restraining intramolecular vibration that expedites non-radiative decay.

To gain insight into the molecular geometries and frontier orbital distributions, density functional theory (DFT) calculations were performed on these HPB-based molecules. The HOMO are mainly distributed on the electron-donating 10-phenyl-phenoxazine (PXZ) and DMAC moieties, while the LUMO are located on the electron-accepting TRZ moiety and partially extend to the central phenyl ring of HPB (**Figure 2B**). On one hand, the phenyls in HPB are aligned tightly in a highly twisted molecular conformation, resulting in the separation of HOMO and LUMO. On the other hand, the molecular orbitals are spatially proximate, allowing through-space charge transfer process to occur, and thus enhance the radiative decay rate. As a result, very small ΔE_{ST} and high PLQY can be expected, which make these materials promising candidates for efficient emitters. According to the time-dependent density functional theory (TD-DFT) calculations, the ΔE_{ST} values of TRZ-HPB-PXZ and TRZ-HPB-DMAC are estimated to be 0.0017 and 0.0013 eV, respectively, which are small enough for RISC process.

The absorption and PL spectra of these HPB-based molecules are depicted in **Figure 3**. There are distinct broad absorption shoulders in the range of 300–350 nm, which are associated with the intramolecular charge transfer (ICT), as confirmed by theoretical calculation (**Figure S2**). Their PL spectra in dilute THF solutions show two peaks. The weak PL bands at 370–390 nm are mainly attributable to the localized state emissions of donor and acceptor moieties (Kubota et al., 2014), while the strong PL peaks at 595 nm for TRZ-HPB-PXZ and 541 nm for TRZ-HPB-DMAC are assigned to the ICT state emissions of the molecules. Similar dual emissions have also been discovered by other research groups (Lee et al., 2015b; Shiu et al., 2017). The PL spectra display an apparent solvatochromic effect in different solvents (**Figure S3**). For example, the maximum PL peak of TRZ-HPB-PXZ shifts from 457 nm in hexane to 595 nm in THF. Analogous spectral movements are also found in TRZ-HPB-DMAC, indicative of their strong ICT characters. Both HPB-based molecules exhibit weak emissions in THF solutions with low PLQY of 5.5 and 9.1% (**Table 1**). However, their emissions are significantly enhanced when fabricated into neat films. The PL peak of TRZ-HPB-PXZ is located at around 576 nm and that of TRZ-HPB-DMAC is blue-shifted to 484 nm. High PLQY of 61.5 and 51.8% are recorded in neat films of TRZ-HPB-PXZ and TRZ-HPB-DMAC, respectively, which are improved by about one order of magnitude compared with those in solutions. The obvious increase in PLQY of TRZ-HPB-PXZ and TRZ-HPB-DMAC in neat films indicates that they should possess AIE character. To further corroborate the AIE nature of TRZ-HPB-PXZ and TRZ-HPB-DMAC, their PL spectra in THF/water mixtures were measured. It can be seen that along with the nanoaggregates formation by adding a large amount of water into THF solutions, the emissions of TRZ-HPB-PXZ and TRZ-HPB-DMAC are enhanced significantly (**Figure 3**), clearly validating the AIE nature (Mei et al., 2015).

To deepen the understanding of their PL properties, the transient PL decay spectra in THF/water mixtures and neat

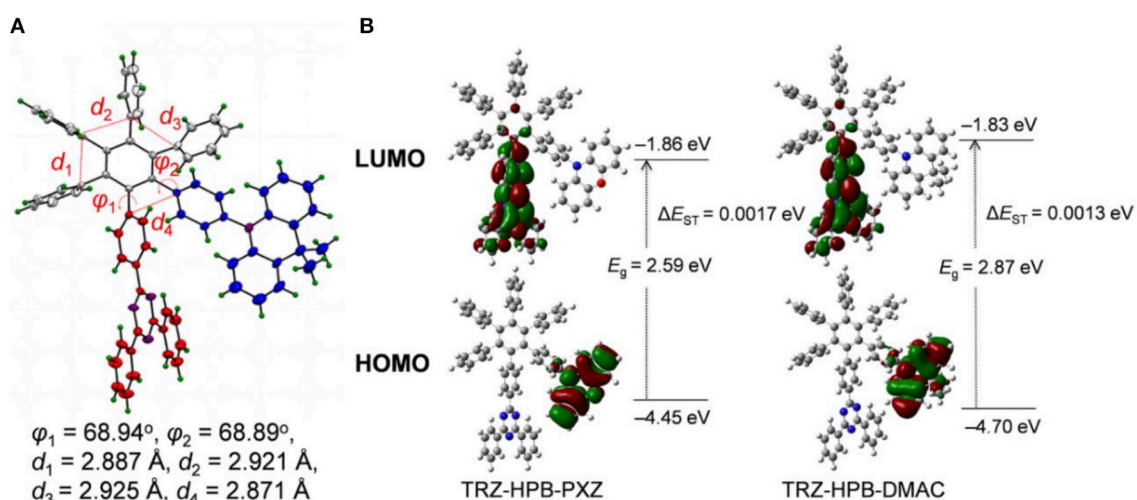


FIGURE 2 | (A) Crystal structure of TRZ-HPB-DMAC. **(B)** Spatial distributions of HOMO and LUMO, and ΔE_{ST} values of the HPB-based molecules, calculated by DFT/TDDFT method.

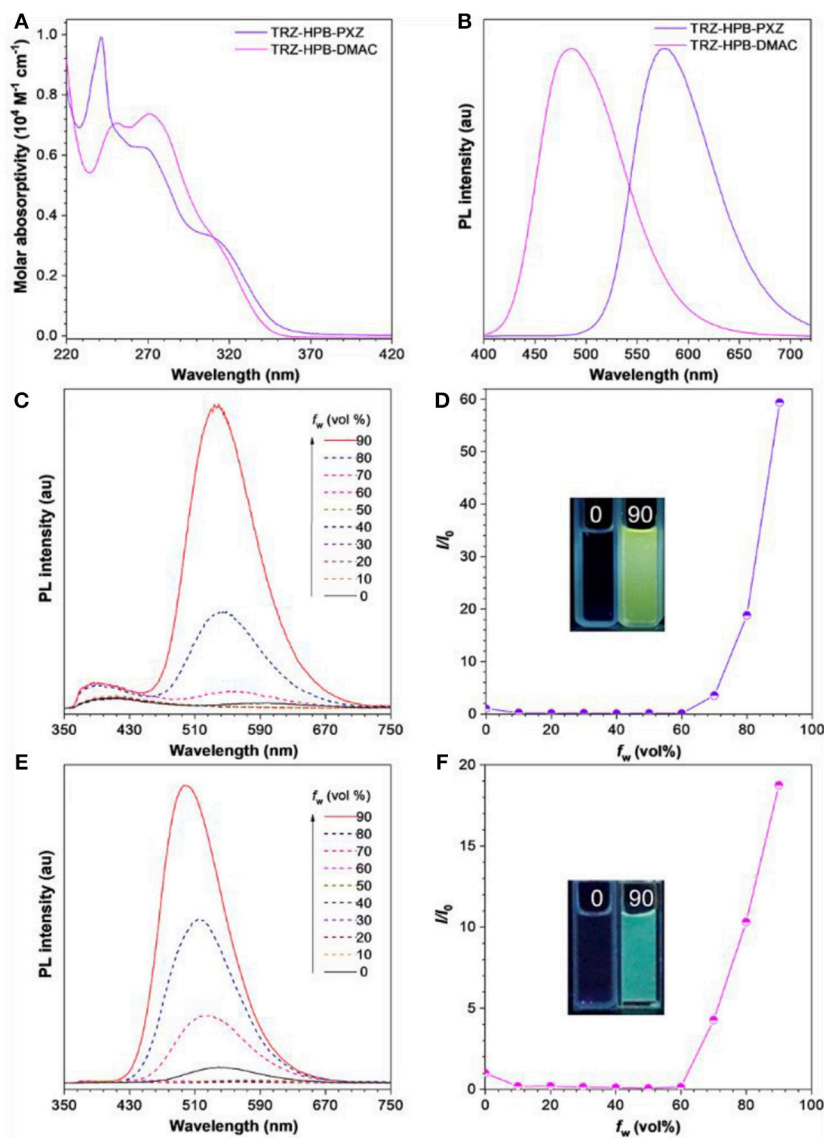


FIGURE 3 | (A) Absorption spectra of these HPB-based molecules in THF solutions (10^{-5} M). **(B)** PL spectra of these HPB-based molecules in neat films. PL spectra of **(C)** TRZ-HPB-PXZ, **(E)** TRZ-HPB-DMAC in THF/water mixtures with different water fractions (f_w). Plots of I/I_0 vs. f_w of **(D)** TRZ-HPB-PXZ, **(F)** TRZ-HPB-DMAC. I_0 is the PL intensity in pure THF. Inset: photographs of these HPB-based molecules in THF/water mixtures ($f_w = 0$ and 90%), taken under 310 nm excitation.

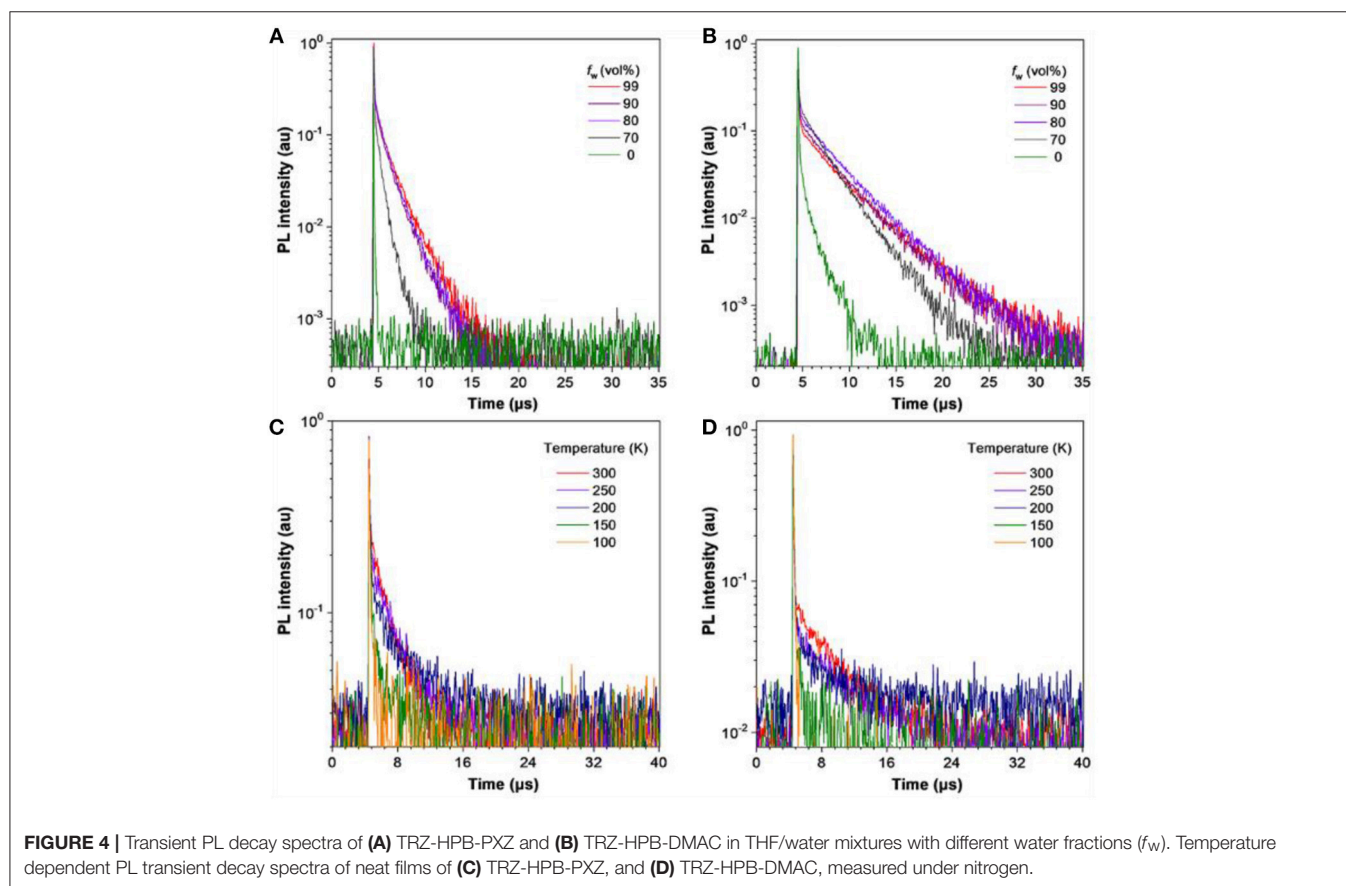
films were measured (Figure 4). Their PL decay profiles consist of two parts: a nanosecond-scale component and a microsecond-scale one, which can be attributed to prompt fluorescence and delayed fluorescence, respectively. In THF solution, TRZ-HPB-PXZ and TRZ-HPB-DMAC possess short mean lifetimes of 15.2 and 357.5 ns, respectively, and the delayed components are hardly recognizable (Table 1). However, prominent delayed components are discovered upon aggregate formation (Table S1), revealing that the delayed fluorescence is induced by aggregation (Aizawa et al., 2017; Gan et al., 2017; Guo et al., 2017a, 2018a; Huang et al., 2017; Liu et al., 2018). The neat films of TRZ-HPB-PXZ and TRZ-HPB-DMAC show long lifetimes in microsecond scale (1.8 and 3.4 μ s), which are significantly longer than those recorded in solutions

(Table S2), further demonstrating their AIDF attributes. When dispersed in good solvents, the intramolecular rotational, and vibrational motions are spiritedly active, and as a result, excited state energy is dissipated in a non-radiative manner via internal conversion (IC) (Li and Li, 2017), leading to faint emission. Besides, rapid IC process will impede intersystem crossing (ISC) and RISC processes, which is responsible for the indiscernible delayed fluorescence. Whereas, in aggregates, the molecular motions are restricted greatly because of the limited physical space, resulting in blocking of non-radiative IC channels and promotion of ISC and RISC processes under the basis of small ΔE_{ST} . Therefore, the molecules can emit strong emission with prominent delayed component (Fan et al., 2017; Guo et al., 2018b). The fluorescence decay is positively

TABLE 1 | Photophysical property of TRZ-HPB-PXZ and TRZ-HPB-DMAC.

	Solution ^a				Neat film ^b							
	λ_{abs} [nm]	λ_{em} [nm]	Φ_F^c [%]	$\langle\tau\rangle^d$ [ns]	λ_{em} [nm]	Φ_F^c [%]	$\langle\tau\rangle^d$ [ns]	τ_{prompt}^e [ns]	τ_{delayed}^e [μs]	R^f_{delayed} [%]	k^g_{RISC} [$\times 10^5 \text{ s}^{-1}$]	ΔE_{ST}^h [eV]
TRZ-HPB-PXZ	310	595	5.5	15.2	576	61.5	1798.4	41.6	2.1	84.8	31.0	0.02
TRZ-HPB-DMAC	310	541	9.1	357.5	484	51.8	3354.8	48.4	4.7	70.6	7.2	0.09

^aMeasured in THF solution (10^{-5} M) at room temperature. ^bVacuum-deposited on a quartz substrate. ^cDetermined by a calibrated integrating sphere under nitrogen at room temperature. ^dMean fluorescence lifetime evaluated at 300 K under nitrogen. ^eFluorescence lifetimes of prompt (τ_{prompt}) and delayed (τ_{delayed}) components evaluated at 300 K under nitrogen. ^fRatio of delayed component. ^gRate constant of RISC calculated from the equations given in the **Supplementary Material**. ^hEstimated from the high-energy onsets of fluorescence and phosphorescence spectra at 77 K.



correlated with temperature and the long-lived component is promoted as temperature increases (Table S3). The ΔE_{ST} values of these molecules were obtained from the singlet and triplet energies calculated from the onset of the fluorescence and phosphorescence spectra, respectively, measured in neat films at 77 K (Figure S4). TRZ-HPB-PXZ and TRZ-HPB-DMAC exhibit small ΔE_{ST} values of 0.02 and 0.09 eV coupled with fast RISC rate constants (k_{RISC}) of 3.1×10^6 and $7.2 \times 10^5 \text{ s}^{-1}$, respectively (Table S4), which are favorable for the occurrence of delayed fluorescence.

In view of excellent solid-state PL efficiencies, prominent delayed fluorescence as well as good thermal stability of

TRZ-HPB-PXZ and TRZ-HPB-DMAC, multilayer non-doped OLEDs were fabricated to investigate their EL properties. The configurations of devices were: ITO/HATCN (5 nm)/TAPC (20 nm)/TCTA (5 nm)/emitter/TmPyPB (55 nm)/LiF (1 nm)/Al, in which the neat films of TRZ-HPB-PXZ (35 nm) (device I) and TRZ-HPB-DMAC (20 nm) (device II) acted as emitters; dipyrzino[2,3-f:2',3'-h]quinoxaline-2,3,6,7,10,11-hexacarbonitrile (HATCN), 1,1'-bis(di-4-tolylaminophenyl)cyclohexane (TAPC), 1,3,5-tri(mpyrid-3-yl-phenyl)benzene (TmPyPB) and 4,4',4''-tris(carbazol-9-yl)-triphenylamine (TCTA) functioned as hole injection, hole-transporting, electron-transporting and

exciton-blocking layers, respectively. Appropriate adjustment of the emitter thickness had been made in order to achieve better device performance. The character curves are presented in **Figure 5** and the key data of the devices are listed in **Table 2**. Devices I and II are turned on at a low voltage of 2.5 and 3.1 V, respectively, implying efficient carrier injection and transport into the emitters. Devices I emits bright yellow light ($\lambda_{\text{EL}} = 544\text{ nm}$) with color coordinates of $\text{CIE}_{x,y}$ (0.39, 0.57). Its maxima current (η_{C}), power (η_{P}) and external quantum (η_{ext}) efficiencies are 41.2 cd A^{-1} , 44.9 lm W^{-1} , and 12.7%, respectively. More significantly, this non-doped device of TRZ-HPB-PXZ enjoys excellent efficiency stability. When the luminance is increased to $1,000\text{ cd m}^{-2}$, the η_{C} , η_{P} , and η_{ext} still remain as 40.1 cd A^{-1} , 31.5 lm W^{-1} , and 12.3%, respectively. The roll-off of current efficiency is only 2.7%. The EL peak of device II is located at 521 nm ($\text{CIE}_{x,y} = 0.28, 0.58$) and the maximum η_{ext} is 6.5%. The

inferior EL performance may be due to the lower PLQY and increased ΔE_{ST} of TRZ-HPB-DMAC compared with those of TRZ-HPB-PXZ. It is noted that the EL spectra are shifted relative to their PL spectra in films. Similar differences are reported by other groups, which may be caused by optical microcavity effect or different excited dipole moments of the molecules under electrical excitation and photoexcitation (Chen et al., 2014; Sun et al., 2015; Zhang et al., 2016).

Theoretical maximum η_{ext} was also calculated in order to evaluate the exciton utilization of TRZ-HPB-PXZ-based device I. According to the values of entire PLQY and lifetime, the PLQY contributed by prompt fluorescence (Φ_{prompt}) and delayed fluorescence (Φ_{delayed}) of TRZ-HPB-PXZ neat film are 9.4 and 52.1% (**Table S4**), respectively. Assuming that the out-coupling efficiency is 20–30% and the charge transport is balanced, the maximum theoretical η_{ext} calculated from photophysical data of TRZ-HPB-PXZ is 12.3–18.5%

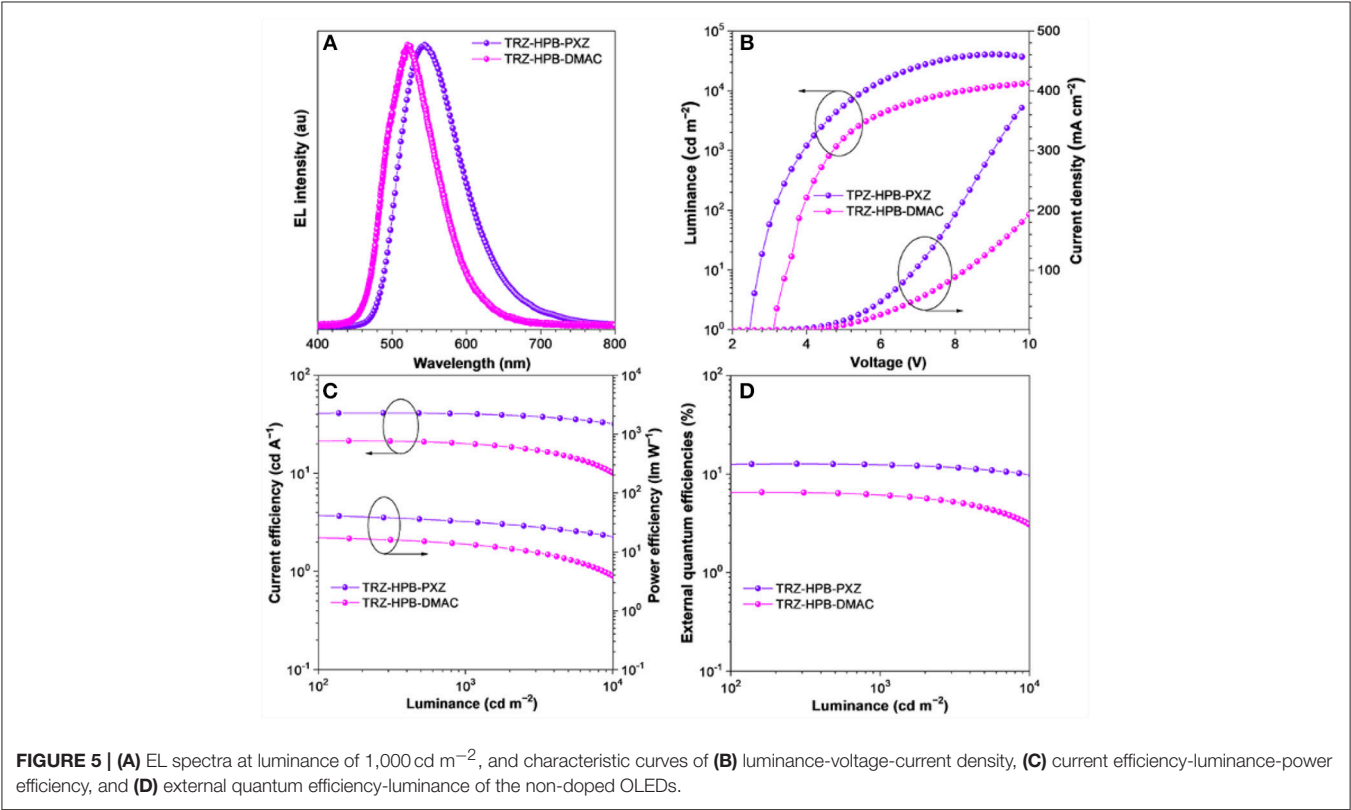


TABLE 2 | EL performances of the non-doped OLEDs based on HPB-based molecules^a.

Device	V_{on} [V]	Maximum values				Values at $1,000\text{ cd m}^{-2}$						
		η_{C} [cd A^{-1}]	η_{P} [lm W^{-1}]	η_{ext} [%]	L [cd m^{-2}]	V [V]	η_{C} [cd A^{-1}]	η_{P} [lm W^{-1}]	η_{ext} [%]	RO [%]	λ_{EL} [nm]	CIE (x, y)
I	2.5	41.2	44.9	12.7	40,382	4.0	40.1	31.5	12.3	2.7	544	(0.39, 0.57)
II	3.1	21.4	17.6	6.5	15,460	4.8	19.9	13.0	6.0	7.0	521	(0.28, 0.58)

^a V_{on} , turn-on voltage at 1 cd m^{-2} ; η_{C} , current efficiency; η_{P} , power efficiency; η_{ext} , external quantum efficiency; L , luminance; CIE, Commission International de l'Eclairage coordinates; λ_{EL} , maxima of electroluminescent spectra; RO, current efficiency roll-off from maximum value to that at $1,000\text{ cd m}^{-2}$. Emitter: TRZ-HPB-PXZ (device I); TRZ-HPB-DMAC (device II).

(Park et al., 2016), which is reasonable according to the experimental data, indicating that the triplet excitons have been sufficiently converted to radiative singlet excitons. However, the experimental η_{ext} of TRZ-HPB-DMAC is inferior to the maximum theoretical η_{ext} (10.3–15.5%). The phenomenon may be attributed to the poorer triplet-to-singlet conversion efficiency of TRZ-HPB-DMAC in EL devices due to the lower k_{RISC} , which is about one-fifth of TRZ-HPB-PXZ's k_{RISC} . In addition, the different carrier transport capabilities of PXZ and DMAC moieties will also influence the carrier balance in EL devices, and thus affect devices' performance. These results demonstrate that through-space charge transfer contributes to a small ΔE_{ST} and thus delayed fluorescence, which allows a high exciton utilization of the emitters. In addition, the intriguing AIDF properties are conducive to suppressing emission quenching and exciton annihilation in neat films. The synergistic effect of these factors ensures non-doped OLEDs with high efficiency and small efficiency roll-off.

CONCLUSIONS

In summary, two HPB-based luminogens TRZ-HPB-PXZ and TRZ-HPB-DMAC with good thermal and electrochemical stabilities are synthesized and characterized. Both luminogens exhibit through-space charge transfer feature between D and A moieties, which brings about efficient separation of HOMO and LUMO, and thus small ΔE_{ST} . TRZ-HPB-PXZ and TRZ-HPB-DMAC are barely fluorescent in solutions but show strong emissions with prominent delayed fluorescence in the aggregated state, that is AIDF property. Their neat films have distinct delayed fluorescence and high PLQY. Non-doped

OLEDs using these luminogens as light-emitting layers have achieved excellent performance with a maximum η_{ext} of 12.7% and very small efficiency roll-off of 2.7% at 1,000 cd m⁻². These results reveal that AIDF luminogens with through-space charge transfer can realize high exciton utilization and suppressed exciton annihilation at high luminance, which could be promising candidates for OLEDs with improved efficiency and stability.

AUTHOR CONTRIBUTIONS

All authors listed have made a substantial, direct and intellectual contribution to the work, and approved it for publication.

ACKNOWLEDGMENTS

This study was financially supported by the National Natural Science Foundation of China (21788102 and 21673082), the National Basic Research Program of China (973 Program, 2015CB655004) Funded by MOST, the Guangdong Natural Science Funds for Distinguished Young Scholar (2014A030306035), the Natural Science Foundation of Guangdong Province (2016A030312002 and 2016B090907001), the Science and Technology Program of Guangzhou (201804020027 and 201704030069) and the Innovation and Technology Commission of Hong Kong (ITC-CNERC14SC01).

SUPPLEMENTARY MATERIAL

The Supplementary Material for this article can be found online at: <https://www.frontiersin.org/articles/10.3389/fchem.2019.00199/full#supplementary-material>

REFERENCES

- Adachi, C., Baldo, M. A., Thompson, M. E., and Forrest, S. R. (2001). Nearly 100% internal phosphorescence efficiency in an organic light-emitting device. *J. Appl. Phys.* 90:5048. doi: 10.1063/1.1409582
- Aizawa, N., Tsou, C.-J., Park, I. S., and Yasuda, T. (2017). Aggregation-induced delayed fluorescence from phenothiazine-containing donor-acceptor molecules for high-efficiency non-doped organic light-emitting diodes. *Polym. J.* 49, 197–202. doi: 10.1038/pj.2016.82
- Baldo, M. A., O'Brien, D. F., You, Y., Shoustikov, A., Sibley, S., Thompson, M. E., et al. (1998). Highly efficient phosphorescent emission from organic electroluminescent devices. *Nature* 395, 151–154. doi: 10.1038/25954
- Balzani, V., Clemente-León, M., Credi, A., Lowe, J. N., Badjić, J. D., Stoddart, J. F., et al. (2003). Controlling multivalent interactions in triply-threaded two-component superbundles. *Chem. Eur. J.* 9, 5348–5360. doi: 10.1002/chem.200304979
- Cao, X., Zhang, D., Zhang, S., Tao, Y., and Huang, W. (2017). CN-Containing donor-acceptor-type small-molecule materials for thermally activated delayed fluorescence OLEDs. *J. Mater. Chem. C* 5, 7699–7714. doi: 10.1039/c7tc02481a
- Chen, L., Jiang, Y., Nie, H., Hu, R., Kwok, H. S., Huang, F., et al. (2014). Rational design of aggregation-induced emission luminogen with weak electron donor-acceptor interaction to achieve highly efficient undoped bilayer OLEDs. *ACS Appl. Mater. Interfaces* 6, 17215–17225. doi: 10.1021/am505036a
- Chen, X. L., Jia, J. H., Yu, R., Liao, J. Z., Yang, M. X., and Lu, C. Z. (2017). Combining charge-transfer pathways to achieve unique thermally activated delayed fluorescence emitters for high-performance solution-processed, non-doped blue OLEDs. *Angew. Chem. Int. Ed.* 56, 15006–15009. doi: 10.1002/anie.201709125
- Cho, S., Li, W. S., Yoon, M. C., Ahn, T. K., Jiang, D. L., Kim, J., et al. (2006). Relationship between incoherent excitation energy migration processes and molecular structures in Zinc (II) porphyrin dendrimers. *Chem. Eur. J.* 12, 7576–7584. doi: 10.1002/chem.200600213
- Endo, A., Ogasawara, M., Takahashi, A., Yokoyama, D., Kato, Y., and Adachi, C. (2009). Thermally activated delayed fluorescence from Sn⁴⁺-porphyrin complexes and their application to organic light emitting diodes—A novel mechanism for electroluminescence. *Adv. Mater. Weinheim.* 21, 4802–4806. doi: 10.1002/adma.200900983
- Fan, J., Lin, L., and Wang, C.-K. (2017). Excited state properties of non-doped thermally activated delayed fluorescence emitters with aggregation-induced emission: a QM/MM study. *J. Mater. Chem. C* 5, 8390–8399. doi: 10.1039/c7tc02541f
- Furue, R., Nishimoto, T., Park, I. S., Lee, J., and Yasuda, T. (2016). Aggregation-induced delayed fluorescence based on donor/acceptor-tethered janus carborane triads: unique photophysical properties of non-doped OLEDs. *Angew. Chem. Int. Ed.* 55, 7171–7175. doi: 10.1002/anie.201603232
- Gan, S., Luo, W., He, B., Chen, L., Nie, H., Hu, R., et al. (2016). Integration of aggregation-induced emission and delayed fluorescence into electronic donor-acceptor conjugates. *J. Mater. Chem. C* 4, 3705–3708. doi: 10.1039/c5tc03588k

- Gan, S., Zhou, J., Smith, T. A., Su, H., Luo, W., Hong, Y., et al. (2017). New AIEgens with delayed fluorescence for fluorescence imaging and fluorescence lifetime imaging of living cells. *Mater. Chem. Front.* 1, 2554–2558. doi: 10.1039/c7qm00286f
- Geng, Y., Fechtenkötter, A., and Müllen, K. (2001). Star-like substituted hexaarylbenzenes: synthesis and mesomorphic properties. *J. Mater. Chem.* 11, 1634–1641. doi: 10.1039/b101163o
- Gong, S., Chen, Y., Luo, J., Yang, C., Zhong, C., Qin, J., et al. (2011). Bipolar tetraarylsilanes as universal hosts for blue, green, orange, and white electrophosphorescence with high efficiency and low efficiency roll-off. *Adv. Funct. Mater.* 21, 1168–1178. doi: 10.1002/adfm.201002066
- Guo, J., Fan, J., Lin, L., Zeng, J., Liu, H., Wang, C. K., et al. (2018b). Mechanical insights into aggregation-induced delayed fluorescence materials with anti-kasha behavior. *Adv. Sci.* 6:1801629. doi: 10.1002/advs.201801629
- Guo, J., Li, X.-L., Nie, H., Luo, W., Gan, S., Hu, S., et al. (2017a). Achieving high-performance non-doped OLEDs with extremely small efficiency roll-off by combining aggregation-induced emission and thermally activated delayed fluorescence. *Adv. Funct. Mater.* 27:1606458. doi: 10.1002/adfm.201606458
- Guo, J., Li, X.-L., Nie, H., Luo, W., Hu, R., Qin, A., et al. (2017b). Robust luminescent materials with prominent aggregation-induced emission and thermally activated delayed fluorescence for high-performance organic light-emitting diodes. *Chem. Mater.* 29, 3623–3631. doi: 10.1021/acs.chemmater.7b00450
- Guo, J., Zhao, Z., and Tang, B. Z. (2018a). Purely organic materials with aggregation-induced delayed fluorescence for efficient nondoped OLEDs. *Adv. Opt. Mater.* 6:1800264. doi: 10.1002/adom.201800264
- Hirata, S., Sakai, Y., Masui, K., Tanaka, H., Lee, S. Y., Nomura, H., et al. (2015). Highly efficient blue electroluminescence based on thermally activated delayed fluorescence. *Nat. Mater.* 14, 330–336. doi: 10.1038/nmat4154
- Huang, J., Nie, H., Zeng, J., Zhuang, Z., Gan, S., Cai, Y., et al. (2017). Highly efficient non-doped OLEDs with negligible efficiency roll-off fabricated from aggregation-induced delayed fluorescence luminogens. *Angew. Chem. Int. Ed.* 56, 12971–12976. doi: 10.1002/anie.201706752
- Kaji, H., Suzuki, H., Fukushima, T., Shizu, K., Suzuki, K., Kubo, S., et al. (2015). Purely organic electroluminescent material realizing 100% conversion from electricity to light. *Nat. Commun.* 6:8476. doi: 10.1038/ncomms9476
- Kanibolotsky, A. L., Perepichka, I. F., and Skabara, P. J. (2010). Star-shaped π -conjugated oligomers and their applications in organic electronics and photonics. *Chem. Soc. Rev.* 39, 2695–2728. doi: 10.1039/b918154g
- Kawasumi, K., Wu, T., Zhu, T., Chae, H. S., Van Voorhis, T., Baldo, M. A., et al. (2015). Thermally activated delayed fluorescence materials based on homoconjugation effect of donor-acceptor triptycenes. *J. Am. Chem. Soc.* 137, 11908–11911. doi: 10.1021/jacs.5b07932
- Kubota, Y., Sakuma, Y., Funabiki, K., and Matsui, M. (2014). Solvatochromic fluorescence properties of pyrazine-boron complex bearing a β -Iminoenolate ligand. *J. Phys. Chem. A* 118, 8717–8729. doi: 10.1021/jp506680g
- Lambert, C. (2005). Hexaarylbenzenes—prospects for toroidal delocalization of charge and energy. *Angew. Chem. Int. Ed.* 44, 7337–7339. doi: 10.1002/anie.200502105
- Lambert, C., Ehbets, J., Rausch, D., and Steeger, M. (2012). Charge-transfer interactions in a multichromophoric hexaarylbenzene containing pyrene and triarylamine. *J. Org. Chem.* 77, 6147–6154. doi: 10.1021/jo300924x
- Lee, D. R., Kim, B. S., Lee, C. W., Im, Y., Yook, K. S., Hwang, S.-H., et al. (2015a). Above 30% external quantum efficiency in green delayed fluorescent organic light-emitting diodes. *ACS Appl. Mater. Interfaces* 7, 9625–9629. doi: 10.1021/acsami.5b01220
- Lee, J., Shizu, K., Tanaka, H., Nakanotani, H., Yasuda, T., Kaji, H., et al. (2015b). Controlled emission colors and singlet-triplet energy gaps of dihydrophenazine-based thermally activated delayed fluorescence emitters. *J. Mater. Chem. C* 3, 2175–2181. doi: 10.1039/c4tc02530j
- Li, Q., and Li, Z. (2017). The strong light-emission materials in the aggregated state: what happens from a single molecule to the collective group. *Adv. Sci.* 4:1600484. doi: 10.1002/advs.201600484
- Liu, H., Zeng, J., Guo, J., Nie, H., Zhao, Z., and Tang, B. Z. (2018). High-performance non-doped OLEDs with nearly 100 % exciton use and negligible efficiency roll-off. *Angew. Chem. Int. Ed.* 130, 9434–9438. doi: 10.1002/ange.201802060
- Mei, J., Leung, N. L. C., Kwok, R. T. K., Lam, J. W. Y., and Tang, B. Z. (2015). Aggregation-induced emission: together we shine, united we soar! *Chem. Rev.* 115, 11718–11940. doi: 10.1021/acs.chemrev.5b00263
- Minaev, B., Baryshnikov, G., and Agren, H. (2014). Principles of phosphorescent organic light emitting devices. *Phys. Chem. Chem. Phys.* 16, 1719–1758. doi: 10.1039/c3cp53806k
- Park, I. S., Lee, S. Y., Adachi, C., and Yasuda, T. (2016). Full-color delayed fluorescence materials based on wedge-shaped phthalonitriles and dicyanopyrazines: systematic design, tunable photophysical properties, and OLED performance. *Adv. Funct. Mater.* 26, 1813–1821. doi: 10.1002/adfm.201505106
- Rajamalli, P., Senthilkumar, N., Gandeepan, P., Huang, P. Y., Huang, M. J., Ren-Wu, C. Z., et al. (2016). A new molecular design based on thermally activated delayed fluorescence for highly efficient organic light emitting diodes. *J. Am. Chem. Soc.* 138, 628–634. doi: 10.1021/jacs.5b10950
- Sasabe, H., and Kido, J. (2013). Recent progress in phosphorescent organic light-emitting devices. *Eur. J. Org. Chem.* 2013, 7653–7663. doi: 10.1002/ejoc.201300544
- Seino, Y., Inomata, S., Sasabe, H., Pu, Y. J., and Kido, J. (2016). High-performance green OLEDs using thermally activated delayed fluorescence with a power efficiency of over 100 lm W⁻¹. *Adv. Mater. Weinheim.* 28, 2638–2643. doi: 10.1002/adma.201503782
- Shao, S., Hu, J., Wang, X., Wang, L., Jing, X., and Wang, F. (2017). Blue thermally activated delayed fluorescence polymers with non-conjugated backbone and through-space charge transfer effect. *J. Am. Chem. Soc.* 139, 17739–17742. doi: 10.1021/jacs.7b10257
- Shiu, Y.-J., Chen, Y.-T., Lee, W.-K., Wu, C.-C., Lin, T.-C., Liu, S.-H., et al. (2017). Efficient thermally activated delayed fluorescence of functional phenylpyridinato boron complexes and high performance organic light-emitting diodes. *J. Mater. Chem. C* 5, 1452–1462. doi: 10.1039/c6tc04994j
- Sun, D., Rosokha, S. V., and Kochi, J. K. (2005). Through-space (cofacial) π -delocalization among multiple aromatic centers: toroidal conjugation in hexaphenylbenzene-like radical cations. *Angew. Chem. Int. Ed.* 44, 5133–5136. doi: 10.1002/anie.200501005
- Sun, J. W., Baek, J. Y., Kim, K.-H., Moon, C.-K., Lee, J.-H., Kwon, S.-K., et al. (2015). Thermally activated delayed fluorescence from azasilene based intramolecular charge-transfer emitter (DTPDDA) and a highly efficient blue light emitting diode. *Chem. Mater.* 27, 6675–6681. doi: 10.1021/acs.chemmater.5b02515
- Sun, J. W., Lee, J.-H., Moon, C.-K., Kim, K.-H., Shin, H., and Kim, J.-J. (2014). A fluorescent organic light-emitting diode with 30% external quantum efficiency. *Adv. Mater. Weinheim.* 26, 5684–5688. doi: 10.1002/adma.201401407
- Tanaka, Y., Koike, T., and Akita, M. (2010). 2-Dimensional molecular wiring based on toroidal delocalization of hexaarylbenzene. *Chem. Commun.* 46, 4529–4531. doi: 10.1039/c0cc00128g
- Tang, C. W., and VanSlyke, S. A. (1987). Organic electroluminescent diodes. *Appl. Phys. Lett.* 51:913. doi: 10.1063/1.98799
- Tao, Y., Yuan, K., Chen, T., Xu, P., Li, H., Chen, R., et al. (2014). Thermally activated delayed fluorescence materials towards the breakthrough of organoelectronics. *Adv. Mater. Weinheim.* 26, 7931–7958. doi: 10.1002/adma.201402532
- Tsujimoto, H., Ha, D. G., Markopoulos, G., Chae, H. S., Baldo, M. A., and Swager, T. M. (2017). Thermally activated delayed fluorescence and aggregation induced emission with through-space charge transfer. *J. Am. Chem. Soc.* 139, 4894–4900. doi: 10.1021/jacs.7b00873
- Vij, V., Bhalla, V., and Kumar, M. (2016). Hexaarylbenzene: evolution of properties and applications of multitailored scaffold. *Chem. Rev.* 116, 9565–9627. doi: 10.1021/acs.chemrev.6b00144
- Waldvogel, S. R., Wartini, A. R., and Rasmussen, P. H. Jr. (1999). A triphenylene scaffold with C_{3v}-symmetry and nanoscale dimensions. *Tetrahedron Lett.* 40, 3515–3518. doi: 10.1016/s0040-4039(99)00545-6
- Wang, H., Xie, L., Peng, Q., Meng, L., Wang, Y., Yi, Y., et al. (2014). Novel thermally activated delayed fluorescence materials-thioxanthone derivatives and their applications for highly efficient OLEDs. *Adv. Mater. Weinheim.* 26, 5198–5204. doi: 10.1002/adma.201401393

- Zhang, J., Ding, D., Wei, Y., and Xu, H. (2016). Extremely condensing triplet states of DPEPO-type hosts through constitutional isomerization for high-efficiency deep-blue thermally activated delayed fluorescence diodes. *Chem. Sci.* 7, 2870–2882. doi: 10.1039/c5sc04848f.
- Zhang, Q., Li, B., Huang, S., Nomura, H., Tanaka, H., and Adachi, C. (2014). Efficient blue organic light-emitting diodes employing thermally activated delayed fluorescence. *Nat. Photonics* 8, 326–332. doi: 10.1038/nphoton.2014.12
- Zhen, S., Mao, J. C., Chen, L., Ding, S., Luo, W., Zhou, X. S., et al. (2018). Remarkable multichannel conductance of novel single-molecule wires built on through-space conjugated hexaphenylbenzene. *Nano Lett.* 18, 4200–4205. doi: 10.1021/acs.nanolett.8b01082

Conflict of Interest Statement: The authors declare that the research was conducted in the absence of any commercial or financial relationships that could be construed as a potential conflict of interest.

Copyright © 2019 Zhang, Zeng, Guo, Zhen, Xiao, Wang, Zhao and Tang. This is an open-access article distributed under the terms of the Creative Commons Attribution License (CC BY). The use, distribution or reproduction in other forums is permitted, provided the original author(s) and the copyright owner(s) are credited and that the original publication in this journal is cited, in accordance with accepted academic practice. No use, distribution or reproduction is permitted which does not comply with these terms.



Design of Efficient Exciplex Emitters by Decreasing the Energy Gap Between the Local Excited Triplet (^3LE) State of the Acceptor and the Charge Transfer (CT) States of the Exciplex

Xiaofang Wei^{1,2}, Yanwei Liu^{2,3}, Taiping Hu^{2,3}, Zhiyi Li^{1,2}, Jianjun Liu^{1,2}, Ruifang Wang^{1,2}, Honglei Gao^{1,2}, Xiaoxiao Hu^{1,2}, Guanhao Liu^{1,2}, Pengfei Wang^{1,2}, Chun-sing Lee⁴ and Ying Wang^{1,2*}

¹ Key Laboratory of Photochemical Conversion and Optoelectronic Materials, Technical Institute of Physics and Chemistry, Chinese Academy of Sciences, Beijing, China, ² School of Future Technology, University of Chinese Academy of Sciences, Beijing, China, ³ Beijing National Laboratory for Molecular Sciences, Key Laboratory of Organic Solids, Institute of Chemistry, Chinese Academy of Sciences, Beijing, China, ⁴ Center of Super-Diamond and Advanced Films (COSDAF), City University of Hong Kong, Hong Kong, Hong Kong

OPEN ACCESS

Edited by:

Shi-Jian Su,
South China University of Technology,
China

Reviewed by:

CaiJun Zheng,
University of Electronic Science and
Technology of China, China
Guohua Xie,
Wuhan University, China

*Correspondence:

Ying Wang
wangy@mail.ipc.ac.cn

Specialty section:

This article was submitted to
Organic Chemistry,
a section of the journal
Frontiers in Chemistry

Received: 27 January 2019

Accepted: 11 March 2019

Published: 09 April 2019

Citation:

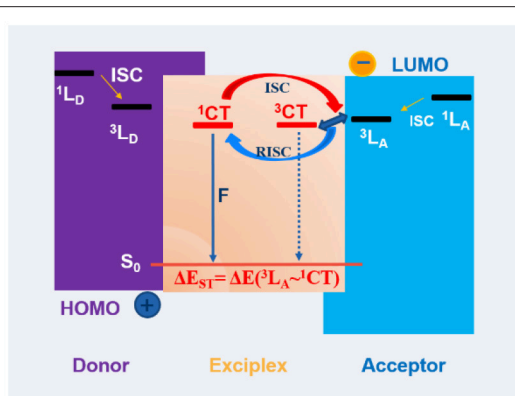
Wei X, Liu Y, Hu T, Li Z, Liu J, Wang R, Gao H, Hu X, Liu G, Wang P, Lee C and Wang Y (2019) Design of Efficient Exciplex Emitters by Decreasing the Energy Gap Between the Local Excited Triplet (^3LE) State of the Acceptor and the Charge Transfer (CT) States of the Exciplex. *Front. Chem.* 7:188. doi: 10.3389/fchem.2019.00188

A series of thermally activated delayed fluorescence (TADF) exciplex based on the TX-TerPy were constructed. The electronic coupling between the triplet local excited states (^3LE) of the donors and acceptor and the charge transfer states had a great influence on the triplet exciton harvesting and Φ_{PL} . Herein, based on this strategy, three donor molecules TAPC, TCTA, and m-MTDATA were selected. The local triplet excited state (^3LE) of the three donors are 2.93, 2.72 and 2.52 eV in pure films. And the ^3LE of TX-TerPy is 2.69 eV in polystyrene film. The energy gap between the singlet charge transfer (^1CT) states of TAPC:TX-TerPy (7:1), TCTA:TX-TerPy (7:1) and the ^3LE of TX-TerPy are 0.30 eV and 0.20 eV. Finally, the Φ_{PL} of TAPC:TX-TerPy (7:1) and TCTA:TX-TerPy (7:1) are 65.2 and 69.6%. When we changed the doping concentration of the exciplex from 15% to 50%, the ratio of the triplet decreased, and Φ_{PL} decreased by half, perhaps due to the increased energy gap between ^1CT and ^3LE . Therefore, optimizing the ^1CT , ^3CT , and ^3LE facilitated the efficient exciplex TADF molecules.

Keywords: organic light emitting diode (OLED), pure thermally activated delayed fluorescence (TADF), exciplex, thioxanthone (TX) derivatives, energy gap

INTRODUCTION

Organic light-emitting devices (OLED) have been widely studied due to their promising applications in large displays and solid-state lighting (Sasabe and Kido, 2013). During recent years, thermally activated delayed fluorescence (TADF) in OLEDs have been desirable due to low-cost fabrication and 100% exciton utilization through the effective intersystem crossing (ISC) and the reverse intersystem crossing (RISC) from triplet state (T_1) to singlet state (S_1), to harness the 25% singlet exciton and the 75% triplet excitons (Tao et al., 2014; Lee et al., 2015; Cui et al., 2016; Wong and Zysman-Colman, 2017; Yang et al., 2017). Hence, an internal quantum efficiency (IQE) of 100% for the TADF-based OLEDs can be achieved. The progress based on the TADF



GRAPHICAL ABSTRACT | Design and prediction of the highly efficient exciplex emitters is desirable to optimize the ^1CT , ^3CT of the exciplex and ^3LE of the donor or acceptor. Here, we studied the newly molecule TX-TerPy as the acceptor blended with TAPC, TCTA and m-MTDATA. The energy gap between the ^1CT and ^3LE in TCTA: 15 wt% TX-TerPy blends film is as small as 0.19 eV. So the Φ_{PL} is the highest one and nearly 100% triplet exciton can be obtained.

emitters reported that the EQEs exceed 30% (Lee et al., 2015; Lin et al., 2016), which is comparable for the phosphorescence OLEDs (PHOLEDs) and much higher than the device based on the traditional fluorescence.

Besides pure TADF emitters, exciplex is an alternative kind of efficient TADF OLED emitters. The efficient separation of the highest occupied molecular orbital (HOMO) and the lowest unoccupied molecular orbital (LUMO) in exciplex located on two different molecules resulted in a smaller ΔE_{ST} (ca. 0–50 meV) which allows the non-radiative different kind of exciplex system showing efficient TADF property have been reported. The efficient separation of the highest occupied molecular orbital (HOMO) and lowest unoccupied molecular orbital (LUMO) in exciplex located on two different molecules results of the smaller ΔE_{ST} (ca. 0–50 meV), which allows the non-radiative T_1 to radiative S_1 via RISC. Many different kinds of exciplex systems showing efficient TADF property have been reported (Graves et al., 2014; Deotare et al., 2015; Liu et al., 2015a,b,c; Wu et al., 2017; Duan et al., 2018; Lin et al., 2018). The EQEs based on them have exceeded 5%, which is the limit for a device based on fluorescent emitters. Moreover, many groups reported that the PHOLEDs and TADF based OLEDs used exciplexes as hosts demonstrating low operating voltages, low efficiency roll-off, and high efficiencies (Li et al., 2014; Liu et al., 2016; Kim et al., 2017; Moon et al., 2017; Shih et al., 2018). However, the exciplex systems generally cannot avoid the relatively lower photoluminescence (PL) quantum yield (PLQY) than the theoretical limit, which is perhaps due to the non-radiative transition of excited state (Goushi et al., 2012; Hung et al., 2013; Park et al., 2013). Exciplex emitters are needed to further efficiency enhancement. Recently, many reports have described that the spin orbital coupling (SOC) is formally forbidden between singlet and triplet CT (^1CT and ^3CT) states. Despite the weakness of the hyperfine coupling (HFC), the ^1CT state can only form a strong couple to a close lying local triplet

state (^3LE) (dos Santos et al., 2016; Etherington et al., 2016; Santos et al., 2016; Samanta et al., 2017; Mamada et al., 2018) despite of the hyperfine coupling (HFC) between ^1CT and ^3CT , the ^1CT state will strongly couple to a close lying local triplet state (^3LE) since the SOC between ^1CT and ^3CT are assumed to be forbidden (dos Santos et al., 2016; Etherington et al., 2016; Santos et al., 2016; Samanta et al., 2017; Mamada et al., 2018). The gap between the ^1CT and ^3LE is the real ΔE_{ST} which requires thermal energy for triplets to cross over to a singlet state meaning that a closed ^3LE is indispensable for the ISC and RISC as shown in **Graphical Abstract**. However, a few reports have clarified the specific value of the energy gap between ^1CT and ^3LE state. Meanwhile, the triplet exciton energy levels should be higher than those of the CT states, in order to prevent “back transfer” loss to a lower-energy triplet exciton of the donors or acceptors (Deotare et al., 2015; Liu et al., 2015c; Mamada et al., 2018).

Herein, three exciplex emitters are designed by adopting our newly molecules Thioxanthone (TX) derivatives 2-([2,2':6',2''-terpyridin]-4'-yl)-9H-thioxanthene-9-one (TX-TerPy) as the acceptor, with the common donors containing the triphenylamine unit to detect the factors leading to high PLQY. The donors are TAPC, TCTA and m-MTDATA, which are common hole-transporting material, namely di-[4-(N,N-di-p-tolyl-amino)-phenyl]cyclohexane, 4,4',4''-Tris(carbazol-9-yl)triphenylamine and 4,4',4''-Tris(N-3-methylphenyl-N-phenyl-amino) triphenylamine, respectively (Graves et al., 2014; Liu et al., 2015c; dos Santos et al., 2016; Shih et al., 2018). The detail chemical structures of these four compounds are shown in **Figure 1A**. The three blended films show green and yellow exciplex emissions which are red shifted greatly compared to their corresponding individual molecules. The TAPC:TX-TerPy, TCTA:TX-TerPy and m-MTDATA:TX-TerPy exciplex system exhibit photoluminescence quantum efficiency (Φ_{PL}) of 65.2, 69.6%, and 10.7% in N_2 atmosphere, respectively, when the doping concentration of TX-TerPy is 15%. In TAPC:TX-TerPy, TCTA:TX-TerPy, the effective exciton confinement of the constituting molecules avoid the exciton leakage due to the high T_1 state. Despite the high T_1 energy level of the two individual molecules of TX-TerPy and m-MTDATA, the energy leakage from the exciplex to the T_1 excited state of m-MTDATA has occurred, which results in a low Φ_{PL} for m-MTDATA:TX-TerPy. Significantly, the ^3LE of TX-TerPy is more close to the ^1CT of TCTA:TX-TerPy compared to TAPC:TX-TerPy, which are 0.19 eV and 0.28 eV, respectively. Thus, the more effective exciton harvesting can be guaranteed by the small energy gap between ^3LE of TX-TerPy and the ^1CT of the exciplex system, especially for TCTA:TX-TerPy. Based on the high Φ_{PL} of TAPC:TX-TerPy and TCTA:TX-TerPy, OLEDs are fabricated to investigate their electrochemical characteristics. The green emitting devices based on TAPC:TX-TerPy and TCTA:TX-TerPy present turn-on voltages of 3.5 V and 3.4 V as well as high maximum current (CE) and power efficiencies (PE) and external quantum efficiencies (EQE) of 7.08 and 8.29 %, 22.18 cd A^{-1} and 25.83 cd A^{-1} , 21.07 lm W^{-1} and 23.19 lm W^{-1} , respectively. And the luminance have reached to 6000 m^{-2} and 8000 cd m^{-2} , respectively. The result is higher than those of the traditional fluorescence emitters but slower than the

expected result from the Φ_{PL} . Therefore, the efficiency of devices can be further improved by optimizing the carrier balance and carrier traps. Thus, in premise of efficient energy transfer from the host to exciplex emitters, the doping concentration of the acceptor should be as low as possible to shift up the 1CT of the exciplex blends. The result above demonstrated a simple way to design the exciplex blends to obtain nearly 100% triplet exciton by decreasing the energy gap between 3LE states of the acceptor and the 1CT of the exciplex emitters.

RESULTS AND DISCUSSION

Synthesis, Thermal Properties, and Photophysical Properties

TX unit is promising as an acceptor unit to construct the efficient pure TADF (Wang et al., 2014; Li et al., 2016). While, TX derivatives have never been used as the acceptor molecule to construct the exciplex, we functionalized the TX unit by bridging it along with the terpyridyl by Suzuki coupling reactions, an electron-withdrawing group, to obtain the molecules TX-TerPy. In exciplex, molecules containing nitrogen heterocycles are always preferred acceptors due to their deep HOMO levels (Shan et al., 2016; Deksnys et al., 2017; Nagai et al., 2017; Wu et al., 2018). TX-TerPy was successfully synthesized as shown in **Scheme S1** and fully characterized by 1H NMR spectroscopy (**Figure S1**), High-resolution EI-mass spectrometry (**Figure S2**), and satisfactory element analysis. Thermal gravimetric analysis (TGA) and differential scanning calorimetry (DSC) were also carried out at a heat rate of $10^\circ C\ min^{-1}$ under a nitrogen atmosphere to observe the thermal stability, respectively. It has an excellent thermal properties with decomposition temperature of $338.8^\circ C$, corresponding to 5 wt% weight loss, which fulfill the requirement of film preparation via vacuum deposition (**Figure S3**) and the glass transition temperature (T_g) of the bulk amorphous film was $141.3^\circ C$. Moreover, **Figure S4** showed the UV/Vis absorption bands and photoluminescence (PL) spectrum of it in different solvents from the low polarity toluene to the high polarity THF. The bands at around 380 nm is the weak intramolecular charge transfer (ICT) transition derived from the TX unit to terpyridyl unit. And the faint red shift of the PL emission in different solvent shows the weak ICT property in the excited state. Then the fluorescent and phosphorescent emissions were examined at 77 K in oxygen-free 2-MeTHF solution and in pure film (shown in **Figures S5, S9**). And the details are shown in **Tables S1, S2**. They exhibited the large ΔE_{ST} of 0.38 and 0.48 eV, respectively. The fluorescence and phosphorescence at 77 K both showed fine structure, which is both attributed to the 1LE and 3LE in solution or in pure film. And the decay lifetime of TX-TerPy is only 5.6 ns. Thus, TX-TerPy is a normal fluorescent molecule. 3LE of the molecule might depend on the polarity of the surrounding media, we not only detected it in neat film in more polar conditions, but also doped the TX-TerPy into polystyrene (PS) to detect it in less polar conditions. Thus, we estimated the S_1 and T_1 energy from the maxima emission of the fluorescent and phosphorescent in the blended films of PS at 77 K, as shown in **Figure S6**. The S_1 and T_1 are 3.03 eV and 2.69 eV, respectively. The details are all

shown in **Table 1**. The energy offset between the donor's HOMO and acceptor's LUMO drive the electron transfer that leads to exciplex formation (Liu et al., 2011; Jankus et al., 2014; Lee et al., 2017; Song et al., 2017). We chose the donor molecules with suitable HOMO or LUMO offset with TX-TerPy and higher 3LE energy level in order to avoid the exciton leakage which was discussed previously (Liu et al., 2011). Meanwhile, choosing the donors with different T_1 energy is an important way to manipulate the exciplex energy level in order to obtain the efficient TADF exciplex emitters. Next three hole-transporting materials of TAPC, TCTA and m-MTDATA were selected to act as the donors.

Exciplex Formation

The three donor molecules are mixed with TX-TerPy by weight of 1:1 to form the exciplexes. **Figures 1B–D** shows the PL spectra of the neat films of TX-TerPy, TAPC, TCTA and m-MTDATA and their corresponding exciplex emitters. The emission for TAPC:TX-TerPy, TCTA:TX-TerPy and m-MTDATA:TX-TerPy exciplex system show the maximum peaks at 538.6 nm, 534.6 nm and 590.6 nm, whereas those for TX-TerPy, TAPC, TCTA and m-MTDATA display the wavelength of 486.6, 373.6, 389.6 and 428.6 nm, respectively. The PL spectrum of the blended films are redshift by 52, 48 and 104 nm relative to the acceptor molecule. Especially for m-MTDATA:TX-TerPy, the interaction between m-MTDATA and TX-TerPy are stronger than the other two exciplex emitters, perhaps since that m-MTDATA holds three triphenylamine units. And the full width at half maximum (FWHM) of the three exciplex emissions is much broader than those of the constituting molecules. The large redshift emission band with broad, featureless structure compared to the emission of the corresponding neat films confirms the formation of exciplex in each of the blend films. The absorption bands of the doped films exhibit only the linear combination of the individual absorption of the donors and acceptors molecules suggesting that there is not a new-state transition in them (as shown in **Figure S7**). The results above all indicate the formation of the exciplex between the individual molecules.

$$E_{exciplex} = E_D^{ox} - E_A^{red} + U_{dest} - U_{stab} - \Delta H_e^{sol} + 0.32\text{eV} \quad (1)$$

$E_{exciplex}$ is the exciplex photon energy. In exciplex, the intermolecular charge transfer derived from the donor and the acceptor leads that the $E_{exciplex}$ has a linear relationship with the oxidation potential of the donor (E_D^{ox}) and the reduction potential of the acceptor (E_A^{red}), as shown in equation (1) (Cocchi et al., 2006; Liu et al., 2015c; Sarma and Wong, 2018). For an exciplex, U_{dest} and U_{stab} is nearly 0, which is, the stabilization and destabilization effects of the exciplex formation (Jankus et al., 2014). ΔH_e^{sol} is the enthalpy of solvation which is nearly 0.17 ± 0.07 eV. Exciplex formation requires a charge transfer from the donor's HOMO to acceptor's LUMO, thus the considerable offset of nearly 0.5 eV between the LUMO levels of the donor and acceptor should be satisfied (Jankus et al., 2014). The $E_{exciplex}$ of TAPC:TX-TerPy, TCTA:TX-TerPy, and m-MTDATA:TX-TerPy are estimated to be 2.30, 2.32 and 2.10 eV. The HOMO energies of the four molecules are determined by Ultraviolet photoelectron spectroscopy (UPS) measurement (**Figure S8**), they were -6.02 ,

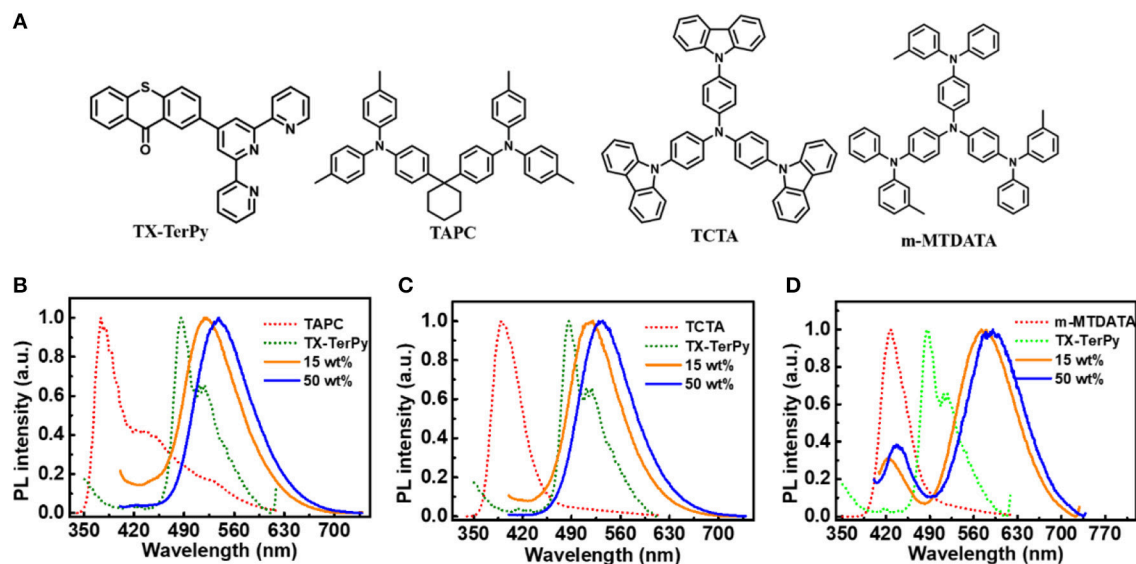


FIGURE 1 | Molecular structures and photoluminescence (PL) spectra of deposited films. **(A)** Molecular structures of TX-TerPy, TAPC, TCTA, and m-MTDATA; **(B)** PL spectra of TAPC, TX-TerPy, TAPC:TX-TerPy (7:1) and TAPC:TX-TerPy (1:1); **(C)** TCTA, TX-TerPy, TCTA:TX-TerPy (7:1) and TCTA:TX-TerPy (1:1); **(D)** m-MTDATA, TX-TerPy, m-MTDATA:TX-TerPy (7:1) and m-MTDATA:TX-TerPy (1:1).

TABLE 1 | Summary of Photophysical properties of exciplex films.

Acceptor	Donor	Conc. ^a [wt%]	Φ_{PL} ^b [%]	Φ_{PL} ^c [%]	Φ_{prompt} ^d [%]	$\Phi_{delayed}$ ^e [%]	λ_{em} ^f [nm]	E_{S1} ^g [eV]	E_{T1} ^g [eV]	$\Delta E(^1CT-^3CT)$ ^h [eV]
TX-TerPy	TAPC	15	59.2	65.2	1.90	63.30	520	2.79	2.75	0.02
		50	37.8	38.5	0.57	37.93	539	2.67	2.65	0.02
	TCTA	15	59.0	69.6	0.02	69.58	521	2.80	2.77	0.03
		50	46.6	47.6	1.43	46.17	535	2.69	2.66	0.03
	m-MTDATA	15	9.6	10.7	1.22	9.48	572	2.15	2.62	/
		50	5.3	6.2	0.84	5.36	590	2.15	2.45	/

^a Acceptor concentration.

^b Absolute PL quantum yield (Φ_{PL}) measured under air flow in an integrating sphere at room temperature.

^c Absolute PL quantum yield (Φ_{PL}) measured under N_2 flow in an integrating sphere at room temperature.

^d The ratio of the prompt component of Φ_{PL} .

^e The ratio of the delayed component of Φ_{PL} .

^f Measured at room temperature.

^g Singlet (E_S) and triplet (E_T) excited energies estimated from the maximum wavelengths of fluorescence and phosphorescence spectra at 77 K in doped film, respectively

^h $\Delta E(^1CT-^3CT) = \Delta E_S - \Delta E_T$.

−5.52, −5.95, and −5.14 eV, respectively. The LUMO levels were then calculated with the optical band gap determined from their absorption spectra. They are −3.15, −1.98, −2.57, and −1.96 eV. Then, $E_D^{ox} - E_A^{red}$ is estimated to be 2.37, 2.80, and 1.99 eV, close to the $E_{exciplex}$ of the three exciplex system, which are indicated the emission of the blend film is formed between the individual donors and the acceptor. For the TAPC:TX-TerPy, $E_{exciplex}$ is 0.07 eV lower than their related $E_D^{ox} - E_A^{red}$. Whereas, TCTA:TX-TerPy is 0.48 eV larger than their corresponding $E_D^{ox} - E_A^{red}$, which indicates the exciplex has a degree charge transfer of < 0.5. The state contains some heteroexcimer and some full ion pair state. For m-MTDATA:TX-TerPy, $h\nu_{max}$ is 0.09 eV larger than their related $E_D^{ox} - E_A^{red}$. The TCTA:TX-TerPy should have good PLQY due to the strongly mixed LE and CT character.

In order to quantify the ΔE_{ST} experimentally, as shown in **Figure S5** and **Table S1**, we investigated the fluorescence and phosphorescence spectra of the individual donors in 2-MeTHF at room temperature and 77K. And we also investigated the fluorescence and phosphorescence spectra of TAPC:TX-TerPy, TCTA:TX-TerPy and m-MTDATA:TX-TerPy in doped films (7:1 and 1:1) (**Figure S11**) and fluorescence and phosphorescence spectra of the individual pure films (**Figure S9**) at 77 k. The details are shown in **Table S2**. The details of the S_1 and T_1 excited state are shown in **Figure 2** and **Table 2**. The TAPC:TX-TerPy and TCTA:TX-TerPy blended films both show the unstructured fluorescence and phosphorescence emission at 77 k. From the maximum emission peaks of the fluorescence and phosphorescence spectra, the S_1 and T_1 state of TAPC:TX-TerPy were calculated to be 2.36 and 2.34 eV, respectively. So the S_1 - T_1

TABLE 2 | Summary of OLEDs Performance.

Exciplex emitters ^a	L _{max} [cd m ⁻²] ^b	V _{on} [V] ^c	CE _{max} [cd A ⁻¹] ^d	PE _{max} [lm W ⁻¹] ^d	EQE _{max} [%] ^d	CIE (x,y) ^e
TAPC:TX-TerPy	6,000	3.4	22.18	21.07	7.08	(0.39, 0.54)
TCTA:TX-TerPy	8,000	3.5	25.83	23.19	8.29	(0.40, 0.54)

^a The devices based on TAPC:20%TX-TerPy in a structure of ITO/ TAPC (35 nm)/mCP (10 nm) /Exciplex (EML) (15 nm)/TmPyPB (50 nm)/LiF (0.9 nm)/Al (100 nm). TCTA:TX-TerPy (1:1) in a structure of ITO / α -NPD (20 nm)/ TCTA (10 nm)/ mCP (10 nm) /Exciplex (EML) (15 nm) / TmPyPB (50 nm) /LiF (0.9 nm)/Al (100 nm).

^b The maximum luminance.

^c Turn-on voltage at 1 cd m⁻².

^d The maximum efficiencies of CE (cd A⁻¹), PE (lm W⁻¹) and EQE (%).

^e The Commission Internationale de L'Eclairage coordinates recorded at 7 V.

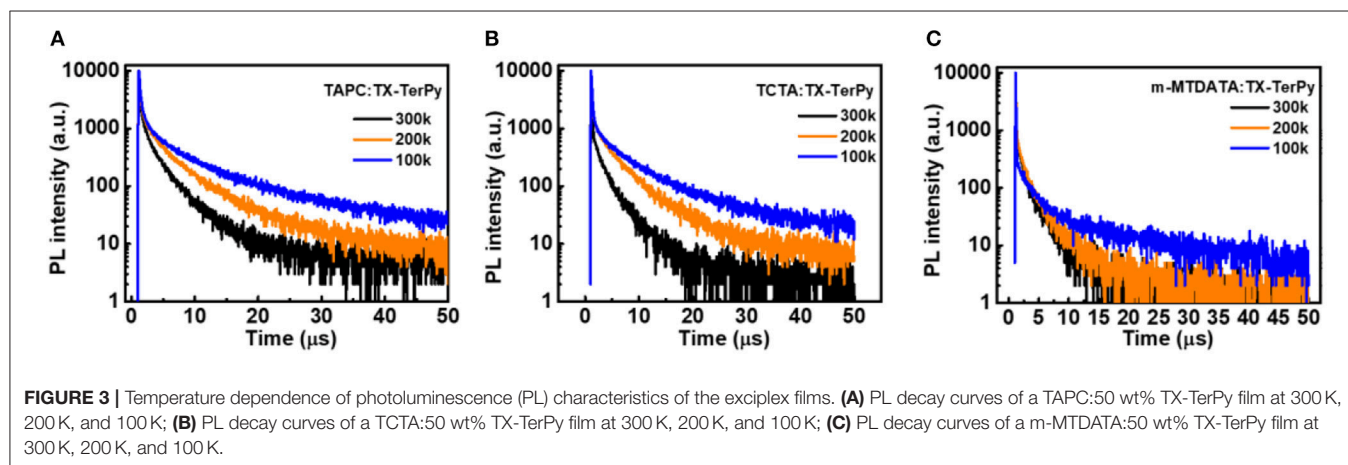
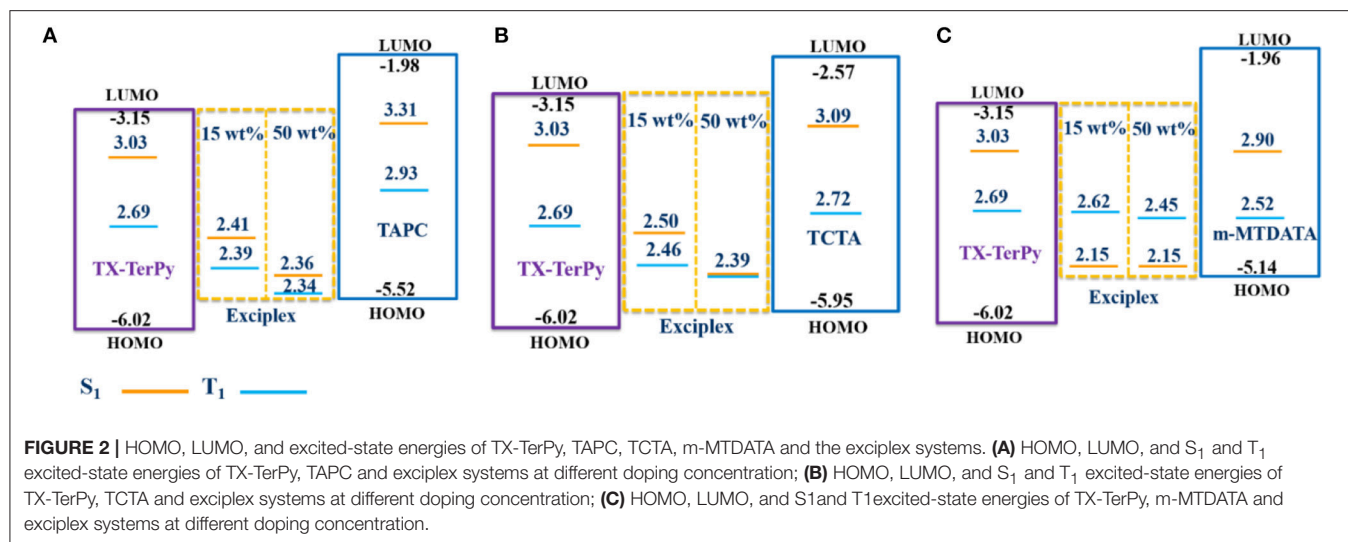
energy gap is 0.02 eV. The blended film displays fluorescence at 77 k with features from both the host and the exciplex emission, but also the unstructured phosphorescence spectra. It is perhaps due to the inefficient energy transfer from TAPC or TX-TerPy to exciplex at low temperature. As for TCTA:TX-TerPy, the S₁ and T₁ are 2.39 and 2.39 eV, which are both lower than that of TAPC:TX-TerPy. And the energy gap is nearly 0. Meanwhile, the phosphorescence of the donors show characteristic vibrational structures with the first highest peaks at 423.6 nm for TAPC, 456.6 nm for TCTA, 491.6 nm for m-MTDATA, so the related T₁ energy is 2.93, 2.72 eV and 2.52 eV, respectively. The ³LE of the donors are all higher than the T₁ state of the corresponding exciplex emitters, so the energy transferring from the exciplex to the donors can be avoided. Surprisingly, the phosphorescence of m-MTDATA:TX-TerPy is arising from m-MTDATA, despite that the T₁ energy of m-MTDATA (2.52 eV) are higher than S₁ energy (2.15 eV) of m-MTDATA:TX-TerPy, perhaps due to the inefficient reverse energy transfer from m-MTDATA to exciplex. Since the ¹CT, ³CT, and ³LE should be match with each other, we optimize the exciplexes at different doping concentrations, which will have an influence on ¹CT and ³CT of the exciplex emitters. As shown in **Figure S11**, the S₁ and T₁ energy of TAPC:TX-TerPy emitters shift up above 0.05 eV when we decrease the concentration of TX-TerPy from 50 to 15 wt%. That will benefit to decrease the energy gap between ¹CT of the exciplex and ³LE of the acceptor and donor. As for TCTA:TX-TerPy (7:1), the S₁ and T₁ shift up above 0.11 eV, larger than TAPC:TX-TerPy. But for the individual molecules, the ³LE changed a little, perhaps due to the insensitive environment dependence of it. That indicated that the RISC process of TCTA:TX-TerPy is more efficient than TAPC:TX-TerPy.

Photoluminescence Decays

In order to look inside into the TADF property of the three exciplex emitters, we conducted a transient photoluminescence experiment. As the different doping concentrations will tune the energy levels of the ¹CT energy of the blend films, we further studied the transient lifetime of the different constituting concentration of TX-TerPy. The choice of the different donors have a great influence on the Φ_{PL} (**Table 1**). When the doping concentration had the weight of 1:1, the Φ_{PL} are 38.5%, 47.6, and 6.2%, respectively. Whilst, the doping concentration for TAPC:TX-TerPy, TCTA:TX-TerPy and m-MTDATA:TX-TerPy had the weight of 7:1 Φ_{PL} of 65.2, 69.6, and 10.7% were for the exciplex emitters. Clearly, TAPC:TX-TerPy and TCTA:TX-TerPy both show higher Φ_{PL} at the weight of 7:1 and are nearly

two times higher than their corresponding doping concentrations of 50%. Notably, the TCTA: 15 wt% TX-TerPy demonstrates that the highest values among the six exciplex system is smaller than those of the other exciplexes as a result of the energy gap between ³LE of TX-TerPy and ¹CT of TCTA:TX-TerPy. As shown in **Figure S10**, the films of the pristine TX-TerPy, TAPC, TCTA, and m-MTDATA all show PL decays with the lifetime of around 2 ns at room temperature. In **Figure S13**, the transient PL decay spectral of the three exciplex emitters (1:1) at room temperature in N₂ flow all demonstrated a clear two-order or three-order exponential decays. The prompt ones refers to the relaxation from S₁ to S₀ and the delayed one refers to the delayed fluorescence (DF) and other persistent luminescence in the exciplex emitters. The DF refers the triplet excitons up-converse to the S₁ state via the RISC process, then decay to S₀. We divided them into two components in order to simplify the comparison. Surprisingly, they all showed a strong delayed emission, as shown in **Figure 3**. Then according to the PL intensity of the different components of TAPC:TX-TerPy (1:1), the Φ_{PL} at room temperature can be divided into 1.5% for the prompt component and 98.5% for the delay component, which indicated that the most triplet exciton can be obtained. For the TCTA:TX-TerPy, the delayed component can be as high as 97.0%, which is due to the smaller energy between ³LE of TX-TerPy and the S₁ and T₁ energy level of the exciplex. Although the Φ_{PL} of m-MTDATA:TX-TerPy is very low, the delayed component is still as large as 86.5%. The prompt fluorescence decay of the TAPC:TX-TerPy, TCTA:TX-TerPy and m-MTDATA:TX-TerPy blended films is 150, 220 and 170 ns, which is much longer than the individual films. As for the constituting concentration of 15% of the three exciplex blended films, the delayed components are higher than that of 50%, which is 97.1% for TAPC:TX-TerPy, 99.9% for TCTA:TX-TerPy and 88.6% for m-MTDATA:TX-TerPy. These are higher than the exciplex systems mentioned previously. The detail of the prompt fluorescence efficiency (Φ_{prompt}) and the delayed emission efficiency ($\Phi_{delayed}$) of the six exciplex emitters are shown in **Table 1**.

Then, the temperature dependence transient decay and PL emission of the three of the exciplex emitters (weight of 1:1) were performed from 300 K to 100 K to determine the nature of the delayed component (**Figure 3**). As shown in **Figure 3**, the PL intensity of the three exciplexes all increased with the decreasing temperature from 300 to 100 K (**Figure S12**), as do the PL intensity of the delay component, perhaps due to the emergence of the phosphorescence or the effect of singlet-triplet recycling.

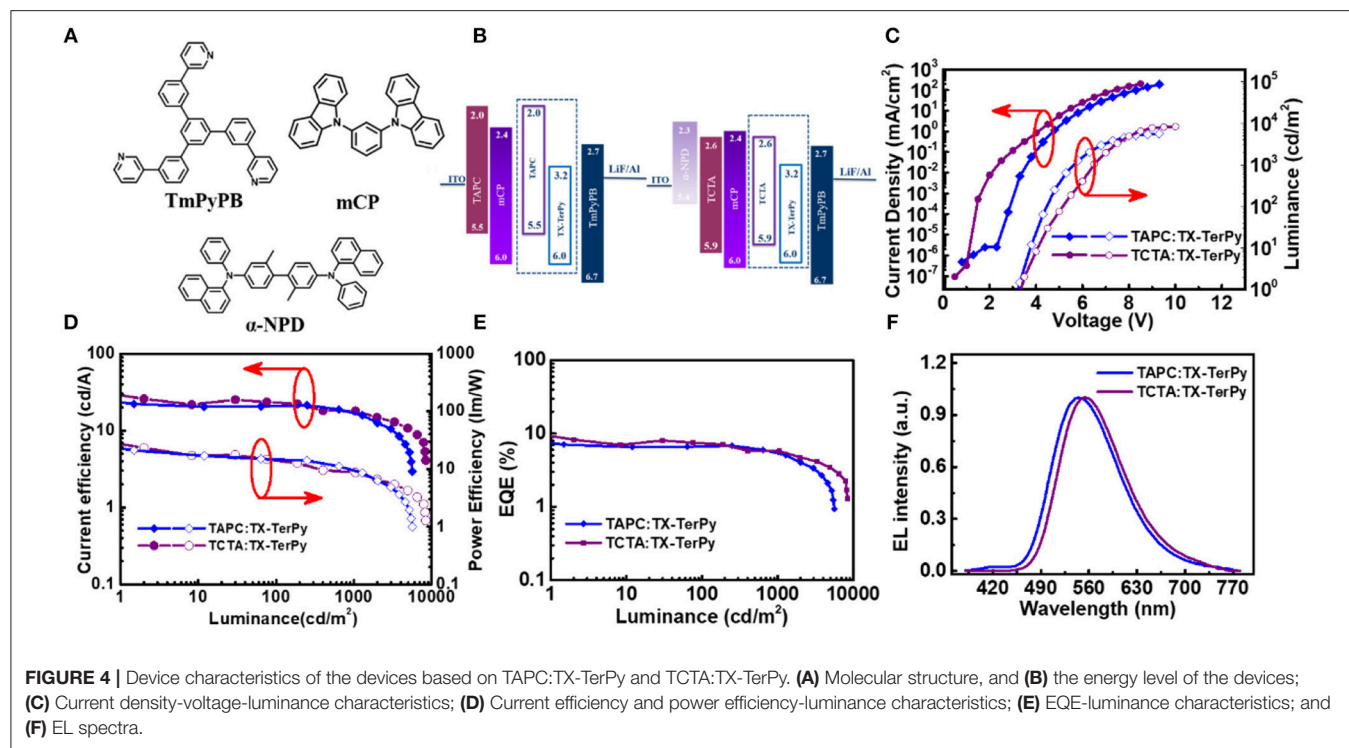


And the two component decay lifetimes of the longer component also varied as the temperature decreased. The lifetime of the delayed fluorescence of the three exciplexes nearly remained the same, namely the second component of the decay, but their ratio decreased a lot as the temperature decreased. On the contrary, for TAPC:TX-TerPy, the longer decay compound lifetime increased from 4.06 to 9.03 μ s. While TAPC:TX-TerPy increased from 3.57 to 8.93 μ s, and for m-MTDATA:TX-TerPy, 2.78 to 15.02 μ s as the temperature varied from 300 K to 100 K. The ratio was at least 79% at 300 K which was beneficial for the triplet exciton to obtain. This does not only verify the origins of the delayed ones, deriving from the recursive S_1 to S_0 transition via the RISC of the T_1 to S_1 by absorbing exothermic heat energy, but also verifies the emergence of the other long decay lifetimes, which was due to the small active energies.

Electroluminescence Properties

In order to further investigate the electrochemical property of the exciplex blend film based on TAPC:TX-TerPy and TCTA:TX-TerPy, OLED devices were fabricated with the following structures: indium tin oxide (ITO)/TAPC(35 nm)/1,3-Bis(carbazol-9-yl)benzene (mCP)

(10 nm)/TAPC:TX-TerPy (15 nm)/1,3,5-tri(m-pyrid-3-yl-phenyl)benzene (TmPyPB) (50 nm)/LiF (1.0 nm)/Al (100 nm) and ITO/ N,N'-Bis(naphthalen-1-yl)-N,N'-bis(phenyl)-2,2'-dimethylbenzidine (α -NPD) (20 nm)/TCTA (10 nm)/mCP (10 nm)/TCTA:TX-TerPy (15 nm)/TmPyPB (55 nm)/LiF (0.9 nm)/Al (100 nm). **Figures 4A,B** show the molecule structure and schematic diagram of the OLEDs and energy levels of the organic materials. Among them, α -NPD acts as the hole injection layer, TAPC or TCTA as the hole transport layer, mCP as the electron-blocking layer, and TmPyPB as the electron transporting and hole blocking layer. The devices based on TAPC:TX-TerPy and TCTA:TX-TerPy show green emission centered at 544 and 556 nm, which are red shifted corresponding to their PL spectrum. In order to optimize the device performance, the donor to acceptor weight ratio (D/A, w/w) in the active layer and the thickness of the active layer were modulated. As depicted in **Figures 4C–F**, the performance of the device with the optical D/A ratio (5:1) for TAPC:TX-TerPy and 1:1 for TCTA:TX-TerPy showed the highest efficiency. The OLED device based on TAPC:TX-TerPy and TCTA:TX-TerPy show the current efficiency (CE) of 22.13 cd A^{-1} and 25.83 cd



A^{-1} , the power efficiency of 21.07 lm W^{-1} and 23.19 lm W^{-1} and a high external quantum efficiency (EQE) of 7.08 and 8.29%, respectively. The details are shown in **Table 2**. The devices show the EQE is much lower than those expected from their Φ_{PL} (D/A ratio 1:1). The efficiency of the devices can be further improved by the optimization of the carrier balance, carrier traps and doping concentration. The device performance will be studied later. The 7.08 and 8.29% of the EQE based on this exciplex is much higher than the theoretical limit of 5% of the conventional fluorescence emitters. This will prove that the efficient triplet is harvesting in exciplex.

CONCLUSIONS

In summary, the three hole transporting molecules containing triphenylamine unit with different T_1 energy were selected as the donors to form exciplex with the newly molecule TX-TerPy. They all displayed a second order decay or third decay transient PL decay curves with the prompt and delayed component or long decay compound. Finally, the exciplex based on TCTA displayed the highest Φ_{PL} due to the appropriate HOMO of TCTA and LUMO of TX-TerPy, the appropriate ^1CT , ^3CT , and ^3LE energy level of them, especially the small energy gap between ^3LE of TX-TerPy and S_1 of TCTA:TX-TerPy. The OLED device based on TAPC:TX-TerPy and TCTA:TX-TerPy displayed the CE of 22.13 and 25.83 cd A^{-1} , the power efficiency of 21.07 and 23.19 lm W^{-1} and a high EQE of 7.08 and 8.29%, respectively. These findings highlight the optimized the ^1CT , ^3CT , and ^3LE in facilitating the efficient exciplex TADF molecules. Further studies on the

adjustment the energy of the three state will open a new way for high performance for OLED device efficiency.

AUTHOR CONTRIBUTIONS

XW, JL, and YW conceived the idea of the study, designed the experiment, and performed most of the optical measurement. XW, JL, RW, XH, and HG synthesized and characterized the molecules under the supervision of YW. YL, ZL, and GL fabricated and measured the devices. XW, YW, CL, and PW wrote the manuscript. TH answered the question about theoretical calculation in comments. All authors contributed to the scientific discussion.

FUNDING

This work was financially supported by the National Key Research and Development Project (No. 2016YFB0401004), the National Science Foundation of China (Grant No. 61420106002, No.51373189, No. 91833304 and No. 21772209), and the National Program for Support of Top-notch Young Professionals.

SUPPLEMENTARY MATERIAL

The Supplementary Material for this article can be found online at: <https://www.frontiersin.org/articles/10.3389/fchem.2019.00188/full#supplementary-material>

REFERENCES

- Cocchi, M., Virgili, D., Sabatini, C., and Kalinowski, J. (2006). Organic electroluminescence from singlet and triplet exciplexes: exciplex electrophosphorescent diode. *Chem. Phys. Lett.* 421, 351–355. doi: 10.1016/j.cplett.2006.01.082
- Cui, L. S., Deng, Y. L., Tsang, D. P., Jiang, Z. Q., Zhang, Q., Liao, L. S., et al. (2016). Controlling synergistic oxidation processes for efficient and stable blue thermally activated delayed fluorescence devices. *Adv. Mater.* 28, 7620–7625. doi: 10.1002/adma.201602127
- Deksnys, T., Simokaitiene, J., Keruckas, J., Volyniuk, D., Bezvikonny, O., Cherpak, V. et al. (2017). Synthesis and characterisation of a carbazole-based bipolar exciplex-forming compound for efficient and color-tunable oleds. *New J. Chem.* 41, 559–568. doi: 10.1039/c6nj02865a
- Deotare, P. B., Chang, W., Hontz, E., Congreve D. N., Shi, L., Reusswig, P. D., et al. (2015). Nanoscale transport of charge-transfer states in organic donor-acceptor blends. *Nat. Mater.* 14, 1130–1134. doi: 10.1038/NMAT4424
- dos Santos, P. L., Dias, F. B., and Monkman, A. P. (2016). Investigation of the mechanisms giving rise to TADF in exciplex states. *J. Phys. Chem. C* 120, 18259–18267. doi: 10.1021/acs.jpcc.6b05198
- Duan, C., Han, C., Du, R., Wei, Y., and Xu, H. (2018). High-efficiency blue dual-emissive exciplex boosts full-radiative white electroluminescence. *Adv. Opt. Mater.* 6:1800437. doi: 10.1002/adom.201800437
- Etherington, M. K., Gibson, J., Higginbotham, H. F., Penfold, T. J., and Monkman, A. P. (2016). Revealing the spin-vibronic coupling mechanism of thermally activated delayed fluorescence. *Nat. Commun.* 7:13680. doi: 10.1038/ncomms13680
- Goushi, K., Yoshida, K., Sato, K., and Adachi, C. (2012). Organic light-emitting diodes employing efficient reverse intersystem crossing for triplet-to-singlet state conversion. *Nat. Photon.* 6, 253–258. doi: 10.1038/NPHOTON.2012.31
- Graves, D., Jankus, V., Dias, F. B., and Monkman, A. (2014). Photophysical investigation of the thermally activated delayed emission from films of m-MTDATA:PBD exciplex. *Adv. Funct. Mater.* 24, 2343–2351. doi: 10.1002/adfm.201303389
- Hung, W. Y., Fang, G. C., Chang, Y. C., Kuo, T. Y., Chou, P. T., Lin, S. W., et al. (2013). Highly efficient bilayer interface exciplex for yellow organic light-emitting diode. *ACS Appl. Mater. Interfaces* 5, 6826–31. doi: 10.1021/am402032z
- Jankus, V., Data, P., Graves, D., McGuinness, C., Santos, J., Bryce, M. R., et al. (2014). Highly efficient TADF OLEDs: how the emitter-host interaction controls both the excited state species and electrical properties of the devices to achieve near 100% triplet harvesting and high efficiency. *Adv. Funct. Mater.* 24, 6178–6186. doi: 10.1002/adfm.201400948
- Kim, H. G., Kim, K. H., and Kim, J. J. (2017). Highly efficient, conventional, fluorescent organic light-emitting diodes with extended lifetime. *Adv. Mater.* 29:1702159. doi: 10.1002/adma.201702159
- Lee, D. R., Kim, B. S., Lee, C. W., Im, Y., Yook, K. S., Hwang, S. H., et al. (2015). Above 30% external quantum efficiency in green delayed fluorescent organic light-emitting diodes. *ACS Appl. Mater. Interfaces* 7, 9625–9629. doi: 10.1021/acsami.5b01220
- Lee, S., Koo, H., Kwon, O., Jae Park, Y., Choi, H., Lee, K., et al. (2017). The role of charge balance and excited state levels on device performance of exciplex-based phosphorescent organic light emitting diodes. *Sci. Rep.* 7:11995. doi: 10.1038/s41598-017-12059-2
- Li, G., Zhu, D., Peng, T., Liu, Y., Wang, Y., and Bryce, M. R. (2014). Very high efficiency orange-red light-emitting devices with low roll-off at high luminance based on an ideal host-guest system consisting of two novel phosphorescent iridium complexes with bipolar transport. *Adv. Funct. Mater.* 24, 7420–7426. doi: 10.1002/adfm.201402177
- Li, Y., Li, X.-L., Chen, D., Cai, X., Xie, G., He, Z., et al. (2016). Design strategy of blue and yellow thermally activated delayed fluorescence emitters and their all-fluorescence white oleds with external quantum efficiency beyond 20%. *Adv. Funct. Mater.* 26, 6904–6912. doi: 10.1002/adfm.201602507
- Lin, T. A., Chatterjee, T., Tsai, W. L., Lee, W. K., Wu, M. J., Jiao, M., et al. (2016). Sky-blue organic light emitting diode with 37% external quantum efficiency using thermally activated delayed fluorescence from spiroacridine-triazine hybrid. *Adv. Mater.* 28, 6976–6983. doi: 10.1002/adma.201601675
- Lin, T. C., Sarma, M., Chen, Y.-T., Liu, S. H., Lin, K. T., Chiang, P. Y., et al. (2018). Probe exciplex structure of highly efficient thermally activated delayed fluorescence organic light emitting diodes. *Nat. Commun.* 9, 3111. doi: 10.1038/s41467-018-05527-4
- Liu, F., Paul Ruden, P., Campbell, I. H., and Smith, D. L. (2011). Exciplex current mechanism for ambipolar bilayer organic light emitting diodes. *Appl. Phys. Lett.* 99:123301. doi: 10.1063/1.3640232
- Liu, W., Chen, J.-X., Zheng, C.-J., Wang, K., Chen, D.-Y., Li, F., et al. (2016). Novel strategy to develop exciplex emitters for high-performance oleds by employing thermally activated delayed fluorescence materials. *Adv. Funct. Mater.* 26, 2002–2008. doi: 10.1002/adfm.201505014
- Liu, X. K., Chen, Z., Qing, J., Zhang, W. J., Wu, B., Tam, H. L., et al. (2015a). Remanagement of singlet and triplet excitons in single-emissive-layer hybrid white organic light-emitting devices using thermally activated delayed fluorescent blue exciplex. *Adv. Mater.* 27, 7079–7085. doi: 10.1002/adma.201502897
- Liu, X. K., Chen, Z., Zheng, C. J., Chen, M., Liu, W., Zhang, X. H., et al. (2015b). Nearly 100% triplet harvesting in conventional fluorescent dopant-based organic light-emitting devices through energy transfer from exciplex. *Adv. Mater.* 27, 2025–2030. doi: 10.1002/adma.201500013
- Liu, X. K., Chen, Z., Zheng, C. J., Liu, C. L., Lee, C. S., Li, F., et al. (2015c). Prediction and design of efficient exciplex emitters for high-efficiency, thermally activated delayed-fluorescence organic light-emitting diodes. *Adv. Mater.* 27, 2378–2383. doi: 10.1002/adma.201405062
- Mamada, M., Tian, G., Nakanotani, H., Su, J., and Adachi, C. (2018). The importance of excited-state energy alignment for efficient exciplex systems based on a study of phenylpyridinato boron derivatives. *Angew. Chem. Int. Educ.* 57, 12380–12384. doi: 10.1002/anie.201804218
- Moon, C. K., Suzuki, K., Shizu, K., Adachi, C., Kaji, H., and Kim, J. J. (2017). Combined inter- and intramolecular charge-transfer processes for highly efficient fluorescent organic light-emitting diodes with reduced triplet exciton quenching. *Adv. Mater.* 29:1606448. doi: 10.1002/adma.201606448
- Nagai, Y., Sasabe, H., Takahashi, J., Onuma, N., Ito, T., Ohisa, S., Kido, J. (2017). Highly efficient deep-red organic light-emitting devices using energy transfer from exciplexes. *J. Mater. Chem. C* 5, 527–530. doi: 10.1039/c6tc04979f
- Park, Y.-S., Kim, K.-H., and Kim, J.-J. (2013). Efficient triplet harvesting by fluorescent molecules through exciplexes for high efficiency organic light-emitting diodes. *Appl. Phys. Lett.* 102:153306. doi: 10.1063/1.4802716
- Samanta, P. K., Kim, D., Coropceanu, V., and Bredas, J. L. (2017). Up-conversion intersystem crossing rates in organic emitters for thermally activated delayed fluorescence: impact of the nature of singlet vs triplet excited states. *J. Am. Chem. Soc.* 139, 4042–4051. doi: 10.1021/jacs.6b12124
- Santos, P. L., Ward, J. S., Data, P., Batsanov, A. S., Bryce, M. R., and Dias, F. B. (2016). Engineering the singlet-triplet energy splitting in a tadf molecule. *J. Mater. Chem. C* 4, 3815–3824. doi: 10.1039/c5tc03849a
- Sarma, M., and Wong, K. T. (2018). Exciplex: an intermolecular charge-transfer approach for TADF. *ACS Appl. Mater. Interfaces* 10, 19279–19304. doi: 10.1021/acsami.7b18318
- Sasabe, H., and Kido, J. (2013). Development of high performance oleds for general lighting. *J. Mater. Chem. C* 1:1699. doi: 10.1039/c2tc00584k
- Shan, T., Liu, Y., Tang, X., Bai, Q., Gao, Y., Gao, Z., et al. (2016). Highly efficient deep blue organic light-emitting diodes based on imidazole: significantly enhanced performance by effective energy transfer with negligible efficiency roll-off. *ACS Appl. Mater. Interfaces* 8, 28771–28779. doi: 10.1021/acsami.6b10004
- Shih, C. J., Lee, C. C., Chen, Y. H., Biring, S., Kumar, G., Yeh, T. H., et al. (2018). Exciplex-forming cohost for high efficiency and high stability phosphorescent organic light-emitting diodes. *ACS Appl. Mater. Interfaces* 10, 2151–2157. doi: 10.1021/acsami.8b08281
- Song, W., Lee, H. L., and Lee, J. Y. (2017). High triplet energy exciplex hosts for deep blue phosphorescent organic light-emitting diodes. *J. Mater. Chem. C* 5, 5923–5929. doi: 10.1039/c7tc01552f
- Tao, Y., Yuan, K., Chen, T., Xu, P., Li, H., Chen, R., et al. (2014). Thermally activated delayed fluorescence materials towards the breakthrough of organoelectronics. *Adv. Mater.* 26, 7931–7958. doi: 10.1002/adma.201402532

- Wang, H., Xie, L., Peng, Q., Meng, L., Wang, Y., Yi, Y., et al. (2014). Novel thermally activated delayed fluorescence materials-thioxanthone derivatives and their applications for highly efficient oleds. *Adv. Mater.* 26, 5198–5204. doi: 10.1002/adma.201401393
- Wong, M. Y., and Zysman-Colman, E. (2017). Purely organic thermally activated delayed fluorescence materials for organic light-emitting diodes. *Adv. Mater.* 29:1605444. doi: 10.1002/adma.201605444
- Wu, Q., Wang, M., Cao, X., Zhang, D., Sun, N., Wan, S., et al. (2018). Carbazole/A-carboline hybrid bipolar compounds as electron acceptors in exciplex or non-exciplex mixed cohosts and exciplex-tadf emitters for high-efficiency oleds. *J. Mater. Chem. C* 6, 8784–8792. doi: 10.1039/c8tc02353k
- Wu, Z., Yu, L., Zhao, F., Qiao, X., Chen, J., Ni, F., et al. (2017). Precise exciton allocation for highly efficient white organic light-emitting diodes with low efficiency roll-off based on blue thermally activated delayed fluorescent exciplex emission. *Adv. Opt. Mater.* 5:1700415. doi: 10.1002/adom.201700415
- Yang, Z., Mao, Z., Xie, Z., Zhang, Y., Liu, S., Zhao, J., et al. (2017). Recent advances in organic thermally activated delayed fluorescence materials. *Chem. Soc. Rev.* 46, 915–1016. doi: 10.1039/c6cs00368k

Conflict of Interest Statement: The authors declare that the research was conducted in the absence of any commercial or financial relationships that could be construed as a potential conflict of interest.

Copyright © 2019 Wei, Liu, Hu, Li, Liu, Wang, Gao, Hu, Liu, Wang, Lee and Wang. This is an open-access article distributed under the terms of the Creative Commons Attribution License (CC BY). The use, distribution or reproduction in other forums is permitted, provided the original author(s) and the copyright owner(s) are credited and that the original publication in this journal is cited, in accordance with accepted academic practice. No use, distribution or reproduction is permitted which does not comply with these terms.



Development of Red Exciplex for Efficient OLEDs by Employing a Phosphor as a Component

Ming Zhang^{1,2†}, Kai Wang^{2†}, Cai-Jun Zheng^{1*}, De-Qi Wang¹, Yi-Zhong Shi², Hui Lin¹, Si-Lu Tao¹, Xing Li² and Xiao-Hong Zhang^{2*}

¹ School of Optoelectronic Science and Engineering, University of Electronic Science and Technology of China, Chengdu, China, ² Institute of Functional Nano & Soft Materials (FUNSOM) and Jiangsu Key Laboratory for Carbon-Based Functional Materials & Devices, Soochow University, Suzhou, China

OPEN ACCESS

Edited by:

Lian Duan,
Tsinghua University, China

Reviewed by:

Qisheng Zhang,
Zhejiang University, China
Toshinori Matsushima,
Kyushu University, Japan

*Correspondence:

Cai-Jun Zheng
zhengcaijun@uestc.edu.cn
Xiao-Hong Zhang
xiaohong_zhang@suda.edu.cn

[†]These authors have contributed
equally to this work

Specialty section:

This article was submitted to
Organic Chemistry,
a section of the journal
Frontiers in Chemistry

Received: 07 November 2018

Accepted: 08 January 2019

Published: 31 January 2019

Citation:

Zhang M, Wang K, Zheng C-J,
Wang D-Q, Shi Y-Z, Lin H, Tao S-L,
Li X and Zhang X-H (2019)
Development of Red Exciplex for
Efficient OLEDs by Employing a
Phosphor as a Component.
Front. Chem. 7:16.
doi: 10.3389/fchem.2019.00016

Exciplexes are ideal candidates as effective thermally activated delayed fluorescence (TADF) emitters. However, efficient orange and red TADF exciplexes have been reported seldomly, because their significant non-radiative (NR) decay of excited states lead to unavoidable energy loss. Herein, we propose a novel strategy to construct efficient red TADF exciplexes by introducing phosphor as one component. Due to the strong spin-orbit coupling of heavy metal (e.g., Ir, Pt, et al.) ion cores, the NR decays will be evidently decreased for both singlet and triplet excitons, reducing the undesired exciton waste. Moreover, compared with the conventional exciplexes, phosphorescence plays an important role for such novel exciplexes, further improving the exciton utilization. Based on this strategy, we fabricated a red exciplex containing 1,3,5-triazine-2,4,6-triyl)tris(benzene-3,1-diyl)tris(diphenylphosphine oxide) (PO-T2T) and tris(2-phenylpyridine) iridium(III) (Ir(ppy)₃) as components and realize a red emission with a peak at 604 nm, a CIE coordinate of (0.55, 0.44), and a high maximum external quantum efficiency of 5% in organic light-emitting device. This efficiency is 2.6 times higher than that of the device based on the conventional red exciplex emitter, proving the superiority of our novel strategy to construct TADF exciplexes with phosphors.

Keywords: exciplex, thermally activated delayed fluorescence, phosphor, spin-orbit coupling, non-radiative decay

INTRODUCTION

Organic light-emitting devices (OLEDs) based on thermally activated delayed fluorescence (TADF) emitters are considered the new generation of OLEDs (Adachi, 2014) and have drawn great attention in recent years (Goushi et al., 2012; Uoyama et al., 2012; Zhang et al., 2014b, 2016; Ban et al., 2015; Hirata et al., 2015; Liu M. et al., 2015, 2017; Liu W. et al., 2015; Chen et al., 2016, 2017; Gómez-Bombarelli et al., 2016; Li et al., 2016, 2017, 2018; Xie et al., 2016; Miwa et al., 2017; Moon et al., 2017; Shiu et al., 2017; Wang K. et al., 2017a; Yang et al., 2017). The TADF emitters can utilize both singlet and triplet excitons for emission by up-converting non-radiative (NR) triplet excitons to radiative singlet excitons via an efficient reverse intersystem crossing (RISC) process from lowest triplet state (T_1) to lowest singlet state (S_1) (Uoyama et al., 2012). Theoretically, an effective RISC process requires that the TADF emitter possesses an extremely small singlet-triplet energy splitting (ΔE_{ST}) between S_1 and T_1 (Uoyama et al., 2012), which needs to isolate its highest occupied molecular

orbital (HOMO) and lowest unoccupied molecular orbital (LUMO) (Chen et al., 2016; Wang D. Q. et al., 2017; Wang et al., 2017b). Clearly, exciplexes are among the ideal candidates as effective TADF emitters, because they meet the requirements mentioned above naturally (Liu et al., 2015a,b, 2016). Formed via intermolecular charge-transfer (CT) transition, the HOMOs and LUMOs of exciplexes are independently located on the electron-donor (D) and electron-acceptor (A) component molecules respectively, possessing extremely small overlaps. Thus, exciplex systems present extremely small energy gaps between their own ^1CT and ^3CT (<0.1 eV). By using high- T_1 component molecules to avoid the triplet excitons loss, exciplexes commonly exhibit TADF characteristics. In the past few years, great progress has been made for exciplex-based TADF OLEDs (Goushi et al., 2012; Li et al., 2014; Liu et al., 2015b,c, 2016; Zhang et al., 2017; Shi et al., 2018). In 2012, Adachi and co-workers firstly reported a yellow-green TADF exciplex, and theoretically proved its great potential (Goushi et al., 2012). In 2015, our group developed a novel strategy to predict and design efficient exciplex with TADF characteristics by using the HOMO and LUMO energy levels of constituting molecules (Liu et al., 2015a). And in 2016, our group further reported highly efficient exciplex-based TADF OLED with an high external quantum efficiency (EQE) of 17.8% (Liu et al., 2016). However, nearly all the currently reported exciplex TADF emitters are limited in short-wavelength (i.e., blue, green, and yellow) emission (Goushi et al., 2012; Li et al., 2014; Liu et al., 2015b,c, 2016; Zhang et al., 2017; Shi et al., 2018). Efficient TADF exciplexes with long-wavelength (i.e., orange and red) emission have rarely been reported (Data et al., 2016). **Figure 1A** illustrates the exciton transfer processes in conventional TADF exciplexes. Both the constituting molecules should have higher S_1 and T_1 energy levels than that of exciplex, ensuring all excitons can be harvested on S_1 and T_1 states of exciplex (Liu et al., 2015a). Therefore, the energy loss of the exciplex-based TADF OLEDs should be mainly caused by the NR decay of both exciplex S_1 and T_1 states. According to photophysical theory, the rate constants of the NR decays are exponentially magnified with the decreased bandgap energy level (Zhang et al., 2014a). For TADF exciplexes with short-wavelength emission, the NR decays of S_1 and T_1 states are almost neglectful compared with the emission process of S_1 state and RISC process of T_1 state, realizing high exciton utilization in the OLEDs (Liu et al., 2016). While for common orange and red TADF exciplexes, the NR decays of excited states become significant due to narrow bandgaps, leading to unavoidable energy loss. Therefore, efficient orange and red TADF exciplexes are hard to be achieved by these common exciplex systems and become the bottleneck of exciplexes development.

In this study, we proposed a novel strategy to construct efficient red exciplexes by introducing a phosphor as one component. As we known, phosphors are generally heavy metal complexes. The spin-orbit coupling (SOC) of heavy metal (Ir, Pt, et al.) ion cores will significantly enhance the energy transfer processes between singlet and triplet states [intersystem crossing process (ISC) from S_1 to T_1 and phosphorescent decay from T_1 to S_0], allowing heavy metal complexes to achieve phosphorescence efficiently (Baldo et al., 1998; Liu X.

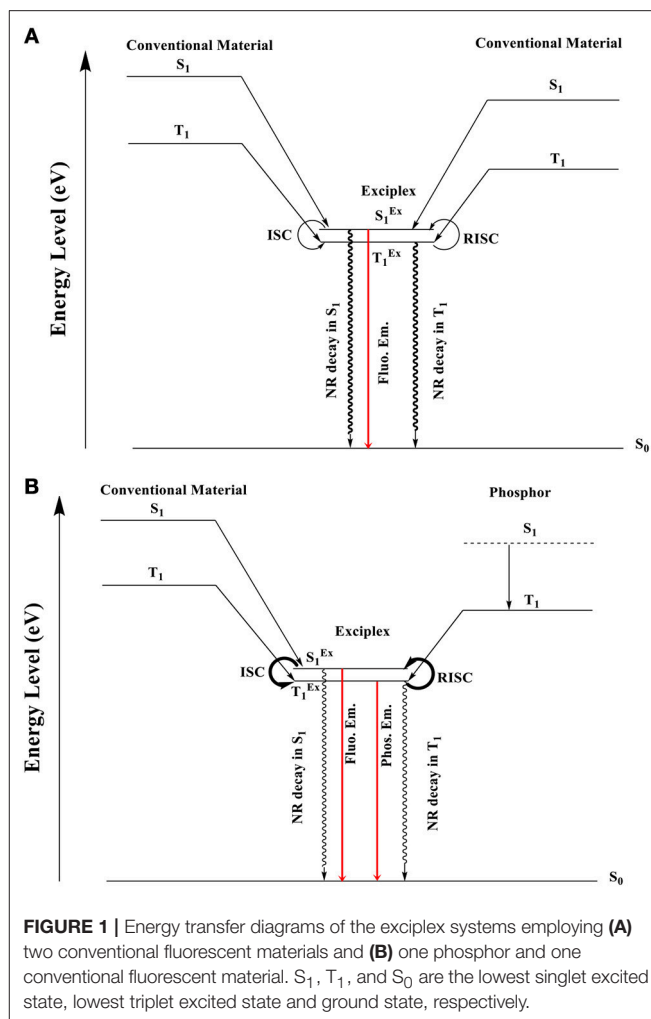


FIGURE 1 | Energy transfer diagrams of the exciplex systems employing (A) two conventional fluorescent materials and (B) one phosphor and one conventional fluorescent material. S_1 , T_1 , and S_0 are the lowest singlet excited state, lowest triplet excited state and ground state, respectively.

et al., 2015; Liu B. et al., 2017). Correspondingly, in new type exciplexes, the decay routes of excited exciplexes will be also affected by the heavy metal phosphor cores. The ISC process from S_1^{EX} to T_1^{EX} , RISC process from T_1^{EX} to S_1^{EX} and phosphorescent decay from T_1^{EX} to S_0^{EX} can be significantly enhanced by the SOC effect. Thus, the proportions of the NR decays will be accordingly decreased for S_1^{EX} and T_1^{EX} states, reducing the undesired exciton waste. Moreover, compared with the conventional exciplexes, phosphorescence may play an important role on such new type of exciplexes with phosphor (Cherpak et al., 2015) (**Figure 1B**), further improving the exciton utilization. Based on this novel strategy, we fabricated a red exciplex containing 1,3,5-triazine-2,4,6-triyl)tris(benzene-3,1-diyl)tris(diphenylphosphine oxide) (PO-T2T) and tris(2-phenylpyridine) iridium(III) ($\text{Ir}(\text{ppy})_3$) as components, which exhibits typical TADF characteristic with an extremely small ΔE_{ST} of 0.026 eV. In device, PO-T2T: $\text{Ir}(\text{ppy})_3$ exciplex shows a red emission with a peak at 604 nm and a CIE coordinate of (0.55, 0.44), and realizes a high maximum external quantum efficiency (EQE) of 5%. As a comparison, the conventional TADF exciplex consisting of PO-T2T and 1,3-di(10H-phenoxazin-10-yl)benzene (13PXZB) only achieves a maximum EQE of 1.9% in

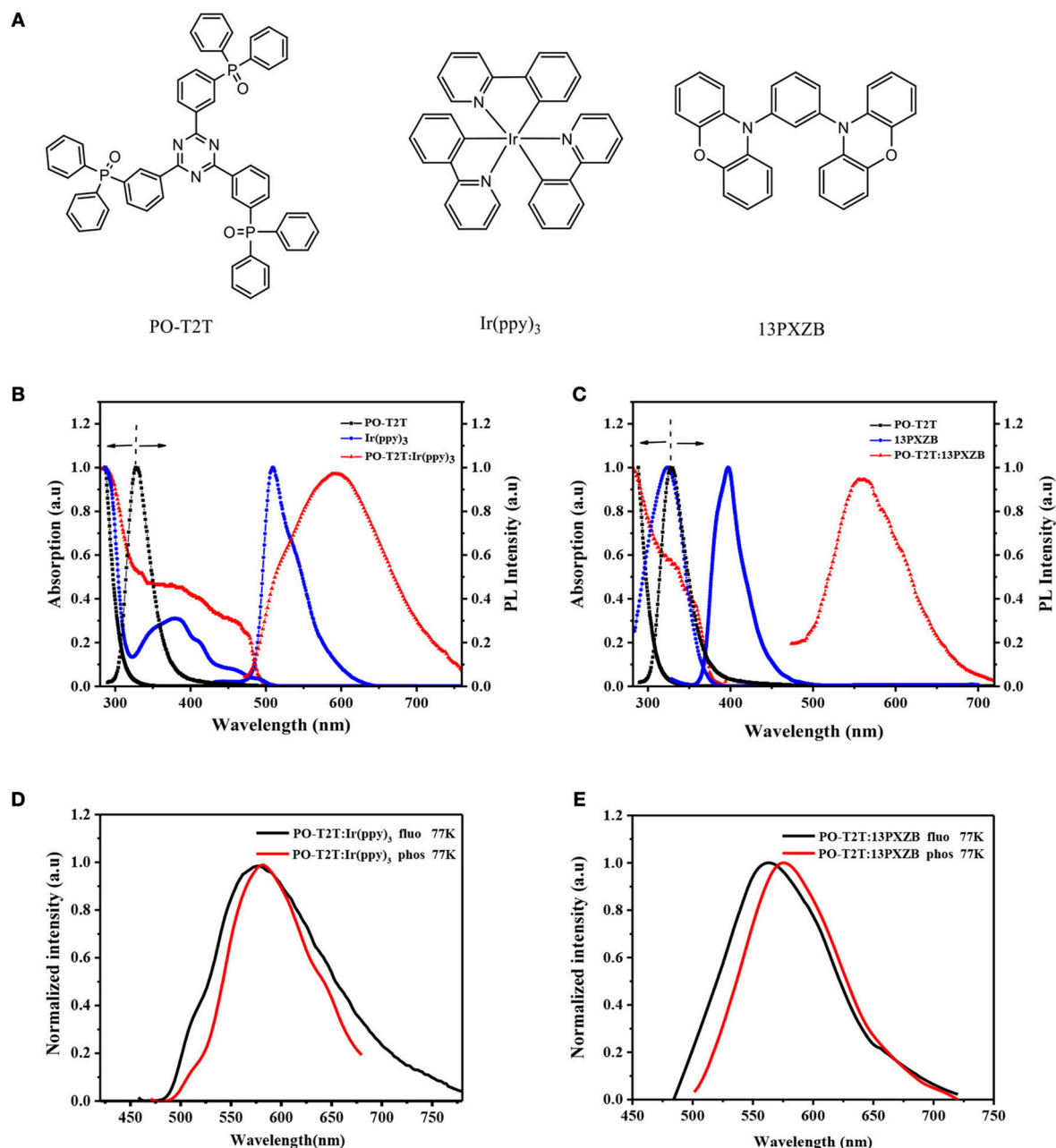


FIGURE 2 | (A) Chemical structures of PO-T2T, Ir(ppy)₃ and 13PXZB; **(B)** Absorption and PL spectra of PO-T2T, Ir(ppy)₃ in toluene solution and POT2T:Ir(ppy)₃ in solid thin film; **(C)** Absorption and PL spectra of PO-T2T, 13PXZB in toluene solution and POT2T:13PXZB in solid thin film; **(D)** the fluorescence and phosphorescence spectra of PO-T2T: 8 wt% Ir(ppy)₃ mixed film and **(E)** PO-T2T: 40 wt% 13PXZB mixed film.

device. These results not only demonstrate exciplexes can also be formed by using a phosphor component, but also indicate that the NR decays of excited states can be significantly suppressed for phosphor-based exciplexes by the SOC effect of heavy metal ion core from phosphor. Although noble metal Ir is contained in our system, we believe efficient but low-cost phosphor-based exciplex emitters can be developed by using other cheap heavy metal-based phosphors, like Cu, et al.

RESULTS AND DISCUSSION

Figure 2A illustrates the molecular structures of PO-T2T, Ir(ppy)₃ and 13PXZB. PO-T2T and Ir(ppy)₃ were directly purchased from commercial sources, and 13PXZB was newly designed and synthesized as shown in **Supporting Information**. The cyclic voltammograms of the three materials are shown in **Figure S1**. Both Ir(ppy)₃ and 13PXZB show nearly identical

oxidation onsets, and their HOMO energy levels are accordingly estimated to be identically at -5.30 eV, while the LUMO energy level of PO-T2T is estimated to be -3.26 eV from the onset of the reduction curve. Combining the energy gaps determined from the onsets of absorption spectra, the LUMO energy levels are estimated to be -2.76 eV for Ir(ppy)₃ and -1.95 eV for 13PXZB, and the HOMO energy level of PO-T2T is -6.93 eV. Based on our previous study, the driving force for exciplex formation can be approximately described as Equation (1) (Liu et al., 2015a)

$$\begin{aligned} -\Delta G_{\text{EX}} &= \text{HOMO}_{\text{D}} - \text{HOMO}_{\text{A}}(\text{for acceptor}) \text{ or} \\ -\Delta G_{\text{EX}} &= \text{LUMO}_{\text{D}} - \text{LUMO}_{\text{A}}(\text{for donor}) \end{aligned} \quad (1)$$

Thus, the driving forces are approximately estimated to be 1.63 eV for PO-T2T and 0.5 eV for Ir(ppy)₃ in the PO-T2T:Ir(ppy)₃ system and 1.63 eV for PO-T2T and 1.31 eV for 13PXZB in the PO-T2T:13PXZB system. These high values can ensure the exciplex formation in both systems. Moreover, as the CT transition of exciplex happens between LUMO of A and HOMO of D, the exciplex energy can be described as Equation (2), where the constant is exciton binding energy and ranges from 0 to 0.20 eV (Kolosov et al., 2002)

$$E_{\text{exciplex}} = e(\text{LUMO}_{\text{A}} - \text{HOMO}_{\text{D}}) + \text{constant} \quad (2)$$

Thus, both exciplexes possess energy of 2.02 eV approximately, ensuring they exhibit red emission. Moreover, the respective T₁ energy levels of PO-T2T, Ir(ppy)₃ and 13PXZB are 2.95 , 2.45 , and 2.73 eV, which are determined from the highest energy vibronic sub-band of their phosphorescence spectra at 77 K (Figure S2). These T₁ energy values of components are much higher than both exciplex energies, which boosts the exciplex to harvest all excitons.

The absorption and photoluminescence (PL) spectra of PO-T2T:Ir(ppy)₃ and PO-T2T:13PXZB exciplexes were investigated first. As shown in Figures 2B,C, the absorption spectra of both PO-T2T:Ir(ppy)₃ and PO-T2T:13PXZB mixed films are nearly identical to their constituting molecules at room temperature, suggesting that there are no extra transitions generated in the ground states. Correspondingly, their PL spectra show broad emissions in the range of 480 – 733 nm with a peak at 590 nm for PO-T2T:Ir(ppy)₃ and in the range of 480 to 670 nm with a peak at 562 nm for PO-T2T:13PXZB, which significantly differ from the PL spectra of the individual constituting molecules, proving the formation of exciplexes for both films during the photoexcitations. And the PL spectrum of PO-T2T:Ir(ppy)₃ is slightly red-shifted compared with that of PO-T2T:13PXZB, indicating PO-T2T:13PXZB actually has higher energy than PO-T2T:Ir(ppy)₃. Particularly, in the PL spectrum of PO-T2T:Ir(ppy)₃ mixed film, a slight shoulder can be observed at

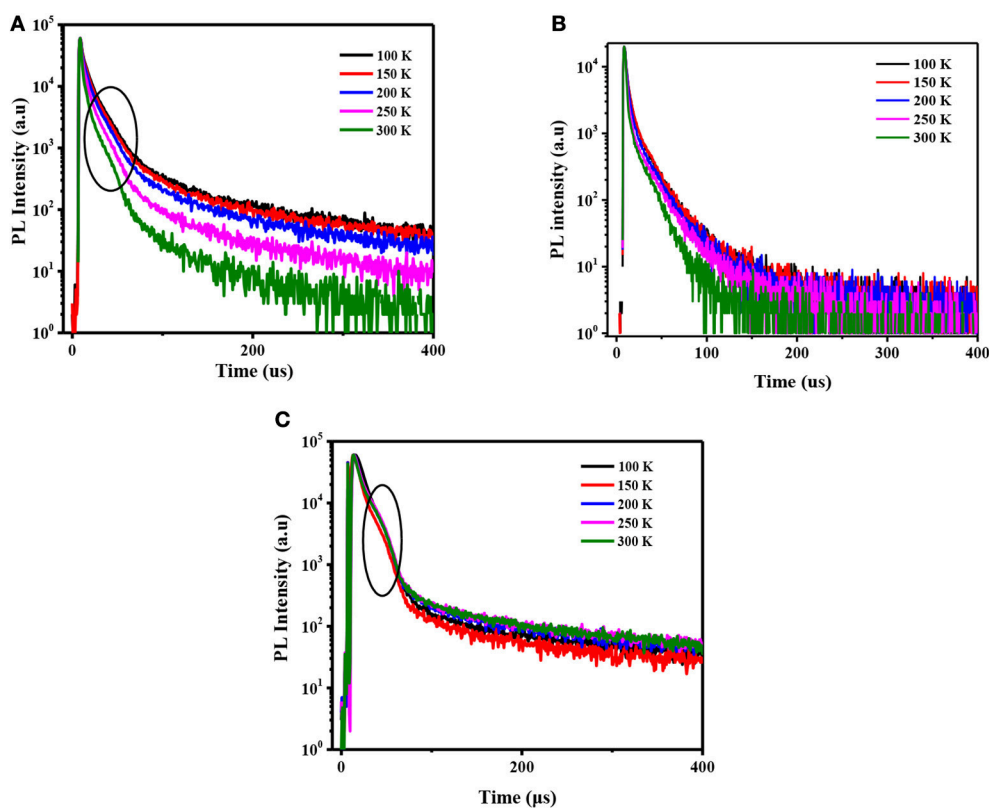


FIGURE 3 | Transient PL decay curves of the (A) PO-T2T:Ir(ppy)₃ film; (B) PO-T2T:13PXZB film; and (C) mCP:Ir(ppy)₃ film at various temperatures by exciting at 300 nm.

the emission area of Ir(ppy)₃, suggesting that the original metal-to-ligand CT transition of Ir(ppy)₃ is still competitive during the photoexcitation.

To study the photophysical properties of both exciplexes, we further measured the fluorescence and phosphorescence spectra of the two mixed films at 77 K. As shown in **Figures 2D,E**, from the peaks in the fluorescence and phosphorescence spectra, the S₁ and T₁ energy levels of both the exciplex systems were estimated to be 2.162 and 2.136 eV for PO-T2T:Ir(ppy)₃ and 2.215 and 2.188 eV for PO-T2T:13PXZB, respectively. Thus, their ΔE_{ST} s are calculated to be 0.026 and 0.030 eV for PO-T2T:Ir(ppy)₃ and PO-T2T:13PXZB, respectively. These extremely small ΔE_{ST} s can lead to efficient RISC process from T₁ to S₁ state, which endow both exciplexes with TADF characteristic. Temperature-dependent transient decay characteristics of these two exciplexes were further measured under nitrogen atmosphere. As shown in **Figure 3** and **Figure S3**, by exciting both the components at 300 nm, the lifetimes of both PO-T2T:Ir(ppy)₃ and PO-T2T:13PXZB exciplexes show significantly decline along with the temperature increasing from 100 to 300 K, indicating their TADF characteristics. At room temperature, PO-T2T:Ir(ppy)₃ shows a

prompt lifetime of 13.2 ns and extremely small delayed lifetime of 2.8 μ s. PO-T2T:13PXZB exciplex has a prompt lifetime of 17.1 ns and a decay lifetime of 13.9 μ s, which is significantly longer than that of PO-T2T:Ir(ppy)₃ film. This phenomenon is caused by the SOC effect of heavy metal core in phosphor, which can effectively enhance the RISC process. Moreover, in the range of <100 μ s (shown in **Figures 3A,C**), significant turning curves can be observed with a similar behavior compared to the initial curve of Ir(ppy)₃, which should indicate the evident contribution of exciplex phosphorescence. PL quantum yields (PLQYs) of PO-T2T:Ir(ppy)₃ and PO-T2T:13PXZB mixed films with a thin thickness of 5 nm were measured via integrating sphere measurements in atmosphere. Both films present a similar low PLQY value of about 4%. Considering that most of triplet excitons can be quenched by oxygen, the PLQY value will be mainly contributed by the prompt component of singlet excitons, and both of the exciplexes should have similar luminescence efficiencies in the devices if we neglect the effect of triplet excitons (M  hes et al., 2012). While under oxygen-free condition, both singlet and triplet excitons make contributions to the emission. As a result, the PLQY values were increased to 23.3 and 8.6%

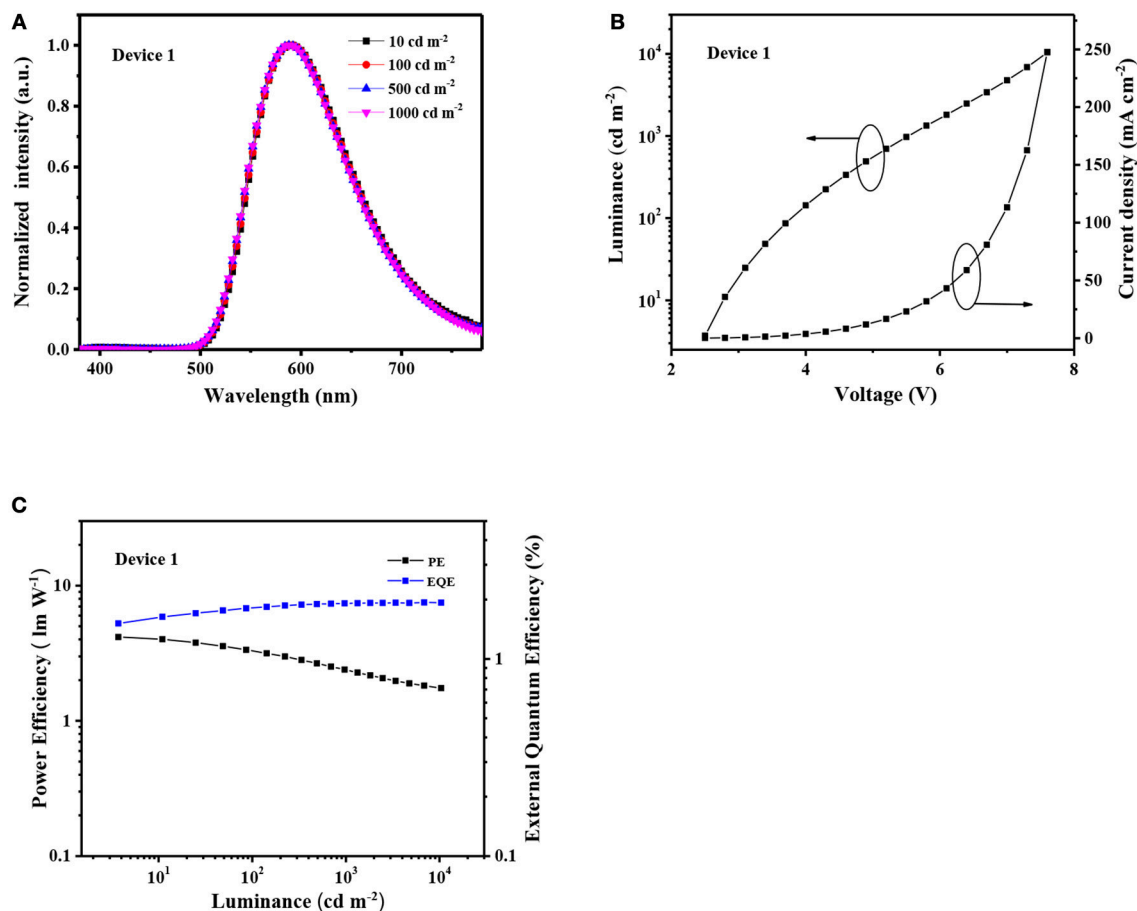


FIGURE 4 | (A) EL spectra of the Device 1 at different luminance; **(B)** Current density-luminance-voltage characteristics of Device 1; **(C)** PE-EQE-luminance plots of the Device 1.

for PO-T2T:Ir(ppy)₃ and PO-T2T:13PXZB, respectively at room temperature. The evidently higher PLQY of PO-T2T:Ir(ppy)₃ should be ascribed to the reduced NR decays of excited states. To further understand this point, PL spectra and delayed transient PL decays at various temperatures were measured and shown in **Figure S4**, and the data are extracted and summarized in **Table S1**. Different from conventional TADF emitters, the PL intensities are decreased from 200 to 300 K for both exciplexes.

This result is because NR decays are significantly enhanced with the increased temperatures. The triplet formation efficiency (Φ_T) and ΔE_{ST} were derived using a Berberan-Santos plot from the temperature-dependent results (in the **Supporting Information**) (Berberan-Santos and Garcia, 1996; Wang H. et al., 2014). The intersystem crossing rate constant (k_{ISC}), the non-radiative rate of singlet excitons constants (k_{nr}^s) and the non-radiative of triplet excitons rate constant (k_{nr}^T) were also calculated assuming

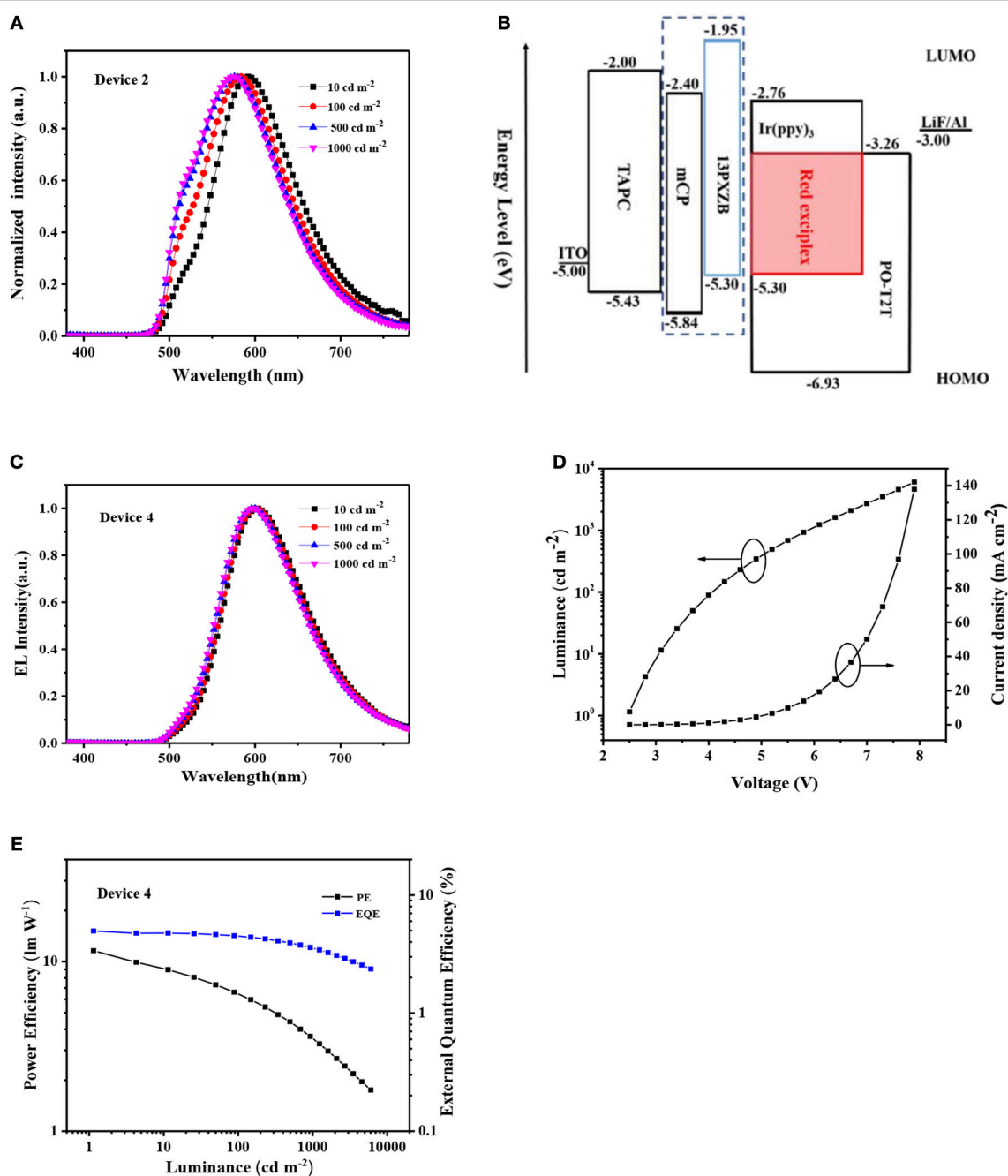


FIGURE 5 | (A) EL spectra of the Device 2 at different luminance; **(B)** Device structures and the energy diagrams of Device 2 and 4; **(C)** EL spectra of the Device 4 at different luminance; **(D)** Current density-luminance-voltage characteristics of Device 4; **(E)** PE-EQE-luminance plots of the Device 4.

that k_{ISC} was independent of temperature, and summarized in **Table S2**. The k_{ISC} of PO-T2T:Ir(ppy)₃ and PO-T2T:13PXZB were calculated to be 6.70×10^7 and 4.93×10^7 s⁻¹. Meanwhile, the k_{nr}^S of PO-T2T:Ir(ppy)₃ and PO-T2T:13PXZB were calculated to be 0.73×10^7 and 0.85×10^7 s⁻¹. Moreover, the k_{nr}^T of the PO-T2T:Ir(ppy)₃ and PO-T2T:13PXZB were estimated to 7.00×10^3 and 1.04×10^4 s⁻¹, respectively. Obviously, the k_{nr}^S and k_{nr}^T of PO-T2T:Ir(ppy)₃ are lower than the PO-T2T:13PXZB, proving the NR decays of S₁ and T₁ states are suppressed in phosphor-based exciplexes.

To evaluate the electroluminescence (EL) performance of the two exciplex, both PO-T2T:Ir(ppy)₃ and PO-T2T:13PXZB exciplexes were used as the emitters to fabricate the devices, respectively. Due to the excellent electron transporting property of PO-T2T and good hole transporting property of 13PXZB (as shown in **Figure S5**), the PO-T2T:13PXZB-based device is constructed with a structure of ITO/TAPC (35 nm)/13PXZB (10 nm)/PO-T2T:x wt% 13PXZB (30 nm)/PO-T2T (45 nm)/LiF (1 nm)/Al (100 nm) (Device 1). In the device, cyclohexylidenebis[*N,N*-bis(4-methylphenyl)aniline] (TAPC) and PO-T2T are respectively used as the hole-transporting layer (HTL) and electron-transporting layer, ITO (indium tin oxide) and LiF/Al work as the anode and the cathode, respectively. A thin layer of 10 nm 13PXZB is inserted between HTL and the emitting layer (EML) aiming to avoid additional exciplex formed between TAPC and PO-T2T. The doping concentration of 13PXZB in EML is optimized to 40 wt% for Device 1. As shown in **Figure 4**, Device 1 exhibits a low turn-on voltage (at the brightness of 1 cd m⁻²) of 2.5 V and stable red EL emission at different luminances with a peak at 592 nm and a CIE coordinate of (0.52, 0.47), indicating that we have successfully constructed a red exciplex with a conventional material system of PO-T2T and 13PXZB. However, the maximum current efficiency (CE), power efficiency (PE), and EQE of Device 1 are only 4.2 cd A⁻¹, 2.0 lm W⁻¹ and 1.9%, respectively. Such low device efficiency should be ascribed to the evident NR decays of S₁ and T₁ states for conventional red exciplexes.

Different from PO-T2T:13PXZB exciplex, both PO-T2T and Ir(ppy)₃ are electron transporting materials. As shown in **Figure S5**, the electron transporting capacity of PO-T2T:Ir(ppy)₃ is significantly better than its hole transporting capacity. Thus, an electron-blocking layer (EBL) is needed to benefit carrier recombination in the device. We first constructed Device 2 with a structure of ITO/TAPC (35 nm)/mCP (10 nm)/PO-T2T:x wt% Ir(ppy)₃ (30 nm)/PO-T2T (45 nm)/LiF (1 nm)/Al (100 nm). 3-bis(9H-carbazol-9-yl)benzene (mCP) is used as EBL due to its unipolar hole transporting capacity. And the doping concentration of Ir(ppy)₃ is optimized to 8 wt%. However, as shown in **Figure 5A**, Device 2 exhibits unsatisfactory EL spectra with additional green emission around 520 nm which should be attributed to the phosphorescence of the initial Ir(ppy)₃. This phenomenon is consistent with the PL spectrum as shown in **Figure 2B**, indicating competition of exciton harvest between Ir(ppy)₃ and PO-T2T:Ir(ppy)₃. In Device 2, the excitons are generated at the interface of mCP/PO-T2T:Ir(ppy)₃. Beyond PO-T2T:Ir(ppy)₃, the excited states of mCP:PO-T2T exciplex

is also unavoidably generated. The energy of mCP:PO-T2T exciplex is around 2.63 eV (Liu et al., 2016), higher than the energies of Ir(ppy)₃ and PO-T2T:Ir(ppy)₃. The competition between Ir(ppy)₃ and PO-T2T:Ir(ppy)₃ should be led by the energy transfers from mCP:PO-T2T to Ir(ppy)₃ and PO-T2T:Ir(ppy)₃.

To avoid the harmful green emission, the exciton harvest of Ir(ppy)₃ should be suppressed. Thus, we designed an optimized a device structure by changing mCP EBL to 13PXZB. At the 13PXZB/PO-T2T:Ir(ppy)₃ interface, the excited states of PO-T2T:13PXZB can also generate. But the energy of PO-T2T:13PXZB is in between that of Ir(ppy)₃ and PO-T2T:Ir(ppy)₃, which can prevent the exciton harvest of Ir(ppy)₃ and thus suppress the green emission. To further prove this point, we also fabricated a device with a structure of ITO/TAPC (35 nm)/13PXZB (10 nm)/PO-T2T (75 nm)/LiF (1 nm)/Al (100 nm) (Device 3). As shown in **Figure S6**, Device 3 exhibits the same EL spectra compared with Device 1 and slightly lower maximum efficiencies of 3.5 cd A⁻¹ for CE, 2.9 lm W⁻¹ for PE and 1.6% for EQE. The reason is that Ir(ppy)₃ cannot harvest the excitons from the red exciplex PO-T2T:13PXZB.

Thus, for PO-T2T:Ir(ppy)₃ exciplex, Device 4 was finally constructed with a structure of ITO/TAPC (35 nm)/13PXZB (10 nm)/PO-T2T:x wt% Ir(ppy)₃ (30 nm)/PO-T2T (45 nm)/LiF (1 nm)/Al (100 nm). And the optimized doping concentration of Ir(ppy)₃ in EML is also 8 wt%. As shown in **Figure 5B**, compared with mCP, 13PXZB also has more appropriate HOMO and LUMO energy levels, which can benefit the hole injection to EML and prevent the electron escape from EML. As shown in **Figure 5C**, a stable red EL emission with a peak at 604 nm and a CIE coordinate of (0.55, 0.44) is successfully generated, and the green emission from Ir(ppy)₃ nearly disappeared in the spectra, indicating the feasibility of our device optimization. As shown in **Figure S7**, the EL spectrum of Device 4 is clearly red-shifted compared with that of Device 1 and 3. Such results indicate that not only the emission is from PO-T2T:Ir(ppy)₃ exciplex, but also effective energy transfer is proved from PO-T2T:13PXZB to PO-T2T:Ir(ppy)₃. As listed in **Table 1** and shown in **Figures 5C–E**, Device 4 realizes a low turn-on voltage of 2.5 V and maximum CE, PE and EQE of 9.3 cd A⁻¹, 11.6 lm W⁻¹ and 5%, respectively. Such high EQE is 2.6 times and 3.1 times higher than that of Device 1 and 3, respectively. And EQE value of 5% is the highest result for red TADF OLEDs based on exciplex emitters. Considering both PO-T2T:13PXZB and PO-T2T:Ir(ppy)₃ possess the same PLQY value of about 4% under triplet excitons quenched condition, the evident efficiency difference between Device 1, 3, and 4 indicates much higher triplet exciton utilization of PO-T2T:Ir(ppy)₃, which should be ascribed to the beneficial effect of heavy metal ion core in the phosphor component. The SOC effect of heavy metal ion core can not only effectively suppress the NR decays of excited states for red TADF exciplexes, but also induce phosphorescence and make great contribution to EL emission. Our study provides a novel approach to develop efficient red TADF exciplexes with phosphors.

TABLE 1 | Summary of performances of the exciplex-based devices.

Device	V_{on}^a [V]	λ_{MAX} [nm]	CE/PE/EQE ^b [cd A ⁻¹ /lm W ⁻¹ /%]			CIE ^c [x, y]
			Maximum	@ 100 cd m ⁻²	@ 1,000 cd m ⁻²	
1	2.5	592	4.2/2.0/1.9	3.9/3.4/1.8	4.2/2.4/1.9	(0.52,0.47)
2	2.6	584	21.6/19.4/9.6	21.3/17.6/9.5	16.1/10.1/7.2	(0.48,0.49)
3	2.6	592	3.5/2.9/1.6	3.4/2.3/1.5	3.0/1.3/1.4	(0.52,0.47)
4	2.5	604	9.3/11.6/5.0	8.4/6.6/4.5	6.7/3.6/3.6	(0.55,0.44)

^a Turn-on voltage, estimated at 1 cd m⁻²; ^b CE, current efficiency; PE, power efficiency; EQE, external quantum efficiency; ^c Estimated at 100 cd m⁻².

CONCLUSION

In summary, we present a novel strategy to construct efficient red TADF exciplexes by introducing phosphor as one component. The SOC effect of heavy metal ion core in phosphor can suppressed the NR decays of excited states and induced phosphorescence makes great contribution to total emission, thus improving the exciton utilization. Red TADF exciplex PO-T2T:Ir(ppy)₃ is constructed accordingly, which exhibits high maximum efficiencies of 9.3 cd A⁻¹ CE, 11.6 lm W⁻¹ PE, and 5% EQE in the device. Such high EQE is 2.6 times higher than that of the device based on the comparative conventional red TADF exciplex PO-T2T:13PXZB and the best performance among reported red TADF OLEDs based on exciplex emitters. These results not only provide a new pathway to develop efficient exciplex emitters with vast phosphors, but also demonstrate the superiority of phosphor-based exciplexes.

AUTHOR CONTRIBUTIONS

C-JZ and X-HZ designed whole work. MZ, KW, and Y-ZS characterize the physical properties of compounds. MZ, KW,

and HL fabricated and optimized the devices. D-QW and XL synthesized the new organic compound. MZ and KW wrote the paper with support from C-JZ, S-LT, and X-HZ. All authors contributed to the general discussion.

FUNDING

This work was supported by the National Natural Science Foundation of China (Grant Nos. 51773029, 51373190 and 51533005), the National Key Research & Development Program of China (Grant No. 2016YFB0401002), the Collaborative Innovation Center of Suzhou Nano Science & Technology, the Priority Academic Program Development of Jiangsu Higher Education Institutions (PAPD), and the 111 Project and Qing Lan Project, P. R. China.

SUPPLEMENTARY MATERIAL

The Supplementary Material for this article can be found online at: <https://www.frontiersin.org/articles/10.3389/fchem.2019.00016/full#supplementary-material>

REFERENCES

- Adachi, C. (2014). Third-generation organic electroluminescence materials. *Jpn. J. Appl. Phys.* 53:060101. doi: 10.7567/jjap.53.060101
- Baldo, M. A., O'Brien, D. F., You, Y., Shoustikov, A., Sibley, S., Thompson, M. E., et al. (1998). Highly efficient phosphorescent emission from organic electroluminescent devices. *Nature* 395:151. doi: 10.1038/25954
- Ban, X. X., Jiang, W., Sun, K., Yang, H., Miao, Y., Yang, F., et al. (2015). Systematically tuning the Δ EST and charge balance property of bipolar hosts for low operating voltage and high power efficiency solution-processed electrophosphorescent devices. *J. Mater. Chem. C*. 3, 5004–5016. doi: 10.1039/c5tc00691k
- Berberan-Santos, M. N., and Garcia, J. M. M. (1996). Unusually Strong Delayed Fluorescence of C70. *J. Am. Chem. Soc.* 118, 9391–9394. doi: 10.1021/ja961782s
- Chen, D. Y., Liu, W., Zheng, C. J., Wang, K., Li, F., Tao, S. L., et al. (2016). Isomeric thermally activated delayed fluorescence emitters for color purity-improved emission in organic light-emitting devices. *ACS Appl. Mater. Interfaces* 8, 16791–16798. doi: 10.1021/acsami.6b03954
- Chen, X. K., Tsuchiya, Y., Ishikawa, Y., Zhong, C., Adachi, C., and Brédas, J. L. (2017). A new design strategy for efficient thermally activated delayed fluorescence organic emitters: from twisted to planar structures. *Adv. Mater.* 29:1702767. doi: 10.1002/adma.201702767
- Cherpak, V., Stakhira, P., Minaev, B., Baryshnikov, G., Stromylo, E., Helzhynsky, I., et al. (2015). Mixing of phosphorescent and exciplex emission in efficient organic electroluminescent devices. *ACS Appl. Mater. Interfaces* 7, 1219–1225. doi: 10.1021/am507050g
- Data, P., Pander, P., Okazaki, M., Takeda, Y., Minakata, S., and Monkman, A. P. (2016). Dibenzo[a,j]phenazine-cored donor–acceptor–donor compounds as green-to-red/NIR thermally activated delayed fluorescence organic light emitters. *Angew. Chem. Int. Ed.* 55, 5739–5744. doi: 10.1002/anie.201600113
- Gómez-Bombarelli, R., Aguilera-Iparraguirre, J., Hirzel, T. D., Duvenaud, D., Maclaurin, D., Blood-Forsythe, M. A., et al. (2016). Design of efficient molecular organic light-emitting diodes by a high-throughput virtual screening and experimental approach. *Nat. Mater.* 15, 1120–1127. doi: 10.1038/nmat4717
- Goushi, K., Yoshida, K., Sato, K., and Adachi, C. (2012). Organic light-emitting diodes employing efficient reverse intersystem crossing for triplet-to-singlet state conversion. *Nat. Photon.* 6, 253–258. doi: 10.1038/nphoton.2012.31
- Hirata, S., Sakai, Y., Masui, K., Tanaka, H., Lee, S. Y., Nomura, H., et al. (2015). Highly efficient blue electroluminescence based on thermally activated delayed fluorescence. *Nat. Mater.* 14, 330–336. doi: 10.1038/nmat4154
- Kolosov, D., Adamovich, V., Djurovich, P., Thompson, M. E., and Adachi, C. (2002). 1,8-naphthalimides in phosphorescent organic LEDs: the interplay between dopant, exciplex, and host emission. *J. Am. Chem. Soc.* 124, 9945–9954. doi: 10.1021/ja0263588

- Li, C., Duan, R., Liang, B., Han, G., Wang, S., Ye, K., et al. (2017). Deep-red to near-infrared thermally activated delayed fluorescence in organic solid films and electroluminescent devices. *Angew. Chem. Int. Ed.* 56, 11525–11529. doi: 10.1002/anie.201706464
- Li, J., Nomura, H., Miyazaki, H., and Adachi, C. (2014). Highly efficient exciplex organic light-emitting diodes incorporating a heptazine derivative as an electron acceptor. *Chem. Commun.* 50, 6174–6176. doi: 10.1039/c4cc01590h
- Li, W., Zhao, J., Li, L., Du, X., Fan, C., Zheng, C., et al. (2018). Efficient solution-processed blue and white OLEDs based on a high-triplet bipolar host and a blue TADF emitter. *Org. Electron.* 58, 276–282. doi: 10.1016/j.orgel.2018.04.027
- Li, Y., Li, L. X., Chen, D., Cai, X., Xie, G., He, Z., et al. (2016). Design strategy of blue and yellow thermally activated delayed fluorescence emitters and their all-fluorescence white OLEDs with external quantum efficiency beyond 20%. *Adv. Funct. Mater.* 26, 6904–6912. doi: 10.1002/adfm.201602507
- Liu, B., Dang, F., Feng, Z., Tian, Z., Zhao, J., Wu, Y., et al. (2017). Novel iridium(III) complexes bearing dimesitylboron groups with nearly 100% phosphorescent quantum yields for highly efficient organic light-emitting diodes. *J. Mater. Chem. C* 5, 7871–7883. doi: 10.1039/c7tc02369c
- Liu, M., Komatsu, R., Cai, X., Sasabe, H., Kamata, T., Nakao, K., et al. (2017). Introduction of twisted backbone: a new strategy to achieve efficient blue fluorescence emitter with delayed emission. *Adv. Opt. Mater.* 5:1700334. doi: 10.1002/adom.201700334
- Liu, M., Seino, Y., Chen, D., Inomata, S., Su, S.J., Sasabe, H., et al. (2015). Blue thermally activated delayed fluorescence materials based on bis(phenylsulfonyl)benzene derivatives. *Chem. Commun.* 51, 16353–16356. doi: 10.1039/c5cc05435d
- Liu, W., Chen, X. J., Zheng, J. C., Wang, K., Chen, Y. D., Li, F., et al. (2016). Novel strategy to develop exciplex emitters for high-performance OLEDs by employing thermally activated delayed fluorescence materials. *Adv. Funct. Mater.* 26, 2002–2008. doi: 10.1002/adfm.201505014
- Liu, W., Zheng, C. J., Wang, K., Chen, Z., Chen, Y. D., Li, F., et al. (2015). Novel carbazol-pyridine-carbonitrile derivative as excellent blue thermally activated delayed fluorescence emitter for highly efficient organic light-emitting devices. *ACS Appl. Mater. Interfaces* 7, 18930–18936. doi: 10.1021/acsami.5b05648
- Liu, X., Wang, S., Yao, B., Zhang, B., Ho, L. C., Wong, Y. W., et al. (2015). New deep-red heteroleptic iridium complex with 3-hexylthiophene for solution-processed organic light-emitting diodes emitting saturated red and high CRI white colors. *Org. Electron.* 21, 1–8. doi: 10.1016/j.orgel.2015.02.016
- Liu, X. K., Chen, Z., Qing, J., Zhang, W. J., Wu, B., Tam, H. L., et al. (2015c). Remanagement of singlet and triplet excitons in single-emissive-layer hybrid white organic light-emitting devices using thermally activated delayed fluorescent blue exciplex. *Adv. Mater.* 27, 7079–7085. doi: 10.1002/adma.201502897
- Liu, X. K., Chen, Z., Zheng, C. J., Chen, M., Liu, W., Zhang, X. H., et al. (2015b). Nearly 100% triplet harvesting in conventional fluorescent dopant-based organic light-emitting devices through energy transfer from exciplex. *Adv. Mater.* 27, 2025–2030. doi: 10.1002/adma.201500013
- Liu, X. K., Chen, Z., Zheng, C. J., Liu, C. L., Lee, C. S., Li, F., et al. (2015a). Prediction and design of efficient exciplex emitters for high-efficiency, thermally activated delayed-fluorescence organic light-emitting diodes. *Adv. Mater.* 27, 2378–2383. doi: 10.1002/adma.201405062
- Méhes, G., Nomura, H., Zhang, Q., Nakagawa, T., and Adachi, C. (2012). Enhanced electroluminescence efficiency in a spiro-acridine derivative through thermally activated delayed fluorescence. *Angew. Chem. Int. Ed.* 51, 11311–11315. doi: 10.1002/anie.201206289
- Miwa, T., Kubo, S., Shizu, K., Komino, T., Adachi, C., and Kaji, H. (2017). Blue organic light-emitting diodes realizing external quantum efficiency over 25% using thermally activated delayed fluorescence emitters. *Sci. Rep.* 7:284. doi: 10.1038/s41598-017-00368-5
- Moon, C. K., Suzuki, K., Shizu, K., Adachi, C., Kaji, H., and Kim, J. J. (2017). Combined inter- and intramolecular charge-transfer processes for highly efficient fluorescent organic light-emitting diodes with reduced triplet exciton quenching. *Adv. Mater.* 29:1606448. doi: 10.1002/adma.201606448
- Shi, Z. Y., Wang, K., Li, X., Dai, L. G., Liu, W., Ke, K., et al. (2018). Intermolecular charge-transfer transition emitter showing thermally activated delayed fluorescence for efficient non-doped OLEDs. *Angew. Chem. Int. Ed.* 57, 9480–9484. doi: 10.1002/anie.201804483
- Shiu, J. Y., Chen, T. Y., Lee, K. W., Wu, C. C., Lin, C. T., Liu, H. S., et al. (2017). Efficient thermally activated delayed fluorescence of functional phenylpyridinato boron complexes and high performance organic light-emitting diodes. *J. Mater. Chem. C* 5, 1452–1462. doi: 10.1039/c6tc04994j
- Uoyama, H., Goushi, K., Shizu, K., Nomura, H., and Adachi, C. (2012). Highly efficient organic light-emitting diodes from delayed fluorescence. *Nature* 492, 234–238. doi: 10.1038/nature11687
- Wang, D. Q., Zhang, M., Wang, K., Zheng, C. J., Shi, Y. Z., Chen, J. X., et al. (2017). Fine-tuning the emissions of highly efficient thermally activated delayed fluorescence emitters with different linking positions of electron-deficient substituent groups. *Dyes Pigments* 143, 62–70. doi: 10.1016/j.dyepig.2017.04.024
- Wang, H., Xie, L., Peng, Q., Meng, L., Wang, Y., Yi, Y., et al. (2014). Novel thermally activated delayed fluorescence materials-thioxanthone derivatives and their applications for highly efficient OLEDs. *Adv. Mater.* 26, 5198–5204. doi: 10.1002/adma.201401393
- Wang, K., Liu, W., Zheng, J. C., Shi, Z. Y., Liang, K., Zhang, M., et al. (2017b). A comparative study of carbazole-based thermally activated delayed fluorescence emitters with different steric hindrance. *J. Mater. Chem. C* 5, 4797–4803. doi: 10.1039/c7tc00681k
- Wang, K., Zheng, J. C., Liu, W., Liang, K., Shi, Z. Y., Tao, L. S., et al. (2017a). Avoiding energy loss on TADF emitters: controlling the dual conformations of d-a structure molecules based on the pseudoplanar segments. *Adv. Mater.* 29, 1701476. doi: 10.1002/adma.201701476
- Xie, G., Li, X., Chen, D., Wang, Z., Cai, X., Chen, D., et al. (2016). Evaporation- and solution-process-feasible highly efficient thianthrene-9,9',10,10'-tetraoxide-based thermally activated delayed fluorescence emitters with reduced efficiency roll-off. *Adv. Mater.* 28, 181–187. doi: 10.1002/adma.201503225
- Yang, Z., Mao, Z., Xie, Z., Zhang, Y., Liu, S., Zhao, J., et al. (2017). Recent advances in organic thermally activated delayed fluorescence materials. *Chem. Soc. Rev.* 46, 915–1016. doi: 10.1039/c6cs00368k
- Zhang, D., Cai, M., Bin, Z., Zhang, Y., Zhang, D., and Duan, L. (2016). Highly efficient blue thermally activated delayed fluorescent OLEDs with record-low driving voltages utilizing high triplet energy hosts with small singlet-triplet splittings. *Chem. Sci.* 7, 3355–3363. doi: 10.1039/c5sc04755b
- Zhang, Q., Kuwabara, H., Potscavage, W. J. Jr., Huang, S., Hatae, Y., et al. (2014a). Anthraquinone-based intramolecular charge-transfer compounds: computational molecular design, thermally activated delayed fluorescence, and highly efficient red electroluminescence. *J. Am. Chem. Soc.* 136, 18070–18081. doi: 10.1021/ja510144h
- Zhang, Q., Li, B., Huang, S., Nomura, H., Tanaka, H., and Adachi, C. (2014b). Efficient blue organic light-emitting diodes employing thermally activated delayed fluorescence. *Nat. Photon.* 8, 326. doi: 10.1038/nphoton.2014.12
- Zhang, Y. X., Wang, B., Yuan, Y., Hu, Y., Jiang, Z. Q., and Liao, L. S. (2017). Solution-processed thermally activated delayed fluorescence exciplex hosts for highly efficient blue organic light-emitting diodes. *Adv. Opt. Mater.* 5, 1700012. doi: 10.1002/adom.201700012

Conflict of Interest Statement: The authors declare that the research was conducted in the absence of any commercial or financial relationships that could be construed as a potential conflict of interest.

Copyright © 2019 Zhang, Wang, Zheng, Wang, Shi, Lin, Tao, Li and Zhang. This is an open-access article distributed under the terms of the Creative Commons Attribution License (CC BY). The use, distribution or reproduction in other forums is permitted, provided the original author(s) and the copyright owner(s) are credited and that the original publication in this journal is cited, in accordance with accepted academic practice. No use, distribution or reproduction is permitted which does not comply with these terms.



N-Benzoimidazole/Oxadiazole Hybrid Universal Electron Acceptors for Highly Efficient Exciplex-Type Thermally Activated Delayed Fluorescence OLEDs

Wenbo Yuan^{1†}, Hannan Yang^{2†}, Mucan Zhang¹, Die Hu¹, Ning Sun^{2*} and Youtian Tao^{1*}

¹ Key Lab for Flexible Electronics and Institute of Advanced Materials (IAM), Nanjing Tech University, Nanjing, China,

² Department of Physics, Yunnan University, Kunming, China

OPEN ACCESS

Edited by:

Lian Duan,
Tsinghua University, China

Reviewed by:

Guohua Xie,
Wuhan University, China
CaiJun Zheng,
University of Electronic Science and
Technology of China, China

*Correspondence:

Ning Sun
ning.sun@ynu.edu.cn
Youtian Tao
iamyttao@njtech.edu.cn

[†]These authors have contributed
equally to this work

Specialty section:

This article was submitted to
Organic Chemistry,
a section of the journal
Frontiers in Chemistry

Received: 17 January 2019

Accepted: 11 March 2019

Published: 03 April 2019

Citation:

Yuan W, Yang H, Zhang M, Hu D,
Sun N and Tao Y (2019)
N-Benzoimidazole/Oxadiazole Hybrid
Universal Electron Acceptors for
Highly Efficient Exciplex-Type
Thermally Activated Delayed
Fluorescence OLEDs.
Front. Chem. 7:187.
doi: 10.3389/fchem.2019.00187

Recently, donor/acceptor type exciplex have attracted considerable interests due to the low driving voltages and small singlet-triplet bandgaps for efficient reverse intersystem crossing to achieve 100% excitons for high efficiency thermally activated delayed fluorescence (TADF) OLEDs. Herein, two N-linked benzoimidazole/oxadiazole hybrid electron acceptors were designed and synthesized through simple catalyst-free C-N coupling reaction. 24iPBIOXD and iTPBIOXD exhibited deep-blue emission with peak at 421 and 459 nm in solution, 397 and 419 nm at film state, respectively. The HOMO/LUMO energy levels were $-6.14/-2.80$ for 24iPBIOXD and $-6.17/-2.95$ eV for iTPBIOXD. Both compounds could form exciplex with conventional electron donors such as TAPC, TCTA, and mCP. It is found that the electroluminescent performance for exciplex-type OLEDs as well as the delayed lifetime was dependent with the driving force of both HOMO and LUMO energy offsets on exciplex formation. The delayed lifetime from 579 to 2,045 ns was achieved at driving forces close to or larger than 1 eV. Two TAPC based devices possessing large HOMO/LUMO offsets of 1.09–1.34 eV exhibited the best EL performance, with maximum external quantum efficiency (EQE) of 9.3% for 24iPBIOXD and 7.0% for iTPBIOXD acceptor. The TCTA containing exciplex demonstrated moderate energy offsets (0.88–1.03 eV) and EL efficiency ($\sim 4\%$), while mCP systems showed the poorest EL performance (EQE $< 1\%$) and shortest delayed lifetime of < 100 ns due to inadequate driving force of 0.47–0.75 eV for efficient exciplex formation.

Keywords: electron acceptor, electron donor, exciplex, oxadiazole, thermally activated delayed fluorescence, OLEDs

INTRODUCTION

Organic light-emitting diodes (OLEDs) have been developed rapidly in recent years since the pioneer work on low-voltage fluorescence electroluminescence by Tang in 1987 (Tang and VanSlyke, 1987; Ma et al., 1998; Gong et al., 2010; Park et al., 2013; Zhang et al., 2016). According to spin statistics, the ratio for singlet and triplet excitons recombined from electrogenerated holes and electrons is 1:3 (Baldo et al., 1999; Segal et al., 2003). Thus, the first generation of traditional fluorescent OLEDs which solely harvest singlet excitons only shows 25% of maximum internal

quantum efficiency (IQE) (Wen et al., 2005). On the other hand, the second generation of phosphorescent OLEDs (PHOLEDs) based on heavy metal complexes and third generation of thermally activated delayed fluorescence (TADF) OLEDs could both reach 100% IQE in theory by utilizing all singlet and triplet excitons through intersystem crossing (ISC) and reverse inter-system crossing (RISC), respectively (Baldo et al., 1998; Adachi et al., 2001; Su et al., 2008; Lo et al., 2009; Goushi et al., 2012; Uoyama et al., 2012; Zhang and Forrest, 2012; Li et al., 2016; Cao et al., 2017; Huang et al., 2018; Wu Q. et al., 2018). However, to avoid consuming noble metals and achieving reliable true-blue light, TADF OLEDs based on low-cost pure organic emitters have attracted increasing interests as an alternative mechanism to PHOLEDs. TADF emission is realized by an up-conversion process from lower energy triplet states to slightly higher energy singlet states by endothermic reverse inter-system crossing process (Li et al., 2016; Cao et al., 2017; Huang et al., 2018; Wu Q. et al., 2018). Therefore, a small singlet-triplet energy bandgap (ΔE_{ST}) is required for TADF emitters.

It is reported that the small ΔE_{ST} could be attained in (i) intramolecular charge transfer featured single molecule with twisted donor-acceptor structured for effective spatial isolation between the highest occupied molecular orbital (HOMO) and lowest unoccupied molecular orbital (LUMO) on the relevant hole and electron transporting moieties, and (ii) bimolecular-exciplex which contains an electron-donor material mixed with an electron-acceptor material through intermolecular charge transfer characteristics (Cai and Su, 2018; Liu et al., 2018; Sarma and Wong, 2018). High external quantum efficiency (EQE) of 20% for red, 29% for orange, 38% for green, and 37% for light-blue TADF OLEDs have been achieved in single-molecule TADF emitters (Lin et al., 2016; Chen et al., 2018; Wu T.-L. et al., 2018; Zeng et al., 2018). However, the development of bimolecular TADF lags far behind. Most exciplex-type TADF OLEDs showed maximum EQE close to 10% (Jankus et al., 2014; Liu et al., 2015a,b; Oh et al., 2015; Zhang L. et al., 2015; Hung et al., 2016, 2017; Jeon et al., 2016), with only one example approaching to 18% (Liu et al., 2016).

In electron donor/acceptor formed exciplex systems, compared with commercially available various electron-donor materials, such as 4,4',4''-tris[3-methylphenyl(phenyl)amino]-triphenylamine (*m*-MTDATA), *N,N'*-bis(1-naphthyl)-*N,N'*-diphenyl-[1,1'-biphenyl]-4,4'-diamine (NPB), 4,4'-(cyclohexane-1,1-diyl)bis(*N*-phenyl-*N*-*p*-tolylaniline) (TAPC), 4,4',4''-tris(*N*-carbazolyl) triphenylamine (TCTA), 4,4'-bis(*N*-carbazolyl)-1,1'-biphenyl (CBP), and *N,N'*-dicarbazolyl-3,5-benzene (mCP) etc., the types of efficient and low-cost electron-acceptor materials are scarce (Goushi and Adachi, 2012; Goushi et al., 2012; Sun et al., 2014; Lee et al., 2015; Liu et al., 2015b). Thus, the exploration of electron accepting materials is essential for constructing exciplex systems with outstanding optoelectronic performance. Therefore, in this work, we designed and synthesized two new electron-acceptors of 2-(2,4-bis(2-phenyl-1*H*-benzo[*d*]imidazol-1-yl)phenyl)-5-phenyl-1,3,4-oxadiazole (24iPBIOXD), and 2-phenyl-5-(2,4,6-tris(2-phenyl-1*H*-benzo[*d*]imidazol-1-yl)phenyl)-1,3,4-oxadiazole (*i*TPBIOXD) through a simple

one-step catalyst-free aromatic nucleophilic substitution reaction. The electron-withdrawing oxadiazole (OXD) unit has been extensively applied in donor-acceptor type bipolar transport host materials, single molecule intramolecular charge transfer type TADF emitters as well as electron transport materials (Tao et al., 2011; Mondal et al., 2013; Olivier et al., 2017; Cooper et al., 2018; Yao et al., 2018; Zhang et al., 2018). By combining OXD building block with our previously reported isomeric *N*-linked benzoimidazole (Hu et al., 2017), both 24iPBIOXD, and *i*TPBIOXD exhibited deep HOMO level of \sim -6.15 eV, facilitating the exciplex formation with general electron donor materials of TAPC, TCTA, and mCP due to the compatible HOMO and LUMO energy levels between donor and acceptor materials. The gradient energy offsets ranging from 0.47 to 1.34 eV correlated well with the delayed lifetime and EL efficiencies in exciplex type TADF OLEDs. The TAPC:24iPBIOXD exciplex with the largest HOMO/LUMO offsets exhibited the best EL performance, with maximum EQE of 9.3% for green TADF OLEDs.

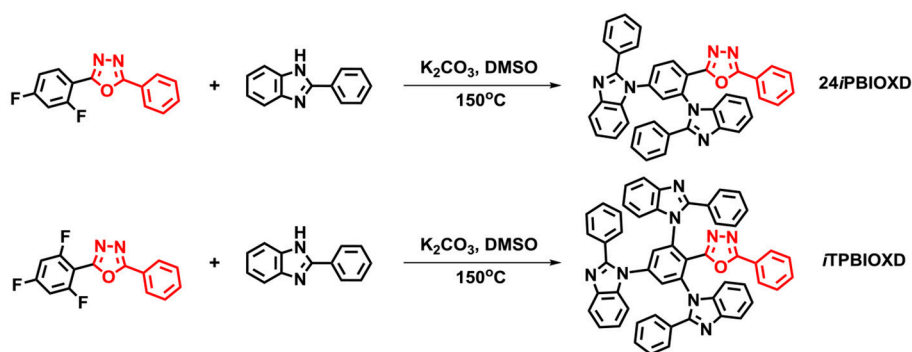
RESULTS AND DISCUSSION

Synthesis and Characterization

Scheme 1 shows the synthetic routes and molecular structures of 24iPBIOXD and *i*TPBIOXD. The two compounds could be facilely synthesized by a simple one-step catalyst free C-N coupling reaction. This nucleophilic substitution reaction was carried out in DMSO solvent with K_2CO_3 base at high yields over 80% by using di/tri-fluorine substituted oxadiazole derivatives as electrophiles and 2-phenyl-1*H*-benzo[*d*]imidazole as nucleophiles. The considerably high yields and environmentally eco-friendly conditions demonstrated the superiority than common metal-catalyzed Ullman reactions (Son et al., 2008; Liu et al., 2011; Volz et al., 2013). In addition, the directly connection of the isomeric *N*-linked benzoimidazole to the central phenyl ring avoided the complicated multistep ring-closing synthetic process for the normal C-linked benzoimidazole in traditional electron transport material of 2,2,2-(1,3,5-phenylene)-tris(1-phenyl-1*H*-benzoimidazole) (TPBI) or its derivatives. The chemical structures of the new compounds were fully characterized by 1H NMR, ^{13}C NMR, mass spectrometry (MALDI-TOF) and element analysis (**Figure S1**). The good thermal stability of the two compounds was confirmed by thermogravimetric analysis (TGA) and differential scanning calorimetry (DSC) (**Figure 1**). The decomposition temperatures (T_d , corresponding to a 5% weight loss) from TGA curves for 24iPBIOXD and *i*TPBIOXD were determined at 443 and 461°C, respectively. Additionally, the melting point (T_m) of *i*TPBIOXD was observed at 327°C, which was much higher than 286°C of 24iPBIOXD. The glass transition temperature (T_g) of both materials can be detected from the second heating cycles from DSC, with values of 126°C for 24iPBIOXD and 165°C for *i*TPBIOXD, indicating their reasonable thermal stability.

Photophysical Properties

The room temperature UV-Vis absorption and photoluminescence (PL) spectra of 24iPBIOXD and *i*TPBIOXD



SCHEME 1 | Synthesis of compounds 24/iPBIOXD and iTPBIOXD.

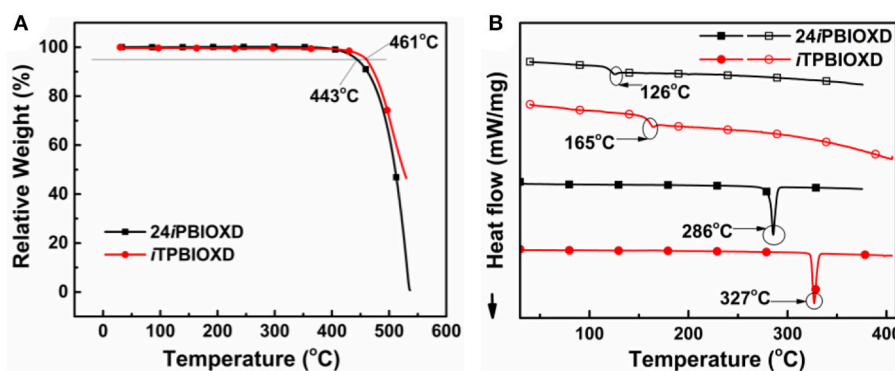


FIGURE 1 | (A) Thermogravimetric analysis (TGA) and (B) differential scanning calorimetry (DSC) (solid symbols represent for first heating scan and open symbols for second heating scan) curves for 24/iPBIOXD and iTPBIOXD.

in CH_2Cl_2 solution are shown in **Figure 2A**. Both compounds exhibited an intense absorption with peaks at 289 and 283 nm in solution, 297 and 288 nm in film, respectively, which can be ascribed to the π - π^* transition of molecules. The optical bandgap (E_g) was calculated to be 3.34 eV for 24/iPBIOXD and 3.22 eV for iTPBIOXD, according to the film-state absorption edge. On the other hand, 24/iPBIOXD and iTPBIOXD showed unimodal photoluminescence peaking at 421 and 459 nm in solution, whereas significantly blue-shift to 397 and 419 nm in film state (**Table 1**). By analyzing the highest-energy vibronic sub-band of low-temperature fluorescence and phosphorescence spectrum (**Figure 2B**), the singlet (E_S) and triplet (E_T) energy levels could be determined to be 3.31/2.55 and 3.18/2.53 eV for 24/iPBIOXD and iTPBIOXD, respectively. In addition, the E_S/E_T energy levels of three hole-transport electron donor materials were also calculated to be 3.54/2.95 eV for mCP, 3.79/2.82 eV for TAPC, and 3.66/2.84 eV for TCTA (**Figure 2C**). The PL spectra for the neat film of electron donors such as mCP, TAPC, and TCTA, the two new electron-acceptors of 24/iPBIOXD and iTPBIOXD as well as their corresponding mixtures in a 1:1 weight ratio were investigated. As shown in **Figure 3** and **Figure S2**, all blended films showed bathochromic shifted PL spectra compared with the emission of neat 24/iPBIOXD/iTPBIOXD and the corresponding donor-material,

indicating the successful formation of exciplex (Zhang T. et al., 2015). In addition, it is found that exciplex based on 24/iPBIOXD acceptors all exhibited about 20–30 nm blue-shifted emission than iTPBIOXD based exciplex systems. The exciplex emission color could be tuned from deep-blue of mCP:24/iPBIOXD with peak at 419 nm to light-blue of TCTA:24/iPBIOXD (501 nm) and further to green of TAPC:24/iPBIOXD (518 nm). Besides, transient photoluminescence (PL) measurements were carried out for all six exciplexes (**Figure 4**). The exciplexes comprising TAPC or TCTA donor all possessed significantly longer delayed decay lifetime, with values of 579 ns for TCTA:24/iPBIOXD, 1,907 ns for TCTA:iTPBIOXD, 1,520 and 2,045 ns for TAPC:24/iPBIOXD, TAPC:iTPBIOXD exciplex, respectively. However, the mCP:24/iPBIOXD and mCP:iTPBIOXD exciplex systems displayed greatly shorter delayed decay lifetime of only 42 and 72 ns (**Table 1**). Besides, the temperature dependent PL transients for the representative TAPC:24/iPBIOXD and TCTA:iTPBIOXD exciplexes (**Figure S3**) both demonstrated a more significant decay from 100 to 300 K at the longer lifetime range, suggesting the potential existence of endothermic reverse inter-system crossing. It is expected the obvious variations on delayed decay time for different exciplexes may demonstrate some relationships with the device efficiency in exciplex-TADF OLEDs.

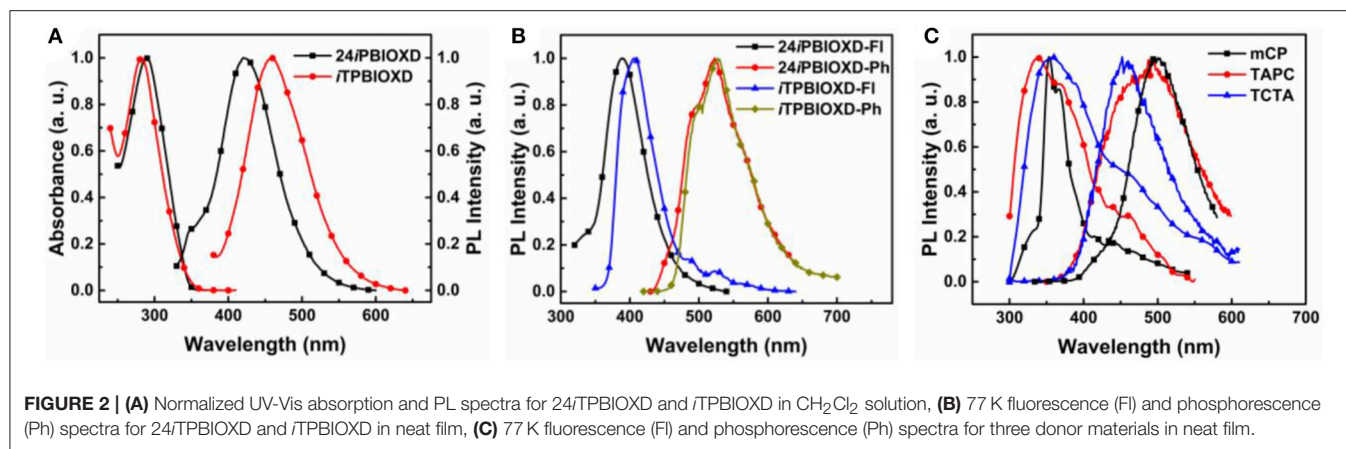


TABLE 1 | Physical properties of compounds 24/PBIOXD and *i*TPBIOXD.

Compounds	$\lambda_{\text{abs}}/\lambda_{\text{em}}^a$ [nm]	$\lambda_{\text{abs}}/\lambda_{\text{em}}^b$ [nm]	E_S/E_T^c [eV]	E_g^d [eV]	HOMO/LUMO ^e [eV]	$T_g/T_m/T_d^f$ [°C]	λ_{CT} (nm)/ E_{CT} (eV)/ τ_d (ns)/ ΔE (eV) ^g		
							mCP	TCTA	TAPC
24/PBIOXD	289/421	297/397	3.31/2.55	3.34	−6.14 (−5.75)/ −2.80 (−2.09)	126/286/443	419/2.96/42 0.47/0.6	501/2.48/579 0.95/0.88	518/2.39/1520 1.09/1.19
<i>i</i> TPBIOXD	283/459	288/419	3.18/2.53	3.22	−6.17 (−5.95)/ −2.95 (−2.05)	165/327/461	443/2.80/72 0.5/0.75	531/2.36/1907 0.98/1.03	544/2.28/2045 1.12/1.34

^aMeasured in CH₂Cl₂ solution at room temperature.

^bMeasured in film.

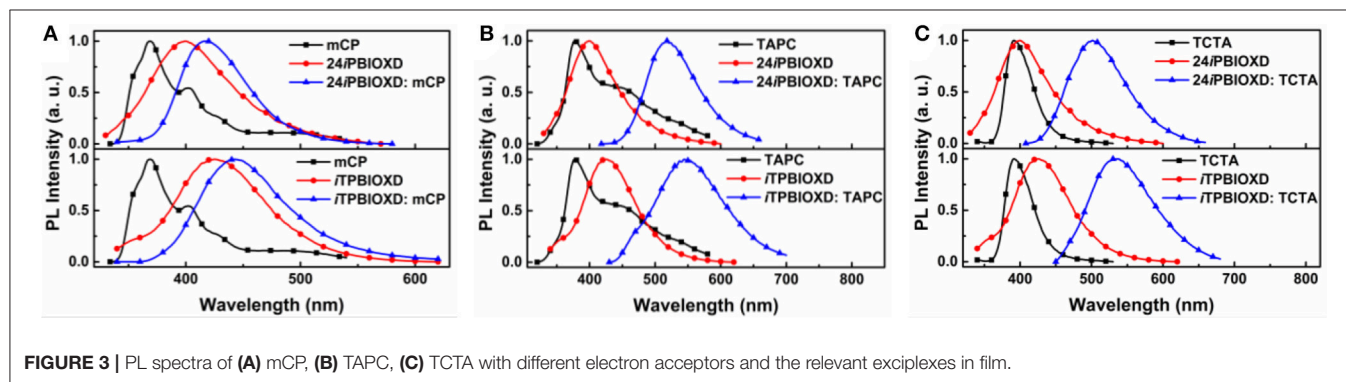
^cSinglet energy and triplet energy was calculated from low temperature (77 K) fluorescence spectra and phosphorescence spectrum.

^dOptical bandgap (E_g) calculated from the absorption edge of film state UV-Vis spectra.

^eLUMO measured from the onset of reduction curves from CV and HOMO calculated from the difference between LUMO and E_g , values in parentheses from DFT calculations.

^fGlass transition temperature/melting point/decomposition temperature.

^gEmission maxima, charge transfer state energy, delayed decay lifetime and HOMO/LUMO energy offsets for various exciplexes.



Theoretical Calculations and Electrochemical Properties

In order to gain insights into the frontier molecular orbital and excited states level distribution of 24/PBIOXD and *i*TPBIOXD, density functional theory (DFT) calculation was conducted at the B3LYP level (Francl et al., 1982; Becke, 1988; Lee et al., 1988). From the optimized geometry shown in **Figure 5**, the dihedral angles between the central phenyl and oxadiazole ring were 22.0 and 50.3° for 24/PBIOXD and *i*TPBIOXD, respectively, the values between the benzoimidazoles and the

central phenyl rings ranged from 50.4 to 77.4°, indicating a twisted structure for both compounds. Furthermore, in the ground state, the highest occupied molecular orbital (HOMO) were almost completely located on one of the ortho-positioned phenylbenzoimidazole units, indicating the electron-donating characteristics of *N*-linked phenylbenzoimidazole, which was quite different from the C-isomerized phenylbenzoimidazole containing TPBI (Hu et al., 2017). And the lowest unoccupied molecular orbital (LUMO) were mainly localized on 2,5-diphenyl-1,3,4-oxadiazole, along with mildly distribution over

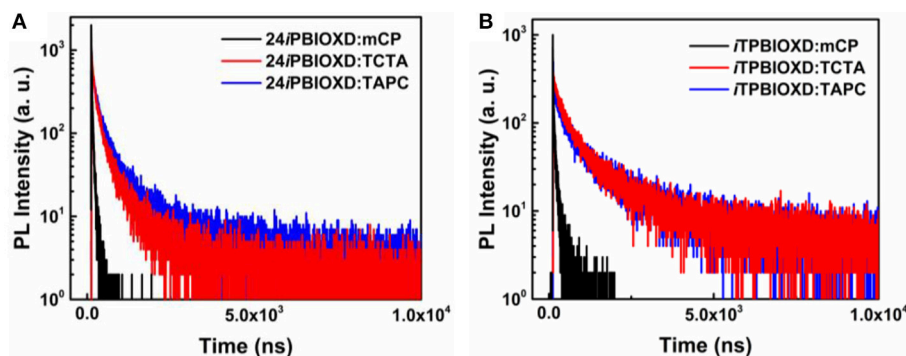


FIGURE 4 | Transient decay curves of (A) 24iPBIOXD and (B) iTPBIOXD-based exciplexes at film state.

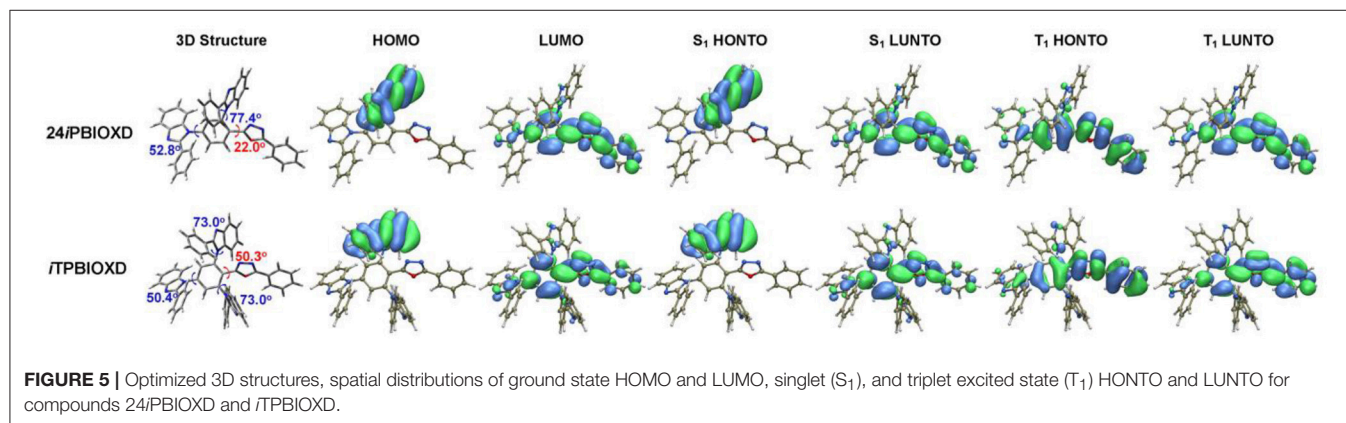


FIGURE 5 | Optimized 3D structures, spatial distributions of ground state HOMO and LUMO, singlet (S_1), and triplet excited state (T_1) HONTO and LUNTO for compounds 24iPBIOXD and iTPBIOXD.

the penta-heterocyclic imidazoles, suggesting the weak electron-withdrawing property to gently participate electron-transport for the imidazoles. Similar distribution can be observed in the highest occupied natural transition orbital (HONTO) and the lowest unoccupied natural transition orbital (LUNTO) at singlet excited state. It should be noted that the HONTO distribution at triplet excited state was completely different from S_0 and S_1 for both compounds, which was mainly delocalized through the 2,5-diphenyl-1,3,4-oxadiazole skeleton, similar with the LUNTO distribution.

The electrochemical features were measured by cyclic voltammetry (CV) (Figure 6). Both compounds exhibited reversible reduction whereas undetectable oxidation behavior. The LUMO energy levels calculated from the onset of reduction curves for 24iPBIOXD and iTPBIOXD were measured to be -2.80 and -2.95 eV, while the HOMO energy levels calculated from the different between the LUMO and optical bandgaps (E_g) were evaluated to be -6.14 and -6.17 eV, respectively. The values were in good agreement with the theoretical calculation. Besides, the energy levels for electron donor materials were also measured, with HOMO estimated from the onset of electro-oxidation curves and LUMO calculated from HOMO and optical bandgaps. The HOMO/LUMO energy level values for mCP, TAPC, and TCTA were $-5.67/-2.20$, $-5.05/-1.61$, and $-5.19/-1.92$ eV, respectively. The deep HOMO and LUMO for

the two new electron acceptors of 24iPBIOXD and iTPBIOXD, provided sufficient driving forces on HOMO/LUMO energy offsets for the exciplex formation (Figure 6A). As shown in Figure 7A, the HOMO energy level offsets between the electron donor of TAPC, TCTA, or mCP and the electron acceptors of 24iPBIOXD/iTPBIOXD were calculated to be 1.09/1.12, 0.95/0.98, or 0.47/0.5 eV, and the corresponding LUMO offsets were 1.19/1.34, 0.88/1.03, or 0.6/0.75 eV, respectively. It is noted in both acceptor systems, the TAPC donor based exciplex presented the highest driving force, followed by TCTA, while the mCP donor demonstrated the lowest HOMO/LUMO offsets.

Electroluminescence Properties

To investigate the charge transport properties of the two new *N*-linked isomeric benzoimidazole containing electron acceptors, single carrier electron-only device was prepared to find out the electron inject and transport properties of 24iPBIOXD and iTPBIOXD. The device structure was ITO/24iPBIOXD, iTPBIOXD, or TPBI (50 nm)/LiF (1 nm)/Al (150 nm), where the commercial electron transport material of 2,2,2-(1,3,5-phenylene)-tris(1-phenyl-1*H*-benzoimidazole) (TPBI) with *C*-linkage in benzoimidazole was selected for comparison. As shown in Figure 8, at the same operating voltage, TPBI based device exhibited the highest current density among all the three devices. Since the LUMO energy of TPBI (2.7–2.9 eV)

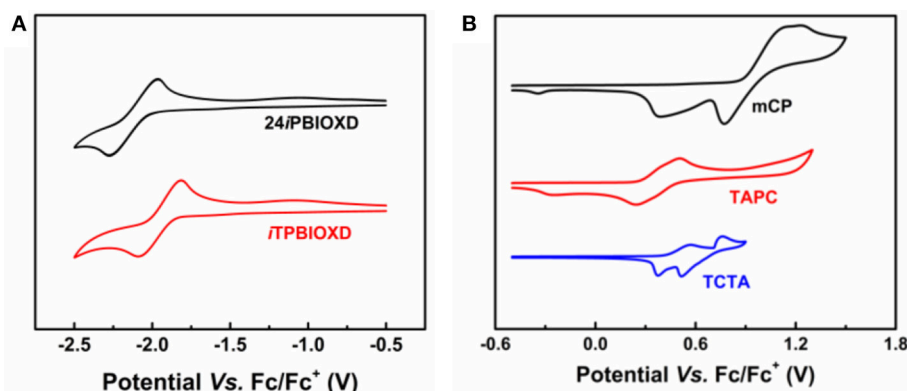


FIGURE 6 | Cyclic voltammograms of (A) 24iPBIOXD and iTPBIOXD in THF solution for reduction scan; (B) conventional electron donors (mCP, TAPC, and TCTA) in CH₂Cl₂ solution for oxidation scan.

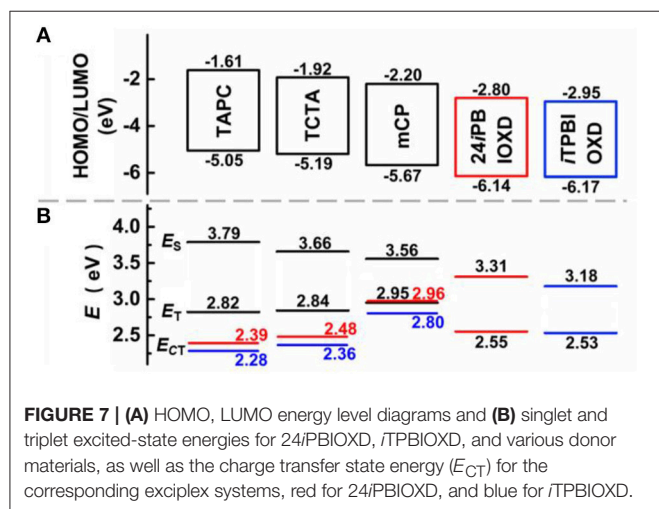


FIGURE 7 | (A) HOMO, LUMO energy level diagrams and (B) singlet and triplet excited-state energies for 24iPBIOXD, iTPBIOXD, and various donor materials, as well as the charge transfer state energy (E_{CT}) for the corresponding exciplex systems, red for 24iPBIOXD, and blue for iTPBIOXD.

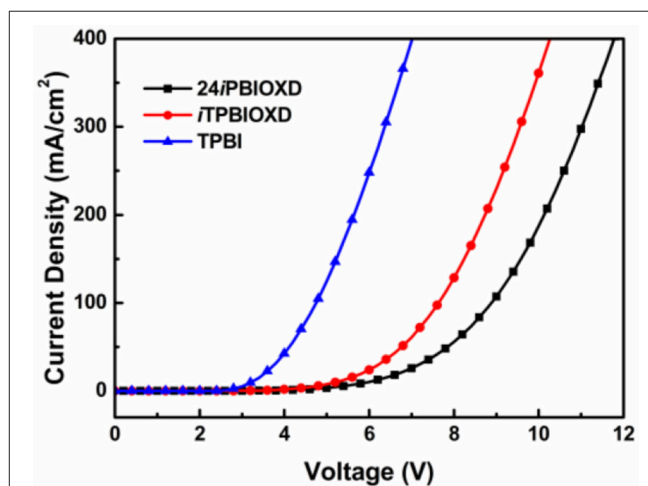


FIGURE 8 | J-V characteristic of nominal single-electron-only devices based on compounds 24iPBIOXD, iTPBIOXD, and TPBI [device structures: ITO/EML (50 nm)/LiF (1 nm)/Al (150 nm)].

(Bian et al., 2018; Jou et al., 2018) was almost the same as 24iPBIOXD and iTPBIOXD, which manifested their similar injection barrier for efficient electron injection. Therefore, the significantly higher current for TPBI indicated better electron transporting property than 24iPBIOXD and iTPBIOXD. On the other hand, the current density in iTPBIOXD device was slightly higher than 24iPBIOXD, as depicted in **Figure 8**, the LUMO level of iTPBIOXD was 0.15 eV lower than 24iPBIOXD, therefore a mildly efficient electron-injection could be attained in iTPBIOXD device due to its lower injection barriers. Thus, the electron-transport performance for both electron acceptors may be comparable.

To conduct a comprehensive comparison on the EL performance for the exciplex-TADF OLEDs among diverse electron-donor and acceptor systems, a series of vacuum deposited devices A-F were fabricated. Due to the highest HOMO level of TAPC for efficient hole-injection, the device configuration for TAPC-based OLEDs was ITO/MoO₃ (1 nm)/TAPC:24iPBIOXD or iTPBIOXD (1:1, 70 nm)/LiF (1 nm)/Al (100 nm). To reduce the hole-injection

barrier, TCTA-based device was constructed by ITO/MoO₃ (1 nm)/TAPC (40 nm)/TCTA:24iPBIOXD or iTPBIOXD (1:1, 30 nm)/TmPyPB (40 nm)/LiF (1 nm)/Al (100 nm), while a further 10 nm TCTA thin film was inserted between the TAPC layer and emissive layer (EML) in mCP-based devices. Among them, MoO₃ and LiF were used as hole- and electron-injection materials, respectively; TAPC and 1,3,5-tri[(3-pyridyl)-phen-3-yl] benzene (TmPyPB) were functionalized as hole- and electron-transport materials, respectively, an extra TCTA layer was aimed to promote the hole-injection and block the electrons.

The current density-voltage-luminance (J - V - L), electroluminescence (EL) spectra, together with the current and power efficiency, external quantum efficiency vs. luminance curves are shown in **Figure 9**. The device fabrication details are stated in Supporting Information. According to the key EL data listed in **Table 2**, the turn-on voltage for TAPC, TCTA, and mCP containing devices was gradually increased from 2.8, 3.0

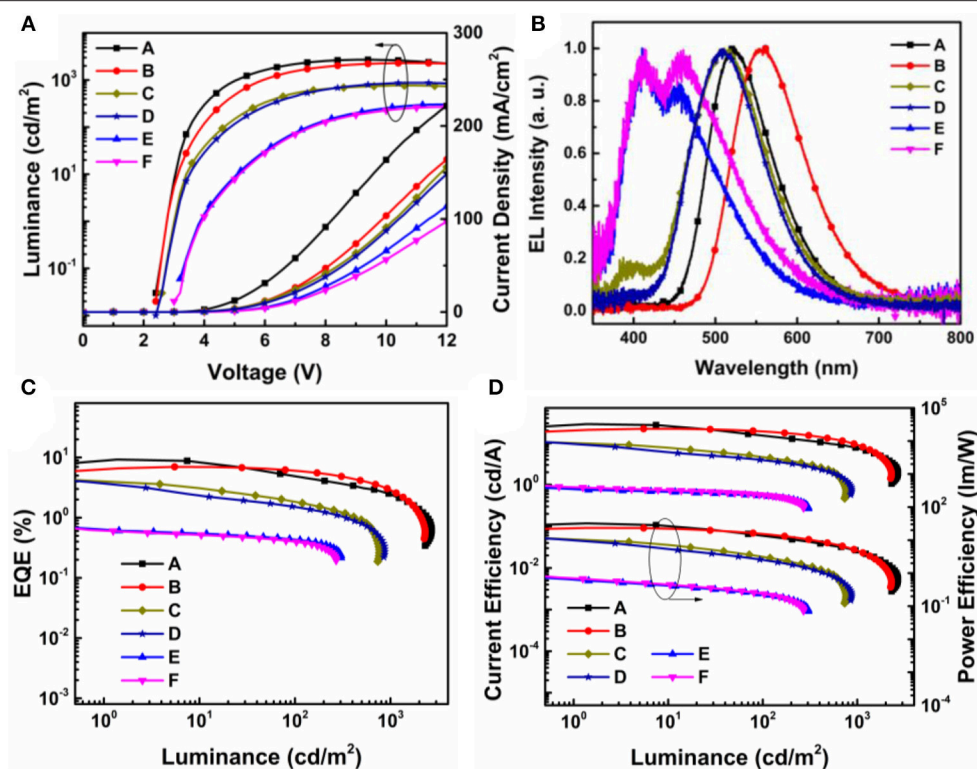


FIGURE 9 | (A) *L*-*V*-*J* characteristics; **(B)** normalized electroluminescent (EL) spectra; **(C)** external quantum efficiency (EQE) vs. luminance curves; **(D)** current efficiency and power efficiency vs. luminance curves of device A–F.

TABLE 2 | Electroluminescence characteristics for the devices.

Device	Emitting layer	V_{on}^a (V)	η_c^b (cd/A)	η_p^c (lm/W)	η_{ext}^d (%)	CIE (x,y)
A	TAPC: 24/PBIOXD	2.8	28.8	32.3	9.3	(0.31, 0.55)
B	TAPC: <i>i</i> TPBIOXD	2.8	22.1	23.4	7.0	(0.43, 0.54)
C	TCTA: 24/PBIOXD	3.0	10.1	10.6	4.0	(0.26, 0.43)
D	TCTA: <i>i</i> TPBIOXD	3.0	10.6	10.2	3.9	(0.25, 0.44)
E	mCP: 24/PBIOXD	3.8	0.8	0.66	0.65	(0.19, 0.20)
F	mCP: <i>i</i> TPBIOXD	3.8	0.9	0.74	0.63	(0.20, 0.23)

^a Turn-on voltage at 1 cd/m².

^b Maximum current efficiency.

^c Maximum power efficiency.

^d Maximum external quantum efficiency.

to 3.8 eV. The as high as 0.48 eV hole-injection barrier between TCTA and mCP lead to the highest operating voltage in devices E and F. The EL performance trend was in consistent with the values of HOMO/LUMO energy offsets, and TAPC-analog bearing the highest driving forces for convenient exciplex formation demonstrated the best highest EL efficiency. The best performance was attained from device A with TAPC:24/PBIOXD exciplex, corresponding to a maximum current efficiency (CE), power efficiency (PE), and external quantum efficiency (EQE) of 28.8 cd/A, 32.3 lm/W, and 9.3%. And the TAPC:*i*TPBIOXD based device B demonstrated slightly poorer EL performance with maximum current efficiency, power efficiency and external

quantum efficiency of 22.1 cd/A, 23.41 m/W, and 7.0%, respectively. Device C and D based on TCTA electron donor showed comparable EL efficiency, with maximum EQE of 4.0 and 3.9% for 24/PBIOXD and *i*TPBIOXD electron acceptors, respectively. The EL performance for mCP device was rather poor, with maximum EQE of <1% in both device E and F. As depicted in **Figure 9B**, devices A and B with TAPC donor depicted smooth exciplex-TADF emission, with EL peak at 519 and 556 nm, respectively, which is in agreement with the relevant PL spectra. Commission Internationale de L'Eclairage (CIE) values for device A and B was measured at (0.31, 0.55) and (0.43, 0.54), corresponding to green and yellow emission,

respectively. The TCTA based device C and D both exhibited blueish-green emission, with a gentle shoulder peak at around 400 nm for 24iPBIOXD. The two mCP-based devices displayed blue emission with CIE x, y each at ~ 0.20 . However, the EL spectra of device E and F revealed bimodal emission showing comparable intensity for the two peaks. It is hypothesized that the inadequate HOMO and LUMO energy offsets ($< \sim 1$ eV) for TCTA:24iPBIOXD, mCP:24iPBIOXD, and mCP:*i*TPBIOXD, resulted in the unexpected shorter wavelength EL emission peak, which was ascribed to pure mCP emission (Chiu and Lee, 2012; Shahalizad et al., 2017). In addition, since the E_{CT} of TAPC and TCTA based exciplexes were lower than the triplet energy of both donor and acceptor materials, which was beneficial to restrict triplet excitons in the exciplex states for the efficient RISC. However, E_{CT} of 2.8–2.96 eV (Figure 7B) for mCP based exciplex was significantly higher than the triplet energy (~ 2.55 eV) of the two electron acceptors, which provided a potential way for energy leakage from exciplex states to the T_1 excited state of 24iPBIOXD and *i*TPBIOXD. Thus, devices based on mCP donors demonstrated the lowest EL efficiency and inadequate TADF emission.

CONCLUSION

In summary, we have designed and synthesized two universal *N*-linked benzoimidazole/oxadiazole hybrid electron acceptors through a simple nucleophilic substitution reaction. Diverse deep-blue to yellow emissive exciplex could be formed between various conventional donor materials and the two acceptors due to their deep HOMO levels of ~ 6.15 eV. The HOMO and LUMO energy level offsets which were also named as the driving forces for exciplex formation were gradiently increased from 0.47 to 1.12 and 0.6 to 1.34 eV in mCP, TCTA, to TAPC based exciplexes. We have found that both HOMO and LUMO offsets ≥ 1 eV was required to form efficient and stable intermolecular charge transfer exciplex. When the driving forces were as low as

0.47–0.75 eV, which is far < 1 eV, the two mCP based exciplex demonstrated considerably short delayed component lifetime, with values of only 42 and 72 ns for 24iPBIOXD and *i*TPBIOXD acceptors, respectively. Additionally, the exciplex-type device EQE was lower than 1%. When the driving forces were slightly lower or approaching 1 eV, the two TCTA exciplexes displayed moderate EL efficiency of about 4%. And the best EL performance was achieved in TAPC containing exciplex-type TADF OLEDs, with relatively low turn-on voltage of 2.8 V, maximum efficiency of 28.8 cd/A CE, 32.3 lm/W PE, and 9.3% for 24iPBIOXD acceptor and 22.1 cd/A CE, 23.4 lm/W and 7.0% for *i*TPBIOXD acceptor. Our results provide guidance on the exploration of efficient exciplex type TADF OLEDs.

AUTHOR CONTRIBUTIONS

WY, MZ, and DH designed and synthesized the materials. WY and MZ did most of the experimental work and data analyses. OLED device fabrication and electroluminescent performance studies were carried out by HY and NS. YT had the idea, led the project. WY and YT prepared the manuscript. All authors contributed to the manuscript preparation.

ACKNOWLEDGMENTS

We declare all sources of funding received for the research being submitted. We thank the National Natural Science Foundation of China (91833304 and 61805211), the Natural Science Foundation of Jiangsu Province (BK20160042 and XYDXX-026) for financial support.

SUPPLEMENTARY MATERIAL

The Supplementary Material for this article can be found online at: <https://www.frontiersin.org/articles/10.3389/fchem.2019.00187/full#supplementary-material>

REFERENCES

- Adachi, C., Baldo, M. A., Thompson, M. E., and Forrest, S. R. (2001). Nearly 100% internal phosphorescence efficiency in an organic light-emitting device. *J. Appl. Phys.* 90, 5048–5051. doi: 10.1063/1.1409582
- Baldo, M. A., O'Brien, D. F., Thompson, M. E., and Forrest, S. R. (1999). Excitonic singlet-triplet ratio in a semiconducting organic thin film. *Phys. Rev. B* 60, 14422–14428. doi: 10.1103/PhysRevB.60.14422
- Baldo, M. A., O'Brien, D. F., You, Y., Shoustikov, A., Sibley, S., Thompson, M. E., et al. (1998). Highly efficient phosphorescent emission from organic electroluminescent devices. *Nature* 395, 151–154. doi: 10.1038/25954
- Becke, A. D. (1988). Density-functional exchange-energy approximation with correct asymptotic behavior. *Phys. Rev. A* 38, 3098–3100. doi: 10.1103/PhysRevA.38.3098
- Bian, M., Wang, Y., Guo, X., Lv, F., Chen, Z., Duan, L., et al. (2018). Positional isomerism effect of spirobifluorene and terpyridine moieties of “(A)*n*–D–(A)*n*” type electron transport materials for long-lived and highly efficient TADF-PhOLEDs. *J. Mater. Chem. C* 6, 10276–10283. doi: 10.1039/c8tc03796e
- Cai, X., and Su, S.-J. (2018). Marching toward highly efficient, pure-blue, and stable thermally activated delayed fluorescent organic light-emitting diodes. *Adv. Funct. Mater.* 28:1802558. doi: 10.1002/adfm.201802558
- Cao, X., Zhang, D., Zhang, S., Tao, Y., and Huang, W. (2017). CN-Containing donor–acceptor-type small-molecule materials for thermally activated delayed fluorescence OLEDs. *J. Mater. Chem. C* 5, 7699–7714. doi: 10.1039/C7TC02481A
- Chen, J.-X., Wang, K., Zheng, C.-J., Zhang, M., Shi, Y.-Z., Tao, S.-L., et al. (2018). Red organic light-emitting diode with external quantum efficiency beyond 20% based on a novel thermally activated delayed fluorescence emitter. *Adv. Sci.* 5:1800436. doi: 10.1002/advs.201800436
- Chiu, T.-L., and Lee, P.-Y. (2012). Carrier injection and transport in blue phosphorescent organic light-emitting device with oxadiazole host. *Int. J. Mol. Sci.* 13, 7575–7585. doi: 10.3390/ijms13067575
- Cooper, M. W., Zhang, X., Zhang, Y., Jeon, S. O., Lee, H., Kim, S., et al. (2018). Effect of the number and substitution pattern of carbazole donors on the singlet and triplet state energies in a series of carbazole-oxadiazole derivatives exhibiting thermally activated delayed fluorescence. *Chem. Mater.* 30, 6389–6399. doi: 10.1021/acs.chemmater.8b02632

- Franci, M. M., Pietro, W. J., Hehre, W. J., Binkley, J. S., Gordon, M. S., DeFrees, D. J., et al. (1982). Self-consistent molecular orbital methods. XXIII. A polarization-type basis set for second-row elements. *J. Chem. Phys.* 77, 3654–3665. doi: 10.1063/1.444267
- Gong, S., Chen, Y., Yang, C., Zhong, C., Qin, J., and Ma, D. (2010). *De Novo* design of silicon-bridged molecule towards a bipolar host: all-phosphor white organic light-emitting devices exhibiting high efficiency and low efficiency roll-off. *Adv. Mater.* 22, 5370–5373. doi: 10.1002/adma.201002732
- Goushi, K., and Adachi, C. (2012). Efficient organic light-emitting diodes through up-conversion from triplet to singlet excited states of exciplexes. *Appl. Phys. Lett.* 101:023306. doi: 10.1063/1.4737006
- Goushi, K., Yoshida, K., Sato, K., and Adachi, C. (2012). Organic light-emitting diodes employing efficient reverse intersystem crossing for triplet-to-singlet state conversion. *Nat. Photon.* 6, 253–258. doi: 10.1038/nphoton.2012.31
- Hu, J., Zhao, C., Zhang, T., Zhang, X., Cao, X., Wu, Q., et al. (2017). Isomeric N-linked benzimidazole containing new electron acceptors for exciplex forming hosts in highly efficient blue phosphorescent OLEDs. *Adv. Optical Mater.* 5:1700036. doi: 10.1002/adom.201700036
- Huang, T., Jiang, W., and Duan, L. (2018). Recent progress in solution processable TADF materials for organic light-emitting diodes. *J. Mater. Chem. C* 6, 5577–5596. doi: 10.1039/C8TC01139G
- Hung, W.-Y., Chiang, P.-Y., Lin, S.-W., Tang, W.-C., Chen, Y.-T., Liu, S.-H., et al. (2016). Balance the carrier mobility to achieve high performance exciplex OLED using a triazine-based acceptor. *ACS Appl. Mater. Interfaces* 8, 4811–4818. doi: 10.1021/acsami.5b11895
- Hung, W.-Y., Wang, T.-C., Chiang, P.-Y., Peng, B.-J., and Wong, K.-T. (2017). Remote steric effect as a facile strategy for improving the efficiency of exciplex-based OLEDs. *ACS Appl. Mater. Interfaces* 9, 7355–7361. doi: 10.1021/acsami.6b16083
- Jankus, V., Data, P., Graves, D., McGuinness, C., Santos, J., Bryce, M. R., et al. (2014). Highly efficient TADF OLEDs: how the emitter–host interaction controls both the excited state species and electrical properties of the devices to achieve near 100% triplet harvesting and high efficiency. *Adv. Funct. Mater.* 24, 6178–6186. doi: 10.1002/adfm.201400948
- Jeon, S. K., Yook, K. S., and Lee, J. Y. (2016). Highly efficient exciplex organic light-emitting diodes using thermally activated delayed fluorescent emitters as donor and acceptor materials. *Nanotechnology* 27:224001. doi: 10.1088/0957-4484/27/22/224001
- Jou, J.-H., Weng, J.-W., Chavhan, S. D., Yadav, R. A. K., and Liang, T.-W. (2018). Investigation of charge-transporting layers for high-efficiency organic light-emitting diode. *J. Phys. D: Appl. Phys.* 51:454002. doi: 10.1088/1361-6463/aad951
- Lee, C., Yang, W., and Parr, R. G. (1988). Development of the Colic-Salvetti correlation-energy formula into a functional of the electron density. *Phys. Rev. B* 37, 785–789. doi: 10.1103/PhysRevB.37.785
- Lee, J.-H., Cheng, S.-H., Yoo, S.-J., Shin, H., Chang, J.-H., Wu, C.-I., et al. (2015). An exciplex forming host for highly efficient blue organic light emitting diodes with low driving voltage. *Adv. Funct. Mater.* 25, 361–366. doi: 10.1002/adfm.201402707
- Li, J., Ding, D., Tao, Y., Wei, Y., Chen, R., Xie, L., et al. (2016). A significantly twisted spirocyclic phosphine oxide as a universal host for high-efficiency full-color thermally activated delayed fluorescence diodes. *Adv. Mater.* 28, 3122–3130. doi: 10.1002/adma.201506286
- Lin, T.-A., Chatterjee, T., Tsai, W.-L., Lee, W.-K., Wu, M.-J., Jiao, M., et al. (2016). Sky-blue organic light emitting diode with 37% external quantum efficiency using thermally activated delayed fluorescence from spiroacridine-triazine hybrid. *Adv. Mater.* 28, 6976–6983. doi: 10.1002/adma.201601675
- Liu, W., Chen, J.-X., Zheng, C.-J., Wang, K., Chen, D.-Y., Li, F., et al. (2016). Novel strategy to develop exciplex emitters for high-performance OLEDs by employing thermally activated delayed fluorescence materials. *Adv. Funct. Mater.* 26, 2002–2008. doi: 10.1002/adfm.201505014
- Liu, X.-K., Chen, Z., Qing, J., Zhang, W.-J., Wu, B., Tam, H. L., et al. (2015a). Remanagement of singlet and triplet excitons in single-emissive-layer hybrid white organic light-emitting devices using thermally activated delayed fluorescent blue exciplex. *Adv. Mater.* 27, 7079–7085. doi: 10.1002/adma.201502897
- Liu, X.-K., Chen, Z., Zheng, C.-J., Liu, C.-L., Lee, C.-S., Li, F., et al. (2015b). Prediction and design of efficient exciplex emitters for high-efficiency, thermally activated delayed-fluorescence organic light-emitting diodes. *Adv. Mater.* 27, 2378–2383. doi: 10.1002/adma.201405062
- Liu, Y., Li, C., Ren, Z., Yan, S., and Bryce, M. R. (2018). All-organic thermally activated delayed fluorescence materials for organic light-emitting diodes. *Nat. Rev. Mater.* 3:18020. doi: 10.1038/natrevmats.2018.20
- Liu, Z., Qayyum, M. F., Wu, C., Whited, M. T., Djurovich, P. I., Hodgson, K. O., et al. (2011). A codeposition route to copper-pyridine coordination complexes for organic light-emitting diodes. *J. Am. Chem. Soc.* 133, 3700–3703. doi: 10.1021/ja1065653
- Lo, S.-C., Harding, R. E., Shipley, C. P., Stevenson, S. G., Burn, P. L., and Samuel, I. D. (2009). High-triplet-energy dendrons: enhancing the luminescence of deep blue phosphorescent iridium(III) complexes. *J. Am. Chem. Soc.* 131, 16681–16688. doi: 10.1021/ja903157e
- Ma, Y., Zhang, H., Shen, J., and Che, C. (1998). Electroluminescence from triplet metal-ligand charge-transfer excited state of transition metal complexes. *Synth. Met.* 94, 245–248. doi: 10.1016/S0379-6779(97)04166-0
- Mondal, E., Hung, W.-Y., Dai, H.-C., and Wong, K.-T. (2013). Fluorene-based asymmetric bipolar universal hosts for white organic light emitting devices. *Adv. Funct. Mater.* 23, 3096–3105. doi: 10.1002/adfm.201202889
- Oh, C. S., Kang, Y. J., Jeon, S. K., and Lee, J. Y. (2015). High efficiency exciplex emitters using donor–acceptor type acceptor material. *J. Phys. Chem. C* 119, 22618–22624. doi: 10.1021/acs.jpcc.5b05292
- Olivier, Y., Moral, M., Muccioli, L., and Sancho-García, J.-C. (2017). Dynamic nature of excited states of donor–acceptor TADF materials for OLEDs: how theory can reveal structure–property relationships. *J. Mater. Chem. C* 5, 5718–5729. doi: 10.1039/C6TC05075A
- Park, Y.-S., Lee, S., Kim, K.-H., Kim, S.-Y., Lee, J.-H., and Kim, J.-J. (2013). Exciplex-forming co-host for organic light-emitting diodes with ultimate efficiency. *Adv. Funct. Mater.* 23, 4914–4920. doi: 10.1002/adfm.201300547
- Sarma, M., and Wong, K.-T. (2018). Exciplex: an intermolecular charge-transfer approach for TADF. *ACS Appl. Mater. Interfaces* 10, 19279–19304. doi: 10.1021/acsami.7b18318
- Segal, M., Baldo, M. A., Holmes, R. J., Forrest, S. R., and Soos, Z. G. (2003). Excitonic singlet-triplet ratios in molecular and polymeric organic materials. *Phys. Rev. B* 68:075211. doi: 10.1103/PhysRevB.68.075211
- Shahalizad, A., D'Aléo, A., Andraud, C., Sazzad, M. H., Kim, D.-H., Tsuchiya, Y., et al. (2017). Near infrared electroluminescence from Nd(TTA)₃phen in solution-processed small molecule organic light-emitting diodes. *Org. Electron.* 44, 50–58. doi: 10.1016/j.orgel.2017.01.044
- Son, K. S., Yabito, M., Imai, T., Yoshizaki, H., and Adachi, C. (2008). Analyzing bipolar carrier transport characteristics of diarylamino-substituted heterocyclic compounds in organic light-emitting diodes by probing electroluminescence spectra. *Chem. Mater.* 20, 4439–4446. doi: 10.1021/cm8004985
- Su, H.-C., Chen, H.-F., Fang, F.-C., Liu, C.-C., Wu, C.-C., Wong, K.-T., et al. (2008). Solid-state white light-emitting electrochemical cells using iridium-based cationic transition metal complexes. *J. Am. Chem. Soc.* 130, 3413–3419. doi: 10.1021/ja076051e
- Sun, J. W., Lee, J.-H., Moon, C.-K., Kim, K.-H., Shin, H., and Kim, J.-J. (2014). A fluorescent organic light-emitting diode with 30% external quantum efficiency. *Adv. Mater.* 26, 5684–5688. doi: 10.1002/adma.201401407
- Tang, C. W., and VanSlyke, S. A. (1987). Organic electroluminescent diodes. *Appl. Phys. Lett.* 51, 913–915. doi: 10.1063/1.98799
- Tao, Y., Yang, C., and Qin, J. (2011). Organic host materials for phosphorescent organic light-emitting diodes. *Chem. Soc. Rev.* 40, 2943–2970. doi: 10.1039/c0cs00160k
- Uoyama, H., Goushi, K., Shizu, K., Nomura, H., and Adachi, C. (2012). Highly efficient organic light-emitting diodes from delayed fluorescence. *Nature* 492, 234–238. doi: 10.1038/nature11687
- Volz, D., Zink, D. M., Bockrocker, T., Friedrichs, J., Nieger, M., Baumann, T., et al. (2013). Molecular construction kit for tuning solubility, stability and luminescence properties: heteroleptic MePyrPHOS-copper iodide-complexes and their application in organic light-emitting diodes. *Chem. Mater.* 25, 3414–3426. doi: 10.1021/cm4010807
- Wen, S. W., Lee, M. T., and Chen, C. H. (2005). Recent development of blue fluorescent OLED materials and devices. *J. Disp. Technol.* 1, 90–99. doi: 10.1109/JDT.2005.852802

- Wu, Q., Wang, M., Cao, X., Zhang, D., Sun, N., Wan, S., et al. (2018). Carbazole/ α -carboline hybrid bipolar compounds as electron acceptors in exciplex or non-exciplex mixed cohosts and exciplex-TADF emitters for high-efficiency OLEDs. *J. Mater. Chem. C* 6, 8784–8792. doi: 10.1039/C8TC02353K
- Wu, T.-L., Huang, M.-J., Lin, C.-C., Huang, P.-Y., Chou, T.-Y., and Cheng, R.-W., et al. (2018). Diboron compound-based organic light-emitting diodes with high efficiency and reduced efficiency roll-off. *Nat. Photon.* 12, 235–240. doi: 10.1038/s41566-018-0112-9
- Yao, C., Yang, Y., Li, L., Bo, M., Peng, C., and Wang, J. (2018). Ge-based bipolar small molecular host for highly efficient blue OLEDs: multiscale simulation of charge transport. *J. Mater. Chem. C* 6, 6146–6152. doi: 10.1039/C8TC00355F
- Zeng, W., Lai, H.-Y., Lee, W.-K., Jiao, M., Shiu, Y.-J., Zhong, C., et al. (2018). Achieving nearly 30% external quantum efficiency for orange-red organic light emitting diodes by employing thermally activated delayed fluorescence emitters composed of 1,8-naphthalimide-acridine hybrids. *Adv. Mater.* 30:1704961. doi: 10.1002/adma.201704961
- Zhang, D., Cai, M., Bin, Z., Zhang, Y., Zhang, D., and Duan, L. (2016). Highly efficient blue thermally activated delayed fluorescent OLEDs with record-low driving voltages utilizing high triplet energy hosts with small singlet–triplet splittings. *Chem. Sci.* 7, 3355–3363. doi: 10.1039/C5SC04755B
- Zhang, D., Cao, X., Wu, Q., Zhang, M., Sun, N., Zhang, X., et al. (2018). Purely organic materials for extremely simple all-TADF white OLEDs: a new carbazole/oxadiazole hybrid material as a dual-role non-doped light blue emitter and highly efficient orange host. *J. Mater. Chem. C* 6, 3675–3682. doi: 10.1039/C7TC04969B
- Zhang, L., Cai, C., Li, K. F., Tam, H. L., Chan, K. L., and Cheah, K. W. (2015). Efficient organic light-emitting diode through triplet exciton reharvesting by employing blended electron donor and acceptor as the emissive layer. *ACS Appl. Mater. Interfaces* 7, 24983–24986. doi: 10.1021/acsami.5b05597
- Zhang, T., Zhao, B., Chu, B., Li, W., Su, Z., Wang, L., et al. (2015). Blue exciplex emission and its role as a host of phosphorescent emitter. *Org. Electron.* 24, 1–6. doi: 10.1016/j.orgel.2015.05.013
- Zhang, Y., and Forrest, S. R. (2012). Triplets contribute to both an increase and loss in fluorescent yield in organic light emitting diodes. *Phys. Rev. Lett.* 108:267404. doi: 10.1103/PhysRevLett.108.267404

Conflict of Interest Statement: The authors declare that the research was conducted in the absence of any commercial or financial relationships that could be construed as a potential conflict of interest.

Copyright © 2019 Yuan, Yang, Zhang, Hu, Sun and Tao. This is an open-access article distributed under the terms of the Creative Commons Attribution License (CC BY). The use, distribution or reproduction in other forums is permitted, provided the original author(s) and the copyright owner(s) are credited and that the original publication in this journal is cited, in accordance with accepted academic practice. No use, distribution or reproduction is permitted which does not comply with these terms.



Efficient Organic Light Emitting Diodes Using Solution-Processed Alkali Metal Carbonate Doped ZnO as Electron Injection Layer

Guo Chen*, Feiyang Liu, Zhitian Ling, Pengpeng Zhang, Bin Wei and Wenqing Zhu*

Key Laboratory of Advanced Display and System Applications, Shanghai University, Ministry of Education, Shanghai, China

OPEN ACCESS

Edited by:

Shi-Jian Su,
South China University of Technology,
China

Reviewed by:

Takayuki Chiba,
Yamagata University, Japan
Hirohiko Fukagawa,
Tokyo University of Science, Japan

*Correspondence:

Guo Chen
chenguo@shu.edu.cn
Wenqing Zhu
wqzhu@shu.edu.cn

Specialty section:

This article was submitted to
Organic Chemistry,
a section of the journal
Frontiers in Chemistry

Received: 31 January 2019

Accepted: 22 March 2019

Published: 16 April 2019

Citation:

Chen G, Liu F, Ling Z, Zhang P, Wei B
and Zhu W (2019) Efficient Organic
Light Emitting Diodes Using
Solution-Processed Alkali Metal
Carbonate Doped ZnO as Electron
Injection Layer. *Front. Chem.* 7:226.
doi: 10.3389/fchem.2019.00226

In this study, we demonstrate highly efficient, inverted organic light-emitting diodes (IOLEDs) using solution-processed alkali metal carbonate doped ZnO as an electron injection layer (EIL) and tris-(8-hydroxyquinoline) aluminum (Alq₃) as an emitter layer. In order to enhance the electron injection efficiency of the IOLEDs, the ZnO EIL layers were modified by doping various alkali metal carbonate materials, including Li₂CO₃, Na₂CO₃, K₂CO₃, and Cs₂CO₃, using the low-temperature wet-chemical method. Compared to the control neat ZnO EIL-based IOLEDs, the alkali metal carbonate doped ZnO EIL-based IOLEDs possess obviously improved device performance. An optimal current efficiency of 6.04 cd A⁻¹ were realized from the K₂CO₃ doped ZnO EIL based IOLED, which is 54% improved compared to that of the neat ZnO EIL based device. The enhancement is ascribed to the increased electron mobility and reduced barrier height for more efficient electron injection. Our results indicate that alkali metal carbonate doped ZnO has promising potential for application in highly efficient solution-processed OLEDs.

Keywords: organic light emitting diodes (OLED), solution process, electron injection layer, doped ZnO, alkali metal carbonate

INTRODUCTION

Organic light-emitting diodes (OLEDs) have been extensively investigated as a promising technology for energy-saving lighting and large-area flexible displays (Kido et al., 1995; Forrest, 2004; Sasabe and Kido, 2010; Higuchi et al., 2015; Li et al., 2016). Typically, there are two kinds of device structures mainly used in OLEDs, i.e., conventional and inverted structures. Compared with the conventional structure, the inverted OLEDs (IOLEDs), which use the air stable metals as top anode and indium-tin-oxide (ITO) as the cathode, have been considered as an advantageous approach to improve the stability and the roll-to-roll fabrication process of flat-panel display (Chu et al., 2006; Morii et al., 2006; Sessolo and Bolink, 2011; Chen et al., 2012; Guo et al., 2017; Fukagawa et al., 2018). Moreover, one benefit of the IOLED is to take advantage of the existing n-type amorphous silicon thin film transistor (a-Si TFT) technology for the development of the active-matrix driving OLED technology (Kabra et al., 2010; Hsieh et al., 2011; Zhong et al., 2011; Park et al., 2015; Hosono et al., 2017).

In an IOLED device, ITO is used as the electron injection cathode while metal electrode acts as hole injection anode. To facilitate electron injection from ITO into the upper electron transporting or light-emitting layers, the electron injection layers (EILs) are usually coated onto the ITO cathode. Moreover, introducing the EIL into the OLED devices can also efficiently reduce the driving voltage

and improve the power efficiency in the same time (Guo et al., 2017). Up to date, some inorganic alkali metal-containing materials (such as LiF and Cs_2CO_3), metal oxide materials (such as TiO_2 , ZnO, and ZrO_2) and ionic π -conjugated polymers have been reported as efficient EIL for high performance OLEDs (Tokmoldin et al., 2009; Kim et al., 2014; Chiba et al., 2015; Zhao et al., 2017). Among all these EIL materials, ZnO has attracted increasing attention for being used in IOLED because ZnO is environmentally stable, low-cost and has high transparency in visible region (Chen et al., 2016). In particular, the solution-processed ZnO film has been widely used as an EIL in the IOLED configuration due to its advantages of optical transparency, low work function, high electron mobility and good electron selective, and hole blocking contact (Bolink et al., 2007; Chiba et al., 2012; Dong et al., 2017). However, the ZnO EIL based IOLED demonstrates ordinary device performance owing to the injection barrier between ZnO EIL and the adjacent electron transporting layers (ETL) caused by the still high work function of ZnO film (Höfle et al., 2014). Thus, there is an urgent need to develop a new technique to improve the injection efficiency of ZnO EIL based IOLEDs.

Some recent reports indicate that doping the low-concentration group I elements into the ZnO host is one of the most efficient methods to enhance the optoelectronic properties of ZnO films for organic electronic devices (Lin et al., 2016; Nho et al., 2016; Wang et al., 2018). The doped ZnO films always demonstrate much higher electron mobility and reduced work function than the bare ZnO film, which are sought-after properties for high efficiency organic electronic devices. For example, the Li ion and LiF have been doped in ZnO films to increase the electron mobility and thus increase the charge collection efficiency and reduce the charge carrier recombination, leading to enhanced photovoltaic performance in organic solar cells (Chang et al., 2013; Lin et al., 2016). To obtain the doped ZnO film, various techniques such as sputting, pulsed laser deposition, sol-gel, chemical vapor deposition, thermal evaporation, spray pyrolysis, and wet-chemical method have been used to dope the dopant into the ZnO host (Chen et al., 2016). Among these doping techniques, wet-chemical doping is the most promising route due to its advantages of low-cost, easy operation and low-temperature (Chang et al., 2015). It has been well used in the research field of organic solar cells and thin film transistors (Chang et al., 2013, 2015). However, to the best of our knowledge, few researchers pay attention to the usage of wet-chemical doping technique to fabricate doped ZnO films as EILs for OLEDs.

In this work, to systemically investigate the effect of group I elements doping on properties of the ZnO films and the doped ZnO film based IOLEDs, we introduced various alkali metal carbonates (M_2CO_3 , $\text{M} = \text{Li, Na, K, and Cs}$) with various doping ratios into ZnO film using the low-temperature wet-chemical doping method. Then the doped $\text{ZnO}:\text{M}_2\text{CO}_3$ films were employed as EIL layers, combined with the tris-(8-hydroxyquinoline) aluminum (Alq_3) emitter layer, to construct the IOLEDs. By controlling the doping concentration of M_2CO_3 in the precursor solution, highly efficient IOLEDs with high current efficiency and power efficiency have been obtained.

EXPERIMENTAL SECTION

Materials

All materials employed in this study were purchased from commercial sources and used without further purification. The ZnO precursor solution was prepared by dissolving ZnO powder (Sigma Aldrich, 99.9%) in an ammonium solution (Sigma Aldrich, 99%) to form a 0.1 M $\text{Zn}(\text{NH}_3)_4^{2+}$ complex precursor saturated solution. The solution was refrigerated for several tens of hours to promote the ZnO powder dissolution. Then, various molar ratios (3, 5, and 10%) of M_2CO_3 were added to the precursor solution to prepare the M_2CO_3 doped $\text{Zn}(\text{NH}_3)_4^{2+}$ complex precursor solution. The patterned indium-tin-oxide (ITO) glass substrates with a sheet resistance of 15 Ω/sq were cleaned in ultrasonic bath with detergent, de-ionized water, acetone, and isopropanol consecutively, then they were dried by keeping them in an oven at 80°C for 12 h before usage.

Film Characterization

The UV-Vis transmittance was recorded at room temperature using an ultraviolet-visible-near infrared spectrophotometer (U-3900H, Hitachi). The work function was determined using a Riken-Keiki AC-3 ultraviolet photoelectron spectrometer. X-ray photoelectron spectroscopy (XPS) measurements were implemented using X-ray photoelectron spectrometer (Kratos Amicus Budget). The surface morphology of the film was investigated by the atomic force microscopy (AFM) technique in contact mode using the Seiko instrument SPA 400 AFM system. The films for the above mentioned measurements were prepared under the same conditions used for fabricating the devices to enable accurate comparisons.

Device Fabrication And Characterization

The IOLEDs were fabricated with a structure of ITO/ $\text{ZnO}:\text{M}_2\text{CO}_3$ (10 nm) /4,7-diphenyl-1,10-phenanthroline (Bphen, 20 nm)/ Alq_3 (20 nm)/N,N'-bis(naphthalen-1-yl)-N,N'-bis(phenyl)-benzidine (NPB, 40 nm)/ MoO_3 (5 nm)/Al (120 nm), as shown in **Figure 1A**. Firstly, the clean ITO substrates were treated by ultraviolet-ozone for 30 min. Then the $\text{ZnO}:\text{M}_2\text{CO}_3$ films were prepared by spin-coating the $\text{Zn}(\text{NH}_3)_4^{2+}:\text{M}_2\text{CO}_3$ precursors on the ITO substrates and subsequently heated at 200°C for 15 min to realize the conversion from $\text{Zn}(\text{NH}_3)_4^{2+}:\text{M}_2\text{CO}_3$ complex to $\text{ZnO}:\text{M}_2\text{CO}_3$ (Chang et al., 2015). Then the substrate was transferred into a high-vacuum chamber (1×10^{-5} Pa), where organic layers and a metal cathode layer were successively evaporated using a shadow mask. The deposition rates for the organic materials, MoO_3 and Al, were 1.0, 0.5, and 5.0 \AA s^{-1} , respectively. The electron-only devices were fabricated with a structure of ITO/ $\text{ZnO}:\text{M}_2\text{CO}_3$ (10 nm)/Bphen (60 nm)/LiQ (1 nm)/Al (120 nm). The device active area was 0.04 cm^2 , defined by the overlap of anode and cathode. The current density-voltage-luminescence (J - V - L) characteristics were measured using a Keithley 2400 source meter and a PR-650 Spectra Colorimeter. The luminance and spectra of each device were measured in the direction perpendicular to the substrate.

All the measurements were performed in air under ambient conditions without device encapsulation.

RESULTS AND DISCUSSION

Figure 1 illustrates the device architecture of ZnO (ZnO:M₂CO₃) based IOLEDs and the corresponding energy-level diagram. In this IOLED device, the Alq₃ film acts as an emitter layer, the NPB and Bphen films are hole-transporting and ETLs, respectively. Additionally, MoO₃ and ZnO (ZnO:M₂CO₃) are employed as hole-injection layer and EIL, respectively. For comparison, all devices have the same emitter layer and functional layers, except that of the ZnO:M₂CO₃ layers. Various M₂CO₃ dopant, including Li₂CO₃, Na₂CO₃, K₂CO₃, and Cs₂CO₃ with various concentration, were doped into the ZnO film to investigate the effect of M₂CO₃ doping on the film properties of the ZnO EIL and the device performance of doped ZnO based IOLEDs.

The ZnO:M₂CO₃ EILs in this study were fabricated by a simple wet-chemical doping method using the blend aqueous solution of M₂CO₃ and Zn-ammine complex as the precursor. The detailed fabrication process includes the following three steps: (1) The Zn(NH₃)₄²⁺ complex precursor was prepared by dissolving ZnO powder in an ammonium solution (Lin et al., 2014). Then various M₂CO₃ aqueous solution with various molar concentration were blended into the Zn(NH₃)₄²⁺ complex aqueous solution to prepare the Zn(NH₃)₄²⁺:M₂CO₃ precursors for the doped films; (2) The doped ZnO:M₂CO₃ films were fabricated by spin-coating the Zn(NH₃)₄²⁺:M₂CO₃ precursors, followed by thermal annealing at 200°C for 15 min to realize the conversion from Zn(NH₃)₄²⁺ complex to ZnO. The fabrication route using the aqueous-based Zn-ammine complex solutions is one of the most promising routes to prepare the ZnO film, owing to its advantages of low-temperature and easy-operation. However, it is difficult to directly dope the metal ion into the ZnO host from the Zn-ammine complex precursor because the ammonium hydroxide tends to precipitate metal salts due to acid–base neutralization reaction (Zhang et al., 2018). Therefore, we choose the M₂CO₃ aqueous solutions with weak alkalinity to

blend into the Zn-ammine complex aqueous solution to make the precursors for the doped ZnO:M₂CO₃ films. Herein, the weak alkalinity of the M₂CO₃ aqueous solution makes it coexist with the Zn-ammine complex. The doping concentration was controlled by blending various amounts of M₂CO₃ into the Zn-ammine complex aqueous solution. As shown in **Figures 2–7**, **Figures S1–S3**, **Tables 1, 2** and **Table S1**, to investigate the effect of alkali metal doping on properties of the ZnO film and doped ZnO film based IOLED devices, we used various tools including UV-vis absorption spectra, AFM, XPS, and AC-3 to characterize the surface morphology and optoelectronic properties of the doped ZnO film, then fabricated and characterized a series of ZnO:M₂CO₃ EILs based IOLEDs.

In the IOLEDs, the transparency of the EIL in the visible wavelength region will greatly affect the output efficiency of devices, since the outgoing light has to pass through the EIL layer before going out. To investigate the M₂CO₃ doping effect on the transparency of the ZnO film, the transmittance spectra of the

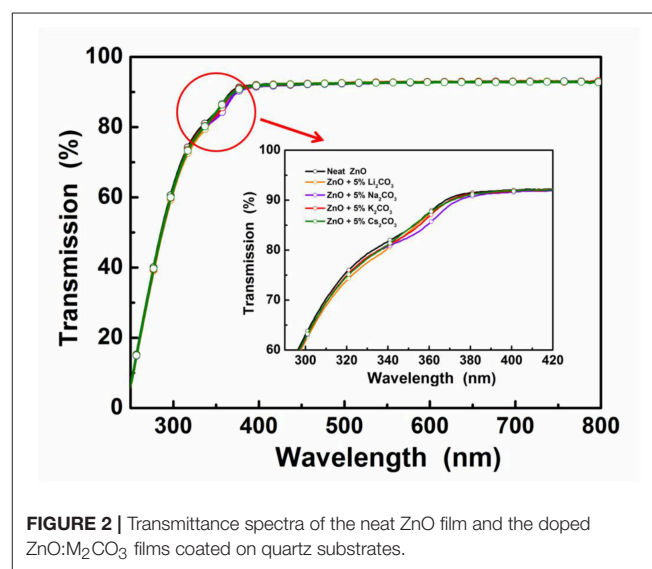


FIGURE 2 | Transmittance spectra of the neat ZnO film and the doped ZnO:M₂CO₃ films coated on quartz substrates.

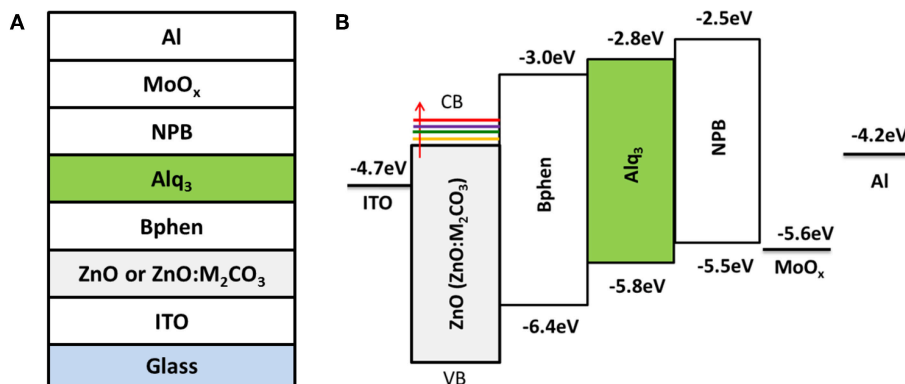


FIGURE 1 | **(A)** Device structure of the alkali metal carbonate doped ZnO (ZnO:M₂CO₃) EIL based inverted organic light-emitting diodes (IOLEDs) and **(B)** the energy-level diagram of the materials under investigation.

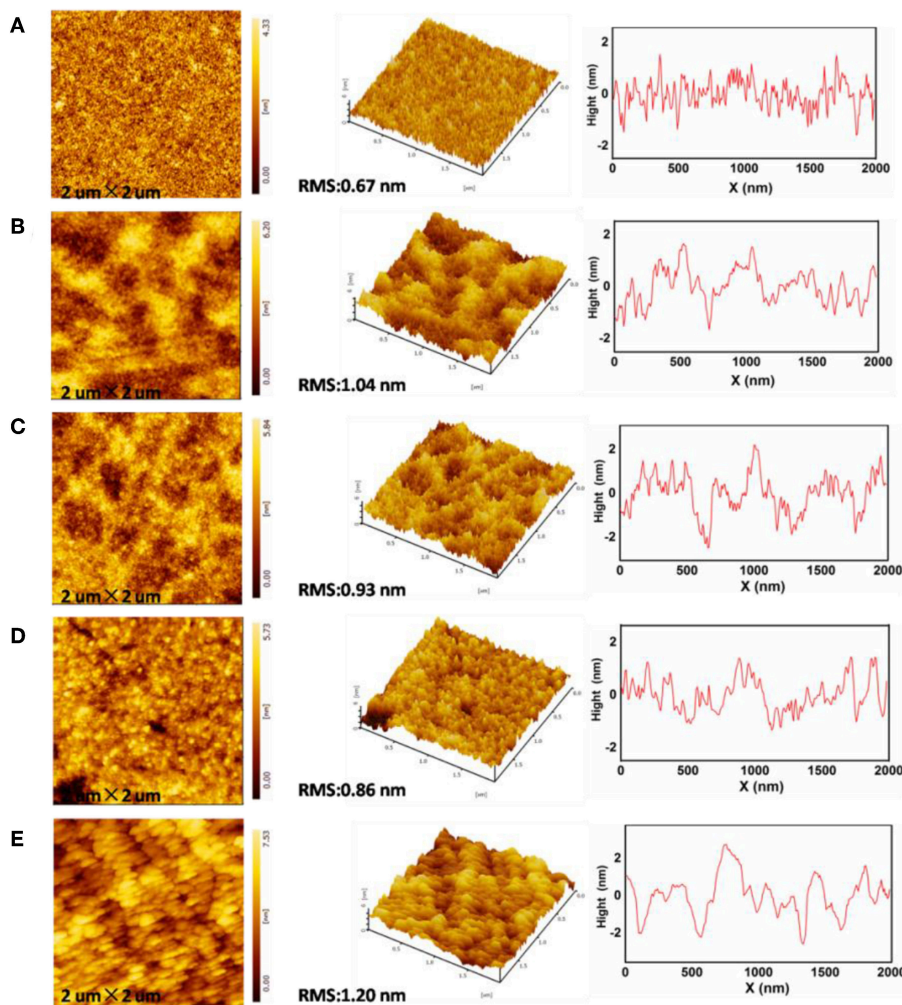


FIGURE 3 | Atomic force microscopy (AFM) topographic and 3D images of (A) neat ZnO film, (B) ZnO:Li₂CO₃ film, (C) ZnO:Na₂CO₃ film, (D) ZnO:K₂CO₃ film, (E) ZnO:Cs₂CO₃ film.

ZnO:M₂CO₃ EIL were characterized. As shown in **Figure 2**, all of the ZnO films exhibit high transparency in the visible wavelength range with transmittance values over 90%. It indicates that doping M₂CO₃ into the ZnO film has a minimal effect on the transmittance of the ZnO thin film, which is a promising property for making highly efficient IOLEDs.

Surface roughness of the ZnO EIL has been proven to have an influence on the device performance. The rough morphology of the EIL may cause partial short circuits and poor electrical contact in the thin flat devices, leading to dark spots in IOLEDs and thus poor device performance (Si et al., 2017). The morphology of the neat ZnO and doped ZnO:M₂CO₃ thin films were investigated by the tapping-mode AFM. As presented in **Figure 3**, the root-mean-square (RMS) roughness of the neat ZnO film is 0.67 nm, whereas, the RMS roughness of the doped ZnO film are 1.04, 0.93, 0.86, and 1.20 nm for ZnO:Li₂CO₃, ZnO:Na₂CO₃, ZnO:K₂CO₃, and ZnO:Cs₂CO₃ films, respectively. It can be seen that the morphologies of

the ZnO:M₂CO₃ doped films are almost as smooth as that of the neat ZnO film, which is also beneficial to achieving high-performance IOLEDs.

To confirm that the M₂CO₃ exists in the doped ZnO films, we investigated the surface chemical composition of the neat ZnO and ZnO:M₂CO₃ using XPS analysis. **Figure 4** shows Zn 2p_{1/2}, Zn 2p_{3/2}, O 1s, Li 1s, Na 1s, K 2p, and Cs 3d XPS spectra in comparison with those of the neat ZnO film. As shown in **Figure 4A**, the difference between Zn 2p_{3/2} and Zn 2p_{1/2} binding energies of both of the neat ZnO and doped ZnO:M₂CO₃ films is ~23 eV, which is in good agreement with the standard value of ~22.97 eV for Zn²⁺ (Hsien et al., 2008). When introducing the M₂CO₃ into the ZnO film, the Zn 2p_{3/2} and Zn 2p_{1/2} binding energies shift to slightly lower level, which may be attributed to the alkali metal cation doping effect (Chen et al., 2016). The O 1s XPS spectra (**Figure 4B**) of the neat ZnO film show a binding energy peak at 530.8 eV, which indicates that Zn-O exists in the neat ZnO film (Hsien et al., 2008). After the introduction

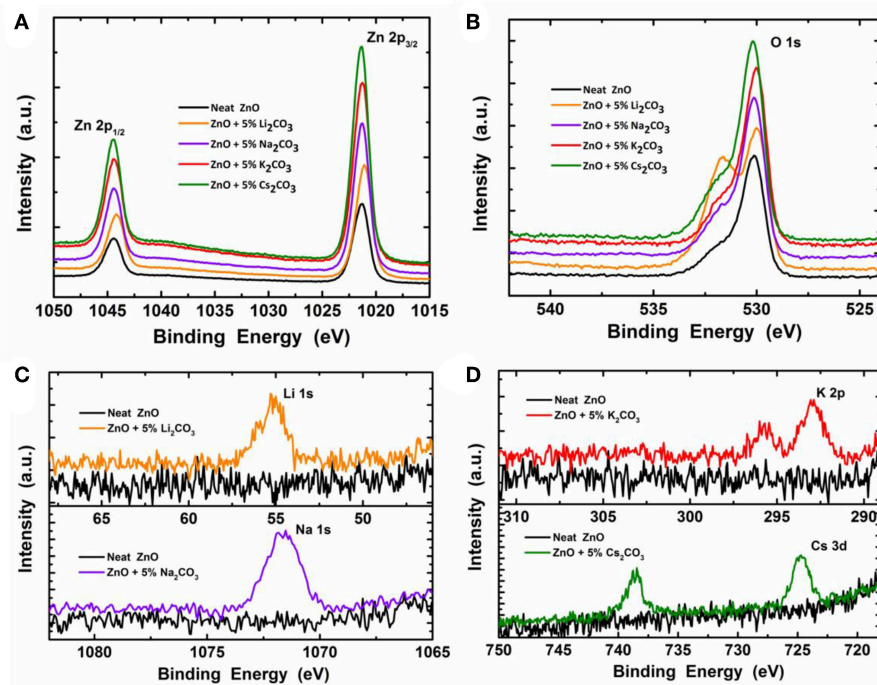


FIGURE 4 | The X-ray photoelectron spectroscopy (XPS) spectra of the neat ZnO film and ZnO: M_2CO_3 doped films coated on Si wafer: **(A)** Zn $2p_{1/2}$ and Zn $2p_{3/2}$; **(B)** O 1s; **(C)** Li 1s, Na 1s, and **(D)** K 2p and Cs 3d.

of M_2CO_3 into the ZnO film, the O 1s binding energy shifts to slightly lower binding level (530.2 eV). In the same time, another binding energy band with a peak at ~ 532.3 eV appears, which indicates that the chemisorbed O_2 molecules exists in the doped ZnO: M_2CO_3 film (Chen et al., 2016). As depicted in **Figures 4C,D**, the Li 1s peak, Na 1s peak, K 2p peak, and Cs 3d peak were clearly detected for the ZnO: Li_2CO_3 film, ZnO: Na_2CO_3 film, ZnO: K_2CO_3 film, and ZnO: Cs_2CO_3 film, respectively, which indicates that the alkali metal cation exists in the relative doped films.

To investigate the effect of M_2CO_3 doping on the device performance of IOLEDs, a series of green IOLEDs based on ZnO: M_2CO_3 EILs, with various doping concentrations (3, 5, and 10%) or various M_2CO_3 dopant (Li_2CO_3 , Na_2CO_3 , K_2CO_3 , and Cs_2CO_3), were fabricated and characterized. **Figure 5** represents the current density–luminance–voltage (J–L–V), the current efficiency and power efficiency characteristics for the IOLEDs, based on the neat ZnO or doped ZnO: K_2CO_3 EILs with various K_2CO_3 doping concentrations. The relative optoelectronic parameters are summarized in **Table 1**. As shown in **Figure 5A** and **Table 1**, the neat ZnO EIL based IOLED demonstrates a driving voltage of 5.2 V, a maximum luminescence of 15,430 cd/m^2 , a maximum current efficiency of 3.92 cd/A and a maximum power efficiency of 1.81 lm/W . By introducing the K_2CO_3 into the ZnO EIL, the devices show obviously enhanced device performance. When increasing the doping concentration of K_2CO_3 , the operational voltage of the device would at first decrease and afterwards increase, whereas, the maximum

luminescence, maximum current efficiency and maximum power efficiency show trends of rising first and then falling. As a result, the doped ZnO:5% K_2CO_3 EIL based IOLED possesses an optimal device performance with a decreased driving voltage of 4.8 V, and an enhanced maximum luminescence of 22,651 cd/m^2 , an increased maximum current efficiency of 6.04 cd/A and an improved maximum power efficiency of 2.61 lm/W . Compared with the neat ZnO based IOLED, the current efficiency of the doped ZnO:5% K_2CO_3 EIL based IOLED increased by 54%, which should be ascribed to the increased electron mobility and reduced barrier height for electron injection due to the doping of K^+ ions, as discussed in a subsequent section.

Figure 6 demonstrates the J–V characteristics, L–V characteristics, current efficiency, and power efficiency characteristics of IOLEDs, based on doped ZnO:5% Li_2CO_3 , ZnO:5% Na_2CO_3 , ZnO:5% K_2CO_3 , and ZnO:5% Cs_2CO_3 EILs, respectively. As shown in **Figure 6** and **Table 2**, similar to the K_2CO_3 doping effect, introducing Li_2CO_3 , Na_2CO_3 , and Cs_2CO_3 into the ZnO EIL will obviously improve the maximum luminescence, maximum current efficiency, and maximum power efficiency of the IOLEDs compared with that of the neat ZnO based IOLED. As a familiar dopant in ZnO, the mechanism of Li ion doping leading to the enhancement of device performance has been well explained: the Li ion doped ZnO film possesses enhanced electron mobility and better band matching with adjoining layer (Chen et al., 2016). Herein, our results show that other alkali metal ions (Na, K, and Cs) can each also act as an efficient dopant in ZnO

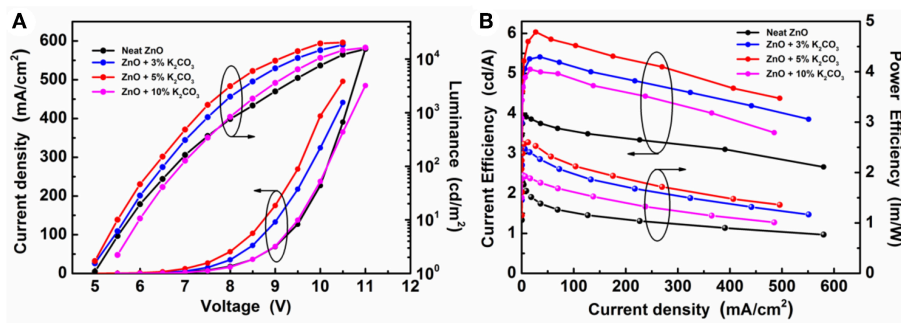


FIGURE 5 | (A) The J-V-L characteristics and **(B)** the current efficiency and power efficiency characteristics of IOLEDs based on the neat ZnO and the doped ZnO:K₂CO₃ EILs with various K₂CO₃ doping concentration.

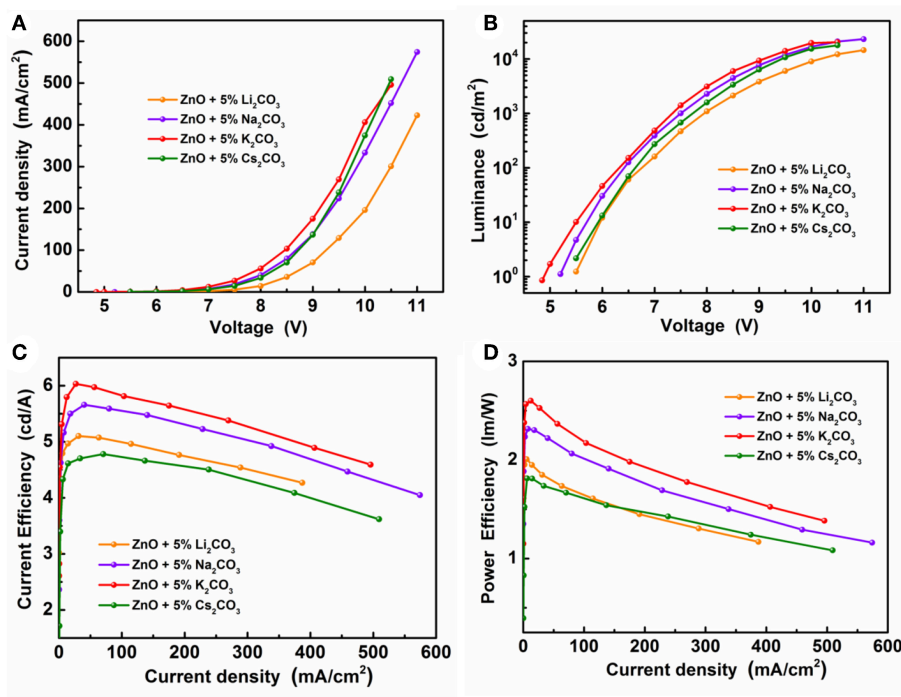


FIGURE 6 | (A) The J-V characteristics, **(B)** the L-V characteristics, **(C)** the current efficiency and **(D)** the power efficiency characteristics of the IOLEDs based on the doped ZnO:Li₂CO₃, ZnO:Na₂CO₃, ZnO:K₂CO₃, and ZnO:Cs₂CO₃ EILs.

film for high efficiency OLED devices. Furthermore, the ZnO:5%K₂CO₃ EIL based IOLED displays the highest device performance. The difference in the device performance should be ascribed to the different electron injection properties of these devices caused by the different electron mobility and work function of the doped ZnO:M₂CO₃ films with various dopant, which may be attributed to them having a different ionic radius: Li (0.76 Å), Na (1.02 Å), K (1.38 Å), and Cs (1.67 Å) cation dopant (Chang et al., 2015). This leads to different interstitial or substitutional sites in the bulk ZnO thin films (Chang et al., 2015).

To compare the electron mobilities in the ZnO:M₂CO₃ EIL with various dopant, the electron-only devices, with a structure

of ITO/ZnO:5%M₂CO₃ (10 nm)/Bphen (60 nm)/Liq (1 nm)/Al (120 nm) (**Figure 7A**), were also prepared and characterized. As depicted in **Figure 7B**, the electron-only device with ZnO:M₂CO₃ EIL exhibits much larger current density at the same voltage than that of the device with neat ZnO EIL. Moreover, the ZnO:K₂CO₃ EIL based electron-only device has the highest current density. This indicates that the electron mobilities of the ZnO:M₂CO₃ EIL are much higher than that of the neat ZnO EIL, and the electron mobility of the ZnO:K₂CO₃ EIL are highest in this series of ZnO:M₂CO₃ EILs. This observation is consistent with the device performance: the enhanced electron mobility will contribute to more efficient electron injection, and thus, higher device performance of the

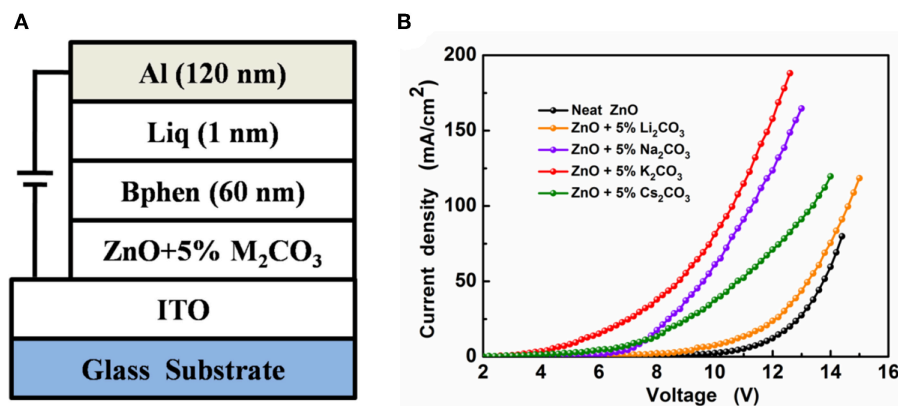


FIGURE 7 | (A) The device structure of the electron-only devices and **(B)** the J-V characteristics of the electron-only devices.

IOLEDs. Additionally, the effect of M_2CO_3 doping on the work function of the ZnO film was also studied. As shown in **Table S1**, the work function of the neat ZnO is 4.02 eV. Doping M_2CO_3 into the ZnO will effectively reduce the work function of the ZnO film. The ZnO: K_2CO_3 EIL has a much shallower work function of 3.61 eV. The obviously reduced work function of the ZnO: M_2CO_3 film has much better energy alignment with the lowest unoccupied molecule orbital (LUMO) level of the Bphen ETL in the IOLEDs. The reduced barrier height between EIL and ETL is beneficial for enhancing the charge injection efficiency, and thus, increasing the device performance of the ZnO: M_2CO_3 EIL based IOLEDs, especially in the ZnO: K_2CO_3 EIL case.

To further study the operational stability of ZnO: M_2CO_3 EIL in the IOLEDs, we chose the ZnO: K_2CO_3 EIL as an example to measure the operation lifetime of ZnO: M_2CO_3 EIL based IOLEDs. As shown in **Figure S1**, the operation lifetime declined to 50% after 25 h. The microscopic picture of the device shows that the dark strains occurred at the edge of the light-emitting areas. The unsatisfactory lifetime of the device may be attributed to the unstable property of the ZnO: K_2CO_3 film, possibly due to the presence of alkali metal K ion. As Takada et al. reported, the alkali metal ion may diffuse into the emitter layer of the OLED device under the action of the external voltage, which will cause quenching of the photoluminescence (Takada et al., 2017). In the same time, the air-stability of ZnO: M_2CO_3 EIL based IOLEDs were also studied. The result shows that

TABLE 2 | Device performance of the IOLEDs based on the doped ZnO: Li_2CO_3 , ZnO: Na_2CO_3 , ZnO: K_2CO_3 , and ZnO: Cs_2CO_3 EILs.

EIL	V_{on}^a (V)	Luminance ^b (cd/m ²)	CE ^b (cd/A)	PE ^b (lm/W)
ZnO:5% Li_2CO_3	5.5	16,320	5.10	2.01
ZnO:5% Na_2CO_3	5.1	21,219	5.66	2.32
ZnO:5% K_2CO_3	4.8	22,651	6.04	2.61
ZnO:5% Cs_2CO_3	5.3	17,830	4.82	1.88

^aThe driving voltage for the luminance of 1 cd/m².

^bThe maximum values.

the operation lifetime declined to 50% after 13 h (**Figure S2**). **Figure S3** shows the image of the light-emitting areas of the ZnO: M_2CO_3 EIL based IOLED at a driving voltage of 9.0 V after 1, 3, and 24 h. The formation of dark spots and shrinkage from the edge of the light-emitting areas is clearly observed for the device without encapsulation kept in air over 3 h. The poor air-stability of the device should be also ascribed to the presence of alkali metal compounds in the IOLED devices. The alkali metal compounds have undesirable properties of strong affinity for moisture and reactivity with oxygen, which will significantly lead to the degradation of the OLED device (Sato et al., 2018).

CONCLUSIONS

In summary, we have reported efficient IOLEDs employed solution-processed ZnO: M_2CO_3 as an EIL and Alq₃ as an emitter layer. A series of M_2CO_3 , including Li_2CO_3 , Na_2CO_3 , K_2CO_3 , and Cs_2CO_3 , were introduced into the ZnO EIL to enhance the electron injection efficiency of the IOLEDs. Our findings demonstrate that the doped ZnO: M_2CO_3 EIL-based IOLEDs possess obviously improved device performance, compared to the control neat ZnO EIL-based IOLEDs. An optimal current efficiency of 6.04 cd A⁻¹ were obtained from the ZnO: K_2CO_3 EIL based IOLED, which is 54% improved than that of the neat ZnO EIL based device. The

TABLE 1 | Device performance of IOLEDs based on the neat ZnO or doped ZnO: K_2CO_3 EILs with various K_2CO_3 doping concentration.

K_2CO_3 doping concentration	V_{on}^a (V)	Luminance ^b (cd/m ²)	CE ^b (cd/A)	PE ^b (lm/W)
0	5.2	15,430	3.92	1.81
3 wt%	4.9	20,500	5.41	2.46
5 wt%	4.8	22,651	6.04	2.61
10 wt%	5.5	16,500	5.01	1.90

^aThe driving voltage for the luminance of 1 cd/m².

^bThe maximum values.

enhancement is ascribed to the increased electron mobility and reduced barrier height for more efficient electron injection. Our results indicate that the doped ZnO:M₂CO₃ EIL has promising potential for application in highly efficient solution-processed OLEDs.

AUTHOR CONTRIBUTIONS

GC and WZ: designed experiments; FL and ZL: carried out experiments; PZ: analyzed experimental results; GC, PZ, BW, and WZ: wrote the manuscript.

REFERENCES

- Bolink, H. J., Coronado, E., Repetto, D., and Sessolo, M. (2007). Air stable hybrid organic-inorganic light emitting diodes using ZnO as the cathode. *Appl. Phys. Lett.* 91:223501. doi: 10.1063/1.2809387
- Chang, J., Lin, Z., Lin, M., Zhu, C., Zhang, J., and Wu, J. (2015). Solution processed F doped ZnO (ZnO:F) for thin film transistors and improved stability through co-doping with alkali metals. *J. Mater. Chem. C* 3, 1787–1793. doi: 10.1039/C4TC02257B
- Chang, J., Lin, Z., Zhu, C., Chi, C., Zhang, J., and Wu, J. (2013). Solution-processed LiF-doped ZnO films for high performance low temperature field effect transistors and inverted solar cells. *ACS Appl. Mater. Interfaces* 5, 6687–6693. doi: 10.1021/am4014488
- Chen, G., Wang, T., Li, C., Yang, L., Xu, T., Zhu, W., et al. (2016). Enhanced photovoltaic performance in inverted polymer solar cells using Li ion doped ZnO cathode buffer layer. *Org. Electroncis* 36, 50–56. doi: 10.1016/j.orgel.2016.05.033
- Chen, J., Shi, C., Fu, Q., Zhao, F., Hu, Y., Feng Y., et al. (2012). Solution-processable small molecules as efficient universal bipolar host for blue, green and red phosphorescent inverted OLEDs. *J. Mater. Chem.* 22, 5164–5170. doi: 10.1039/C2JM16463A
- Chiba, T., Pu, Y. J., Hirasawa, M., Masuhara, A., Sasabe, H., and Kido, J. (2012). Solution-processed inorganic-organic hybrid electron injection layer for polymer light-emitting devices. *ACS Appl. Mater. Interfaces* 4, 6104–6108. doi: 10.1021/am301732m
- Chiba, T., Pu, Y. J., and Kido, J. (2015). Solution-processable electron injection materials for organic light-emitting devices. *J. Mater. Chem. C* 3, 11567–11576. doi: 10.1039/C5TC02421H
- Chu, T. Y., Chen, J. F., Chen, S. Y., Chen, C. J., and Chen, C. H. (2006). Highly efficient and stable inverted bottom-emission organic light emitting devices. *Appl. Phys. Lett.* 89:053503. doi: 10.1063/1.2268923
- Dong, D., Wang, Y., Lian, L., Feng, D., Wang, H., and He, G. (2017). Novel solution-processed ZnO-based electron injection layer for organic light-emitting diodes. *Phys. Status Solidi A* 214:1700583. doi: 10.1002/pssa.201700583
- Forrest, S. R. (2004). The path to ubiquitous and low-cost organic electronic appliances on plastic. *Nature* 428, 911–918. doi: 10.1038/nature02498
- Fukagawa, H., Sasaki, T., Tsuzuki, T., Nakajima, Y., Takei, T., Motomura, G., et al. (2018). Long-lived flexible displays employing efficient and stable inverted organic light-emitting diodes. *Adv. Mater.* 30:1706768. doi: 10.1002/adma.201706768
- Guo, K., Si, C., Han, C., Pan, S., Chen, G., Zheng, Y., et al. (2017). High-performance flexible inverted organic light-emitting diodes by exploiting MoS₂ nanopillar arrays as electron-injecting and light-coupling layer. *Nanoscale* 9, 14602–14611. doi: 10.1039/C7NR03920D
- Guo, K., Wang, H., Wang, Z., Si, C., Peng, C., Chen, G., et al. (2017). Stable green phosphorescence organic lightemitting diodes with low efficiency roll-off using a novel bipolar thermally activated delayed fluorescence material as host. *Chem. Sci.* 8, 1259–1268. doi: 10.1039/C6SC03008D
- Higuchi, T., Nakanotani, H., and Adachi, C. (2015). High-efficiency white organic light-emitting diodes based on a blue thermally activated delayed fluorescent emitter combined with green and red fluorescent emitters. *Adv. Mater.* 27, 2019–2023. doi: 10.1002/adma.201404967
- Höfle, S., Schienle, A., Bruns, M., Lemmer, U., and Colmann, A. (2014). Enhanced electron injection into inverted polymer light-emitting diodes by combined solution-processed zinc oxide/polyethylenimine interlayers. *Adv. Mater.* 26, 2750–2754. doi: 10.1002/adma.201304666
- Hosono, H., Kim, J., Toda, Y., Kamiya, T., and Watanabe, S. (2017). Transparent amorphous oxide semiconductors for organic electronics: application to inverted OLEDs. *Proc. Natl. Acad. Sci. U.S.A.* 114, 233–238. doi: 10.1073/pnas.1617186114
- Hsieh, S. H., Tsai, T. T., Chang, C. Y., Hsu, S. F., Chuang, C. S., and Lin, Y. (2011). Active-matrix organic light-emitting diode displays with indium gallium zinc oxide thin-film transistors and normal, inverted, and transparent organic light-emitting diodes. *J. Soc. Inf. Disp.* 19, 323–328. doi: 10.1889/JSID19.4.323
- Hsien, P. T., Chen, Y. C., Kao, K. S., and Wang, C. M. (2008). Luminescence mechanism of ZnO thin film investigated by XPS measurement. *Appl. Phys. A* 90, 317–321. doi: 10.1007/s00339-007-4275-3
- Kabra, D., Lu, L. P., Song, M. H., Snaith H. J., and Friend, R. H. (2010). Efficient single-layer polymer light-emitting diodes. *Adv. Mater.* 22, 3194–3198. doi: 10.1002/adma.201000317
- Kido, J., Kimura, M., and Nagai, K. (1995). Multilayer white light-emitting organic electroluminescent device. *Science* 267, 1332–1334. doi: 10.1126/science.267.5202.1332
- Kim, Y. H., Han, T. H., Cho, H., Min, S. Y., Lee, C. L., and Lee, T. W. (2014). Polyethylene imine as an ideal interlayer for highly efficient inverted polymer light-emitting diodes. *Adv. Funct. Mater.* 24, 3808–3814. doi: 10.1002/adfm.201304163
- Li, X. L., Xie, G. Z., Liu, M., Chen, D. C., Cai, X. Y., Peng, J. B., et al. (2016). High-efficiency WOLEDs with high color-rendering index based on a chromaticity-adjustable yellow thermally activated delayed fluorescence emitter. *Adv. Mater.* 28, 4614–4619. doi: 10.1002/adma.201505963
- Lin, Z., Chang, J., Jiang, C., Zhang, J., Wu, J., and Zhu, C. (2014). Enhanced inverted organic solar cell performance by post-treatments of solution-processed ZnO buffer layers. *RSC Adv.* 4, 6646–6651. doi: 10.1039/c3ra46702c
- Lin, Z., Chang, J., Zhang, C., Zhang, J., Wu, J., and Hao, Y. (2016). Low temperature aqueous solution-processed Li doped ZnO buffer layers for high performance inverted organic solar cells. *J. Mater. Chem. C* 4, 6169–6175. doi: 10.1039/C6TC00760K
- Morii, K., Ishida, M., Takashima, T., Shimoda, T., Wang, Q., Nazeeruddin, M. K., et al. (2006). Encapsulation-free hybrid organic-inorganic light-emitting diodes. *Appl. Phys. Lett.* 89:183510. doi: 10.1063/1.2374812
- Nho, S., Baek, G., Park, S., Lee, B. R., Cha, M. J., Lim, D. C., et al. (2016). Highly efficient inverted bulk-heterojunction solar cells with a gradiently-doped ZnO layer. *Energy Environ. Sci.* 9, 240–246. doi: 10.1039/C5EE03045E
- Park, C. H., Lee, H. J., Hwang, J. H., Kim, K. N., Shim, Y. S., Jung, S. G., et al. (2015). High-performance hybrid buffer layer using 1,4,5,8,9,11-hexaazatriphenylenehexacarbonitrile/molybdenum oxide in inverted top-emitting organic light-emitting diodes. *ACS Appl. Mater. Interfaces* 7, 6047–6053. doi: 10.1021/am5091066
- Sasabe, H., and Kido, J. (2010). Multifunctional materials in high-performance OLEDs: challenges for solid-state lighting. *Chem. Mater.* 23, 621–630. doi: 10.1021/cm1024052
- Sato, S., Ohisa, S., Hayashi, Y., Sato, R., Yokoyama, D., Kato, T., et al. (2018). Air-stable and high-performance solution-processed organic light-emitting devices

FUNDING

This work is financially supported by the National Key Research and Development Program of China (No. 2016YFB0401303).

SUPPLEMENTARY MATERIAL

The Supplementary Material for this article can be found online at: <https://www.frontiersin.org/articles/10.3389/fchem.2019.00226/full#supplementary-material>

- based on hydrophobic polymeric ionic liquid carrier-injection layers. *Adv. Mater.* 30:1705915. doi: 10.1002/adma.201705915
- Sessolo, M., and Bolink, H. J. (2011). Hybrid organic–inorganic light-emitting diodes. *Adv. Mater.* 23, 1829–1845. doi: 10.1002/adma.201004324
- Si, C., Chen, G., Guo, K., Pan, S., Peng, C., and Wei, B. (2017). Enhanced performance in inverted organic light-emitting diodes using Li ion doped ZnO cathode buffer layer. *Mol. Cryst. Liq. Cryst.* 651, 118–125. doi: 10.1080/15421406.2017.1338067
- Takada, M., Nagase, T., Kobayashi, T., and Naito, H. (2017). Electron injection in inverted organic light-emitting diodes with poly(ethyleneimine) electron injection layers. *Org. Electron.* 50, 290–295. doi: 10.1016/j.orgel.2017.07.049
- Tokmoldin, N., Griffiths, N., Bradley, D. D. C., and Haque, S. A. (2009). A hybrid inorganic-organic semiconductor light-emitting diode using ZrO_2 as an electron-injection layer. *Adv. Mater.* 21, 3475–3478. doi: 10.1002/adma.200802594
- Wang, Z., Wang, Z., Zhang, R., Guo, K., Wu, Y., Wang, H., et al. (2018). Urea-doped ZnO films as the electron transport layer for high efficiency inverted polymer solar cells. *Front. Chem.* 6:398. doi: 10.3389/fchem.2018.00398
- Zhang, Q., Peng, R., Zhang, C., Chen, D., Lin, Z., Chang, J., et al. (2018). Inverted organic solar cells with low-temperature Al-doped-ZnO electron transport layer processed from aqueous solution. *Polymers*. 10:127. doi: 10.3390/polym10020127
- Zhao, X. D., Li, Y. Q., Xiang, H. Y., Zhang, Y. B., Chen, J. D., Xu, L. H., et al. (2017). Efficient color-stable inverted white organic light-emitting diodes with outcoupling-enhanced ZnO layer. *ACS Appl. Mater. Interfaces* 9, 2767–2775. doi: 10.1021/acsami.6b14778
- Zhong, C. M., Liu, S. J., Huang, F., Wu, H. B., and Cao, Y. (2011). Highly efficient electron injection from indium tin oxide/cross-linkable amino-functionalized polyfluorene interface in inverted organic light emitting devices. *Chem. Mater.* 23, 4870–4876. doi: 10.1021/cm2025685

Conflict of Interest Statement: The authors declare that the research was conducted in the absence of any commercial or financial relationships that could be construed as a potential conflict of interest.

Copyright © 2019 Chen, Liu, Ling, Zhang, Wei and Zhu. This is an open-access article distributed under the terms of the Creative Commons Attribution License (CC BY). The use, distribution or reproduction in other forums is permitted, provided the original author(s) and the copyright owner(s) are credited and that the original publication in this journal is cited, in accordance with accepted academic practice. No use, distribution or reproduction is permitted which does not comply with these terms.

Advantages of publishing in Frontiers



OPEN ACCESS

Articles are free to read
for greatest visibility
and readership



FAST PUBLICATION

Around 90 days
from submission
to decision



HIGH QUALITY PEER-REVIEW

Rigorous, collaborative,
and constructive
peer-review



TRANSPARENT PEER-REVIEW

Editors and reviewers
acknowledged by name
on published articles

Frontiers

Avenue du Tribunal-Fédéral 34
1005 Lausanne | Switzerland

Visit us: www.frontiersin.org

Contact us: info@frontiersin.org | +41 21 510 17 00



REPRODUCIBILITY OF RESEARCH

Support open data
and methods to enhance
research reproducibility



DIGITAL PUBLISHING

Articles designed
for optimal readership
across devices



FOLLOW US

@frontiersin



IMPACT METRICS

Advanced article metrics
track visibility across
digital media



EXTENSIVE PROMOTION

Marketing
and promotion
of impactful research



LOOP RESEARCH NETWORK

Our network
increases your
article's readership